ISSN 0386-5878
Technical Memorandum
of PWRI No.3542

PROCEEDINGS OF THE 13TH U.S. -JAPAN BRIDGE ENGINEERING WORKSHOP

OCTOBER 2 AND 3,1997

PUBLIC WORKS RESEARCH INSTITUTE
MINISTRY OF CONSTRUCTION

1, Asahi, Tsukuba-shi, Ibaraki-ken, 305-0804 Japan

Copyright © (1998) by P.W.R.I.

All rights reserved. No part of this book may be reproduced by any means, nor transmitted, nor translated into a machine language without the written permission of the Director General of P.W.R.I.

この報告書は、土木研究所長の承認を得て刊行したものである。したがって、本報告書の全部又は一部の転載、複製は、土木研究所長の文書による承認を得ずしてこれを行ってはならない。

永久保存

建設省土木研究所
10. 4. 24
図書館

Technical Memorandum
of PWRI No.3542

PROCEEDINGS OF THE 13TH U.S. -JAPAN BRIDGE ENGINEERING WORKSHOP

by

Kazuhiro Nishikawa

Snopsis:

The proceedings document the results of the the thirteenth U.S. -Japan Bridge Engineering Workshop which was held at Tsukuba, Japan, on October 2 and 3, 1997, under the auspices of the Panel on Wind and Seismic Effects, UJNR. The Workshop was organized by Task Committee J "Wind and Earthquake Engineering for Transportation Systems" (U. S. side chairman: Mr. J. D. Cooper, FHWA, Japan side chairman: Mr. K. Nishikawa, PWRI) of the Panel.

Key Words: Bridge Seismic Retrofit, Bridge Management, Bridge Maintenance, Wind, Advanced Materials, UJNR

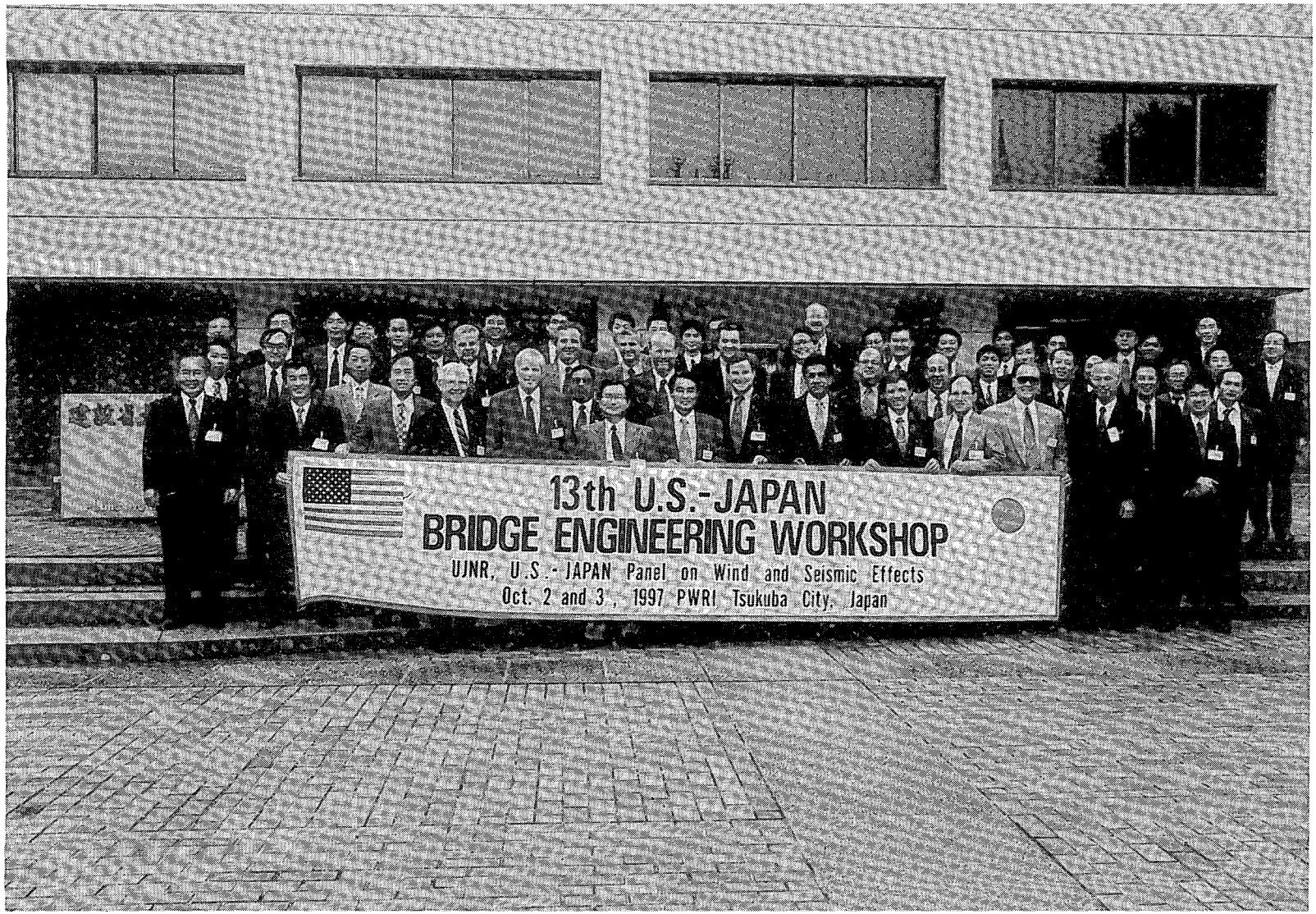
FOREWORD

The 13th U.S.- Japan Bridge Engineering Workshop is a continuation of a series of technical interchanges between the United States and Japan on all topics related to bridge engineering. This series of Workshops have been conducted under the auspices of Task Committee "J" of the U.S.-Japan panel on Wind and Seismic Effects, which is one of 16 panels making up the United States-Japan Cooperative Program in Natural Resources (UJNR). The previous workshops are indicated in the table.

WORKSHOP	DATE	PLACE
First	February 20-22, 1984	Tsukuba, *Japan*
Second	August 19-20, 1985	San Francisco, CA, *United States*
Third	May 8-9, 1987	Tsukuba, *Japan*
Fourth	May 11-12, 1988	San Diego, CA, *United States*
Fifth	May 9-10, 1989	Tsukuba, *Japan*
Sixth	May 7-8, 1990	Lake Tahoe, NV, *United States*
Seventh	May 8-9, 1991	Tsukuba, *Japan*
Eighth	May 11-12, 1992	Chicago, IL, *United States*
Ninth	May 10-11, 1993	Tsukuba, *Japan*
Tenth	May 10-11, 1994	Lake Tahoe, NV, *United States*
Eleventh	May 30-31, 1995	Tsukuba, *Japan*
Twelfth	October 29-30, 1996	Buffalo, NY, *United States*
Thirteenth	October 2-3, 1997	Tsukuba, *Japan*

The steering committee for the 13th U.S.- Japan Workshop consisted of Kazuhiro Nishikawa, James D. Cooper, Jun Murakoshi, Yasushi Josen, Emmanuel Maragakis and David Sanders. The principal funding for the workshop was provided by PWRI.

The workshop proper was held in the PWRI, Tsukuba. The study tour was held in three locations: Nara, Kobe and Nagoya City. The first leg of the study tour started on the Horyuji Temple, Nara. The second leg of the study tour, held in Akashi Kaikyo Bridge, Kobe City, was organized by Honshu-Shikoku Bridge Authority. The third leg of the study tour, held in Tokai-Obu Viaduct, Yatomi Viaduct, Meiko Three Bridges and Kurokawa Rump, etc., Nagoya, was organized by Japan Highway Public Cooperation and Nagoya Expressway Public Cooperation.



Participants of the Workshop

TABLE OF CONTENTS

FOREWORD

PAPERS

SESSION 1: OPENING SESSION 1

SESSION 2: SEISMIC ISSUES (1) 5
(1) Technology to Restore a PC Viaduct Damaged by the Great Hanshin Earthquake 9
(M. Yoshikawa and H. Kanaji)
(2) Seismic Retrofitting of Bridges in New York 25
(Ayaz H. Malik)
(3) A seismic Behavior Assessment of Composite Extradossed Bridge 41
(H. Komatsu, Y. Suzuki and K. Mizuguchi)

SESSION 3: SEISMIC ISSUES (2) 55
(1) Experimental Study of the Effects of Liquefaction-Induced Ground Flow on Bridge Foundation.. 59
(K. Tamura and T. Azuma)
(2) Seismic Vulnerability Studies of Highway Structures 73
(W. Phillip Yen, John D. O'Fallon, James D. Cooper and Ian M. Friedland)
(3) Evaluation of Seismic Performance of Japanese Bridge Piers Designed by the Previous Codes..... 83
(K. Kawashima, J. Sakai and H. Takemura)

SESSION 4: SEISMIC ISSUES (3) 99
(1) Interaction of Hysteretic Behavior between Isolator/Damper and Pier in an Isolated Bridge 103
(K. Kawashima and G. Shoji)
(2) Nonlinear Seismic Response Characteristics of Two-Story Frame Piers 119
(T.Terayama, S.Unjoh and K.Tasaki)
(3) Displacement Issues of Seismically Loaded R/C Bridge Columns..... 133
(Nadim I.Wehbe, M.Saiid Saiidi and David H.Sanders)
(4) Damping Characteristics of a Long-Span Suspension Bridge Identified by Strong-motion Data..... 147
(Y.Adachi and S.Unjoh)

SESSION 5: SEISMIC ISSUES (4) 163
(1) Ductility Improvement of Steel Bridge Columns Based on Large-Scale Cyclic Loading Tests 167
(K. Nishikawa, J. Murakoshi, Y. Josen and M. Takahashi)
(2) Lap Splice and Shear Enhancements in Composite-Jacketed Bridge Columns 189
(Medhat A. Haroun and Maria Q. Feng)
(3) Experimental Studies on Ductility Properties of Steel Rectangular Piers 201
(H. Hanno, H. Tajima and K. funamoto)
(4) A Comparative Study of Elastic-Plastic Seismic Response Analysis
and Pseudo-Dynamic Testing of Steel Bridge Piers 211
(T. Takaku, S. Ikeda, T. Okamoto, H. Matsuda, H. Noto and Y. Kawai)

SESSION 6: MANAGEMENT (1) 227
(1) Network Level Comprehensive Bridge Safety Assurance and Management..... 231
(Arunprakash M. Shirole)
(2) Bridge Alternatives for Low Volume Roads..... 241
(F. Wayne Klaiber, Terry J. Wipf, Brent M. Phares and Jeff R. Reid)

SESSION 7: MANAGEMENT (2) 257
(1) Net-Capable Informatics for Instrumented Bridges 261
(Stuart S. Chen and Michael F. Lamanna)
(2) Development of a Bridge Management System 277
(H. Sato and K. Ogihara)
(3) Optimal Bridge Management under Uncertainty in a Life-Cycle Perspective 287
(Dan M. Frangopol, Allen C. Estes and Kai-Yung Lin)
SESSION 8: MANAGEMENT (3) 301
(1) Evaluation of Bridges by Field Testing 305
(Andrzej S. Nowak, Sangjin Kim and Vijay Saraf)
(2) Development of Survey Method for Bridge Foundations 321
(M. Ishida, N. Akita, A. Watanabe and J. Fukui)
(3) Detection of Concrete Bridges Using Micropower Impulse Radar and Multi-Frequency Diffraction Tomography 335
(Terry D. Philbin)
(4) Hydrogen Embrittlement and Deterioration Effects on Wires in Cable-Supported Bridges 343
(Raimondo Betti, Maciej P. Bieniek, Paul F. Duby, Alan C. West, Scott C. Barton and Garry Veermaas)

SESSION 9: ADVANCED MATERIALS 353
(1) The Use of High Performance Materials in Virginia's Bridges 359
(Malcolm T. Kerley and Jose P. Gomez)
(2) Test Methods and Long-Behavior of Polymer Composites for Bridge Structures 373
(A. Zureick)
(3) Experimental Study on Strengthening Effect of High-Modulus Carbon Fiber Sheet on Damaged Concrete Deck Slab 381
(T. Hoshijima, H. Sakai, H. Otaguro and S. Matsui)
(4) Preliminary Evaluation of an Aluminum Bridge Deck Design for Highway Bridges 395
(Adam Matteo, Peter Massarelli, Jose Gomez, William Wright and James Cooper)
(5) The Design and Construction of Composite-Material Bridges in Delaware 405
(Dennis R. Mertz, John W. Gillespie,Jr. and William A. Edberg)

SESSION 10: SEISMIC ISSUES (5) 415
(1) Compressive Behavior of Concrete Stub Columns Confined by Carbon Fiber Composite Jackets 421
(Y. Xiao and H. Wu)
(2) Design Considerations on the Retrofit of RC Columns with CFRP Sheet 437
(F. Hakamada)
(3) California's Program for the Use of Composite Materials for Seismic Retrofit 453
(Thomas Post and Mohsen Sultan)
(4) Evaluation of Foundations on the Hanshin Expressway Kobe Route Damaged by the Great Hanshin Earthquake 461
(H.Hayashi, K. Kosa, Y. Kimura and H. Kitahara)
(5) Retrofitting of Railway Bridges 473
(E. Manos Maragakis, Bruce M.Douglas, Qingbin Chen and Ray Zelinski)

SESSION 11: WIND 487
(1) Development of Expert System for Wind Resistant Design of Highway Bridges 491
(H. Sato and T. Mabuchi)
(2) Wind Characteristics for Structural Design in Osaka City 507
(Y. Inoshita and T. Yokota)
(3) Very Long Suspension Bridges Using the Temporary Mass Method 523
(S. Nakazaki and H. Yamaguchi)
(4) On Aerodynamic Stability of a Suspension Bridge with Box Girder during Erection Stage 531
(R. Toriumi and M. Takeguchi)

SESSION 12: CLOSING SESSION 545

RESOLUTION 547

APPENDICES

Workshop Program 551
List of Participants 559
Photos of Study Tour 575

SESSION 1: OPENING SESSION

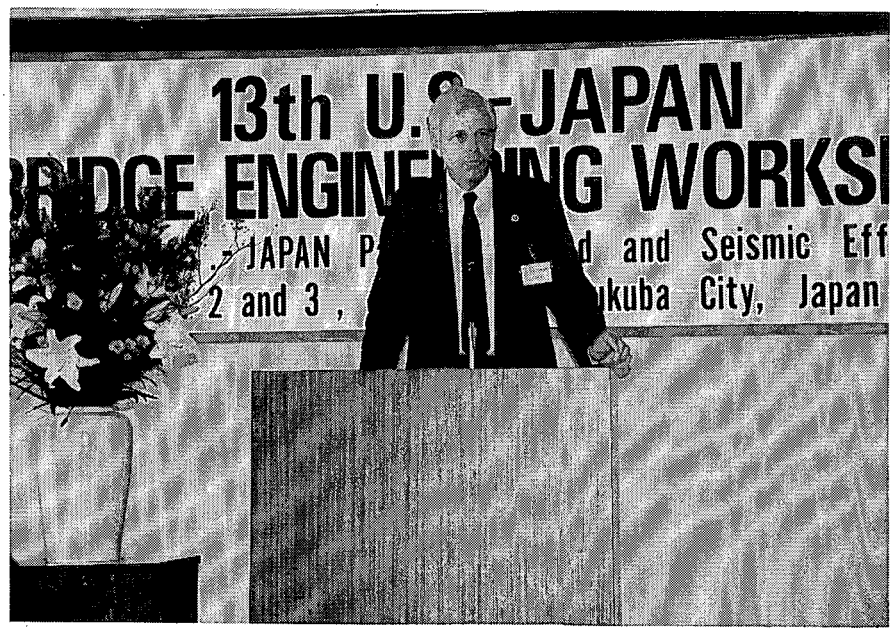
Welcome Remarks: Seizo Tsuji (Director General, PWRI)

Remarks: James D.Cooper (Chairman for the U.S. Side)

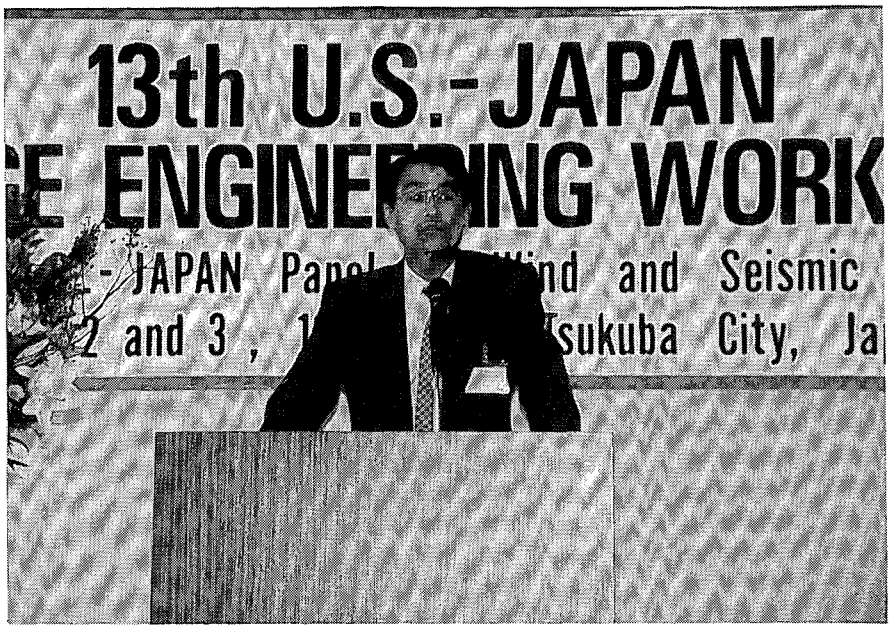
Remarks: Kazuhiro Nishikawa (Chairman for the Japan Side)



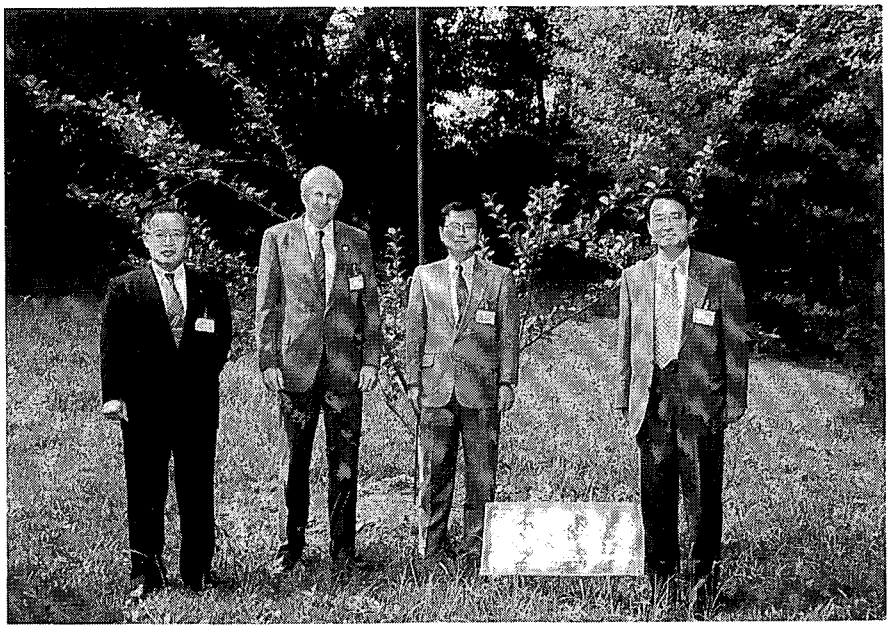
SESSION 1 : Seizo Tsuji



SESSION 1: James D. Cooper



SESSION 1 : Kazuhiro Nishikawa



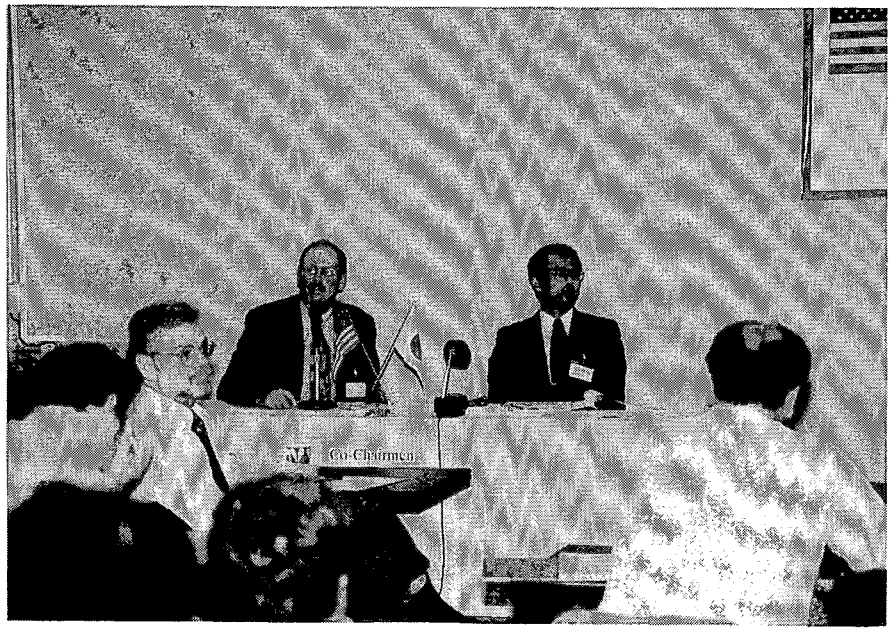
Snap Photograph

SESSION 2: SEISMIC ISSUES (1)

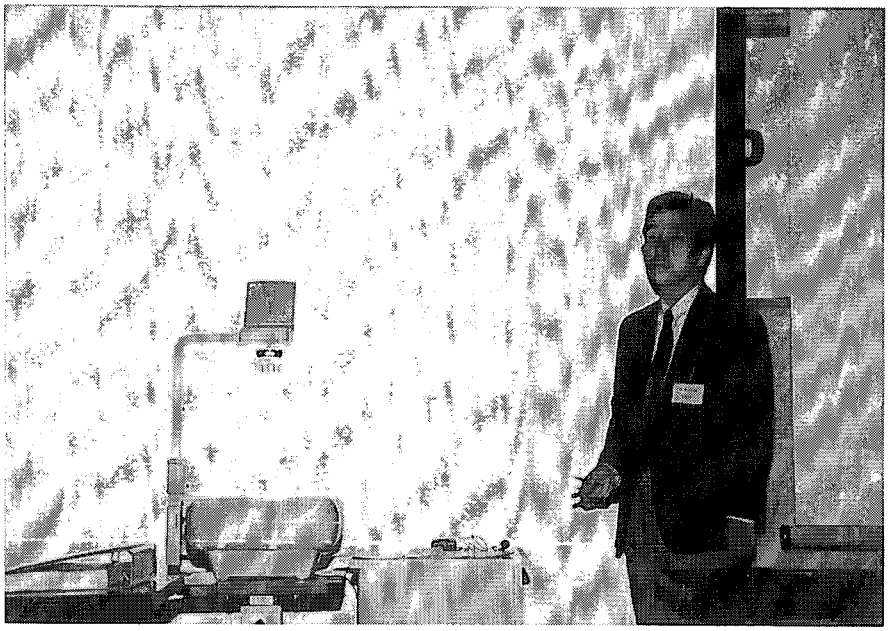
(1) Technology to Restore a PC Viaduct Damaged by the Great Hanshin Earthquake
(M. Yoshikawa and H. Kanaji)

(2) Seismic Retrofitting of Bridges in New York
(Ayaz H. Malik)

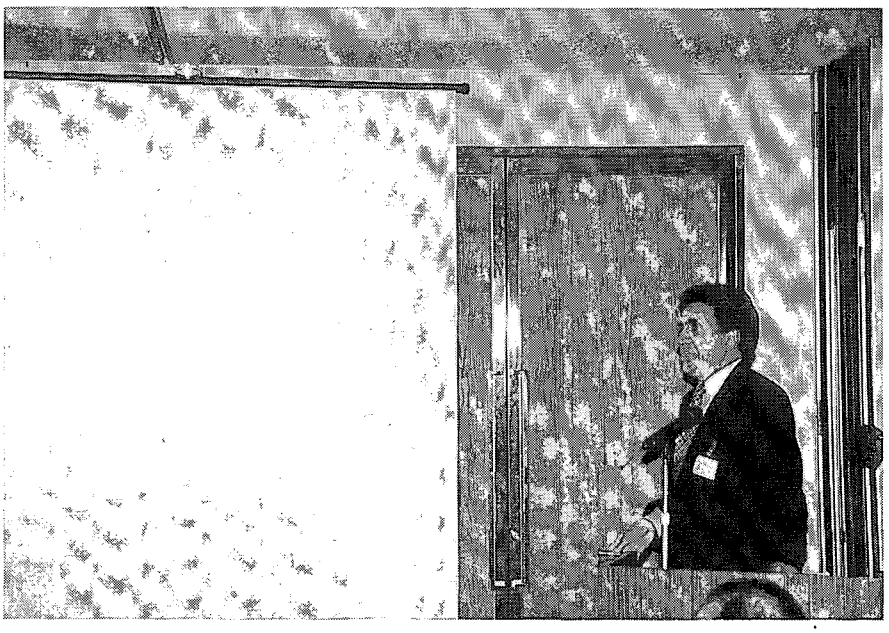
(3) A seismic Behavior Assessment of Composite Extradossed Bridge
(H. Komatsu, Y. Suzuki and K. Mizuguchi)



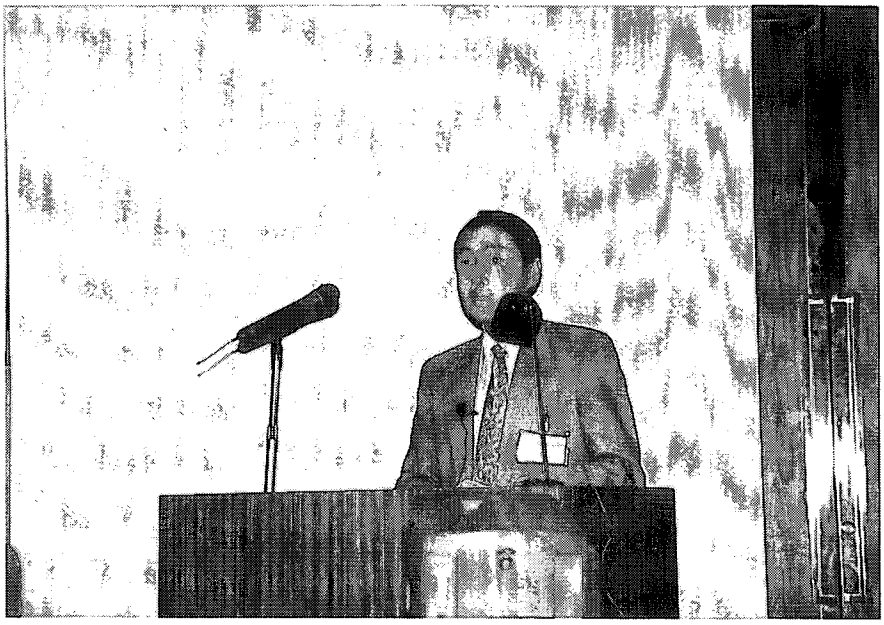
Co-Chairmen : Masahiro Kaneko, David Sanders



SESSION 2 : Hidesada Kanaji



SESSION 2 : Ayaz Malik



SESSION 2 : Kazuyuki Mizuguchi

TECHNOLOGY TO RESTOR A PC VIADUCT DAMAGED BY THE GREAT HANSHIN EARTHQUAKE

Minoru YOSHIKAWA
Manager, Kobe First Construction Division
Hanshin Expressway Public Corporation
Hidesada KANAJI
Engineer, Osaka First Construction Division
Hanshin Expressway Public Corporation

ABSTRACT

The bridge discussed in this paper has simple composite PC girders supported by six RC T-beam piers and one RC rigid frame pier. It was severely damaged by the Great Hanshin Earthquake. The damage included inclination of the eccentric piers and the damage to the end cross beams. To repair the bridge, a jointless girder system with isolators was applied to distribute and reduce inertia force. Specifically, the slab-rubber-hinge type girder connection method was developed; base isolators with both lead-rubber bearings and sliding rubber bearings and restrainers having rubber-sheathed chains were also used. The inclination of the RC T-beam piers was corrected successfully by applying plastic hinges to them.

1. INTRODUCTION

The bridge discussed in this paper is located in Midorocho, Nada Ward, Kobe (see **Figure 1**). At the time of the Great Hanshin Earthquake, the substructure consisted of six RC T-beam piers and one RC rigid frame pier (Piers No.294 to 300), and piles while the superstructure was composed of six simple PC girders. The positioning of piers had been limited due to houses and other structures under the bridge, and some of the T-beam piers were eccentric, having different cantilever lengths.

Eccentric Pier No.297 was found to be severely damaged and leaning in the lateral direction immediately after the Great Hanshin Earthquake. In the meantime, a permanent restoration plan was formulated and the work was finally completed about 10 months after the earthquake.

In formulating the plan, the focus was placed on developing a jointless girder structure and employing omnidirectional seismic isolation or "menshin" devices to increase the seismic resistance of the eccentric piers whose reinforcement possibilities were limited. In addition to RC jacket with steel plate to reinforce piers, which was implemented as a

standard method for the restoration of the Hanshin Expressway[1], new structures and equipment were developed, including base isolators using both lead-rubber bearings (LRB) and sliding rubber bearings (SRB), slab-rubber-hinge to connect each girder and restrainers having rubber-sheathed chains. Tests to verify the validity of these methods and equipment were also conducted.

The preliminary design was first drawn up by applying the seismic coefficient method and a method to check the lateral bearing capacity of reinforced concrete piers. The final, comprehensive design was based on the nonlinear dynamic analysis of the seismic record of the Great Hanshin Earthquake at the Japan Meteorological Agency (JMA) Kobe station. In addition, to verify the validity of the adopted isolated structures, the cumulative strain energy was calculated by analysis of the entire bridge, obtaining the proportions of seismic energy shared by the foundation, piers and isolation bearings.

During restoration, a jacking technique was employed to correct the piers which had inclined approximately 2.2 degrees in the lateral direction by rotating around the plastic hinges near the lower ends of the piers.

In this paper, we report on the damage caused by the earthquake, design of the structural framework and its validation results, LRB-SRB isolation structures, characteristic components and the inclination correction technique.

2. DAMAGE DUE TO THE EARTHQUAKE AND ITS CAUSES

2.1 Outline of the survey

A survey of the piers was conducted as the first step in investigating damage due to the earthquake. A survey of the arrangement of rebar (intervals between rebar, thickness of cover concrete and the positions of joints) and concrete material tests (carbonization, strength and alkali-aggregate reaction) were then conducted and the conditions of the pile foundations (visual inspection of cracks) were examined.

2.2 Girders

The PC girders of the superstructure moved by up to 10 cm north in the lateral direction and the concrete around the anchor bars, which was placed at the end cross beams to prevent the girders from moving, flaked off and had cracks. Such anchor bars were found to have deformed as the concrete moved. No damage, including cracks, was observed in the main girders.

2.3 Piers

Damage to the seven piers ranged from minor, such as extremely small cracks, to severe

such as the 2.2-degree inclination in the lateral direction observed in Pier No.297. The survey of the rebar arrangement using radar found that the intervals between rebar and the thickness of cover concrete were as specified by their design. It also found no difference between the type and positioning of the exposed rebar joints of Pier No.297 and those of adjacent piers. The concrete material tests showed that carbonization had occurred on the surface of the concrete. However, the measured concrete strength was sufficiently higher than the design strength and no harmful substances indicating alkali-aggregate reactions were found.

Our survey was focused, then, on Pier No.297 which was the most severely damaged. It inclined by rotating around the plastic hinge, and the concrete around the hinge flaked off. This damage spread throughout the area between two and four meters above the upper surface of the footing, and the rebar of the outer lap joints were forced away from each other (see **Figure 2**). The results of a survey of the arrangement of rebar and material tests indicate that such damage was mainly caused by the actual seismic force exceeding the design seismic force in the lateral direction. The process proceeded as follows: first, the cover concrete around the main rebar joints at the bottom of the column was damaged, next, the tie hoops that were not anchored inside the concrete then loosened, and finally, the upper and lower rebar of the lap joints broke at their lapped sections.

2.4 Foundations

The cores of the four piles of the two piers were bored to inspect the degree of damage visually and indirectly by inserting a camera into the piles. This found minute cracks in some piles, which did not affect their strength[2]. No damage was observed in the exposed footings.

3. DESIGN OF STRUCTURAL FRAMEWORK AND NONLINEAR DYNAMIC ANALYSIS

3.1 Design plan

The following are the basic design plans of each load level.

- Level I (seismic coefficient method level): Applying the design horizontal seismic coefficient (see the Specifications for the Design of Highway Bridges[3]) of K_h=0.25, the pier cross-sections were determined employing the allowable stress design method.
- Level II (bearing capacity for lateral force): Following the Specifications for the Design of Highway Bridges[3], the lateral bearing capacity of reinforced concrete piers was checked using a design external force of K_{hc}=0.85.
- Level Ⅲ: A time history analysis was conducted using the seismic wave record at the

JMA Kobe station to ensure safety in the ultimate state.

3.2 Structural Framework Plan

The objectives of the structural framework plans were as follows:

- As shown in **Figure 3**, all the PC girders (Piers No.294 to 300) were connected so that they moved together, transferring some of the load applied to Piers No.296 to 299, which had limited reinforcement possibilities, to the other piers that could be reinforced easily.
- Isolation bearings were employed to reduce the reinforcement required by the piers and foundations.
- An omnidirectional isolation structure that would be useful for earthquakes at Level II or above was adopted. This reduces the reinforcement required by eccentric piers, which are prone to severe damage when they are subjected to horizontal forces in the lateral direction during a major earthquake.
- A concrete jacket with a thin steel plate was employed to reinforce the piers. The secondary purpose of this method was to increase the amount of energy absorbed by the isolation bearings whilst increasing pier stiffness.

3.3 Implementation of Design

The cross-section of the piers was designed by setting the stiffness and damping capacity of isolation bearings so that stress would be dispersed correctly during a Level I earthquake. In the longitudinal direction, the horizontal force shared by the pier in the bridge center was changed little even though the design seismic coefficient in the longitudinal direction increased from 0.20 to 0.25.

Checking the pile foundations revealed that their stress had not changed much from the initial design value partially due to the isolation effect. A static cone penetration test found that the actual bearing capacity was higher than the calculated one, so no additional piles were necessary.

For piers under Level III, the movement during such an earthquake was studied by conducting nonlinear dynamic analysis considering the characteristics of isolation bearings, piers and foundations (see **Figure 4**). The record of the Hanshin Earthquake at the JMA Kobe station was used as the input data. The results showed that the maximum shear strain of LRBs and shear force and bending moment of piers were within their allowable values.

When designing the superstructure, the thickness of the end cross beams was increased from 50 cm to 80 cm to increase resistance to external force at Levels I to III. They were fastened from the sides to the main girders by PC wires.

3.4 Energy Dissipation Ratio

To check the overall safety of the bridge, the ratio of cumulative stress energy shared by foundations, piers and isolation bearings was calculated (see **Figure 5**). The energy at short intervals of time was obtained by calculating and summing the values of time history curves of each structural component.

Taking the structural components of the entire bridge as a whole, approximately 70% of the energy was shared by the isolation bearings, 25% by the piers and 5% by the foundations. From this it is deduced that the structure is relatively ideal for the earthquake record at the JMA Kobe station.

4. LRB-SRB COMBINED ISOLATION SYSTEM

4.1 Isolation System[4]

Two kinds of bearings, shown in **Figure 6**, were applied to the bridge. One was the SRB that was placed under the main girders to support the vertical load, and the other was the LRB that was placed in the gap left under the end cross beams by removing part of their underside to absorb inertia force during an earthquake.

New bridges usually have isolating bearings under the main girders for their vertical bearing capacity and to absorb inertia force. This method, however, could not applied to the bridge in this paper which had rubber pad bearings. The reason is that the thickness of these isolators changes considerably the vertical level of that part of the bridge. The above method, which used SRB having a similar thickness to that of the bearings they replaced, was therefore employed.

To support the vertical load, SRB having sliding surfaces made of PTFE and SUS were used so that they would offer little resistance to the horizontal inertia force during an earthquake. In addition, they were placed with their bearing surface on top to prevent debris from covering it. LRB had a low-stiffness rubber layer at the top of them so that the end cross beams only needed to have a little vertical bearing capacity.

4.2 Performance Test[4]

Performance tests were conducted on the LRB and SRB. The purpose of the tests was to study the characteristic features of the isolation structure discussed in this paper, including the properties of the LRB under no vertical load, that of LRB in the diagonal direction and the friction-resistant properties of SRB.

The following are the results verified by the tests :

- The horizontal spring constant and damping capacity of LRB depended on the vertical load, but they were within the design limit regardless of the vertical load (see **Figure 7**).
- There were no significant changes in horizontal spring constant or damping capacity, regardless of the direction of vibration.
- The friction coefficient of SBR was approximately 0.1.

5. CHARACTERISTIC STRUCTURE COMPONENTS

5.1 Connected Girder Structure[5]

The girder connecting sections were designed to satisfy the following conditions: (1) the rotation of the joint section (girder end) due to live load deflection would not be restricted, and (2) inertia force in the longitudinal direction and thermal expansion would be transmitted through the joints. Accordingly, new slab-rubber-hinge types to connect girder members where the end cross beams could be reconstructed was adopted (see **Figure 8**). In this connection method, a buffer rubber was placed on the slab and the upper parts of the end cross beams were connected tightly by PC steel wires.

5.2 Restrainers[6]

A restrainer which could work in directions both longitudinal and lateral to the bridge axis was required for an omnidirectional isolation system. Rubber-sheathed chains as shown in **Figure 9** were adopted. Their impact absorbing properties can also minimize the probability of destruction due to impact . A impact-tension test was conducted to check the impact-absorbing capability of the above chains by applying a maximum load of 80 tf at 150 mm/s by a high-speed tension tester (see **Figure 10**). The design load of the chains was determined so that they could support the girders even if the girders were to separate from their piers.

5.3 Expansion Joints

Expansion joints that can expand in both longitudinal and lateral directions were preferred. However, placing priority on durability under usual traffic loads, steel finger joints were adopted. When a Level Ⅲ earthquake occurs, the tapered edge of one joint's jaw plate runs over the other and a knock-off mechanism works (see **Figure 11**). It is expected that the jaw plate edge will break easily at its foot due to the inertia force when lateral motion is added.

6. TECHNIQUE TO CORRECT THE INCLINATION OF RC PIERS

6.1 Correcting Inclination by the Jack-up Method[7]

This jack-up method was employed to correct the inclination of the RC column by

pushing up an inclined beam. Considering the resistivity of the plastic hinge occurred on the lower part of the column, an additional method was required. Two possible methods were increasing the strength of the beam by the addition of reinforcement and reducing the stiffness of the plastic hinge of the column. The latter was chosen since it could be constructed more safely and was more reliable.

The load was applied in steps of 10 tf at a loading rate of 30 to 60 seconds. Two 200 tf capacity jacks with a horizontally sliding function were used (see **Figure 12**). The target value of the pier inclination was 1/500 radian both in the longitudinal and lateral directions, while the control value of the width of any cracks during correction was 0.5 mm.

The inclination was corrected successfully to within the target value without further reducing the stiffness of the severely damaged hinge, and without cutting through the concrete and rebar (see **Figure 13**). In addition, control values remained within limits during correction, so that the pier was not damaged further.

6.2 Repairing the Plastic Hinge

The plastic hinge of the corrected pier was severely damaged, as could be expected from its rotating movement. Crushed concrete was removed by breaking it into pieces with small rock drills, picks and hammers. The exposed lap joints were cut and removed so they were staggered, and new rebar were connected with existing rebar by butt weld. Concrete was then placed and fine particle cement was poured into previously-inserted pipes to repair internal cracks. This completed the repairs to the plastic hinge.

7. CONCLUSIONS

In this paper we have reported the techniques we used to restore a PC viaduct damaged by the Great Hanshin Earthquake. The following results were obtained through the restoration:

- Employing girder-connecting technology, isolation technology and steel-RC combined jacket technology, a well-balanced design was implemented for safety at the ultimate state. The effects were verified by calculating the cumulative strain deformation energy.
- To increase seismic resistance of the eccentric T-beam piers, an omnidirectional isolation structure is preferable. As practical methods, the isolators and restrainers in this paper are effective.
- To maintain the specified vertical level, a combined LRB-SRB isolation system was adopted. The results of the performance test verified the validity of this method.
- To restore RC pier having plastic hinge with residual deformation, the inclination

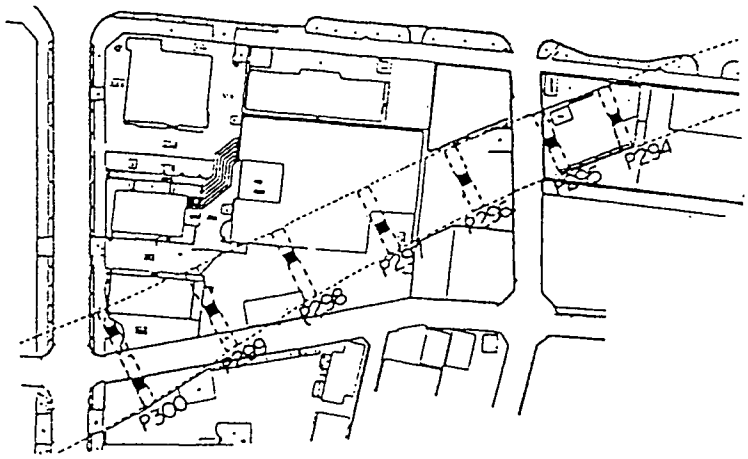
correction method implementing jacks as used on this bridge is effective.

8. ACKNOWLEDGEMENTS

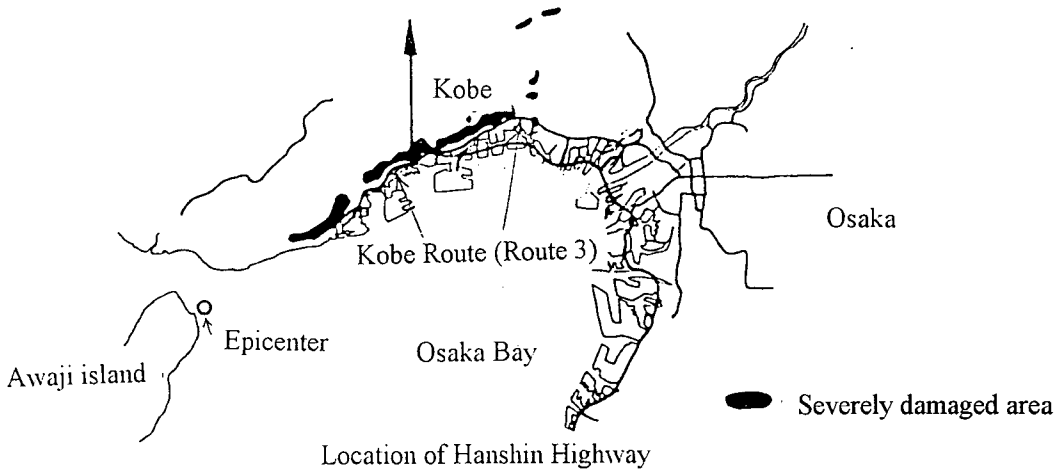
Restoration of the bridge in this paper could only be carried out with the great efforts of the large number of people involved. We would like to take this opportunity to express our sincere gratitude, especially to the members of the Concrete Structure Subcommittee of Hanshin Expressway Earthquake Damage Restoration Technology Committee (Chairperson: Professor Fujii of Kyoto University), as well as Mr. K.Nishimori and Mr. H.Uno of Sogo Engineering Inc., and Mr. T.Shimoda of Hazama Corporation, Ltd. for their efforts in design, analysis and other technical matters.

9. REFERENCES

1. Hanshin Expressway Public Corporation, "Specification for the reconstruction design of Kobe route of Hanshin Expressway", March 1995 (in Japanese).
2. Hanshin Expressway Public Corporation, "Report on the Restoration of Kobe Route Foundations", February 1997 (in Japanese).
3. Japan Road Association, "Specifications for the Design of Highway Bridges", February 1990.
4. Uno, Kanaji, Suzuki, "Development of Menshin System for the Existing Bridge", Proceedings of Annual Japan Society of Civil Engineering, September 1996 (in Japanese).
5. Nomura, Kanaji, Uno, "Performance Test for the Girder Connecting Method of Slab-Rubber-Hinge Type for Existing PC Girder", Proceedings of Annual Japan Society of Civil Engineering, September 1997 (in Japanese).
6. Uruta, Nishioka, Kanaji, Uno, "Development of a Restrainer Having Shock Absorbing Property", Proceedings of Annual Japan Society of Civil Engineering, September 1996 (in Japanese).
7. Shimoda, Yoshikawa, Kanaji, "Correcting the Inclination of RC Piers Damaged by the Hanshin Earthquake", Proceedings of Annual Japan Society of Civil Engineering, September 1996 (in Japanese).



Location of the bridge



Location of Hanshin Highway

Figure 1 Location

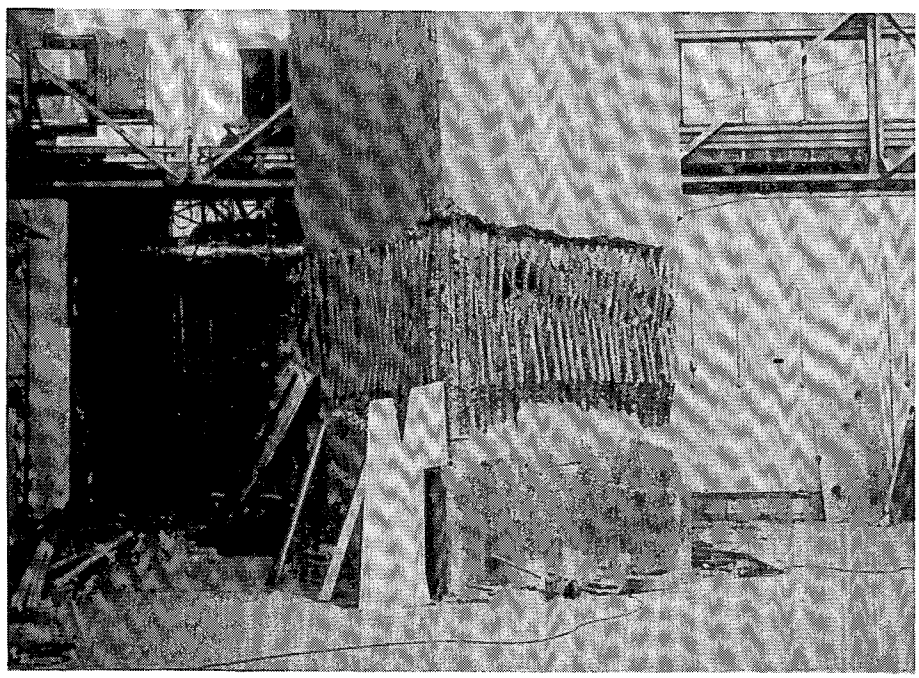


Figure 2 Condition of Pier 297 (near the ground)

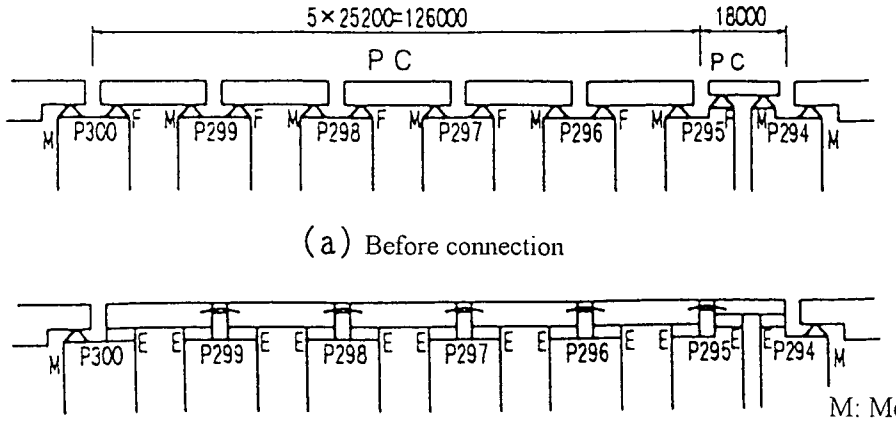
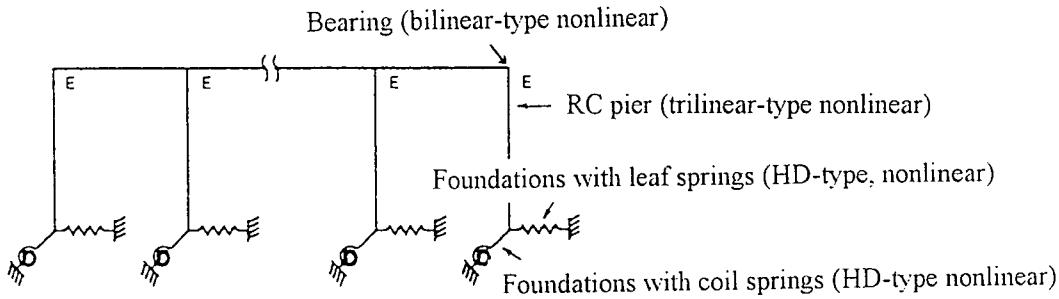
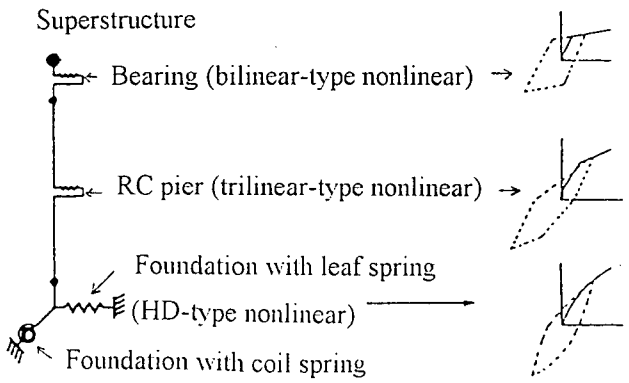


Figure 3 Bearings after/before connecting girders



(a) Models in the longitudinal direction



(b) Models in the lateral direction

Figure 4 Spring-mass models

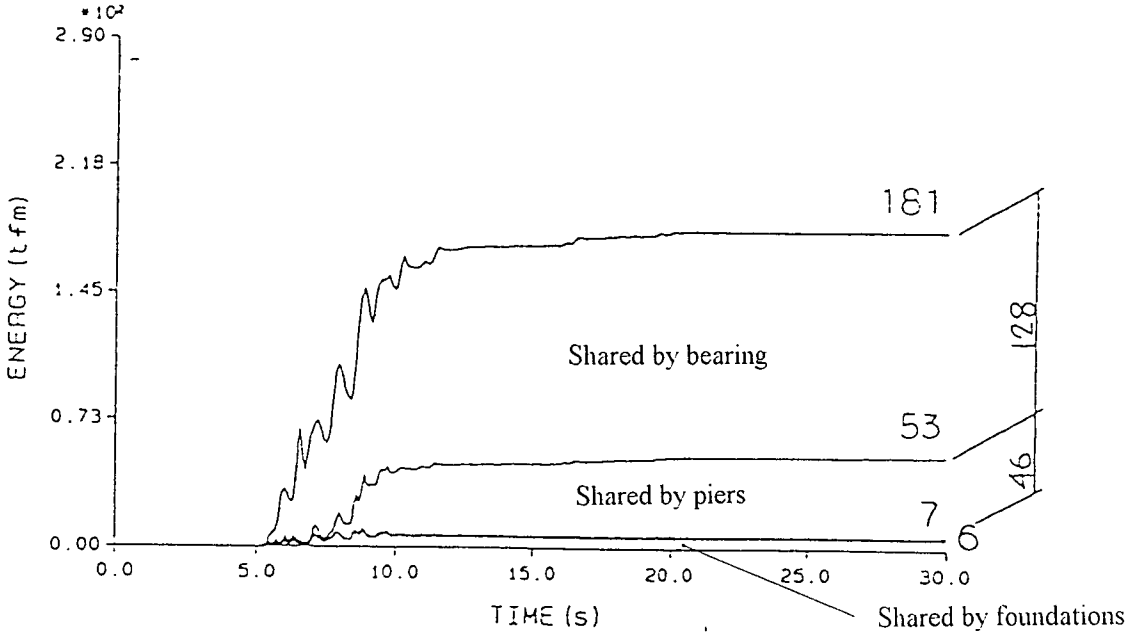


Figure 5 Time history records of cumulative strain energy of Pier 297

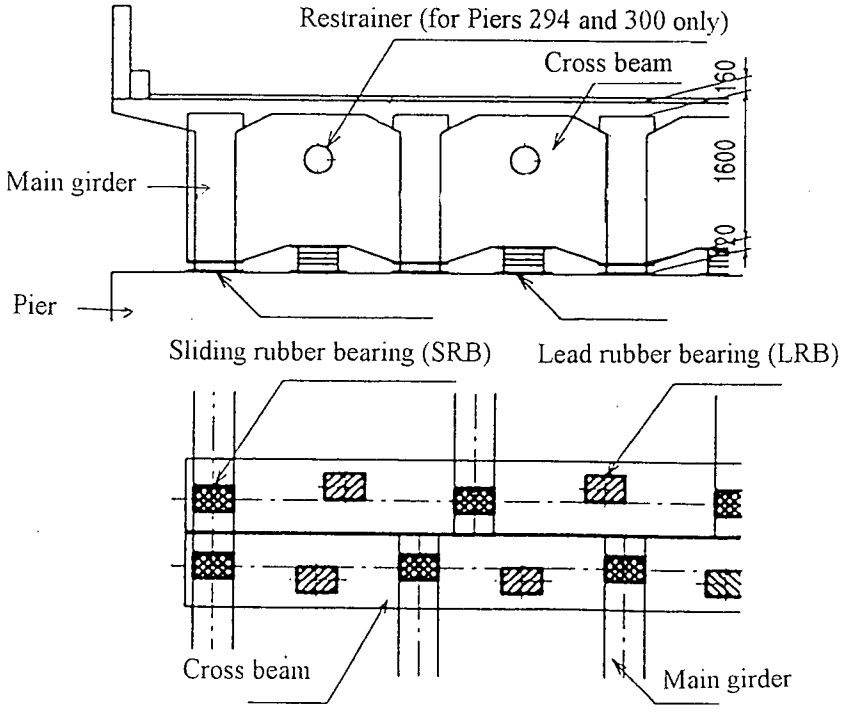


Figure 6 Isolation system with LRB and SRB

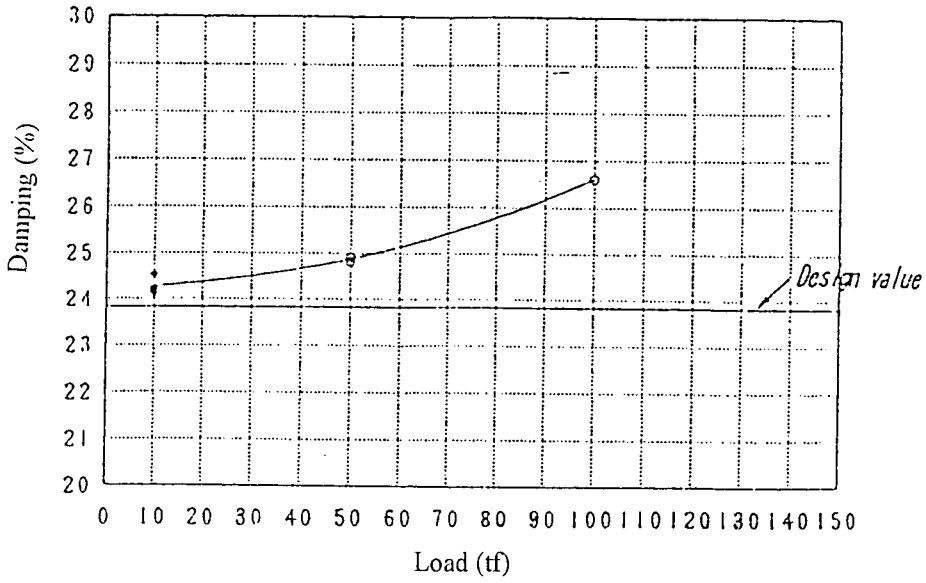


Figure 7 Relationship for LRB between vertical load and damping properties

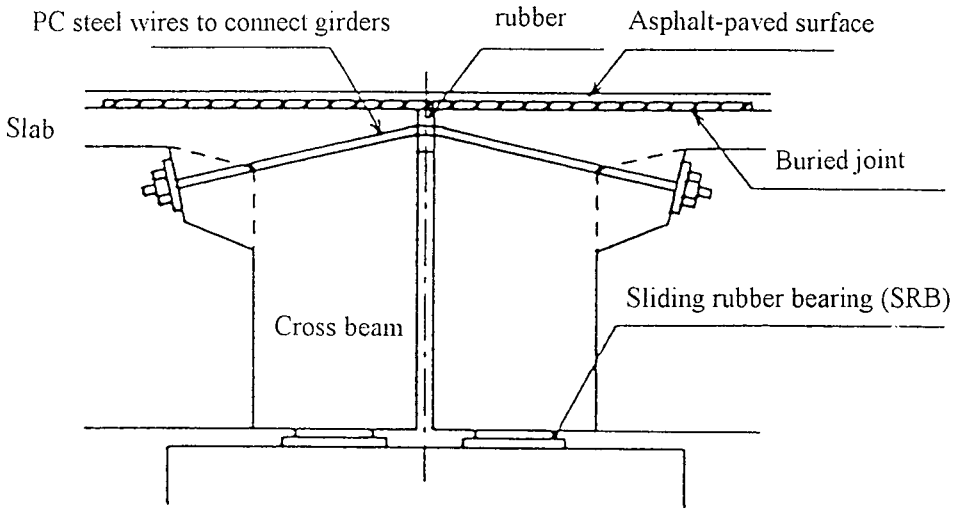


Figure 8 Slab-rubber-hinge type connection structure

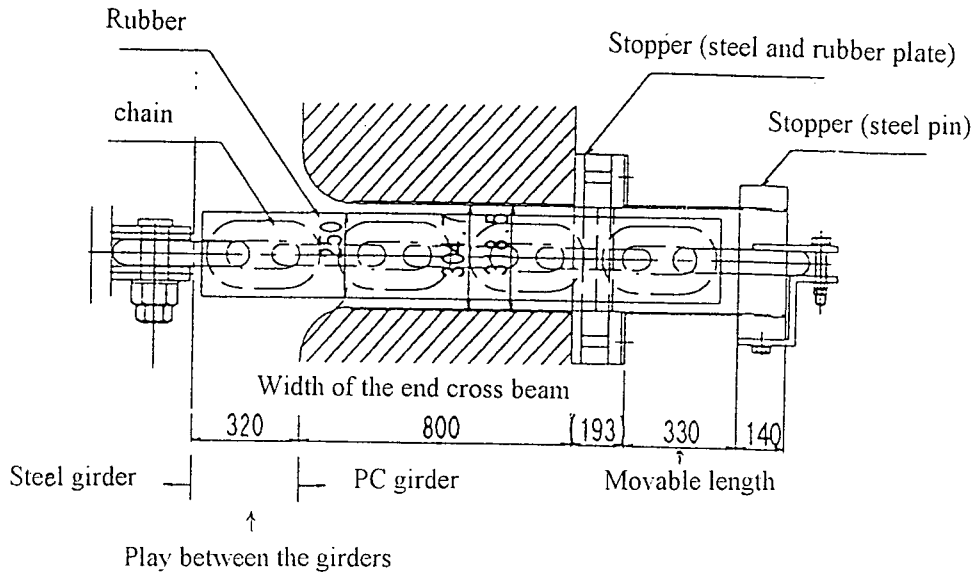


Figure 9 Restrainer with rubber-sheathed chain

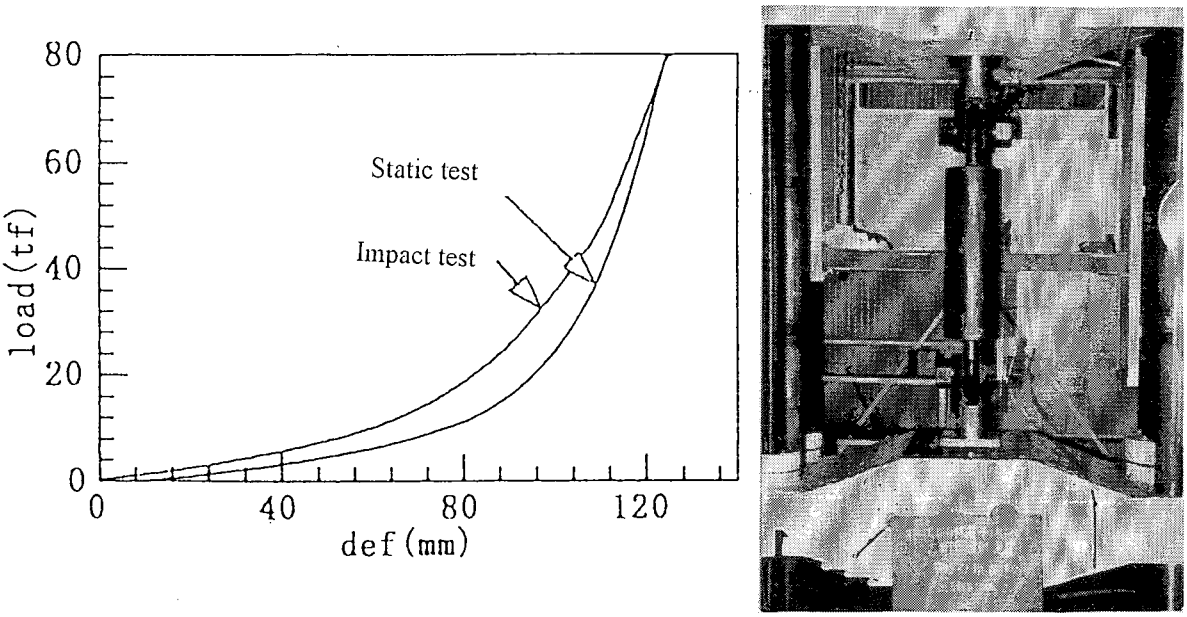


Figure 10 Performance test results of the rubber-sheathed chain

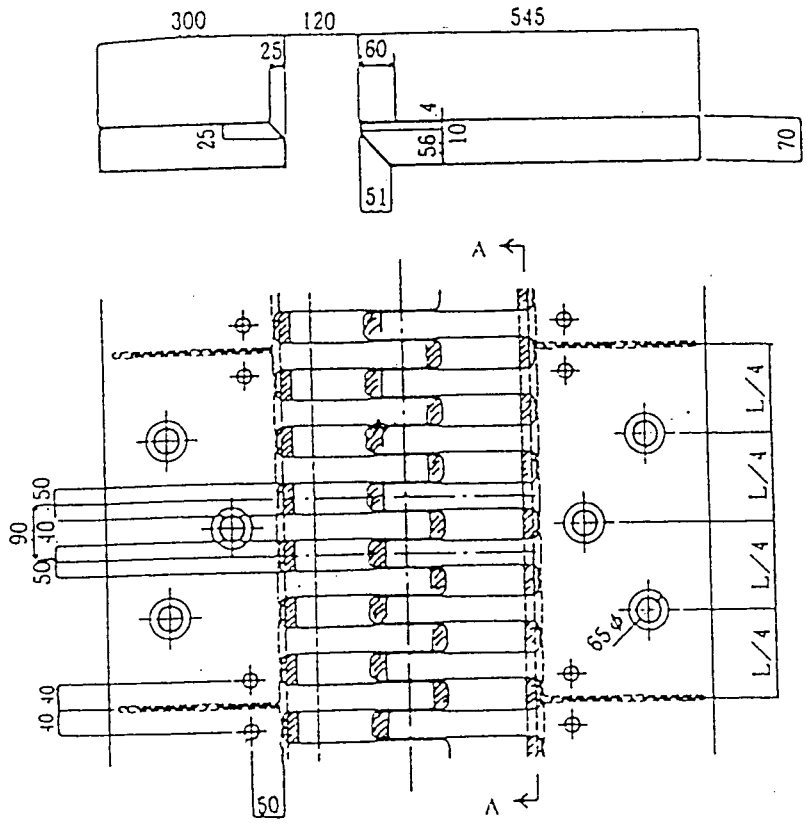


Figure 11 Finger joint with a tapered edge

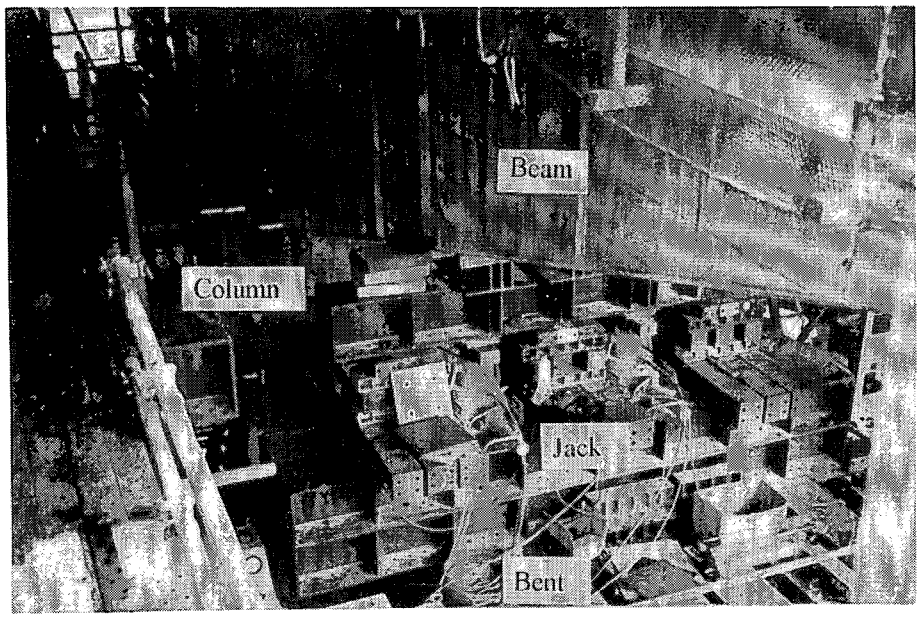


Figure 12 Correcting inclination of Pier 297 (near the jack-up point)

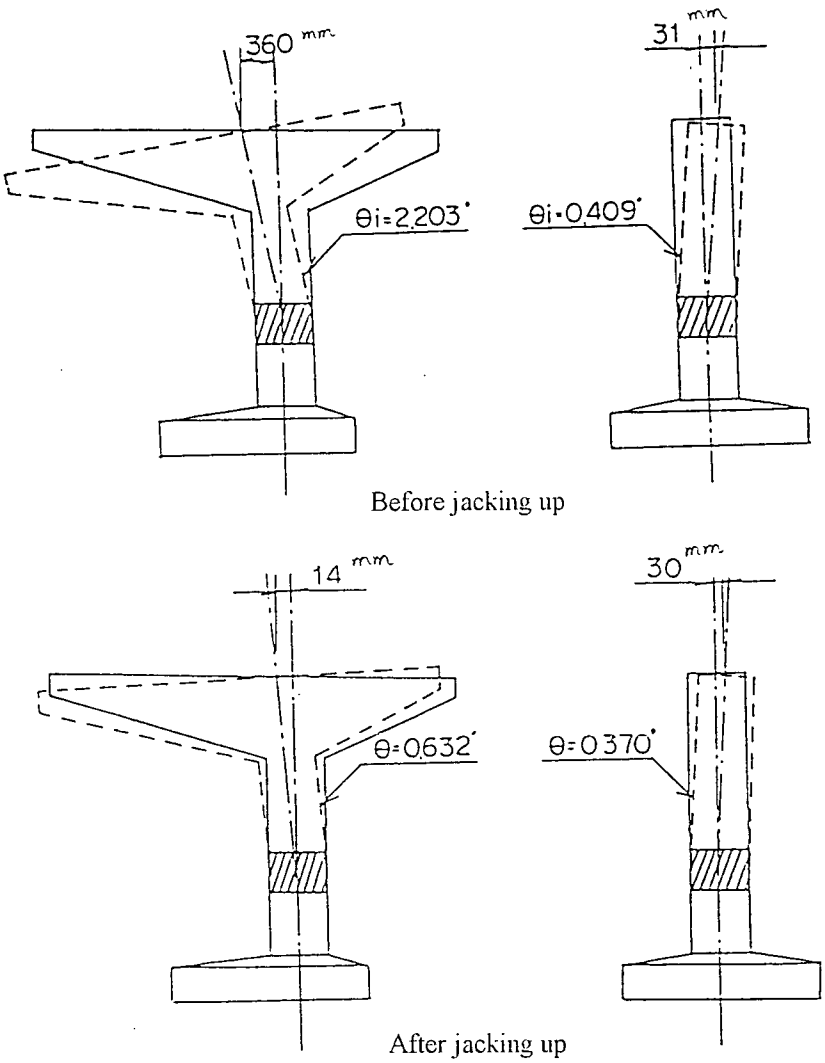


Figure 13 Inclined pier before/after jack-up correction

SEISMIC RETROFITTING OF BRIDGES IN NEW YORK

Ayaz H. Malik, P.E.[1]

ABSTRACT

The N.Y.S.D.O.T. has established policies covering minimum requirements for resisting the seismic forces for new and existing structures. Based on the importance, location and other pertinent features, additional requirements are considered on a project-to-project basis. This paper presents an overview of the seismic design criteria for new structures and seismic retrofitting of conventional existing highway structures as part of the rehabilitation program of New York State. The scope of rehabilitation work considers the seismic vulnerability of the existing elements and aims at improving the seismic resistance and overall performance by retrofitting. Additionally, for larger and complex type of structures more sophisticated analysis techniques have been utilized for evaluating seismic vulnerability of these important structures.

INTRODUCTION

There are currently about 20,000 bridges in New York State under the jurisdiction of State, Bridge Authorities and Local governments. These bridges vary in structural types and materials. Many of these structures are more than fifty years old and the majority of these structures were constructed without any consideration for earthquake loadings. Any moderate to major seismic event can cause severe damage to the structures, endangering public safety and interrupting vital life lines. The New York State Department of Transportation has adopted measures to minimize the potential for catastrophic failure of its bridges (5). It is intended to maintain the retrofitted structures functional after the event, requiring a certain degree of repairs.

SEISMIC ACTIVITY

With the increased frequency of earthquake occurrences elsewhere, the probability of a significant seismic event occurring in the northeastern part of the United States is being given careful consideration. Over the past three centuries, the eastern United States experienced several major earthquakes. Historical evidence indicates that the largest earthquake ever occurred in the United States of America was in the eastern United States, at New Madrid, Missouri, in 1811, equivalent to 8.0 on the Richter scale.

The biggest earthquake ever recorded in New York State was in Messina, New York, two hundred miles northwest of Albany. It occurred on September 5, 1944, measuring 6.0 on the

---

[1] Associate Civil Engineer, New York State Department of Transportation, Albany, New York, USA 12232.

Richter scale. Since 1884, New York State has experienced four earthquakes with Richter Magnitudes greater than 5.0. The neighboring Canadian Provinces have experienced earthquakes of magnitude up to 7.0, which also affected New York State and adjacent areas.

Certain parts of the United States have traditionally ignored the potential for seismic damage, since evidence of past earthquakes of significance was relatively rare. The Northeast, including New York, was among those areas. Continuing advances in seismology and the increased public attention have caused scientists and engineers to look more closely at the threat that earthquakes pose to this area.

NEW YORK STATE DEPARTMENT OF TRANSPORTATION SEISMIC CRITERIA

New York State Department of Transportation has developed "guidelines" to assist in the design of new structures and evaluate vulnerability of existing structures. They are summarized below.

Seismic Criteria for Design of New Structures

The seismic design requirements of Division 1A of the 1994 AASHTO Specifications are incorporated into the New York State Standard Specifications for Highway Bridges (1), with the following modifications:

- Although New York State comes under Seismic Performance Category 'A' (SPC 'A') and SPC 'B' on the AASHTO rock acceleration map, designers shall use a rock acceleration coefficient equal to 0.19 for the design of all new highway bridges.

- Seismic analysis shall consider the gravity load as the sum of the dead load plus live load.

- Continuous structures on a multiple span bridge shall be used rather than a series of simply-supported single spans.

- Steel rocker or steel sliding bearings shall not be used. Elastomeric pads (plain, or laminated with or without load plates) or multi-rotational (pot type or disc type) shall be used. Multi-rotational expansion bearings shall always be provided with guide bars, to allow limited lateral movement.

- Bridge bearings shall be anchored on the bridge seat. Anchor bolts shall be provided with a minimum of 200 mm (8 inch) edge cover with reinforced concrete substructures.

- Abutments shall be provided with a continuous bridge seat. Stub type abutments with isolated bearing seats shall not be used.

♦ Skewed layout of substructures shall be minimized as much as possible.

Superstructures and substructures are first designed for non-seismic group loadings specified by AASHTO. Seismic analysis is conducted on the "designed" structure. Designers have access to the SEISAB bridge seismic analysis program. Conventional structures are analyzed by modeling fixity condition at the substructure foundations. Multiple span bridges are analyzed by Response Spectrum Method, using the AASHTO Ground Motion Spectra and an acceleration coefficient of 0.19. Capacities of the designed structure are checked against the seismic forces (demand) and adjustments are made to the design as warranted. In all cases (whether seismic forces control or not), standard seismic details for: reinforcement, connections between superstructure and substructure, support length, column confinement, and footing anchorage details conforming to the AASHTO Division 1A are utilized.

Seismic Criteria for Design of Existing Structures

♦ Existing bridges programmed for rehabilitation are evaluated for seismic failure vulnerability and retrofitting measures are incorporated into the rehabilitation contract.

♦ Initial seismic evaluations and seismic element analysis are based on the actual rock acceleration coefficient from AASHTO's rock acceleration map, attributable to the bridge site. In New York, AASHTO rock acceleration coefficients vary from .09 to .15.

♦ If retrofitting is deemed necessary, then all retrofitted elements are designed to meet NYSDOT 'new bridge' specifications.

♦ Capacity Demand ratios are computed for all elements of the bridge as outlined in FHWA's Seismic Retrofitting Manual for Highway Bridges (7).

Bearing Retrofitting

As observed in the previous earthquakes, as well as in the recent Kobe (Hanshin-Awaji, Japan) earthquake, steel bearings performed very poorly and bearing failure was the cause of the many structural failures (3, 9). During an earthquake, bearings are subjected to displacements, rotation and lateral forces in various directions, resulting in brittle failure of the unidirectional steel high rocker and low sliding bearings (Figures 1 and 2).

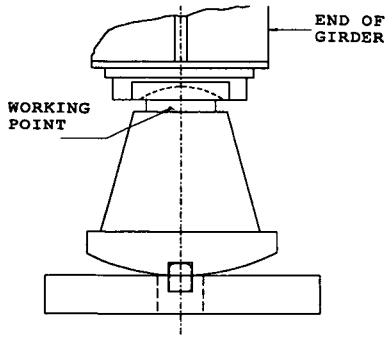


Figure 1 Steel Rocker Bearing

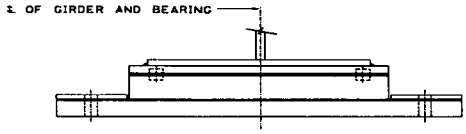


Figure 2 Steel Sliding Bearing

Replacing these bearings with ductile, multi-rotational and multi-directional bearings provide safety against potential unseating of the superstructure (Figures 3 and 4).

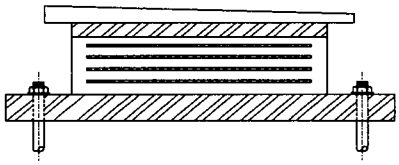


Figure 3 Elastomeric Bearing with Laminated Load Plates

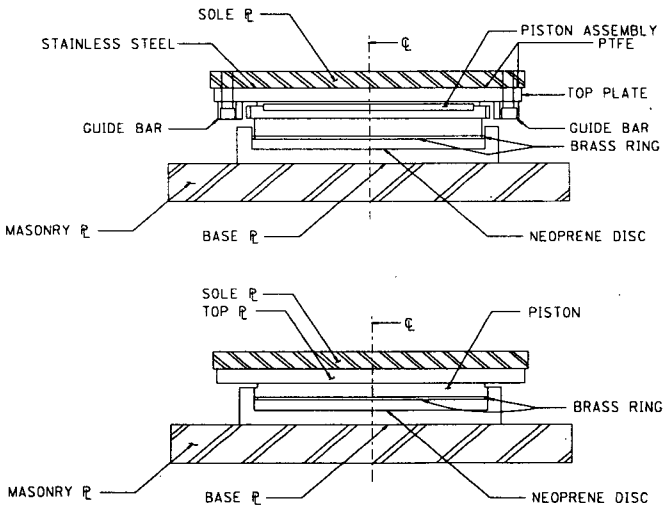


Figure 4 Expansion and Fixed Multi-Rotational Bearings

During the rehabilitation work, existing structures are jacked to remove the existing steel rocker or low sliding bearings. Due to the height difference between the elastomeric bearings and the existing rocker bearings, existing pedestals are built up to higher elevation, as recommended in the FHWA Retrofitting Manual (7). Alternately, steel extensions bolted to the bottom flange are used to adjust the height difference. Fixed steel bearings are replaced in a similar manner with fixed elastomeric bearings. New anchor bolts are set into the built up pedestals or drilled into the existing pedestals.

Depending upon the capacity of the existing substructure, various options have been considered to reduce the seismic design demand by adjusting the bearing configurations in one of the following manners:

- Providing fixed bearings at one of the abutments, and expansion bearings at the piers and the other abutment. This will help to reduce the seismic demand at the piers (Figure 6a).

- Providing all expansion bearings with lateral restrainers (Figure 5), thus reducing the transverse force demand by distributing it to all the substructures through expansion and fixed bearings (Figure 6b). Additionally, to further improve the longitudinal resistance, one abutment can be provided with fixed bearings and the other abutment can be provided with expansion bearings along with lockup devices (Figure 6b).

- Providing conventional laminated elastomeric bearings at the expansion supports and using a lead core base-isolation bearing at the fixed support. This will reduce the seismic demand, even at the fixed substructure (Figures 6c). For thermal expansion and contraction, the lead core bearing acts as a fixed bearing.

- Providing guided pot bearings at the expansion supports and a lead core base-isolation bearing at the fixed support. Since the coefficient of friction for expansion pot bearing is less than the elastomeric bearing, it will further cut down the demand in the longitudinal direction on the substructures (Figure 6d).

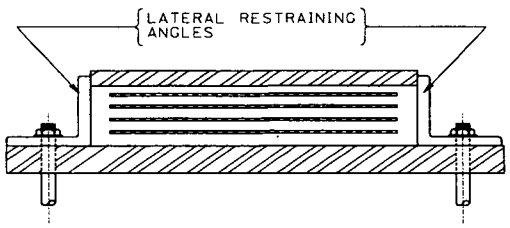


Figure 5 Elastomeric Bearing with Lateral Restraining Angles

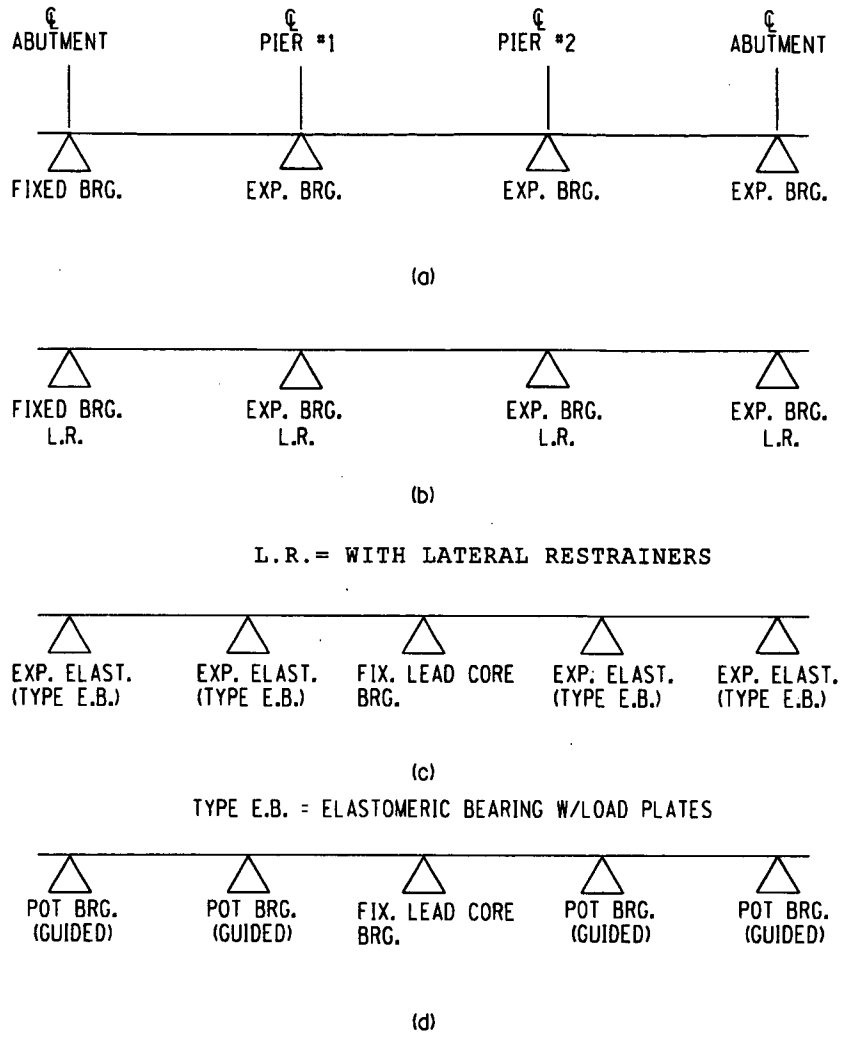


Figure 6 Various Lockup Devices

RETROFITTING FOR CONTINUITY

Simply supported spans are made continuous, when feasible to provide redundancy (8). Continuity enhances the seismic response by distributing the in-plane forces to the piers and abutments and prevents loss of end support at piers due to longitudinal movement. When connecting the unrestrained ends of the two girder spans it is important to provide a complete splice between the flanges and the webs. Bolted splices are used since they provide ductility to the connection (Figure 7).

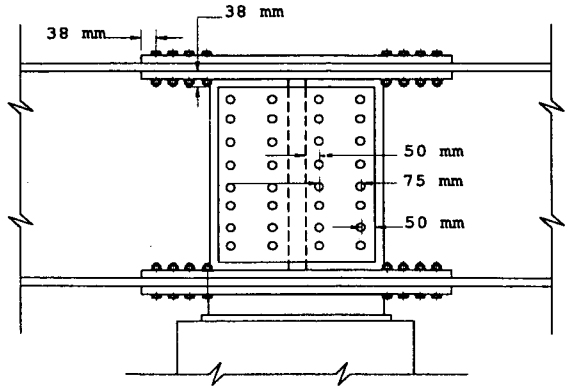
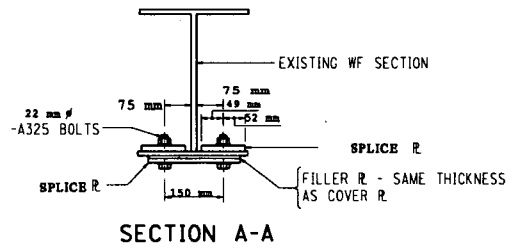


Figure 7 Typical Elevation at Piers

The use of slotted holes to allow any movement in the connection may cause brittle failure of the connection. Since continuity will introduce stress reversal, fatigue critical details at the end of bottom flange partial cover plates (if any) are retrofitted by a bolted splice (Figure 8) as per the AASHTO Standard Specification (1).



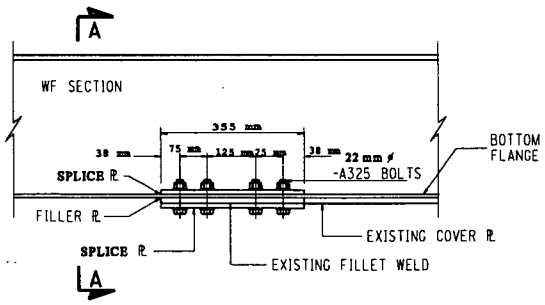


Figure 8 Bottom Flange Cover Plate Retrofit

Overstressing due to the continuity is controlled by using a lightweight deck. The two lines of bearings at the piers are replaced with a single elastomeric bearing, thus eliminating the dead load and/or live load eccentricity on the pier column(s) (Figure 9).

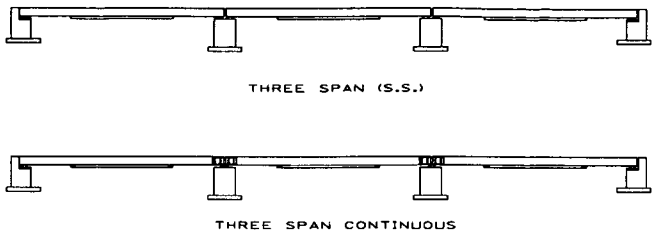


Figure 9 Continuity

For structures with pin and hanger systems, the suspended spans are fully-spliced with the cantilever to eliminate the vulnerable pin and hanger system (Figure 10).

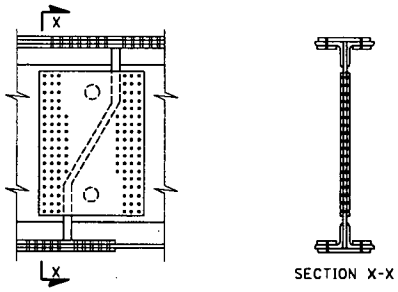


Figure 10 Splice Details

Where continuity is not feasible, restrainers and shear blocks (Figure 11) as recommended in the FHWA Retrofitting Manual (7) are used to prevent unseating of the superstructure girders.

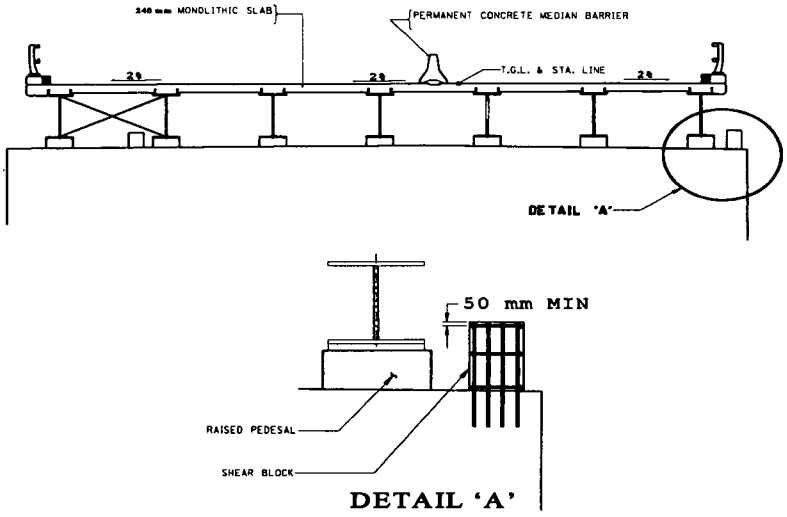


Figure 11 Shear Restrainers

Column Retrofitting

The current practice for earthquake resistance design of columns for bridge piers is to provide sufficient confinement of the potential plastic hinge locations by ties or spirals. Almost 90% of the existing pier columns are not provided with sufficient confinement necessary to improve the compressive strain and provide proper lateral support to the primary reinforcement. Hence, the failure of the column due to flexure or shear (in case of a short column) can be avoided by providing adequate confinement. In New York, this is typically done by retrofitting columns with steel or concrete jacketing and adding ties.

Steel Jacketing

By analyzing the existing columns for the design earthquake, the columns are checked for the flexural strength and the shear strength demands. Circular columns have been retrofitted with 10 mm (3/8") thick steel casing to provide passive confinement. To avoid excessive moment demand on the adjacent cap beam/footing a 10 mm (3/8") rubber sheet is placed between the in-fill grout and the steel casing around the column top/bottom. Figure 12 shows the details of the steel jacket retrofitting.

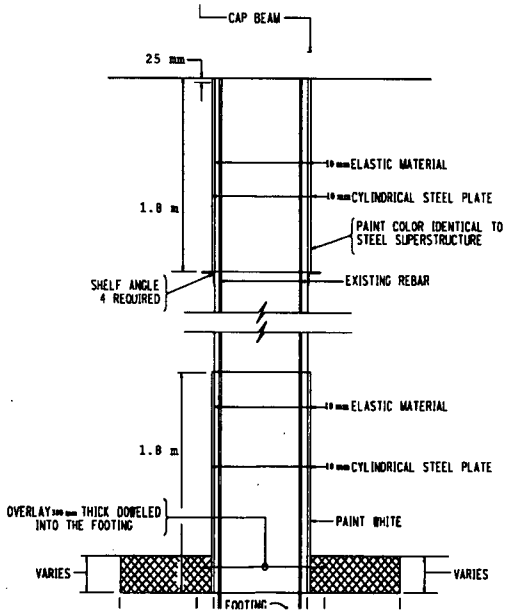


Figure 12 Seismic Retrofit for Pier Columns

Reinforced Concrete Jacketing

For solid (wall type) piers, a 305 mm (12 inch) thick layer of reinforced concrete is used as a jacket to provide flexural (longitudinal) as well as confinement reinforcement for the existing pier. A 1.2 m (4 foot) by 1.2 m (4 foot) grid pattern of drilling and grouting is used to dowel the

concrete jacket to the existing pier. Figure 13 shows details of the retrofitted pier.

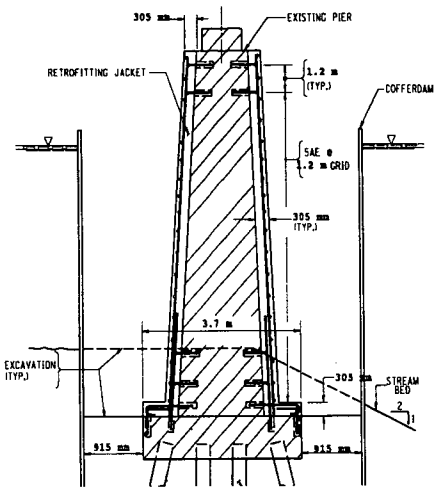


Figure 13 Reinforced Concrete Jacketing

Adding Ties

Adding of ties increases the shear strength of the column section along with the confinement for the column. This causes the flexural failure to occur before the shear failure, thus premature shear failure can be avoided. At the bottom of flared columns, adequate confinement is provided by adding ties (hoops) spaced equally between the existing 305 mm (12") centered ties. First the concrete cover is removed from the plastic hinge area and #5 hoops are tied around the existing flexural (longitudinal) reinforcement, alternating with the existing ties (Figure 14).

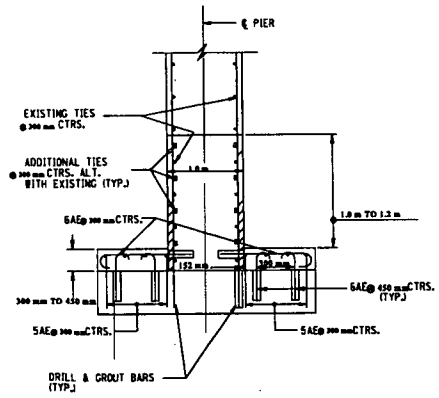


Figure 14 Footing Retrofit

Additionally, a 460 mm (18") thick reinforced concrete overlay is doweled into the existing footing. The retrofitted column has ties going 460 mm (18") into the retrofitted footing. Concrete cover is placed to match the existing column dimensions.

Foundation Retrofitting

Adding Piles

To satisfy the seismic demand for the design earthquake, piles are added to the existing foundation along with extension of the pile cap doweled into the existing cap. Additional piles with twice the capacity (soil and structural) are driven at the corners. By simple analysis of the pile group under the seismic load (plus any new load due to rehabilitation work) pile loads are computed by the following equation: Seismic load on pile = $P_s/n \pm M_{yy}/S_{xx} \pm M_{xx}/S_{yy}$; where P_s is the seismic axial load , n is the number of piles, M_{yy} and M_{xx} are the seismic longitudinal and transverse moment combinations, respectively, S_{xx} and S_{yy} being the corresponding section modulii. Existing pile loads plus the additional load due to earthquake, computed above, should not exceed the ultimate capacity of the existing piles. (Figure 15).

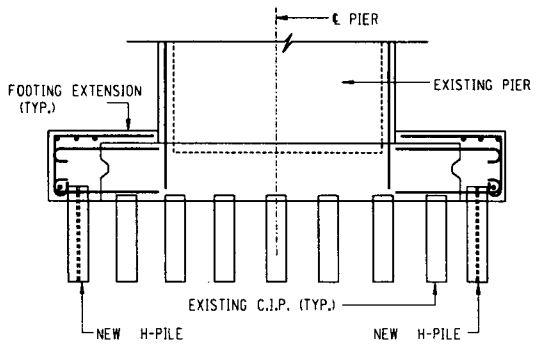


Figure 15 Foundation Retrofit

Bridging the Liquefiable Layer

To determine the liquefaction potential of cohesionless soils NYSDOT's Geotechnical Engineering Bureau uses two procedures (6). They are: 1) The empirical correlation based on the SPT blow count and field performance; and 2) a simplified steady-state strength procedure for analyzing stability of embankments and slopes against flow failures.

Depending on the thickness of the potential liquefiable layer at the existing pile foundation, additional steel piles are driven to rock to sustain the seismic loads under liquefiable conditions. The steel piles are over designed to carry the design loads below their buckling load capacity

(Figure 16). This is determined by approximating the end conditions of the pile, to figure out the effective length factor,'K'. For example, for steel piles with a reinforced concrete footing and driven to bearing on rock, 'K' value of 1.0 will be used to determine $P_{ultimate}$ equal to $\Pi^2 AE/(Kl/r)^2$, where A is defined as the cross sectional area, E is the elastic modulus, Kl is the effective length, and r is the radius of gyration. Once the size is selected, Geotechnical Bureau performs the lateral analysis of the pile using FHWA's 'COM624' analysis program and its proprietary versions 'L-Pile' and 'Group' (distributed by Ensoft Products) to verify the adequacy of the selected pile(s).

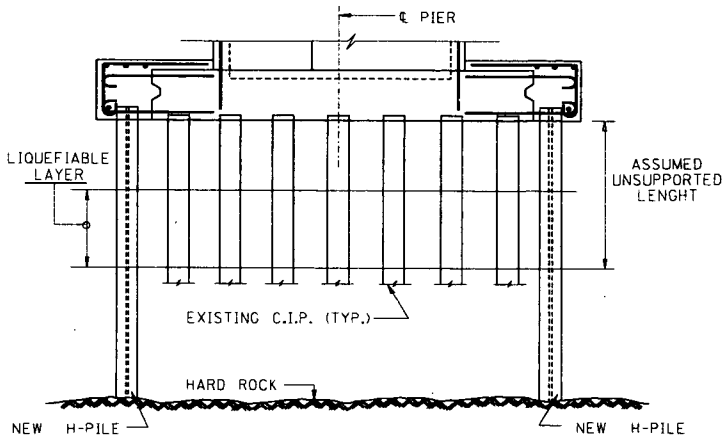


Figure 16 Bridging the Liquefiable Layer

Retrofitted Projects

Following are the number of projects, retrofitted for various elements of the existing structures, between 1991 and the end of 1995.

Table 3 Seismic Retrofits of NY Bridges

DESCRIPTION	TOTAL NUMBER OF STRUCTURES
Replacement of existing rocker and low steel bearings with elastomeric or multi-rotational pot bearings	431
Cable restrainers as seismic retrofit measure	29
Extension of bearing seat	28
Introduction of continuity on simple span stringers (No. of spans)	152
Pier column jacketing (steel or reinforced concrete)	21
Pin and hanger retrofit (continuity)	8

Retrofitting of Special Non-conventional Existing Structures

There are several structures in New York City which are more than 75 years old and are essential transportation network links for the city with a population of more than 10 million. These structures are maintained and upgraded by ongoing contracts for various elements of the bridge. As a supplement to these contracts 'Request For Proposal' are advertised, outlining the scope of seismic work to be performed. The performance goals are set based on the importance and location of the structure.

A good example of such a project is Queensboro bridge, connecting the boroughs of Queens and Manhattan, with a daily traffic count of about 147,000 vehicles. As part of an ongoing seismic retrofit program, the design consultant was required to provide seismic evaluation and retrofit recommendations for the main bridge 1135 m long (3724 ft.), and Queens 813 m (2667 ft.) and Manhattan 330 m (1082 ft.) long approaches of the Queensboro bridge (2). The Queensboro bridge, 18.3 m (60 ft.) wide, is a two level double cantilever truss structure, opened to traffic in 1909.

The performance goals were set for two levels of site-specific earthquake as follows:

- The bridge must remain functional, which implies that it shall be capable to carry normal traffic almost immediately, with minimal or no damage to structural elements during a low to moderate hazard event, called an Operation Basis Earthquake (OBE) . This is an earthquake with a 10% probability of exceedence in 50 years, or a return period of approximately 500 years.

- The bridge shall be capable to carry limited traffic within days and full traffic within months. Damage shall be repairable without complete closure for extended periods during a high hazard event, called a Structural Safety Earthquake (SSE). This is an earthquake with a 10% probability of exceedence in 250 years, or a return period of approximately 2,500 years.

Following are the specific tasks included in this study:

- Review subsurface geotechnical conditions and determine soil profiles at the bridge site. Conduct soil exploration (drilling) and perform specialized field and laboratory tests supplement the soil data from existing records. Assess the potential for soil liquefaction and the likely effect of the structure.

- Modify the bedrock ground motions for the effect of soil profiles beneath the bridge to develop the ground motions at the level of the foundations. Provide two horizontal and one vertical component of design spectra and time histories.

- Provide input regarding the spatial coherence or spatial variation of ground motions for

calculations of the effect of out-of-phase motions on the performance of the bridge superstructure.

- Conduct field measurements of ambient bridge and ground (foundation) motions due to traffic or wind, to determine the modal behavior of the Queensboro Bridge. The mode shapes, frequencies and damping were compared with those obtained from computer models of the dynamic response of the bridge. Where discrepancies were found, the computer models were adjusted regarding their mass and stiffness until the observed and computed modes converged within reasonable limits of error.

- Perform detailed structural analysis of various portions of the bridge, using the multimode response spectrum procedure with uniform support excitation. Structural analysis were performed using the computer program SAP90.

- Make recommendations for retrofitting and provide preliminary construction costs for the AASHTO and site-specific earthquakes. The costs are to be based on conceptual retrofit details and qualitative retrofit strategies.

The seismic condition assessment of the bridge was performed for the above two levels of site-specific earthquakes and for AASHTO type earthquake, which is used for the majority of bridges in the country.

DESIGN CONSIDERATIONS ON THE HORIZON

In order to achieve a better estimation of the distribution of seismic forces in a structure, equivalent stiffness factors for foundation systems are required. At present, we are analyzing our conventional structures for seismic loads, assuming in most cases fixity condition at the foundation. By using the spring constants for the foundation system, we will be achieving relatively realistic estimates of forces acting on the structure when analyzing for the design earthquake.

NYSDOT's Geotechnical Engineering Bureau will investigate and develop the Stiffness matrix for shallow and deep foundations and soil parameters needed for the Mononobe-Okabe method of analysis.

Better understanding of current and new materials, better modeling techniques, innovative retrofit details and development of more sophisticated software will enhance overall performances of highway structures under seismic and non-seismic loadings.

The research work now in progress at the National Center for Earthquake Engineering Research (NCEER) on the Federal Highway Administration (FHWA's) sponsored project, (Contracts DTFH61-92-C-00106 and 00112) represents a major step in earthquake engineering

and will have significant impact on the future design of new highway structures as well as retrofitting of existing structures.

SUMMARY

NYSDOT's seismic design performance goals are similar to AASHTO Specification requiring the earthquake forces to be resisted within the elastic range of the members without significant damage during a moderate earthquake. Under a severe earthquake, catastrophic failure should not occur and any damage should be detectable and can be repaired. For the new structures, design criteria requires elastic forces to be determined from a single mode spectral method of analysis as a minimum. In many cases, single mode method gives satisfactory results but it uses various approximations and it may compute some questionable results. Standard seismic details for reinforcement, connections, support length, column confinement and anchorages are provided, conforming to the AASHTO Division 1A, for all structures.

Seismic failure vulnerability of bridges programmed for rehabilitation are investigated to assess options and costs of seismic retrofit measures, and incorporate with the rehabilitation work to eliminate or mitigate catastrophic failure. A cost increase for seismic retrofit in the range of 10% to 15% of the rehabilitation cost is typical for conventional type of structures (4).

ACKNOWLEDGMENTS

The cooperation and assistance given by Lisa Bariteau (NYSDOT) in preparing this paper is greatly appreciated.

REFERENCES

1. AASHTO Standard Specifications for Highway Bridges, Division 1A Seismic Design (1994) with NYSDOT "Blue Pages"- New York State Department of Transportation's Engineering Instructions 94-026, (July 1994)
2. Arzoumanidis, S., Gager, R.B., Malik, A.H., Queensboro Bridge: Seismic Condition Assessment and Retrofit of a Landmark Bridge presented at the Third U.S.- Japan Workshop on Seismic Retrofit of Bridges, Osaka, Japan, December 10-11, 1996.
3. Kawashima K., Damage of Highway Bridges by Hashin/Awaji, Japan, Earthquake and Seismic Design and Seismic Strengthening, proceedings of the International Conference on Retrofitting of Structures, Columbia University, New York City, NY March 11-13, 1996 (pages 187-207).
4. Malik, A. H., Seismic Retrofitting of Conventional Bridges, proceedings of the International Conference on Retrofitting of Structures, Columbia University, New York City, NY March 11-13, 1996 (pages 208-224).
5. New York State Department of Transportation's Engineering Instruction "SEISMIC CRITERIA- Bridge Rehabilitation Projects, # EI 92-046 issued October 14, 1992.
6. New York State Department of Transportation- Geotechnical Engineering Bureau Manual- 'Liquefaction Potential of Cohesionless Soils' Geotechnical Design Procedure GDP-9 January 1995.
7. Seismic Retrofitting Manual for Highway Bridges- F.H.W.A. RD-94-052, May 1995
8. Shirole, A. M. and Malik, A. H. Increasing the Seismic Failure Resistance of Highway Structures presented at the Second U.S.- Japan Workshop on Retrofit of Bridges, Berkeley, California, January 18-20,1994
9. Yashinsky, M., Lessons Learned from the January 17, 1995 Kobe Earthquake, proceedings of the National Seismic Conference on Bridges and Highways, sponsored by FHWA and CALTRANS, San Diego, California December 10-13, 1995.

Aseismic Behavior Assessment of Composite Extradossed Bridge

--- Assessment Example Assuming Active Fault ---

Hideki Komatsu[1)] , Yuji Suzuki[1)] & Kazuyuki Mizuguchi[1)]
[1)]*Nagoya Construction Bureau, Japan Highway Public Corporation*

ABSTRACT

This paper presents a methodology to assess the aseismic behavior of a composite extradossed bridge assuming active faults. The objective bridge is Kisogawa bridge, which is a 5-span composite extradossed bridge with length of 1145m. The strong ground motions at stiff diluvial deposits are synthesized by semi-empirical method, attenuation formula using equivalent hypocentral distance and normal mode method. A 2D FEM model of bridge-foundation-soil system is established in order to evaluate the seismic motion at top of foundation, using the synthesized strong ground motions at stiff diluvial deposits. The evaluation methodology of strong ground motion and the modeling of 2D FEM model are described in detail, and the topics for further study are presented.

1. INTRODUCTION

As a road bridge of New Meishin Expressway, Kisogawa bridge is planned to be constructed across Kisogawa river in Mie Prefecture. The bridge is designed as a composite extradossed one with length of 1145m. The construction site is with soft surface ground, and locates in a region close to several active faults. Therefore, it is very important to assess the strong ground motions due to active faults, and to evaluate the aseismic behavior of the bridge taking the bridge-soil interaction into account.

This paper attempts to establish a methodology to assess the aseismic behavior of Kisogawa bridge during large earthquakes caused by active faults. First, the strong ground motions at stiff diluvial layer are synthesized by following three methods: 1) semi-empirical method; 2) attenuation formula using equivalent hypocentral distance; and 3) normal mode method. Then a 2D FEM model of the bridge-foundation-soil system is developed to evaluate the input motion at top of foundation using the synthesized strong ground motions at stiff diluvial deposits. The seismic motion at top of foundation will be adopted for aseismic behavior investigation of the bridge at the next step. The evaluation methods of strong ground motion based on active models and the modeling of FEM model are described in detail, and the topics for further study are also presented.

2. OUTLINE OF KISOGAWA BRIDGE

Figure 1 shows the location of the construction site. The bridge is designed as a 5-span continuous composite extradossed bridge across the Kisogawa river. A extradossed bridge is a kind of prestressed concrete bridge which has large bonded external cables outside of girders. The outline of the bridge is indicated in Fig. 2. The whole length of the bridge is 1145m, and

the maximum span is 275m. The pylons are 30m high above the deck, which are supported by 14m tall piers. The main girder consists of prestressed concrete girder part and steel girder part with complex box section. The height and width of the girder are 7m and 33m, respectively.

Figure 3 represents a typical soil profile at the construction site. Soft silty sand and clay layers with whole thickness of 41.18m are overlying relatively hard sandy and gravel layers. Steel pipe sheet pile is adopted as foundation, which rests onto the hard sandy and gravel layers. The section of the foundation is shown in Fig. 2. The widths in longitudinal and transverse direction are 30m and 27m, respectively.

3. FLOW OF ASEISMIC ASSESSMENT

The flow chart for aseismic behavior assessment of Kisogawa bridge is shown in Fig. 4. First, the seismic activities around the construction site are investigated, and the geological structure is clarified. Based on these results, strong ground motions at stiff diluvial deposits are synthesized using three types of methods considering the spreading of fault rupture. Then a 2D FEM model of bridge-foundation-soil is established, and the input motion at top of foundation is evaluated taking the nonlinearity of soil into account. Finally, nonlinear response analysis of bridge will be performed, and the aseismic behavior of upper structure, pier and foundation are evaluated. This paper mainly presents the methodology of evaluation of strong ground motions and the modeling of 2D FEM model.

4. EVALUATION OF STRONG GROUND MOTION AT STIFF DILUVIAL DEPOSITS

4.1 Outline of the evaluation of strong ground motion

The flow chart for the evaluation of strong ground motion is shown in Fig. 5. As indicated by the flow chart, the first step is to decide subject earthquakes based on the past earthquakes and active fault circumstances around the construction site. In this study, the results of past researches are investigated to determine the subject earthquakes. A number of earthquakes, which have large effects on the seismic motion at the construction site, are determined taking account of the characteristics of geological structure around active faults. The parameters (such as magnitude, fault size, seismic moment and rupture velocity) are decided based on the past researches.

For the evaluation of strong ground motion, following three methods based on fault models are used. All these three methods can include the effects of the rupture spreading of active faults during earthquakes.

(1) Semi-empirical method using a hybrid of stochastic and deterministic fault (Takemura & Ikeura, 1988)
(2) Attenuation formula using equivalent hypocentral distance (Ohno et al., 1993)
(3) Normal mode method (for evaluation of surface waves)

Although all the three methods are used, the semi-empirical method is adopted as the basic evaluation method in this study. The applicable frequency range of the semi-empirical method is up to about 10Hz, and is the most stable and reliable evaluation method among various proposed methods based on the fault models. However, as the semi-empirical method is mainly for body waves, it is difficult for this method to be used in the cases when the

surface waves are predominant. Therefore, for evaluation of surface waves, normal mode method is adopted. The subsurface structure model needed in normal mode method are obtained from the results of the past researches.

For the evaluation of inland active fault, attenuation formula of response spectra is also used, which is obtained from the regression analysis of strong-motion records in California. The validity of the method has been verified in the simulation of Hyogo-Ken Nanbu earthquake.

When adopting semi-empirical method and normal mode method, the time history of seismic wave can be synthesized, and thus the maximum acceleration and response spectrum can also be computed. However, the attenuation formula can only give the maximum acceleration and 5% damping response spectrum.

The overall evaluation based on the results by the above three methods is finally conducted to determine the time history and spectrum of strong ground motion corresponding to large earthquake for checking horizontal bearing capacity.

4.2 Determination of subject earthquakes

(1) Past strong earthquakes

There are 4 strong past earthquakes with clarified fault parameters, which are shown in Fig. 6 (Sato, 1989). In addition, the effects of all the past earthquakes with epicenter within 100km from the construction site are evaluated using Kanai's relation (Kanai, 1966). The first ten most affective earthquakes are shown in Table 1. According to the results indicated in Fig. 6 and Table 1, 4 past earthquakes as shown in Table 2 are finally selected in this study.

(2) Earthquakes caused by active faults

Figure 7 shows the location of active faults that are within 50km from the construction site, which are selected according to the past results of active faults in Japan (Research Group on Active Faults, 1991). The earthquakes with activity degree of A and B, and certainty degree of I and II are adopted. In the cases where many faults are very close, the biggest one is selected if it is clearly larger than others. In this study, 5 faults as shown in Table 2 are adopted based on the faults shown in Fig. 7, referring to the earthquake circumstance in Japan (Kakimi, 1994) as shown in Fig. 8.

4.3 Evaluation methods of strong ground motion based on fault models

(1) Semi-empirical method using a hybrid of stochastic and deterministic fault

The semi-empirical method is to synthesize strong ground motions using observed seismograms from small events as Green functions. Figure 9 indicates the outline of the method. As this method can avoid the difficulty concerning the heterogeneity of the earth's structure, a number of semi-empirical methods have been proposed. In this study, the semi-empirical method proposed by Takemura & Ikeura is applied. The method could estimate strong ground motions over a wide frequency range with the assumption of hybrid deterministic and stochastic fault models. The deterministic model is based on the kinematic source model of Haskell and the similarity law of earthquakes, and the stochastic model is described by a specific distribution function of displacement on the fault plane. In this method, as shown in Fig. 10 and 11, the displacement Dij is expressed as the sum of D0 and $\triangle$Dij,

where D0 is the average displacement over the fault plane and $\triangle$Dij the deviation from D0. The strong ground motion is computed by summing the seismic waves due to D0 and those due to $\triangle$Dij, as indicated by eq(1).

$$Ssy(t) = \sum_{i=1}^{nL} \sum_{j=1}^{nW} \frac{re}{rij} \left(\sum_{k=1}^{nD} Se(t - tij - \{k-1\}\tau e) + \kappa ij\, Se(t - tij) \right) \qquad (1)$$

where Se(t) is the recorded small earthquakes used for superposition, re is the source-to-site distance of element earthquake, and τc is the time interval for the superposition of ramp functions. i,j and k are the indexes expressing the superposition of fault length, fault width and ramp function, respectively, and nL, nW and nD are the number of superposition. rij is the distance from ij segment on the fault plane to the site, and tij is the time from the starting of the fault rupture to the arriving of the wave caused by ij segment at the site. kij is assumed to be a probabilistic parameter of normal distribution with an average of 0 and a standard deviation of SD. If the distance from the starting point of fault rupture to the rupture point of the ij segment is denoted by dij, and the rupture propagation velocity and S wave velocity are denoted by VR and β , respectively, tij can be obtained by the following equation.

$$tij = dij/VR + rij/\beta \qquad (2)$$

If the strong ground motion is synthesized considering the radial component and the transverse component, it can be expressed by eq(3).

$$Ssy(t) = \sum_{i=1}^{nL} \sum_{j=1}^{nW} Cij \frac{re}{rij} \left(\sum_{k=1}^{nD} Se(t - tij - \{k-1\}\tau e) + \kappa ij\, Se(t - tij) \right) \qquad (3)$$

Where Ssy(t) and Se(t) represent the vectors of synthesized wave and element wave, respectively. The first and the second element of Ssy(t) are NS component and EW component, and the first and the second element of Se(t) indicate radial component and transverse component, respectively. Cij is the matrix for coordination transformation.

(2) Attenuation formula using equivalent hypocentral distance

To predict the spectrum of strong motion, many studies have been conducted using attenuation formula as a function of magnitude, source-to-site distance and soil classification. The coefficients have been obtained by performing regression analysis of observed data. This kind of method is known as empirical estimation. The major advantages of the method are: 1) the number of parameter is small; 2) the method can be applied to almost any location; and 3) the results are stable. The main disadvantage is that it cannot be used to predict complicated site-dependent phenomena such as the effect of local topography. Therefore, the method is mainly adopted for prediction of the maximum response and response spectra. In this study, the attenuation formula using equivalent hypocentral distance proposed by Ohno et al. is used to evaluate the maximum acceleration and response spectrum. The formula is expressed by eq(4).

$$\log S(T) = a(T)Mw - \log Xeq - b(T)Xeq + c(T) + \delta \triangle s(T) \qquad (4)$$

Where S(T): response spectrum
Mw: moment magnitude

Xeq: equivalent hypocentral distance
a(T), b(T), c(T): regression coefficients
$\triangle$s(T): residual (equivalent of amplification ratio)
δ : dummy variable (pre-Quaternary: 0; Quaternary: 1)

This formula is obtained through regression analysis of strong-motion records in California including many near-source data, and the equivalent hypocentral distance is introduced so that it can be applied over a wide range of earthquakes from near-source ones to far-source ones. Figure 12 demonstrates the concept of the equivalent hypocentral distance. Xeq indicates the hypocentral distance from a virtual point source that provides the same energy to the site as does a finite-size fault, and thus it can be used for evaluating the near-source strong-spectrum without changing the form of attenuation formula. Figure 13 represents the explanation of the method.

To verify the applicability of the attenuation formula in Japan, it has been used in the simulation of Hyogo-Ken Nanbu earthquake. The simulated results are compared with the observed ones in Fig. 14 and 15. It can be seen that the predicted and observed results are in good agreement over the period range shorter than 1 second. The peak at period of around 1-2 seconds reflects the effects of directivity effect, which cannot be modeled by attenuation formula. From the above comparisons, it is confirmed that the attenuation formula using equivalent hypocentral distance can predict the average characteristics of strong-motion for practical use.

(3) Normal mode method

The concept and procedure of the normal mode method are shown in Fig. 16 and 17, respectively. This method synthesizes seismic wave by superposing the normal mode solutions in multilayered elastic half space assuming point double couple force. The amplitude characteristics at the site is expressed by eq(5).

$$U(\omega) = S(\omega) \cdot \sum_{j} [D_j(\omega) \cdot X_j(\theta, d) \cdot \kappa_j^{1/2} \cdot A_j] / (2\pi r)^{1/2} \qquad (5)$$

Where $U(\omega)$: displacement at the surface of the site
$S(\omega)$: source properties (seismic moment, ramp function)
$Dj(\omega)$: effects of directivity (rupture velocity)
$Xj(\theta,d)$: radiation pattern coefficient, where θ is the angle between the site and the rupture proceeding direction of fault, and d the depth of source
kj: wave number
Aj:wave amplitude factors
r: epicentral distance
j: j order

For each mode of surface waves, the solution to source $S(\omega)$ is first solved considering the radiate characteristics $Xj(\theta,d)$ determined according to the location of source and the site, the propagation characteristics of surface waves $kj^{1/2}$ and Aj decided by subsurface structure, and the geometric attenuation term $r^{1/2}$. Then the effects of source moving $Dj(\omega)$ is included, and finally the results of all modes are superposed. The strong ground motion is computed through inverse Fourier transform of $U(\omega)$.

The subsurface structure is determined referring to the results of past researches (e.g., Aoki et al., 1972). Figure 18 represents the subsurface structure.

4.4 Evaluation of strong motion for design

In this study, the strong ground motion for design is defined as the strong motion at the stiff diluvial deposit. The strong motions at stiff diluvial deposit are synthesized using the three methods described in 4.3 for the selected subject earthquakes indicated in 4.1, and are evaluated considering following three aspects: 1) maximum acceleration and maximum velocity; 2) 5% damping response spectrum; and 3) the variation of amplitude with the time and the duration. Fig. 19 represents the detailed flow chart of the evaluation of strong ground motions. The semi-empirical method is mainly used, and normal mode method is adopted for synthesizing the strong ground motions with surface waves being predominant.

As the example of synthesized strong ground motions with body waves being predominant, the strongest one among the synthesized motions with period range from 0.2 to 2.0 seconds is indicated in Fig. 20, which is obtained using semi-empirical method assuming Yoro-Iseiwan-Fault earthquake. The maximum acceleration is 885 Gal.

Fig. 21 represents the strongest synthesized strong ground motion using normal mode method, with period range from 2.0 to 5.0 seconds. The maximum acceleration is 56.7Gal.

5. EVALUATION OF INPUT MOTION FOR ASEISMIC DESIGN

5.1 Outline of evaluation of input motion for bridge

Fig. 22 represents the flow chart for evaluation of input motion at top of foundation using the strong ground motion at stiff diluvial deposits.

To correctly reflect the effects of soil-structure interaction, 3D analysis is the best choice. However, as the 3D nonlinear and equivalent linear response analysis of structure-soil system is still very difficult for now, 2D equivalent linear analysis method is selected to evaluate the seismic motion at the top of foundation in this study.

5.2 Modeling of foundation

(1) Modeling of surface ground

To find the appropriate equivalent stiffness and damping ratio of surface ground corresponding to the objective large earthquakes, the equivalent linear response analysis of surface ground is performed using the synthesized strong ground motion due to hypothetical Youro-Iseiwan-Fault earthquake as input. The code SHAKE is adopted for the computation. The initial stiffness of soils is computed based on the results of P-S logging. As for the G/G0-γ, and h-γ curves, the results presented in related report are adopted. Table 3 indicates the averaged equivalent shear modulus and damping ratio for each layer of soil, which are used for following static and dynamic analysis.

(2) Modeling of steel pipe sheet pile foundation

The steel pipe and the joint between pipes can be modeled as beam element and spring element. In response evaluation of bridge-foundation-soil system, however, the behavior of

whole foundation is of greater concern than that of single steel pipe, and thus it is an appropriate method to model the foundation using equivalent shell elements. In this study, the above two modeling methods are compared through 3D linear analysis of a single foundation inside soil with a horizontal load applying at the center of top of the foundation. It has be confirmed that the two models give very similar results. Therefore, in the following analysis, the modeling method using equivalent shell elements is adopted.

(3)Effective width of foundation in 2D analysis

In order for 2D analysis to reflect the behavior of 3D structure-foundation-soil model, it is essential to appropriately determine the effective width of foundation in transverse direction. In this study, to find the appropriate effective width in 2D analysis, 3D linear dynamic analysis and 2D linear dynamic analysis are performed with the effective width as parameter, and the transfer functions at top of foundation computed by 3D and 2D analysis are compared.

The 3D model is indicated in Fig. 23. The soil is modeled by 8-node solid elements, and the foundation by shell and solid elements. The bridge is modeled by beam elements. The boundary conditions are indicated in Table 4. As the analysis here is for determining equivalent 2D model, the damper is not used at boundary at this stage. The 2D model is demonstrated in Fig. 23, which is simply the projection of 3D model. The effective width of foundation in transverse direction is adjusted to make 2D analysis and 3D analysis give close results. In addition, to add damper in transverse direction is also considered as an option to improve the behavior of 2D model. The concept of effective width is shown in Fig. 24. In total, four cases are considered. The first three cases are without damper, and the effective widths are 1B, 3B and 10B, respectively. The fourth case is with damper, and has effective width of 1B.

The computed transfer functions for the four cases are compared with that obtained by 3D analysis in Fig. 25. It can be seen that the results of the fourth case, where the effective width is 1B and the damper is used, are in the best agreement with the results obtained by 3D analysis. Therefore, in the 2D analysis, the effective width is set as 1B, and the damper is adopted in transverse direction.

As the joint between steel pipes may fail during large earthquakes, it is necessary to comprehend the effects of joint stiffness. The transfer functions of the cases with and without joint stiffness have been compared, and no significant difference has be found between the two results. As the response in the case without joint stiffness is slightly larger than that in the case with joint stiffness, it is appropriate to consider only the case without joint stiffness.

5.3 2D model of bridge-foundation-soil system

Base on the above results, 2D model of bridge-foundation-soil system is established. Figure 26 indicates the FEM model. Considering the symmetry of the bridge, only the left half is modeled. To mitigate the effects of ground boundary, the left side of ground is set as energy transfer boundary, and the basement is treated as viscous boundary. The right side of surface ground is modeled as horizontal roller.

Using the 2D FEM model shown in Fig. 26, the seismic motion at top of foundation can be computed by inputting the strong ground motion at stiff diluvial deposits.

6. CONCLUSIONS

A methodology is presented to assess the aseismic behavior of a composite extradossed bridge during large earthquakes caused by active faults. The strong ground motions at stiff diluvial layer are synthesized by semi-empirical method, attenuation formula using equivalent hypocentral distance and normal mode method. 2D FEM model of bridge-foundation-soil system is established to evaluate the seismic motion at top of foundation, which will be adopted for aseismic behavior assessment of bridge. It is demonstrated that the methodology presented here can appropriately evaluate the aseismic behavior of bridges during large earthquakes caused by active faults.

In this study, the strong ground motions are synthesized assuming heterogeneous rupture over whole active faults. However, many recent investigations on source characteristics have indicated that not all parts of faults generate strong seismic motion. Only less than 40% of the fault generate strong seismic motion, which is called as asperity, while some region of fault generate almost no seismic motion. Therefore, further study will be performed considering the asperity in evaluation of strong ground motion.

ACKNOWLEDGMENTS

The authors would like to thank the members of the committee on the aseismic behavior assessment of Kisogawa bridge for their very helpful suggestions during the present study.

REFERENCES

Aoki, H. et al., 1972, Crustal structure in the profile across central Japan as derived from Exposion seismic observations, J. Phys. Earth, 20, 197-223.

Kakimi, T. et al., 1994, Earthquake Circumstance in Japan and Maximum Scale of Earthquake, Proc. of Conference on Earth and Planet, 302 (in Japanese).

Kanai, K. et al., 1966, Observation of strong earthquake motions in Matsushiro area, Part1, Bull. Earthq. Res. Inst., 44, 1269-1296.

Ohno et al., 1993, Revision of attneuation formula considering the effect of fault size to evaluate strong motion spectra in near field, Tectonophys. 218, 69-81.

Research Group on Active Faults, 1991, Active Faults in Japan: Map and Information, Publish Bureau of Univeristy of Tokyo (in Japanese).

Sato, 1989, Handbook of fault parameters in Japan.

Takemura, M. and Ikeura, T., 1988, A semi-empirical method using a hybrid of stochastic and deterministic fault models: simulation of strong ground motions during large earthquake, J. Phys. Earth, 36, 89-106.

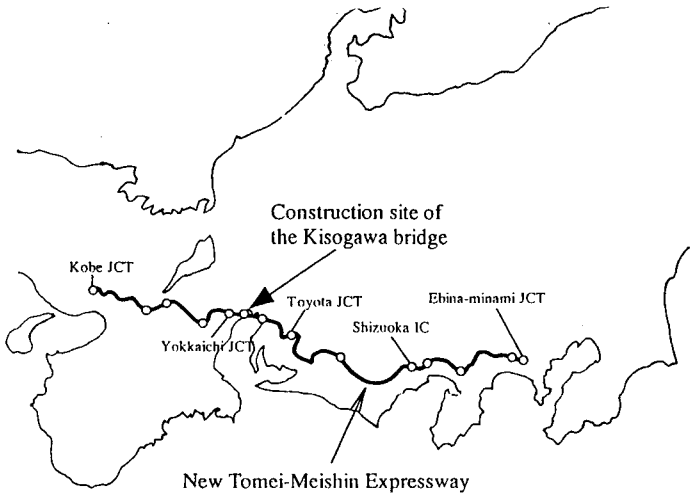


Fig. 1 Location of the construction site

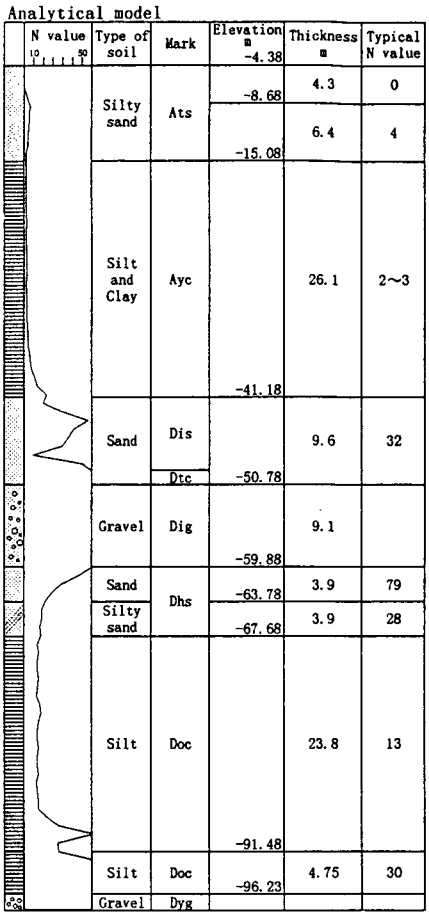


Fig. 3 Typical soil profile at the construction site

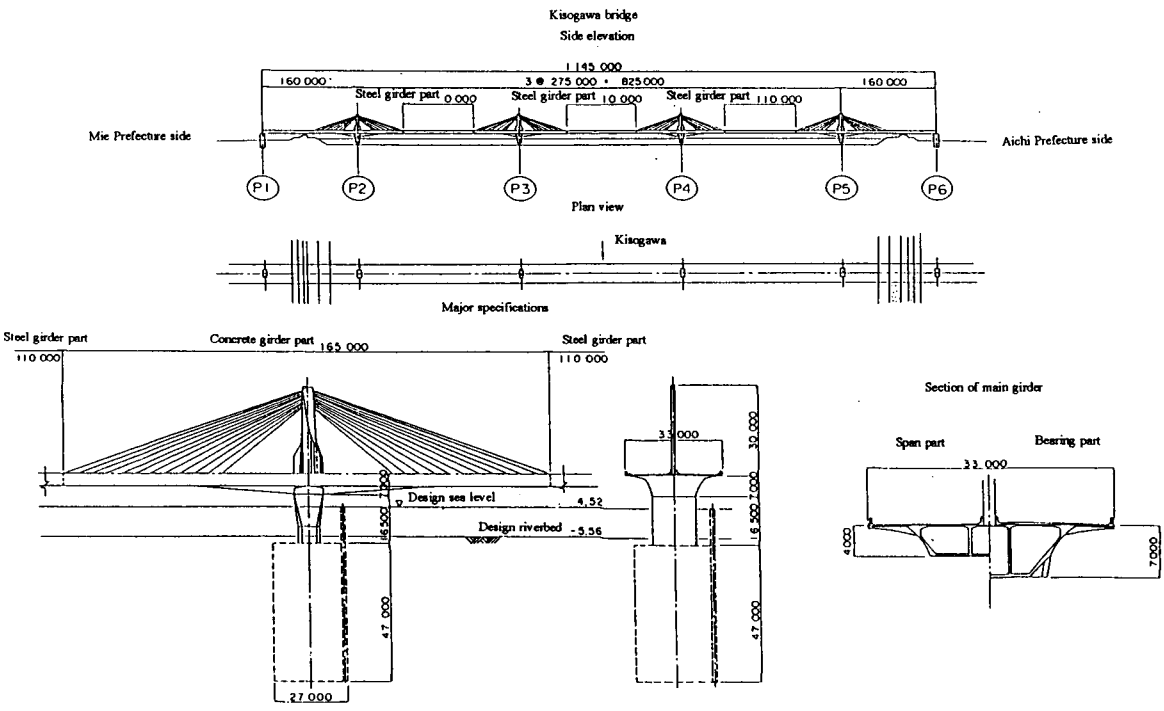


Fig. 2 Outline of Kisogawa bridge

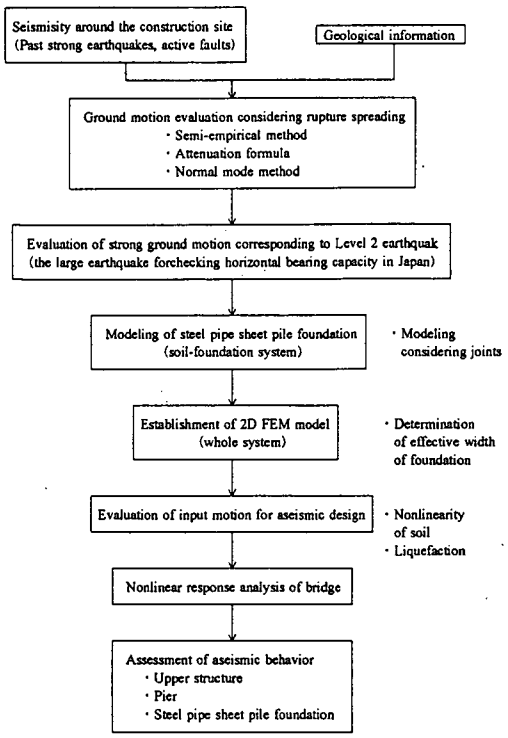


Fig. 4 Flow chart of the study

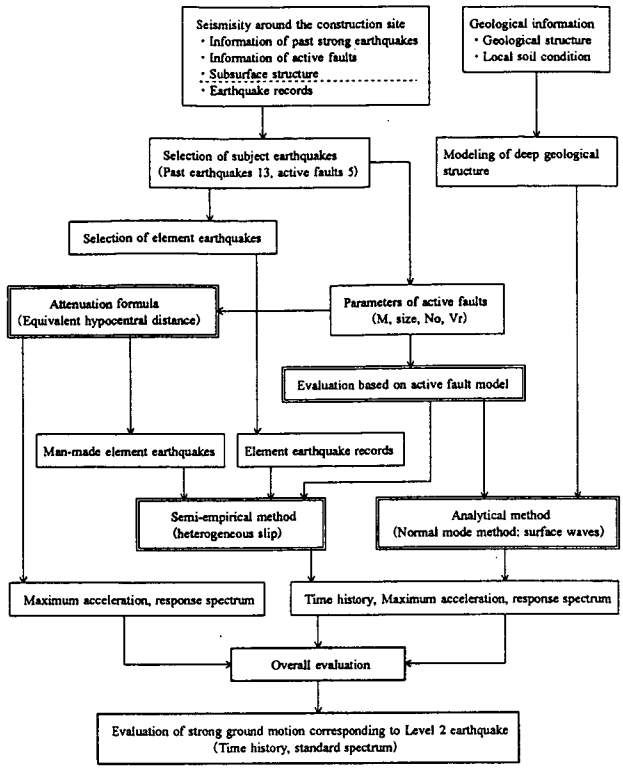


Fig. 5 Flow chart for the evaluation of strong ground motion

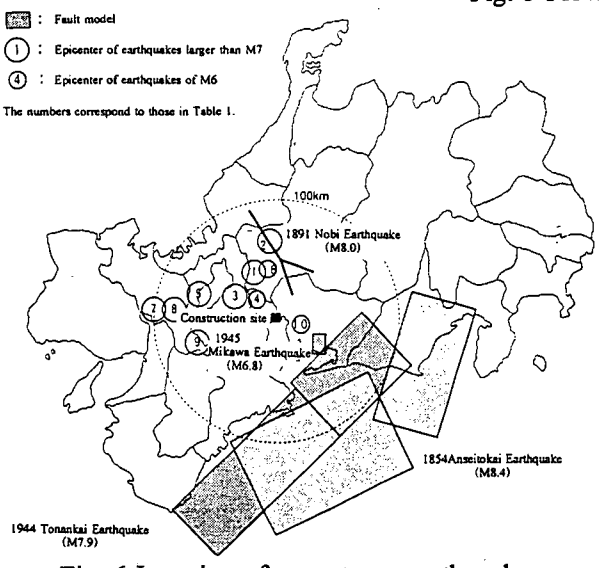


Fig. 6 Location of past strong earthquakes

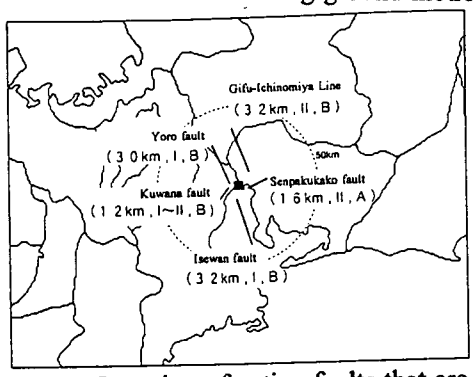


Fig. 7 Location of active faults that are within 50km from the construction site

Table 1 Most affective past earthquakes

No.	Time	Region	Magnitude	Epicenter distance (km)	Maximum velocity (cm/s)
1	745	Mino	7.9	44	16.54
2	1891	Nobi Earthquake	8.0	62	13.62
3	1819	Ise Mino Oumi	7.3	43	7.54
4	1802	Kinai Nagoya	6.8	27	6.68
5	1662	Yamashiro ~ Shinano	7.4	74	4.72
6	1715	Ogaki Nagoya	6.8	41	4.11
7	827	Kyoto	7.5	90	3.92
8	1185	Oumi Yamashiro Yamato	7.4	85	3.68
9	1854	Iga Ise Yamato	7.3	75	3.61
10	1945	Chubu-Chiho-Nanbu	6.3	51	3.48

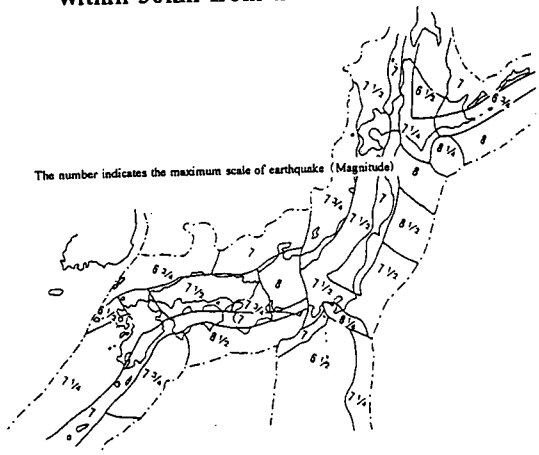


Fig. 8 Subsurface structure (Kakimi, 1994)

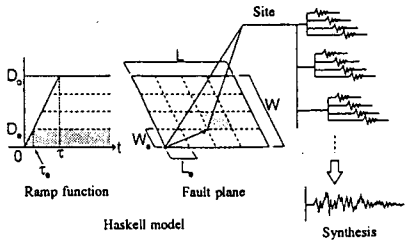


Fig. 9 Outline of semi-empirical method

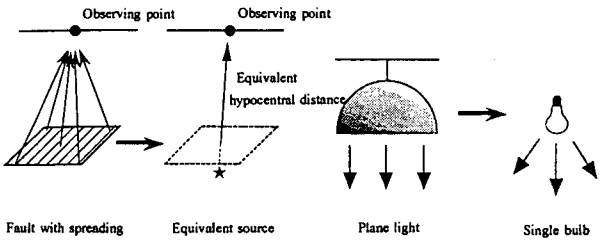


Fig. 12 Concept of equivalent hypocentral distance

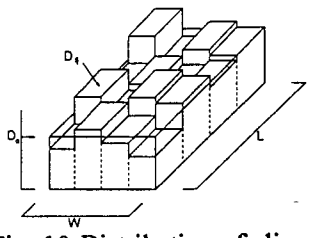


Fig. 10 Distribution of slip on the fault plane

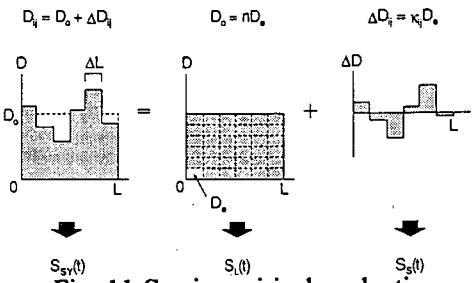


Fig. 11 Semi-empirical evaluation of heterogeneous slip

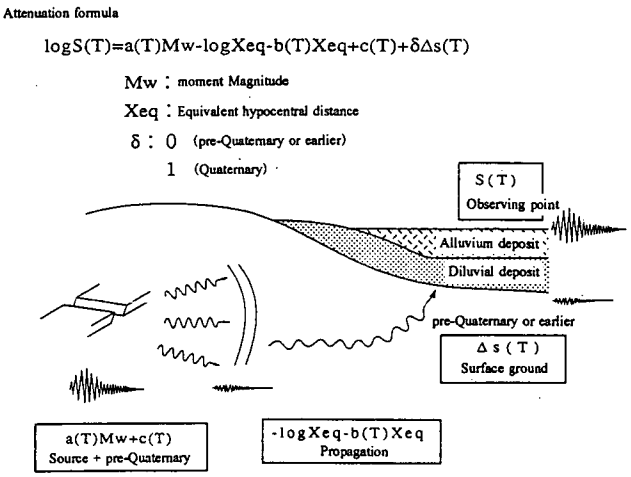


Fig. 13 Modeling of response spectrum by attenuation formula

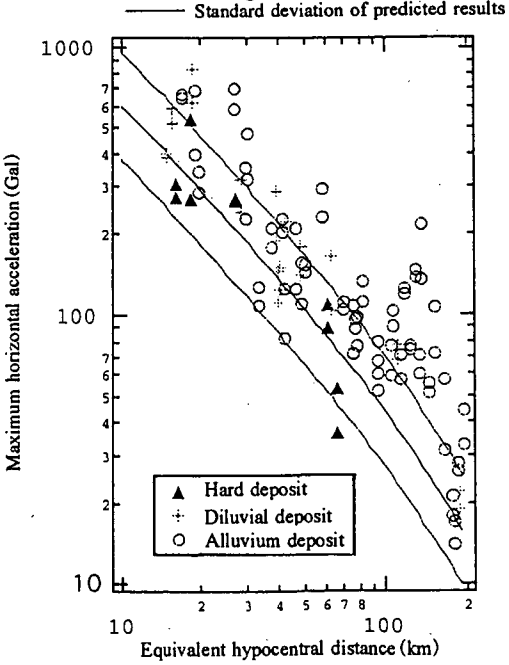


Fig. 14 Comparison between predicted and observed results (maximum acceleration)

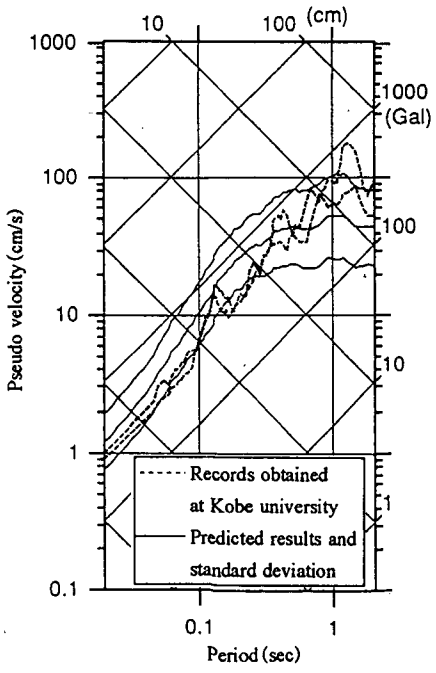


Fig. 15 Comparison between predicted and observed results (response spectrum)

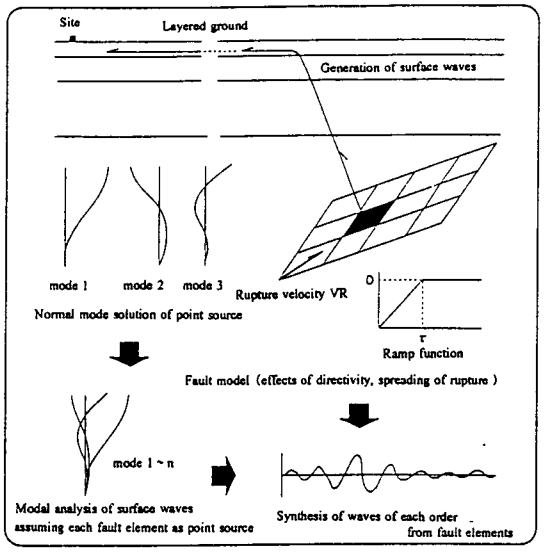


Fig. 16 Concept of normal mode method

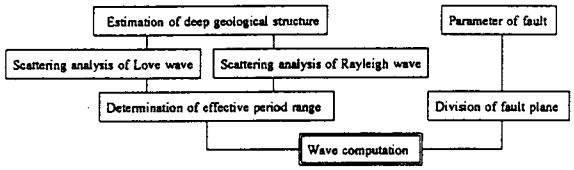
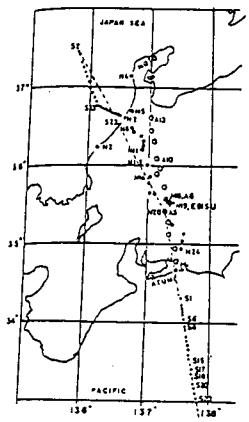


Fig. 17 Analysis procedure of normal mode method



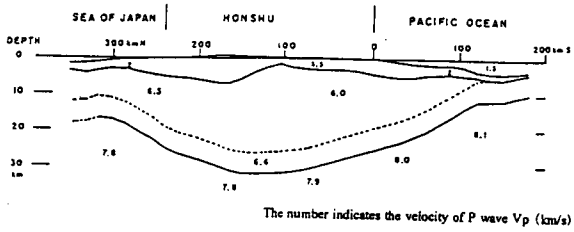


Fig. 18 Subsurface structure around construction site

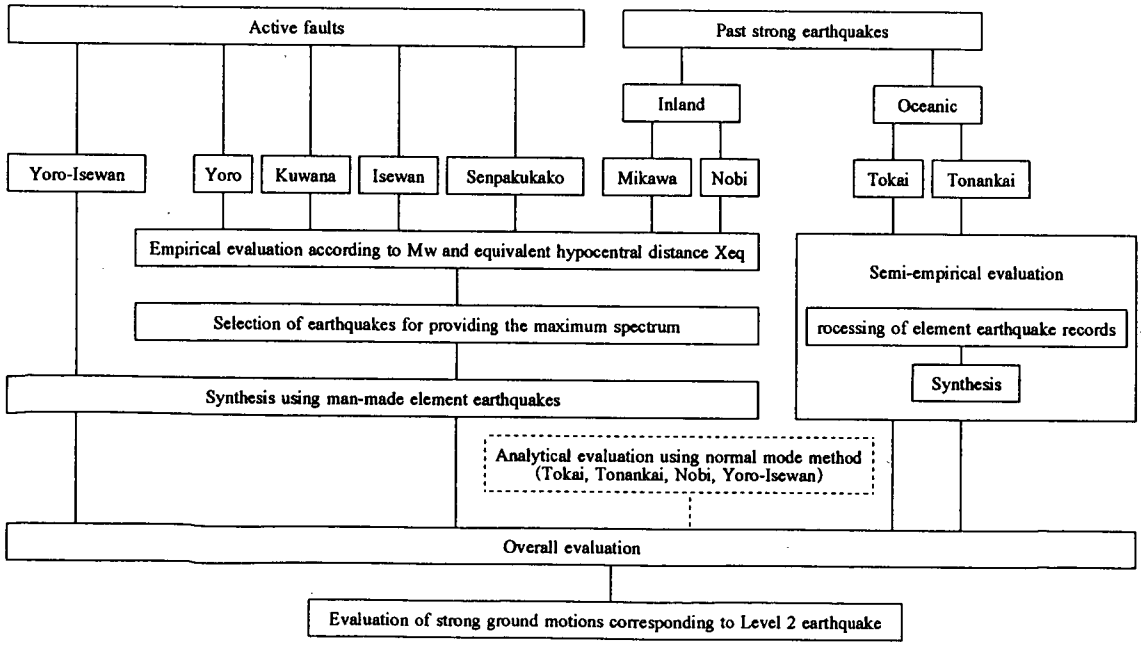


Fig. 19 Detailed flow chart of the evaluation of strong ground motions

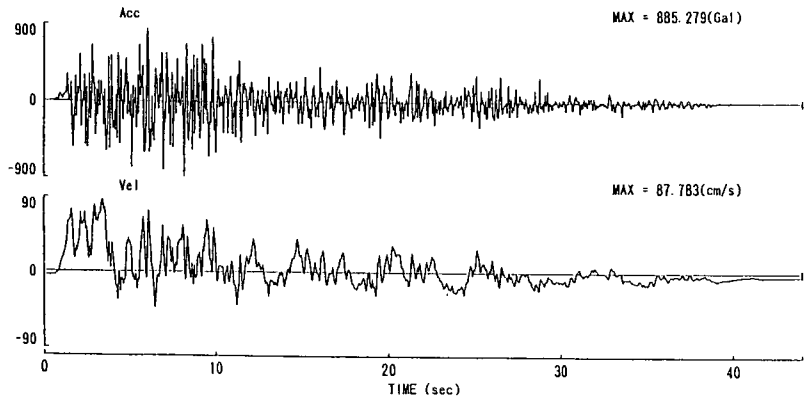


Fig. 20 Synthesized waves caused by virtual Yoro-Isewan-Fault earthquake

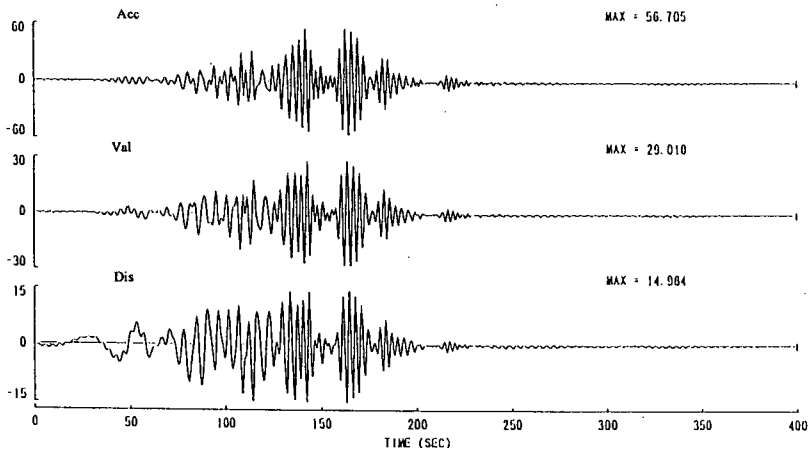


Fig. 21 Synthesized waves caused by virtual Tokai earthquake

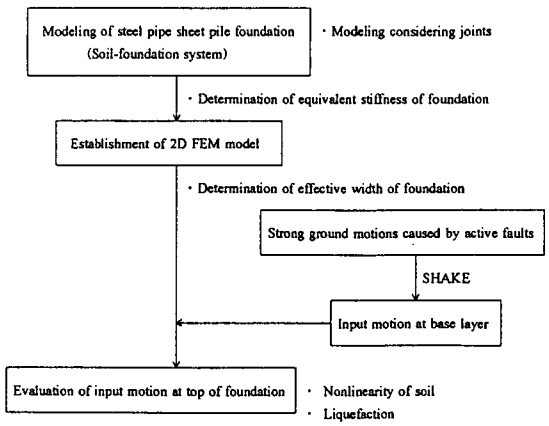


Fig. 22 Flow chart of the evaluation of input motion at top of foundation

Table 2. Selected virtual earthquakes

	Virtual earthquakes	Scale	Reason for being selected
Virtual earthquakes determined according to past earthquakes	Virtual Tokai Earthquake	M8.4	Ansei-Tokai Earthquake (1854, M8.4)
	Virtual Tonankai Earthquake	M7.9	Tonankai Earthquake (1944, M7.9)
	Virtual Nobi Earthquake	M8.0	Nobi Earthquake (1891, M8.0)
	Virtual Mikawa Earthquake	M6.8	Mikawa Earthquake (1945, M6.8)
Virtual earthquakes determined according to active faults	Virtual Senpakukako-Fault Earthquake	M6.8	Senpakukako fault(Ⅱ,A,L=16km)
	Virtual Yoro-Fault Earthquake	M7.5	Yoro fault(Ⅰ,B,L=41km)
	Virtual Kuwana-Fault Earthquake	M7.0	Kuwana fault(Ⅰ,B,L=21km)
	Virtual Isewan-Fault Earthquake	M7.7	Isewan fault(Ⅰ,B,L>32km)
	Virtual Yoro-Isewan-Fault Earthquake	M8.1	Yoro-Isewan fault(Ⅰ,B,L>77km)

Table 3 Averaged equivalent shear modulus and damping ratio

Layer No.	Altitude (m) -7.5	Thickness (m)	G (tf/m^2)	γ (tf/m^3)	ν	h (%)	Vs (m/s)
1	-8.7	1.2	101.6	1.6	0.495	21.3	25.0
2	-15.1	6.4	633.8	1.7	0.495	21.4	60.4
3	-41.2	26.1	928.8	1.65	0.495	19.4	74.3
4	-50.8	9.6	2215.0	1.8	0.490	23.0	109.8
5	-59.9	9.1	17329.6	2.0	0.474	14.4	291.4
6	-63.8	3.9	15711.1	2.0	0.474	15.7	277.5
7	-67.7	3.9	1193.0	1.8	0.481	25.2	80.6
8	-91.5	23.8	2514.9	1.7	0.481	19.3	120.4
9	-96.3	4.8	3479.6	2.0	0.476	19.0	130.6
10	-108.0	11.7	53700.0	2.1	0.458	3.0	500.0

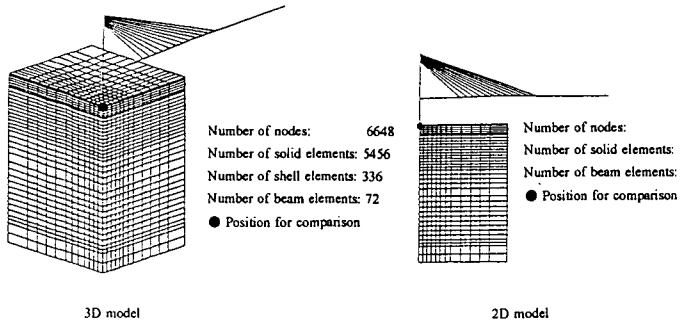


Fig. 23 FEM model

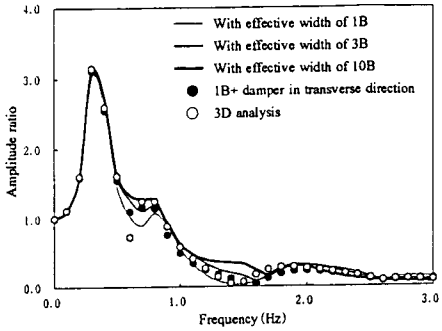
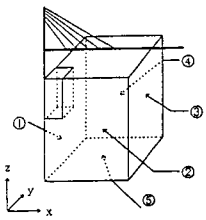


Fig. 25 Comparison of transfer functions of acceleration (at top of foundation)

Table 4 Boundary condition (Fixed degree of freedom)

Boundary	Excitation in longitudinal direction	Excitation in transverse direction
①	Y,Z,XR	X,YR,ZR
②	Y,XR,ZR	X,Z,YR
③	Z,XR,YR,ZR	Z,XR,YR,ZR
④	Z,XR,YR,ZR	Z,XR,YR,ZR
⑤	All degrees fixed	All degrees fixed



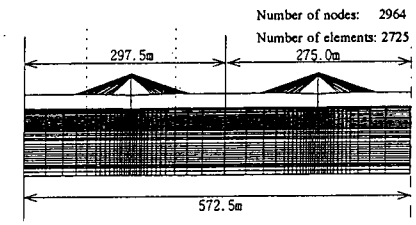


Fig. 26 2D FEM model of bridge-foundation-soil system

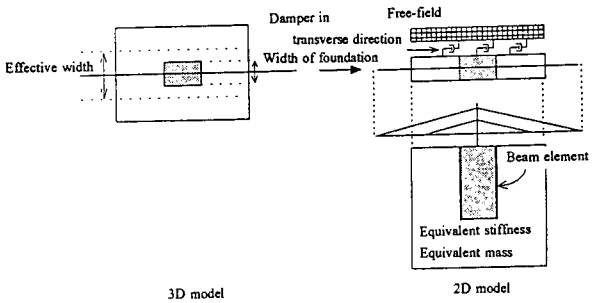


Fig. 24 Concept of effective width

SESSION 3: SEISMIC ISSUES (2)

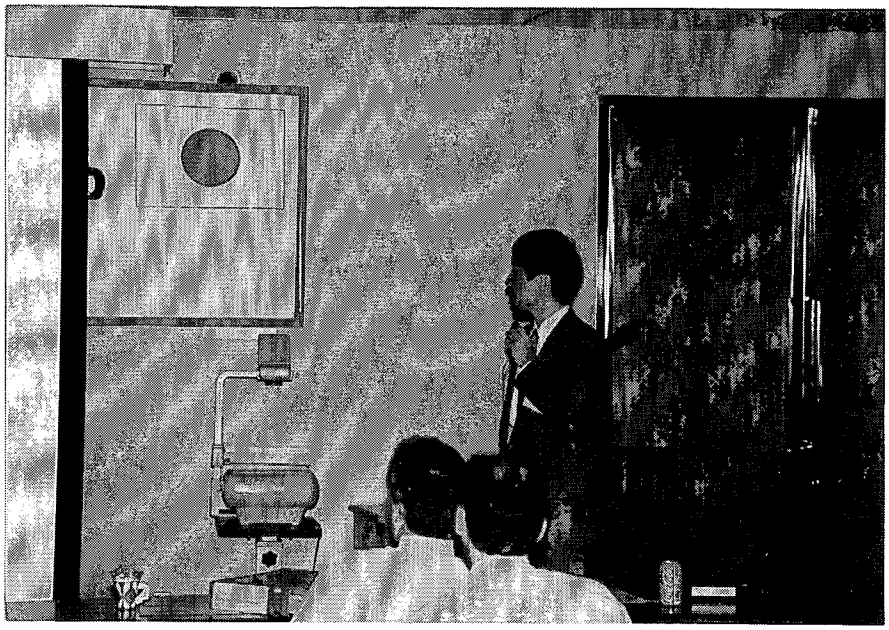
(1) Experimental Study of the Effects of Liquefaction-Induced Ground Flow on Bridge Foundation
(K. Tamura and T. Azuma)

(2) Seismic Vulnerability Studies of Highway Structures
(W. Phillip Yen, John D. O'Fallon, James D. Cooper and Ian M. Friedland)

(3) Evaluation of Seismic Performance of Japanese Bridge Piers Designed by the Previous Codes
(K. Kawashima, J. Sakai and H. Takemura)



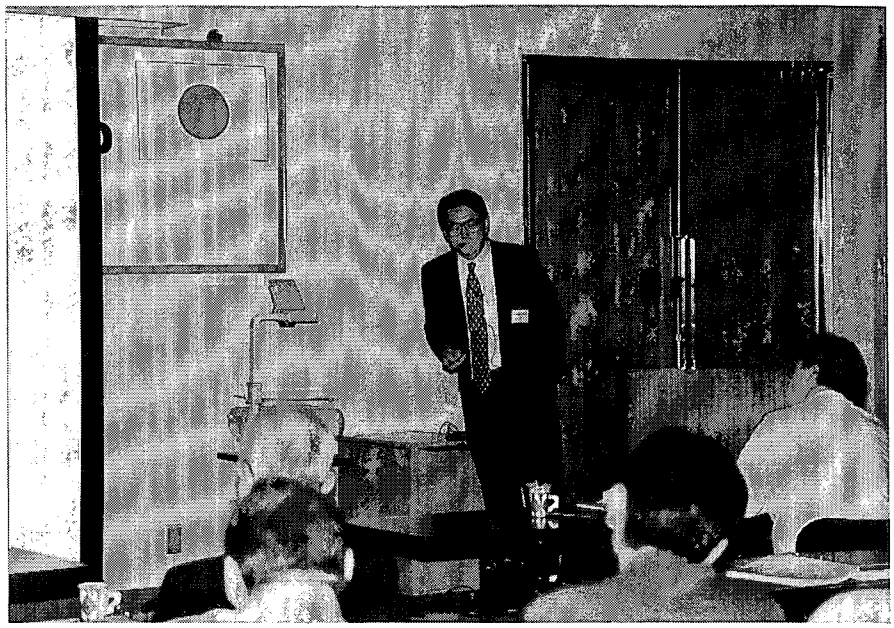
Co-Chairmen : Yukio Adachi, Medhat Haroun



SESSION 3 : Keiichi Tamura



SESSION 3 : Phillip Yen



SESSION 3 : Kazuhiko Kawashima

EXPERIMENTAL STUDY OF THE EFFECTS OF LIQUEFACTION-INDUCED GROUND FLOW ON BRIDGE FOUNDATION

Keiichi Tamura [1] and Takuo Azuma [2]

1 Head, Ground Vibration Division, Public Works Research Institute
Ministry of Construction, 1 Asahi, Tsukuba-shi, Ibaraki-ken 305 Japan
2 Research Engineer, ditto

ABSTRACT

The liquefaction-induced ground flow inflicted serious damage to various engineering structures including highway bridges in the Hyogo-ken Nanbu Earthquake of 1995. After this earthquake, the Specifications for Highway Bridges were revised, in which the effects of liquefaction-induced ground flow were incorporated. This was mainly based on the analytical study of damaged highway bridge foundations. From an experimental approach, shaking table tests are in progress at the Public Works Research Institute, Ministry of Construction. This paper presents the preliminary results of experiments on the liquefaction-induced ground flow. A quaywall and the ground behind it were modeled in a large container, and shaking table tests were carried out. Two different ground conditions were considered, and the effects of liquefaction-induced ground flow were studied.

INTRODUCTION

The Hyogo-ken Nanbu Earthquake, which occurred on January 17, 1995, caused extensive soil liquefaction over a wide area of offshore reclaimed lands and natural deposits [1, 2]. Besides that, near the water's edge, liquefaction induced ground flow with the movement of quaywalls and seawalls. Aerial photogrammetry revealed that the maximum residual displacement due to ground flow reached 3 to 4m [3, 4]. Liquefaction and its associated ground flow exerted serious influence on various engineering structures. Although highway bridges did not suffer fatal damage due to liquefaction, liquefaction-induced ground flow caused large deformation of bridge foundations. For example, a pier of the Shin-Shukugawa Bridge, which crosses a watercourse between reclaimed lands, was moved toward the watercourse by approximately 1m, which resulted in rupture of bearings on the pier [5]. This pier was supported by cast-in-place concrete piles, 1.5m in diameter. The piles were constructed in the reclaimed soil and supported by a diluvial sandy layer.

Considering large influence of the liquefaction-induced ground flow on the seismic safety of highway bridges, its seismic design treatment has been incorporated into the newly revised "Specifications for Highway Bridges" [6, 7], which was mainly based on the back analysis of bridges that suffered residual displacements by the Hyogo-ken Nanbu

Earthquake [8]. The effect of liquefaction–induced ground flow is idealized as the static force acting on structure in the Specifications. This premises that the surface soil is of the non–liquefiable and liquefiable layers, and the forces equivalent to the passive earth pressure and 30% of the overburden pressure are applied to the structure in the non–liquefiable layer and liquefiable layer, respectively, as shown in Figure 1. Since the magnitude of ground flow decreases as the distance from the water's edge increases, modification by distance is incorporated in the estimation of ground flow force. Modification by the degree of liquefaction is also introduced.

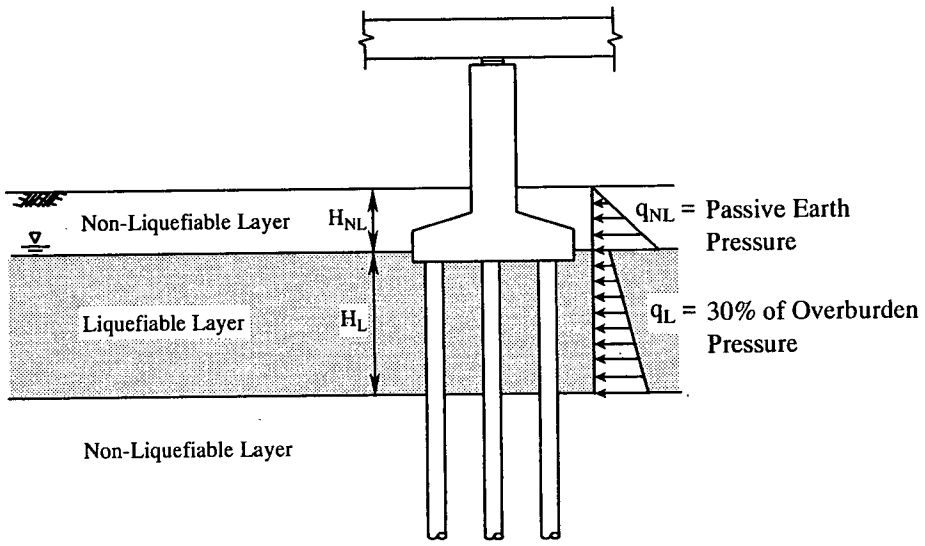


Figure 1 Idealization of Ground Flow Force for Seismic Design of Bridge Foundations

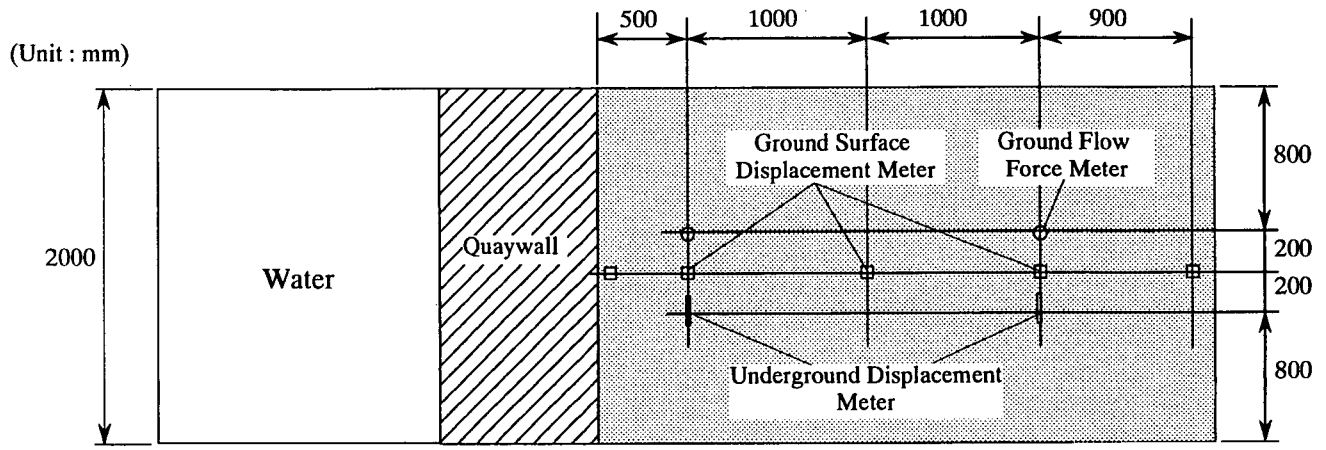
Presented in this paper are preliminary results of shaking table experiments on the liquefaction–induced ground flow [9]. Experiments were conducted for two different ground conditions and characteristics of ground displacement and ground flow force were analyzed.

METHODS OF EXPERIMENTS

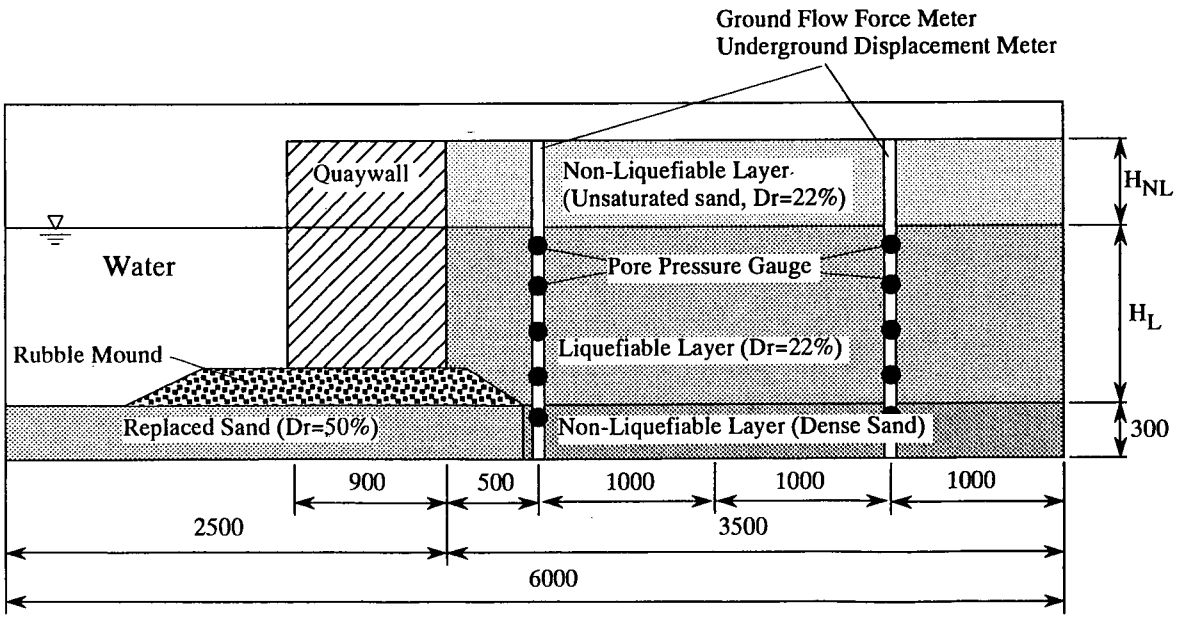
Experiment Models

A caisson type quaywall and the ground behind it were modeled in a large container (6m long, 2m wide and 2m deep), which was placed on a shaking table. An overall view of experiment model is given in Figure 2. The quaywall model was 0.9m wide, 2m long and 1.3m high. The ground model was composed of three layers, that is, base layer, liquefiable layer and non–liquefiable layer. The base layer was of dense sand. The upper two layers were of loose sand, and were made by putting clean sand into the water. The relative density of these layers was 22 %, and the other physical properties of the sand are listed in Table 1. The liquefiable and non–liquefiable layers were distinguished by adjusting the water level. Two cases of tests, i.e., Case 1 and Case 2, were carried out, in which the thicknesses of liquefiable layer H_L and non–liquefiable layer H_{NL} were

changed. H_L and H_{NL} were set as H_L=100cm, H_{NL}=50cm in Case 1 and H_L=50cm, H_{NL}=100cm in Case 2, respectively. The ground models had vertical lines on their sides so that ground deformation could be observed through the transparent glass of the container. These lines were made of colored sand. Photos 1 and 2 show the side views of experiment models.



(a) Plan



(b) Elevation

Figure 2 Overall View of Experiment Model

Table 1 Physical Properties of Sand

Specific Gravity of Soil Particle	2.633
Maximum Dry Density	1.350 gf/cm ^{3}
Maximum Void Ratio	0.944
Minimum Void Ratio	0.593
60% Grain Size	0.195 mm
10% Grain Size	0.130 mm
Mean Grain Size	0.180 mm
Coefficient of Uniformity	1.500

Instrumentation

Acceleration, displacement, pore water pressure and ground flow force were measured in the experiments. An overall instrumentation layout was presented in Figure 2. Displacements on the ground surface were measured by wire−reel type displacement meters. Figure 3 shows the instruments to measure displacement in the ground and ground flow force. The displacement meter is of nine 2 mm thick stainless steel plates connected by hinges. These plates follow deformation of the ground. An accelerometer is attached to each plate, and the displacement is estimated from the change of gravity acceleration by incline of plate. The ground flow force meter consists of nine separate polyvinyl chloride pipes and a rigid shaft that goes through pipes. Each pipe is 20cm long. A load gauge is installed between pipe and shaft so that the force acted on each pipe can be measured.

Test Procedures

In the experiments, liquefaction and its induced ground flow were generated by shaking the container on a shaking table. Sinusoidal waves with frequency of 5Hz were inputted in both Case 1 and Case 2 tests. For each case, the test was first conducted with acceleration level of 0.15G on the shaking table, and the acceleration level was then increased to 0.5G, after confirming that the excess pore water pressure induced by the first test disappeared. The duration of excitation was 5 seconds for both tests with 0.15G and 0.5G.

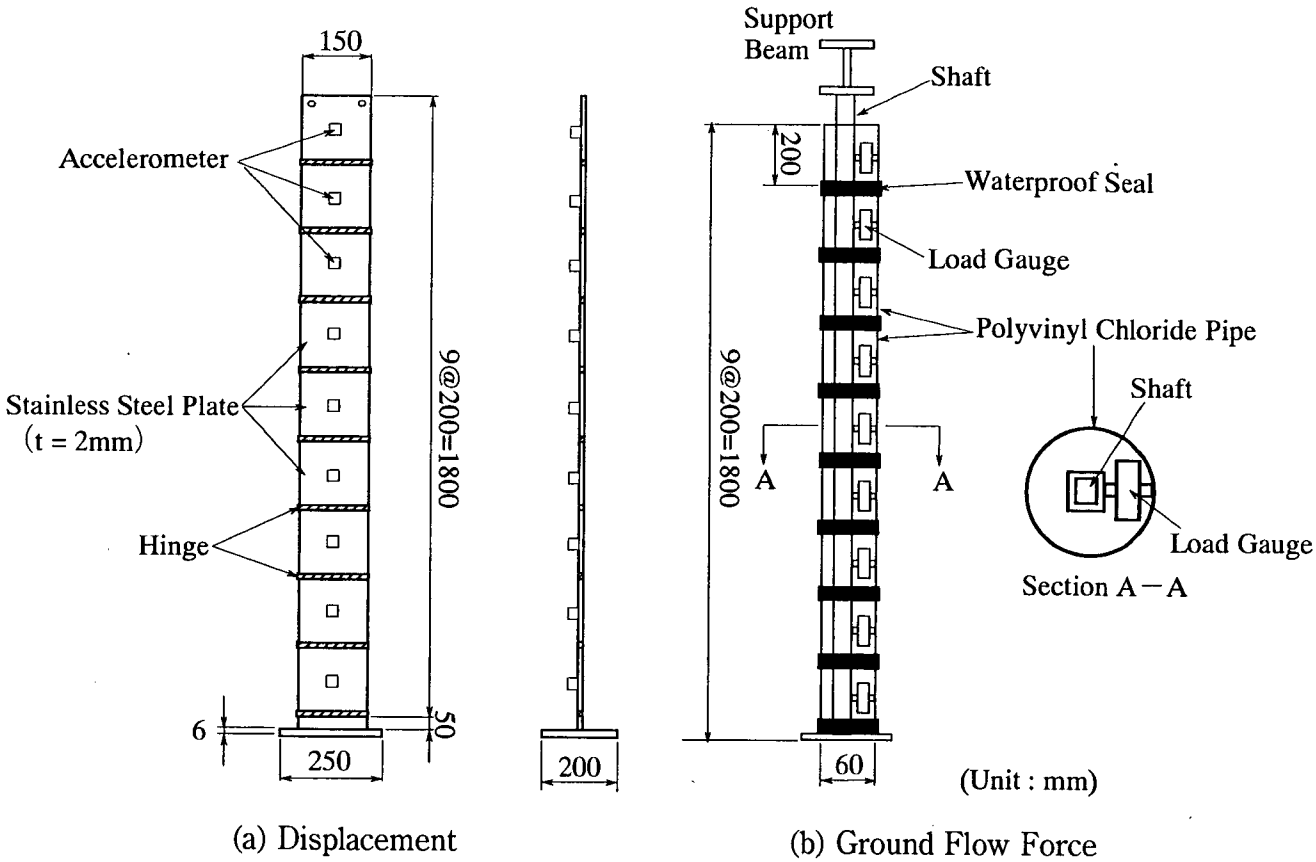
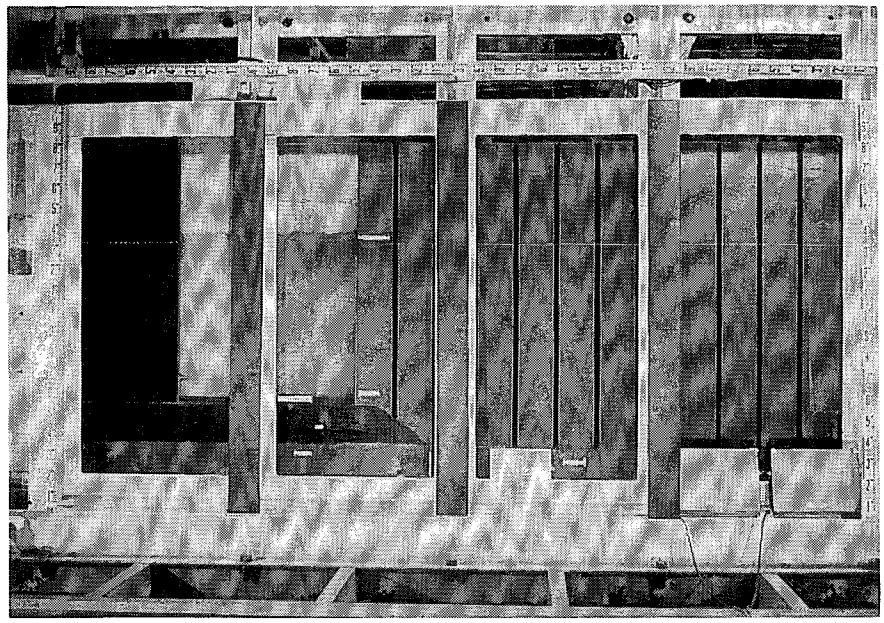


Figure 3 Instruments to Measure Displacement in the Ground and Ground Flow Force

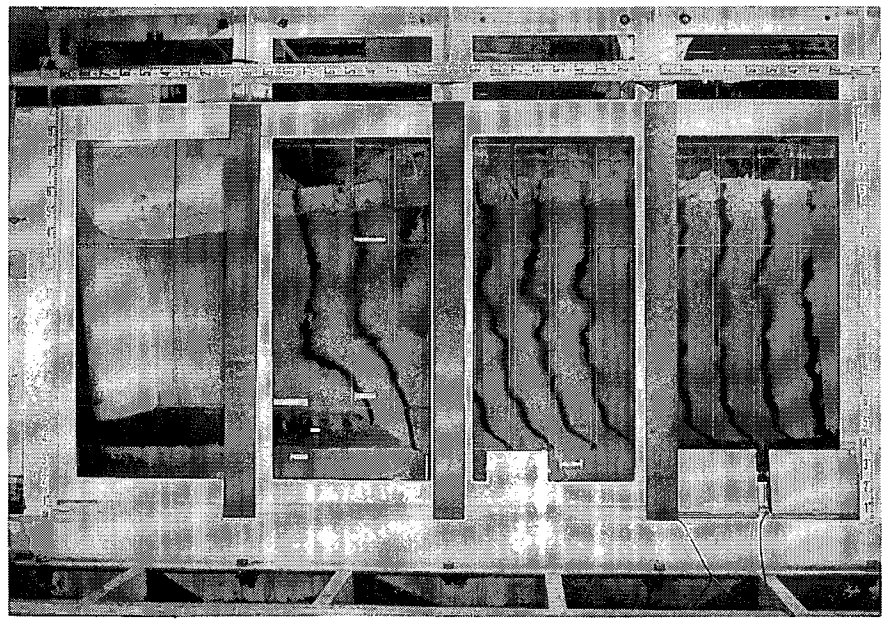
PRELIMINARY RESULTS OF EXPERIMENTS

Failure Modes

Photos 1 and 2 show the ground failure after 0.5G excitation for Case 1 and Case 2 tests, respectively. The quaywall was moved toward the water, and the liquefied layer with the overlain non-liquefied layer followed it. Deformation of vertical lines on the side of ground model indicates that lateral displacement of the ground increases from the bottom of the liquefied layer to the middle of it, and it is almost uniform for the upper part of the ground. Comparing the magnitude of ground deformation for Case 1 and Case 2, the former is larger than the latter. This may be attributed to the difference of the thickness of liquefied layer H_L.

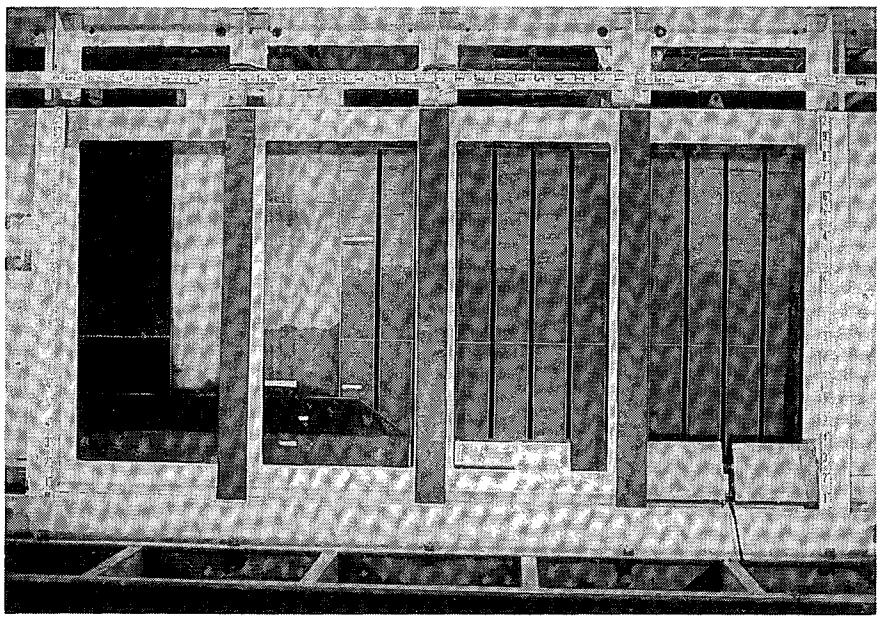


(a) Original Form

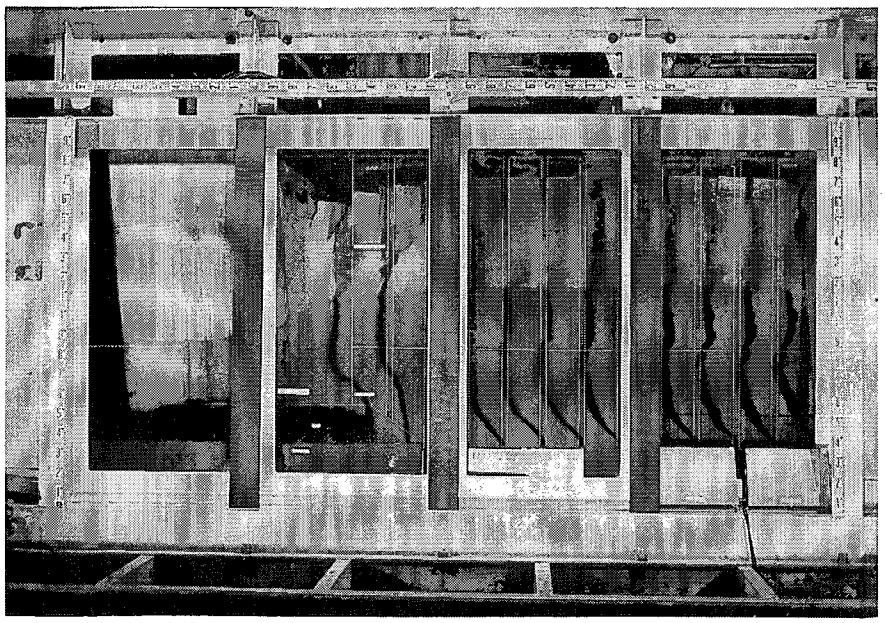


(b) After Excitation with 0.5G

Photo 1 Failure Mode of Case 1 Test (H_L=100cm, H_{NL}=50cm)



(a) Original Form

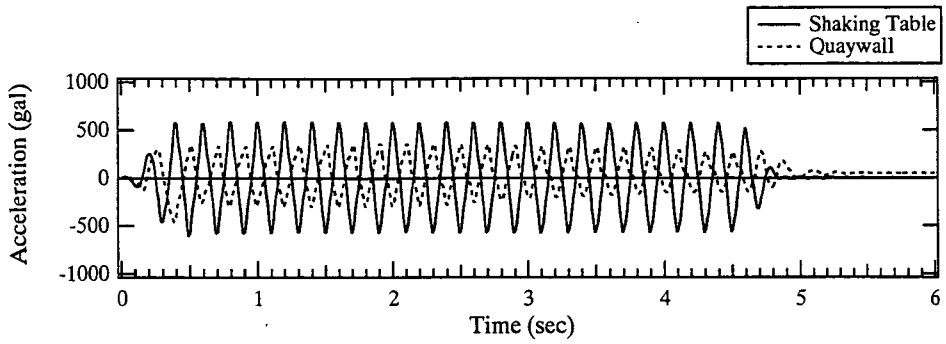


(b) After Excitation with 0.5G

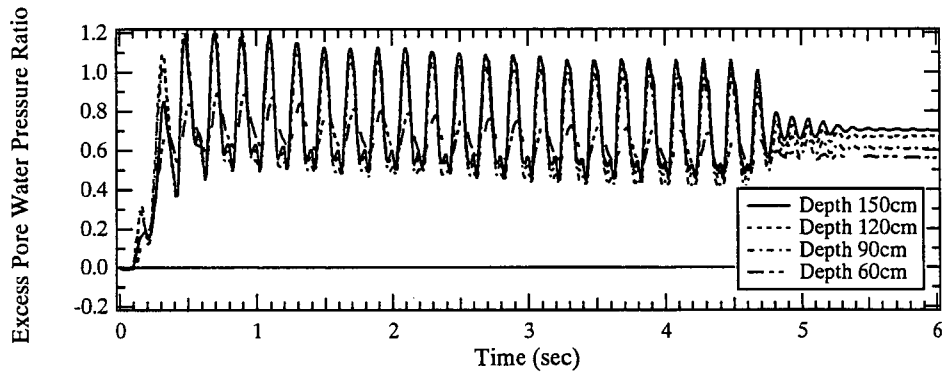
Photo 2 Failure Mode of Case 2 Test (H_L=50cm, H_{NL}=100cm)

Recorded Time Histories

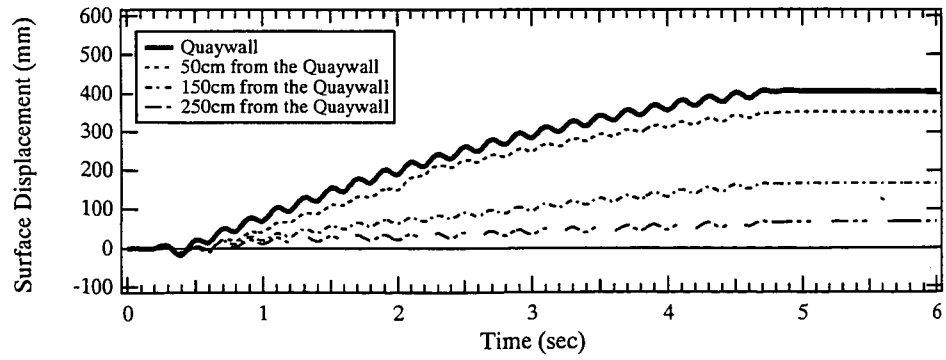
Time histories of acceleration, excess pore water pressure ratio which is the ratio of excess pore water pressure to effective overburden pressure, and ground surface displacement from Case 1 test with acceleration of 0.5G are shown in Figure 4. The accelerations were recorded on the shaking table and the quaywall. The excess pore water pressure ratios were measured at four depths, which were horizontally 150cm from the quaywall. The ground displacement begins to increase at about 0.5 seconds when the excess pore water pressure ratio becomes about 0.6 or greater. Displacement keeps to increase during excitation, and stops to increase when excitation ends. The residual displacement decreases as the distance from the quaywall increases.



(a) Acceleration



(b) Excess Pore Water Pressure Ratio



(c) Displacement

Figure 4 Time Histories of Case 1 Test with Acceleration of 0.5G

Ground Flow Displacement

Figure 5 illustrates the relationship between the residual displacement on the ground surface, which was caused by the ground flow, and the distance from the water's edge. The displacement at the left end indicates the residual displacement of quaywall. The ground flow displacement decreases as the distance from the water's edge increases. Comparing displacements for the same distance, it is larger as the thicknesses of liquefied layer H_L or level of input motion is larger.

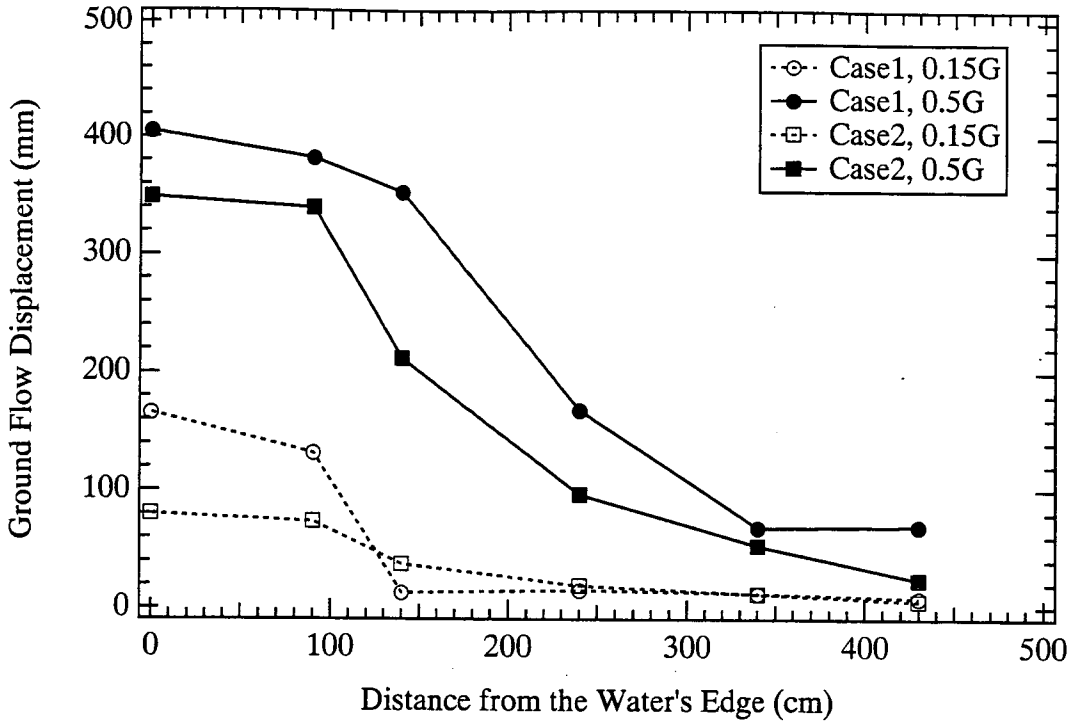


Figure 5 Relationship between the Ground Flow Displacement and the Distance from the Water's Edge

Based on Figure 5, Figure 6 shows the normalized relationship between the ground flow displacement and the distance from the water's edge, where the ground flow displacement and distance are normalized by the residual displacement of quaywall and the height of quaywall, respectively [10, 11]. The measured ground flow displacements at reclaimed lands in Kobe from the Hyogo-ken Nanbu Earthquake are also shown in this figure. They are also normalized by the same way. Although considerable scatter exists, the trends of ground flow displacement obtained from experiments agree with those estimated from the in situ measured data.

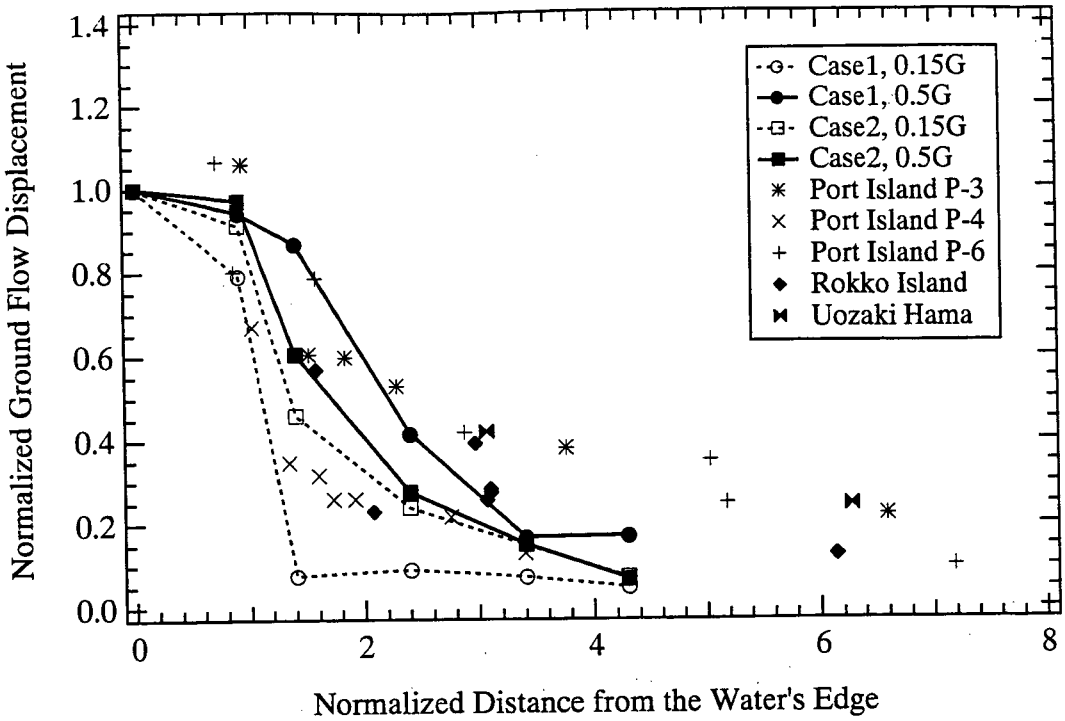
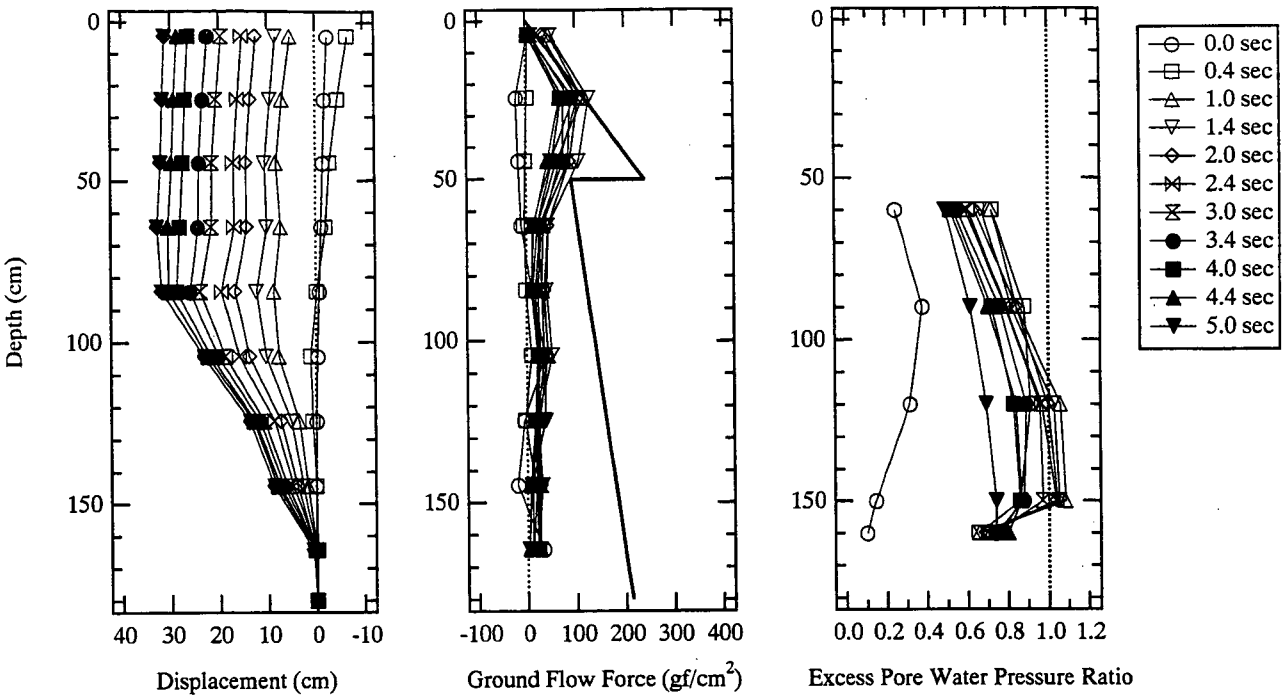


Figure 6 Normalized Relationship between the Ground Flow Displacement and the Distance from the Water's Edge

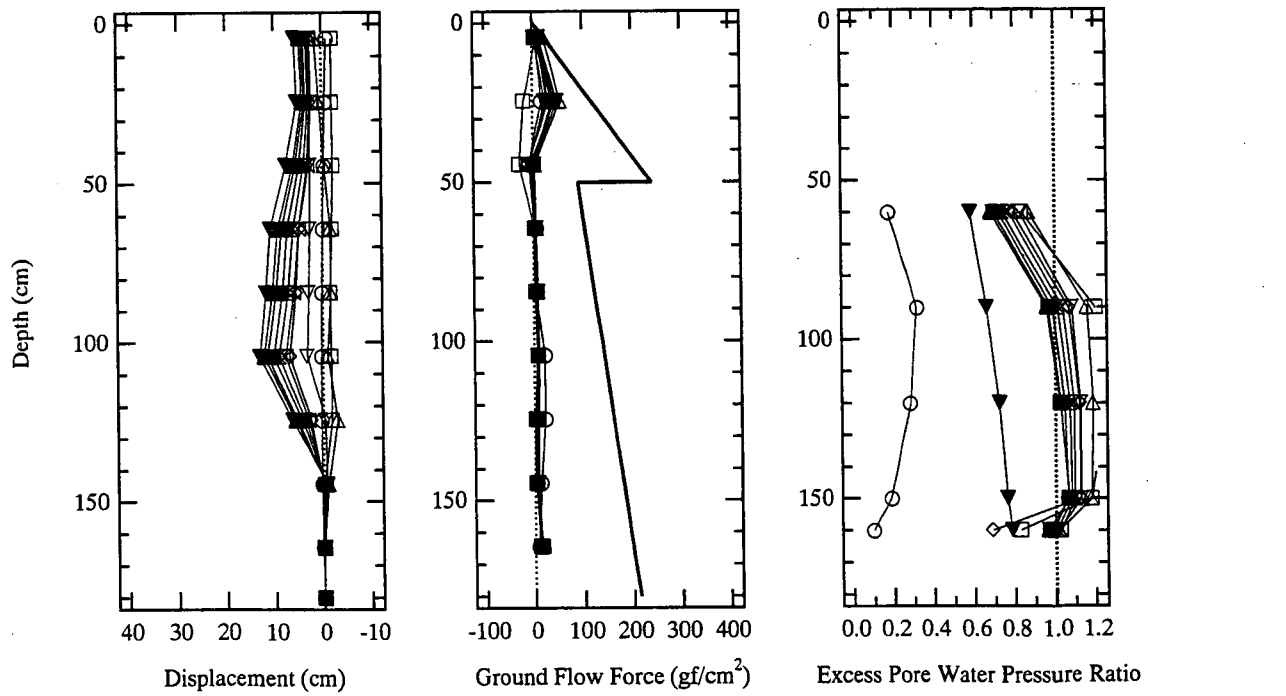
Ground Flow Displacement and Force in the Ground

Distributions of ground displacement, ground flow force and excess pore water pressure ratio in the ground are shown in Figures 7 and 8. These were recorded at 50cm and 250cm from the quaywall, and the results are presented for various times. Near the quaywall, the surface non−liquefied layer was moved toward the water with the underlain liquefied layer, on the other hand, the ground deformation far from the quaywall was mainly concentrated in the liquefied layer.

The ground flow force generated in the non−liquefied layer is larger than that in the liquefied layer. In the figures, the passive earth pressure and overburden pressure are also shown for the non−liquefied and liquefied layers, respectively. In case of 50cm from the quaywall, ground flow force in the non−liquefied layer almost reached the passive earth pressure, and it was smaller than the overburden pressure in the liquefied layer. In case of 250cm from the quaywall, however, the ground flow force was small and did not reach the passive earth pressure in the non−liquefied layer. It should be noted that the excess pore water pressure ratio for Case 2 did not exceed 1.0, which signifies that the complete liquefaction did not take place, nevertheless, large ground flow force was induced in the surface non−liquefied layer.

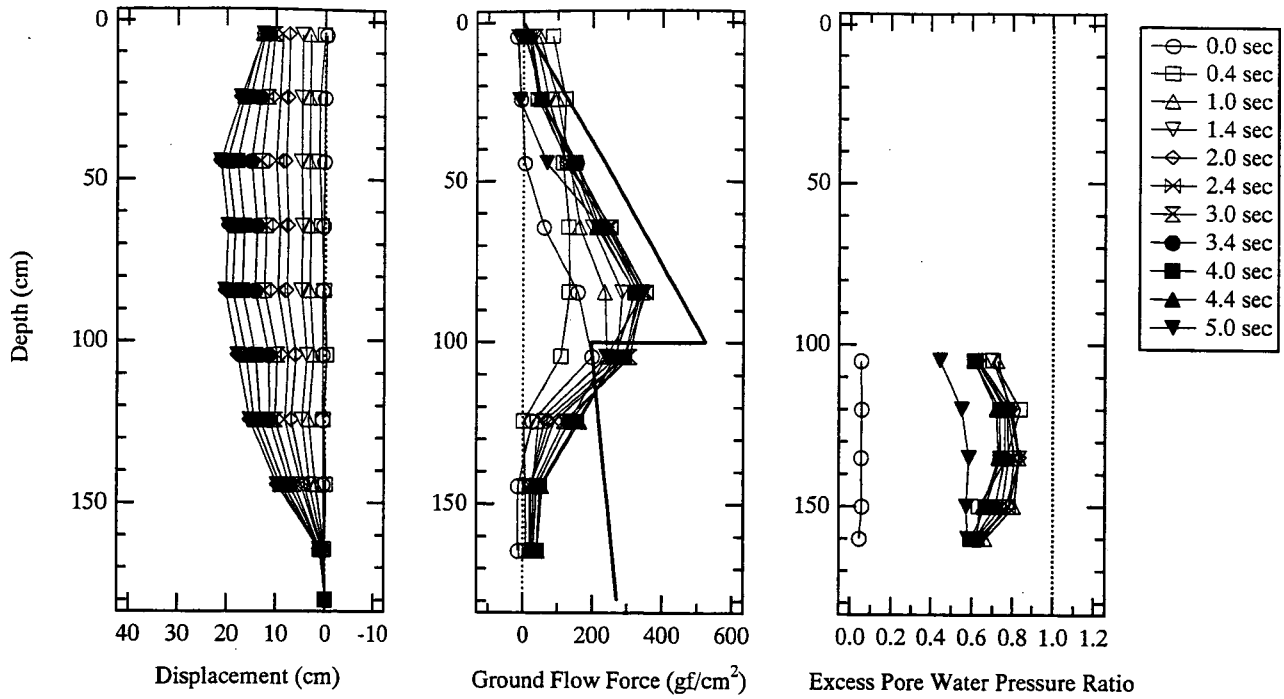


(a) 50cm from the Quaywall

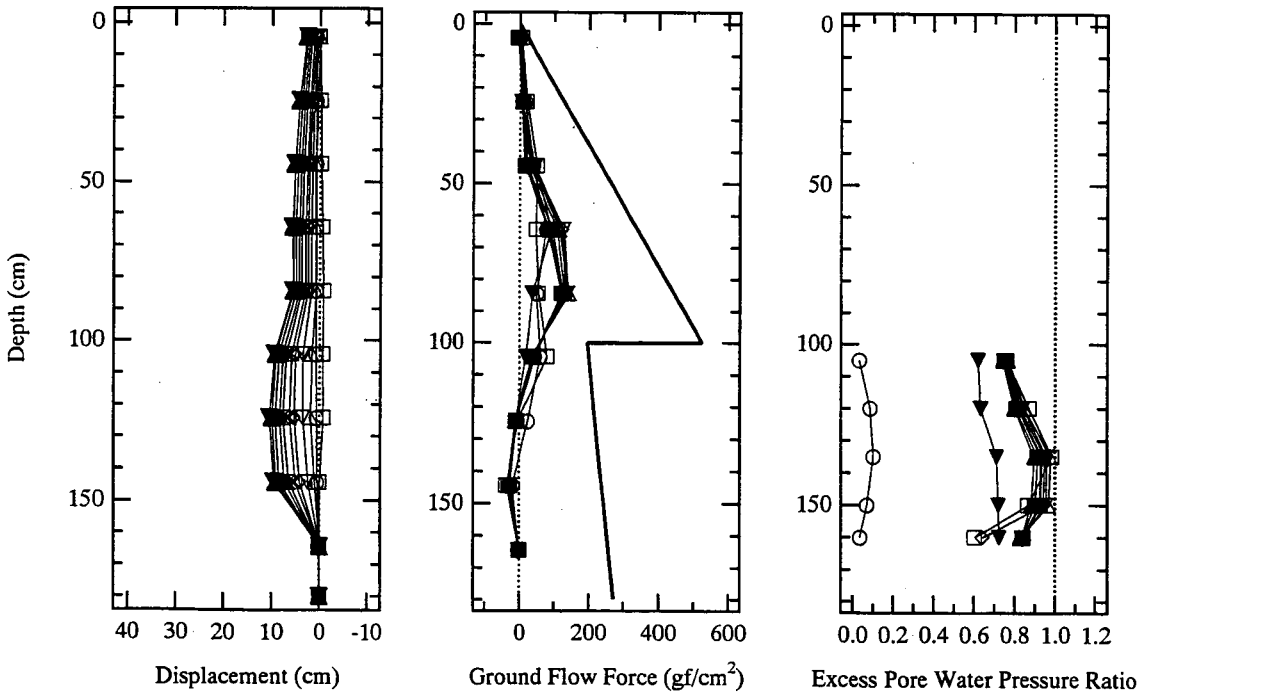


(b) 250cm from the Quaywall

Figure 7 Distribution of Displacement, Ground Flow Force and Excess Pore Water Pressure Ratio in the Ground of Case 1 Test (H_L=100cm, H_{NL}=50cm)



(a) 50cm from the Quaywall



(b) 250cm from the Quaywall

Figure 8 Distribution of Displacement, Ground Flow Force and Excess Pore Water Pressure Ratio in the Ground of Case 2 Test (H_L=50cm, H_{NL}=100cm)

CONCLUSIONS

The following conclusions may be deduced from the present study:

1) Ground flow was principally induced by the movement of liquefied layer with the overlain non-liquefied, following the movement of the quaywall. The normalized ground flow displacements obtained from experiments are consistent with those observed from the Hyogo-ken Nanbu Earthquake.

2) The ground flow force in the surface non-liquefied layer is almost equivalent with the passive earth pressure, and that in the liquefied layer is smaller than the overburden pressure.

REFERENCES

1) Japanese Geotechnical Society: Special Issue on Geotechnical Aspects of the January 17 1995 Hyogoken-Nambu Earthquake, 1996

2) Japan Society of Civil Engineers: The 1995 Hyogoken-Nanbu Earthquake - Investigation into Damage to Civil Engineering Structures -, 1996

3) Hamada, M., Isoyama, R. and Wakamatsu, K.: The 1995 Hyogoken-Nanbu (Kobe) Earthquake, Liquefaction, Ground Displacement and Soil condition in Hanshin Area, Association for Development of Earthquake Prediction, 1995

4) Committee for Investigation on the Damage of Highway Bridges by the Hyogo-ken Nanbu Earthquake, 1995: Report on the Damage of Highway Bridges by the Hyogo-ken Nanbu Earthquake, 1995 (in Japanese)

5) Otsuka, H. et al.: Report on the Disaster Caused by the 1995 Hyogoken Nanbu Earthquake, Chapter 5, Damage to Highway Bridges, Report of PWRI, No.196, 1996 (in Japanese)

6) Japan Road Association: Specifications for Highway Bridges, Part V Seismic Design, 1996 (in Japanese)

7) Kawashima, K. et al.: The 1996 Seismic Design Specifications of Highway Bridges, Proc. of 29th Joint Meeting, U.S.-Japan Panel on Wind and Seismic Effects, UJNR, 1997

8) Yokoyama, K., Tamura, K. and Matsuo O.: Design Method of Bridge Foundations against Soil Liquefaction and Liquefaction-Induced Ground Flow, Proc. of Second

Italy–Japan Workshop on Seismic Design and Retrofit of Bridges, 1997

9) Azuma, T. and Tamura, K.: Study on Ground Displacement and Force Acted on Bridge Foundations due to Liquefaction–Induced Ground Flow, Proc. of 24th JSCE Earthquake Engineering Symposium, 1997 (in Japanese)

10) Ishihara, K.: Soil Liquefaction and Effects of Lateral Flow on Foundations, 51st JSCE Annual Meeting, 1996 (in Japanese)

11) Inatomi, T. et al.: Mechanism of Damage to Port Facilities during 1995 Hyogo–ken Nanbu Earthquake, Technical Note of Port and Harbour Research Institute, No.813, 1995 (in Japanese)

SEISMIC VULNERABILITY STUDIES OF HIGHWAY STRUCTURES

By
W. Phillip Yen[1], John D. O'Fallon[2], James D. Cooper[3] and Ian M. Friedland[4]

ABSTRACT

This paper summarizes the progress of a current FHWA seismic vulnerability research program for existing and new highway constructions. Research is being conducted under this program in the subject areas of: *Seismic Hazards and Ground Motion, Geotechnical Engineering, Intelligent and Protective Systems, and Structures and Systems.* This program will result in the development of an improved understanding of the seismic hazard in the eastern and central United States, the behavior and response of foundations and soils under seismic excitation, and the overall response of highway structures and systems during earthquakes. This program is also developing retrofitting technologies appropriate for bridges and other highway structures in low-to-moderate seismic zones and design criteria and philosophies intended to reduce the vulnerability of future highway construction nationally.

BACKGROUND

There are approximately 600 thousand bridges in the U.S. About 70 percent of these bridges were constructed prior to 1971 with little or no consideration given to seismic resistance. The damage resulting from recent large earthquakes shows the need for a significant research effort to develop refined seismic retrofitting and design procedures for bridges. In recognition of this need, the Federal Highway Administration (FHWA) initiated a comprehensive Seismic Research Program for bridges and highways in the fall of 1992. This program is being conducted in cooperation with the National Center for Earthquake Engineering Research (NCEER) which is headquartered on the campus of the State University of New York at Buffalo.

The seismic research program being conducted by NCEER consists of two separate projects. Both projects involve research studies on the seismic vulnerability of highway construction in the United States including bridges, tunnels, retaining structures, slopes and embankments, culverts and pavements. One project focuses on existing transportation infrastructure while the other is concerned with future (new) highway construction.

The motivation for these two studies comes from the fact that the present guidelines for seismic design and retrofit of highway bridges are 10-15 years old, and that there are no national seismic design or retrofit

1 Research Structural Engr., Structures Division, FHWA Turner-Fairbank Highway Research Center, 6300 Georgetown Pike, McLean, VA 22101
2 Manager, Structures Program, ditto.
3 Chief, Structures Division, ditto.
4 Assistant Director for Bridges and Highways, National Center for Earthquake Engineering Research, State University of New York at Buffalo, 102 Red Jacket Quadrangle, Buffalo, NY 14261-0025

standards for the other components of typical highway systems. In addition, recent experience in California, Costa Rica, the Philippines, and Japan has provided new insight into bridge and highway response during earthquakes.

Significant progress has also been made in understanding the seismic risk of the United States, in geotechnical engineering terms and in seismic resistant design, such that a comprehensive review of design and retrofit philosophies and procedures can now be undertaken. However, although much has been learned, there are still many gaps in basic knowledge. Furthermore, not all existing knowledge can be immediately applied to the highway arena and further studies are required to facilitate the transfer of this technology.

As a result, the FHWA initiated the two studies comprising the NCEER Highway Project. The existing transportation infrastructure study is a six-year project concentrating on the development of revised and up-to-date seismic *retrofit guidelines* in order to provide cost-effective tools for improved evaluation and seismic-upgrading of the existing highway network. The new construction study is a four-year project in which improved seismic *design guidelines* for future highway construction will be developed. Research on these two projects was initiated by NCEER in the spring and summer of 1993, respectively.

Both studies being conducted under the NCEER Highway Project have a national focus and are intended to address differences in seismicity, bridge types, and typical design details between eastern and central U.S. bridges and those which have been studied in California. Furthermore, unlike the western U.S., design and retrofit strategies for the eastern and central U.S. need to reflect the probability that an earthquake significantly larger than the design earthquake can occur.

Critically important bridges on vital transportation routes or those providing access to emergency care facilities are being evaluated for their performance under these conditions. In such cases, California design and retrofit practice may need modification before being implemented in the eastern and central U.S. Another vital need is guidance on the evaluation and retrofit of long span bridges such as those crossing major rivers, ports, and harbors. This is especially critical for the eastern U.S. as there are many more such structures there, and a large number of these are relatively old and constructed of non-ductile cast iron or supported on uncemented masonry piers. The development of appropriate retrofit schemes for such structures will be a serious challenge.

A range of studies is therefore being carried out which encompass research into seismic hazard, foundations and soils properties and response, and the response of structures and systems. NCEER is coordinating a consortium of researchers through the various tasks of these projects. The consortium includes more than 20 academic institutions and consulting engineering firms, bringing together more than 30 earthquake and bridge engineers and scientists, to work on the project. This consortium provides a balance between University researchers and practicing professionals from the eastern and western United States.

Technical issues in the NCEER Highway Project have been grouped into several key subject areas. Within these subject areas, a number of research tasks are being conducted under each project (existing construction and new construction) as shown in Table 1.

Table 1 Subject Areas and Research Tasks in the NCEER Highway Project

Subject Areas	Research tasks	
	New Construction	Existing Construction
Vulnerability Assessment • Seimic hazard and ground motion • Soil and foundations • Systems and components	• Hazard Exposure Review • Spatial Variation • National Hazard Exposure	• Seismic Hazard • Ground Motion • Spatial Variation • Soil & Foundation Components, Structures, Systems.
Design Issues • Foundations and soils • Structures and special issues • Design issues and details • Design criteria	• Ductility Requirements • Structure Importance • Foundation and Soil-Structure-Interaction • Soils Behavior and Liquefaction • Seismic Detailing • Structural Response • Structural Analysis • Existing Design Criteria Review • Impact Assessment	
Retrofit Technologies • Soils and foundations • Systems and components • Special studies • Demonstration projects		• Soils & Foundations, Components, Structures, Systems • Special Studies • Demonstration Projects
Performance Criteria, Guidelines, and Education	• Existing Design Criteria Review	• State-of-the-art Review • Bridge retrofit Guidelines (Interim) • Performance Criteria • Retrofit Manuals • Cost Impact Studies • Technology transfer
Oversight, Coordination, and Reporting	• Project Administration & Highway Seismic Research Council	• Project Administration & Highway Seismic Research Council

An overview of the tasks and subject areas being researched in the new and existing construction projects are shown in Figures 1 and 2, respectively. As noted in these figures and Table 1, there is a significant amount of overlap between the two projects in several areas, requiring close coordination.

CURRENT RESEARCH

The research initiated to date under the NCEER Highway Project is fairly broad and covers a number of important technical studies. In subsequent years, work will focus on synthesizing the results of these studies into comprehensive seismic design and retrofitting guides, specifications, and implementation aids. The following briefly describes some of the current research and the agencies involved in the tasks.

Seismic Hazards and Ground Motion - Researchers at Geomatrix Consultants, the Lamont-Doherty Earth Observatory of Columbia University, the University of Southern California, and Princeton University are evaluating current methods to determine the seismic hazard and exposure of highway systems and bridges. They are compiling national and regional maps to develop more comprehensive strategies for representing seismic hazards, developing methods to quantify these hazards in a systematic way, and devising methodologies to determine when and how 3-dimensional basin effects, ground motion duration, and the spatial variation of ground motion should be considered during seismic hazard evaluations of bridges.

Geotechnical Engineering - A series of studies is being conducted by researchers at the University at Buffalo, University of Southern California, University of California at Berkeley, Virginia Polytechnic Institute, Brigham Young University, Rensselaer Polytechnic Institute and Earth Mechanics, Inc., to develop tools and technologies to identify and quantify various earthquake-related effects on soils and foundations. Of particular importance is the liquefaction potential of foundation soils beneath approach fills, bridge piers and abutments; the influence of pile groups on surrounding soils; and the post-liquefaction residual stiffness and strength of soils in providing support for pile foundation systems. Ground remediation techniques for liquefiable soils are being developed and improved. Studies are also being conducted to assess soil site coefficients, and the vulnerability of existing foundations for long-span bridges including large pile groups and caissons.

Structures and Systems - Researchers at the University at Buffalo, Imbsen & Associates, Inc., Modjeski and Masters, the National Institute of Standards and Technology, Iowa State University, the University of California at Berkeley, Dynamic Isolation Systems, and the University of Nevada at Reno are investigating and evaluating design and construction details commonly found in eastern and central U.S. bridges. Research is focused on understanding the flexure and shear performance characteristics of bridge columns and pier walls, joints and connection details, steel super- and substructures, and steel and elastomeric bridge bearings. Criteria and technologies are under development for the retrofit of tunnels, and columns, piers, joints, and bearings for highway bridges. In addition, these researchers, together with others from the Applied Technology Council and Geomatrix Consultants, are developing design criteria for new highway construction which focuses on detailing columns, pier walls, and joints for ductility and shear, and bridges and tunnels for structural movements.

NCEER researchers, with assistance from Modjeski and Masters and Imbsen & Associates, Inc., produced

the *Seismic Retrofitting Manual for Highway Bridges.* This manual was published by the FHWA in May 1995 as FHWA Report No. FHWA-RD-94-052, and contains a screening and evaluation procedure for seismically deficient highway bridges and outlines various measures to upgrade such structures. The manual is an update and revision to a 1983 FHWA report.

A system-wide seismic vulnerability assessment methodology is being developed by researchers at Dames and Moore, Inc., Seismic Systems & Engineering Consultants, and the University of Southern California to consider the seismic vulnerability and traffic impacts resulting from earthquake damage on a region or highway network: e.g., the city and surrounding counties around Memphis, Tennessee, or the Los Angeles, California, basin.

Intelligent and Protective Systems - A variety of earthquake protective systems are being evaluated by researchers at the University at Buffalo, University of California at Berkeley, University of California at Irvine, and University of Southern California to determine their applicability to highway bridges. Systems being studied include high-damping and lead-rubber bearings, sliding isolation systems, and viscous, visco-elastic, and friction damper systems. In addition, a study is being performed to provide a comparative assessment of the various types of protective systems currently available, and to identify the range of performance characteristics and limitations for each of these systems. NCEER Highway Project researchers have also been involved in the development of the new AASHTO "Guide Specifications for Seismic Isolation Design," which was adopted by AASHTO in 1997 and will be published in early 1998, and are developing response modification factors (R-factors) for seismically-isolated bridges.

Earthquake Reconnaissance - Within hours of the January 17, 1994, Northridge earthquake in California, a bridge reconnaissance team was organized. The team was on-site for two days after the event to survey and document damage to bridges and highways. The reconnaissance team provided reports on seven highway bridges that suffered partial collapses and another 170 bridges that suffered damage ranging from minor cracking to slumping within abutment fills. NCEER Technical Report NCEER-94-0008, "The Northridge, California Earthquake of January 17, 1994: Performance of Highway Bridges," documents the results of this effort.

A reconnaissance team was also assembled and sent to Kobe, Japan, following the January 17, 1995, Hanshin-Awaji earthquake, as part of the UJNR site visit, which was organized by the National Institute of Standards and Technology.

Many of the lessons learned from these reconnaissance visits, both with respect to damaged and undamaged structures in both the Kobe and Northridge earthquakes, have resulted in changes to Highway Project research tasks and overall program objectives. For example, special studies on the performance of superstructure restrainers was initiated following the Northridge earthquake, and a study on pier wall reinforcing and performance was started following the Kobe earthquake.

Demonstration Projects - NCEER was employed as sub-consultant to Steinman Engineers of New York City to assist in a seismic hazard analysis of the Queensboro Bridge. Using the results of several generic Highway Project studies, NCEER researchers reviewed past and current information on the seismicity, geology, and fault patterns in the region, to determine the seismic exposure of the bridge, and to provide

quantitative ground motion data suitable for a detailed structural analysis of the bridge.

As discussed under "Structures and Systems" above, a system-wide seismic vulnerability assessment methodology is being developed, in order to provide tools to identify the transportation impacts of earthquakes on a region or highway network. In order to demonstrate the draft methodology, a case study using the highway network in the city of Memphis, Tennessee and the surrounding Shelby County was conducted during the second year of work on the Highway Project. The demonstration identified the expected damage and minimum restoration times to all highway bridges contained within the region, under four different scenario earthquakes which could be expected to occur within the New Madrid Seismic Zone. During subsequent years, the traffic modeling and bridge damage models have been improved, and the Memphis demonstration will be shortly re-run using the improved methodologies.

Under Highway Project work on foundations and soils, a draft guide intended to assist bridge owners in screening and identifying liquefaction potential at bridge sites was developed by researchers from Brigham Young University. The draft guide has been tested through a demonstration project with the Utah Department of Transportation on the I-15 corridor in the Salt Lake City region, in order to validate the procedures contained in the guide and identify areas in need of further improvement. It is expected that this liquefaction hazard screening guide will be published and distributed by NCEER during the winter of 1997.

Workshops and Conferences - The *Second, Third, and Fourth U.S.- Japan Workshops on Earthquake Protective Systems for Bridges* were held in Tsukuba, Japan in December 1992. Berkeley, California in January 1994, and Osaka, Japan in December 1996, respectively. All three workshops focused on the application and improvement of seismic isolation systems to bridges, and have resulted in ongoing cooperation between U.S. and Japanese researchers and practitioners.

The *Second and Third U.S.-Japan Workshops on Seismic Retrofit of Bridges* were also held in Berkeley, California in January 1994, and Osaka, Japan in December 1996, respectively. These workshops were organized by the University of California at Berkeley and NCEER, respectively, and were both supported by NCEER.

The NCEER *Long-Span Bridge Seismic Research Workshop* was held in San Francisco, California, in December 1994. The objective of the workshop was to identify and discuss issues critical to the seismic performance and retrofitting of long-span bridges, including suspension, truss, cable-stayed, and arch bridges. The results of the workshop have assisted in identifying research needs specific to long, monumental bridges. Work on several of these issues, including the response of large pile groups in soft soils and the response of large caisson foundations under seismic excitation, was initiated as a result of this workshop.

The NCEER *Workshop on Seismic Damage Quantification and Performance of Structures* was held in San Francisco, California, in February 1995. The workshop was jointly supported by the NCEER Highway Project and the NCEER Building Project (which has the National Science Foundation as its primary sponsor). The objective of the workshop was to define the most desirable qualities of numerical damage indicators in order to link expected structural damage with structural performance in terms

suitable for use by practicing engineers and decision makers.

Additional workshops to be conducted under the NCEER Highway Project in the next year include a workshop to assist in finalizing recommendations to AASHTO on changes for portraying the national seismic hazard exposure in the U.S. in AASHTO specifications, a workshop on highway system risk and post-earthquake damage assessment, a U.S.-Italy workshop on seismic retrofitting for bridges, a workshop to quantify seismic ground motion parameters and modeling for the Eastern U.S., and a workshop on seismic retrofitting of highway bridges based on the FHWA bridge retrofitting manual, targeted toward State Bridge engineers.

PRODUCTS

The primary product resulting from the Highway Project contract on existing transportation infrastructure will be a manual for assessing and retrofitting the major components of the existing highway system in the U.S., including bridges, tunnels, retaining structures, slopes, culverts, and pavements. The manual, which will be presented in three volumes will be comprised of:

Volume I - Seismic Risk Assessment of Highway Systems
Volume II - Seismic Retrofitting Manual for Highway Bridges
Volume III - Seismic Retrofitting Manual for Retaining Structures, Slopes, Tunnels, Culverts, and Pavements

The 1995 FHWA *Seismic Retrofitting Manual for Highway Bridges* (publication No. FHWA-RD-94-052), which was developed during the first year of the NCEER Highway Project, is an interim version of the second volume of this three volume manual. This Manual will be updated and re-issued near the end of the Highway Project, based on the results of research conducted under the project.

Draft "strawmen" manuals were prepared in the fall of 1996 for Volumes I and III. The Volume I strawmen provides the methods, models, data needs, and procedures for conducting a system-wide analysis of scenario earthquake impacts on a highway system or sub-network, e.g. primary and secondary highways within a city, county or other geographic region. This assessment methodology describes expected damage to the highway elements and the resulting impacts on vehicular travel flows between various origins and destinations within the network.

The Volume III strawman contains recommended methods for screening, detailed evaluation, and retrofitting of critical highway structures other than bridges. The material contained in the strawman is based on current practice and ongoing research, and is expected to be significantly enhanced by the results of ongoing studies being conducted under the Highway Project and by others including the FHWA and Caltrans. It should be noted that at the current time, no standardized national guidance is currently available for the evaluation or retrofitting of these other highway system structures.

Secondary products resulting from the research on the existing transportation infrastructure project will be reports emanating from each of the major research tasks, reports synthesizing the results of various tasks in major technical areas (for example, in the areas of liquefaction screening and mitigation, substructure

performance and improvement technologies, and earthquake protective systems), other end-user guides and manuals, workshops, educational materials and training courses intended to aid in the implementation of the newly developed technologies.

The results of research on the new highway construction contract will provide the basis for the development of new design criteria and specifications in the near future. Secondary products, again, will include task reports and synthesis reports describing the advancements made in seismic vulnerability screening and design for transportation systems and components.

SEISMIC VULNERABILITY OF NEW HIGHWAY CONSTRUCTION
FHWA Contract DTFH61-92-C-00112

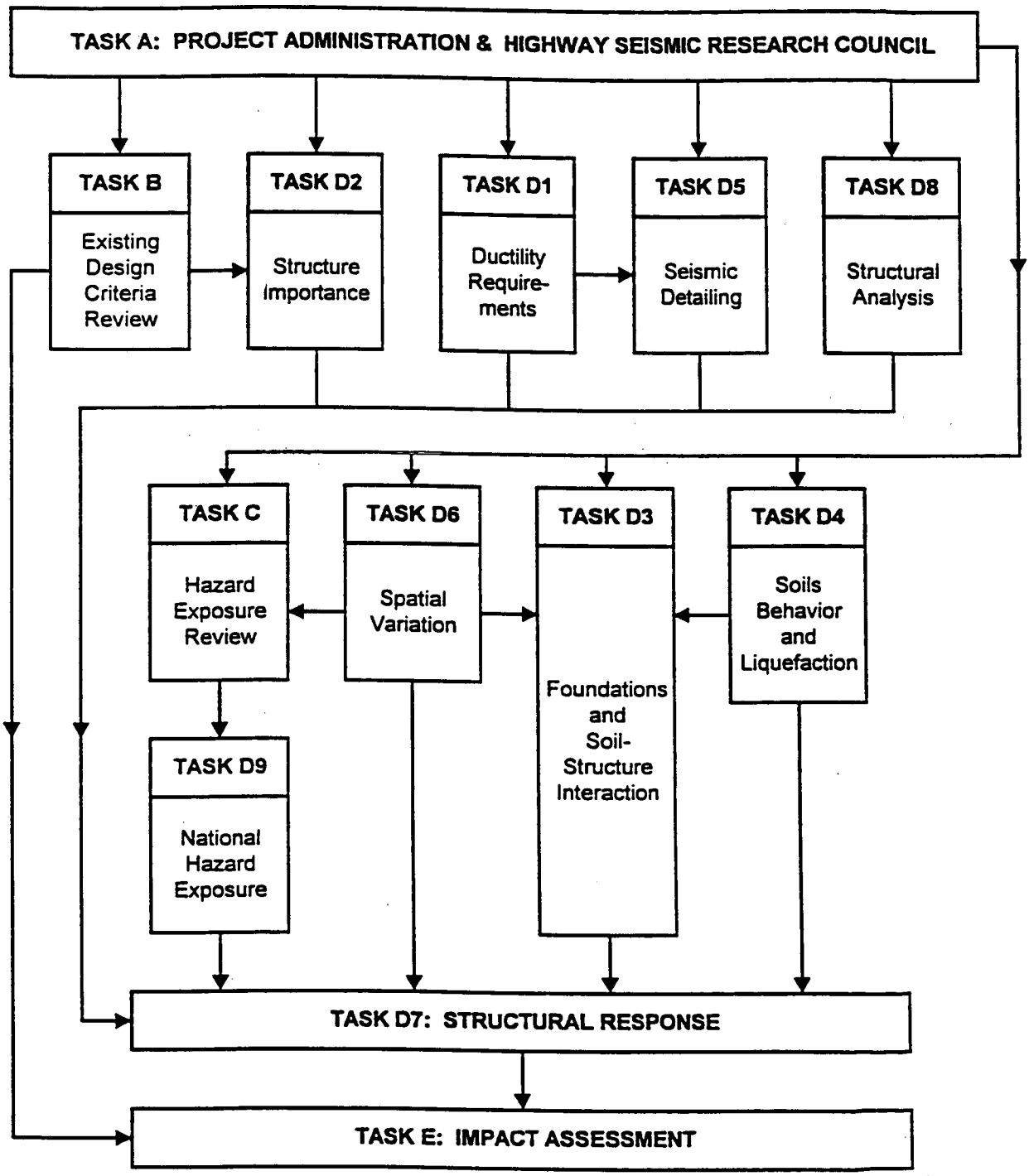


Figure 1. Project 112 - New Highway Construction.

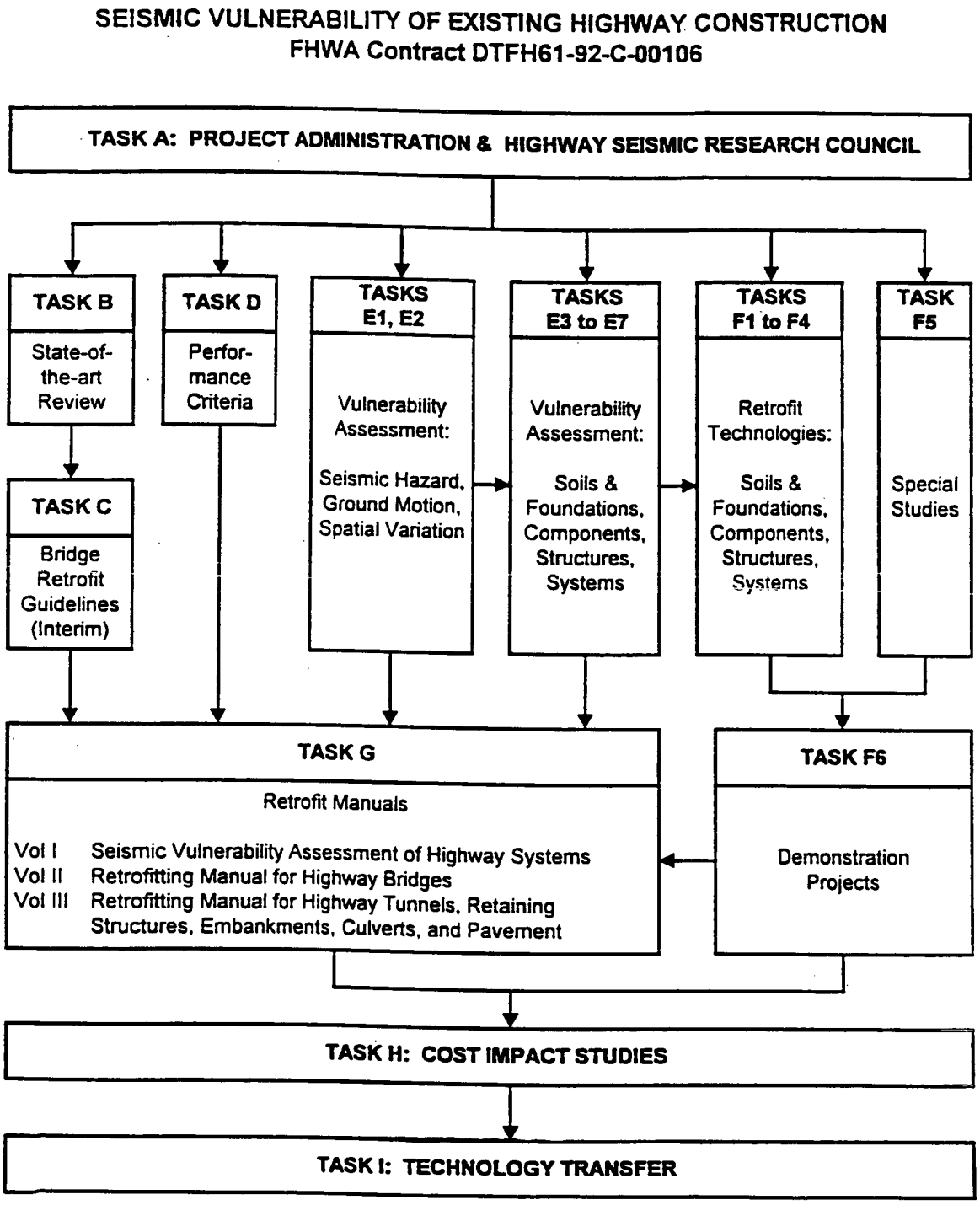


Figure 2. Project 106 - Existing Highway Construction.

EVALUATION OF SEISMIC PERFORMANCE OF JAPANESE BRIDGE PIERS DESIGNED BY THE PREVIOUS CODES

Kazuhiko Kawashima[1], Jun-ichi Sakai[2] and Hiroshi Takemura[3]

1) Professor, Department of Civil Engineering, Tokyo Institute of Technology
2) Graduate Student, Department of Civil Engineering, Tokyo Institute of Technology
3) Research & Development Department, P.S. Concrete Ltd.

ABSTRACT

This paper presents the seismic performance of Japanese bridges designed by the previous design codes. Four bridge piers which support the same superstructure were designed by the Design Specifications issued in 1964, 1980, 1990 and 1995. They were clarified by the Ductility Design Method and nonlinear dynamic response analysis. It was found that significant difference exists in the seismic performance of four piers.

1. INTRODUCTION

Highway bridges in Japan have been considered safe even against extreme earthquakes such as the Great Kanto Earthquake (M7.9) in 1923, because various past bitter experiences have been accumulated to formulate the seismic design method. Large lateral force coefficient ranging from 0.2g to 0.3g has been adopted in the allowable design approach. Various provisions for preventing damage due to instability of soils such as soil liquefaction have been used. Furthermore, design details including the unseating prevention devices have been adopted. In fact, reflecting those provisions, numbers of highway bridges which caused complete collapse was only 15 since the 1923 Great Kanto Earthquake. Based on this evidence, it has been regarded that the seismic damage of highway bridges has been decreasing in recent year.

The Hyogo-ken Nanbu Earthquake took place at Kobe and Awaji Island on January 17, 1995, and it caused destructive damage to highway bridges. Collapse and near collapse occurred at 9 sites, and other destructive damage occurred at 16 sites. Destructive earthquakes have not occurred at urban areas in recent years, and the earthquake revealed that there are various critical issues in seismic design and seismic strengthening of bridges in urban areas (9).

This paper tries to estimate the seismic performance of Japanese bridge piers, which were designed by the previous design codes, through dynamic response analysis. A bridge with the same dimensions is analyzed.

2. PAST SEISMIC DESIGN CODES OF BRIDGES

The first seismic provisions for highway bridges were introduced in 1926 after experiencing destructive damage in the 1923 Great Kanto Earthquake. Since the first stipulations, the seismic regulations have been reviewed and amended several times. The Design Specifications of Steel Highway Bridges was issued in 1939 and was revised in 1956 and 1964 (1964 Specifications). Because few concrete bridges were constructed at those days, stipulations were provided only for steel bridges. Only the seismic lateral force of 20% of the gravity force was described, and no other seismic design related provisions were presented in these Specifications. The 20% gravity force has been used as a basic design lateral force since then.

The first comprehensive seismic design provisions were issued by the Ministry of Construction in 1971 in the form of "Guide Specifications for Seismic Design of Highway Bridges." This is called hereinafter as the 1971 Specifications. It was described in the 1971 Guide Specifications that the lateral force shall be determined depending on zone, importance and ground condition in the static lateral force method (seismic coefficient method) and structural response shall be further considered in the modified static lateral force method (modified seismic coefficient method). Evaluation of soil liquefaction was incorporated in view of the damage caused by the 1964 Niigata Earthquake. Design details to increase the seismic safety such as the devices for preventing unseating of a superstructure from substructures were introduced. Design methods for substructures were also unified between 1964 and 1971 in the form of "Guide Specifications of Substructures." Therefore, it is considered that

seismic safety was considerably increased in the highway bridges designed according to the post-1971 Specifications.

The 1971 Guide Specifications of Substructures and the 1971 Guide Specifications for Seismic Design were revised in 1980 in the form of "Part IV Substructures" and "Part V Seismic Design" of the "Design Specifications of Highway Bridges." This is called here as 1980 Specifications. Part I, II and III are for "Common Part", "Steel Bridges" and "Concrete Bridges." The Part V was essentially the same with the 1971 Guide Specifications for Seismic Design, but an updated evaluation method for predicting soil liquefaction as well as a practical design method for foundations in liquefying sands was included.

The 1980 Design Specifications were revised in 1990. This is called here as the 1990 Specifications. Various major revisions were included in the revised Part V (3, 6). The first was an unification of the seismic coefficient method and the modified seismic coefficient method. This included the revision of the lateral force coefficient. The second was the introduction of the check of dynamic strength and ductility for reinforced concrete piers. Depending on the failure mechanism, dynamic strength of reinforced concrete piers was checked based on the ductility. The elastic response spectra with as high as 1 g that is presented as Type-I in Fig. 1 (a) has been used in the ductility check. The design spectra were determined from the attenuation equation of response acceleration for a design earthquake. Subduction fault type major earthquake such as the 1923 Kanto earthquake was considered for the design earthquake. This was the first practice in bridges that checked the behavior after yielding of structural members. Although this provision was not mandatory for all reinforced concrete piers, this had been effective to increase the ductility of piers. The third was the introduction of the static frame method to accurately evaluate the lateral force distribution of multi-span continuous bridges. This enables to consider three dimensional behavior of bridges in the equivalent static analysis. The fourth was the provisions for design response spectra for dynamic response analysis.

The Guide Specifications for Reconstruction and Repair of Highway Bridges which suffered Damage in the Hyogo-ken Nanbu Earthquake was issued by the Ministry of Construction on February 27, 1995, 41 days after the earthquake (10). This is called herein as the 1995 Specifications. It was later applied to all new construction and seismic strengthening of highway bridges in all sections of Japan (3), until the 1990 Specifications were revised in November 1996. The check of ductility which was incorporated in the 1990 Specifications was extended to apply to all structural components in which seismic effect is predominant. The elastic response acceleration as high as 2 g that is shown in Fig. 1 (a) as Type-II Ground Motion was included as well as the 1g response acceleration. This typically represents the ground motion at Kobe in the Hyogo-ken Nanbu earthquake.

The 1990 Specifications were revised in 1996 so as to include the essence of the 1995 Specifications. This is called hereinafter as the 1996 Specifications. Various effort to realize the concept of the 1995 Specifications was made to draft the 1996 Specifications. Although they are essentially the same in the concept level, several modifications and upgrading were included in the 1996 Specifications. The check of ductility was upgraded in the 1996 Specifications as the "ductility design method," and this became a major seismic design method as well as the traditional seismic coefficient method. The 1 g and 2 g elastic response spectra were named as "type I ground motion" and "type II ground motion" as shown in Fig. 1. It should be noted that reflecting the difference of the target earthquakes, the type I ground motion has much longer duration than the type II ground motion. Because the ultimate displacement of reinforced concrete pier subjected to cyclic lateral loading depends on the number of loading cycles (repletion), the dependence of ductility of reinforced concrete pier on the type of ground motion (type I and type II) was included. The similar dependence of soil strength against liquefaction on the type of ground motions was also introduced.

Referring to the above-mentioned history of seismic design, it should be noted that a major part of bridges which suffered damage in the Hyogo-ken Nanbu earthquake were designed by the 1964 and 1971 Specifications. Because few scientific knowledge on modern earthquake engineering was available at those days, only lateral force coefficient based on the allowable stress design approach was specified in those Specifications. Lack of shear capacity as well as the short anchoring length of longitudinal reinforcement at mid-height contributed to the damage.

There were two important problems in the 1964 and 1971 Design Specifications (7). First was the allowable stress for shear. The allowable stress at those days for a load combination of seismic effect and dead weight was 13.8 MPa (135 kgf/cm^2) for concrete and 275.5 MPa (2,700 kgf/cm^2) for reinforcements. This had been used without modification for long time. The important point was the allowable shear stress of concrete. Because reinforced concrete piers with large concrete sections such

as wall-type piers had been commonly adopted, check for shear stress of concrete was not so important in most piers. However it was critical in design of single columns with small concrete section. It was 1966 when the stipulations on the shear strength of concrete were incorporated at the first time in the Guide Specifications of Substructures (Part for Investigation and Design). Prior to 1966, the check for shear stress was conducted by referring to the Standard Specifications of Concrete by the Japan Society of Civil Engineers issued in 1931, 1940, 1949 and 1956 (4). In the JSCE Standard Specifications, the allowable shear strength of concrete was provided in two ways, i.e., if only concrete section resists shear, the allowable shear stress of concrete should be τ_{a1}, and if both concrete and reinforcements resist shear, the allowable stress of concrete should be τ_{a2}. The allowable stresses τ_{a1} and τ_{a2} depend on the design strength of concrete, and were 0.714 MPa (7 kgf/cm^2) and 2.04 MPa (20 kgf/cm^2), respectively, for concrete with design strength of 24.5 MPa (240 kgf/cm^2). Those values had been used until the JSCE Standard Specifications were revised in 1980, and τ_{a1} was reduced from 0.714 MPa (7 kgf/cm^2) to 0.459 MPa (4.5 kgf/cm^2) for concrete with design strength of 24.5 MPa (240 kgf/cm^2). As described above, in the same year, the 1980 Specifications incorporated τ_{a1} and τ_{a2} by referring to the JSCE Standard Specifications. The allowable stresses τ_{a1} and τ_{a2} were specified a little smaller than those specified in the JSCE Standard Specifications, and were 0.338 MPa (3.9 kgf/cm^2) and 1.735 MPa (17 kgf/cm^2) for concrete with design strength of 24.5 MPa (240 kgf/cm^2), and 0.429 MPa (4.2 kgf/cm^2) and 1.337 MPa (18 kgf/cm^2) for concrete with design strength of 27.55 MPa (270 kgf/cm^2). This revision was made reflecting the evidence that significant damage occurred at reinforced concrete piers in the 1978 Miyagi-ken-oki Earthquake.

Second was the anchoring length of longitudinal reinforcements of piers terminated at mid-height. Because moment of columns is critical at bottom and decreases with height, number of longitudinal reinforcements are gradually decreased by terminating a part of reinforcements at several heights. Problem was the short anchoring length of longitudinal reinforcements when they were terminated at mid-height. Because there were not a clear stipulation on the anchoring length in the Guide Specifications of Substructures until 1980, it was common to refer to the JSCE Standard Specifications of Concrete (4). It was stipulated in the JSCE Standard Specifications that reinforcements had to be anchored by either providing "enough" anchoring length or hooks/mechanical terminators. Because there was not stipulation on what was the "enough" anchoring length, the stipulations on splice length was alternatively used. The splice length depended on type and strength of reinforcements and bond stress, and was about 20 times diameter of reinforcements. Therefore, only 20 times diameter of longitudinal reinforcements had been adopted for the anchoring length of terminated bars until 1980.

However, similar to the problem on the overestimated allowable shear stress, because reinforced concrete piers with large concrete sections had been constructed in most cases, the problem was not evidently identified until recent time. The problem was first recognized in the 1978 Miyagi-ken-oki Earthquake when several reinforced concrete piers suffered extensive damage at the terminated points. More attention was paid on this problem in 1982 when the Shizunai Bridge suffered significant damage at piers in the Urakawa-oki Earthquake (11). In the 1980 Specifications, it was revised that from the height where longitudinal reinforcements can be terminated from calculation, longitudinal reinforcements had to be elongated with a length equivalent to an effective width of a column plus the splice length (about 20 x diameter of reinforcements). In fact, in the reinforced concrete pier supporting 18 span piltz bridge at Fukae, Route 3 Kobe Line of the Hanshin Expressway that collapsed in the Hyogo-ken Nanbu Earthquake, 60 among 180 longitudinal reinforcements were terminated at 2.5 m from the bottom in the piers. .If this requirement was applied to the piers, the longitudinal reinforcements terminated at 2.5 m from the bottom had to be further elongated with a length of 3.1 m.

3. PROCEDURE FOR EVALUATING SEISMIC PERFORMANCE

Seismic performance of bridge piers designed by the 1964, 1980, 1990 and 1995 Specifications was evaluated based on the nonlinear response analysis. The procedure follows on the 1995 Specifications. Because it is similar to the 1996 Specifications, outline of the procedure is presented based on the 1996 Specifications in the following.

In the 1996 Specifications, a bridge in which principal plastic hinge forms at the bottom of the pier is designed so that the following requirement be satisfied.

$$P_a \geq k_{he} W \tag{1}$$

where

$$k_{he} = \frac{k_{hc}}{\sqrt{2\mu_a - 1}} \tag{2}$$

$$W = W_U + c_P W_P \tag{3}$$

in which P_a= lateral capacity of a pier, k_{he}= equivalent lateral force coefficient, W= equivalent weight, k_{hc}= lateral force coefficient, μ_a= allowable displacement ductility factor of a pier, W_U= weight of a part of superstructure supported by the pier, W_P= weight of a pier, and c_P= coefficient depending on the type of failure mode. The coefficient c_P is 0.5 for a pier in which either flexural failure or shear failure after flexural cracks occurs, and 1.0 for a pier in which shear failure occurs. The lateral capacity of a pier P_a is defined as a lateral force at the gravity center of a superstructure.

The lateral force coefficient k_{hc} in Eq. (2) is given as

$$k_{hc} = c_Z \cdot k_{hc0} \tag{4}$$

in which c_Z = modification coefficient for zone, and is 0.7, 0.85 and 1.0 depending on zone, and k_{hc0}= standard modification coefficient. Fig. 1 (b) shows the standard lateral force coefficients k_{hc0} for the Type-I and the Type-II ground motions. The Type-I ground motions have been used since 1990 (1990 Specifications), while the Type-II ground motions were introduced in the 1996 Specifications.

In the important bridges (Type-B bridges), residual displacement developed at a pier after an earthquake must be checked as

$$\delta_R \leq \delta_{Ra} \tag{5}$$

where

$$\delta_R = c_R(\mu_R - 1)(1 - r)\delta_y \tag{6}$$

$$\mu_R = \frac{1}{2}\left\{\left(\frac{k_{hc} W}{P_a}\right)^2 + 1\right\} \tag{7}$$

in which δ_R= residual displacement of a pier after an earthquake, δ_{Ra}= allowable residual displacement of a pier, r= bilinear factor defined as a ratio between the first stiffness (yield stiffness) and the second stiffness (post-yield stiffness) of a pier, c_R= factor depending on the bilinear factor r, μ_R= response ductility factor of a pier, and δ_y= yield displacement of a pier. Eq. (6) depends on the residual displacement response spectra (8). The δ_{Ra} should be 1/100 of a distance between the bottom of a pier and a gravity center of a superstructure.

Although the acceleration response spectral intensity at short natural period is higher in the Type-II ground motions than in the Type-I ground motions, the duration of extreme acceleration excursion is longer in the Type-I ground motions than the Type-II ground motions. As will be described later, such a difference of the duration is taken into account to evaluate strength of piers and soils vulnerable to liquefaction.

Failure mode is required to be evaluated in determining the strength and ductility of a reinforced concrete pier. A pier is divided into several segments, and moment vs. curvature relation is evaluated for each segment assuming a stress vs. strain relation of both concrete and reinforcing bars. By assuming an elastic-plastic lateral force vs. lateral displacement relation for flexural deformation of pier, ultimate flexural strength of a pier P_u is evaluated. The yielding displacement δ_y is defined as a displacement at an intersection between a line connecting an origin and the first yielding displacement δ_{y0} and a line representing perfect elastic stiffness.

On the other hand, shear capacity of a pier subjected to cyclic loading P_s is evaluated as

$$P_s = S_c + S_s \tag{8}$$

$$S_c = 10 c_c c_e c_{pt} \tau_c b d \tag{9}$$

$$S_s = \frac{A_w \sigma_{sy} d(\sin\theta + \cos\theta)}{10 \times 1.15a} \tag{10}$$

in which, S_c= shear capacity of concrete (tf), S_s= shear capacity carried by reinforcing bars (tf), τ_c= averaged shear strength of concrete (kgf/cm^2) as shown in Table 1, c_c= effect of cyclic loading (=0.6 for the Type I ground motion and 0.8 for the Type II ground motion), c_e= modification for effective height d as shown in Table 2, c_{pt}= modification for tensile reinforcement ratio p_t as shown in Table 3, b= width of a pier (m) perpendicular to a direction for which shear capacity is computed, d= length of a pier (m) parallel to a direction for which shear capacity is computed, and A_w= area of tie reinforcement placed with an interval of a and an angle of θ.

It should be noted in Eq. (8) that the type of ground motion is included in terms of the coefficient c_c. Shear capacity of a pier against static loading P_{s0} is evaluated from Eq. (8) by substituting c_c=1.0.

Failure mode of a pier is determined based on the ultimate capacity P_u, the shear capacity for cyclic loading P_s and the shear capacity for static loading P_{s0} as;

(1) Flexural failure

$$P_u \le P_s \tag{11}$$

(2) Shear failure triggered by flexural failure

$$P_s < P_u \le P_{s0} \tag{12}$$

(3) Shear failure

$$P_{s0} < P_u \tag{13}$$

Based on the failure mode, the lateral capacity P_a and the design displacement ductility factor of a pier μ_a in Eqs. (1) and (2) are evaluated as

$$P_a = \begin{cases} P_u & \text{for flexural failure and shear failure triggered by flexural failure} \\ P_{s0} & \text{for shear failure} \end{cases} \tag{14}$$

$$\mu_a = \begin{cases} 1 + \dfrac{\delta_u - \delta_y}{\alpha \delta_y} & \text{for flexural failure} \\ 1 & \text{for shear failure triggered by flexural failure and shear failure} \end{cases} \tag{15}$$

in which α= safety factor, δ_y= yield displacement of a pier, and δ_u= ultimate displacement of a pier. As well as the lateral capacity of a pier P_a in Eq. (1), the δ_y and δ_u are defined at the gravity center of a superstructure.

In a reinforced concrete single pier in which a plastic hinge is formed at bottom, the ultimate displacement δ_u is evaluated as

$$\delta_u = \delta_y + (\phi_u - \phi_y)(h - L_p/2)L_p \tag{16}$$

in which ϕ_y= yield curvature of a pier at a plastic hinge zone, ϕ_u= ultimate curvature of a pier at a plastic hinge zone, h= height of a pier, and L_p= plastic hinge length of a pier. The plastic hinge length is given as

$$L_p = 0.2h - 0.1D \qquad (0.1D \le L_p \le 0.5D) \tag{17}$$

in which D is a width or a diameter of a pier.

The yield curvature ϕ_y and the ultimate curvature ϕ_u in Eq. (16) are evaluated assuming a stress-strain relation of reinforcements and concrete as shown in Fig. 2. The stress σ_c - strain ε_c relation of concrete with lateral confinement (5) is assumed as

$$\sigma_c = \begin{cases} E_c \varepsilon_c \left\{ 1 - \dfrac{1}{n} \left(\dfrac{\varepsilon_c}{\varepsilon_{cc}} \right)^{n-1} \right\} & (0 \le \varepsilon_c \le \varepsilon_{cc}) \\ \sigma_{cc} - E_{des}(\varepsilon_c - \varepsilon_{cc}) & (\varepsilon_{cc} \le \varepsilon_c \le \varepsilon_{cu}) \end{cases} \tag{18}$$

$$n = \frac{E_c \varepsilon_{cc}}{E_c \varepsilon_{cc} - \sigma_{cc}} \tag{19}$$

in which σ_{cc}= strength of confined concrete, E_c= elastic modulus of concrete, ε_{cc}= strain at maximum strength, and E_{des}= gradient at descending branch. In Eq. (18), the σ_{cc}, ε_{cc} and E_{des} are determined as

$$\sigma_{cc} = \sigma_{ck} + 3.8\alpha\rho_s\sigma_{sy} \tag{20}$$

$$\varepsilon_{cc} = 0.002 + 0.033\beta\frac{\rho_s\sigma_{sy}}{\sigma_{ck}} \tag{21}$$

$$E_{des} = 11.2\frac{\sigma_{ck}{}^2}{\rho_s\sigma_{sy}} \tag{22}$$

in which σ_{ck}= design strength of concrete, σ_{sy}= yield strength of reinforcements, α and β= coefficients depending on the shape of a pier (α=1.0 and β=1.0 for a circular pier, and α=0.2 and β=0.4 for a rectangular pier), and ρ_s= volumetric tie reinforcement ratio defined as

$$\rho_s = \frac{4A_h}{s \cdot d} \tag{23}$$

in which A_h= area of tie reinforcements, s= space of tie reinforcements, and d= effective width of tie reinforcements.

The ultimate curvature ϕ_u is defined as a curvature when concrete strain at longitudinal reinforcing bars in compression reaches an ultimate strain ε_{cu} defined as

$$\varepsilon_{cu} = \begin{cases} \varepsilon_{cc} & \text{for Type I ground motions} \\ \varepsilon_{cc} + \dfrac{0.2\sigma_{cc}}{E_{des}} & \text{for Type II ground motions} \end{cases} \tag{24}$$

It is important to note here that the ultimate strain ε_{cu} depends on the types of ground motions; the ε_{cu} for the Type-II ground motions is larger than that for the Type-I ground motions. Based on a loading test, it is known that a certain level of failure in a pier such as a sudden decrease of lateral capacity occurs at smaller lateral displacement in a pier subjected to a loading hysteresis with more number of load reversals (13). To reflect such a fact, it was decided that the ultimate strain ε_{cu} should be evaluated by Eq. (24), depending on the type of ground motions. Therefore, the allowable ductility factor μ_a also depends on the type of ground motions; the μ_a is larger in a pier subjected to the Type-II ground motions than a pier subjected to the Type-I ground motions.

It should be noted that the safety factor α in Eq. (15) depends on the type of bridges as well as the type of ground motions as shown in Table 4. This is to preserve higher seismic safety in the important bridges, and to take account of the difference of recurrent time between the Type-I and the Type-II ground motions.

In the following, a bridge pier was designed by the 1964, 1980, 1990 and 1995 Specifications. Although the 1995 Specifications are similar to the 1996 Specifications, the followings were not included:

(a) The ultimate strain ε_{cu} for the Type I ground motion was not determined by Eq. (25) but the stress vs. strain relation of concrete specified in the 1990 Specifications.
(b) The ultimate displacement was not evaluated by Eq. (16) but computed by integrating the curvature multiplied by the distance from the gravity center of the deck
(c) The difference of shear capacity for cyclic and static loading was not considered. Thus, the coefficient c_c in Eq. (9) was taken as 1.0.
(d) Internal ties are anchored by 90 degree hook at one end and 135 degree hook at the other end, while both ends are anchored in the core concrete by the 135 degree hook in the 1996 Specifications.

4. BRIDGE DESIGNED BY THE PREVIOUS CODES

A cantilever reinforced concrete pier, P3 of a four span continuous bridge with 4@35 m long as

shown in Fig. 3 was analyzed. The bridge is supported by fixed steel bearings at P2, P3 and P4 with P1 and P5 being supported by steel movable bearings. The total deck weight is 70,882 kN, and a part of the deck of 23,627 kN is laterally supported by P3. Fig. 4 shows the dimension of P3. It is 9.7 m high with a section of 4.0 m deep and 3.5 m wide, and is supported by a footing with 16 cast-in-place reinforced concrete piles with 1.5 m-diameter. The surround soil is of alternation of sandy and clayey layers up to 25 m below the ground surface. It is identified as Type 4 ground in the 1980 Specifications and Type III ground in the 1990 Specifications. The bridge was originally designed by the 1980 Specifications.

The P3 was re-designed by the 1964, 1990 and 1995 Specifications assuming that only the size and reinforcement of the pier can be changed with other conditions such as the height of substructure, length and weight of superstructure, soil condition and nominal design strength of concrete and reinforcement being unchanged.

Fig. 5 compares the section and reinforcement of the four piers. The pier designed by the 1964 Specifications, which is called hereinafter as the 1964 Pier, is 3 m deep in longitudinal direction and 3.5 m wide in transverse direction. In the 1964 Pier, 92 x 29 mm-diameter deformed bars and 60 x 29 mm-diameter deformed bars are placed along each surface perpendicular and parallel to the bridge axis, respectively. Longitudinal reinforcement ratio is 1.21 %. The piers designed by the 1980, 1990 and 1995 Specifications, which is called here as 1980 Pier, 1990 Pier and 1995 Pier, respectively, are 4 m deep and 3.5 m wide. In both the 1990 Pier and 1995 Pier, 108 x 38 mm-diameter deformed bars and 84 x 32 mm-diameter deformed bars are placed along each surface perpendicular and parallel to the bridge axis, respectively. The longitudinal reinforcement ratio is 1.36 % in the both piers. The longitudinal reinforcement ratio in the 1980 Pier is a little smaller, and is 1.25 %. Thus, the longitudinal reinforcement ratio in the four piers are not so much different, and it is in the range of 1.21 - 1.36 %.

However, it is obvious that the amount of tie is significantly different in the four piers. In the 1964 Pier, 16 mm-diameter deformed bars are placed in each 300 mm with the volumetric ratio of tie ρ_s of only 0.09 %. It should be noted that ties are anchored in the cover with 90 degree hook. The anchorage length follows the lap splice length in the 1956 JSCE Specifications. The same detailing of the anchor is used in the 1980 and 1990 Piers. The 19 mm-diameter bars with interval of 150 mm are used in both 1980 and 1990 Piers. In addition to the ties, 16 mm-diameter and 19 mm-diameter bars are placed along the inner longitudinal bars in the 1980 and 1990 Piers, respectively. It should be noted that 19 mm-diameter bars are placed inside the core. It was common that some reinforcements were placed inside the core for fabrication, but they were not intended to be the intermediate ties. Although they should not be considered effective for the confinement in design of new bridges, it was assumed here that they are effective for the confinement in evaluating the existing piers, because they were placed with an interval of 150 mm and lateral space of 1.2 m, and because the lap splice length was taken at the splice zone at center. In the 1995 Pier, the 22 mm-diameter ties with interval of 150 mm are placed. Ends of the ties are anchored in the core concrete by the 135 degree hook. Furthermore, 22 mm-diameter internal ties with 90 degree hook at one end with the other end by 135 degree hook are placed 150 mm interval. Lateral space between the internal ties are less than 1 m. Thus, the volumetric ratio of ties ρ_s is 0.32%, 0.64 % and 1.03 % in the 1980, 1990 and 1995 Piers, respectively.

5. EVALUATION OF SEISMIC PERFORMANCE BASED ON STATIC ANALYSIS

Table 5 shows the design process of the four piers by the traditional seismic coefficient method. Reflecting the increase of seismic coefficient, it is seen that the design lateral force increases in the 1990 and 1995 Piers than the 1964 Pier and 1980 Pier. All the computed stress satisfy the required allowable stress, and thus it is apparent that they are properly designed by the previous codes.

Fig. 6 shows the moment vs. curvature relation at the bottom of the piers and the lateral force vs. lateral displacement relation at the gravity center of the superstructure. Seismic performance evaluated by Eq. (1) is shown in Table 6. Because the shear capacity of the 1964 Pier is smaller than the flexural capacity, it is evaluated that the 1964 Pier fails in shear. Thus, because design displacement ductility factor should be 1.0 from Eq. (15), it is obvious that the 1964 Pier is unsafe. Other piers do not fail in shear, but have some problem except the 1995 Pier. For example, the 1980 Pier has the design flexural capacity of 12,083 kN and 11,103 kN in longitudinal and transverse direction, respectively, while the demanded lateral capacity is 16,003 kN and 12,652 kN. It is thus evaluated

that the 1980 Pier fails in flexure in both directions. Similarly, the 1990 Pier has the design flexural capacity of 12,818 kN in longitudinal direction, while the demanded lateral capacity is 13,642 kN. Because the ultimate flexural capacity is 12,818 kN, and is slightly larger than the demand, the 1980 Pier may be safe for collapse although it suffers major flexural damage. The 1995 Pier is safe in both directions.

6. EVALUATION OF PERFORMANCE BASED ON DYNAMIC RESPONSE ANALYSIS

To evaluate the seismic performance of the piers, the deck-pier-foundation system was idealized as shown in Fig. 7. Nonlinear hysteretic behavior of the pier was idealized by the degrading trilinear Takeda model (12). Effect of surrounding soil was models by soil springs with the equivalent linear stiffness. Damping ratio of 0.02 and 0.2 was assumed for the pier and the foundation, respectively. After computing the modal damping ratio for each mode by the strain proportional method, the two coefficients of Rayleigh damping were determined.

The ground motion measured in the Hyogo-ken Nanbu Earthquake at ground surface near the Higashi-Kobe Bridge (Higashi-Kobe Bridge record) was used as an input ground motion for the analysis. The soil condition at the Higashi-Kobe Bridge site is the Type III, and is similar to that at the bridge. However, because the elastic response spectrum of the Higashi-Kobe Bridge record is smaller than the design spectrum as shown in Fig. 8 (b), the record was scaled up by a factor of 1.5. The record at Higashi-Kobe Bridge is designated hereinafter as the 1.5 x Higashi-Kobe Bridge record. It has the peak acceleration of 0.5 g as shown in Fig. 8 (a).

Because the 1964 Pier fails in shear, the rest piers were analyzed here. Figs. 9 and 10 show the response of 1980 and 1995 Piers against the 1.5 x Higashi-Kobe Bridge record. Table 8 summarized the peak responses. In the 1980 Pier, the response ductility factor is 5.04 and 2.38 in longitudinal and transverse direction, respectively, while the design displacement ductility factor is 2.97 and 3.15. Therefore, the response displacement in longitudinal direction exceeds 70 % of the design displacement. Because the ultimate ductility factor is 3.95 in this direction, the response displacement also exceeds 28 % of the ultimate ductility factor. Thus, the 1980 Pier is evaluated unsafe in longitudinal direction. It should be noted that residual drift of 24 mm and 12 mm is developed at the gravity center of the deck in the 1980 Pier. The drift ratio is 0.25% and 0.10 %. It should be noted that the residual drift is sensitive to the bilinear factor (8).

The longitudinal response is also critical in the 1990 Pier. While the design ductility factor is 3.86, the response ductility factor 4.70, 22 % exceeding the design ductility factor. The response ductility factor is however slightly less that the ultimate ductility factor of 5.29. Thus, it may be said that the 1990 Pier does not collapse but suffers major flexural failure. The response ductility factor of the 1995 Pier is less that the design ductility factor in both directions.

To identify the response of the piers against other ground motions, an analysis was conducted for the 1995 Pier. Three typical ground motions as shown in Table 9 and Fig. 11 were used for this purpose. First is the JMA Kobe record that was measured at the JMA (Japan Meteorological Agency) Kobe Marine Observatory in the 1995 Hyogo-ken Nanbu earthquake. It has the peak acceleration of 0.83 g (NS component). The second is the record measured at the Sylmar Parking Lot in the 1994 Northridge earthquake (1). It has the peak acceleration of 0.84 g (NS component). Third is the Kushiro record measured at the JMA Kushiro Observatory during the Kushiro-oki earthquake in 1993. The earthquake was induced by an interplate-type fault with magnitude of 7.8. The ground motion has the peak acceleration of 0.94 g (EW component), and has long duration. It should be noted here that soil condition was not considered in selecting the ground motion. This is because the purpose of the analysis is to know the response of the 1995 Pier against the "typical" records. Fig. 11 (d) compares the elastic response acceleration for the three records and the 1.5 x Higashi-Kobe Bridge record.

Fig. 12 shows the 1995 Pier subjected to the JMA Kobe and Sylmar records. The response displacement of 1995 Pier is larger when it is subjected to the JMA Kobe record than the Sylmar record.

Fig. 13 compares the lateral force vs. lateral displacement hysteresis at the gravity center of the deck. The response ductility factor is 1.12, 4.59, 3.23 and 2.76 for the 1.5 x Higashi-Kobe Bridge record, the JMA Kobe record, the Sylmar record and the JMA Kushiro record, respectively. Because the design ductility factor is 5.33, the 1995 Pier performs well against those records. However, the residual drift is 41 mm against the JMA Kobe record, that corresponds to the drift ratio of 0.35 %.

7. CONCLUSIONS

A series of design check and nonlinear dynamic response analysis were conducted to clarify the seismic performance of Japanese bridge piers designed by the 1964, 1980, 1990 and 1995 design codes. Although the analysis was limited for only one pier and only few ground motions were used, the following conclusions were delivered from the analysis presented herein:

1) Because of lower seismic coefficient (0.2) in the seismic coefficient method and the higher allowable shear stress, the 1964 Pier has smaller section. Furthermore, the volumetric tie reinforcement ratio is only 0.09 %. Because shear capacity is smaller than the flexural capacity, it is estimated that the pier fails in shear.

2) The rest piers fail in flexure, and the response in longitudinal direction is critical. Against the 1.5 x Higashi-Kobe Bridge record, the response ductility factor of the 1980 Pier in this direction is 5.04, 70 % exceeding the design ductility factor. The response ductility factor of the 1990 Pier is 4.70, 22 % exceeding the design ductility factor (3.86), but is less than the ultimate ductility factor (5.29). Thus, the 1980 Pier could be significantly damaged, although it does not collapse. The response ductility factor of the 1995 Pier is less than the design ductility factor in both directions.

3) Residual drift is developed in the piers. Even in the 1995 Pier, it is 26 mm, which corresponds to the drift ratio of 1/380, against the 1.5 x Higashi-Kobe Bridge record. Residual drift is an important item to be checked in design.

4) The response displacement of the 1995 Pier in transverse direction becomes largest when the pier is subjected to the JMA Kobe record. The response displacement of the pier when it is subjected to the JMA Kushiro record and the Sylmar record is 60 % and 70 %, respectively, less than the response against the JMA Kobe records. The intensity of the Kobe record is significant for nonlinear response of the pier.

ACKNOWLEDGMENTS

For conducting the analysis, invaluable support was provided by Messrs. Nomura, S. and Sato, K., P. S. Concrete, Yabe, M., Chodai Consultant, and Hosotani, M., Taisei Construction Co. Their support is greatly appreciated.

REFERENCES

1) California Department of Conservation: Processed CSMIP Strong Motion Records from the Northridge, California Earthquake of January 17, 1994, Office of Strong Motion Studies, 1994
2) Japan Road Association: Design Specifications of Highway Bridges- Part I Common Part, Part II Steel Bridges, Part III Concrete Bridges, Part IV Substructures, and Part V Seismic Design, 1990
3) Japan Road Association: Reference for Applying the Guide Specifications for Reconstruction and Repair of Highway Bridges Which Suffered Damage in the Hyogo-ken Nanbu Earthquake, 1995
4) Japan Society of Civil Engineers: Standard Specifications of Concrete, 1931, 1940, 1949, 1956, 1967, 1974, 1977, 1980
5) Hoshikuma, J., Kawashima, K. and Nagaya, K.: A Stress-Strain Model for Reinforced Concrete Bridge Piers Confined by Hoop Reinforcement, Proc. 2nd US-Japan Workshop on Seismic Retrofit of Bridges, Berkeley, CA, USA, 1994
6) Kawashima, K. and Hasegawa, K: New Seismic Design Specifications of Highway Bridges in Japan, Earthquake Spectra, Vol.10, No.2, 1994
7) Kawashima, K.: Impact of Hanshin/Awaji Earthquake on Seismic Design and Seismic Strengthening of Highway Bridges, Report No. TIT/EERG 95-2, Tokyo Institute of Technology, 1995
8) Kawashima, K., MacRae, G. A., Hoshikuma, J. and Nagaya, K. : Residual Displacement Response Spectrum and Its Application to Reinforced Concrete Bridge Piers, Proc. 28th Joint Meeting, Wind and Seismic Effect, NIST SP 904, pp.185-204, National Institute of Standards and Technology, Gaithersburg, MD, USA, 1996.
9) Ministry of Construction: Report on the Damage of Highway Bridges by the Hyogo-ken Nanbu Earthquake, Committee for Investigation on the Damage of Highway Bridges in the Hyogo-ken Nanbu Earthquake, 1995

10) Ministry of Construction: Guide Specifications for Reconstruction and Repair of Highway Bridges Which Suffered Damage in the Hyogo-ken Nanbu Earthquake, 1995
11) Narita, N., Murakami, M. and Asanuma, H.: Report of the Investigation on Earthquake Damage to Shizunai Bridge, 15th Joint Meeting, US-Japan Panel on Wind and Seismic Effects, UJNR, Tsukuba, Japan, 1983
12) Takeda, T., Sozen, M. A., and Nielsen, N. N.: Reinforced Concrete Response to Simulate Earthquakes, Journal of Structural Engineering, ASCE, 96-12, 1970
13) Takemura, H.and Kawashima, K.: Effect of Loading Hysteresis on Ductility Capacity of Reinforced Concrete Bridge Piers, Journal of Structural Engineering, Vol.43A, pp.849-858, Japan Society of Civil Engineers, 1997.

Table 1 Averaged shear stress τ_c (kgf/cm^2) of concrete

Concrete strength	210	240	270	300	400
τ_c	3.3	3.5	3.6	3.7	4.1

Table 2 Modification for effective height c_e

Effective height (m)	less than 1	3	5	larger than 10
c_e	1.0	0.7	0.6	0.5

Table 3 Modification for tensile reinforcement ratio c_{pt}

Tensile reinforcement ratio	0.2	0.3	0.5	larger than 1.0
c_{pt}	0.9	1.0	1.2	1.5

Table 4 Safety factor α in Eq. (15)

Type of bridges	Type-I ground motion	Type-II ground motion
Type-B	3.0	1.5
Type-A	2.4	1.2

Table 5 Check of Design by the Seismic Coefficient Method

	1964 Pier		1980 Pier		1990 Pier		1995 Pier	
	LG	TR	LG	TR	LG	TR	LG	TR
Seismic Coefficient	0.20		0.27		0.30		0.30	
Design Lateral Force (kN)	4724	3430	6380	4635	7085	5145	7085	5145
Section Size	3.5m×3.0m		4.0m×3.5m		4.0m×3.5m		4.0m×3.5m	
Longitudinal Reinforcement Ratio (%)	1.21		1.25		1.36		1.36	
Volumetric Ratio of Ties ρ_s (%)	0.09		0.32		0.64		1.03	
Compression Stress (MPa)	12.4	12.1	11.3	11.0	11.7	10.7	11.7	10.7
Allowable Compression Stress (MPa)	14.7							
Shear Stress (MPa)	0.58	0.43	0.61	0.47	0.66	0.51	0.66	0.51
Allowable Shear Stress (MPa)	1.03	1.03	0.73	0.74	0.72	0.74	0.72	0.74
Tension Stress (MPa)	263	275	281	290	278	259	278	259
Allowable Tension Stress (MPa)	294							

Table 6 Evaluation of Seismic Performance based on Ductility Check

	1964 Pier		1980 Pier		1990 Pier		1995 Pier	
	LG	TR	LG	TR	LG	TR	LG	TR
Flexural Strength (kN)	8595	7997	12897	12064	13730	12848	13769	12897
Shear Strength (kN)	6478	6919	15827	15259	16974	18728	23422	23255
Failure Mode	Shear	Shear	Flexure	Flexure	Flexure	Flexure	Flexure	Flexure
Capacity P_a (kN)	6478	6919	12083	11103	12818	11780	12828	11789
Design Ductility Factor μ_a	1.00	1.00	2.97	3.15	3.86	4.01	5.17	5.33
Ultimate Ductility Factor	-----	-----	3.95	4.22	5.29	5.51	7.26	7.49
Equivalent Design Seismic Coefficient k_{he}	1.50	1.50	0.61	0.64	0.52	0.56	0.44	0.48
Lateral Force $k_{he}W$ (kN)	41777	32075	16003	12652	13642	11074	11544	9486
Evaluation of Safety	×	×	×	×	×	○	○	○

Table 7 Ground Motions used for Analysis

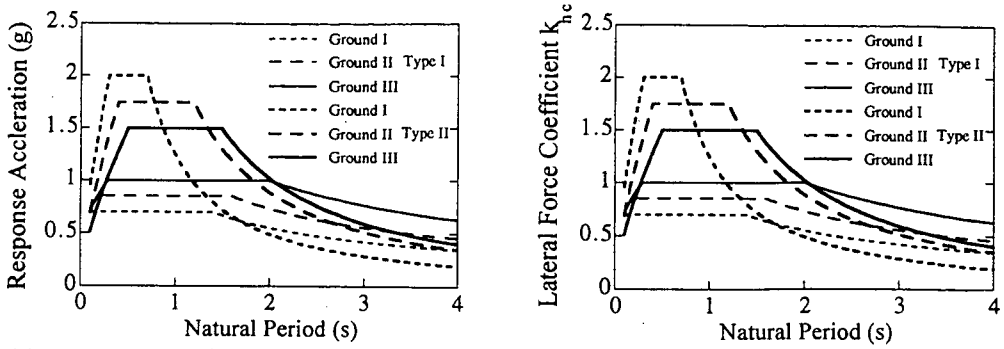
Record Name	Earthquake	Date	Magnitude	Observed Location (Direction)	Peak Acceleration (g)
Higashi-Kobe Bridge Record	Hyogo-ken Nanbu	1995.1.17	7.2	Higashi-Kobe Bridge (TR)	0.334
JMA Kobe Record				JMA Kobe Observatory (NS)	0.834
JMA Kushiro Record	Kusiro-oki	1993.1.15	7.8	JMA Kushiro Observatory (EW)	0.941
Sylmar Record	Northridge	1994.1.17	6.7	Sylmar Country Hospital Parking (NS)	0.844

Table 8 Evaluation of Seismic Performance based on Dynamic Response Analysis

	1980 Pier		1990 Pier		1995 Pier	
	LG	TR	LG	TR	LG	TR
(1) Response Displacement (mm)	95	70	92	65	96	68
(2) Response Ductility Factor	5.04	2.38	4.70	2.14	4.86	2.21
(3) Design Ductility Factor	2.97	3.15	3.86	4.01	5.17	5.33
(2)／(3)	1.70	0.76	1.22	0.53	0.94	0.42
(4) Ultimate Ductility Factor	3.95	4.22	5.29	5.51	7.26	7.49
(2)／(4)	1.28	0.56	0.89	0.39	0.67	0.30
(5) Residual Displacement (mm)	24	12	23	10	26	11
(6) Demand Lateral Force(kN)	13279	11015	13328	11084	12946	10849
(7) Capacity P_a (kN)	12083	11103	12818	11780	12828	11789
(6)／(7)	1.10	0.99	1.04	0.94	1.01	0.92

Table 9 Effect of Different Ground Motion on Response of P3 Designed by 1995 Specifications

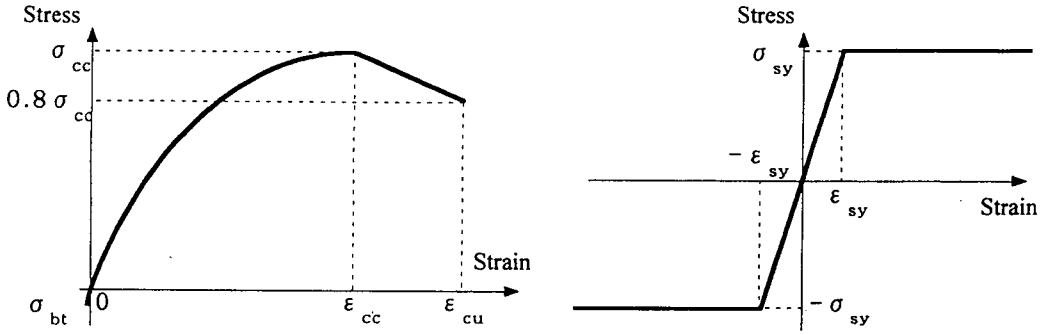
	Higashi-Kobe Bridge Record	JMA Kobe Record	Sylmar Record	JMA Kushiro Record
(1) Response Displacement (mm)	68	142	100	85
(2) Response Ductility Factor	2.21	4.59	3.23	2.76
(3) Design Ductility Factor	5.33			
(2)／(3)	0.42	0.86	0.61	0.52
(4) Residual Displacement (mm)	11	41	24	1
(5) Demanded Lateral Force(kN)	10849	12054	11486	11123
(6) Capacity P_a (kN)	11789			
(5)／(6)	0.92	1.02	0.97	0.94



(a) Response Acceleration for Dynamic Response Analysis (h=0.05)

(b) Lateral Force Coefficient

Fig.1 Design Force in Ductility Design



(a) Concrete

(b) Reinforcing Bars

Fig.2 Material Strength to Compute Moment vs. Curvature Relation

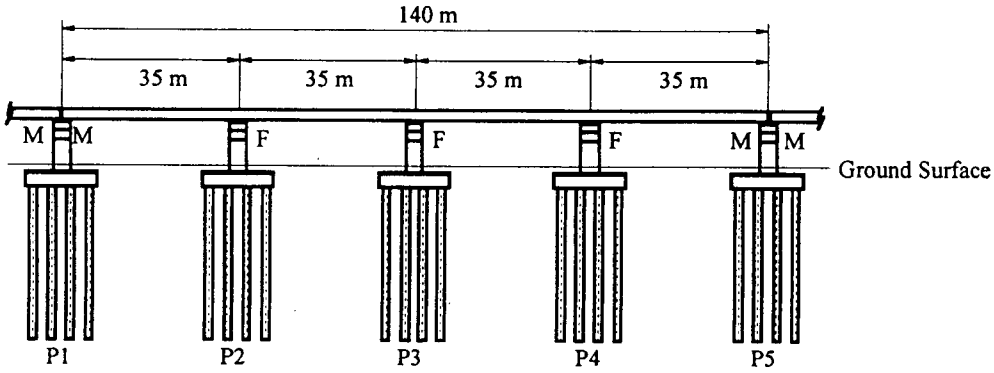
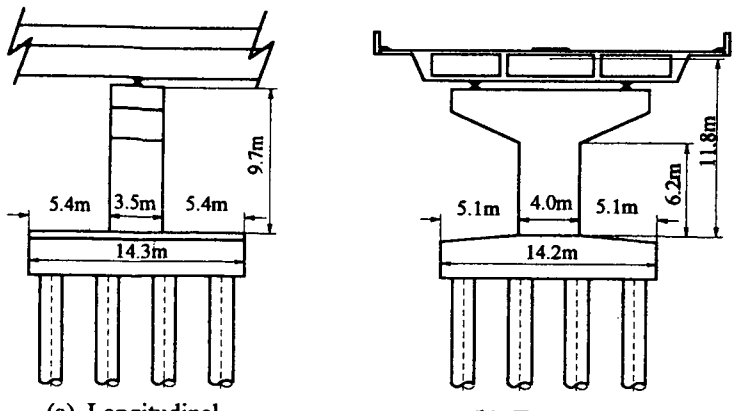


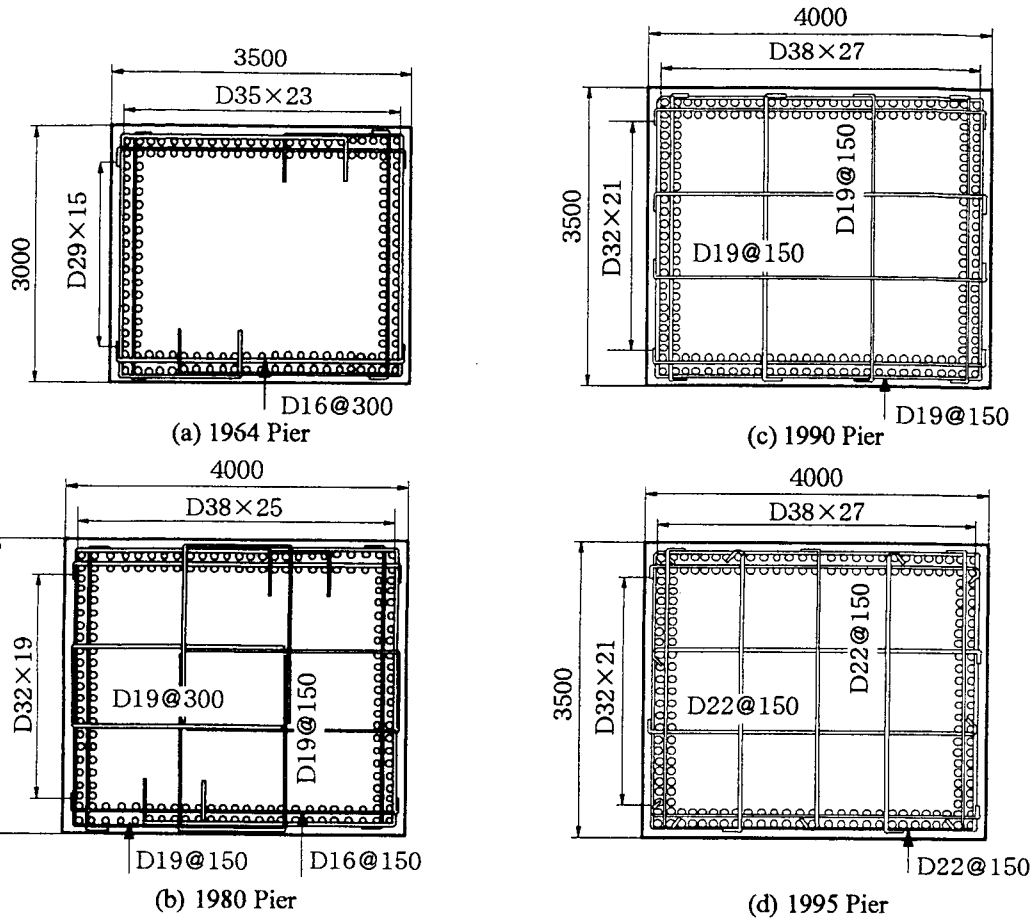
Fig. 3 4-span Continuous Prestressed Concrete Bridge Analyzed



(a) Longitudinal

(b) Transverse

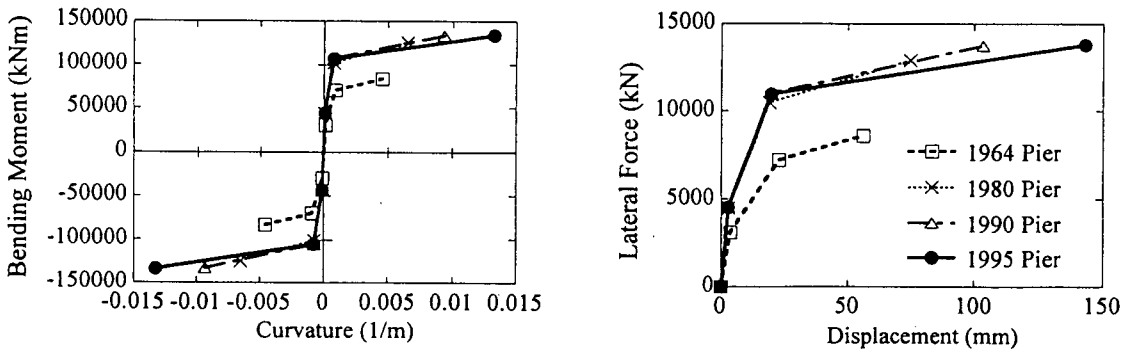
Fig. 4 Pier No. 3 (P3)



(a) 1964 Pier (c) 1990 Pier

(b) 1980 Pier (d) 1995 Pier

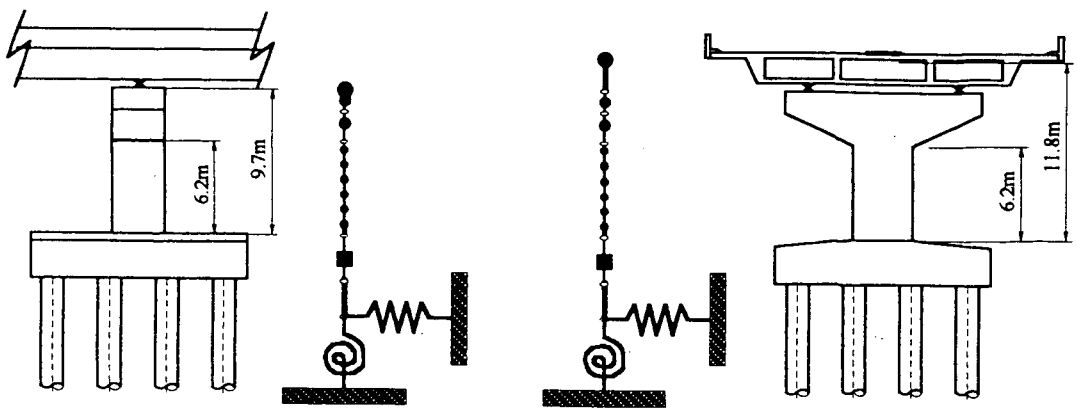
Fig. 5 P3 Designed by 1964, 1980, 1990 and 1995 Specifications



(a) Moment - Curvature Relation at Bottom of Pier

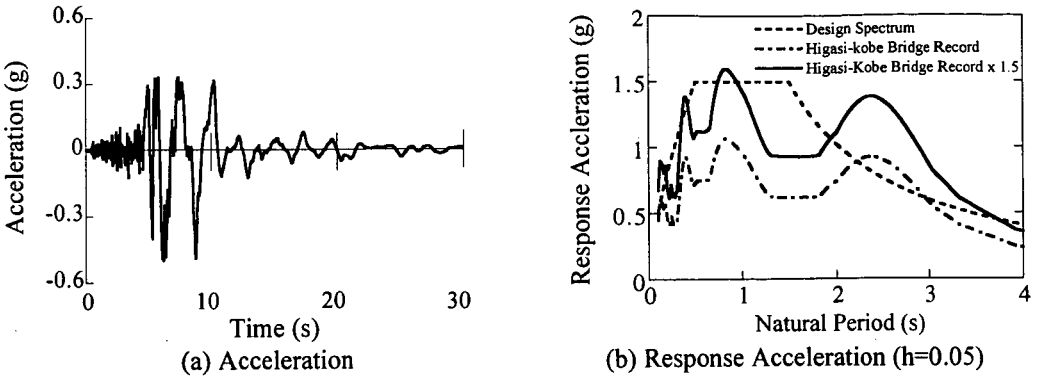
(b) Lateral Force - Lateral Displacement Relation at Gravity Center of Deck

Fig.6 Comparison of Hysteretic Behavior of P3



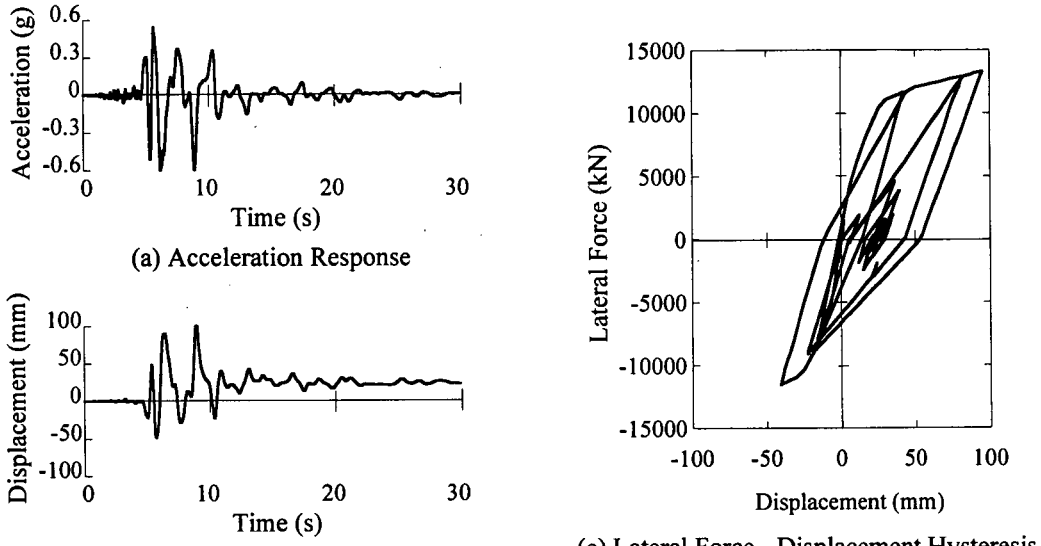
(a) Longitudinal Response (b) Transverse Response

Fig. 7 Analytical Models



(a) Acceleration (b) Response Acceleration (h=0.05)

Fig.8 1.5 x Higasi-Kobe Bridge Record

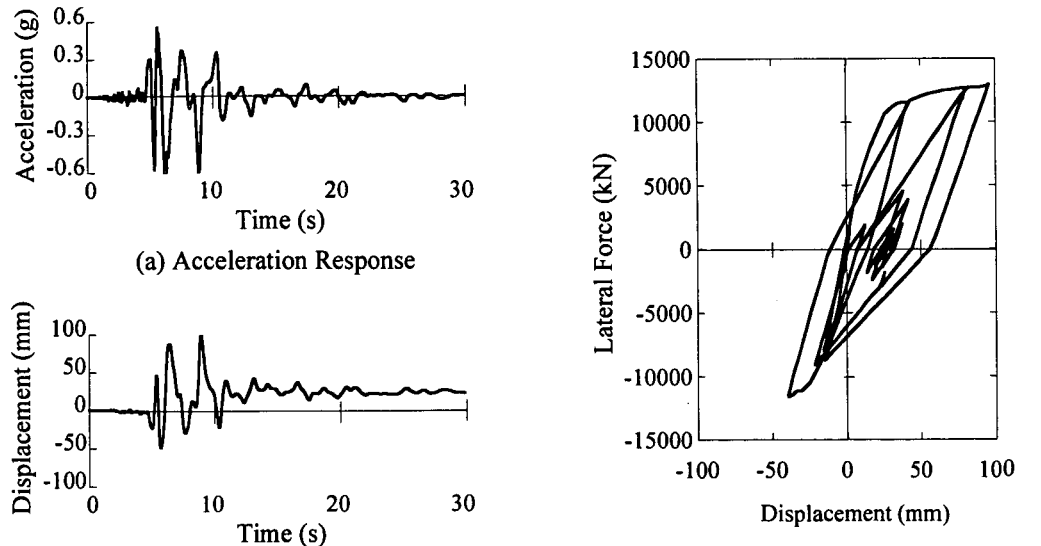


(a) Acceleration Response

(b) Displacement Response

(c) Lateral Force - Displacement Hysteresis

Fig. 9 Response at Top of the1980 Pier Subjected to the 1.5 x Higashi-Kobe Bridge Record



(a) Acceleration Response

(b) Displacement Response

(c) Lateral Force - Displacement Hysteresis

Fig. 10 Response at Top of the1995 Pier Subjected to the 1.5 x Higashi-Kobe Bridge Record

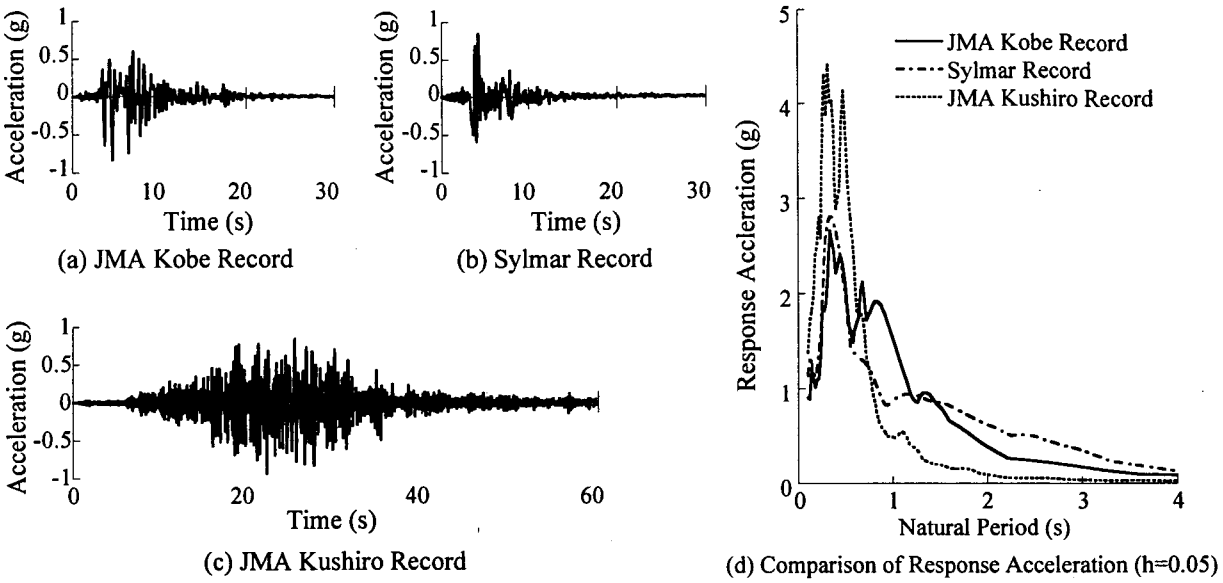


Fig. 11 Ground Motions

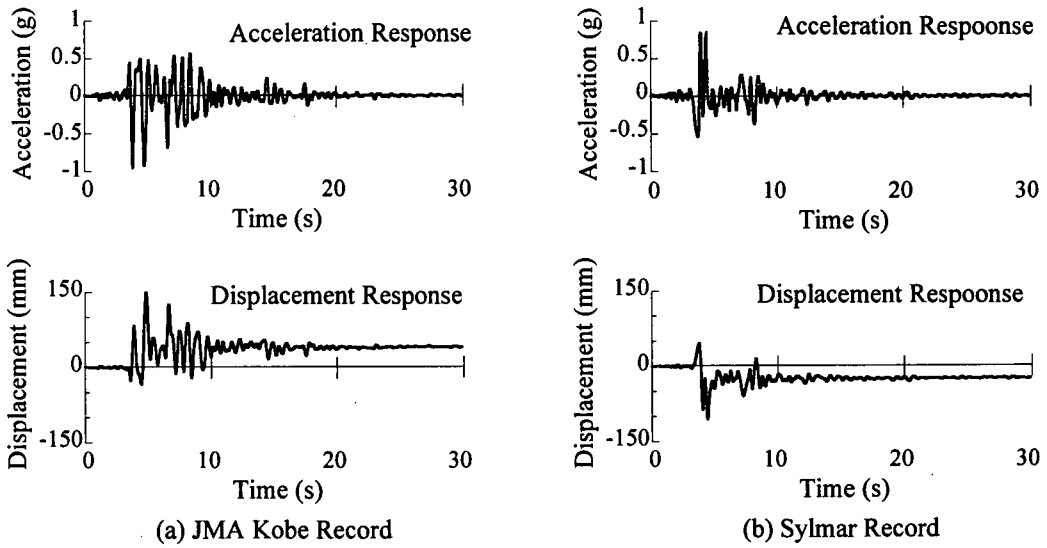


Fig. 12 Response Acceleration and Response Displacement at Top of the 1995 Pier

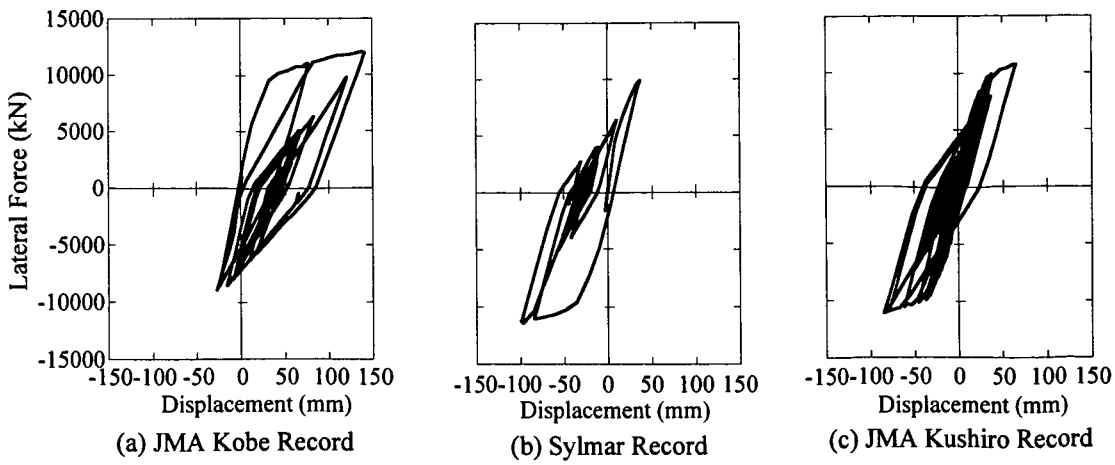


Fig. 13 Comparison of Lateral Force vs. Lateral Displacement Hysteresis

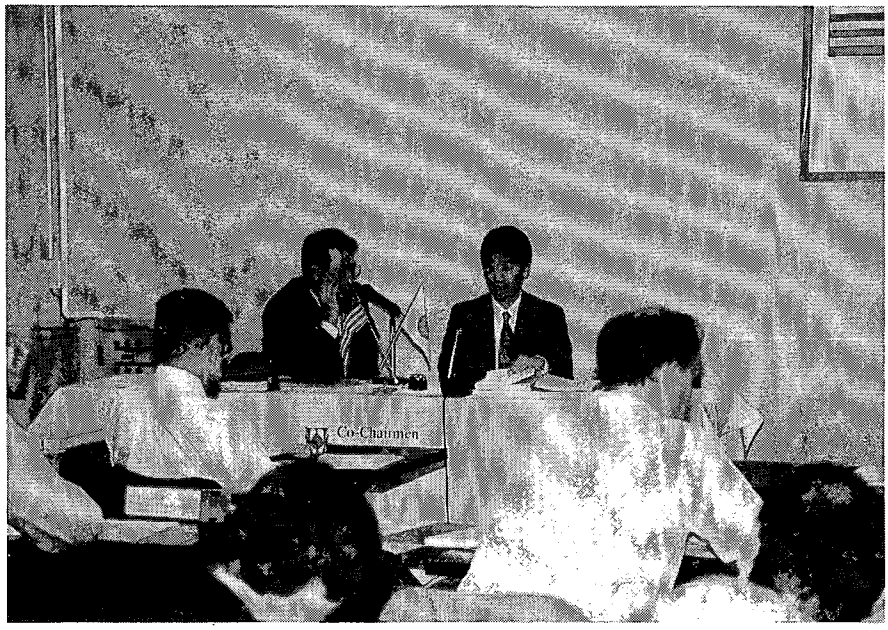
SESSION 4: SEISMIC ISSUES (3)

(1) Interaction of Hysteretic Behavior between Isolator/Damper and Pier in an Isolated Bridge
(K. Kawashima and G. Shoji)

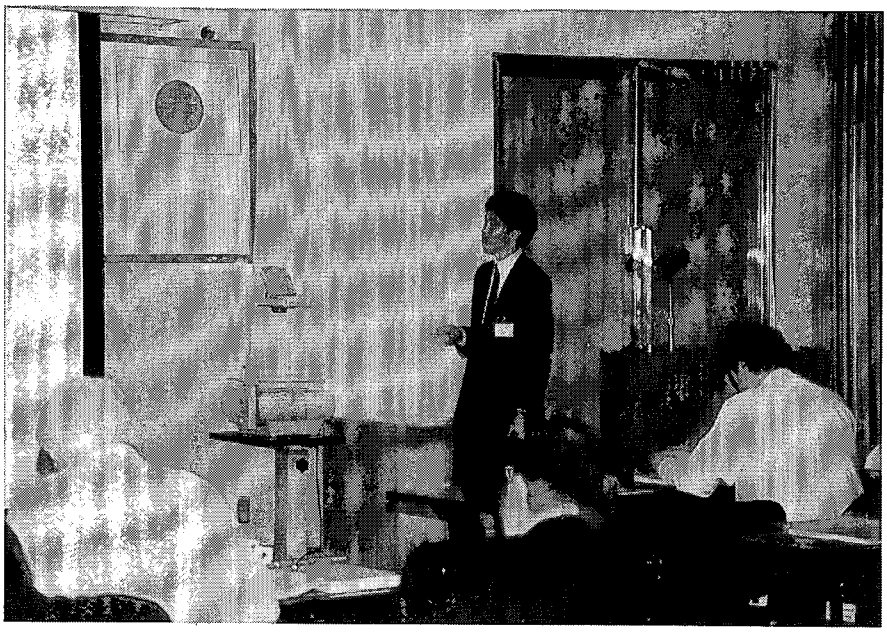
(2) Nonlinear Seismic Response Characteristics of Two-Story Frame Piers
(T.Terayama, S.Unjoh and K.Tasaki)

(3) Displacement Issues of Seismically Loaded R/C Bridge Columns
(Nadim I.Wehbe, M.Saiid Saiidi and David H.Sanders)

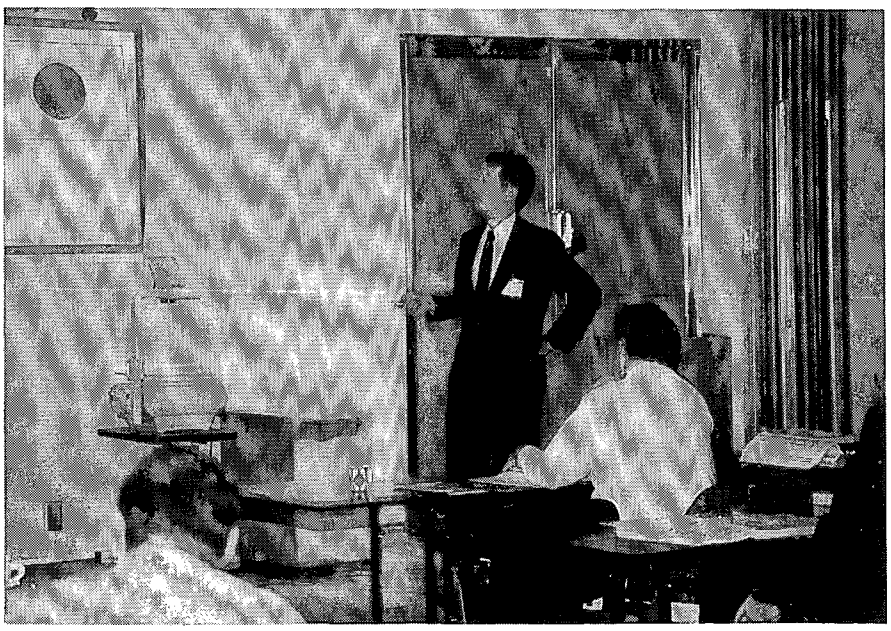
(4) Damping Characteristics of a Long-Span Suspension Bridge Identified by Strong-motion Data
(Y.Adachi and S.Unjoh)



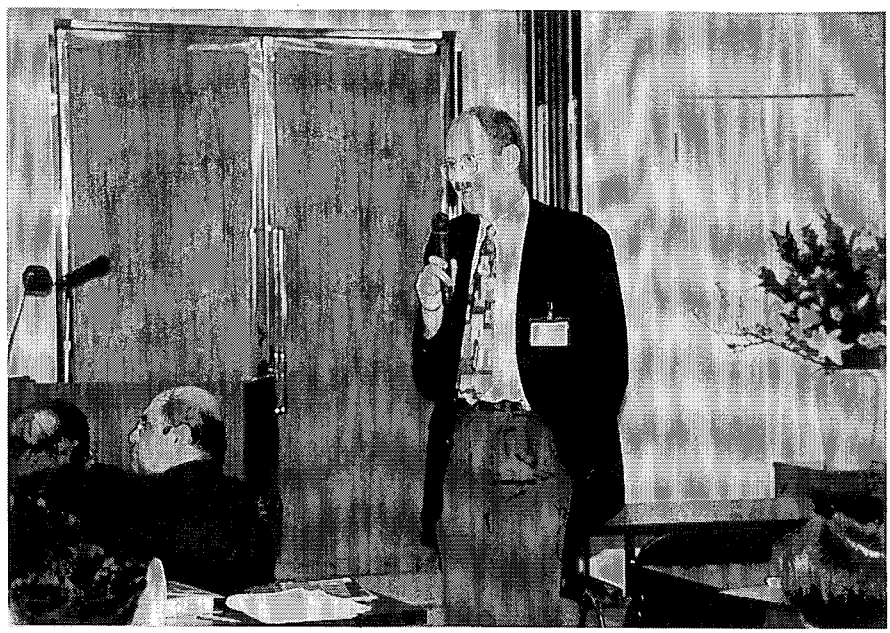
Co-Chairmen : Keiichi Tamura, Phillip Yen



SESSION 4 : Gaku Shoji



SESSION 4 : Toru Terayama



SESSION 4 : David Sanders



SESSION 4 : Yukio Adachi

INTERACTION OF HYSTERETIC BEHAVIOR BETWEEN ISOLATOR/DAMPER AND PIER IN AN ISOLATED BRIDGE

Kazuhiko Kawashima [1] and Gaku Shoji [2]

1) Professor, Department of Civil Engineering, Tokyo Institute of Technology, Tokyo, Japan

2) Research Associate, Department of Civil Engineering, Tokyo Institute of Technology, Tokyo, Japan

ABSTRACT

Because nonlinear hysteretic response occurs in both the isolator / damper and the pier in an isolated bridge subjected to an extreme ground motion, there must be an interaction between the device and the pier. This paper presents an analysis on the interaction with emphasis on the yield force level of the device and the elongation of natural period required for the seismic isolation bridges.

1. INTRODUCTION

Since the 1995 Hyogo-ken Nanbu earthquake, the Menshin design (seismic isolation) has been extensively adopted for new bridge construction. The technical development which was compiled in a form of the "Guidelines of Menshin Design of Highway Bridges" in 1989 (8) and the "Manual of Menshin Design of Highway Bridges" in 1993 (4,5) have been effectively used. The Menshin design was included in the Design Specifications of Highway Bridges revised in 1996 (2). It was the first time that the Menshin design was incorporated in a code of bridges.

The Menshin design is the seismic isolation with the limited increase of natural period by placing emphasis on the increase of energy dissipation and the distribution of lateral force to as many substructures as possible (3,4). The slightly distorted application of the seismic isolation has been adopted in Japan, because significant increase of natural period causes the increase of deck displacement (3). This requires to either adopt large expansion joint or accept large pounding force at joints. Soil condition is generally weaker in Japan than other countries. Large ground motions induced by the subduction-type fault earthquake with magnitude as large as 8 could result in the ground motions with predominant long period component. Thus, it is recommended in the Design Specifications of Highway Bridges that excessive elongation of natural period should not be made, and that the natural period of a menshin bridge may be less than about 2 times the natural period of the same bridge supported by the conventional bearings. This is one of the requirement for the minimum stiffness and the yielding force in design of isolator/energy dissipator.

It is ideal in an isolated bridge that the energy is dissipated at only device so that the substructure does not cause any hysteretic response during a design earthquake (6,7). However, in the Menshin design concept, it is not feasible that the menshin bridge responses with energy dissipation only at the device when the bridge is subjected to an extreme earthquake. Hysteretic response therefore occurs at the pier as well as the device. Thus, nonlinear interaction between the piers and the devices should be carefully considered in design of the isolated bridge.

This paper discusses an analysis of the nonlinear response of bridges with hysteresis behavior at both the pier and the device with an emphasis on the effect of yielding force level and the post-yielding stiffness of the device .

2. ANALYTICAL MODEL AND ANALYTICAL CONDITIONS

In an isolated bridge, the response displacement at the gravity center of the deck u_D may be represented as (refer to Fig. 1)

$$u_D = u_F + H\theta_F + (H - \frac{L_P}{2})\theta_P + u_{PB} + u_B \tag{1}$$

in which u_F and θ_F: translation and rotation of footing, θ_P: plastic rotation at plastic hinge of a pier, u_{PB}: flexural deformation of a pier, u_B: displacement of the device, H: distance from the bottom of pier to the gravity center of the deck and L_P: plastic hinge length.

The lateral force vs. lateral displacement relation of the pier and the device may be represented as shown in Figs. 2 and 3. It should be noted in Figs. 2 and 3 that the lateral force is defined at the gravity center of deck. Two types of isolator/energy dissipator are considered here for analysis. The first is the sliding-type isolator with zero post-yield stiffness, and the other is the lead-rubber bearings (LRB) and high damping rubber bearings (HDR) which have positive post-yield stiffness. In such devices, the level of yield force P_y^b may be a controlling factor for the bridge response. It is obvious that the yield force of the device P_y^b should be less than the yield force of pier P_y^p to achieve favorable response reduction in seismic isolation. It is anticipated that the nonlinear interaction between the device and the pier depends on the yield force ratio P_y^b / P_y^p.

Assuming that the soil is stiff, the response of bridge may be idealized as a two-degree-of-freedom system as shown in Fig. 4. The lateral force vs. lateral displacement hysteresis of the pier and the device is idealized as the bilinear hysteresis models for simplicity of the analysis. Considering a reinforced concrete bridge pier with 10 m high, 2.2 m deep in longitudinal direction and 5 m wide in transverse direction, the cracked stiffness k_1^p and the yield force of pier P_y^p are assumed as 94800 kN/m and 3000 kN, respectively.

The initial stiffness of the devices is assumed here as 47400 kN/m. This corresponds to the

LRB and HDR with 200 mm high and 650 mm diameter. The post-yield stiffness of LRB and HDR is assumed as 7290 kN/m, which is 1/6.5 of the initial stiffness (7).

It is also assumed that the mass of deck is 1000 ton (weight = 9800 kN) and that the mass of pier is 1/5 of the mass of deck. Thus the bridge has the fundamental natural period of 0.71 second. Damping ratio of 2 % is assumed for the pier and the device. Hysteretic damping is further considered for the device in the nonlinear analysis. After modal damping ratios are computed based on the strain-proportional method (2), two coefficients of the Layleigh damping are determined.

Three ground accelerations which were spectrally fitted to a design response spectrum are used for the analysis. The design response spectrum for the Type I ground motion (2) at Soil Group III (soft soil site) is considered here. Spectral fitting was conducted by varying the amplitude of ground acceleration with the phase angle being unchanged (1). Fig. 5 shows the three ground acceleration thus generated.

3. RESPONSE OF BRIDGES ISOLATED BY THE DEVICE WITH ZERO POST-YIELD STIFFNESS

Fig. 6 shows the lateral force vs. lateral displacement hysteresis of the pier and the device for typical combinations of the yield force of pier P_y^p and the yield force of the device P_y^b. As anticipated, the pier response decreases and the device response increases as the yield force ratio P_y^b / P_y^p decreases. Fig. 7 shows how the responses of the pier and the device varies as the yield force ratio P_y^b / P_y^p changes. The responses of the pier and the device are represented in terms of the ductility factor defined as

$$\mu^p = u^p{}_{\max} / u_y^p \tag{2}$$

$$\mu^b = u^b{}_{\max} / u_y^b \tag{3}$$

in which $u_{\max}$ and u_y represent the peak and the yield displacement, respectively. The superscripts b and p denote the device and the pier.

Although the results for three ground motions are presented in Fig. 7, they are almost the same. It is important in Fig. 7 that the pier response starts to reduce from P_y^b / P_y^p of about 1.4, but that nonlinear response at the pier occurs even at P_y^b / P_y^p of 0.4. Finally at P_y^b / P_y^p of about 0.1, the pier response becomes elastic. Because the weight of the deck which is laterally supported by the pier is 9800 kN, this means that linear response of pier can be achieved when the yield force of the device P_y^b is less than 3 % of the deck weight. It is obvious that this is difficult in most cases, and thus the nonlinear response of the pier is inevitable.

To evaluate the degree of nonlinear deformation of the pier and the device, the total energy

dissipation was evaluated as

$$W^p = \oint P^p du^p \tag{4}$$

$$W^b = \oint P^b du^b \tag{5}$$

in which W^p and W^b : the total energy dissipated in the pier and the device, respectively P^p and P^b: restoring force developed in the pier and the device, respectively, and u^p and u^b: lateral displacement of the pier and the device, respectively. The total energy of the bridge is then evaluated as

$$W = W^p + W^b \tag{6}$$

To represent the damage degree of the pier, a parameter r^p defined by Eq. (7) is introduced.

$$r^p = \frac{W^p}{W} \tag{7}$$

Fig. 8 shows the total dissipated energy W^p and W^b as well as the damage ratio parameter r^p. While the total dissipated energy in the pier and the device is smaller for the record 3 than the record 1 and 2, the damage ratio parameter r^p is almost free from the difference of ground accelerations. It is seen in Fig. 8 (a) that the total dissipated energy in the pier W^p decreases and, on the contrary, the total dissipated energy in the device W^b increases as the yield force ratio P_y^b / P_y^p decreases from about 1.4 . Such relation is similar to Fig. 7. Only difference from Fig. 7 is that W^b in Fig. 8 (a) starts to decrease again at P_y^b / P_y^p less than 0.6. This may be understood from Fig. 9. Although the peak displacement of the device (μ^b) increases as the yield force ratio P_y^b / P_y^p decreases, the total amount of energy dissipated in the device decreases.

4. RESPONSE OF BRIDGES ISOLATED BY THE DEVICE WITH POSITIVE POST-YIELD STIFFNESS

Similarly, the nonlinear interaction between the device and the pier was analyzed for the bridge isolated by the device with positive post-yield stiffness. Fig. 10 shows the lateral force vs. lateral displacement hysteresis of the pier and the device. Although the general trend that the total energy dissipated in the pier decreases as the yield force ratio P_y^b / P_y^p decreases is the same with the bridge isolated by the device with zero post-yield stiffness, it is important to note that the total energy dissipated in the pier starts to increase at small yield force ratio as shown in Fig. 10 (d). This is because the small yield force of the device P_y^b results in the increase of displacement of the device, and this in turn causes that the peak lateral force induced in the device exceeds the yield force of the pier P_y^p.

Figs. 11 and 12 show the dependence of the ductility factor, the total dissipated energy and the damage ratio parameter on the yield force ratio. It is seen that the total dissipated energy of the pier W^p and the damage ratio parameter r^p start to increase at P_y^b / P_y^p less about 0.4. This is unique characteristics of the device with positive post-yield stiffness, and has to be carefully

considered in design.

It is common to set the yield force of the device P_y^b at about 0.1 ~ 0.2 of the deck weight. This corresponds to the yield force ratio P_y^b / P_y^p of 0.3 ~ 0.6. It is seen in Figs. 7 and 8 that this yield force level is appropriate in design.

5. ELONGATION OF NATURAL PERIOD REQUIRED FOR ISOLATION

From the peak response of the pier and the device, the equivalent stiffnesses of the pier and the device, K_e^p and K_e^b, may be evaluated as shown in Fig. 13. The fundamental natural period of the bridge (pier-device-deck system) may be computed as

$$T = 2\pi\sqrt{\frac{W}{g \cdot K_e}} \tag{8}$$

in which K_e is the effective stiffness of the bridge, and is given as

$$K_e = \frac{K_e^p \cdot K_e^b}{K_e^p + K_e^b} \tag{9}$$

Fig. 14 (a) shows the natural period T vs. total energy dissipated in the pier W^p relation for the bridge isolated by the device with positive post-yield stiffness. It is seen in Fig. 14 (a) that the total dissipated energy of the pier W^p sharply decreases as the natural period T increases from 2 second. Because of the flexibility of device, natural period of the bridges is longer than 2 second in all cases. It should be noted that the data at natural period longer than 2.5 second corresponds to the bridges isolated by the device with low yield forces. Therefore the larger response displacement of the devices with low yield force results in the larger energy dissipation in the pier.

When the deck is supported by the normal bearing, the natural period of the bridge is

$$T_f = 2\pi\sqrt{\frac{W}{g \cdot K_e^p}} \tag{10}$$

and the energy dissipation of the bridge is

$$W_f = \oint P_f^p \, du_f^p \tag{11}$$

in which P_f^p and u_f^p are the lateral force and the lateral displacement of the pier when the deck is supported by the normal bearing.

In Fig. 14 (b), natural period T and the total energy dissipated in the pier W^p are normalized by T_f and W_f, respectively. Because T_f and W_f are constant, the shape of Fig. 14 (b) is the same with that of Fig. 14 (a). If it is considered that the use of device is favorable at W^p / W_f less than 1.0, natural period of the isolated bridge T should be longer than 2 second, which corresponds to T/T_f of about 3.

As previously described, it is recommended in the Design Specification of Highway Bridges that natural period of a menshin bridge may be about 2 times the natural period of non-menshin bridges. However, it is assumed in the Specification that natural periods of both menshin bridge and non-menshin bridge are computed with use of the cracked stiffness of the pier. Because the equivalent stiffness of the pier depending on the peak response displacement as shown in Fig. 13 (a) is used in Fig. 14, the W^p/W_f vs. T/T_f relation was computed using the cracked stiffness of pier following the procedure of the Design Specifications. This result is shown in Fig. 15. It is observed that T/T_f of 2 is appropriate to reduce the response of the bridges. Although further elongation of natural period reduces the energy dissipation of the pier, it brings larger response of the deck as shown in Fig.16. However because the ground motions which decrease response spectral amplitude used for the analysis, the appropriateness of the T/T_f of 2 needs to be studied for other type of ground motion.

6. CONCLUSIONS

A series of analysis was conducted for the menshin bridges to clarify the yield force of the device. From the analysis presented herein, the following conclusions may be deduced:

(1) When the device with zero post-yield type device is used, the ductility factor of and energy dissipation of the pier decrease as the yield force ratio P_y^b/P_y^p decreases from 1.4. However, even at P_y^b/P_y^p less than 0.4, hysteretic response occurs in the pier, and P_y^b/P_y^p has to be less than 0.1 for making the pier response elastic.

(2) Although the general trend is the same with (1) for the bridges isolated by the device with positive post-yield stiffness, the ductility factor of and the energy dissipated in the pier are large at P_y^b/P_y^p less than about 0.4. This is because large nonlinear response occurs in the device when the yield force P_y^b is small, and this results in the lateral force in the device larger than the yield force of the pier P_y^p. Thus, yield force of the device has to be carefully evaluated in design.

(3) About two times the natural period of a bridge supported by the normal bearing may be an appropriate estimation for the natural period of a menshin bridge isolated by the device with positive post-yield stiffness. However this has to be further studied for other types of ground motion.

REFERENCES

1) Arakawa, T., Kawashima, K. and Aizawa, K.: Spectral Fitting Method for Generating Ground Motion for Dynamic Response Analysis, Civil Engineering Journal, Vol. 26-7, pp. 392-397, 1984

2) Japan Road Association: Design Specifications of Highway Bridges, 1996

3) For example, Kawashima, K., Hasegawa, K. and Nagashima, H. : A Perspective of Menshin Design of Highway Bridges in Japan, Proc. First US-Japan Workshop on Earthquake Protective Systems for Bridges, Technical Report NCEER 92-4, pp. 3-25, National Center for Earthquake Engineering, State University of New York at Buffalo, 1992

4) Kawashima, K.: Manual for Menshin Design of Highway Bridges, Proc. 2nd US-Japan Workshop on Earthquake Protective Systems of Bridges, Technical Memorandum No. 3196, pp. 195-219, Public Works Research Institute, Tsukuba, Japan. 1992
5) Ministry of Construction: Manual of Menshin Design of Highway Bridges, Technical Note, No. 60, Public Works research Institute, 1993. English translation is available by Sugita, H. and Mahin, S.: Manual for Menshin Design of Highway Bridges: Ministry of Construction, Japan, Report No. EERC 92-10, Earthquake Engineering Research Center, University of California, Berkeley, 1994
6) Priestley, M.J.N., Seible, F. and Calvi, G.M.: Seismic Design and Retrofit of Bridges, John Wiley & Sons, 1996.
7) Skinner, I., Robinson, W. H. and McVerry, G. H.: An Introduction to Seismic Isolation, John Wiley & Sons, 1993.
8) Technical Research Center for National Land Development: Guidelines for Menshin Design of Highway Bridges, 1993

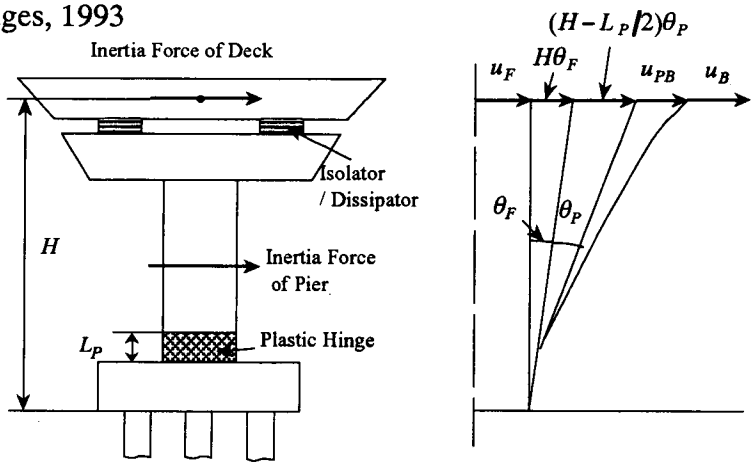
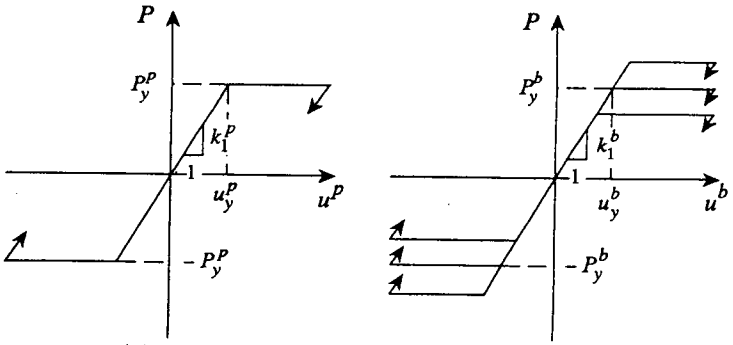
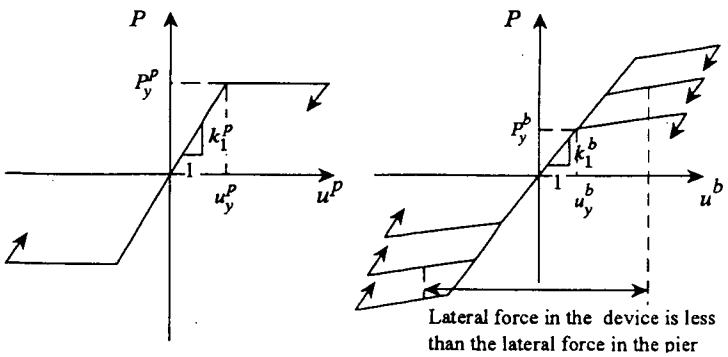


Fig. 1 Deformation of an Isolated Bridge



(a) Pier (b) Isolator / Energy Dissipator

Fig. 2 Hysteresic Behavior of Pier and Device with Zero Post-Yield Stiffness



(a) Pier (b) Isolator / Energy Dissipator

Fig. 3 Hysteresis Behavior of Pier and Device with Positive Post-Yield Stiffness

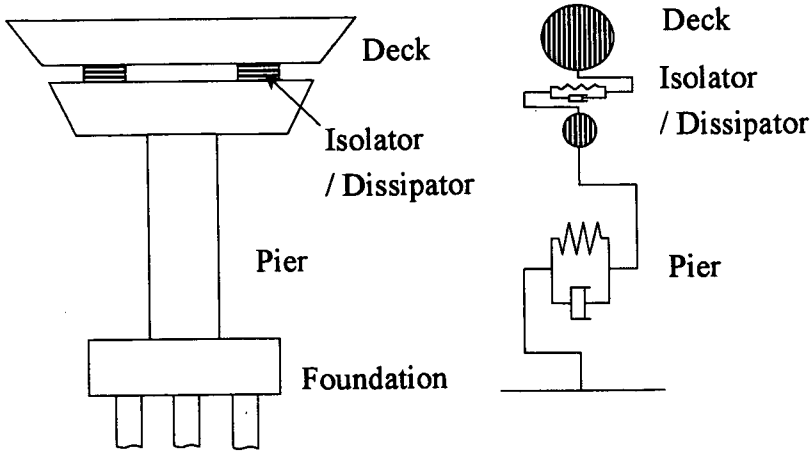
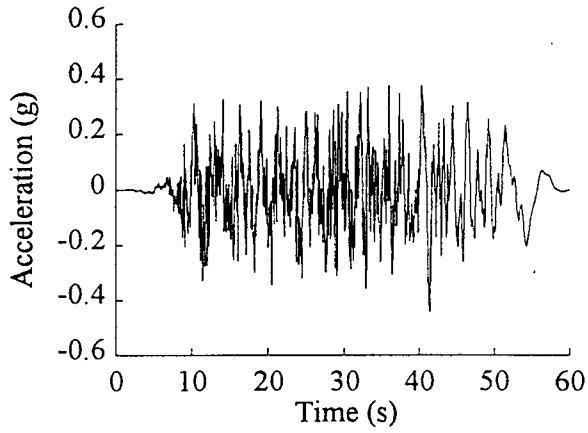
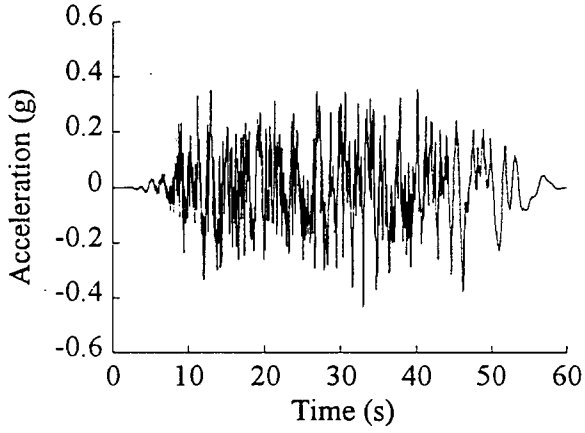


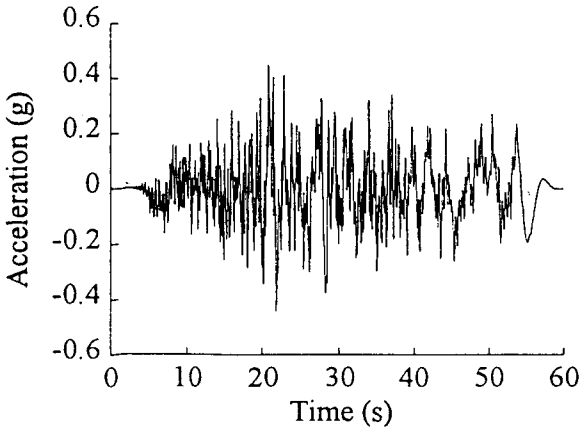
Fig. 4 Analytical Model of an Isolated Bridge



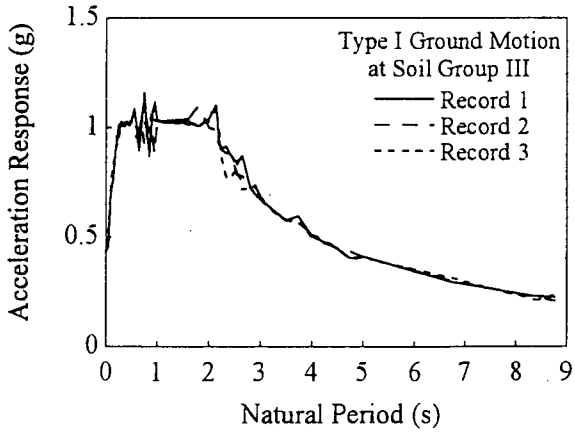
(a) Record 1



(b) Record 2

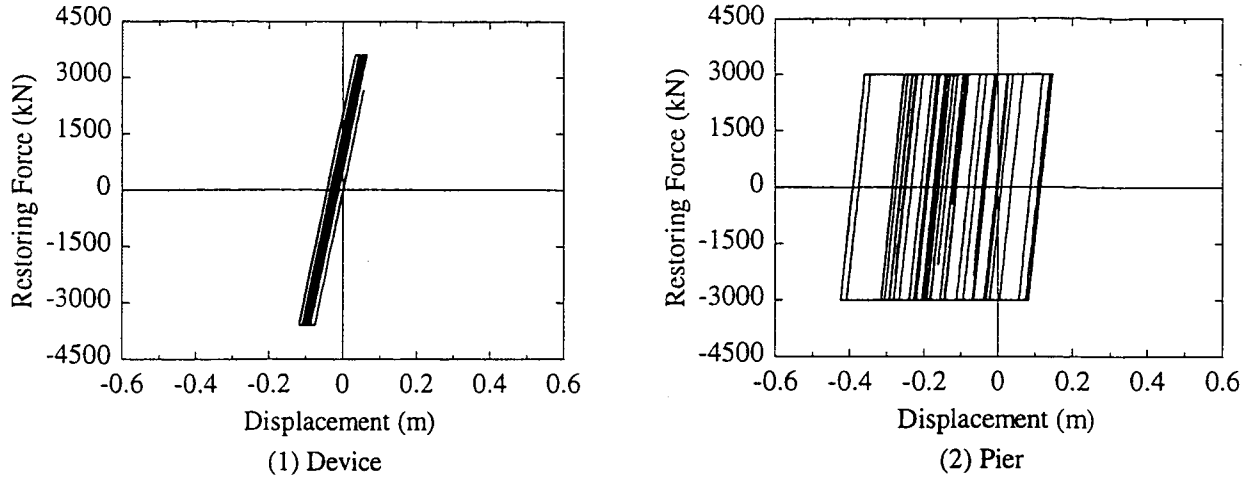


(c) Record 3



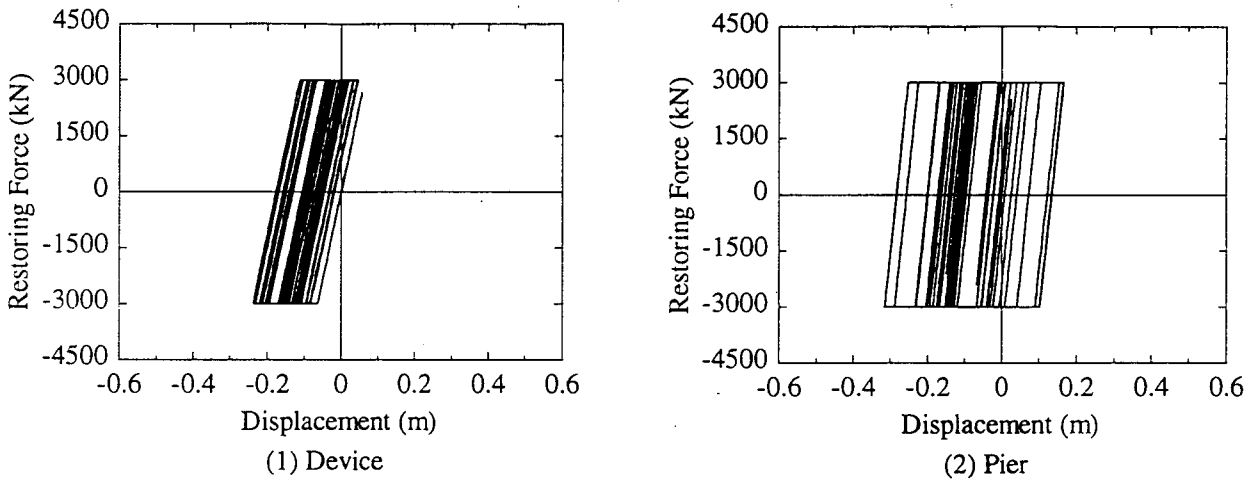
(d) Acceleration Response Spectra (h=0.05) of three Ground Accelerations used for Analysis

Fig. 5 Ground Accelerations used for Analysis and Response Sperctra (h=0.05)



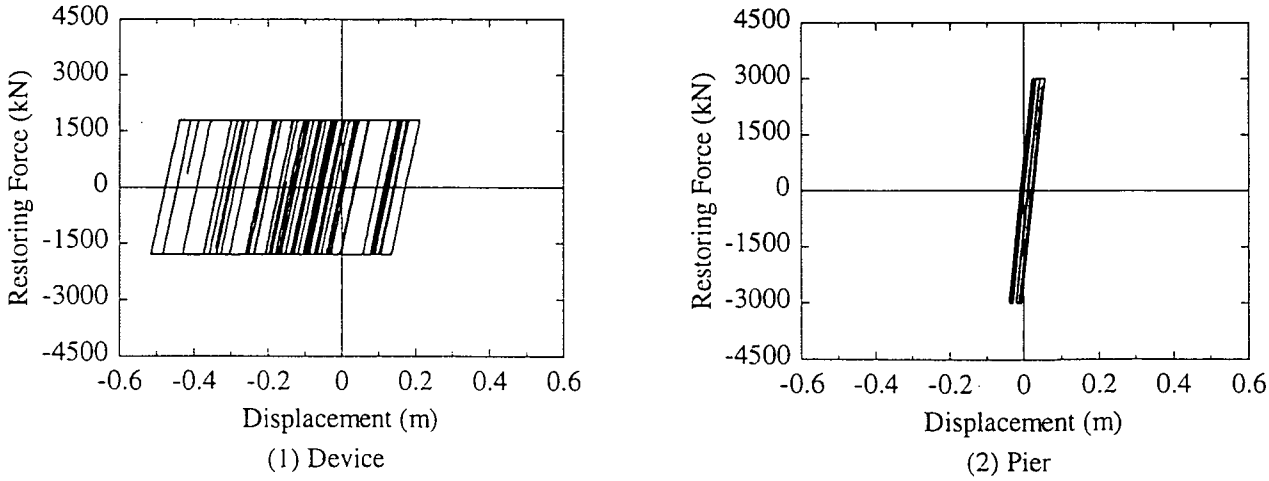
(1) Device　　(2) Pier

(a) $P_y^b > P_y^p$　(P_y^b=3600kN, P_y^p=3000kN)



(1) Device　　(2) Pier

(b) $P_y^b \approx P_y^p$　(P_y^b=3000kN, P_y^p=3000kN)



(1) Device　　(2) Pier

(c) $P_y^b < P_y^p$　(P_y^b=1800kN, P_y^p=3000kN)

Fig. 6　Lateral Force vs. Lateral Displacement Hysteresis for Pier and Device (Device with Zero Post-Yield Stiffness)

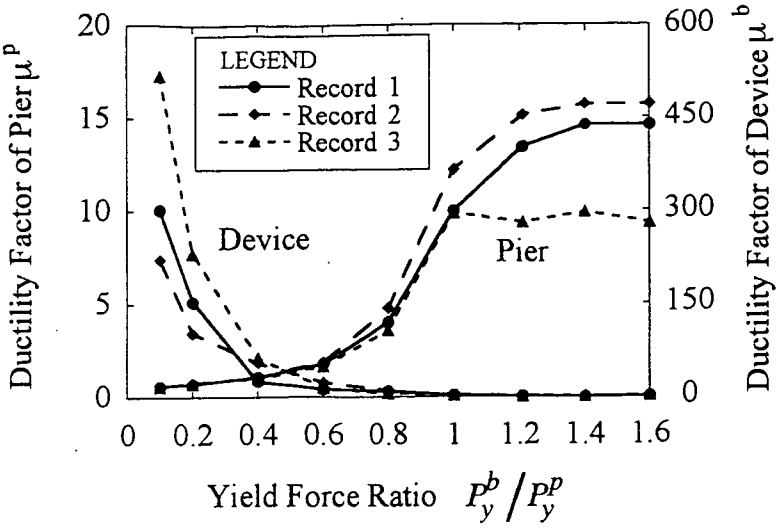
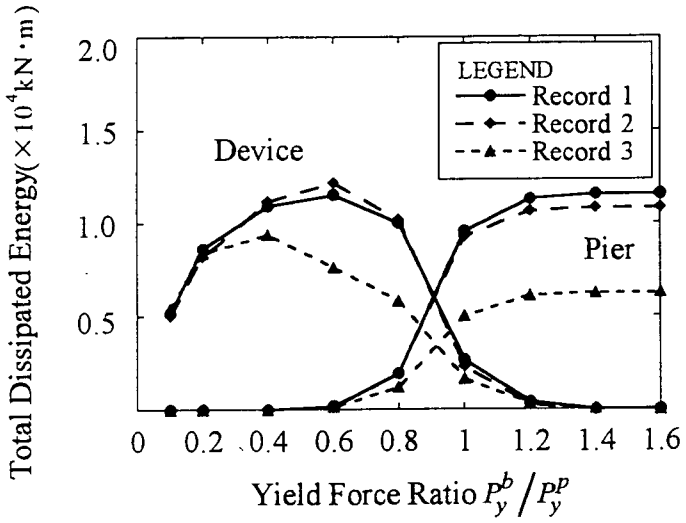
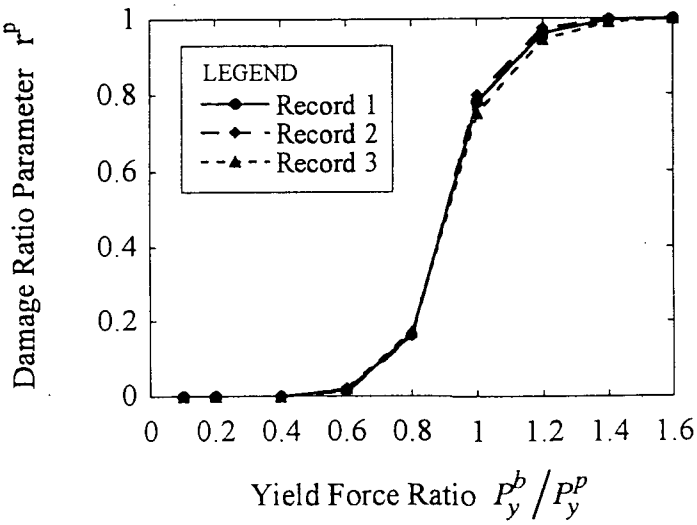


Fig. 7 Effect of the Yield Force of the Pier and the Device, P_y^p and P_y^b, on the Ductility Factor of the Pier and the Device (Device with Zero Post-Yield Stiffness)

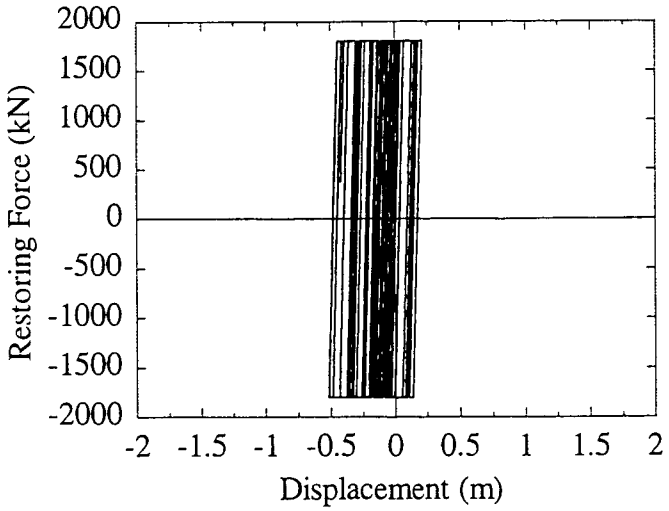


(a) Total Dissipated Energy

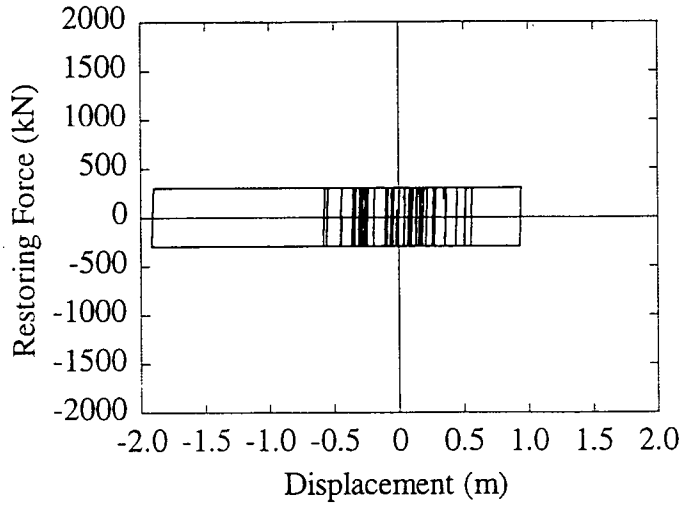


(b) Damage Ratio Parameter

Fig. 8 Effect of the Yield Forece of the Pier and the Device, P_y^p and P_y^b, on the Damage Degree (Device with Zero Post-Yield Stiffness)

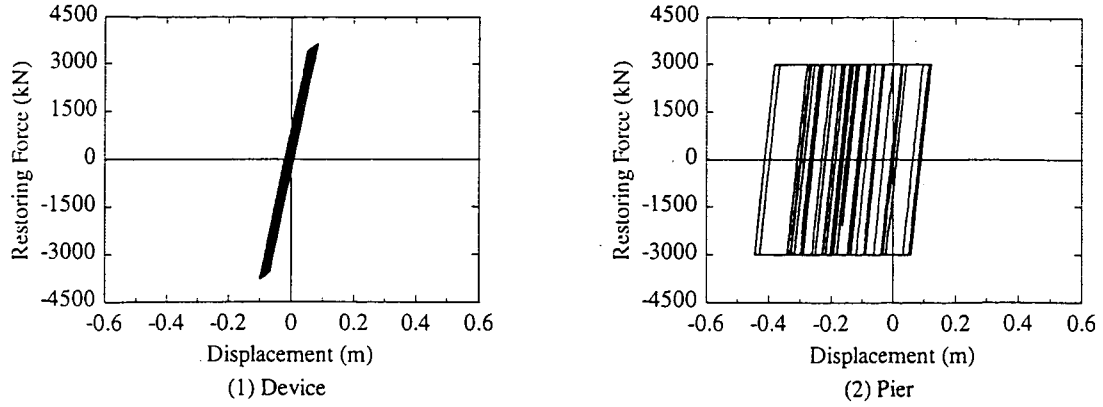


(a) $P_y^b < P_y^p$ (P_y^b=1800kN, P_y^p=3000kN)

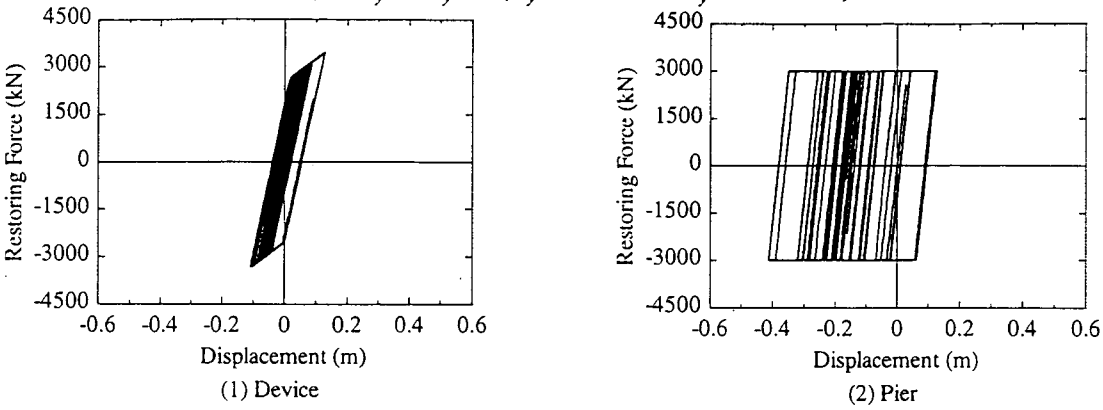


(b) $P_y^b << P_y^p$ (P_y^b=300kN, P_y^p=3000kN)

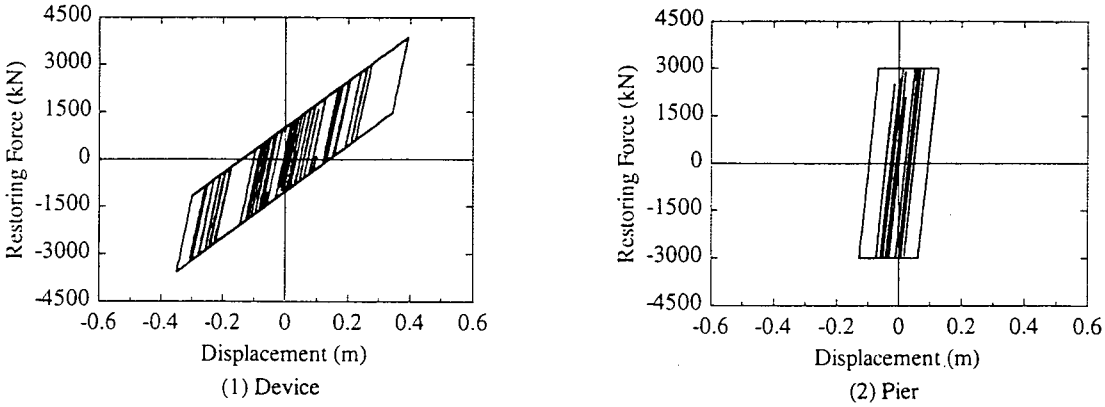
Fig.9 The Energy Dissipated in the Device with Small Yield Force



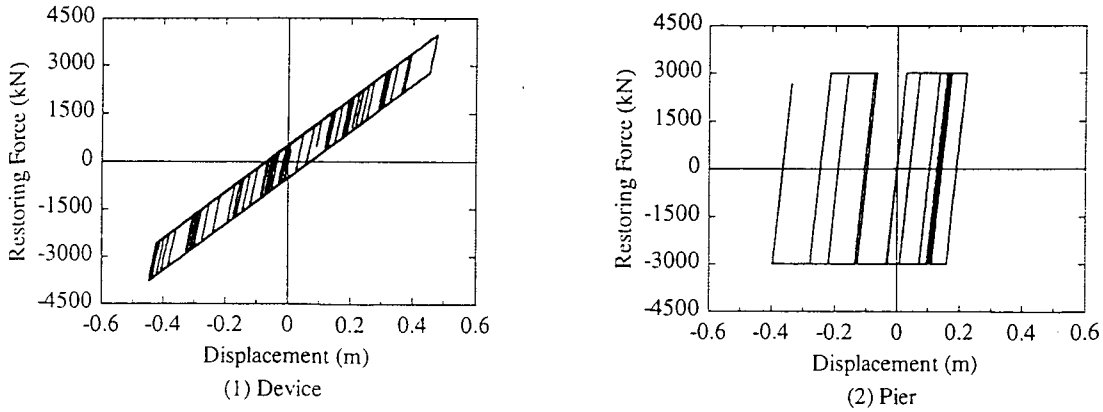
(a) $P_y^b > P_y^p$ (P_y^b=3600kN, P_y^p=3000kN)



(b) $P_y^b \approx P_y^p$ (P_y^b=3000kN, P_y^p=3000kN)



(c) $P_y^b < P_y^p$ (P_y^b=1200kN, P_y^p=3000kN)



(d) $P_y^b << P_y^p$ (P_v^b=600kN, P_v^p=3000kN)

Fig. 10 Lateral Force vs. Lateral Displacement Hysteresis for Pier and Device (Device with Positive Post-Yield Stiffness)

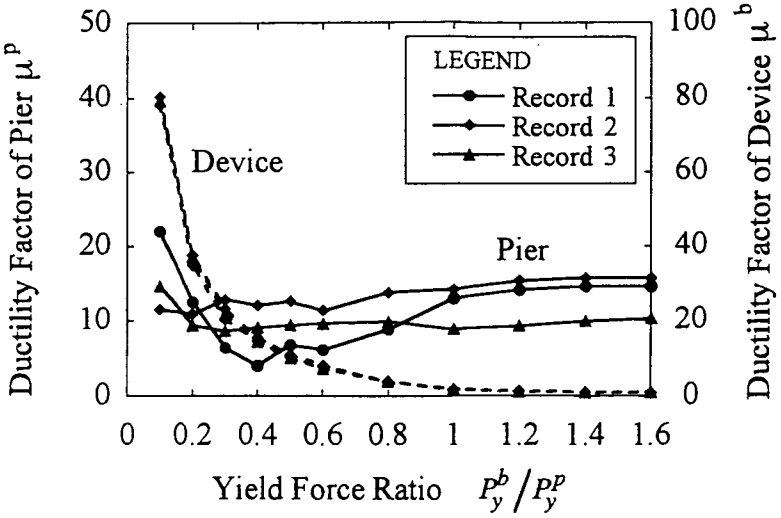
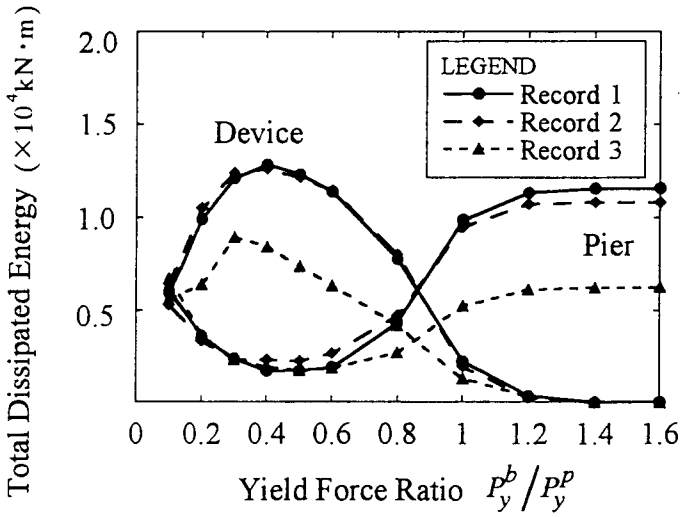
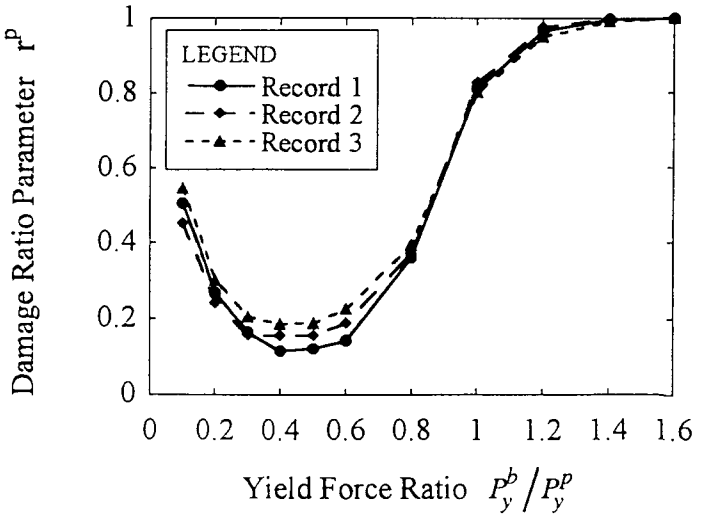


Fig. 11 Effect of the Yield Force of the Pier and the Device, P_y^p and P_y^b, on the Ductility Factor of the Pier and the Device (Device with Positive Post-Yield Stiffness)

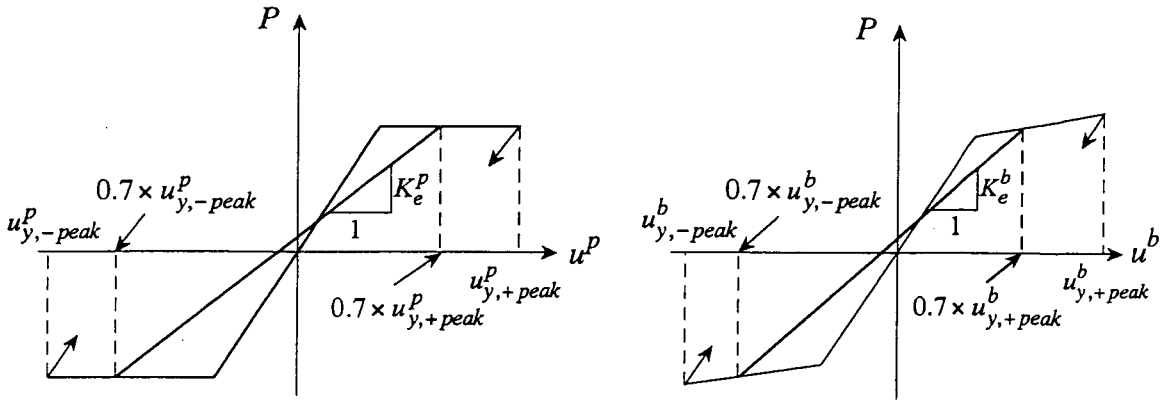


(a) Total Dissipated Energy



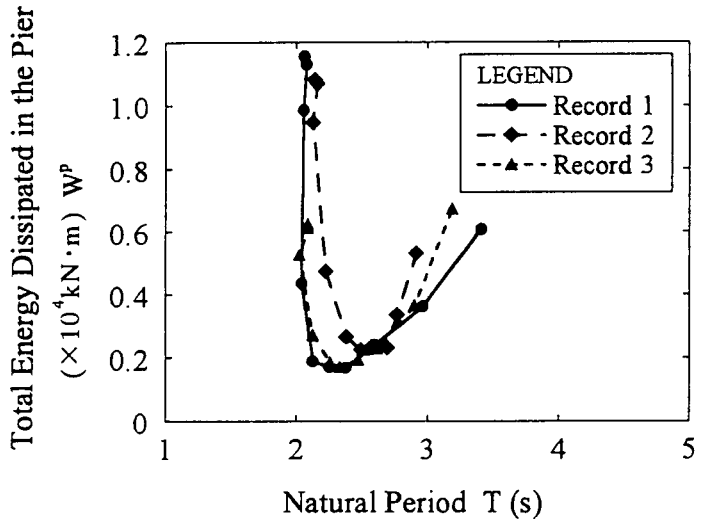
(b) Damage Ratio Parameter

Fig. 12 Effect of the Yield Force of the Pier and the Device, P_y^p and P_y^b, on the Damage Degree (Device with Positive Post-Yield Stiffness)

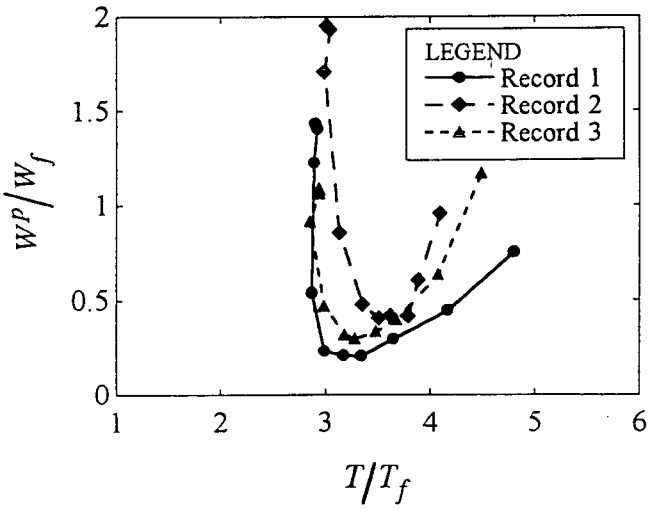


(a) Equivalent Stiffness of Pier (b) Equivalent Stiffness of Device

Fig.13 Definition of Equivalent Stiffness of Pier and Device

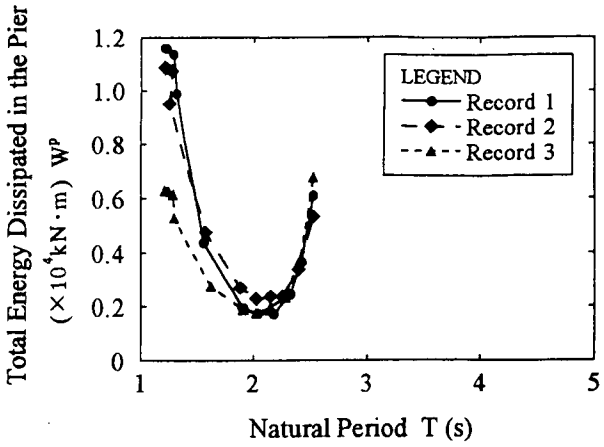


(a) Natural Period T vs. Total Dissipated in the Pier W^{p}

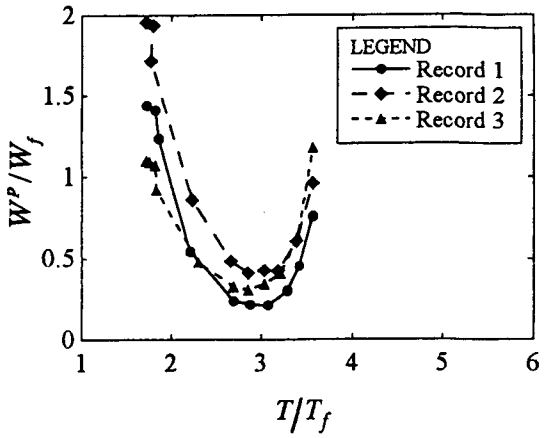


(b) Normalized Natural Period vs. Normalized Enregy Dissipated in the Pier

Fig. 14 Dependence of Total Energy Dissipated in the Pier on the Natural Period (Device with Positive Post-Yield Stiffness)

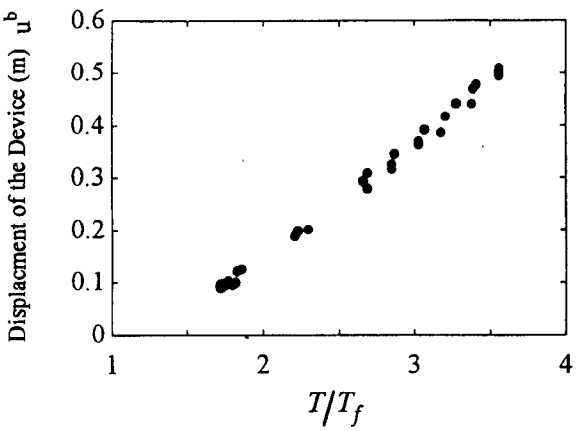


(a) Natural Period T vs. Total Energy Dissipated in the Pier W^p

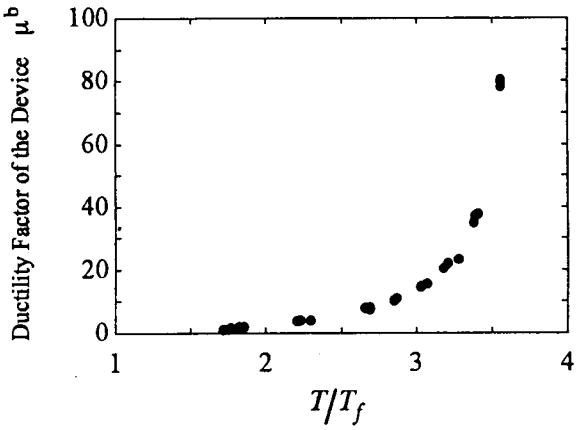


(b) Normalized Natural Period T/T_f vs. Normalized Total Energy Dissipated in the Pier W^p/W_f

Fig. 15 Dependence of Total Energy Dissipated in the Pier on the Natural Period computed with use of Cracked Stiffness of the Pier (Device with Positive Post-Yield Stiffness)



(a) Normalized Natural Period T/T_f vs. Displacement of the Device u^b



(b) Normalized Natural Period T/T_f vs. Ductility Factor of the Device μ^b

Fig. 16 Displacement of the Device vs. Natural Period computed with use of Cracked Stiffness of the Pier (Device with Positive Post-Yield Stiffness)

Nonlinear Seismic Response Characteristics of Two-Story Frame Piers

Toru Terayama[1], Shigeki Unjoh[2], Kenji Tasaki[3]

ABSTRACT

This paper describes a seismic response characteristics of two-story frame piers in the transverse direction. Firstly, the past specifications for highway bridges on the frame structures are reviewed. Secondly, static push-over analyses and non-linear dynamic analyses are carried out in order to examine the effects of the various parameters of beams and columns. The results of static analyses reveals that the failure mode can be changed from the shear failure to the flexural failure by increasing the volumetric ratio of the mid-beams, but a large amount of transverse reinforcement are needed. The results of the dynamic analyses indicate that the increase of yield stiffness if mid-beams or columns is more effective to improve the seismic performance than the increase of yield stiffness of upper-beams. Lastly, an accuracy of the equivalent energy method is evaluated by comparing the results of static analysis and dynamic analysis.

INTRODUCTION

Recently, three large destructive earthquakes have occurred in the United States and Japan. These earthquakes, the Lama Prieta earthquake in 1989, the Northridge earthquake in 1994, and the Kobe earthquake in 1995, have severely damaged a number of highway bridges, and have cost many lives and billions of dollars. In the Kobe earthquake, not only the single-column bents but also the frame structures were damaged by the seismic responses, see Fig.1. The major reasons of the damage are considered to be insufficient ductility and inadequate shear reinforcement.

In the United States, especially in California, the multi-column bents tends to be integral cap beam/superstructure type rather than bearing supported superstructure type. In order to analyze these structure, the push-over analysis method has been already developed, such as

1 Senior Research Engineer, Earthquake Engineering Division, Earthquake Disaster Prevention Research Center, Public Works Research Institute, Ministry of Construction
2 Head, ditto
3 Visiting Research Engineer, ditto

DRAIN-3D[1].

After 1990, the single-column bents for highway bridges in Japan basically must be checked by the horizontal dynamic capacity, which is a kind of limited stage design, in the Design Specifications for Highway Bridges Part V. Seismic Design, 1990[2], but frame structures need not be checked. After the Kobe earthquake, the intensive work has been done[3] in the Public Work Research Institute to develop the method of analysis to check the horizontal dynamic capacity and the ductility for the 1-story frame structures and a kind of push-over analysis method was introduced in the newly revised Design Specifications for Highway Bridges Part V. Seismic Design, 1996[4]. Using this method, the locations of plastic hinges and the comparison of the flexural strength between the foundation, the columns and the bearings can be clarified. But this method was verified by the test data only for the 1-story two-column bents and few research has been done for the two-story frame piers. Based on these facts, this paper examines seismic response characteristics of the two-story frame piers in the transverse direction with a static analysis as well as a non-linear dynamic analysis. In order to examine the effects of the ratios of the transverse reinforcement, the stiffness and the flexural strength of beams and columns, parametric study will be done and the results are discussed.

HISTORY OF THE PAST SEISMIC DESIGN CODES FOR FRAME STRUCTURE

History of the specifications and the codes for the design of concrete columns in Japan have been discussed by K. Kawashima, et al. [5][6] Although the checking method of the ductility, namely the check of the horizontal dynamic capacity, was introduced in the specifications of 1990 [2] for the single-column bent, the frame structures had been designed by the allowable stress design and the seismic coefficient method until the new Design Specifications for Highway Brides, 1996 [4] was issued. In this specifications, the checking method of the horizontal dynamic capacity for the multi-column bents was introduced, and with that the transverse reinforcement should be arranged adequately preventing from the shear failure or the brittle failure due to the insufficient ductility.

Reinforcement details were specified in the past specifications for highway bridges. In the Design Specifications for Highway Bridges Part IV Substructure, 1980[7], the minimum diameter of transverse reinforcement was specified as 13mm and the spacing should be less than 300mm, less than the twelve times of the diameter of the longitudinal reinforcement and also less than the half of the diameter or the shorter dimension of the column. In the Design Specifications

for Highway Bridges Part IV Substructure, 1990[2], the appropriate ratio of the transverse reinforcement was suggested. The ratio of transverse reinforcement should be 0.15% for the column with a longitudinal tensile reinforcement ratio from 0% to 0.5%, 0.2% for the column with a longitudinal tensile reinforcement ratio from 0.5% to 1.0% and 0.25% for the column with a longitudinal tensile reinforcement ratio bigger than 1.0%. The ratio of the transverse reinforcement is calculated by dividing the area of the transverse reinforcement by width of the column and the spacing of the transverse reinforcement. The Design Specifications for Highway Bridges, Part III Concrete Bridges, 1990 [2] specifies the reinforcement details for the frame structure as shown in Fig.2. For the frame structure, the ratio of the transverse reinforcement is specified as 0.2% for the part A and the part B, 0.25% for the part C and 0.15% for the part D.

MODEL FOR ANALYSIS

Fig.3 describes the model of the two-story frame reinforced concrete structure with plastic hinges, elastic member and rigid member. The superstructure is supported by the bearings on the upper-beam and no superstructure is supported on the mid-beam. Each elastic member has the yield stiffness which is based on the axial load by the dead load of the superstructure and the column itself. The plastic hinges are placed at the end regions of beams and columns. The location of the plastic hinge is a half distance of the plastic hinge length off from the end edge of each elastic member, where plastic hinge length Lp is calculated by the following equation (1).

$$Lp = 0.2h - 0.1D \quad and \quad 0.1D \le Lp \le 0.5D \tag{1}$$

where h is a half distance of the member and D is the dimension of the columns or the beams. Fig. 4 shows the moment and curvature relationship, which is based on the stress- strain relationship developed by Hoshikuma et al.[8] The effect of axial force on flexural strength is taken into account by axial load-moment interaction curve shown in Fig.5.

CASES OF ANALYSIS

To examine the effects of volumetric ratios of the transverse reinforcement, the stiffness and the flexural strength of beams and columns on the seismic response of the two-story frame pier, parametric study has been carried out. Varying parameter are as follows.

1. Volumetric ratio of transverse reinforcement of mid-beam 0.28%-1.77%
2. Yield stiffness of mid-beam 0.38×10^6-1.03×10^6 tf-m^2
3. Yield stiffness of upper-beam 0.67×10^6-1.37×10^6 tf-m^2

4. Yield stiffness of column $0.95x10^6$-$1.79x10^6$ tf-m^2

Tables 1, 2 and 3 show parameters of each case. It is noted that when the stiffness of beams changes, the flexural strength and the shear strength changes as well, because the sections and the volume of longitudinal reinforcement are changed.

STATIC PUSH-OVER ANALYSIS

The horizontal force is applied statically at the height of upper-beam of the frame model in Fig.1. As the horizontal force increases, six plastic hinges out of twelve plastic hinges(A to L) gradually yield. Furthermore, as the horizontal displacement increases, the rotations of the yielded plastic hinges increase and reach to the ultimate rotation which is calculated by the equation(2).

$$\theta_{pu} = \left(\frac{\phi_u}{\phi_y} - 1\right) \times L_p \times \phi_y \qquad (2)$$

where θ_{pu} is the ultimate rotation, ϕ_y is the yield curvature, ϕ_u is the ultimate curvature and L_p is the plastic hinge length. Fig. 6 shows one case of the horizontal force- horizontal displacement relationship derived from a static push over analysis. Plastic hinges occurred at both ends of mid-beam firstly, and at both ends of upper-beam next. Lastly plastic hinges formed at the bottom ends of columns. Once six plastic hinge formed, the horizontal force became constant.

Fig.7 shows the relation between S/Ps and volumetric ratio of mid-beams where S is the shear force at the plastic hinge of the mid-beams and Ps is the shear strength. Whether the expected failure mode is a flexural failure or a shear failure can be determined by the parameter of S/Ps. If S/Ps is larger than 1.0, then the failure mode will be a shear failure. On the other hand, if S/Ps is smaller than 1.0, then failure mode will be a flexural failure. Fig.7 shows that volumetric ratio should be larger than 1.77% if a flexural failure is required.

The relation between S/Ps versus the yield stiffness of the mid-beams, the upper-beams and the columns are plotted in Figs. 8, 9 and 10, respectively. The failure mode cannot be changed from the shear failure to the flexural failure by increasing the yield stiffness of the mid-beam, see Fig. 8. This is because the shear force increases even though the shear strength increases by enlarging the stiffness of the mid-beam. Fig. 9 shows that S/Ps at the upper-beam increases as the stiffness of the upper-beam increases, and the failure mode changed from the flexural failure to the shear failure in Case 8. It can be seen in Fig.10 that S/Ps is almost constant as the stiffness of the columns increases, and that the failure mode does not change to the shear mode.

It can be said from the study above that the shear strength can be increased by increasing the stiffness of the individual member. But since the shear force increases at the same time, it is not easy to change the failure mode from the shear failure to the flexural failure.

NON-LINEAR DYNAMIC ANALYSIS

Non-linear dynamic time-history analysis was carried out by using the model depicted in Fig.3. The suggested three ground motions for each soil condition in the Design Specifications for Highway Bridges Part V. Seismic Design, 1996[4] were used for the input ground motions. The response was evaluated by the average value obtained by the analyses using three input motions. The bi-linear model without degradation of stiffness was used for the hysteresis model. But this model can include the effects of the varying axial load. Newmark's method was used for the direct integration and the sampling time was determined as 0.005sec. Rayleigh damping was used for the damping matrix. Table 4 shows the effective mass and the period of each mode. The effective mass of the first mode is 87% and the first mode governs the response of this structure. Considering the first and the second mode, the sum of the effective mass is 93%. The Rayleigh damping was determined by the first mode and the second mode.

$\phi max/\phi u$ versus the yield stiffness of the mid-beam, the upper-beam and the column are plotted in Figs. 11, 12 and 13, respectively, where ϕmax is the maximum curvature response and ϕu is the ultimate curvature. As mentioned above, ϕmax is the average value of three responses by the analysis using three input ground motions. It can be seen in Fig.11 that $\phi max/\phi u$ can be decreased by increasing the yield stiffness of the mid-beam. The response curvature was decreased because the total stiffness increased by increasing the stiffness of the mid-beam. On the other hand, it can be seen in Fig. 12 that $\phi max/\phi u$ increased by increasing the yield stiffness of the upper-beam. The reason of this is that the response of the columns increased because the stiffness of the columns decreased comparing with the stiffness of the upper-beams. The balance of stiffness affected the response of the individual member. It can be seen in Fig. 13 that $\phi max/\phi u$ at the columns decreases drastically but $\phi max/\phi u$ at the beams are almost constant as the stiffness of the columns increases.

As a consequence, to increase the stiffness of the mid-beam and to increase the stiffness of the columns are more effective than to increase the stiffness of the upper-beam for improving the seismic performance of two-story frame piers.

EQUIVALENT ENERGY METHOD

Since Table 4 shows the first mode governs the response of this structure, the vibration of this structure can be assumed as a vibration of single-degree of freedom. Based on this fact, the equivalent energy method[9] can be applied to estimate the inelastic displacement of this structure and the accuracy of this method will be examined in this section. The displacement response δ_{EL} can be calculated by the equation (3) based on the equivalent energy method. δ_{EL} will be compared with the displacement response obtained by the non-linear time history analysis, see equation(4).

$$\delta_{EL} = \frac{1}{2}\delta_y\left[\left(\frac{k_{hc}\times W}{P_u}\right) + 1\right] \tag{3}$$

$$\alpha = \frac{\delta_{EL}}{\delta_{NL}} \tag{4}$$

where δ_{EL} is the displacement response calculated by the equivalent energy method using the elastic response, δ_{NL} is the maximum displacement based on the non-linear dynamic analysis, δ_y is the yield displacement, k_{hc} is the seismic coefficient for the elastic response, W is the equivalent weight, Pu is the flexural strength of the two-story frame pier, and α is the ratio of the accuracy of the equivalent energy method, .

Fig. 14 shows α for the varying yield stiffness. If α equals 1.0, the equivalent energy method is accurate and if α is larger than 1.0, the displacement calculated by the equivalent energy method is larger than the displacement analyzed by the non-linear dynamic analysis. Here it is noted that the first mode period is 0.6sec. to 0.7sec., where the equivalent energy method can be applied to estimate the inelastic response. The values α scatters slightly in the range from 0.9 to 1.6 in Fig.14, but it can be said that the accuracy of the equivalent energy method is not too bad.

CONCLUDING REMARKS

The purpose of this study was to examine the seismic response characteristics of two-story frame piers. Based on the parametric analyses, the following conclusions were reached.

1. The failure mode can be changed from the shear failure to the flexural failure by increasing the volumetric ratio of the mid-beam, but a large amount of transverse reinforcement is needed to change the failure mode.
2. The shear strength can be increased by increasing the stiffness of the individual member such

as the mid-beam, the upper-beam or the column. But since the shear force increases at the same time, it is not easy to change the failure mode from the shear failure to the flexural failure.

3. To increase the stiffness of the mid-beam and to increase the stiffness of the columns are more effective on the improvement of the seismic performance of two-story frame piers than to increase the stiffness of the upper-beam.
4. The accuracy of the equivalent energy method was examined. The ratio α representing the accuracy of the equivalent energy method scatters 0.9 to 1.6, which means that the accuracy is not too bad.

REFERENCES

[1] V. Prakash, G.H. Powell, S. Campbell, DRAIN-3D, Base Program Description and User Guide, Report No. UCB/SEMM-94/07, University of California, August 1994.

[2] Japan Road Association, Design Specifications for Highway Bridges, Part III Concrete Bridges, Part IV Substructure, Part V Seismic Design, 1990.

[3] T. Terayama, H. Otsuka, K. Nagaya, Strength and Ductility Characteristics of Two-Column Bents, Proceedings of the Second Italy-Japan Workshop on Seismic Design and Retrofit of Bridges, Italy, February 1997.

[4] Japan Road Association, Design Specifications for Highway Bridges, Part V Seismic Design, 1996.

[5] K. Kawashima, Seismic Design, Seismic Strengthening and Repair of Highway Bridges in Japan, Proceedings of the First U.S.-Japan Workshop on Seismic Retrofit of Bridges, Tsukuba, December 1990.

[6] T. Akimoto, Design Details of Reinforced Concrete Bridges in Japan, Proceedings of the First U.S.-Japan Workshop on Seismic Retrofit of Bridges, Tsukuba, December 1990.

[7] Japan Road Association, Design Specifications for Highway Bridges, Part IV Substructure, 1980.

[8] Hoshikuma, J., Kawashima K., Nagaya K.,"A Stress-Strain Model for Reinforced Concrete Bridge Piers Confined by Hoop Reinforcement," Proceedings of 2nd International Workshop on Seismic Design and Retrofitting of Reinforced Concrete Bridges, 365-385, Edited by R. Park, University of Canterbury, New Zealand, 1994.

[9] A. S. Velotsos, N. M. Newmark, Effects of Inelastic Behavior on the Response of Simple

Systems to Earthquake Motions, Proceedings of the 2nd World Conference on Earthquake Engineering, 1960

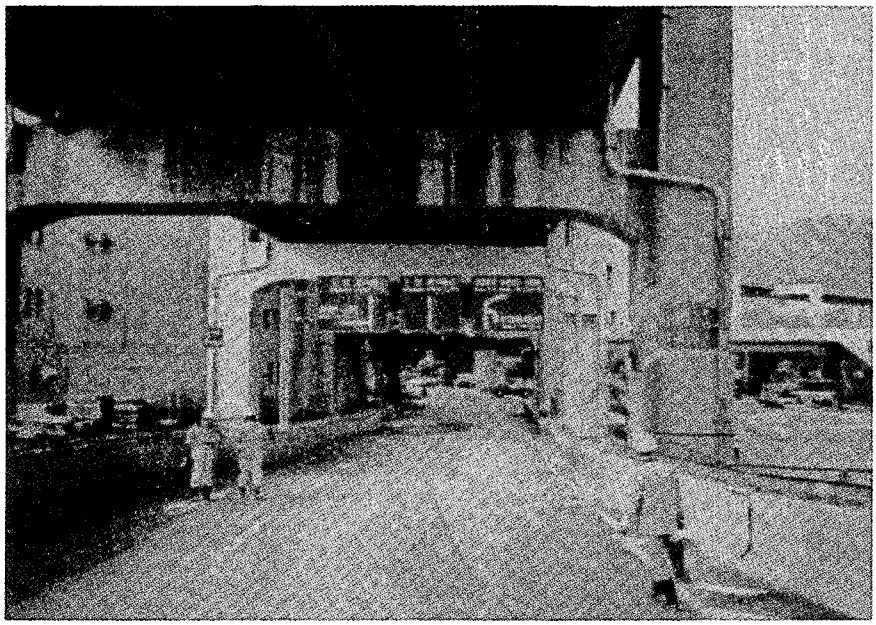


Fig. 1 Damage of Two-story frame Pier During Kobe Earthquake

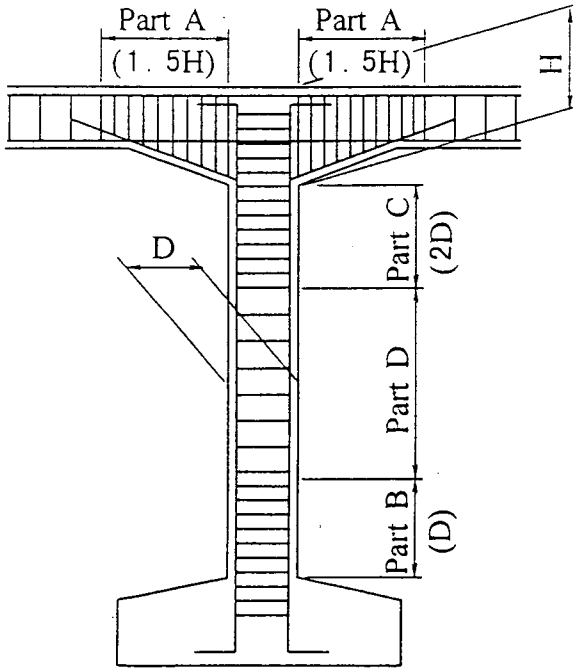


Fig. 2 Reinforcement Details in the Specifications, 1990

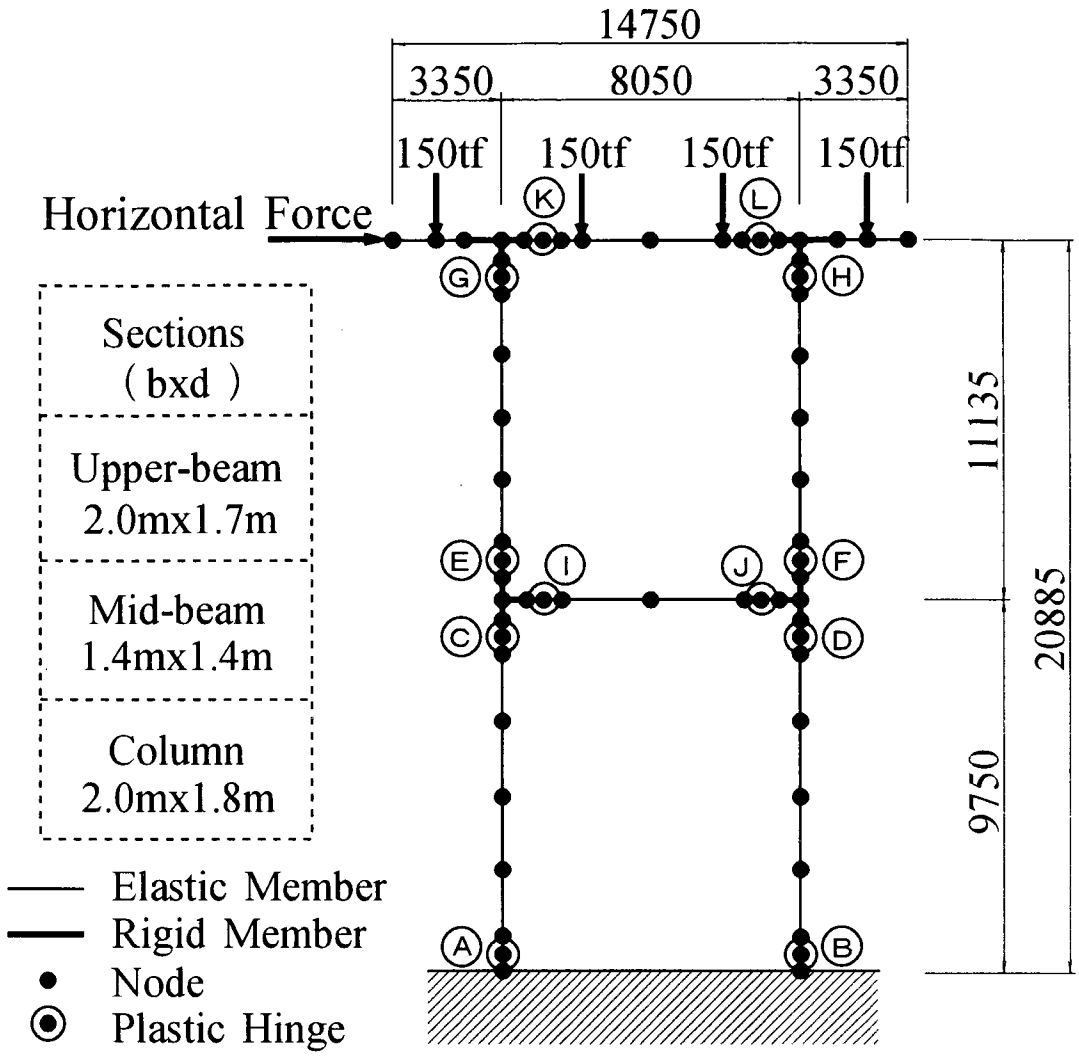


Fig. 3 Analytical Model of Two-story frame Pier

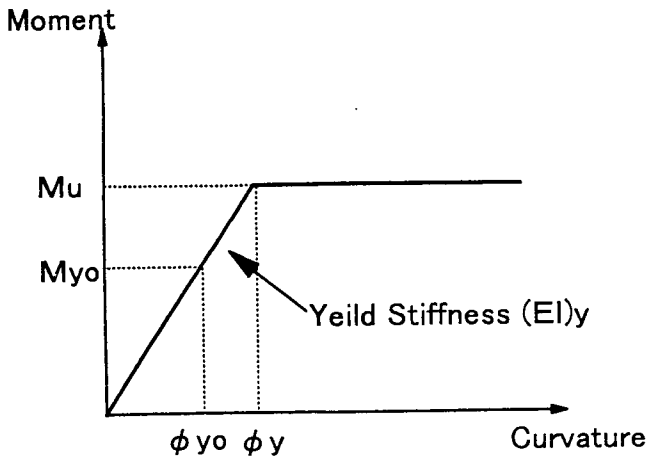


Fig. 4 Moment-Curvature Relationship

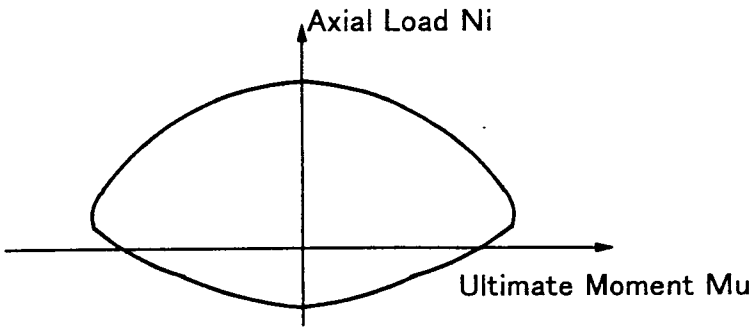


Fig. 5 Axial Load-Moment Interaction

Table 1 Stiffness and Strength of Structural Member (Yield Stiffness of Mid-Beam Varies)

Structural Member		Yield Stiffness ($tf\text{-}m^2$)	Shear Strength (tf)	Flexural Strength (tf-m)	Volumetric Ratio (%)
Column		$1.26x10^6$	383.2	3004.9	0.56
Upper-Beam		$0.97x10^6$	614.6	1417.8	1.06
Mid-Beam	Case 1	$0.38x10^6$	324.6	868.6	1.77
	Case 2	$0.55x10^6$	355.8	1243.3	1.77
	Case 3	$0.77x10^6$	409.0	1465.7	1.77
	Case 4	$1.03x10^6$	461.1	1727.0	1.77

Table 2 Stiffness and Strength of Structural Member (Yield Stiffness of Upper-Beam Varies)

Structural Member		Yield Stiffness ($tf\text{-}m^2$)	Shear Strength (tf)	Flexural Strength (tf-m)	Volumetric Ratio (%)
Column		$1.26x10^6$	383.2	2941.5	0.56
Mid-Beam		$0.38x10^6$	324.6	868.6	1.77
Upper-Beam	Case 5	$0.67x10^6$	599.0	1092.9	1.06
	Case 6	$0.82x10^6$	607.2	1356.5	1.06
	Case 7	$0.97x10^6$	614.6	1648.9	1.06
	Case 8	$1.37x10^6$	680.6	2043.9	1.06

Table 3 Stiffness and Strength of Structural Member (Yield Stiffness of Column Varies)

Structural Member		Yield Stiffness ($tf\text{-}m^2$)	Shear Strength (tf)	Flexural Strength (tf-m)	Volumetric Ratio (%)
Upper-Beam		$0.97x10^6$	614.6	1648.9	1.06
Mid-Beam		$0.38x10^6$	324.6	868.9	1.77
Column	Case 9	$0.95x10^6$	379.1	2216.9	0.56
	Case 10	$1.10x10^6$	383.2	2569.8	0.56
	Case 11	$1.26x10^6$	383.2	2953.3	0.56
	Case 12	$1.79x10^6$	424.8	3710.7	0.56

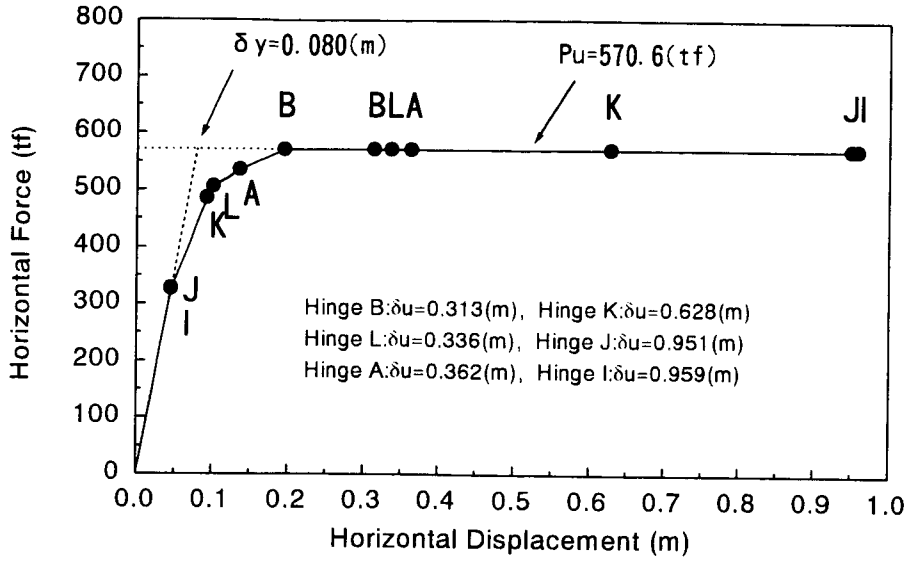


Fig. 6 Horizontal Force - Horizontal Displacement Relationship

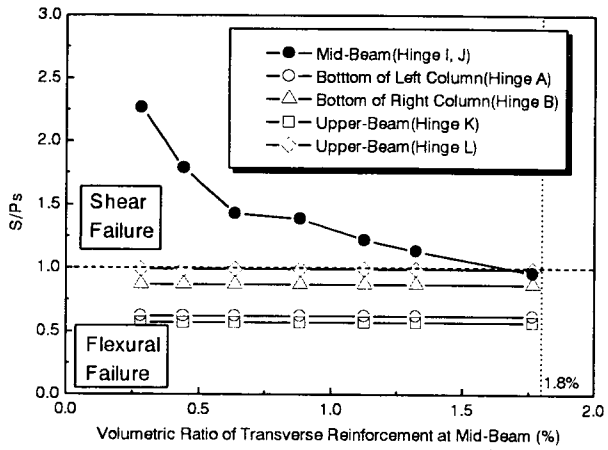


Fig. 7 S/Ps versus Volumetric Ratio of Mid-Beam

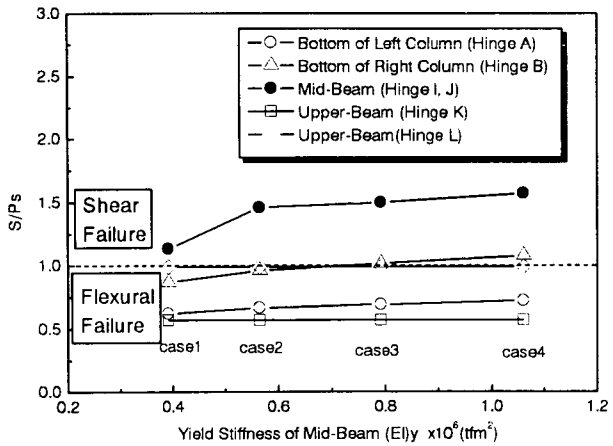


Fig. 8 S/Ps versus Yield Stiffness of Mid-Beam

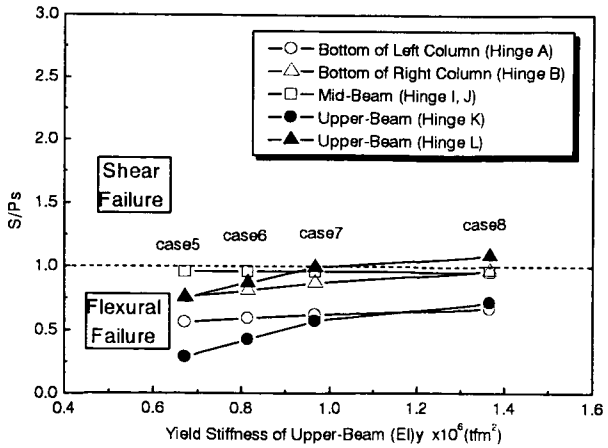


Fig. 9 S/Ps versus Yield Stiffness of Upper-Beam

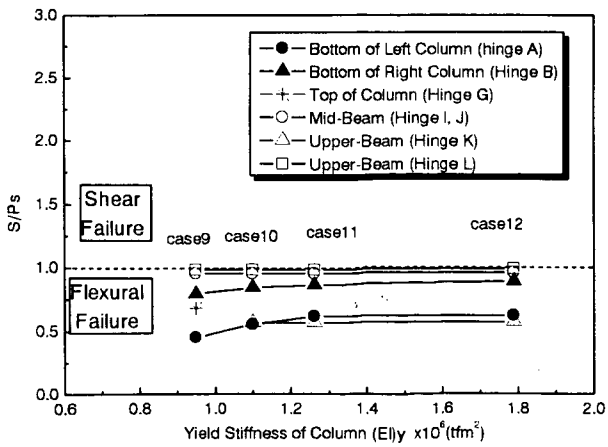


Fig. 10 S/Ps versus Yield Stiffness of Column

Table 4 Effective Mass and Period of Each Mode

Mode	Effective Mass (%)	Accumulated Effective Mass(%)	Period(sec.)
1	87	87	0.704
2	6	93	0.107
3	0	93	0.087
4	1	94	0.065
5	0	94	0.062

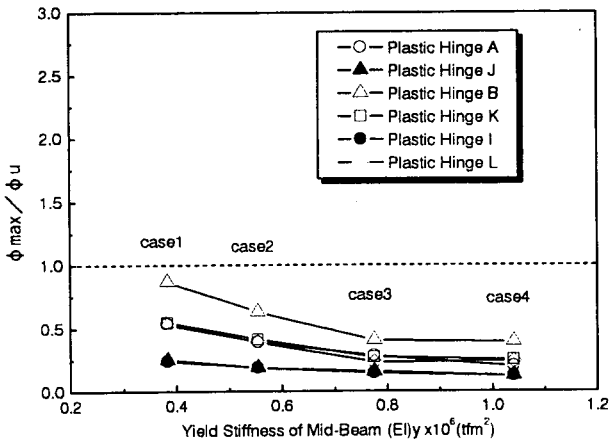


Fig.11 ϕmax/ϕu versus Yield Stiffness of Mid-Beam

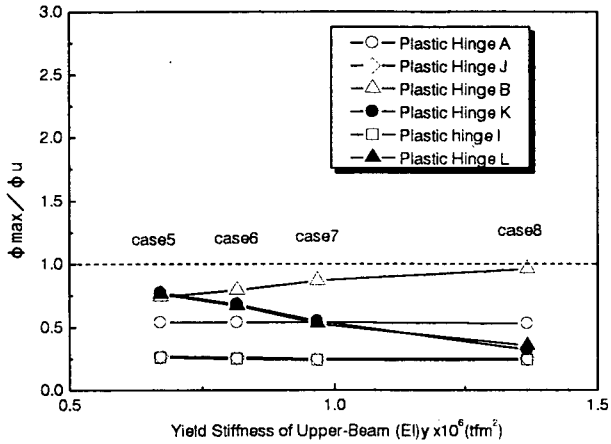


Fig.12 ϕmax/ϕu versus Yield Stiffness of Upper-Beam

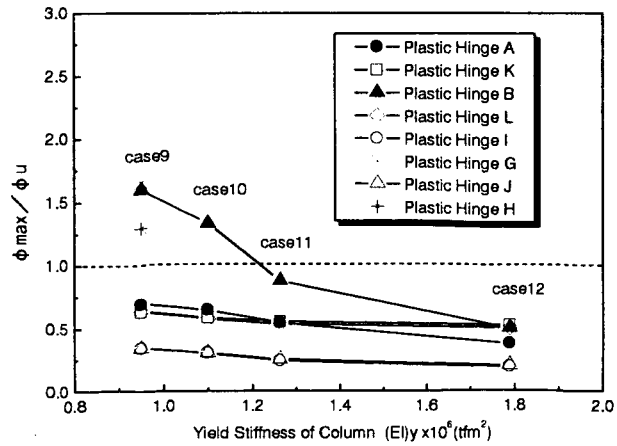


Fig.13 ϕmax/ϕu versus Yield Stiffness of Column

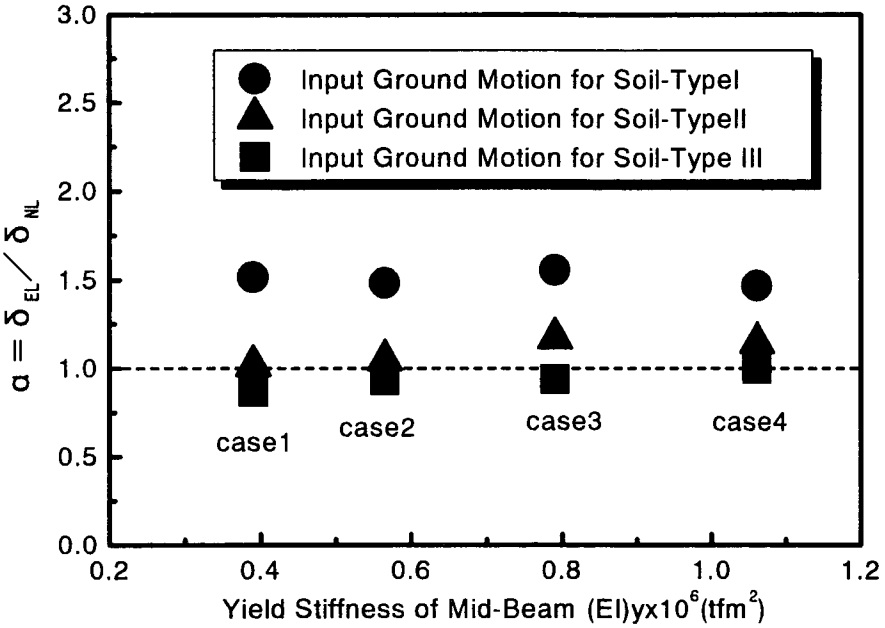


Fig. 14 Accuracy of Energy Equivalent Method

DISPLACEMENT ISSUES OF SEISMICALLY LOADED R/C BRIDGE COLUMNS

Nadim I. Wehbe[1], M. Saiid Saiidi[2] and David H. Sanders[3]

Abstract:

This paper describes an investigation into the deformation of reinforced concrete bridge columns subjected to lateral loads. Lateral deflections due to flexure, shear, and bond slip are discussed. Analytical models, based on monotonic lateral loading, are presented and used to predict the response envelopes of cyclically loaded columns. Consideration is given to the effects of confinement steel and other relevant details on the performance of columns with uniform and non uniform shapes. Analytical predictions are compared to experimental data obtained from tests of rectangular and flared column specimens. The results indicate that elastic and inelastic lateral deflections of reinforced concrete bridge columns can be estimated with good accuracy.

Introduction

Performance based design philosophy of structures relates the strength of structural members to target damage levels set for different loading conditions. When no permanent damage is allowed, structural members should be designed to remain elastic under the imposed loads. For most structures, however, inelastic deformations form an economical means to dissipate the energy induced by strong earthquake motions. For bridge structures, it is well established that inelastic deformations should be accommodated through the formation of plastic hinges in the columns (Priestley and Park, 1987). The degree of damage in the plastic hinge region of a reinforced concrete column is mainly dependent on the attained deformation relative to the column deformation capacity.

In current U.S. codes (ACI, 1995; UBC, 1997; AASHTO, 1992), the seismic design of structural members is based on specified forces. This approach is rather suitable for elastic members. The U.S. codes (AASHTO, 1992; UBC, 1997) address the ductility of structural members indirectly through force reduction factors applied to the forces obtained from elastic analysis of structures. If structural members are expected to sustain inelastic deformations under induced seismic loads, it may be more appropriate to employ a displacement-based approach for the seismic design of structures. Recently, a displacement-based approach has been suggested for the seismic design of reinforced concrete bridges (Kowalsky and Priestley, 1996). Any displacement-based method entails that the load-deformation relationships of structural members be known. The ability to obtain reasonable estimates of lateral deflections of reinforced concrete

[1] Ph.D. Candidate and Graduate Research Assistant, University of Nevada, Reno, NV.

[2] Professor, University of Nevada, Reno, NV.

[3] Associate Professor, University of Nevada, Reno, NV.

columns has been doubted by some researchers (Konwinsky, 1996). The experimental and the analytical results presented in this paper show that the load-displacement relationships of reinforced concrete bridge columns can be predicted with reasonable accuracy.

Analytical Lateral Deflections

The total lateral deflection, Δ_t, of reinforced concrete columns subjected to lateral loads may be expressed as:

$$\Delta_t = \Delta_f + \Delta_s + \Delta_{sh} \quad (1)$$

where Δ_f is deflection due to flexure, Δ_s is deflection due to reinforcement bond slip, and Δ_{sh} is deflection due to shear. In Equation 1, it is assumed that footing or joint rotation is prevented.

Flexural Deflection

Flexural deflections (Δ_f) can be found by applying the moment area theorem as follows

$$\Delta_f = \int_0^l \varphi \, x \, dx \quad (2)$$

where ϕ is the theoretical curvature profile along the column height for a given lateral load. The analytical moment-curvature relationships must be based on considering the following effects:

(a) Confined properties of the core concrete
(b) Spalling of the cover concrete (unconfined properties)
(c) Strain hardening of main reinforcing steel

The unconfined concrete properties may be modeled using the Kent and Park concrete model (Kent and Park, 1971) with an ultimate concrete strain, ϵ_u, equal to 0.004. The confined concrete constitutive relationship may be modeled using the Mander et al. model (Mander, Priestley, and Park, 1988) with an ultimate strain as recommended by Paulay and Priestley (Paulay and Priestley, 1992). The steel stress-strain behavior may be idealized with a tri-linear relationship.

When premature buckling of longitudinal bars is prevented by proper detailing, flexural failure can be considered when either the confined concrete reaches its ultimate strain or when the longitudinal steel strain attains the rupture strain, whichever occurs first.

Bond Slip Deflection

Bond slip deflection is defined as the lateral deflection due to the elongation of the developed main steel beyond the critical section.

The following method has been developed for calculating bond slip deflection. The method is based on compatibility and equilibrium of the developed tensile bars. The applicability of this method is limited to columns with tensile bars having sufficient development length or anchorage so as to prevent bar pull out. The bond slip rotation (θ_s) is assumed to occur about the neutral axis of the column cross section at the connection interface as is shown in

Figure 1. The neutral axis location and the strain and stress in the tensile steel corresponding to the desired lateral load are determined from moment-curvature analysis of the section. The additional longitudinal bar extension (δl), due to slippage, at the interface is calculated at the outermost tensile steel layer in the column by integrating the theoretical strain profile along the embedded bar length inside the connection (Figure 1). Thus, the bond slip rotation, θ_s, can be found as δl divided by the distance of the neutral axis to the center of the outermost tensile steel layer. The corresponding lateral deflection at the top of the column (Δ_s) is obtained as $\Delta_s = \theta_s \cdot L$, where L is the column shear span. In finding the theoretical strain profile along the embedded bar length, uniform bond stress is assumed along a length required to develop a force equal to the bar tensile force at the bottom of the column. For ϕ 35 mm (#11) or smaller deformed bars with sufficient concrete confinement, the basic bond strength, u, of tension bars can be found using the following equations (ACI, 1963)

$$u = \frac{20\sqrt{f_c'}}{d_b} \leq 5.5 \quad (MPa); \qquad u = \frac{9.5\sqrt{f_c'}}{d_b} \leq 800 \quad (psi) \tag{3}$$

where d_b is the bar diameter in consistent units.

The two strain profiles shown in Figure 1 are based on tri-linear steel stress-strain model. Depending on the calculated strain in the outermost steel layer of the column section at the interface, the strain profile along the development length may assume one of the two profiles presented in Figure 1. The two strain profiles represent the following cases:

Calculated steel strain is less than or equal to strain hardening, $\epsilon_{s.h.}$, ($f_s \leq f_y$):

When the calculated strain is less than the yield strain (ϵ_y), the steel stress (f_s) at the interface would be equal to $E\,\epsilon_s$ which is less than the yield stress (f_y). Since the bond stress is assumed to be constant, the gradient of the strain profile along the embedded bar will have to be constant. In this case, the maximum strain would be equal to the calculated strain. When the calculated strain is greater than ϵ_y but less than or equal to the strain hardening of steel ($\epsilon_{s.h.}$), the steel stress would be equal to f_y. Since the stress along the development length is changing at a constant rate, the maximum strain of the bar at the interface would have to be equal to ϵ_y. From equilibrium of forces, the development length, l, can be calculated as follows:

$$l = \frac{f_s d_b}{4u} \tag{4}$$

Calculated steel strain is greater than strain hardening, $\epsilon_{s.h.}$, ($f_s > f_y$):

In this case, the strain profile follows two strain gradients along the embedded lengths l_1 and l_2 (see Figure 1). The strain at the interface would be equal to the calculated strain ϵ_s from the moment-curvature analysis. The strain reduces from ϵ_s to ϵ_y and from ϵ_y to zero along l_1 and l_2, respectively. The absence of the yield plateau is due to the fact that the steel stress along the

development length changes at a constant rate. Therefore, the yield plateau and the strain hardening region are approximated by a single line with moderate slope. l_1 and l_2 can be found as follows

$$l_1 = \frac{(f_s - f_y)d_b}{4u} \tag{5}$$

$$l_2 = \frac{f_y d_b}{4u} \tag{6}$$

Shear Deflection

Shear deflections can be found using the shear stiffness expression derived by Park and Paulay (Park and Paulay, 1975). For assumed 45° diagonal cracks, the shear stiffness may be expressed as

$$K_{v,45} = \frac{\rho_v}{1 + 4n\rho_v} E_s b_w d \tag{7}$$

where

$K_{v,45}$ = shear stiffness per unit length along the column height
E_s = elastic modulus of shear reinforcement
b_w = section width perpendicular to applied shear
d = effective section depth parallel to applied shear
n = E_s/E_c (modular ratio)
E_c = elastic modulus of concrete
ρ_v = A_v/sb_w (shear reinforcement ratio)
A_v = area of shear reinforcement
s = spacing of shear reinforcement sets along the member longitudinal axis

Having the shear stiffness per unit length, the total shear deflection, Δ_{sh}, for the column would be

$$\Delta_{sh} = \frac{VL}{K_{v,45}} \tag{8}$$

where V is the applied shear force and L is the shear span. For a column with varying shear stiffness along its height, the total shear deflection can be found as follows

$$\Delta_{sh} = \sum_{i=1}^{i=m} \left[\frac{L_i}{(K_{v,45})_i} \right] V \tag{9}$$

where m is the total number of column segments with different unit shear stiffness and L_i and $(K_{v,45})_i$ are the length and stiffness of segment i, respectively.

Test Specimens

The experimental results of four rectangular column specimens and two flared column specimens are included in this paper. The tests were conducted at the University of Nevada, Reno. The objectives of the tests were to study the ductility of rectangular bridge columns with moderate confinement and to assess the seismic vulnerability of bridge columns with structural flares. However, the discussion of the experimental results in this paper is limited to issues related to lateral displacements.

Rectangular Column Specimens

Four one-half scale rectangular column specimens (referred to as A1, A2, B1, and B2) were designed, constructed and tested. The parameters varied in the tests were the transverse steel reinforcement amount and the axial load level. All four specimens had the same cross sectional dimensions and column height, and were reinforced with identical longitudinal steel. Details of the column specimens are shown in Figure 2. Each column was 380 millimeters (15 in.) wide by 610 mm (24 in.) deep and was reinforced with 18- ϕ19 mm (#6) bars, resulting in longitudinal reinforcement ratio, ρ_l, of 2.2 percent. The column height was 2050 mm (6.7 ft.).

Lateral steel consisted of ties and cross ties engaging longitudinal bars. Except for the lateral steel ratio and hoop set spacing, detailing of ties and cross ties was in accordance with current seismic requirements (ACI, 1995; AASHTO, 1992). Each tie set in the potential plastic hinge zone of the test specimens consisted of 1- ϕ 6 mm (#2) perimeter hoop, 2- ϕ 6 mm (#2) cross ties in the long direction, and 2- ϕ 10 mm (#3) cross ties in the short direction. To prevent premature bar buckling, the tie set vertical spacing was kept below six times the longitudinal bar diameter (6 d_b). For specimens A1 and A2 the tie set spacing was set at 110 mm (4.25 in.). For Specimens B1 and B2, the spacing of the tie sets was reduced to 83 mm (3.25 in). The tie set arrangement and spacing was maintained the same along the column height. However, ϕ 10 mm (#3) bars were used outside the potential plastic hinge region (Figure 2) because of the limited availability of ϕ 6 mm (#2) bars. The lateral steel ratios are summarized in Table 1. Measured concrete and steel properties for the rectangular column specimens are presented in Table 2.

Flared Column Specimens

Two flared column specimens, referred to as HS and LS, were designed to represent 40 percent scaled models of prototype columns of an existing bridge in Northern Nevada.

Details of Specimens LS and HS are presented in Figures 3 and 4, respectively. Each specimen was configured to represent an inverted position of the prototype column. Thus, the specimen footing corresponded to the bridge bent cap whereas the top of the specimen represented the hinge connection between the prototype column and its footing. The specimen height between the footing and the loading block on top of the column was 2007 mm (79 in.). The lower 1956 mm (77 in.) segment of the column represented the 4.88 m (16 ft) parabolic flare transition of the prototype.

The main reinforcement in the columns consisted of ϕ16 mm (#5) bars. The longitudinal steel ratios at the largest cross section (bottom of specimen column) were 1.02 percent and 1.79 percent for specimens LS and HS, respectively. The lateral steel in specimens LS and HS was identical and comprised ϕ6 mm (#2) ties and cross ties. The lateral steel ratios in the models and the corresponding prototypes were maintained the same. The tie set spacing was 64 mm (2.5 in) in both specimens. The lateral steel ratios for cross sections at different locations along the column height of the test specimens are presented in Table 3. Summary of the measured concrete and steel properties is presented in Table 4.

Experimental Procedure

The experimental procedure was nearly identical for all six specimens. Each specimen was tested under constant axial load while subjected to lateral drift reversals along the column strong direction. The test setups for the rectangular and the flared column specimens are shown in Figures 5 and 6, respectively. The footings were tied to the laboratory floor to prevent rocking under the overturning moments during the test. The axial load was applied by means of two prestressing bars. The lateral load was applied by means of a hydraulic actuator.

The lateral load was monotonic, load controlled up to ±75 percent the calculated "effective" lateral yield load [$\pm 0.75\ (F_y)_{eff.}$] and displacement controlled afterward. The effective lateral yield load corresponded to the theoretical effective yield moment taken at the column critical section. The effective yield moment for each specimen was obtained from moment-curvature analysis using tri-linear and parabolic stress-strain relationships for steel and concrete, respectively. In the analysis, the confinement of core concrete and the spalling of cover concrete were accounted for. The effective yield moment was based on idealized elastoplastic moment-curvature relationship. The elastic segment of the idealized relationship was assumed to pass through the point of first yield and the plastic segment was assumed to terminate at the section theoretical ultimate curvature. The effective yield moment was then obtained by equating the areas under the idealized and the theoretical moment-curvature relationships.

The measured yield displacements (Δ_y) were determined experimentally by extrapolating the average measured displacements at $+0.75\ (F_y)_{eff.}$ and $-0.75\ (F_y)_{eff.}$ (Priestley and Park, 1987).

Rectangular Column Specimens

Specimens A1, A2, B1 and B2 were subjected to initial axial loads of 615 kN (138 Kips), 1505 kN (338 Kips), 601 kN (135 Kips) and 1514 kN (340 Kips), respectively. Based on measured concrete strengths, these loads correspond to axial load ratios, $P/(f_c' \cdot A_g)$, of 0.1, 0.24, 0.09 and 0.23. The axial load ratio in bridge columns is normally below 0.3.

Each specimen was subjected to one full cycle at post-cracking moment (M_{cr}), one full cycle at $\pm 0.75\ (F_y)_{eff.}$, two full cycles at a displacement ductility μ_Δ of ±1, and two full cycles at a displacement ductility μ_Δ of ±2. Afterward, in general, specimens with the lower axial load (A1 and B1) were then cycled at displacement ductility increments of 2 whereas those with higher axial loads (A2 and B2) were cycled at displacement ductility increments of 1, until failure. At

each ductility level, the specimen was taken through at least two full excursions.

In all four specimens, plastic hinges developed at the bottom of the columns. The observed concrete deterioration extended for approximately 610 mm (24 in.) above the footing. Failure of the specimens was initiated by opening of the 90° cross tie hooks in the plastic hinge region, mainly, in the second and the third hoop sets above the footing. This was followed by buckling of the outer longitudinal steel due to loss of confinement.

Flared Column Specimens

Specimens LS and HS were subjected to initial axial loads of 632 kN (142 Kips) and 713 kN (160 Kips), respectively. The axial loads were scaled representations of the dead loads in the prototype columns.

Each specimen was subjected to one full cycle at post-cracking moment (M_{cr}), one full cycle at $\pm 0.75\ (F_y)_{eff.}$ and two full cycles at a displacement ductility μ_Δ of ± 1. Afterward, the specimens were cycled through two full excursions at displacement ductility increments of 1, until failure.

Because of the varying flexural strength along the column height, plastic hinges in the flared column specimens did not occur at locations of maximum bending moments, but were rather initiated at approximately 737 mm (29 in.) above the footing. This was consistent with the analytical predictions that were established based on calculated flexural capacities at different cross sections along the column height (Wehbe, 1997). The axial load ratio at the critical section was approximately 0.05 for each specimen. Failure of the specimens was initiated by bar buckling of the outermost longitudinal bars. The bars buckled at locations that ranged between 635 mm (25 in.) and 838 mm (33 in.) above the footing. It was observed that bar buckling followed extensive deterioration of the core concrete in the vicinity of the buckled bar segments.

Analytical and Measured Results

The lateral deflections due to flexure, bond slip, and shear were calculated according the analytical models presented earlier in this paper. However, for the rectangular column specimens, consideration was given to the "clamping" effect imparted by the footing on the flexural response of the columns. The experimental data and observations showed that the footing provided additional confinement to the column segment next to the footing (Wehbe, 1997). This additional confinement allowed for the development of a critical column segment, rather than one discrete critical section, that was capable of attaining ultimate curvatures. For columns with properly detailed lateral steel, the length of the critical segment may primarily depend on the axial load, but can be approximated as twice the tie spacing (Wehbe, 1997). Thus, the ultimate lateral load was based on a reduced shear span which is equal to the original shear span less two tie spacings. The corresponding theoretical curvature profile along the column height was assumed as a parabolic curve along the reduced shear span followed by a constant curvature line (ultimate curvature) along the column critical segment next to the fixed column end.

In the analysis of the flared column specimens, consideration was given to the effect of concrete deterioration in the plastic hinge region on the development of the longitudinal bars that terminated at 737 mm (29 in.) and 1092 mm (43 in) above the base. Theoretically, the plastic hinge initiates at 737 mm (29 in.) above the footing and concrete deterioration spreads to approximately half a section depth in either direction. Thus, bars developed within the deteriorated column segment would lose anchorage. Prior to concrete deterioration, the terminated bars were considered to be fully effective at sections located at one development length below the terminated ends. At ultimate, however, the flexural deflections were based on neglecting the area of the terminated bars in the moment-curvature analysis.

The calculated and the measured lateral deflections at yield and ultimate are summarized in Table 5. Figures 7 and 8 present the calculated and the measured response envelopes for the rectangular and the flared column specimens, respectively. For proper comparison between the measured and the calculated values, the measured envelopes presented in Figures 7 and 8 reflect the portion of the applied lateral load resisted by the columns rather than the absolute lateral loads registered by the actuator load cell. The necessity for adjusting the measured lateral loads arise from the fact that when the column specimens were subjected to higher drift levels, the resulting inclinations along the applied axial load generated lateral force components that opposed the actuator force.

Comparison of the analytical and experimental results reveals that the predicted and the measured values are in very good agreement. The ratio of the calculated to the measured yield displacements were 0.91, 0.97, 0.90, 0.92, 1.00, and 0.99 for specimens A1, A2, B1, B2, LS, and HS, respectively. The calculated maximum drift ratios deviated from the measured ones by 14 percent, 9 percent, 7 percent, 9 percent, 12 percent and 14 percent for specimens A1, A2, B1, B2, LS and HS, respectively.

Conclusions

Lateral load-deflection envelopes of cyclically loaded reinforced concrete columns can be predicted with reasonable accuracy using methods of monotonic loading analysis. The analytical models presented in this study for calculating lateral deflections due to flexure, bond slip, and shear can be used for uniform and non-uniform (such as flared) columns. Estimation of lateral deflections should include, whenever applicable, the clamping effect provided by footings (or bent caps) and/or de-bonding of longitudinal bars that are developed in the plastic hinge region.

Acknowledgment

The study of rectangular columns was sponsored by Federal Highway Administration (FHWA) and administered through Highway Project 112 at the National Center for Earthquake Engineering Research (NCEER) at Buffalo. The study of the flared columns was funded by the Nevada Department of Transportation. The opinions presented in this paper do not necessarily represent those of the sponsors.

References

American Association of State Highway and Transportation Officials, *"Standard Specifications for Highway Bridges,"* Fifteenth Edition, Washington, D.C., 1992.

American Concrete Institute Committee 318, *"Building Code Requirements for Reinforced Concrete and Commentary,"* American Concrete Institute, Detroit, Michigan, 1995.

American Concrete Institute Committee 318, *"Building Code Requirements for Reinforced Concrete,"* American Concrete Institute, Detroit, Michigan, 1963.

Kent, D. C. and Park, R., *"Flexural Members with Confined Concrete,"* ASCE Journal of the Structural Division, Vol. 97, No. ST7, July 1971, pp. 1969-1990.

Konwinski, C., *"Shear Strength of Concrete Bridge Piers Subjected to Earthquake Loading,"* M.S. Thesis, Department of Civil Engineering, Purdue University, 1996, 152p.

Kowalski, M. J. and Priestley, M. J. N., *"A Direct Displacement-Based Design Approach for Reinforced Concrete Bridges,"* The Fourth CALTRANS Seismic Research Workshop, July 9, 10 and 11, 1996, Sacramento, California.

Park, R. and Paulay, T., *"Reinforced Concrete Structures,"* John Wiley & Sons, New York, 1975.

Paulay, T. and Priestley, M. J. N., *"Seismic Design of Reinforced Concrete and Masonry Buildings,"* John Wiley & Sons, Inc., New York, 1992.

Priestley M. J. N., and Park, R., *"Strength and Ductility of Concrete Bridge Columns under Seismic Loading,"* ACI Structural Journal, January-February 1987, pp. 61-75.

International Conference of Building Officials, *"Uniform Building Code,"* 5360 South Workman Mill Road, Whittier, California 90601, 1997.

Wehbe, N. I., *"Effects of Confinement and Flares on the Seismic Performance of Reinforced Concrete Bridge Columns,"* Ph.D. Dissertation, University of Nevada, Reno, December 1997.

Table 1 Plastic Hinge Lateral Steel Ratios for Rectangular Column Specimens

Specimen	Lateral Steel Ratio, $A_{sh}/(s \cdot h_c)$	
	Long Direction	Short Direction
Group I (Specimens A1 & A2)	0.0037	0.0035
Group II (Specimens B1 & B2)	0.0048	0.0046

Table 2 Measured Material Properties for Rectangular Column Specimens

Specimen	Concrete f'_c MPa (Ksi)	Longitudinal Steel				Lateral Steel			
		ϵ_y	f_y, MPa (Ksi)	ϵ_u	f_u, MPa (Ksi)	ϵ_y	f_y, MPa (Ksi)	ϵ_u	f_u, MPa (Ksi)
A1 & A2	27.2 (3.95)	0.0022	448 (65)	0.110	731 (106)	0.0023	455 (66)	0.160	676 (98)
B1 & B2	28.1 (4.08)	0.0022	448 (65)	0.110	731 (106)	0.0023	455 (66)	0.160	676 (98)

Table 3 Lateral Steel Ratio for Flared Column Specimens

Distance to Top of Footing	Lateral Ties Ratio	
	Long Direction	Short Direction
0 mm (0 in.)	0.00412	0.00269
127 mm (5 in.)	0.00412	0.00289
254 mm (10 in.)	0.00411	0.00310
381 mm (15 in.)	0.00410	0.00333
737 mm (29 in.)	0.00409	0.00302
1092 mm (43 in.)	0.00409	0.00356
1295 mm (51 in.)	0.00409	0.00385
1499 mm (59 in.)	0.00410	0.00409
1702 mm (67 in.)	0.00410	0.00425
2007 mm (79 in.)	0.00410	0.00433

Table 4 Measured Material Properties for Flared Column Specimens

Specimen	Concrete f'_c MPa (Ksi)	Longitudinal Steel				Lateral Steel			
		ϵ_y	f_y, MPa (Ksi)	ϵ_u	f_u, MPa (Ksi)	ϵ_y	f_y, MPa (Ksi)	ϵ_u	f_u, MPa (Ksi)
LS & HS	51.7 (7.50)	0.0022	438 (63.5)	0.150	710 (103)	0.0023	455 (66)	0.160	676 (98)

Table 5 Measured and Calculated Displacements at Yield and Ultimate

Specimen	Measured Displacements				Calculated Displacements			
	Δ_y, mm (in)	Δ_u, mm (in.)	μ_Δ	Drift Ratio %	Δ_y, mm (in)	Δ_u, mm (in.)	μ_Δ	Drift Ratio %
A1	23 (0.92)	121 (4.76)	5.3	5.2	21 (0.84)	141 (5.54)	6.6	6.0
A2	19 (0.75)	100 (3.93)	5.2	4.3	19 (0.73)	90 (3.56)	4.9	3.9
B1	24 (0.94)	161 (6.32)	6.7	6.9	22 (0.85)	173 (6.80)	8.0	7.4
B2	20 (0.79)	123 (4.83)	6.1	5.3	19 (0.73)	112 (4.40)	6.0	4.8
LS	23 (0.89)	173 (6.80)	7.6	7.1	23 (0.90)	151 (5.95)	6.7	6.2
HS	27 (1.05)	159 (6.27)	6.0	6.6	26 (1.04)	136 (5.37)	5.2	5.6

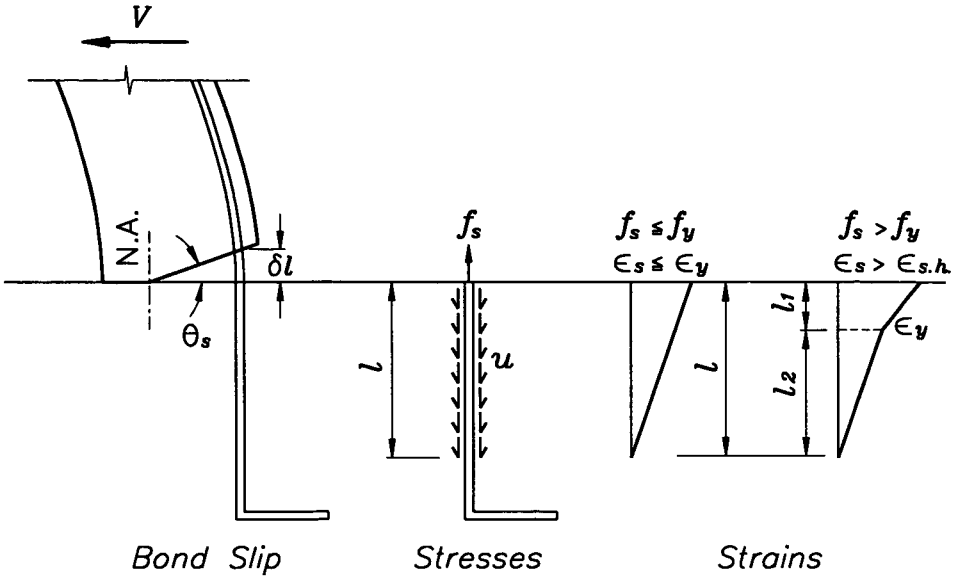


Figure 1 Bond Slip of Developed Bars

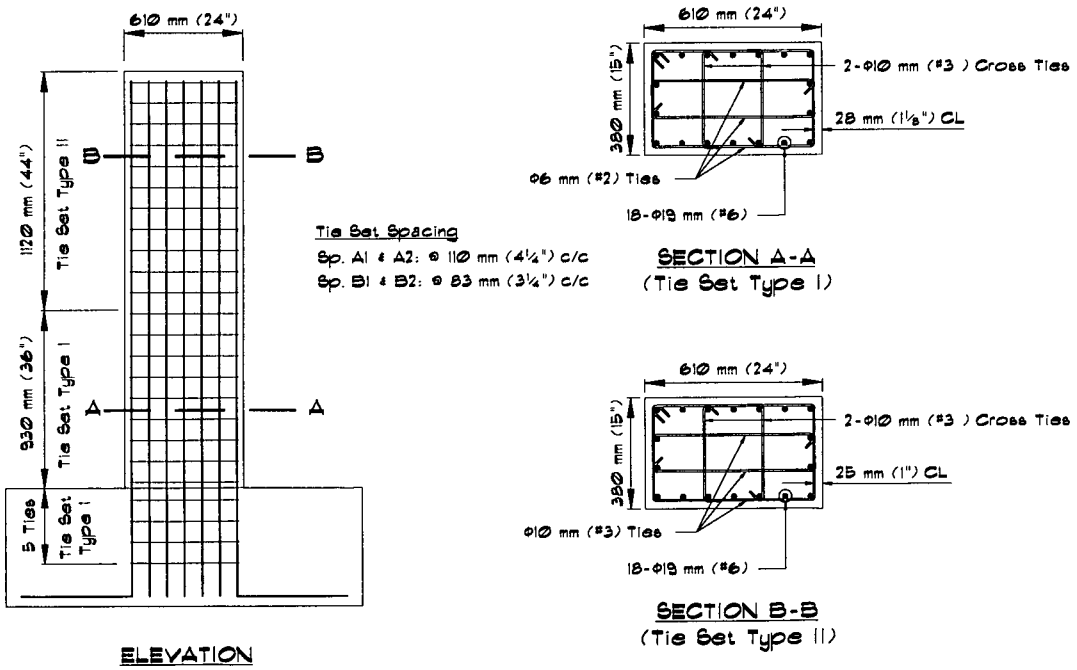


Figure 2 Column Details for Rectangular Column Specimens

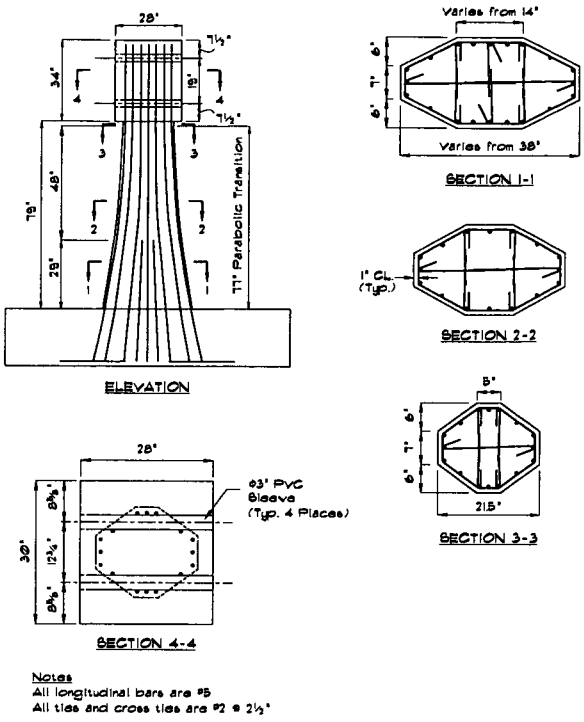


Figure 3 Column Details for Specimen LS

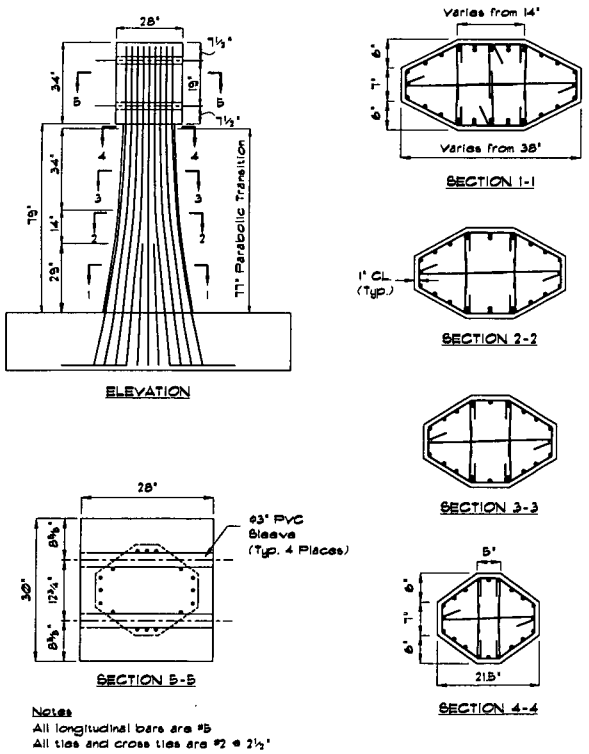


Figure 4 Column Details for Specimen HS

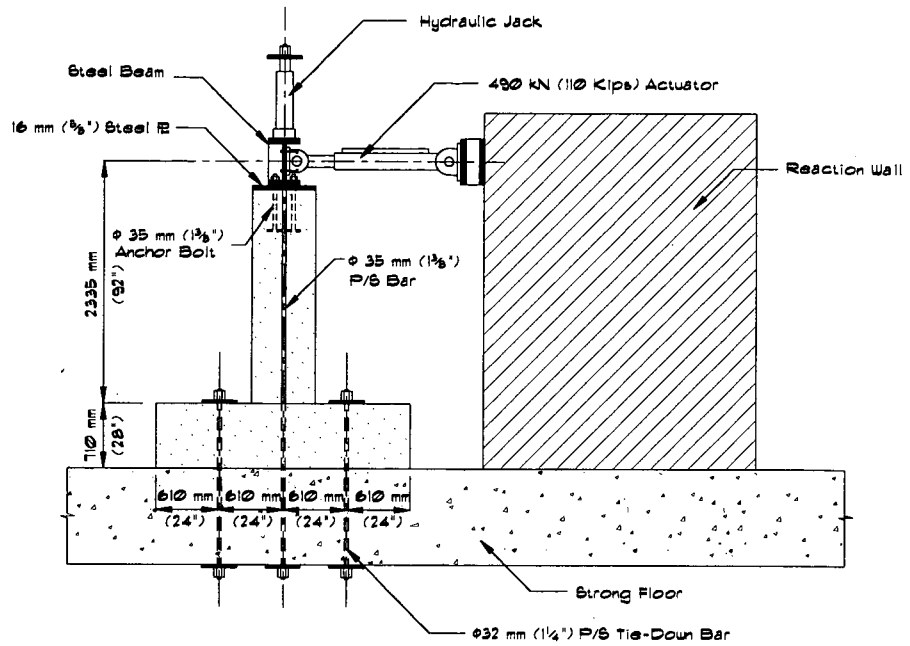


Figure 5 Test Setup for Rectangular Columns

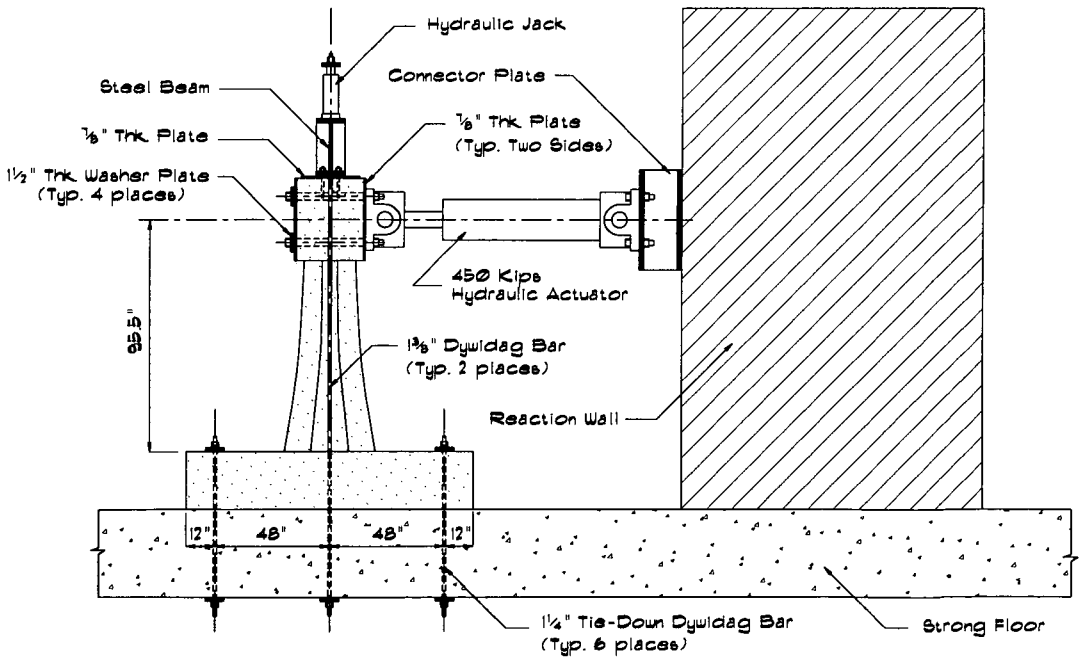
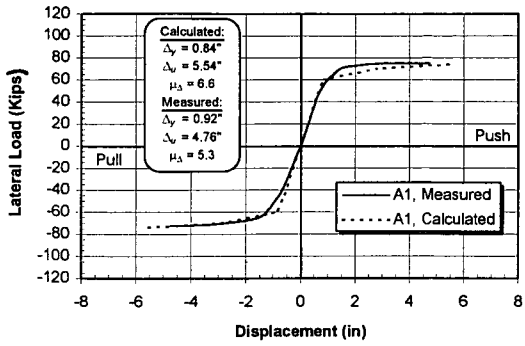
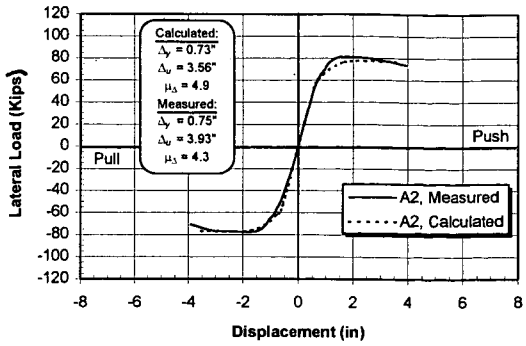


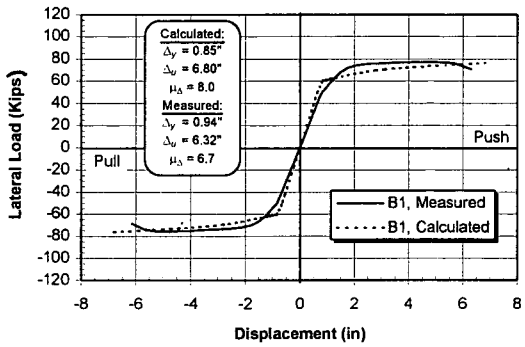
Figure 6 Test Setup for Flared Columns



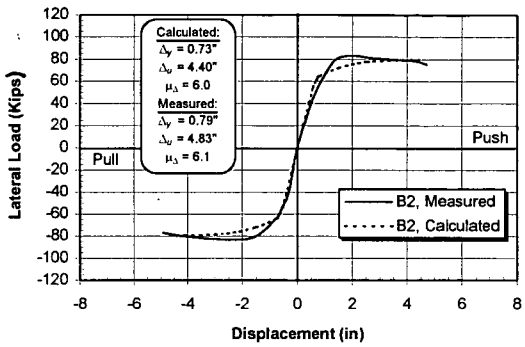
(a) Specimen A1



(b) Specimen A2

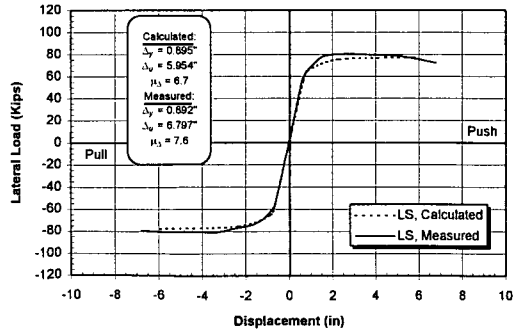


(c) Specimen B1

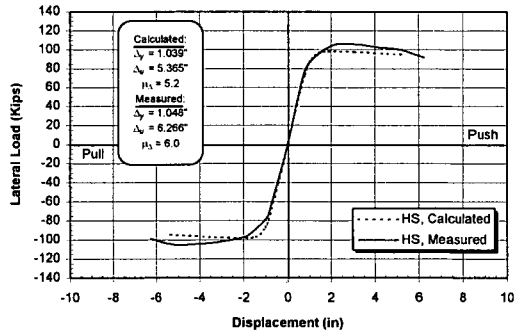


(d) Specimen B2

Figure 7 Measured and Calculated Lateral Load-Deflection Envelopes for Rectangular Column Specimens



(a) Specimen LS



(b) Specimen HS

Figure 8 Measured and Calculated Lateral Load-Deflection Envelopes for Flared Column Specimens

Damping Characteristics of a Long-Span Suspension Bridge Identified by Strong-motion Data

Yukio ADACHI*, Shigeki UNJOH**

*Senior research engineer,
Earthquake Engineering Division, Public Works Research Institute, MOC
**Head, ditto

ABSTRUCT

There is uncertainty in damping characteristics when making seismic resistant designing of long-span bridges. In general, damping ratio of 2% has been employed for seismic design of long-span bridges. However, smaller damping characteristics had been observed according to the results of vibration test of suspension bridges. A well-instrumented suspension bridge in Los Angels was shaken by two major earthquakes, the 1987 Whittier earthquake and the 1994 Northridge earthquake, which generated the most comprehensive data on not only the seismic response of the super structure but also support excitation. Using these precious data, system identification was conducted to study damping characteristics of this bridge. As the result of this study, Identified damping ratios were generally around 2% or more. Smaller damping values were also found in some modes.

INTRODUCTION

Long-span bridges are relatively flexible structures and have generally small damping characteristics. There is uncertainty in damping characteristics when making seismic design of long-span bridges. In general, damping ratio of 2% has been employed for seismic design. However, smaller damping ratio had been observed according to the results of vibration test of suspension bridges. The damping characteristics of long-span bridges are significantly affects the seismic response of super structures and force transmitted to substructures from super structures. Therefore identification of the damping characteristics of long-span bridges is needed to minimize the difference between the design seismic response and the actual response. In this paper, analytical studies were conducted on the damping characteristics of a long-span suspension bridge using measured earthquake data. The suspension bridge named "The Vincent Thomas bridge" which was located southwest of Los Angels, California, was shaken by two major earthquake, the Oct 1, 1987 Whittier Earthquake and the Jan 17, Northridge Earthquake. The main shocks generated the most comprehensive sets of data on not only the seismic response of the super structure but also support excitation. Therefore, the study on the damping characteristics was carried out using these sets of data. The analytical methods for estimating the damping ratio of long-span suspension bridges using measured data have not yet been firmly established. In this study, the following methods were employed for identifying the damping characteristics: the half-power method applying to the power spectrum or the transfer function spectrum of measured acceleration data, free-vibration decay method, and estimating

damping ratio which gave better agreement with measured response in the earthquake response analysis in terms of peak acceleration and displacement.

THE VINCENT-THOMAS BRIDGE AND ITS OBSERVED DATA

The Vincent-Thomas suspension bridge was located southwest of Los-Angels, California. This was a toll bridge which connected the Terminal island and California state road 47. Figure 1 shows the general feature of this bridge. The center, side, and total length of this bridge are 457m, 154m, and 766m respectively. The bridge was designed in 1959, and completed the construction in 1964. The suspended structure consists of two stiffening trusses, floor trusses and lower chords. The deck is 15.6m (4 lanes) wide and made from non-composite concrete slab. The each main steel tower was connected at 5 locations at mid height by lateral beams. 26 accelerometers were instrumented at the stiffening trusses, the towers, the tower bases, and the ground as shown in Figure 2.

This bridge had suffered two major earthquake: the Whittier earthquake and the Northridge earthquake. Those acceleration data were very important and very precious to study the damping characteristics and seismic response behavior of long-span bridges. Figure 3 shows the location of the Vincent-Thomas bridge and the epicenters of the both earthquakes. The measured peak acceleration data and displacement of which was calculated by integrating measured acceleration at major points are shown in the Table 1 and also Figure 4.

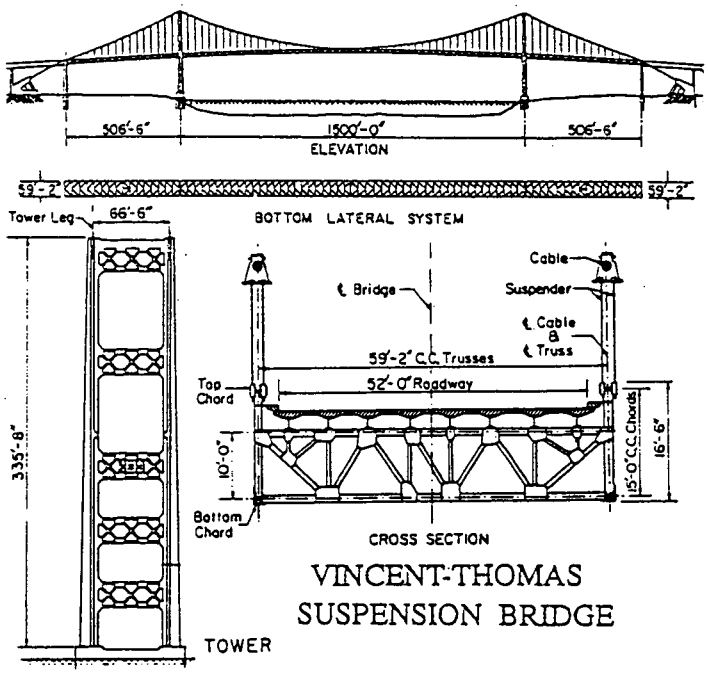


Figure 1 The Vincent-Thomas bridge[2)]

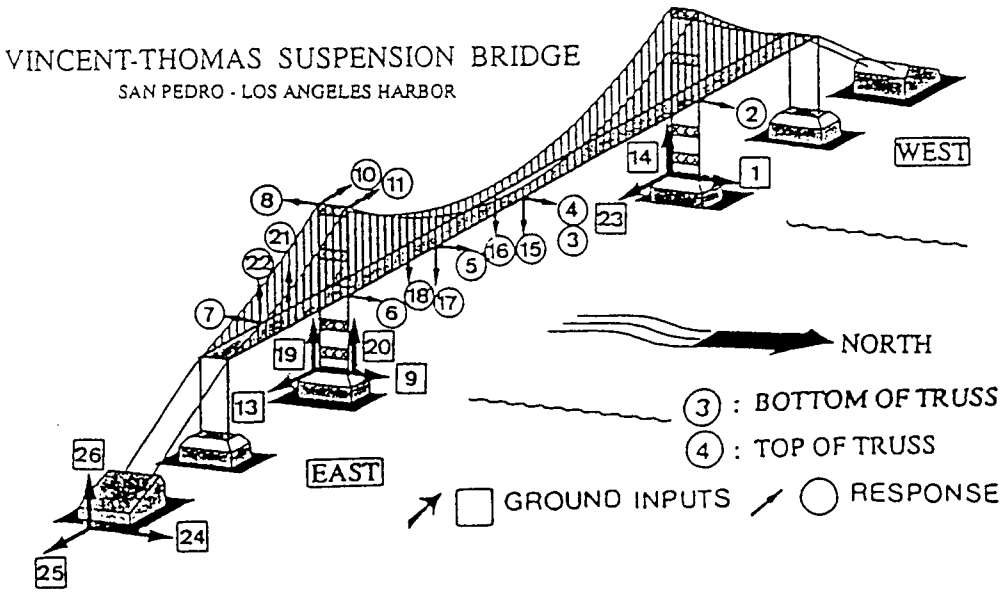


Figure 2 Instrumentation of the Vincent-Thomas bridge[5)]

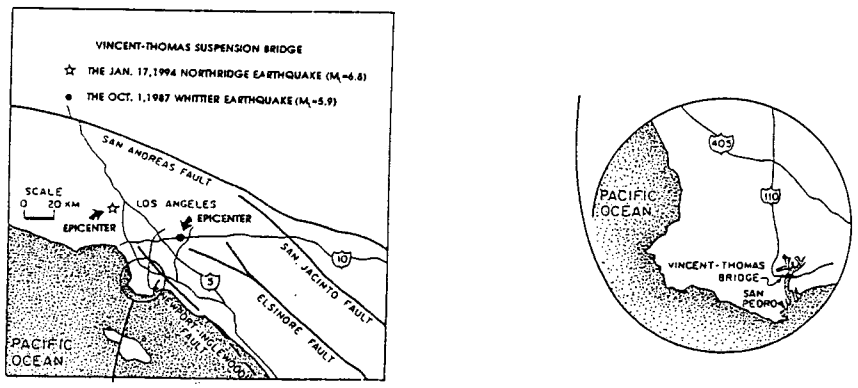


Figure-3 Location of the Vincent-Thomas bridge[5)]

Table-1 The maximum displacement amplitude at the major measuring locations

	Whittier earthquake	Northridge earthquake
The center of the center span (Transverse direction)	4.6 (0.00010)#	4.5 (0.00010)#
The center of the center span (Vertical direction)	5.8 (0.00013)#	17.7 (0.00039)#
The center of the side span (Transverse direction)	3.3 (0.00007)#	4.7 (0.00010)#
The center of the side span (Vertical direction)	8.7 (0.00019)#	20.6 (0.00045)#
The top of the tower (Longitudinal direction)	2.8 (0.00006)#	4.8 (0.00011)#
The top of the tower (Transverse direction)	3.1 (0.00007)#	4.4 (0.00010)#

UNIT: cm, # (The maximum displacement) / (The center span length=457m)

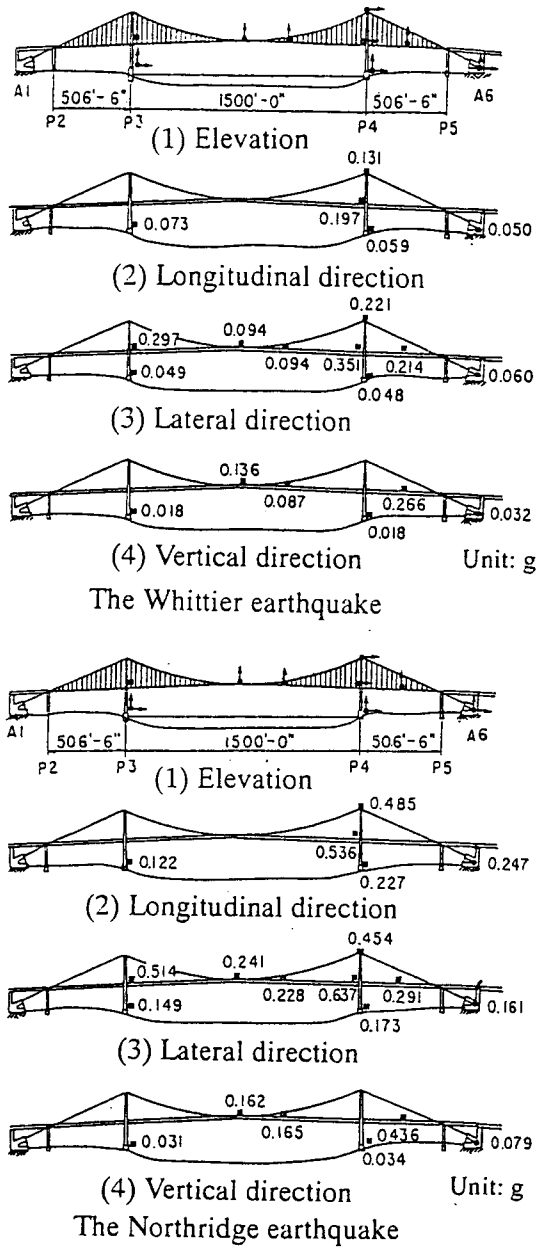


Figure-4 The maximum observed acceleration data

Figure-5 (1), (2), (3) shows the measured acceleration and displacement, which is produced by integrating the acceleration, at major points of the Northridge earthquake. The vibration characteristics of this bridge can be summarized as follows:

1) Longitudinal direction

The measured maximum acceleration at the tower base was around 0.23g. The acceleration was amplified by 2.4 times at the deck and 2.1 times at the top of the tower. The observed acceleration was greater at the deck level than that at the top. The cables restrained the tower top displacement in the longitudinal direction so that the mode that amplified the deck level of the tower was dominant.

2) Transverse direction

The measured maximum acceleration at the base was around 0.17g. The acceleration was amplified by 3.6 times at the deck level and 2.6 times at the top of the tower. As seen in the longitudinal direction, the measured acceleration was greater at the deck level of the tower than at the top. The maximum acceleration at the center of the center span of the stiffening truss girder was 0.241g. The maximum acceleration at the center of the side span was 0.291g. Those acceleration data were amplified by 1.4-1.7 times compared to the those data at the tower base. Some impact pulse can be observed in the time history of acceleration data at the deck. This might be results of Impacts between the tower and the girder.

3) Vertical direction

The measured maximum acceleration at the foundation was very small around 0.03-0.08g. The acceleration was amplified to 0.152g at the center of the center span and to 0.417g at the center of the side span. Compared to those at the tower base, the 2-5.2 times of amplifying can be observed, especially at the side span. The natural period of the stiffening truss girder was 5 sec at the center span and the 2 sec at the side span. The principal ground motion was finished around the time of 20 sec but the vertical vibration of the girder still oscillated and had the peak amplitude around 80-90 sec. According to this observation, the damping of the stiffening truss girder can be estimated very small.

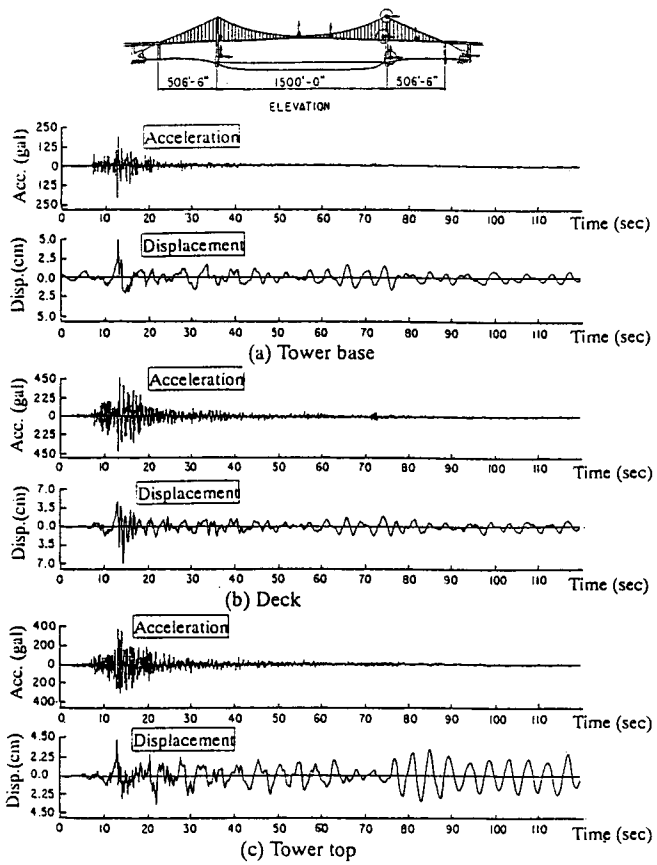


Figure 5 (1) Measured Acceleration data of the Northridge earthquake
Tower, Longitudinal direction

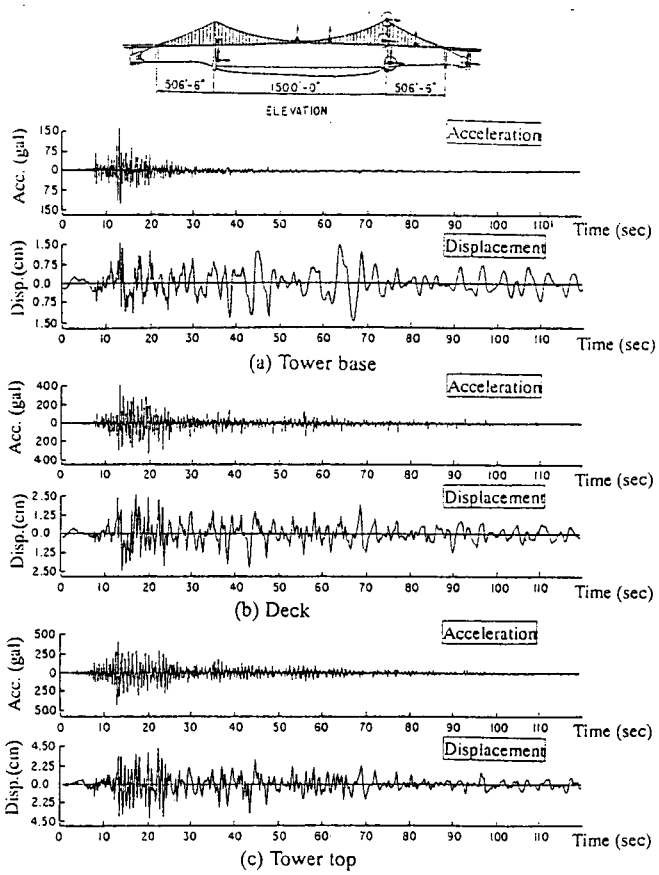


Figure 5 (2) Measured Acceleration data of the Northridge earthquake
Tower, Lateral direction

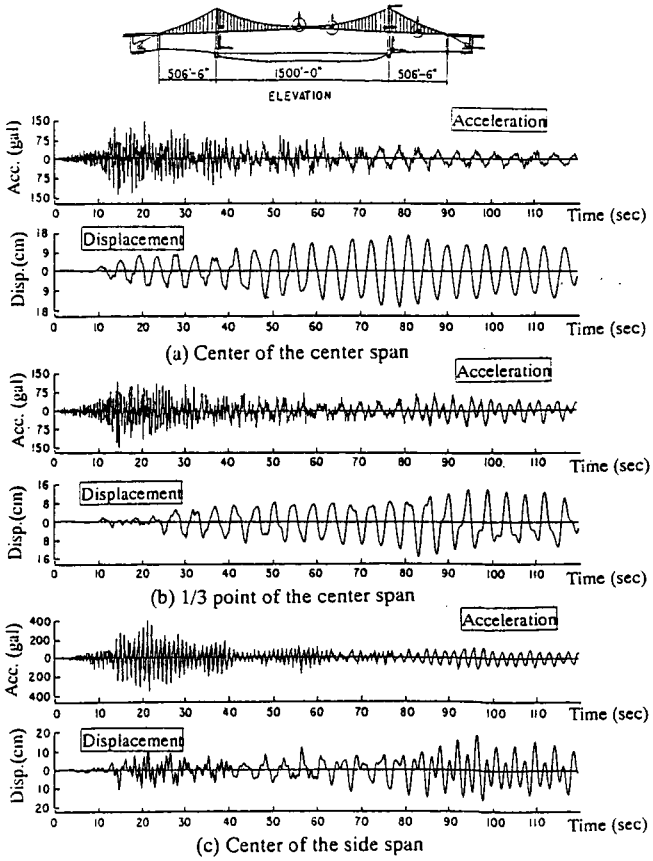


Figure 5 (3) Measured Acceleration data of the Northridge earthquake
The stiffening trusses, Vertical direction

THE DAMPING CHARACTERISTICS IDENTIFICATION BY HALF POWER METHOD

The analytical methods to estimate the damping ratio have not been firmly established. This chapter shows the first try of identifying the damping ratio of each mode using the half power method applied to the measured acceleration data in the frequency domain. In this case, the transfer function and the power spectrum were employed for the identification. The identification of the damping ratio of each vibration mode is very difficult because different damping values are estimated at each location and each mode. Therefore the identification works were carried out for each mode and each measuring point. No smoothing work was conducted for observed data.

The table 2 shows the mean value of the each damping ratio calculated from the power spectrum and the transfer function. According to the identification results from the transfer function of the Northridge earthquake, the identified damping ratios are 1-3 % for the lower vertical vibration mode, 1-4% for the lateral vibration mode, and only 1% for the torsional mode of the girder. According to the results from the power spectrum, smaller damping values were estimated because the power spectrum is the transformed data of the measured acceleration whereas the transfer function is the ratio of the input and output data in the frequency domain. The estimated damping ratios calculated using transfer function from the Northridge earthquake data are 1-4% for the vertical and lateral vibration mode and the damping values are estimated smaller in the lower modes and greater in the higher modes when compared to the result from the Whittier earthquake.

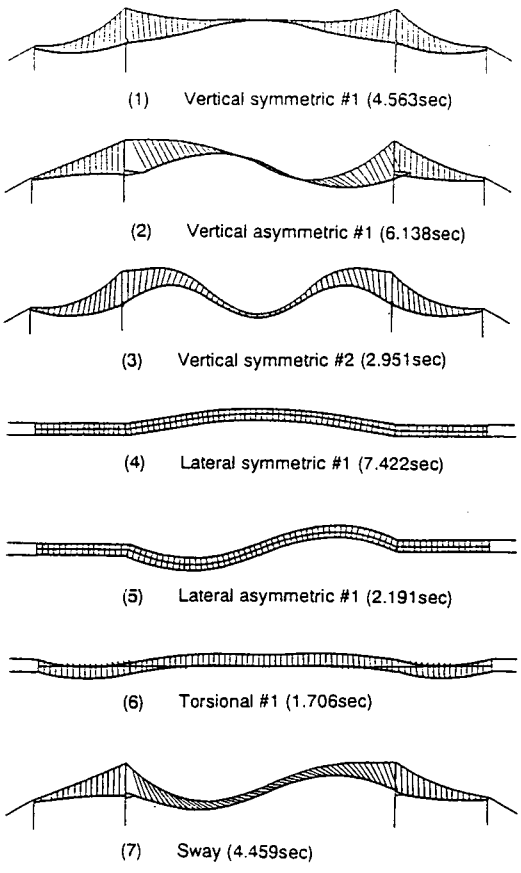


Figure 6 Dominant vibration modes

Table 2 The damping ratios estimated from the observed data

	Power spectrum		Transfer function	
	Frequency(Hz)	Damping ratio	Frequency(Hz)	Damping ratio
Whittier earthquake				
Vertical symmetric #1	0.226	0.053	0.229	0.023
Vertical symmetric #2	0.372	0.028	0.378	0.014
Vertical asymmetric #1	0.183	0.039	0.177	0.014
Lateral symmetric #1	0.134	0.079	0.138	0.042
Lateral asymmetric #1	0.427	0.021	0.421	0.008
Sway	0.232	0.043	0.232	0.048
Torsional #1	0.510	0.019	0.507	0.007
Northridge earthquake				
Vertical symmetric #1	0.226	0.020	0.226	0.019
Vertical symmetric #2	0.342	0.011	0.339	0.022
Vertical asymmetric #1	0.159	0.035	0.165	0.031
Lateral symmetric #1	0.134	0.058	0.140	0.041
Lateral asymmetric #1	0.419	0.017	0.421	0.007
Sway	0.244	0.059	0.238	0.040
Torsional #1	0.530	0.017	0.528	0.007

Figure 7 shows the relation between the Fourier amplitude of each mode and identified damping ratio at the center of the center span in order to study the amplitude dependency of the damping ratio. The difference of the two earthquake expressed as the difference of the Fourier amplitude. The damping ratios of the vertical vibration modes are around 2%. It seems that the damping ratio increases as the Fourier amplitude increases but the smaller damping ratio can be observed when the Fourier amplitude is over 100m•sec. The non-composite concrete deck or friction at the bearings may influence the damping characteristics of this bridge. As concern for the first torsional mode of the girder, the damping ratios are around 1% and show no amplitude dependency. As concern for the lateral vibration mode of the girder, the damping ratios are relatively large but there is no difference of the Fourier amplitude of each earthquake so that amplitude dependency could not be studied. The previous study shows that the smaller damping ratios were identified when analyzing the results of vibration tests of real long-span bridges but in this study, larger damping ratios were identified. However, the damping ratios of some modes were identified below 2% which is now taken for the design of long-span bridges.

THE DAMPING CHARACTERISTICS IDENTIFICATION BY USING EARTHQUAKE RESPONSE ANALYSES

Another identification method of damping characteristics ratios is to search the damping ratio which gives better agreement with measured peak acceleration or displacement data in the earthquake response analyses using a proper bridge model. In order to match the measured peak data and the analyzed data, proper modal damping should be given. However, it was impossible to set the best or the most proper modal damping for each mode so that unique damping ratio, 0,1,2,3,5%, was set to each mode. The identification of the damping ratio was made by comparing the maximum measured acceleration or displacement data and the maximum calculated data.

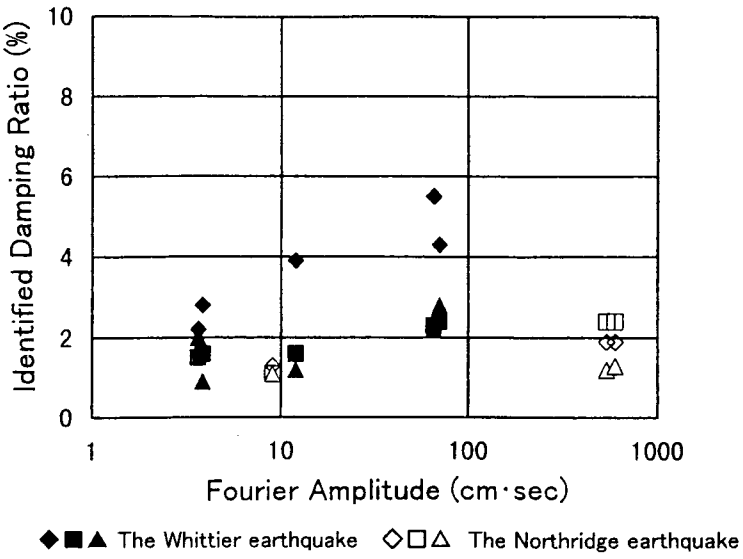


Figure 7(1) Amplitude dependency of the damping ratio (Vertical mode)

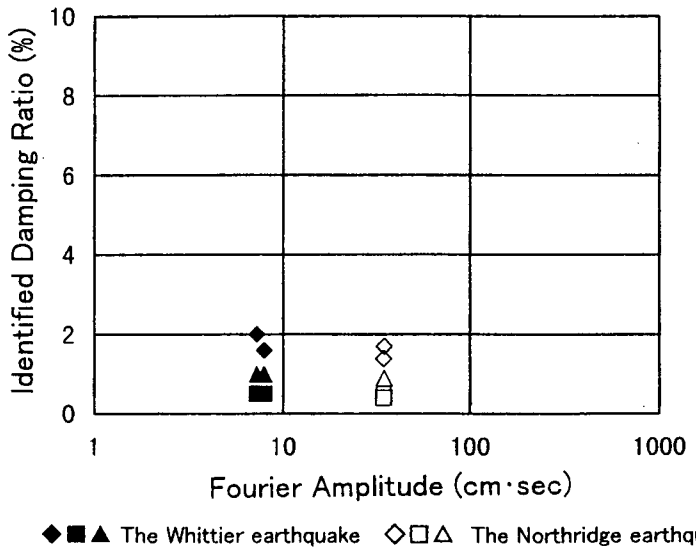


Figure 7(2) Amplitude dependency of the damping ratio (Torsional mode)

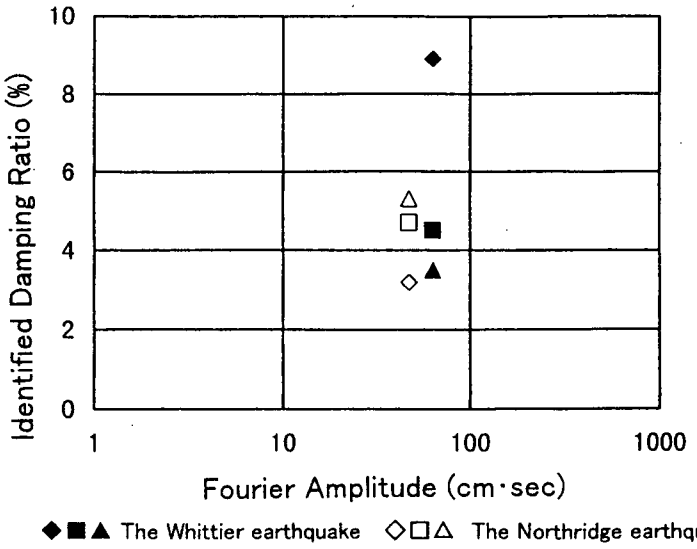


Figure 7(3) Amplitude dependency of the damping ratio (Lateral mode)

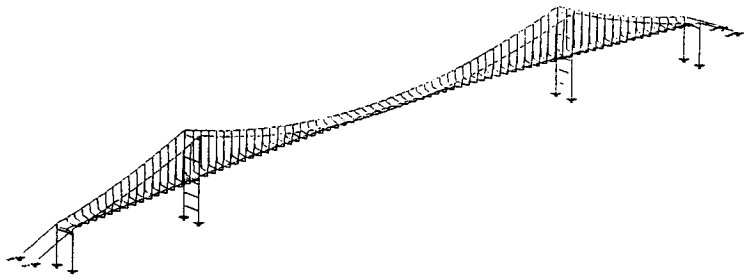
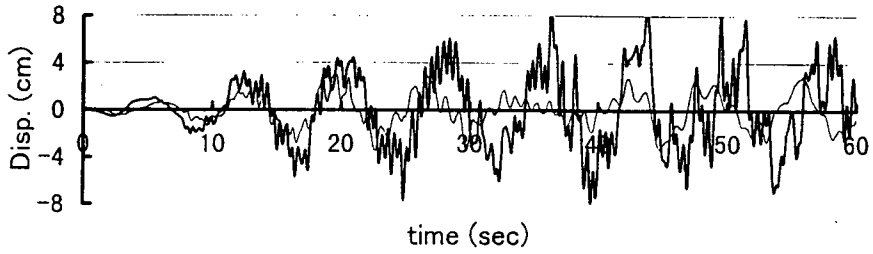
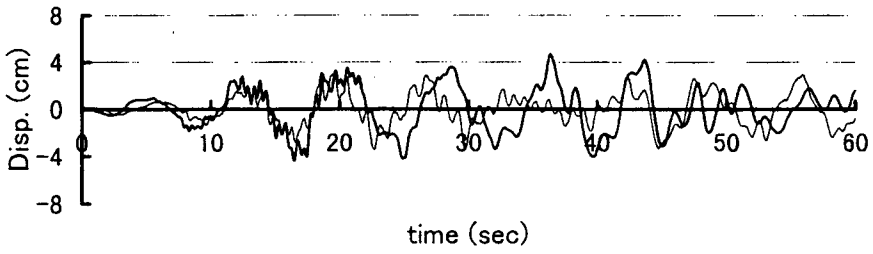


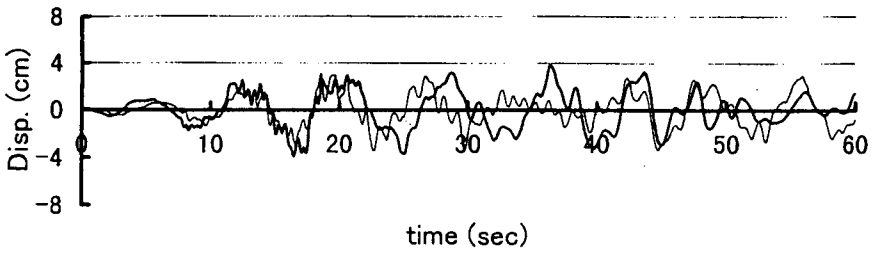
Figure 8 Fish bone model of the Vincent-Thomas bridge



(a) h=0%



(b) h=3%



(c) h=5%

Figure 9 Displacement time history data (Analytical and measured data, Northridge earthquake)

Table 3 Natural period of each mode estimated from the observed data and the mode analysis

	Mode analysis	Whittier earthquake	Northridge earthquake
Girder:			
Lateral symmetric #1	7.422	7.407	7.463
Lateral asymmetric #1	2.191	2.336	2.375
Torsional #1	1.706	1.949	1.883
Vertical asymmetric #1	6.138	5.814	6.289
Vertical symmetric #1	4.563	4.630	4.425
Vertical symmetric #2	2.951	2.732	2.924
Sway	4.459	4.310	4.098
Tower:			
Longitudinal direction	1.162	1.159	1.164
Lateral direction	1.780	1.567	1.742

Unit: sec

The super structure of the bridge was model by a fish bone model as shown in Figure 8. The deck was non-composite concrete slab. It is assumed in this study that 40% of the stiffness contribute the lateral stiffness of the girder. The accuracy of the model was verified by comparing the natural frequencies obtained by the measured data. The natural frequency of the measured data were obtained from the Fourier transform analysis. Table 3 shows the natural period obtained by the measured data and the mode analysis using the fish bone model. According to the table, both periods have quite good agreement so that the accuracy of the model was verified. Using the verified model, a series of time history analyses were conducted by changing the modal damping ratio. The number of the modes that was considered in this study was 1st to 292th mode. The total summed equivalent mass of those modes was 95%.

Figure 9 shows an example of an analytical result comparing the observed data. Figure 8 shows the lateral displacement time history at the center of the center span of the Northridge earthquake and the analytical results by changing the damping ratios. According to this figure, the first lateral vibration mode was dominant and the analytical wave can express the measured data. Compared to the peak measured and analyzed data, the damping ratio can be identified 5% or more. In this way, the damping ratios were identified if the maximum response of each data were agreed each other in terms of acceleration or displacement. Table 4 shows the identified damping ratios estimated using this method. The time history analyses were carried out by changing the damping ratios as 0,1,2,3,5% so that Table 4 shows the nearest damping values or range if the maximum response data do not match the observed ones.

Table 4 The damping ratios identified by time history analysis which gives the same maximum acceleration and displacement as the observed data

	Whittier earthquake		Northridge earthquake	
	Disp.	Acc.	Disp.	Acc.
Lateral Mode				
The center point of the center span	5%~	1%	5%~	3~5%
The 1/3 point of the center span	5%~	1%	5%~	2%
Vertical Mode				
The 1/3 point of the center span	5%~	1~2%	1~2%	3~5%
The center point of the center span	1~2%	1~2%	0~1%	5%~
The tower point of the center span	2%	0%	3~5%	0%
Tower				
Transverse, The top of the tower	2%	0~1%	5%~	5%~
Longitudinal, The top of the tower	5%~	5%	3%	5%~

The followings considerations can be made according to Table 4:

1) The identified damping ratios varied by each data and each earthquake. According to the Identification results using peak displacements, following damping ratios were generally identified: 0-2% for vertical direction of the center span of the girder and 2-5% for other vibration mode and the location.

2) The identification results were different whether using acceleration data or displacement data. One possible reason is that some impulse were found in the measured data so that smaller damping ratio was needed when fitting the maximum response. This assumption is also verified from the fact that the analytical maximum displacements occurs almost at the same time as measured one whereas the analytical maximum accelerations occurs almost at the same time as measured one.

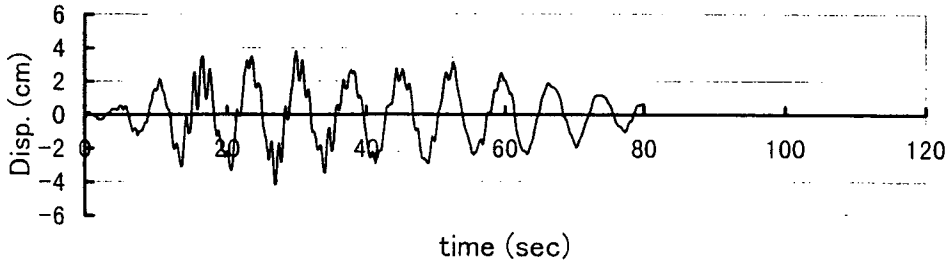
3) Compared to both identified damping ratios, the damping ratios identified from the Northridge earthquake is relatively larger than those from the Whittier earthquake.

DAMPING IDENTIFICATION FROM FREE VIBRATION DECAY

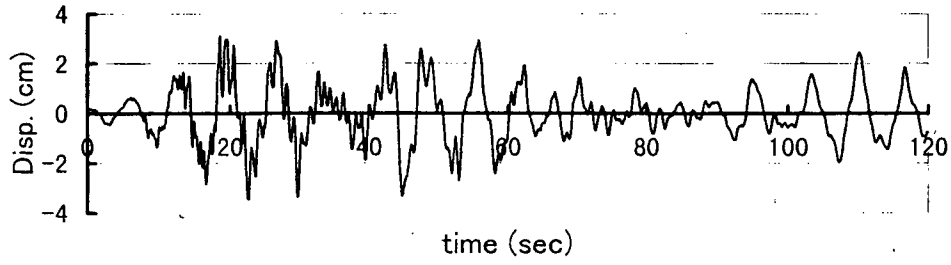
The measured data has long free vibration part after principal excitation so that damping ratio can be identified using the free vibration decays. Figure 10 shows the lateral vibration time history at the center of the center span. According to this figure, it is recognized that the principal excitation was almost ceased 20 second or so but a long free vibration was followed and continued until 80-120 second.

The target frequency component of measured data were extracted by band-pass filtering in the frequency domain and the damping ratio was identified the free vibration decay in the time domain. The filtering width were determined by trial and error basis. The damping identification can be made every measuring point but the data recorded at dominant excitation were employed for this identification work. Figure 10 shows some examples of extracted displacement response of the lateral #1 mode of the stiffening trusses in the time domain. Table 5 shows the list of the identified damping ratios of each vibration mode. Star mark (*) was put if beating was not clearly removed when extracting the target frequency component. According to the results of the Wittier earthquake, the damping ratio of lateral #1 vibration mode was identified as 5.5% but the rest shows smaller values. On the other hand, the larger damping ratio of vertical #1 and sway vibration mode were identified in case of the Northridge earthquake.

The identified damping values using free vibration decay are relatively small compared to the result of other estimation methods. Moreover, the identified damping ratios were less than 2% in most of the vibration modes

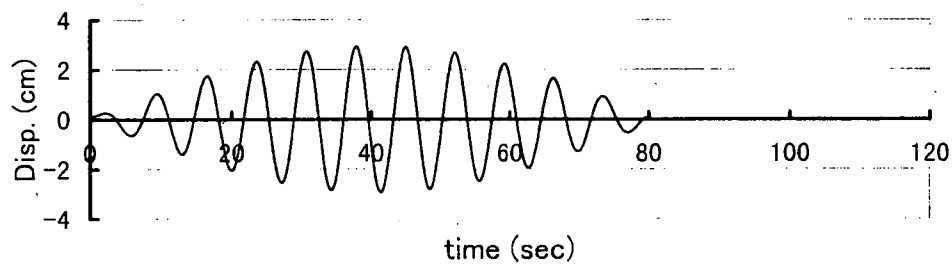


(a) Whittier earthquake

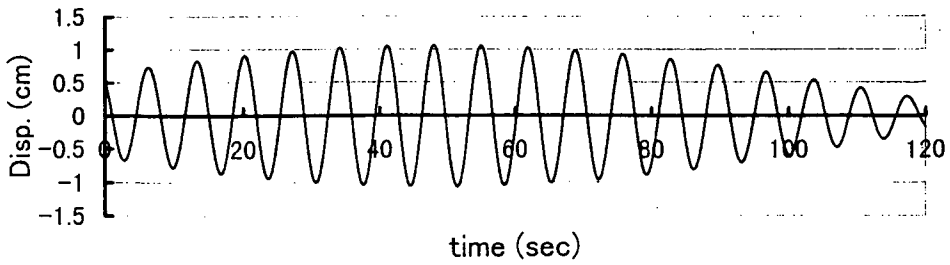


(b) Northridge earthquake

Figure 10 Measured displacement time history at the center of the center span in the lateral direction



(c) Whittier earthquake



(d) Northridge earthquake

Figure 11 Extracted displacement time history of the target frequency of lateral #1 vibration mode at the center of the center span in the lateral direction

Table 5 The damping ratios identified by free vibration decay

		Whittier earthquake	Northridge earthquake
Girder:			
Lateral symmetric #1	Center of the center span	5.5%	2.6%
Lateral asymmetric #1	1/3 point of the center span	1.4%	1.4%
Torsional #1	Center of the center span	0.8%	0.9%
Vertical asymmetric #1	1/3 point of the center span	1.4%*	0.9%
Vertical symmetric #1	Center of the center span	1.5%*	2.9%
Vertical symmetric #2	Center of the center span	2.0%*	0.6%
Sway	Tower point	1.7%	3.4%
Tower:			
Longitudinal direction	Top of the tower	0.7%	1.6%
Lateral direction	Top of the tower	0.3%	0.6%

SUMMERY

Using the measured response data obtained at the Vincent-Thomas bridge, damping identification was carried out to study the damping characteristics of long-span bridges. Identification tools of damping ratios were the following methods: the half-power method applying to the power spectrum or the transfer function spectrum of measured acceleration data, free-vibration decay method, and estimating damping ratio which gave better agreement with measured response in the earthquake response analysis in terms of peak acceleration and displacement.

Following results can be summarized in this study.

1.The damping identified from the three method shown in this paper are varied. The identification results using free vibration decay after the cease of the principal ground motion is considered to yield the most reliable estimation. The results of this method show that the identified damping ratios are 0.3-5.5% but the values vary by each location and each mode. Comparing the all results each other by vibration direction, the damping ratios of the higher vibration modes seem to have higher values comparing to those of lower vibration modes.

2. The damping ratios of vertical modes show amplitude dependency but the tendency is not clear. No other amplitude dependency except vertical modes can be clearly recognized in this study.

3. The identified damping ratios are generally 1-5% even though the values vary by each data and each earthquake. These values verified that the damping ratio of 2% which is now practically used is reasonable. However this study also shows that smaller or larger damping ratios are identified in some modes such as some vertical and torsional modes of the girder, and the longitudinal mode of the tower so that careful considerations are needed in this point.

ACKNOWLEDGEMENT

The authors acknowledge Dr. Mark Yashinsky, California Department of Transportation, and Dr. Bob Darraugh, California Department of Conservation, to kindly help to obtain the strong-motion data of the Vincent-Thomas bridge.

REFERENCES

1) Kawashima, Ohtsuka, and Unjoh: Dynamic behavior and damping characteristics of long-span bridge according to shaking tests of real bridges, Civil engineering journal, Vol.37, No.3, 1995.3

2) Abdel-Gaffar, et al: An Analysis of the Dynamic Characteristics of a Suspension Bridge by Ambient Vibration Measurements, EERL Report, No.77-01 CALTECH, 1977

3) Abdel-Gaffar, et al: Ambient Vibration Tests of Suspension Bridge, J of the Engineering Mechanics Division, Proc. of ASCE, Vol.104, No.EM5, Oct. 1978

4) Abdel-Gaffar, et al: Seismic Performance Evaluation of Suspension Bridge, Proc. of 10th WCEE, Madrid, Spain, July, 1992

5) Abdel-Gaffar, et al: Seismic Behavior of Cable-Stayed and Suspension Bridges, Ponts Suspendus Et AHaubans, Cable-Stayed and Suspension Bridges, Deauville, France, 12-15 Oct. 1994

6) California Department of Conservation: CSMIP Strong-Motion Records from the Northridge, California Earthquake of 17 January 1994, Report No. OSMS94-07, Feb.18, 1994

7) California Department of Conservation: Processed CSMIP Strong-Motion Records for the Los Angels from the Whittier, California Earthquake of 1 October 1987: Vincent Thomas Bridge, Report No. OSMS-/NA, 3/30/1989

8) California Department of Conservation: Processed CSMIP Strong-Motion Records for the Los Angels from the Northridge Earthquake of 17 January1994: Vincent Thomas Bridge, Report No. OSMS 95-01S, 6/1/1995

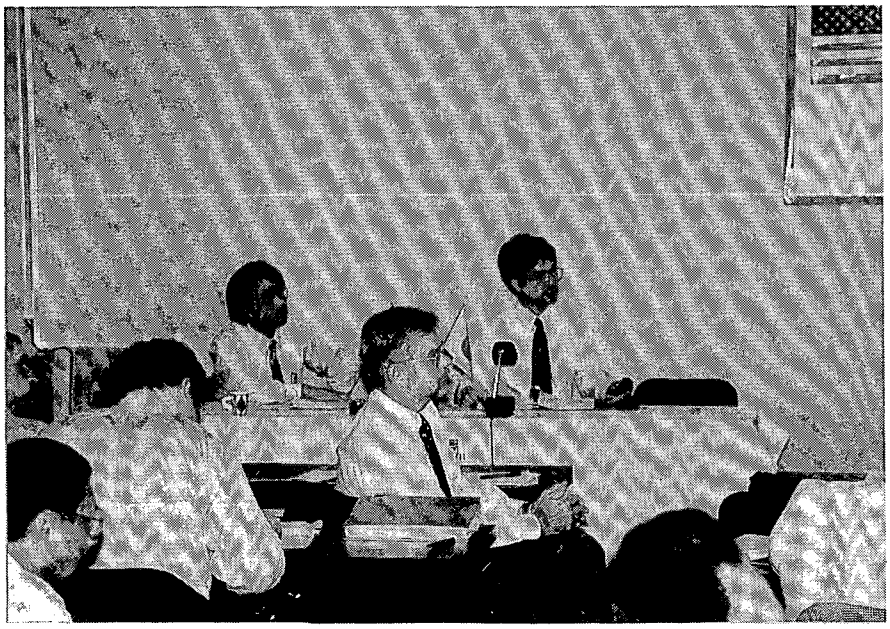
SESSION 5: SEISMIC ISSUES (4)

(1) Ductility Improvement of Steel Bridge Columns Based on Large-Scale Cyclic Loading Tests
(K. Nishikawa, J. Murakoshi, Y. Josen and M. Takahashi)

(2) Lap Splice and Shear Enhancements in Composite-Jacketed Bridge Columns
(Medhat A. Haroun and Maria Q. Feng)

(3) Experimental Studies on Ductility Properties of Steel Rectangular Piers
(H. Hanno, H. Tajima and K. funamoto)

(4) A Comparative Study of Elastic-Plastic Seismic Response Analysis and Pseudo-Dynamic Testing of Steel Bridge Piers
(T. Takaku, S. Ikeda, T. Okamoto, H. Matsuda, H. Noto and Y. Kawai)



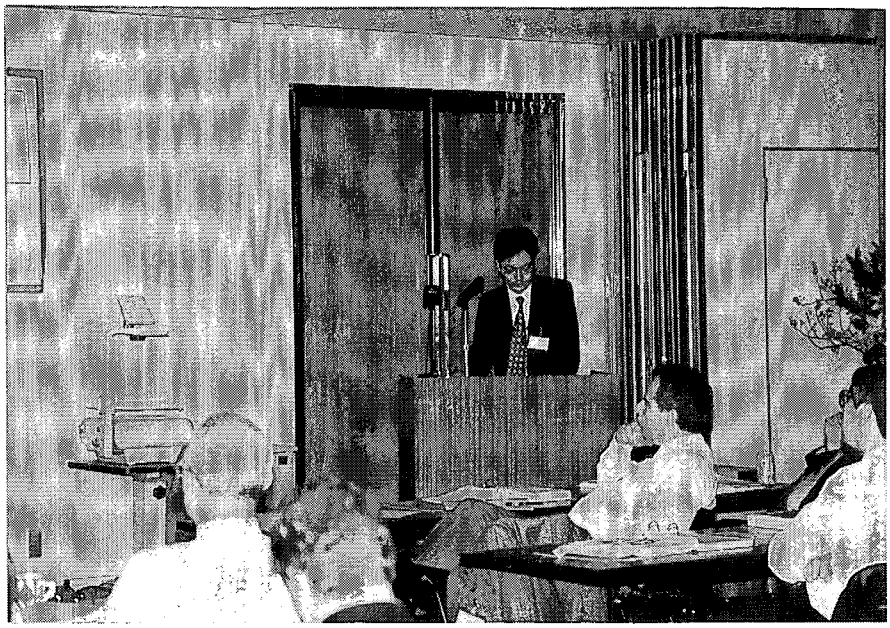
Co-Chairmen : Shigeki Unjoh, Yan Xiao



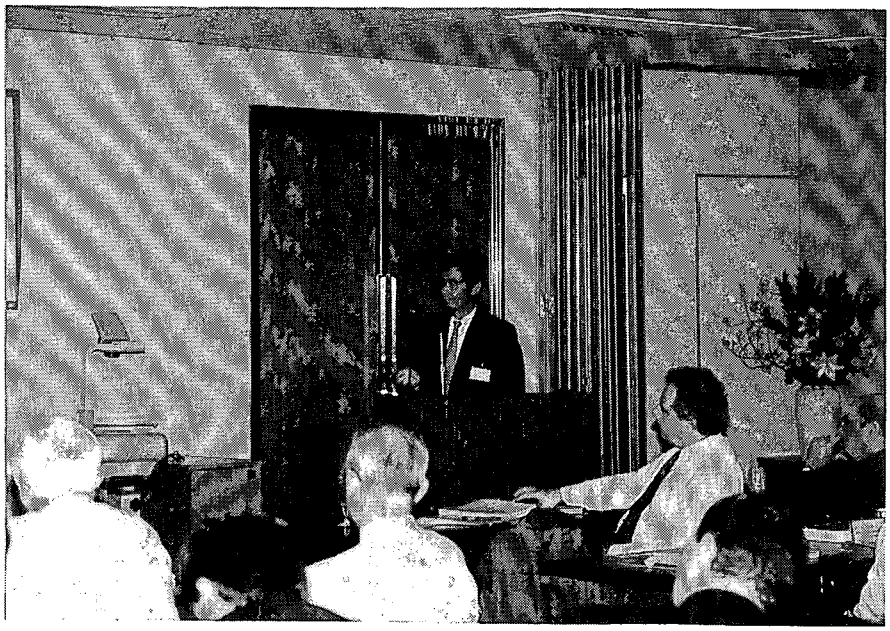
SESSION 5 : Jun Murakoshi



SESSION 5 : Medhat Haroun



SESSION 5 : Hitoshi Tajima



SESSION 5 : Tatsumasa Takaku

DUCTILITY IMPROVEMENT OF STEEL BRIDGE COLUMNS BASED ON LARGE-SCALE CYCLIC LOADING TESTS

Kazuhiro Nishikawa
Head, Bridge Division, Public Works Research Institute, Ministry of Construction
Jun Murakoshi
Senior Research Engineer, Ditto
Yasushi Josen
Research Engineer, Ditto
Minoru Takahashi
Assistant Research Engineer, Ditto

ABSTRACT

This paper deals with methods of seismic retrofit for existing steel bridge columns. Based on the investigation of damaged steel columns, authors identify the failure modes which should be avoided to prevent steel columns from failure, and propose retrofit methods of steel bridge columns. In order to investigate the effectiveness of proposed retrofit methods, cyclic loading tests were carried out on rectangular specimens with section of 900mm×900mm and circular specimens with diameter of 900mm. Test results indicate the effectiveness for rectangular columns to strengthen corners by corner plates and for circular columns to build outer pipe around the existing column with a small clearance.

INTRODUCTION

Steel bridge columns are widely used in the urban area in Japan, since the sections of them are smalller than those of reinforced concrete columns. In the Hyogo-ken Nanbu earthquake, there were examples of buckling of stiffened plates or fracture of welding. The damage includes of collapse of two steel columns. After the earthquake, the "Guide Specifications for Reconstruction and Repair of Highway Bridges Which Suffered Damage due to the Hyogo-ken Nanbu Earthquake"[1] was issued by the Ministry of Construction on February 27, 1995. In this specifications, it was specified that dynamic strength and ductility shall be assured not only for concrete colimns but also for steel columns and it was decided to tentatively use steel columns with infilled concrete for reconstruction and repair. This approach of concrete infill is certainly one of the most effective and practical methods to improve the ductility of steel columns, however, one of the demerits is that it also increase the flexural capacity greatly and weight of columns, which will be imposed on anchors and foundations. Most of steel columns are used in the urban area in Japan, so that retrofit work including anchors must be difficult to do from the point of view of constructibility and economy.

Considering these restriction, PWRI started a joint research with Metropolitan Expressway Public Corporation, Hanshin Expressway Public Corporation, Japan Association of Steel Bridge Construction and The Kozai(steel material) Club in order to develop methods to strengthen both existing and newly constructed steel bridge columns. In this research, more than 70 large scale specimens, which are about one-third scale models of actual bridge columns, have been tested under a constant compressive axial load and cyclic horizontal load during 1995 and 1996. This

paper deals with a part of the research mainly conducted by PWRI for developing seismic retrofit methods of existing steel bridge columns. Authors briefly show the damage of steel columns by the Hyogo-ken Nanbu Earthquake, identifies failure modes which should be avoided to prevent piers from failure according to the features of the damages, propose retrofit methods of steel columns and describe the effectiveness of proposed methods from the results of cyclic loading tests.

DAMAGE OF STEEL COLUMNS AND BASIC CONCEPTS OF SEISMIC RETROFIT

Outline of the Damage of Steel Bridge Columns

The earthquake caused damage to elevated highway bridges on National Highway Route(NHR) 2, 43 and 171, the Meishin Expressway(JHM), Chugoku Expressway(JHC), and the Route 3 Kobe Highway and Route 5 Harbor Highway of the Hanshin Expressway(HER3 and HER5). Among these bridges, the number of steel columns inspected was 355. Damage were classified into 5 classes from As to class D for steel bridge. **Table 1** shows the damage definition of steel columns. Class A is categorized for falling off or collapse, A is major damage , B is moderate damage, C is minor damage and D is very slight or no damage. **Table 2** shows the number and the percentage of damaged columns by class. Among them, the percentage of the steel columns judged to be class B or higher are about 14%. Two rectangular columns were crushed in compression due to the rupture of the welding at the corners.

Fig. 1(a) shows an example of local buckling in the bottom of a rectangular column. Many stiffened plates in columns with rectangular section buckled and out-of-plane deformation occurred in the bottom or the mid height of the columns. **Fig. 1(b)** shows the collapse of the rectangular column of HER3. This pier have T-shaped steel frame supported by two reinforced concrete columns. It was estimated four stiffened plates composing rectangular section of the column failured from the corner along the weld lines after the local buckling of the stiffened plates at the bottom of the columns. In case of pipe columns, **Fig. 1(c)** shows a typical elephant foot buckling. **Fig. 1(d)** shows the cracking along the circumference after progress of deformation. **Fig. 1(e)** is another damage of pipe columns in HER3. The residual displacement is remarkable in this columns.

Failure Modes

As a result of detail survey of the damaged steel columns, it was clear that occurrence of local buckling, which was supposed as an ultimate state of steel columns in the previous Japanese design code, is not always an actual ultimate limit state and that it is essential to avoid the failure mode which causes sudden decrease of flexural capacity or unstable state and to increase the ductility after the buckling. From the deformation and fracture patterns of steel columns damaged in the earthquake, the failure modes which should be avoided, can be identified as follows (see **Fig. 2**) :

(1) Rectangular columns

For rectangular section, it can be proposed that breaking of corners or buckling of corners should be failure modes. Such failure mode was observed in the two columns which completely collapsed in the Hyogo-ken Nanbu earthquake. Actually, it is known that corners

have a higher buckling strength than other parts. If the breaking of corners occurs, it can cause sudden decrease of flexural capacity after the maximum horizontal load, and ductility can't be expected. Fig. 3 shows an example of breaking of corners of a specimen after the cyclic loading test. Since the specimen was filled with concrete at a certain height, breaking of corners are likely to occur. It was observed that the specimen rapidly lost flexural capacity as soon as the corners started to partially break with the progress of the local buckling of stiffened plates. This failure mode is similar to shear failure of concrete piers, therefore it is important to avoid this kind of failure mode.

(2) Circular columns

In the Hyogo-ken Nanbu earthquake, local deformation due to buckling of circular columns was observed at the limited portion of the pipe for the vertical direction, therefore progress of deformation resulted in the large residual displacement, or cracking along the circumference, which are considered unstable state for supporting superstructure. Such large residual displacement and/or cracking due to buckling should be considered as a failure mode.

Above identification of failure modes focuses on the deformation and accompanying fracture patterns of steel bridge columns. There were examples of the breaking and cracking of steel members, probably due to brittle fracture or low-cycle fatigue, reported as other types of damage to steel bridge piers in the Earthquake. How to evaluate such damage patterns and how to cope with them are also important, however, this paper does not discuss such failures because they are considered exceptional cases.

Basic Concepts of Seismic Retrofit

The general countermeasures presented in the previous studies[4],[5] for improving the seismic performance of steel bridge columns are as follows:

1) To improve structural parameters related to buckling strength.
   (To decrease the width-thickness ratio of stiffened plates or the diameter-wall thickness ratio of steel pipes, to increase the stiffness of stiffeners, or reduce the diaphragm spacing.)
2) To fill steel columns with concrete, or to combine the steel columns with concrete into composite structures.

The former method aims at preventing the local buckling of steel bridge piers and improving the ductility, and consequently increase the ductility and the flexural capacity at the same time. However, considering features of the damage as mentioned above, there is no need to stick to these conventional countermeasures, and other ideas can be proposed. The latter method is one of the most effective and easiest methods to enhance both strength and ductility from the previous studies and our experiments. This approach has been used on many steel columns for the reconstruction and repair of damaged highway bridges by the earthquake. However, most of the existing steel columns are located in the urban area in Japan, such that concrete filling method is not a good solution since the retrofit work of anchors may be needed. Fig. 4 illustrates image of relationship between flexural capacity and ductility before and after the retrofit of steel columns. If the ductility of steel columns is increased without much increase of the flexural capacity, their seismic performance can be ensured without retrofitting the anchors. Consequently, the following requirements are considered to be necessary for retrofit methods of steel columns.

- Avoid failure modes
- Improve ductility

- Less increase in flexural strength (Less increase in seismic force to anchors)
- Easy retrofit work on site

Fig. 5 illustrates the image of the seismic retrofit methods. Fig. 6 shows the behaviors after local buckling of retrofitted columns. As to rectangular columns, four corners are strengthened with corner plates or angle plates to prevent cracking or fracture after local buckling. The concept is that even after the local buckling of the stiffened plates at the maximum load, the steel column can sustain its flexural capacity in a similar mechanism as a rigid frame structure consisting of the four corners acting as columns and stiffened panels acting as bracings. As to circular columns, an outer pipe is set around the bottom part of the pier with a small space between the existing pipe and the outer pipe. This outer pipe can restrain the progress of deformation of the existing pipe and help the pipe column to keep the flexural capacity and improve ductility.

CYCLIC LOADING TESTS

Outline of Test Specimens

Cyclic loading tests were carried out to examine the seismic behavior of as-built and retrofitted steel columns in a different structural parameters. Test specimens are described in Table 3. "As-built" types are simulating typical existing steel columns and the other types are simulating retrofitted ones. σ_y is a measured yield stress. Structural parameters of each specimen for buckling are given based on the measured yield stress. Fig. 7 shows dimensions of each specimen. Specimens are around one-third scale models of existing columns. Dimensions of the cross section are determined to be large enough to simulate the effect of corner plates and size of welding. The height of retrofitting is 1,800mm from the base of the column for rectangular specimens. The outer pipe of circular specimens is installed to the height of 600mm to cover the base region where the column is expected to be buckled.

The values of structural parameters of stiffened panels were determined by referring to those for existing steel bridge piers designed by the past design codes. R_F of the specimen No.20 were set at approximately 0.55. The stiffened plates of the specimen M8 have a larger width-thickness ratio than that of No.20. R_F of M8 is 0.85, close to maximum value in existing steel columns. The specimen T1 has almost the same structural parameters as those of No.20, but the column slenderness ratio differs.

Retrofit for Rectangular Specimens

Except for specimen No.5 and No.12, four corners are strengthened with corner plates. In case of corner plates, a triangle closed section of each corner is considered to have relatively high flexural stiffness and torsional stiffness as a column. Corner plates are connected with high-strength bolts between the vertical stiffeners at the inside of each corner. The specimen K3, No.11, K4 and No.25 differ in the size of corner plates. Their moments of inertia are about 1.1, 1.2, 1.4, 1.9 times as large as that of the specimen No.20, respectively. The specimen No.5 and No.12 are strengthened with angle plates, which are relatively flexible strengthening. The specimen No.12 has smaller size of angle plates than that of No.5.

Retrofit for Circular Specimens

The specimen No.6 and No.8 are differ in radius-wall thickness ratio. Outer pipe of retrofitted specimens is placed outside the existing pipe with small spacing to control out-of-plane deformation after the buckling. The outer pipe is completely separated from the exisiting pipe. The outer pipe does not contribute to increase the stiffness and the flexural capacity of the existing pipe. When the pipe locally buckles and deforms to a certain degree, the outer pipe restrains the further deformation at initial buckling section. The spacing between the two pipes is set at 10mm for both the specimen No.7 and No.9. In case of the specimen No.15, the gap is set at 5mm.

In case of actual retrofit work, the outer pipe is divided into several arc members at the shop and welded on site. The gap should be filled with soft sealant or elastic material in order to prevent the corrosion.

Loading Method

All test specimen were loaded with two hydraulic jacks installed in the horizontal and vertical direction respectively in a fully rigid frame as shown in Fig. 8. Fig. 9 shows the experimental setup. With the axial force kept constant by the vertical jack, the cyclic lateral load was applied by the horizontal jack at the loading point of the head of specimen to simulate the selfweight of the superstructure. The axial force was basically set at 15% of the full-section yield load calculated from the nominal yield stress, which is generally taken as average value of axial force in existing steel bridge columns. The horizontal loading pattern is shown in Fig. 10, where δ_{y0} is the displacement of the loading point when the specimen yields at the lower end. The specimen was first alternately loaded up to δ_{y0} and then alternately loaded by gradually increasing the amplitude as integral multiples of the displacement δ_{y0} like $\pm 2\,\delta_{y0}$, $\pm 3\,\delta_{y0}$, until the horizontal load dropped fully below the yield horizontal load. One cycle number was applied at each level of $n\,\delta_{y0}$. The basic displacement δ_{y0} under cyclic loading is calculated by

$$\delta_{y0} = \frac{H_y h}{3EI} \qquad \cdots\cdots(1)$$

$$P_y = \left(\sigma_y - \frac{N}{A}\right)\frac{z}{h} \qquad \cdots\cdots(2)$$

where σ_y is the yield stress of the steel, z is the section modulus of the specimen.

Test Results

Failure Process

Fig. 11 shows examples of failure processes of as-built specimens. As to the rectangular specimen, the deformation of stiffened panels gradually increased beyond $+4\,\delta_{y0}$. As to the circular specimen, convex local buckling in the column base on the compression side occurred just before the maximum load. Subsequent cyclic loading gradually increased the out-of-plane deformation and extended it into the circumferential direction. Finally, it resulted in the elephant foot buckling mode.

Fig. 12 shows the difference of appearance after the maximum load between the as-built specimens No.20 and the retrofit specimen No.11. With the progress of deformation of the stiffened plates, the corners of the specimen No.20 gradually lost straightness and twisted. Consequently, the fracture occurred at the corner between the web and the flange at +6 δ_{y0}.. On the other hand, the specimen No.11 kept straightness of each corner even after the maximum load for a while.

Fig. 13 shows the downward view of inside of the retrofit specimen No.15 from the upper side after the test. Because of restriction of out-of-plane deformation by the outer pipe, deformed area of the existing pipe spread in the direction of its upper side. After the contact of the existing pipe with the outer pipe, the progress of the deformation due to the first buckling mode was prevented, and next buckling occurred as the second deformation mode.

Horizontal Load - Horizontal Displacement Relations

Table 4 shows the test results. δ_u is defined as the displacement at 97% of the ultimate horizontal load. In other words, δ_u is a value defined as the displacement where the horizontal load hardly drop down. Fig. 14 and Fig. 15 show the horizontal load-horizontal displacement relationship(hysteresis curve). The load-displacement envelopes of as built sections are also shown by dotted lines in the figures. The maximum displacement at which the corners can be kept straight are indicated by the inverted triangle symbol (∇) in the hysteresis curves of Fig. 14. Encircled figures on the hysteresis loops indicate multiples of δ_y. Fig. 16 and Fig. 17 shows the envelope curves of the horizontal load-horizontal displacement relations among all the speimens.

As to rectangular sections, deterioration of the specimen No.20, M8 and T1, which are representing as-built steel columns, after the maximum horizontal load is considerable. Compared to this, it can be said retrofit specimens have more ductility. The specimen No.5 and No.22 sustain the straightness of corners until the displacement reached about -6 δ_{y0}. In this way, strengthening of corners by corner plates is considered to change the original structure into a stable rigid frame structure composed of four corner columns and web panel bracings as shown in Fig. 6 after the local buckling of the stiffened panels and to delay the decrease of the flexural capacity. Fig. 18 shows the effect of corner plates bolted at corners on ductility. δ_u / δ_y is the displacement ductility factor. $I_{\text{retrofit}} / I_{\text{as-built}}$ is a ratio of moment of inertia of retrofit specimen to that without corner plates. For the retrofit specimen No. 11 with corner plates, with the increase of the ratio of moment of inertia up to 1.2, the ductility factor increases from 3 to around 5.5. It is not so difficult to increase the ratio up to 1.2 in practical retrofit design. Also shown in this figure, the specimen No. 20 has more ductility compared to the specimen M8 and T1. Regarding the effects of the column slenderness ratio $\bar{\lambda}$ and flange width-thickness ratio R_F, it can be said that the bigger these structural parameters become, the less ductility the steel column will have.

As to circular sections, the ductilities of specimens with outer pipe are improved after the maximum loading point. Deterioration slope in envelope of specimen No.7 and No.15 after the peak are gentle compared to specimen No.6 and No.8 respectively. As to specimen No.7 and No.15, the deformed portion of the column body was considered to have contacted the outer pipe around the maximum load. However, the outer pipe of the specimen No.9 did not function effectively just at the maximum load. The reason is that the gap between the outer pipe and the existing pipe of No.9 was relatively large so that the out-of-plane deformation due to local

buckling progressed. According to the test results and the findings from the FEM analysis on the effect of the gap size, it can be said the about half of thickness of the existing pipe is appropriate for the gap size.

Design recommendations

For rectangular columns, to take into account of the effects of the axial load ratio N/N_y, the column slenderness ratio $\bar{\lambda}$ and the flange width-thickness ratio R_F, C_R is defined by the equation (3).

$$C_R = \frac{N}{N_y} \times R_F \times \bar{\lambda} \qquad \cdots\cdots(3)$$

The displacement ductility factor δ_u / δ_y versus C_R for as-built and retrofitted specimens with corner plates are plotted in **Fig. 19**. The solid line in the figure can be proposed to predict the ductility factor for the retrofitted column with corner plates of $1.2 I_{\text{retrofit}} / I_{\text{as-built}}$.

As to circular columns, the displacement ductility factor versus pipe radius-thickness ratio R_t for retrofit specimens with outer pipe are plotted in **Fig. 20**. In case of circular columns, it was found that pipe radius-thickness ratio R_t greatly affects on the ductility factor compared to N/N_y and $\bar{\lambda}$. From the practical point of view, the ductility factor is given by R_t.

CONCLUSIONS

Concepts of retrofit methods of steel bridge columns were described in the paper. Loading tests were carried out to clarify the effectiveness of the proposed retrofit methods for rectangular and circular columns respectively. Based on the field study about the damaged piers and the findings from the experiments results, the following conclusions were reached.

1) As to rectangular steel columns, strengthening of the four corners by corner plates is effective to improve the ductility with few increase of flexural strength of columns as well as to prevent fracture at corners. Even after local buckling of stiffened flange panles after the maximum horizonatal load, retrofitted columns can sustain flexural strength in a similar mechanism as a kind of rigid frame structure composed of the four corners acting as columns and stiffened flange panels as bracings.
2) As to circular steel columns, installation of an additional outer pipe around the bottom of the existing column with a certain gap between them is effective to improve the ductility without changing the initial stiffness and the flexural strength of the column. This outer pipe can restrain the amount of out-of-plane deformation due to local buckling, and help the column to improve the ductility.
3) For design recommendations, the simple equations were proposed to predict the displacement ductility factors of the retrofitted rectangular and circular columns respectively.

REFERENCES

[1] Ministry of Construction : Guide Specifications for Reconstruction and Repair of Highway Bridges Suffered Damage due to the Hyogo-ken Nanbu Earthquake, 1995.2.
[2] Committee for Investigation on the Damage of Highway Bridges Caused by the Hyogo-ken Nanbu Earthquake : Final Report on the Damage of Highway Bridges by the Hyogo-ken

Nanbu Earthquake, 1995.12.

[3] Japan Road Association : Reference for Applying the "Guide Specifications for Reconstruction and Repair of Highway Bridges which Suffered Damage due to the Hyogo-ken Nanbu Earthquake", 1995.6.

[4] Japan Society of Civil Engineers, Committee of Steel Structures, Sub-Committee on Inelastic Behavior of Steel Structures : Inelastic Behavior of Steel Structures and Earthquake Resistant Design Methods, Journal of Structural Mechanics and Earthquake Engineering, No.489/I-27, 1994.4.

[5] Japan Society of Civil Engineers, Committee of New Technologies in Steel Structures : The Report of New Technologies for Steel Structures, 1993.3.

[6] Japan Road Association : Design Specifications of Highway Bridges - Part V Seismic Design, 1990.2.

[7] Terayama, T., Otsuka, H., Nishikawa, K. and Murakoshi, J. : Ductility Improvement of Steel Columns with Corner Plates Based on Large-Scale Cyclic Loading Tests, Proceedings of the 5th International Colloquium on Stability and Ductility of Steel Structures, Vol.2, 1997.7.

Table 1 Definition of Damage Degree of Steel Columns

Damage Degree	Definition
As	Collapsed. Extremely serious damage or deformation.
A	Cracking, buckling or serious deformation.
B	Partial buckling or deformation of members.
C	Localized light buckling or deformation.
D	No damage, or if there is, extremely minor damage that will not effect the load bearing capacity.

Table 2 Damage Degree of Steel Columns (number)

Damage Degree					Total
As	A	B	C	D	
4 (1%)	11 (3%)	36 (10%)	138 (39%)	166 (47%)	355 (100%)

Table 3 Test Specimens

(a) Rectangular Section

Specimen	Type	Dimension of Corner or Angle Plates	Steel Grade	σ_y (kgf/cm²)	$\frac{N}{Ny}$	R_R	R_F	$\bar{\lambda}$
No.20	As-Built		SM490	4,160	0.125	0.585	0.611	0.272
No.18	As-Built		SM490	3,900	0.197	0.567	0.591	0.264
No.11	Corner Plates (Bolted)	4-PL 295X6 (1.2I)	SM490	3,770	0.128	0.557	0.581	0.259
No.33	Corner Plates (Bolted)	4-PL 295X6 (1.2I)	SM490	3,750	0.154	0.556	0.580	0.258
K3	Corner Plates (Bolted)	4-PL 220X4.5 (S) (1.1I)	SM490	3,940	0.122	0.570	0.594	0.265
K4	Corner Plates (Bolted)	4-PL 220X4.5(S), 8-PL 135X4.5	SM490	3,750	0.128	0.556	0.580	0.258
No.25	Corner Plates (Bolted)	4-PL 295X6, 8-PL 200X12	SM490	4,060	0.118	0.578	0.603	0.269
No.5	Angle Plates (Bolted)	4-L 90X90X9, 8-Fill 90X9	SM490	3,770	0.128	0.557	0.581	0.258
No.12	Angle Plates (Bolted)	4-L 75X75X6, 8-Fill 75X4.5 (S)	SM490	3,770	0.128	0.557	0.581	0.259
M8	As-Built		SM490	3,590	0.134	0.652	0.847	0.251
No.28	Corner Plates (Bolted)	4-PL 295X6 (1.2I)	SM490	3,780	0.134	0.669	0.869	0.257
T1	As-Built		SM490	4,070	0.118	0.579	0.566	0.393
T3	Corner Plates (Bolted)	4-PL 282X6 (1.2I)	SM490	4,070	0.118	0.579	0.566	0.393

(b) Circular Section

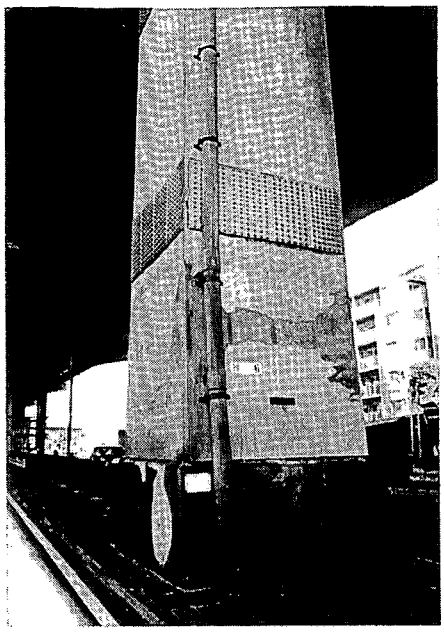
Specimen	Type	Steel Grade	σ_y (kgf/cm²)	$\frac{N}{Ny}$	R_t	$\bar{\lambda}$
No.6	As-Built	SM490	3,510	0.137	0.0763	0.283
No.7	Outer Pipe (Gap=10mm)	SM490	3,540	0.136	0.0769	0.285
No.8	As-Built	SS400	2,960	0.122	0.115	0.258
No.29	As-Built	SS400	3,150	0.199	0.123	0.268
No.9	Outer Pipe (Gap=10mm)	SS400	2,850	0.126	0.111	0.253
No.15	Outer Pipe (Gap= 5mm)	SS400	3,130	0.115	0.122	0.267
No.31	Outer Pipe (Gap= 5mm)	SS400	3,150	0.199	0.123	0.268

Note : σ_y = Yield Stress, N/N_y = Axial Force Ratio, $\bar{\lambda}$ = Column Slenderness Ratio $(=1/\pi\sqrt{(\sigma_y/E)\cdot(l/r)})$
R_R = Width-Thickness Ratio of Flange Panel $(= b/t\cdot\sqrt{(\sigma_y/E)\cdot 12(1-\nu^2)/\pi^2 k_R})$
R_F = Width-Thickness Ratio between Longitudinal Ribs $(= b/t\cdot\sqrt{(\sigma_y/E)\cdot 12(1-\nu^2)/\pi^2 k_F})$
R_t = Radius-Thickness Ratio $(= (R/t)\cdot(\sigma_y/E)\cdot\sqrt{3(1-\nu^2)})$

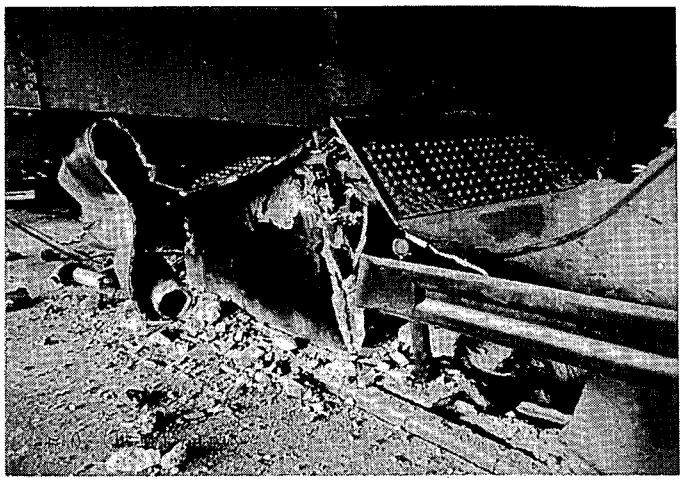
Table 4 Test Results

Specimen			$\frac{N}{N_y}$	P_y (tf)	P_u (tf)	$\frac{P_u}{P_y}$	δ_y (mm)	δ_m (mm)	δ_u (mm)	$\frac{\delta_m}{\delta_y}$	$\frac{\delta_u}{\delta_y}$
Rectangular Section	No.20	As-Built	0.125	114	140	1.23	14.0	38	42	2.7	3.0
	No.18	As-Built	0.197	98	130	1.33	12.6	28	36	2.2	2.9
	No.11	Corner Plates (Bolted)	0.128	103	153	1.49	12.7	60	72	4.7	5.7
	No.33	Corner Plates (Bolted)	0.154	99	148	1.49	13.2	54	65	4.1	4.9
	K3	Small Corner Plates (Bolted)	0.122	108	151	1.40	13.3	47	56	3.5	4.2
	K4	Corner Plates (Bolted)	0.128	102	165	1.62	12.4	60	69	4.8	5.6
	No.25	Corner Plates (Bolted)	0.118	112	193	1.73	10.7	76	83	7.1	7.8
	No.5	Angle Plates (Bolted)	0.128	103	175	1.70	11.4	49	62	4.3	5.4
	No.12	Small Angled Plates (Bolted)	0.128	103	150	1.46	12.5	43	53	3.4	4.2
	M8	As-Built	0.134	101	111	1.10	17.3	33	34	1.9	2.0
	No.28	Corner Plates (Bolted)	0.134	106	153	1.44	13.3	44	55	3.3	4.1
	T1	As-Built	0.118	77	99	1.29	27.9	69	72	2.5	2.6
	T3	Corner Plates (Bolted)	0.118	77	107	1.40	27.0	85	102	3.1	3.8
Circular Section	No.6	As-Built	0.137	86	157	1.83	14.2	51	72	3.6	5.1
	No.7	Outer Pipe (Gap=10mm)	0.136	87	161	1.86	15.5	59	98	3.8	6.3
	No.8	As-Built	0.122	42	61	1.43	10.1	26	32	2.6	3.2
	No.29	As-Built	0.199	41	54	1.31	8.5	24	28	2.8	3.3
	No.9	Outer Pipe (Gap=10mm)	0.126	41	61	1.51	10.7	26	35	2.4	3.3
	No.15	Outer Pipe (Gap=5mm)	0.115	45	66	1.47	10.2	36	48	3.5	4.7
	No.31	Outer Pipe (Gap=5mm)	0.199	41	55	1.35	8.5	34	40	4.0	4.7

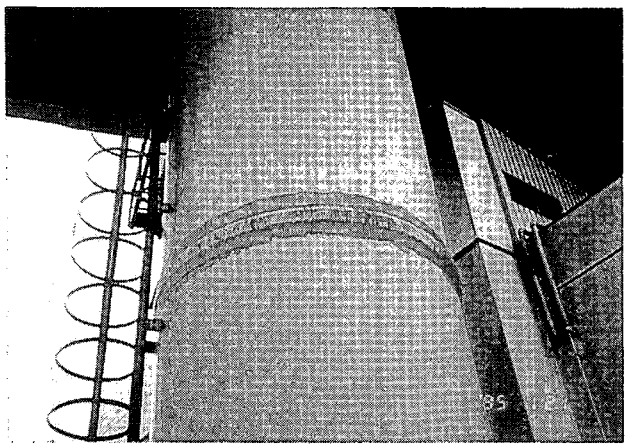
Note : N/N_y = Axial Force Ratio, P_y = Horizontal Yield Load, P_u = Maximum Horizontal Load
δ_y = Yield Horizontal Displacement, δ_m = Horizontal Displacement at P_u, δ_u = Displacement at 97% of P_u



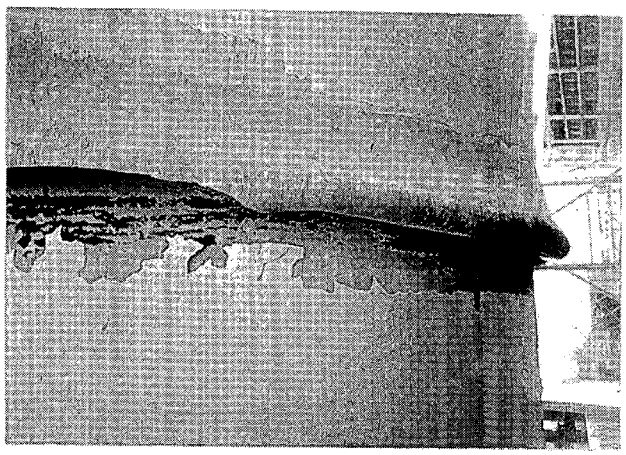
(a) Local buckling
at the bottom part



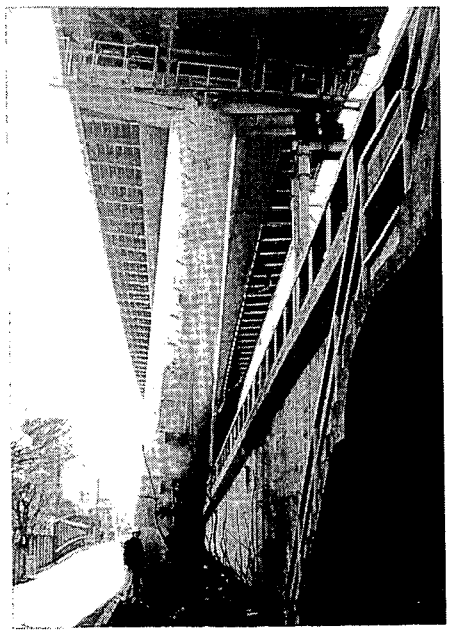
(b) Collapsed pier
(Breaking of corners)



(c) Elephant foot buckling
at the changing part of sections

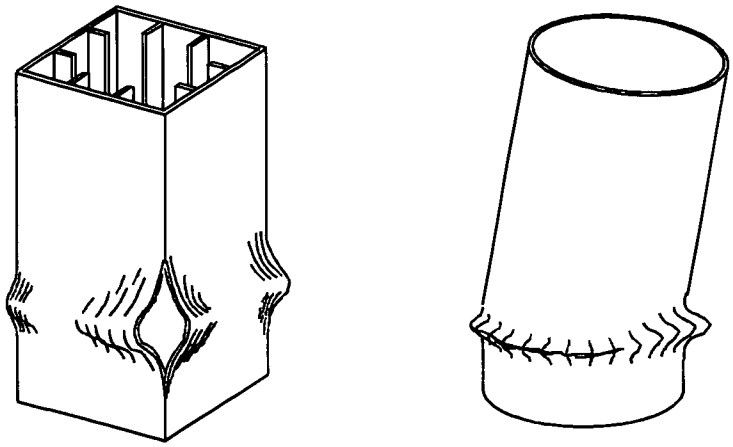


(d) Cracking due to progress
of local bucklong



(e) Residual Displacement
Due to Local Buckling

Fig. 1 Damage of Steel Piers



(a) Breaking of Corners

(b) Progress of Local Deformation, Large Residual Displacement, Cracking at Deformed Point

Fig. 2 Failure Mode

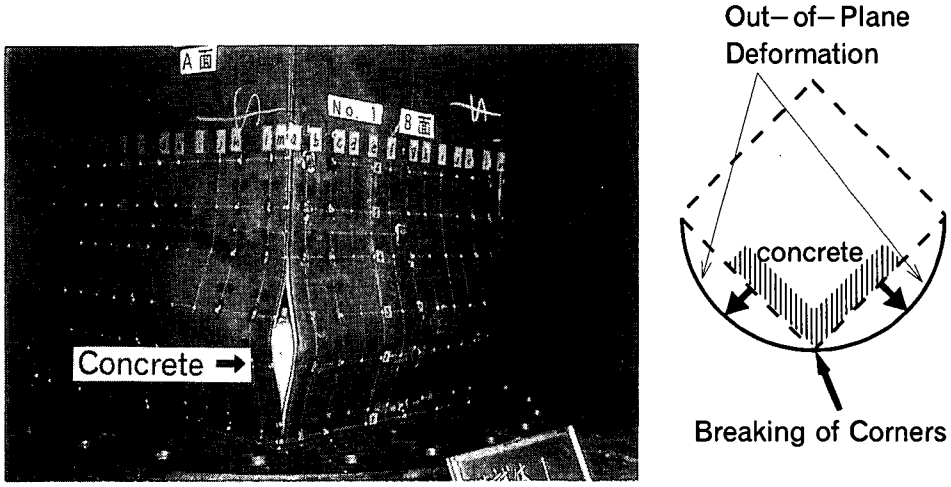


Fig. 3 Breaking of Corners of a Specimen under Cyclic Loading Test

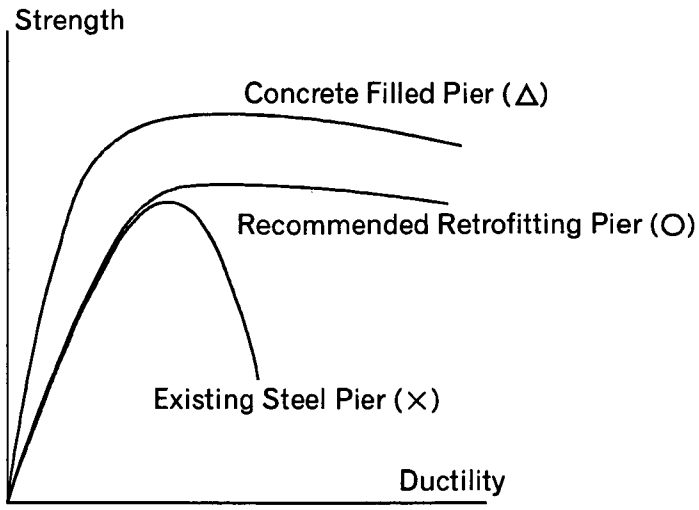
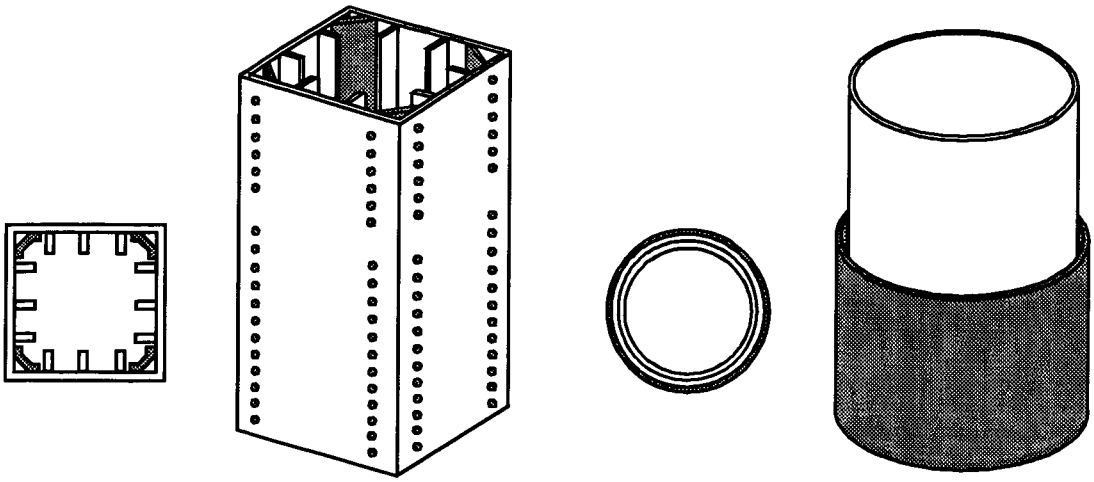
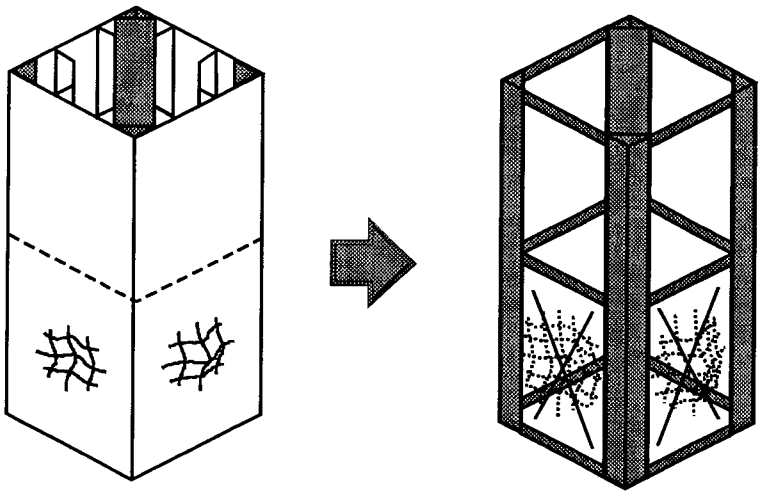


Fig. 4 Effect of Retrofit of Steel Piers

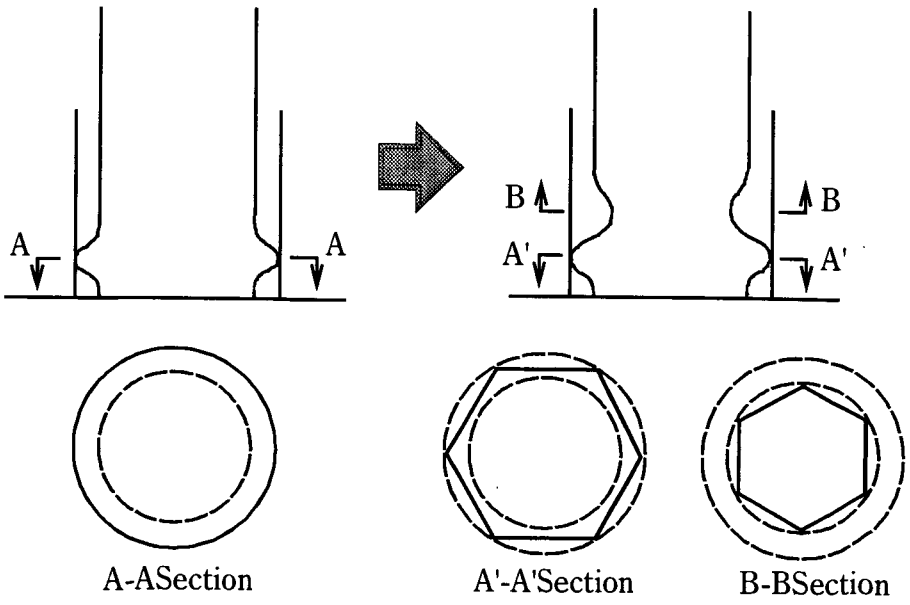


(a) Rectangular Piers (b) Circular Piers

Fig. 5 Image of Proposed Seismic Retrofit of Steel Piers



(a) Rectangular Piers



(b) Circular Piers

Fig. 6 Behaviors After Local Buckling

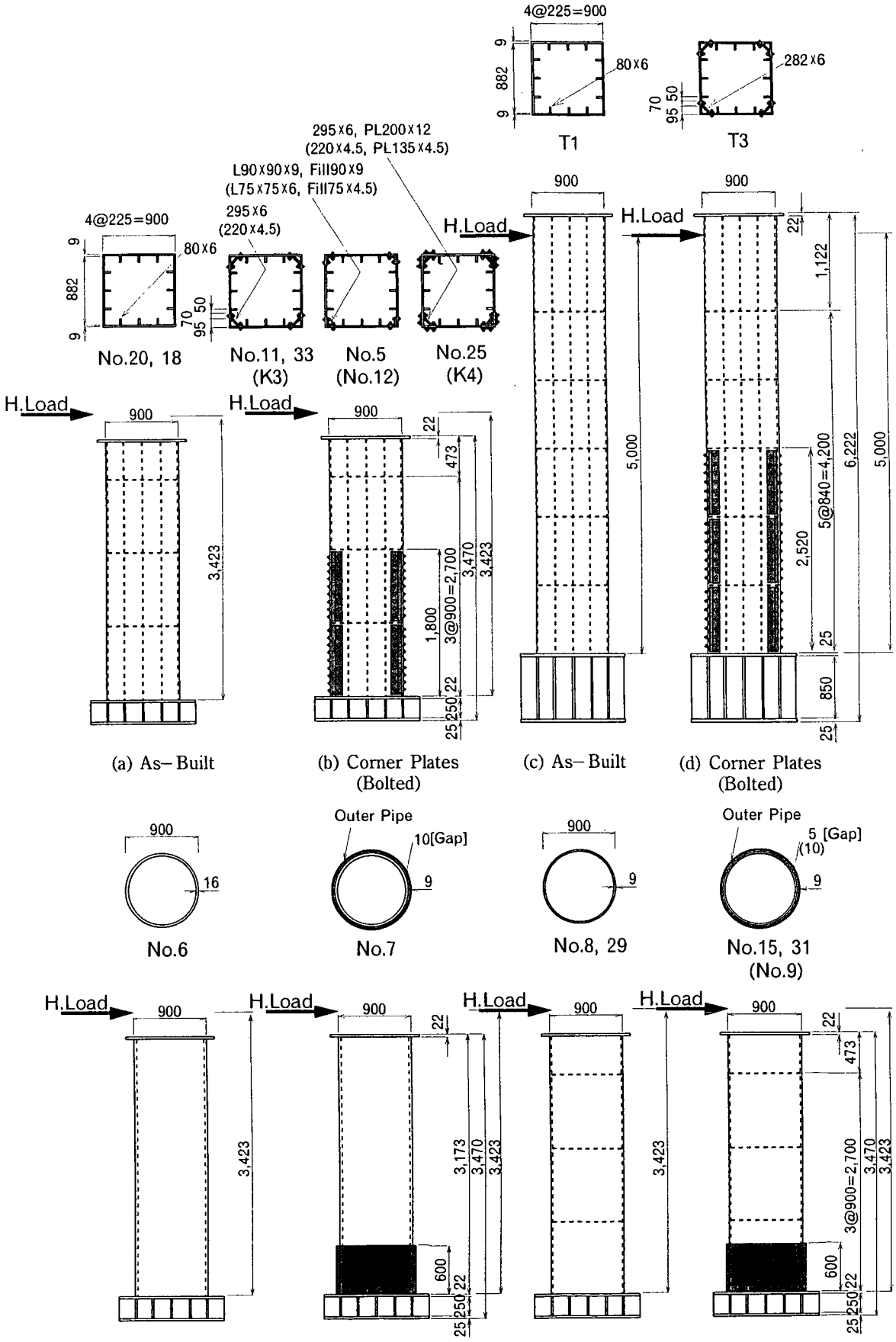


Fig. 7 Shape and Size of Specimens

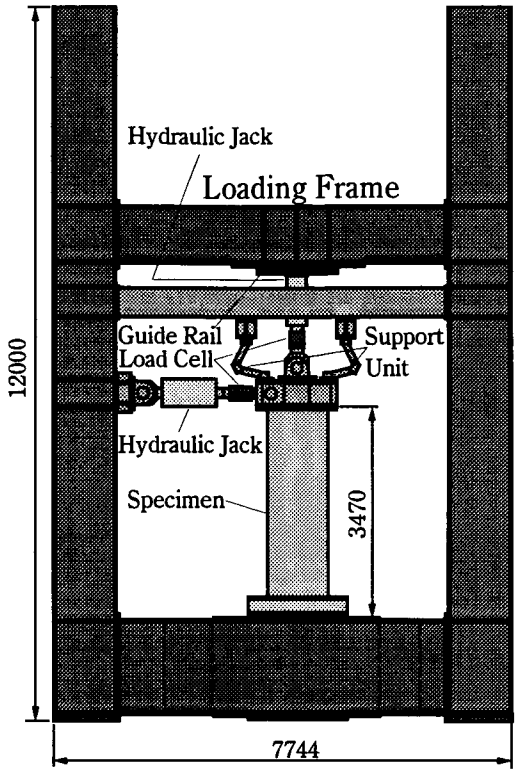


Fig. 8 Test Specimen and Detail of Load Application

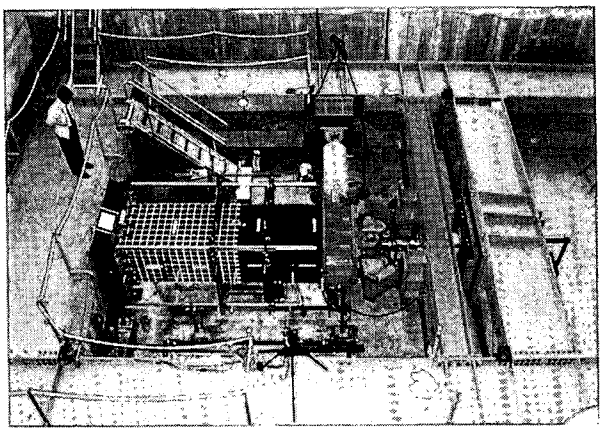


Fig. 9 Test Setup

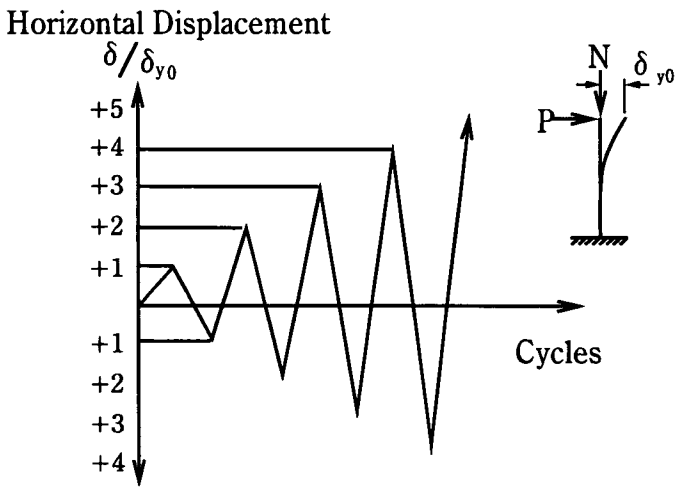
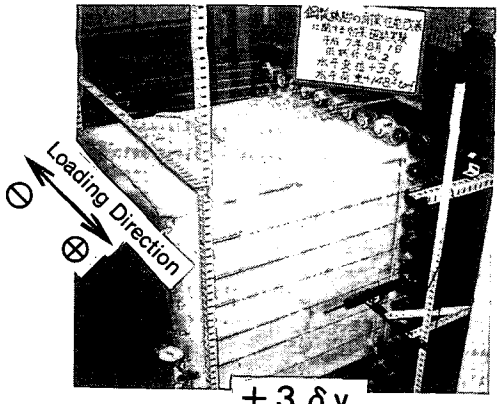
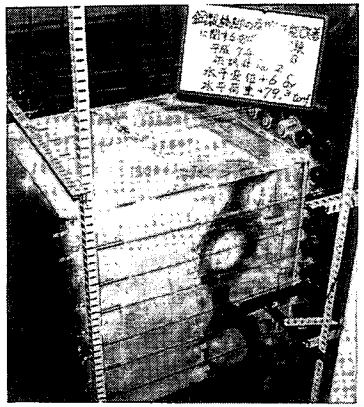


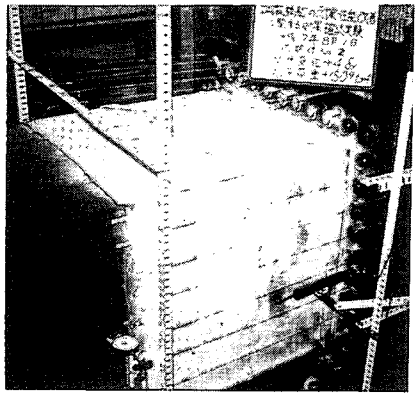
Fig. 10 Type of Horizontal Loading



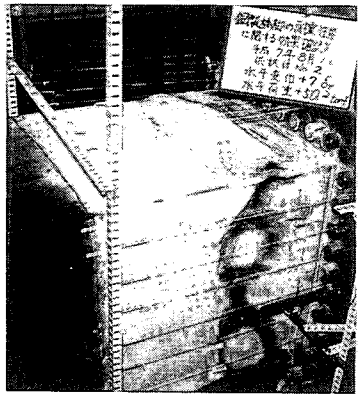
+3 δy



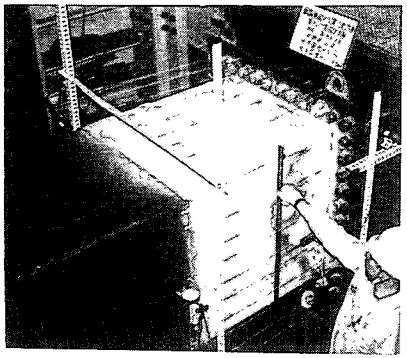
+6 δy



+4 δy Around Peak Load

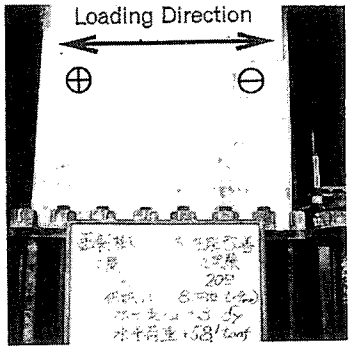


+7 δy

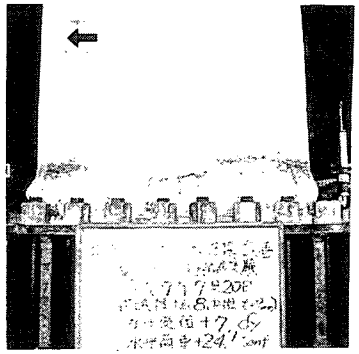


+5 δy Just before the Loss of Straightness of Corners

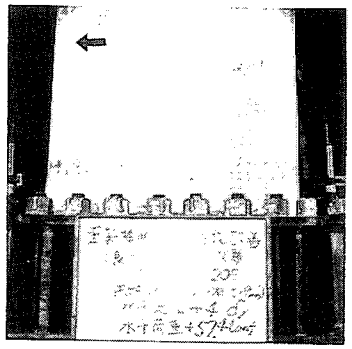
Fig. 11(a) Process of Failure of Rectangular Section (No.2 : the same as No.20)



+3 δy



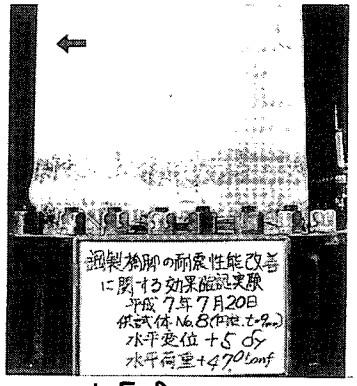
+7 δy



+4 δy Around Peak Load

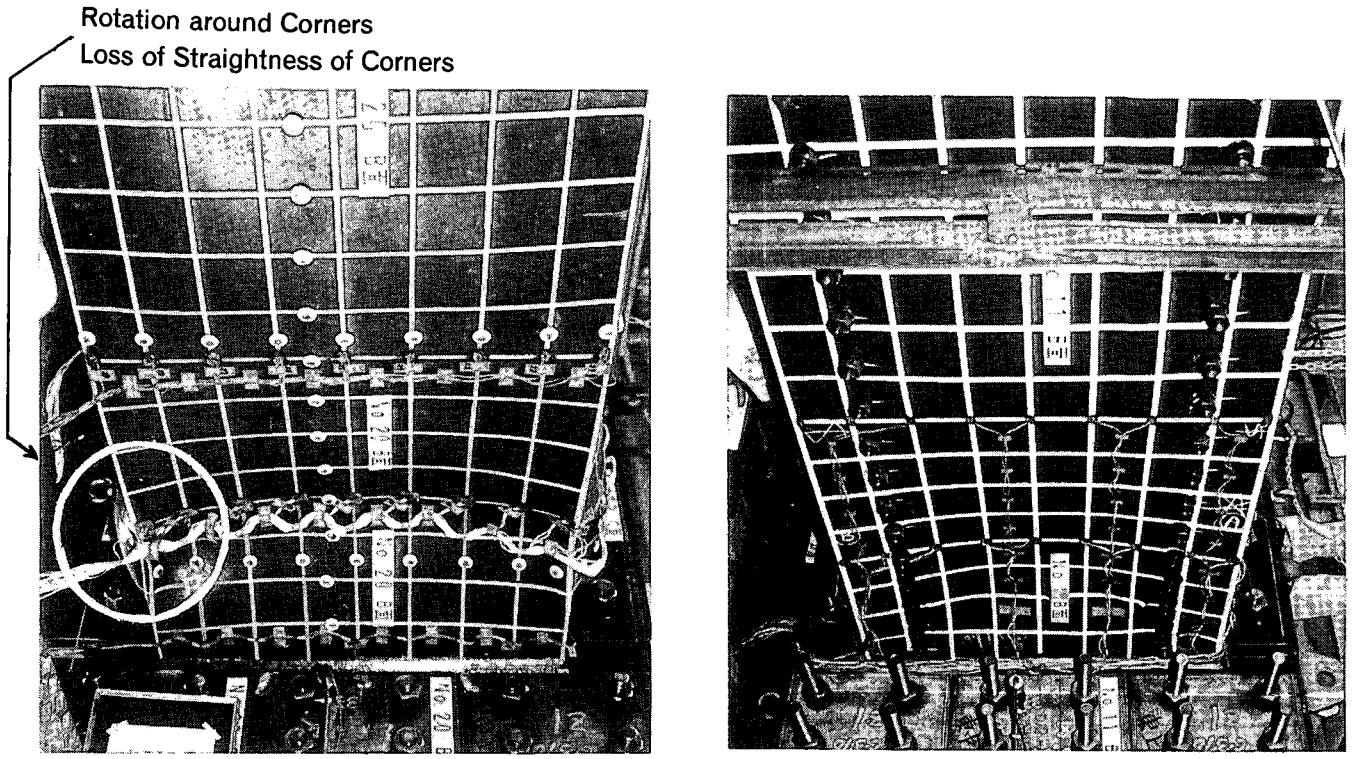


−7 δy Occurrence of Elephant Buckling



+5 δy

Fig. 11(b) Process of Failure of Circular Section (No. 8)



No. 20 −5δy
(a) As−Built Type

No. 11 −6δy
(b) Retrofit Type by Corner Plates

Fig. 12 Effect of Coner Plates

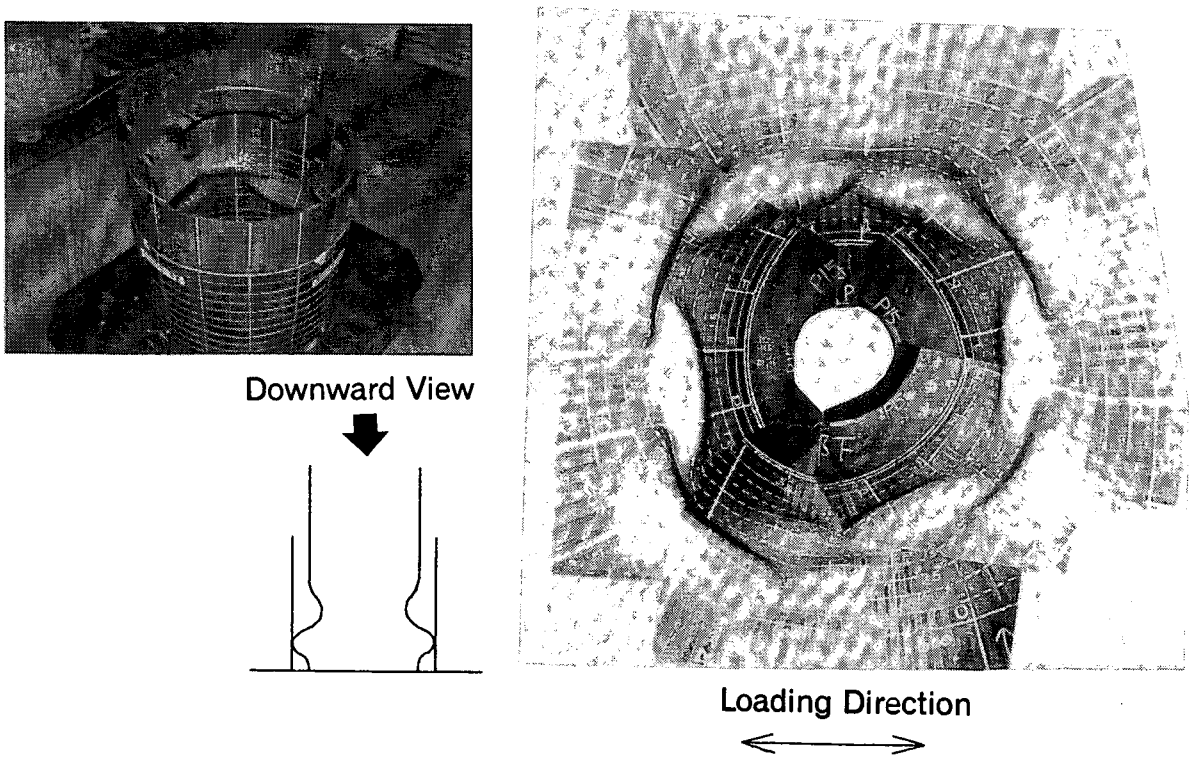
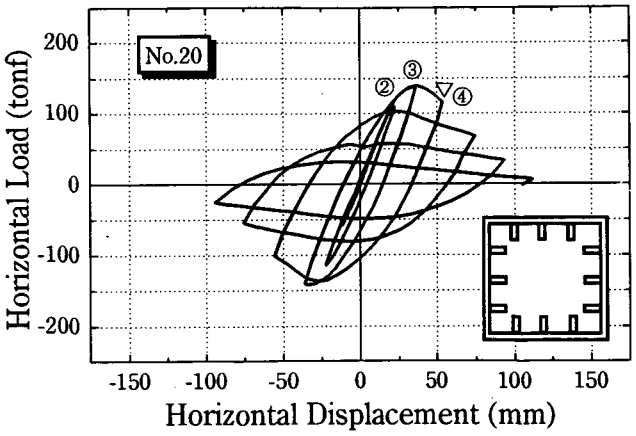
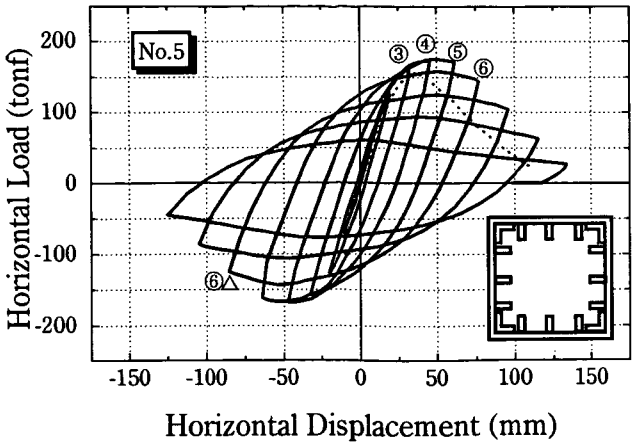


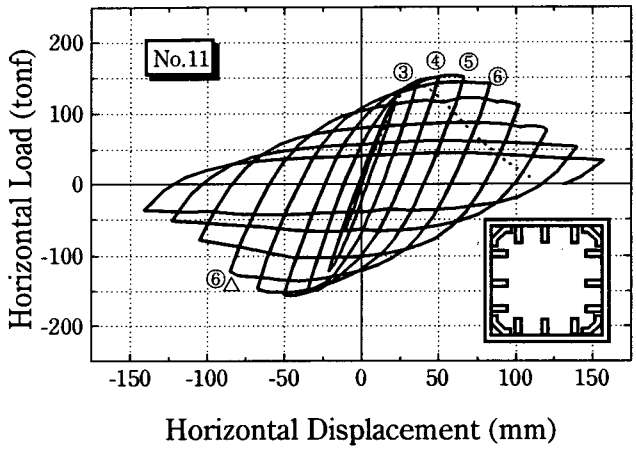
Fig.13 View of the Inside of Retrofit Specimen After the Test



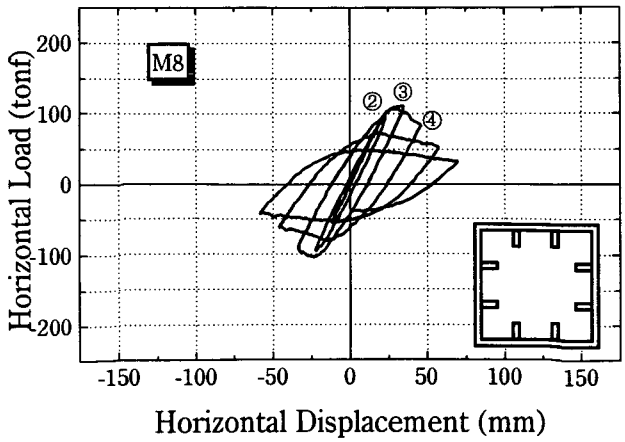
(a)



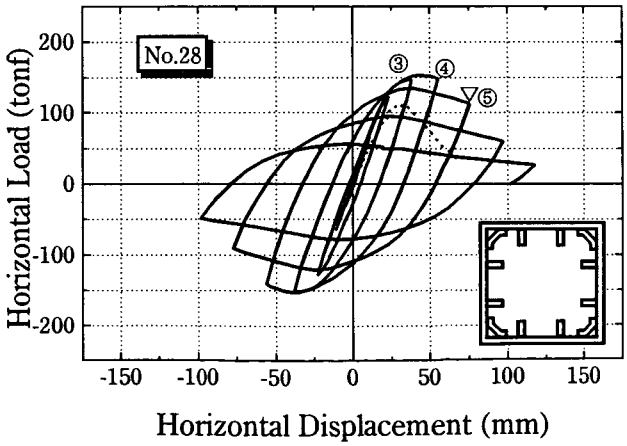
(b)



(c)



(d)



(e)

Fig. 14 Relation between Horizontal Load and Horizontal Displacement (Rectangular Section)

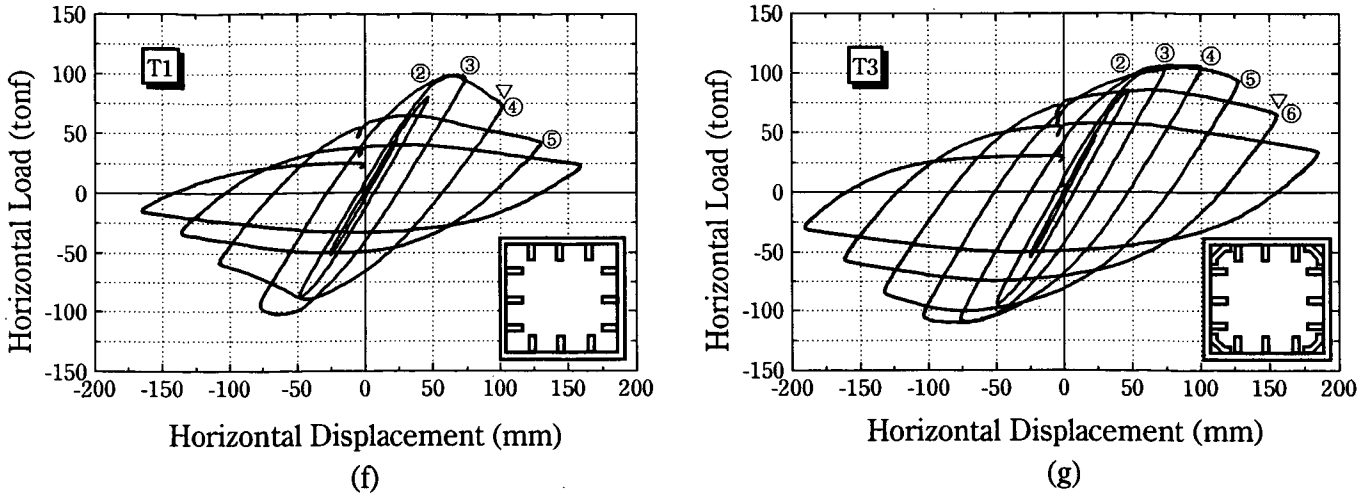


Fig. 14 Relation between Horizontal Load and Horizontal Displacement (Rectangular Section)

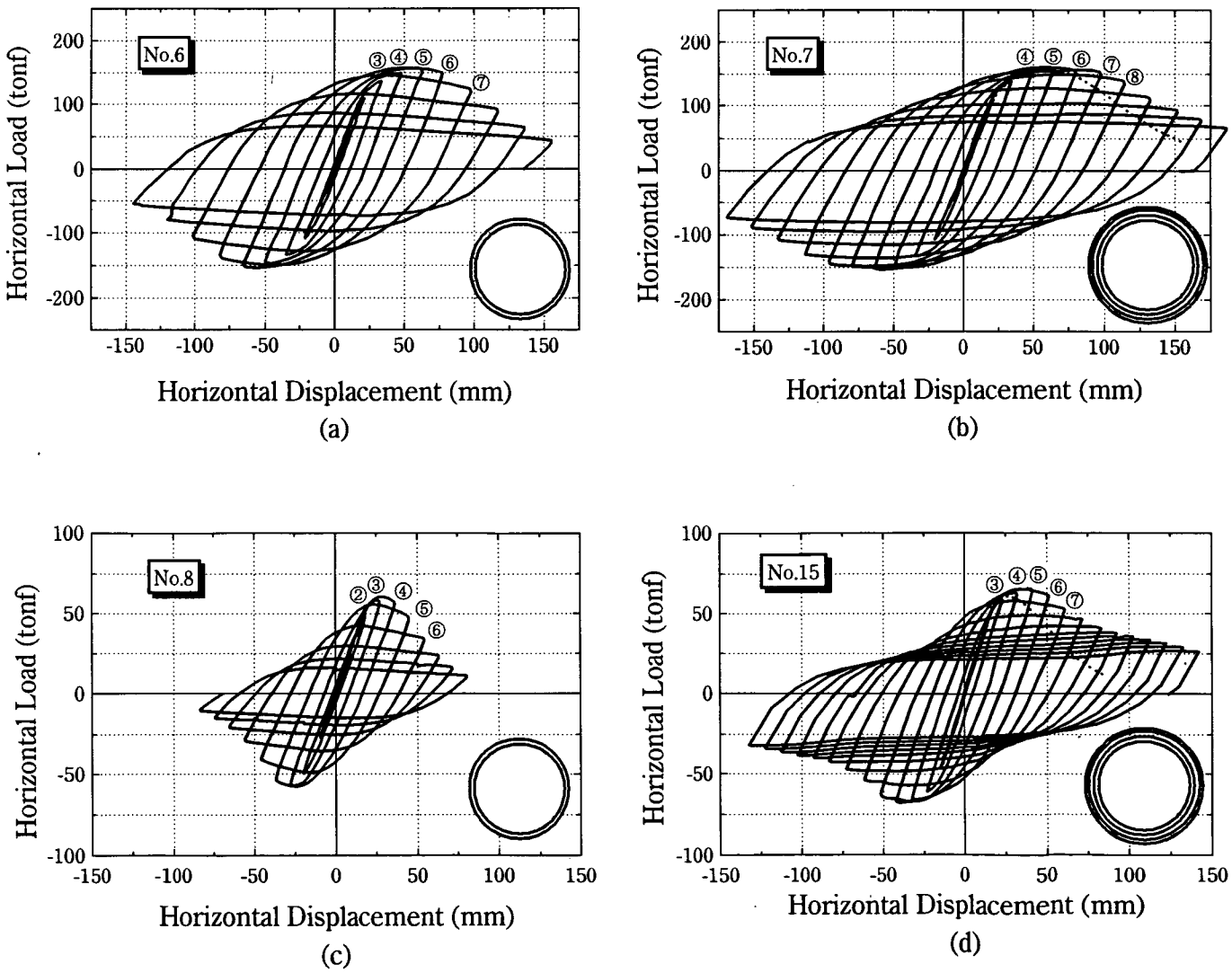
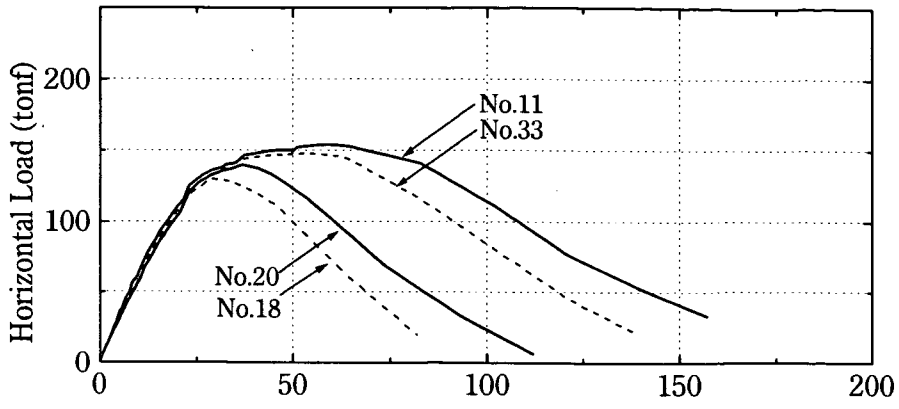
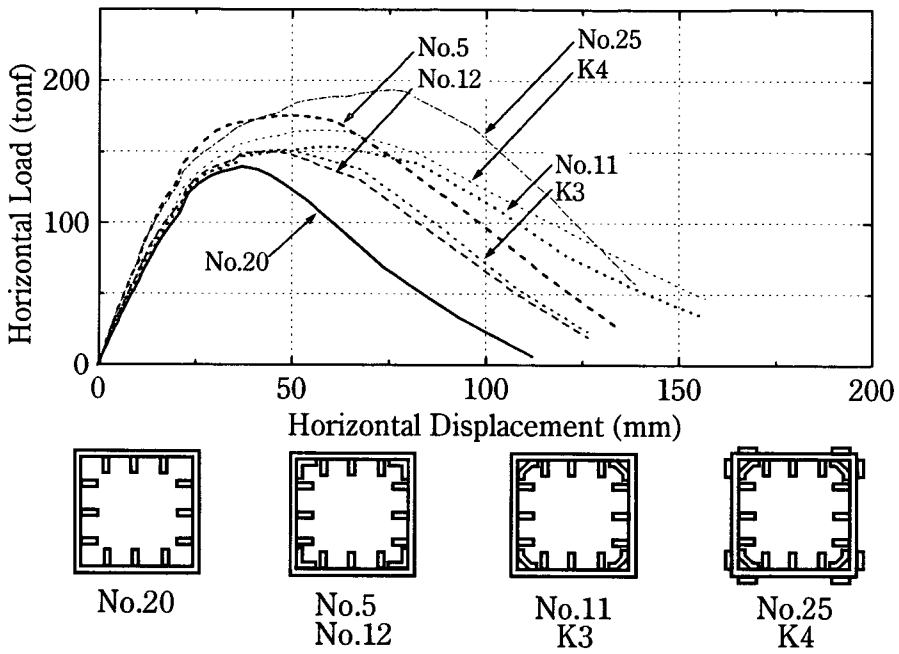


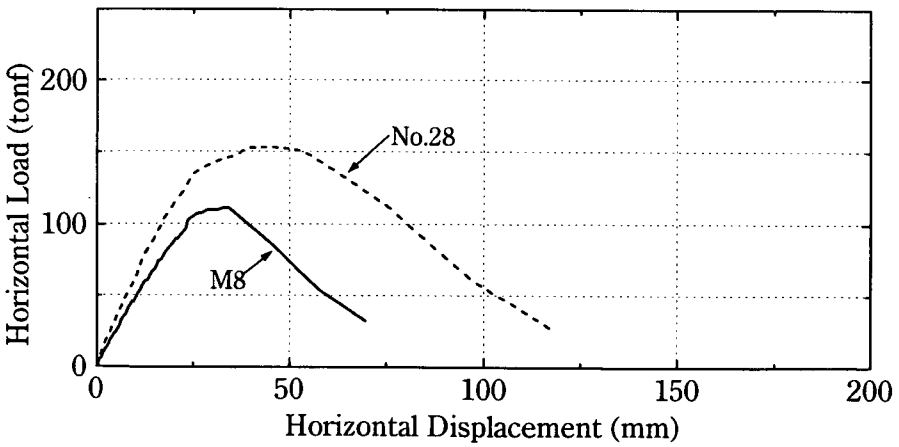
Fig.15 Relation between Horizontal Load and Horizontal Displacement (Circular Section)

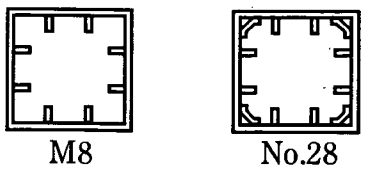


(a) Effect of Axial Force



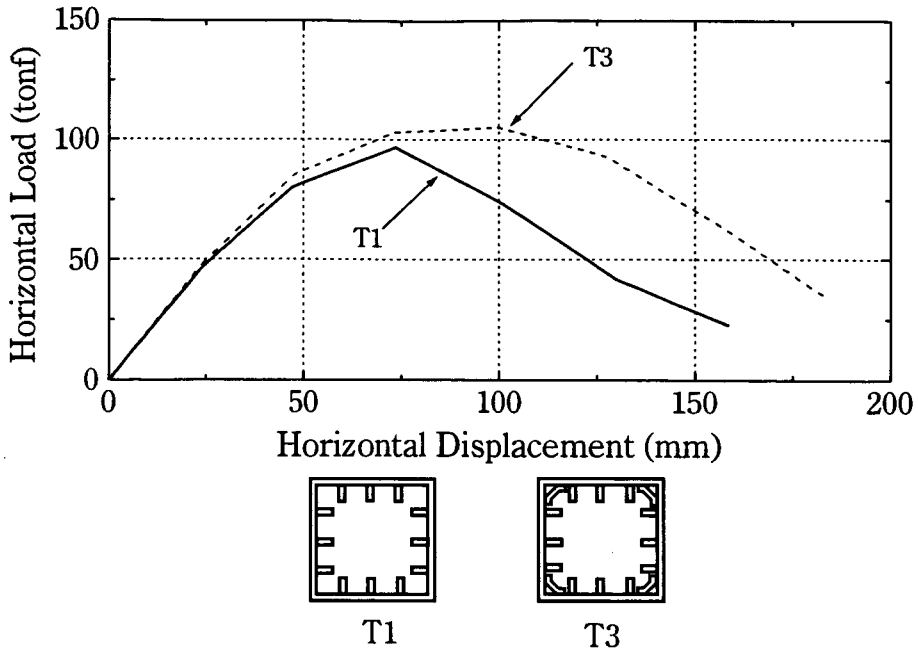
(b) Effect of Retrofit for No.20





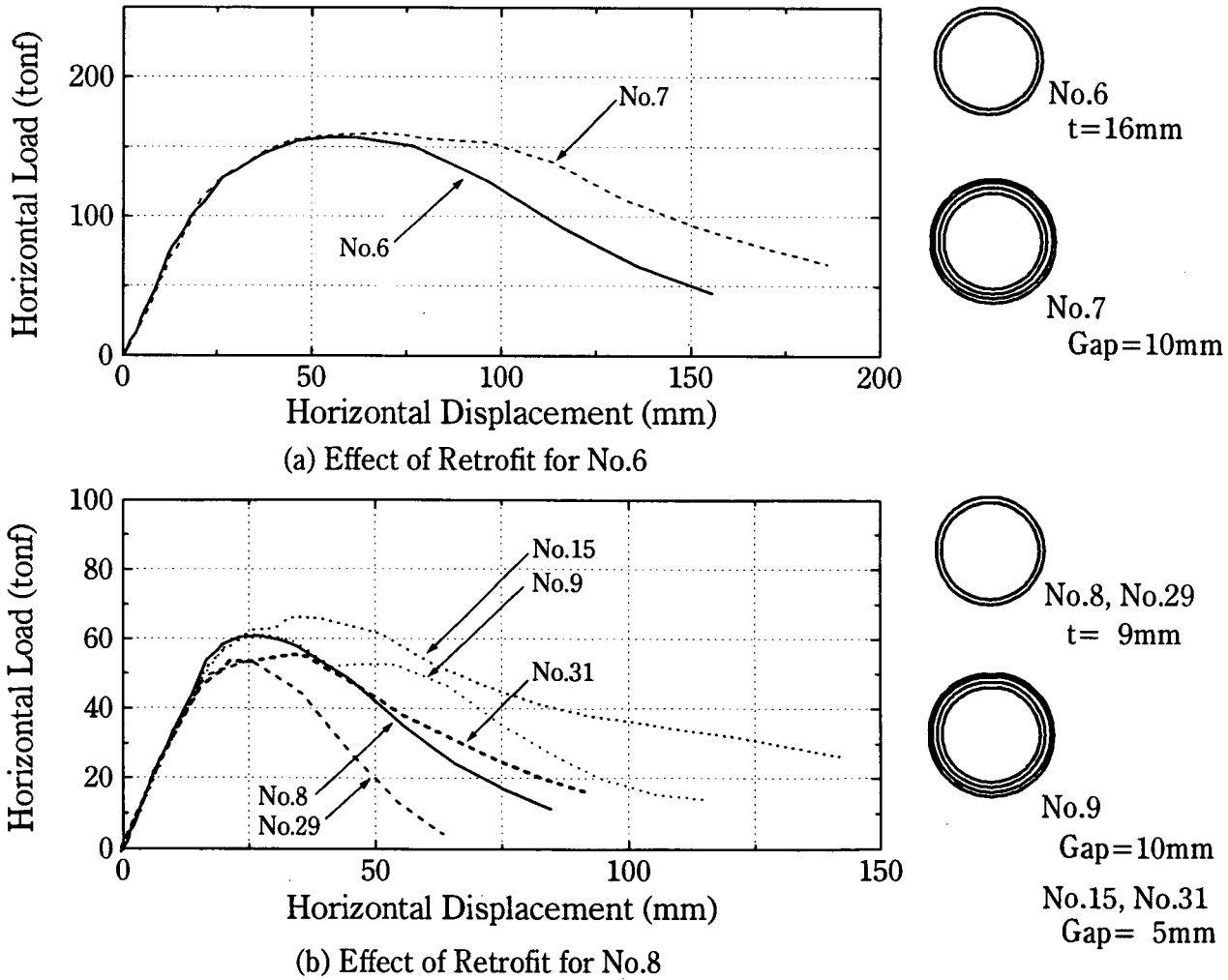
(c) Effect of Retrofit for M8

Fig. 16 Horizontal Load - Horizontal Displacement Envelope (Rectangular Section)



(d) Effect of Retrofit for T1

Fig. 16 Horizontal Load - Horizontal Displacement Envelope (Rectangular Section)



(a) Effect of Retrofit for No.6

(b) Effect of Retrofit for No.8

Fig. 17 Horizontal Load - Horizontal Displacement Envelope (Circular Section)

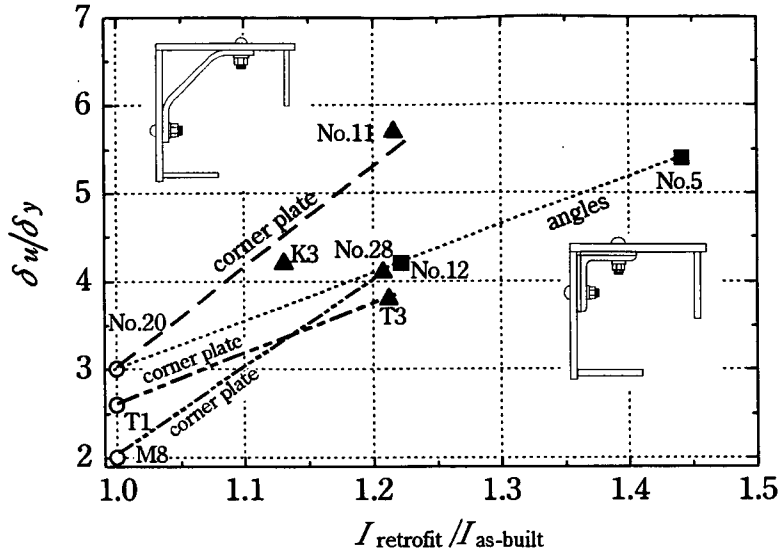


Fig. 18 Effect of Corner Plates on Ductility

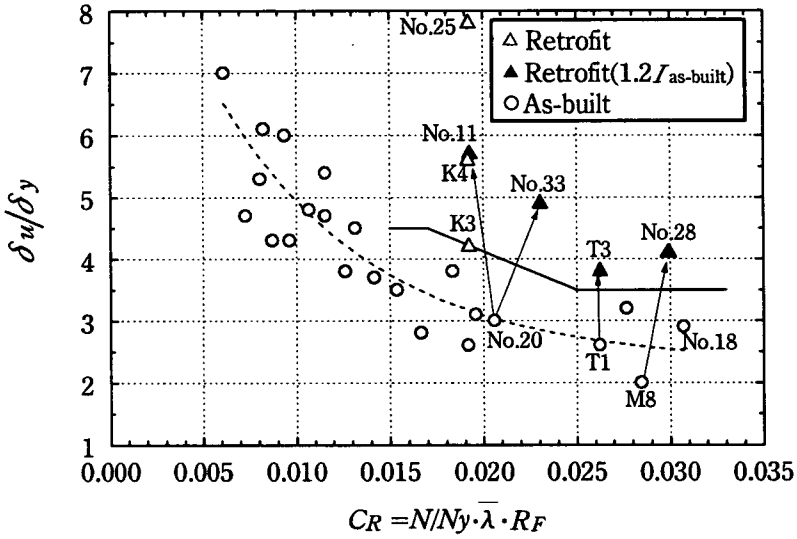


Fig. 19 Ductility Factor $\delta u/\delta y$ versus C_R for rectangular specimens

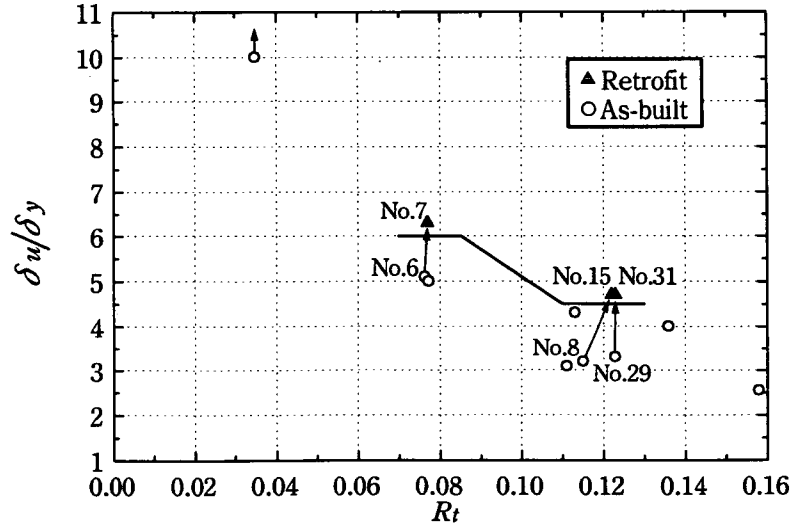


Fig. 20 Ductility Factor $\delta u/\delta y$ versus R_t for circular specimens

LAP SPLICE AND SHEAR ENHANCEMENTS IN COMPOSITE-JACKETED BRIDGE COLUMNS

Medhat A. Haroun[1] and Maria Q. Feng[2]

ABSTRACT

A structural assessment and qualification testing program, coupled with a material testing program, are being conducted to verify the performance of bridge columns retrofitted with composite jackets. The testing program conforms to the guidelines of the Caltrans Program for the Evaluation of Fiber Reinforced Plastics for Seismic Retrofit and Rehabilitation of Structures. Tests include the evaluation of lap splice enhancement and shear enhancement of both circular and rectangular columns. The tests completed so far on ten circular columns, retrofitted by either carbon fiber or E-glass composite jackets, have shown significant enhancement of the column ductility in comparison with the as-built columns.

INTRODUCTION

Existing reinforced concrete bridge columns designed and constructed according to older seismic design provisions may suffer from the following potential problems:

- Insufficient Lap Splice Length: Lap splices were often used to extend the longitudinal steel. Typically, the length of lap splices was equal to 20 times the bar diameter and the transverse reinforcement was provided by hoops spaced at every 12 inches. This may not be sufficient to develop a satisfactory strength due to debonding and slip at the lap splices, and subsequently, such columns may have undependable flexural capacity.

- Insufficient Shear Strength: Columns with continuous longitudinal steel bars may still have problems due to insufficient confinement reinforcement and shear reinforcement. Such columns may not exhibit enough ductility to dissipate the earthquake energy and may become vulnerable to failure by buckling of the longitudinal steel, concrete crushing, and shear failure.

Proven as an effective technology for alleviating these problems and for enhancing the seismic performance of old bridge columns, steel jacketing has been widely implemented for their seismic retrofit. Recently, advanced composite materials have shown great potential to becoming a viable alternative to steel jackets. The light weight, high strength, corrosion resistance, and more importantly the ease of installation make such materials most suitable for retrofitting bridge columns.

[1] Professor, Department of Civil and Environmental Engineering, University of California, Irvine
[2] Associate Professor, Dept. of Civil and Environmental Engnr., University of California, Irvine

In order to examine and qualify the seismic performance of bridge columns retrofitted with composite material jackets, an experimental study is being conducted at the University of California, Irvine, on both circular and rectangular columns. The columns with lap splices are tested in flexure to evaluate the effectiveness of the composite jackets on the enhancement of lap splice clamping, while the columns with the continuous longitudinal steel are tested for shear enhancement in a fixed-fixed condition.

CIRCULAR TEST SPECIMENS

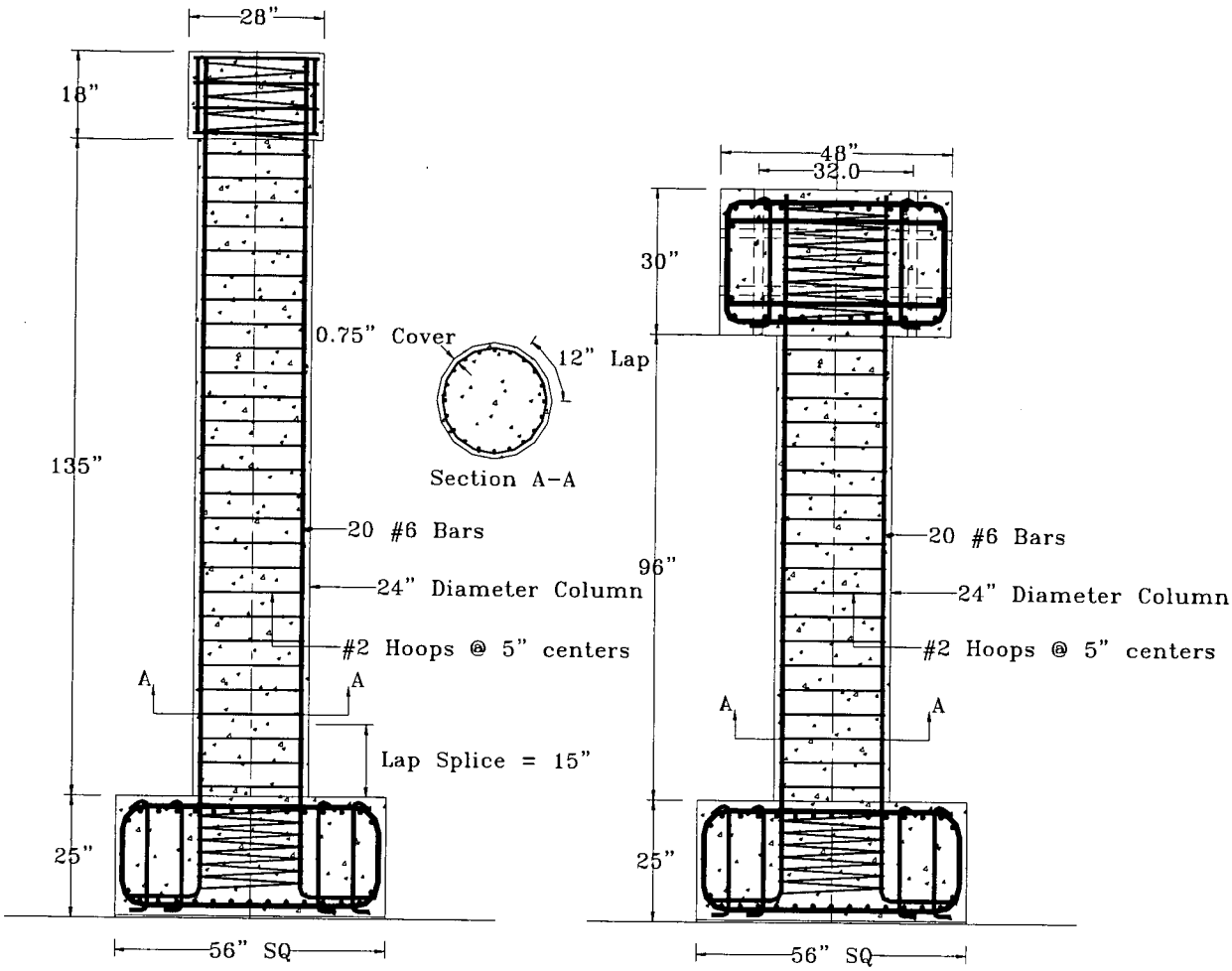
Ten circular columns have been tested so far: two as-built in flexure (CF-1 and CF-2), five retrofitted by five different types of jackets in flexure (CF-3 to CF-7), one as-built in shear (CS-1), and two retrofitted by two different jackets in shear (CS-2 and CS-3). It should be noted that the letter 'C' denotes circular columns, and the letters 'F' and 'S' denote flexure and shear testing, respectively.

Lap Splice Enhancement Columns: Seven reduced scale columns were built with a lap splice. Each column was reinforced longitudinally by 20 #6 (d_b = 1.905 cm) as well as #2 hoops (d_b = 0.635 cm) spaced at 5 inch (12.7 cm). Steel grade 40 was used to accurately reflect the field condition in most existing columns with lap-splices. The footings, however, were reinforced with grade 60 steel. The columns have a circular cross-section with a diameter of 24 inch (60.96 cm). Other details are as shown in Figure 1 and Table 1. These columns were tested in single bending simulating a fixed-free condition with a moment arm of 144 inch (3.66 m).

Table 1. Properties of Circular Column Specimens

Diameter of section	24.00 inch (60.96 cm)
Concrete strength	5.00 ksi (34.5 MPa)
Yield stress of longitudinal steel	43.41 ksi (299.3 MPa)
Number of longitudinal bars	20
Longitudinal steel bar size	#6 (d_b = 1.905 cm)
Clear cover to confinement steel	0.75 in (1.905 cm)
Confinement steel bar size	#2 (d_b = 0.635 cm)
Yield stress of confinement steel	30.5 ksi (210.3 MPa)
Spacing of confinement steel	5.00 in (12.7 cm)

Shear Enhancement Columns: Three reduced scale columns with continuous longitudinal reinforcement were also tested. The reinforcement and cross-section details were identical to the lap-spliced columns except that the column height was 96 inch (2.44m) and the tests were conducted under fixed-fixed conditions. Reinforcement details are displayed in Fig. 1.



(a) Lap Splice Enhancement Column (b) Shear Enhancement Column

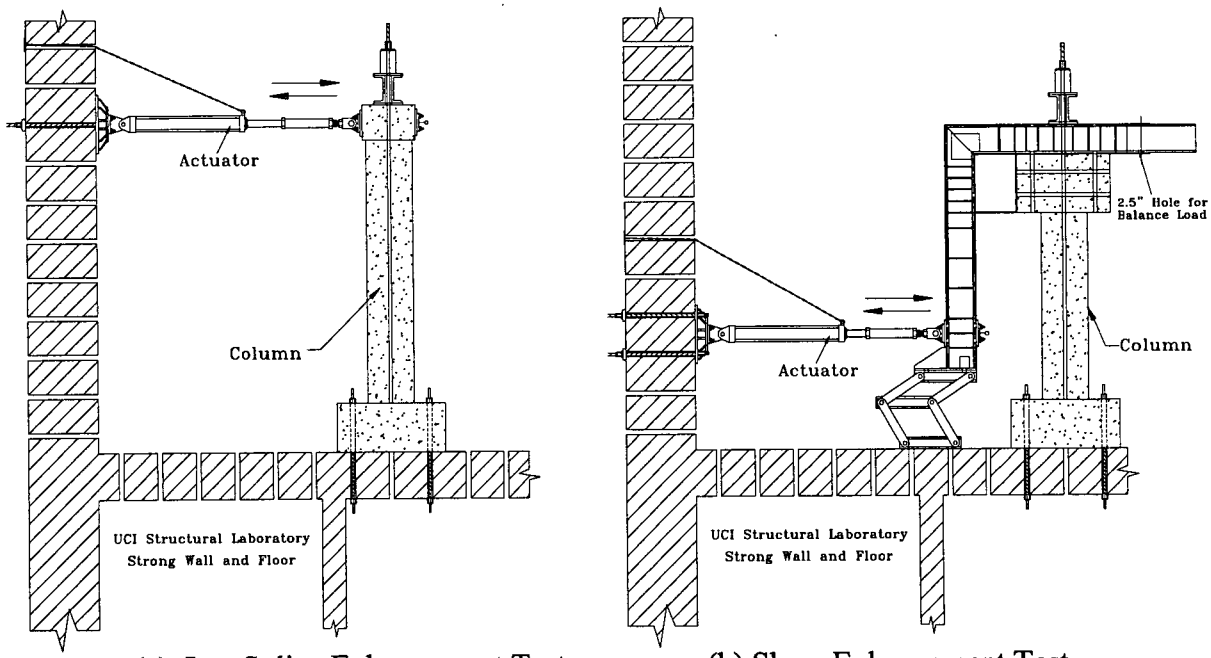
Fig. 1. Details of Tested Circular Columns.

Retrofitted Columns: Three of the column specimens were tested without a jacket (henceforth referred to as 'as- built' columns). Two of the lap splice enhancement columns in flexure and one of the shear enhancement columns were tested in the as-built state. The installation of the composite jackets was performed by crews from each of the participating manufacturers of composite jackets strictly following their own field installation practice. Five of the lap splice columns were retrofitted by five different types of composite jackets. The first three samples, CF-3, CF-4, and CF-5, were carbon fiber jackets whereas the last two, CF-6 and CF-7, were E-glass jackets. So far, only carbon fiber jackets have been installed on columns CS-2 and CS-3, and tested for shear enhancement.

TEST SET-UP AND PROCEDURE

Test Set-up: The test set-up was designed to subject the columns to a constant axial compressive load and cyclic horizontal loads. As shown in Fig. 2(a), each of the lap splice enhancement columns was subjected to a horizontal loading directly applied at the top of the column, by an actuator installed on the strong wall of the Structural Test Hall, to simulate the fixed-free condition. As shown in Fig. 2(b), each of the shear enhancement columns was subjected to a lateral load applied by a specially-designed test rig using a pantagraph arrangement to restrain the rotation at the top of the column, thereby simulating the fixed-fixed condition.

The columns were instrumented with strain gages on the longitudinal reinforcement as well as the hoop reinforcement. The composite jacket was also strain-gaged to monitor its performance. During the test, string potentiometers were used to monitor the displacements at various heights.



(a) Lap Splice Enhancement Test (b) Shear Enhancement Test

Figure 2: Test Set-up.

Test Procedure: An axial load was applied to each column specimen by post-tensioning two steel rods with a hydraulic jack at the top of the column. The ratio of the applied axial load to the column axial load capacity is among the range of those typically used in multi-column bent bridges in California. The horizontal loading regime used in the tests (Table 2) is based on the

guidelines of the California Department of Transportation (Caltrans). The initial loading cycles were controlled by the peak force until the column developed the lateral force corresponding to the first yield of the longitudinal steel, H_y. Then, the test was stopped and the yield displacement was determined from

$$\Delta_y = \frac{H_i}{H_y}\Delta_1 \tag{1}$$

where Δ_1 is the average of the measured peak displacements corresponding to the first-yield lateral load, H_y, in the push and pull directions. The ideal flexural lateral load capacity, H_i, is computed based on an extreme concrete compressive strain of 0.004 (0.005 for the jacketed columns) and on measured material properties. After the column developed the first yield capacity, loading cycles were controlled by the peak displacement.

Table 2: Horizontal Loading Regime

Load	Displacement	No. of Cycles
$0.25H_y$		3
$0.50H_y$		3
$0.75H_y$		3
H_y		3
	Δ_y	3
	$1.5\Delta_y$	3
	$2\Delta_y$	3
	$3\Delta_y$	3
	.....	.....

PREDICTION OF COLUMN PERFORMANCE

The performance of as-built and jacketed columns can be reasonably predicted using standard methods of analysis [4]. For the jacketed columns, the analysis is conducted based on an equivalent steel jacket. A moment-curvature study of the column section provides the first yield moment, the ultimate moment, the lateral load capacity, and the expected displacement ductility. For example, the as-built lap splice enhancement circular column was theoretically expected to achieve a displacement ductility factor of only 2.15. In addition, the column was to exhibit a flexural failure since both shear strengths of the column in the brittle shear failure mode and in the flexural shear failure mode exceeded the expected lateral load capacity of the column. The as-built shear enhancement circular column was designed so that a flexural shear failure would be induced. Example analyses of as-built and jacketed columns can be found in [2].

LAP SPLICE ENHANCEMENT COLUMNS

For lap splice enhancement columns, the as-built samples failed at a displacement ductility factor of about 2, whereas the jacketed columns performed much better reaching ductility greater than 6. The hysteresis loops for both as-built columns, CF-1 and CF-2, were virtually identical, and those of the sample CF-2 are shown in Fig. 3. The hysteresis loops for two of the retrofitted columns, CF-5 and CF-6, are displayed in Figs. 4 and 5, respectively. Note that column CF-5 was retrofitted by a carbon fiber jacket whereas column CF-6 was retrofitted by an E-glass jacket.

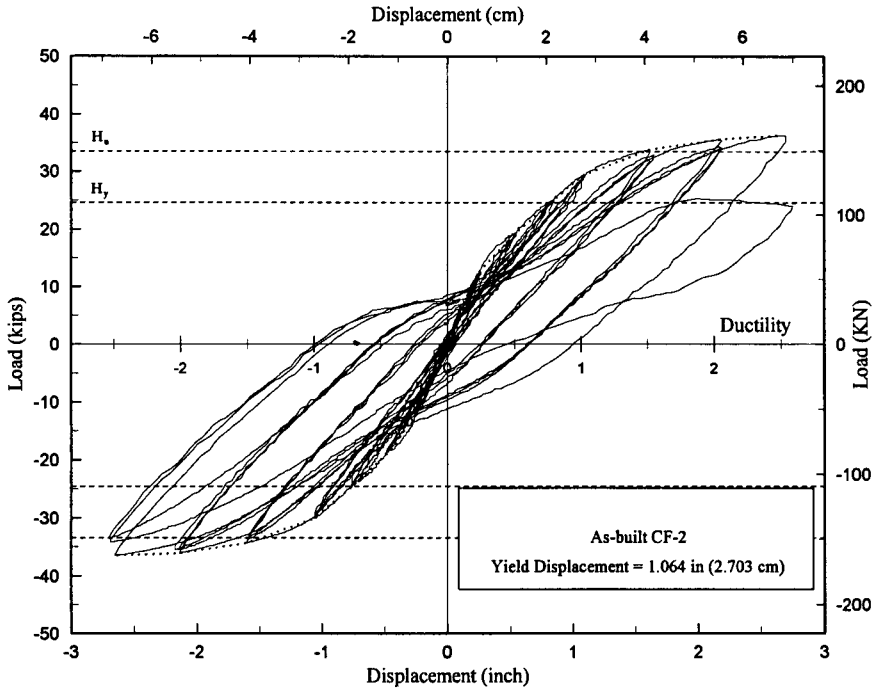


Fig. 3. Hysteresis Loops of As-built Lap Splice Enhancement Column.

For a comparison of the relative performance of all retrofit jackets, the envelopes of the hysteresis loops were constructed and displayed for both the absolute displacements and the displacement ductility factors in Figs. 6 and 7, respectively. It is clear from these figures that all tested jackets were generally successful in clamping on the lap splice in the columns. It should be noted, however, that a quality control of the installation procedure of the composite jackets is of significant importance. For example, the originally-wrapped sample CF-7 performed relatively poorly due to delamination, contrary to the expectations before the test was conducted. An identical virgin column was retrofitted by a similar composite jacket of same design, made from same material, and installed by same crew, except that care was thoroughly exercised in the

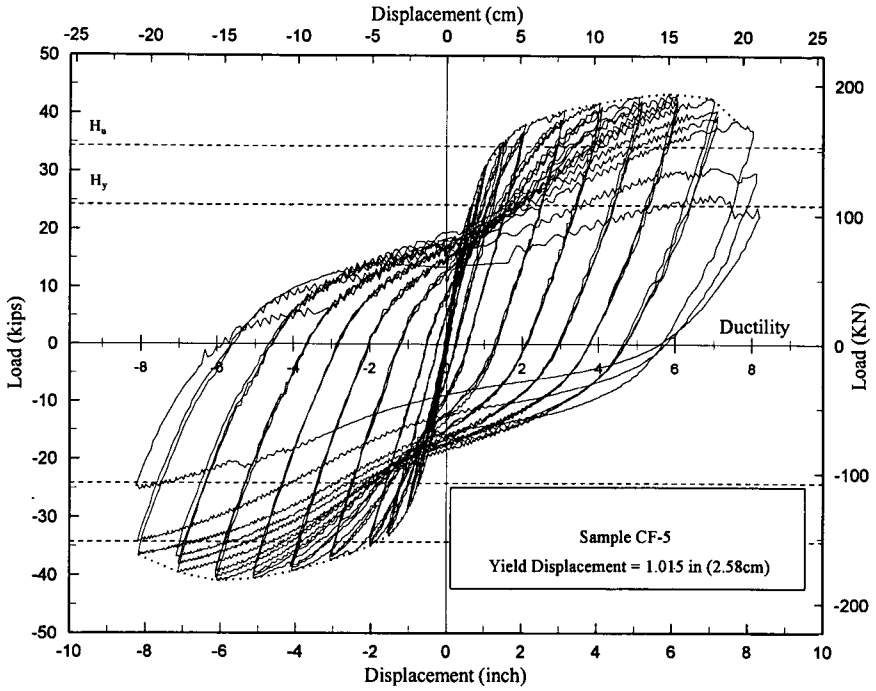


Fig. 4. Hysteresis Loops of a Retrofitted Lap Splice Column with Carbon Fiber Jacket.

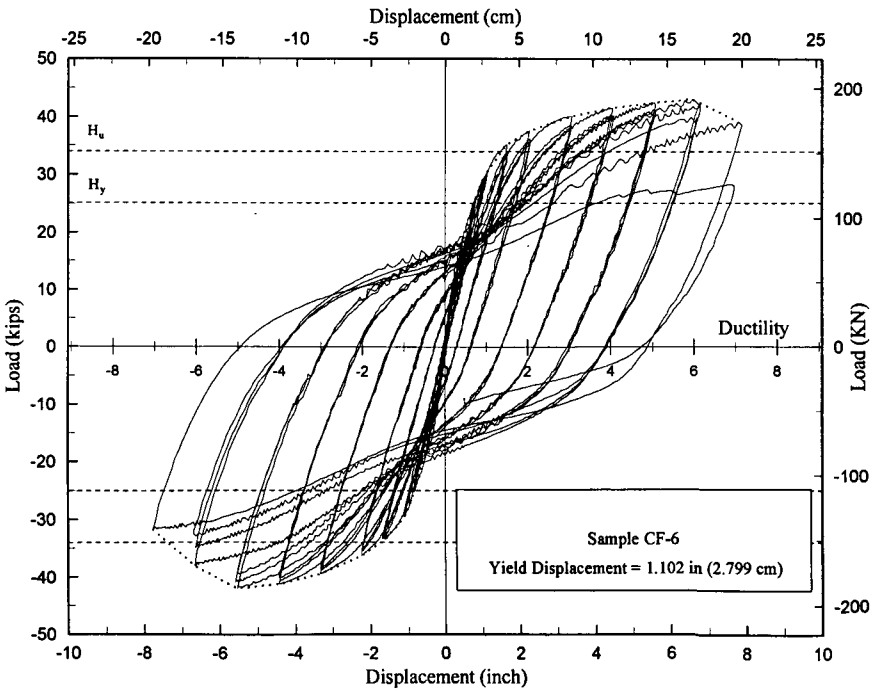


Fig. 5. Hysteresis Loops of a Retrofitted Lap Splice Column with E-glass Jacket.

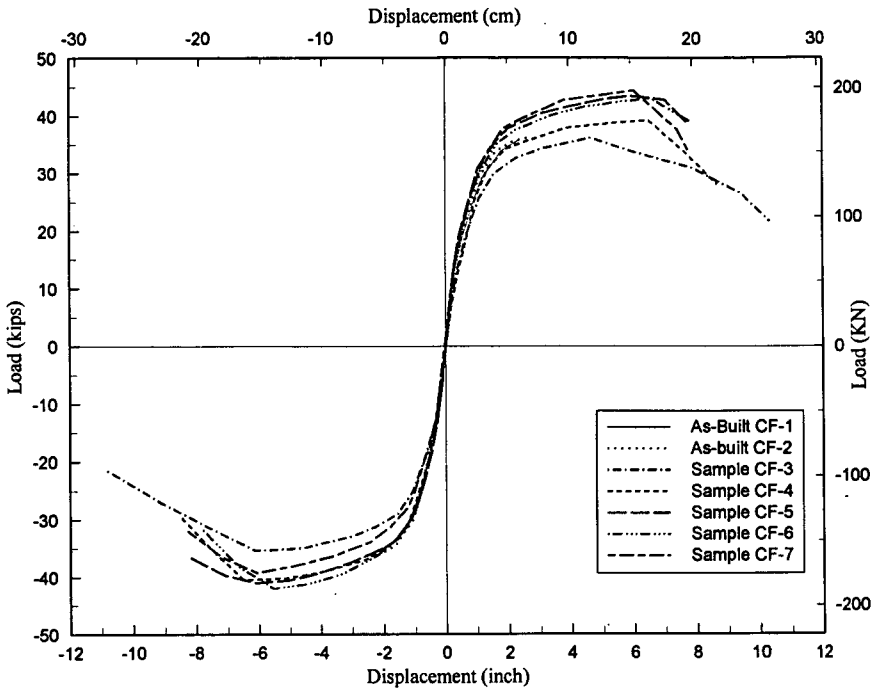


Fig. 6. Load-Displacement Envelopes of Lap Splice Enhancement Columns.

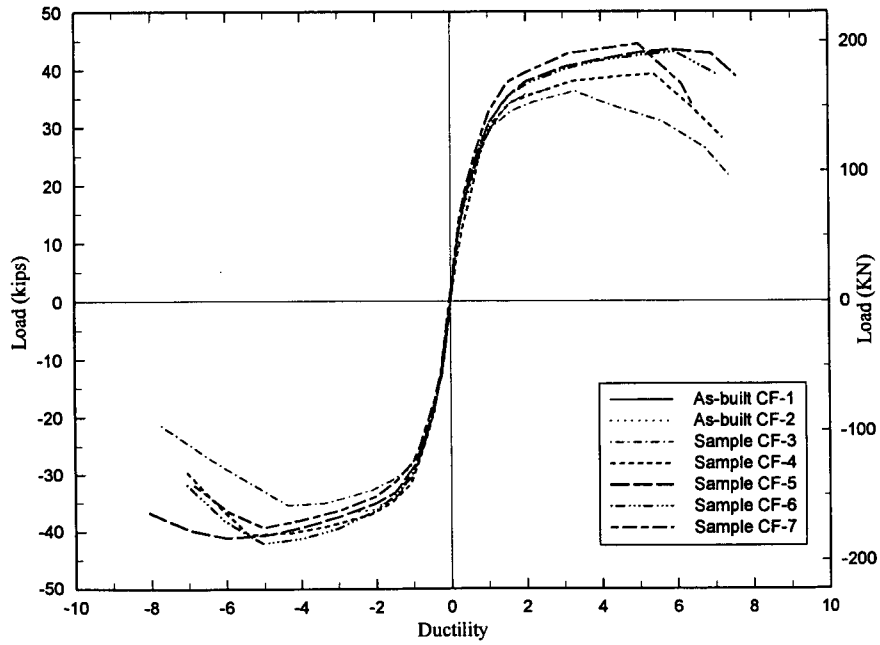


Fig. 7. Load-Ductility Envelopes of Lap Splice Enhancement Columns.

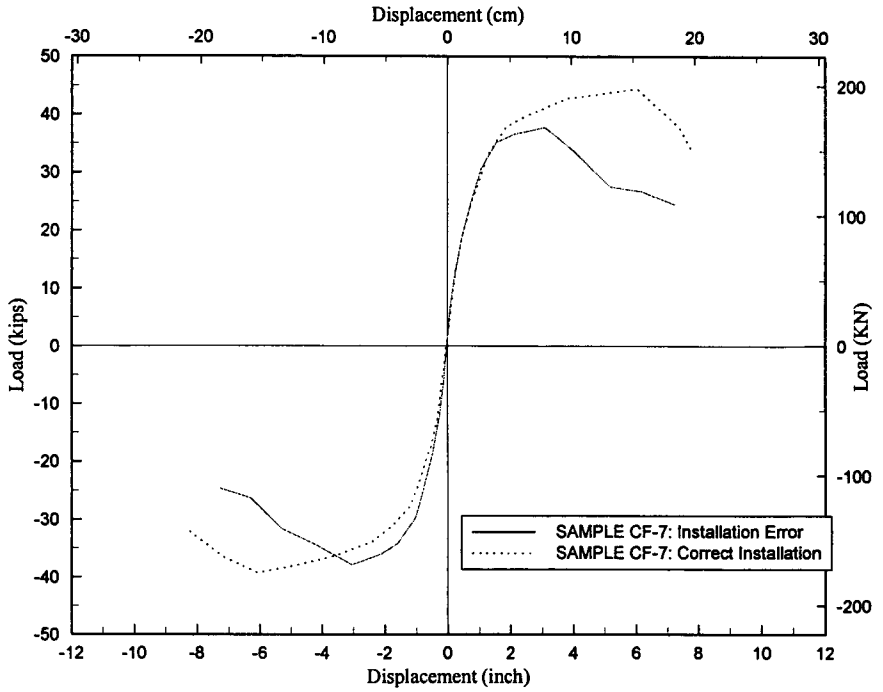


Fig. 8. Quality Control Effect on the Performance of a Retrofitted Column.

installation process. Indeed, the latter sample performed very well, emphasizing the need for quality control of the installation process. Figure 8 shows a comparison between the performance of column CF-7 samples under the same test conditions.

It should be noted that the jacket thickness for columns CF-3 and CF-4 was designed inappropriately by the manufacturers for a design strain of 0.004 rather than the recommended value of 0.001. Had the column jackets been designed for the lower strain, the columns would have achieved a higher ductility factor. It was also noted, and verified by modal analysis tests, that the installation of the advanced composite jackets has very little effect on the column stiffness and its dynamic characteristics.

SHEAR ENHANCEMENT COLUMNS

The shear enhancement columns were tested following the same test protocol as that for the lap splice confinement columns except that the former were tested in a fixed-fixed condition. The enhancement of the column ductility was even more dramatic. Figure 9 shows the hysteresis loops of the shear enhancement column, CS-3, which clearly demonstrate a very stable performance with a preserved ultimate load for large displacement values. Figure 10 displays a comparison of the envelopes of the hysteresis loops for the retrofitted column samples with the as-built specimen.

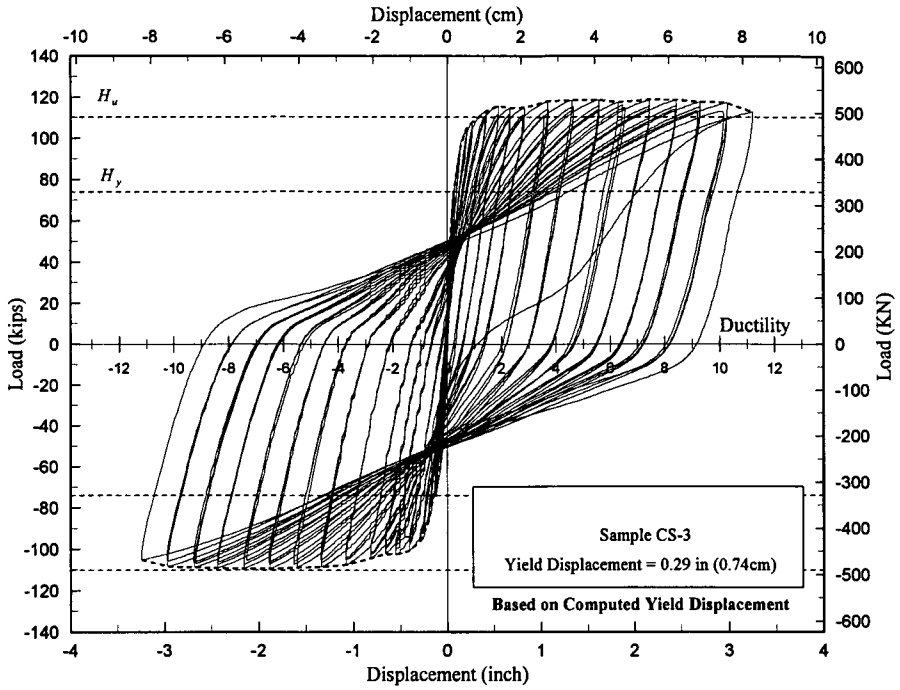


Fig. 9. Hysteresis Loops of a Retrofitted Shear Enhancement Column.

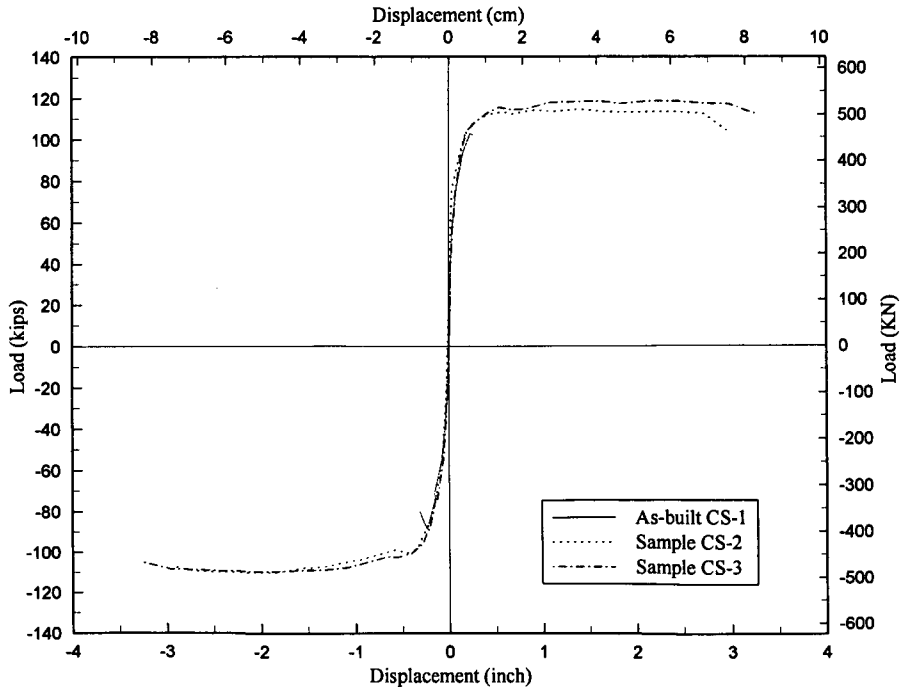


Fig. 10. Load-Displacement Envelopes for Shear Enhancement Columns.

RECTANGULAR COLUMNS

For a complete qualification of columns retrofitted by composite jackets, the testing program also evaluates square/rectangular columns in flexure and shear similar to the circular columns shown before. For lap splice enhancement columns, the cross-section is square with a side length of 24 inch (60.96 cm). The column is reinforced by 20 #6 (d_b = 1.905 cm) as the main longitudinal reinforcement with #2 (d_b = 0.635 cm) spaced at 5 inch (12.7 cm). Each column is tested in single bending simulating a fixed-free condition with a moment arm of 144 inch (3.66 m).

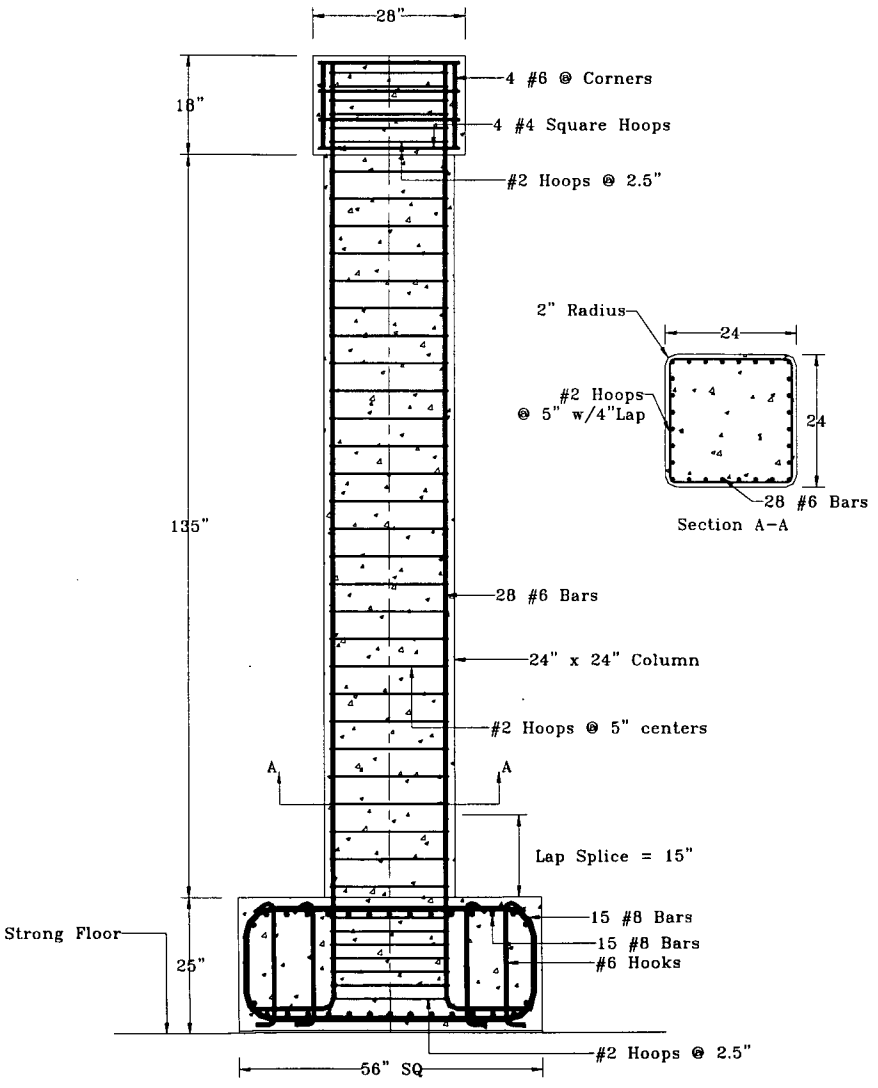


Fig. 11. Reinforcement Details for Lap Splice Enhancement Square Column.

For the shear enhancement columns, the cross section is rectangular with side lengths of 24 x 18 inch, and these columns are tested in double bending to simulate a fixed-fixed condition as shown earlier. The limited tests on lap-spliced square columns in flexure showed a poor performance of the as-built column and very limited improvement in enhancing the column ductility by the direct wrapping of the square column by the carbon fiber jackets.

CONCLUSIONS

This experimental study has demonstrated that advanced composite jackets can significantly enhance the ductility performance of old circular bridge columns with poor lap splice details and insufficient shear reinforcement. Such performance can be predicted by a standard analysis using an equivalent steel jacket. It was also observed from the testing results that the lateral stiffness of the columns is not affected by the composite jackets contrary to steel jackets which alter the lateral stiffness, and consequently, the bridge dynamic characteristics.

The study reported herein is a phase of a comprehensive testing program currently underway at the University of California, Irvine. More columns of different cross-sections and of different types of composite material systems are yet to be tested.

ACKNOWLEDGMENTS

This research is partly supported by the California Department of Transportation through a research funding from the Federal Highway Administration. The research is also supported by the Society for the Advancement of Material and Process Engineering. All tests are monitored by Caltrans engineers. The composite materials are supplied and installed by each manufacturer participating in the qualification testing program.

REFERENCES

1. California Department of Transportation, Bridge Design Specifications, Sacramento, California, 1993.
2. Haroun, M.A., Feng, M.Q., Bhatia, H., Sultan, M., Hoshijima, T., and Kobatake, Y., "Testing Bridge Columns Enhanced by Fiber Composite Jackets," Recent Advances in Bridge Engineering, US-Canada-Europe Workshop on Bridge Engineering, Zurich, July 1997.
3. Haroun, M.A., Haggag, H.A., and Salama, A.E., "Enhanced Seismic Design of Reinforced Concrete Bridge Supporting Elements," 4th US Conf. on Lifeline Earthquake Engineering, August 1995, pp. 439-446.
4. Priestley, M.J.N., Seible, F., and Calvi, G.M., Seismic Design and Retrofit of Bridges, John Wiley and Sons, Inc., 1996.
5. Xiao, Y., Martin, G.R., Yin, Z., and Ma, R., "Bridge Column Retrofit using Snap-Tite Composite Jacketing for Improved Seismic Performance," University of Southern California, Structural Engineering Research Report No USC-SERR95/02, June 1995.

EXPERIMENTAL STUDIES ON DUCTILITY PROPERTIES OF STEEL RECTANGULAR PIERS

H. Hanno[1], H. Tajima[2] and K. Funamoto[3]

ABSTRACT: A series of cyclic loading tests were carried out to investigate the seismic properties of rectangular steel piers of bridges. Retrofitting methods for existing piers such as additional transverse stiffeners, additional flanges welded at the top of the longitudinal stiffeners and concrete filling were proposed. All the specimens presented improvement on their ductility, together with an increase in their load carrying capacity. Relationship between the panel width-thickness ratio R_F and the deformation capacity was also investigated.

1. INTRODUCTION

In view of the damage cases in Hyogo-ken Nanbu Oki Earthquake, it is necessary for Metropolitan Expressway Public Corporation to investigate the seismic property of the steel piers of bridges and improve their resistant capacity to the severe earthquake. The Metropolitan Expressway were mainly constructed in Tokyo area as the city expressway. The current length of the Metropolitan Expressway is 247.8kilometer, of which 202kilometer, about 81% of the total length, are constructed with bridge structure. The number of the piers to support these bridges is 7100, where the steel piers are 2280 bases with about 32% of the total piers as show in Table-1. Since the cross-section of the steel piers is smaller, the steel piers were adopted in narrow places where the construction space is limited, that is the reason why so many steel piers were constructed in Metropolitan Expressway in Tokyo area. The structural form of the steel piers are mainly in single-column and frame, where the frame structure occupies about 60%. Moreover, for the section of the steel piers, about 70% are rectangular section and 30% are circular pipe section. With the investigation of the period when these steel piers were constructed, it is found that about 54%, half of the whole were made before the Specifications for Highway Bridge was published in 1972. Since the design code for the steel stiffened plates of the rectangular steel piers was established in the Specification for Highway Bridge in 1972, the cross-section of the steel piers prior to 1972 was designed in consideration of various parameters of the stiffened plates. However, even for the steel piers constructed after 1972, although the property of stiffened plate is examined for the allowable stress and load, the investigation of the seismic property of the steel piers, especially for the severe earthquake such as the Hanshin great earthquake, was not carried out sufficiently.

Table 1 Number of the Steel Piers in Metropolitan Expressway

	Single-column			Frame			Total
	C. pipe	Rect.	Sum	C. pipe	Rect.	Sum	
Before 1972	190	220	410	190	620	810	1,200 (54%)
After 1972	240	230	470	90	500	590	1,060 (46%)
Total	430	880 (39%)	880	280	1120	1,400 (61%)	2,280

C. pipe: piers with Circular pipe section
Rect. : piers with Rectangular section

[1] Assistant Manager, Design and Research Division, Engineering Department, Metropolitan Expressway Public Corporation, Tokyo, Japan
[2] Section Chief, same as above
[3] Senior Engineer, same as above

In the present paper, the parameters of the stiffened plate and the ductility of the rectangular steel piers are investigated with the experiment in order to develop the retrofitting method and improve the seismic property of the steel piers. Moreover, the experimental results of the rectangular steel piers will be reported here. The experiments were part of a joint research headed by the Public Works Research Institute of the Japanese Ministry of Construction and consisting of the Metropolitan Expressway Public Corporation, the Hanshin Expressway Public Corporation, Japan Association of Steel Bridge Construction and the Kozai Club. Thus, comparisons of the present work results and the experimental results obtained by the other members of this joint research are also provided in the present paper.

2. OUTLINES OF THE DAMAGE IN STEEL PIERS AND PHILOSOPHY OF IMPROVING THEIR SEISMIC PROPERTIES

From what was observed in a survey on actual cases of rectangular piers damaged during the referred earthquake, it could be confirmed that the post-buckling decrease of the load carrying capacity of these piers was due to the increasing progress of the out-of-plane deformation of the stiffened plates, which form the walls of the box cross-sections. Moreover, with the increase of the out-of-plane deformations in the stiffened plates, which comprises the walls of the box cross-section, the corners of the cross-section lose their straightness until the structural collapse, with cracks or rupture at the corners. Therefore, the following three methods are proposed to improve the seismic properties of steel piers with rectangular steel cross-section.

2.1 Improvement of the Stiffened Plate Buckling Strength

If progression of the out-of-plane deformation after buckling in the stiffened plates, causes the decrease in the strength of steel piers, as described in the above lines, improvement of the buckling properties of the stiffened plate can be presented as an alternative to improve the steel pier seismic properties. Generalized panel buckling parameter, width-thickness ratio of the stiffened panel plate, R_F, and the width-thickness ratio of the unstiffened panel between longitudinal stiffeners represented by R_R, can be named as buckling parameters of stiffened plates. Effects of the parameter R_F on the ductility of steel piers have been already discussed by the authors [1][4] in former publications and R_F and R_R are defined as follows:

$$R_F = \frac{b}{t}\sqrt{\frac{12(1-\nu^2)}{\pi^2 \kappa_F}}\sqrt{\frac{\sigma_y}{E}} \qquad (1)$$

and

$$R_R = \frac{b}{t}\sqrt{\frac{12(1-\nu^2)}{\pi^2 \kappa_R}}\sqrt{\frac{\sigma_y}{E}} \qquad (2)$$

where κ_F is the buckling coefficient of the stiffened plate

$$\kappa_F = \frac{(1+\alpha^2)^2 + n\gamma_l}{\alpha^2(1+n\delta_l)}, \text{ for } \alpha \le \alpha_0 \quad \text{and} \quad \kappa_F = \frac{2(1+\sqrt{1+n\gamma_l})}{1+n\delta_l}, \text{ for } \alpha > \alpha_0$$

κ_R is the buckling coefficient of the unstiffened panel between longitudinal stiffeners, $\kappa_R = 4n^2$.
b= plate width; t= plate thickness; σ_y= yield stress; E= Young's modulus; ν= Poisson's ratio;
$\alpha = a/b$; $\alpha_0 = \sqrt[4]{1+n\gamma_l}$; $\gamma_l = \frac{I_l}{bt^3/11}$ and $\delta_l = \frac{A_l}{bt}$.

2.2 Concrete Fill

With the same purpose of restraining the excessive out-of-plane deformation of the stiffened plates, concrete can be filled into the steel piers [2]. Thus, the filled-in concrete confined by the diaphragms and the pier walls, besides inhibiting the lower buckling modes of the stiffened plates, induce the composite steel-concrete action, restraining the out-of-plane displacement of the stiffened plates. Thus, improving also the ductility of the pier. However, it has to be noted

that this composite action causes also a considerable increase in the structural strength.

3. OUTLINES OF THE EXPERIMENTS

3.1 Loading Method

The test specimens were loaded in an experimental setup as shown in Fig. 1.

A constant load of P=0.15 P_y (P_y=yield load at the specimen bottom cross-section) was applied in the specimen axial direction and a variable lateral load (in the direction of the bending moment due to earthquake) was simultaneously applied. As lateral load, a cyclic triangular load, whose amplitude increased linearly, every cycle, in integral multiples of δ_y (δ_y= displacement corresponding to P_y), as shown in the left side of Fig. 1, was applied.

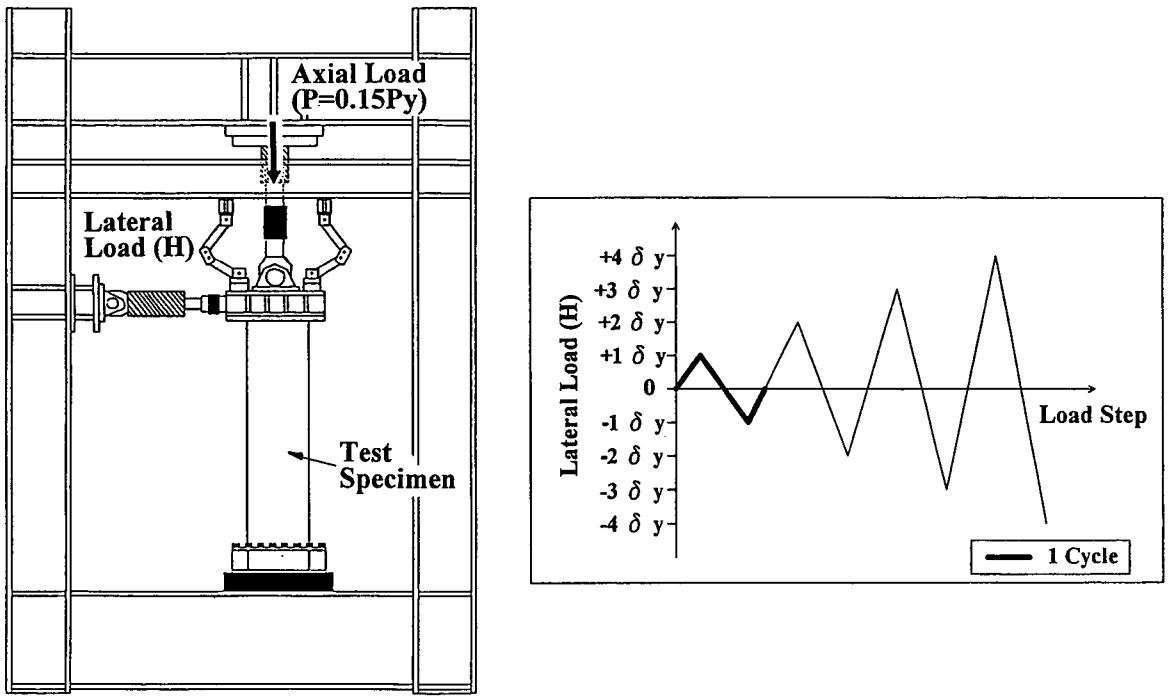


Fig.1 Experimental Setup

3.2 Test Specimen

In order to investigate on the ductility improvement of rectangular piers, the tests were carried out on specimens, whose dimensions were about 1/3 of the average dimensions of the existing piers. The main dimensions of the specimens were 900 mm x 900 mm x 3,470 mm, as it is shown in Fig. 2, where specimen types and their properties are also shown.

A brief description of the specimens is given in the following lines.

3.2.1 Stiffened Plate with Improved Buckling Strength

Increase in the stiffened plate buckling strength can be achieved by improving its width-thickness ratio parameter R_F. In case of piers to be constructed in future, the panel thickness, width-length ratio (aspect ratio), as well as longitudinal stiffener stiffness and distribution are to be defined so as to obtain the required R_F. On the other hand, in retrofitting piers, additional transverse stiffeners and strengthened longitudinal stiffeners (e.g., by adding a flange to the existing longitudinal stiffeners) can be considered to obtain the same effect. In both cases, the improvement of the panel buckling parameter width-thickness ratio is achieved by increasing the longitudinal stiffener stiffness. In the present test, retrofitted structures were mainly focused.

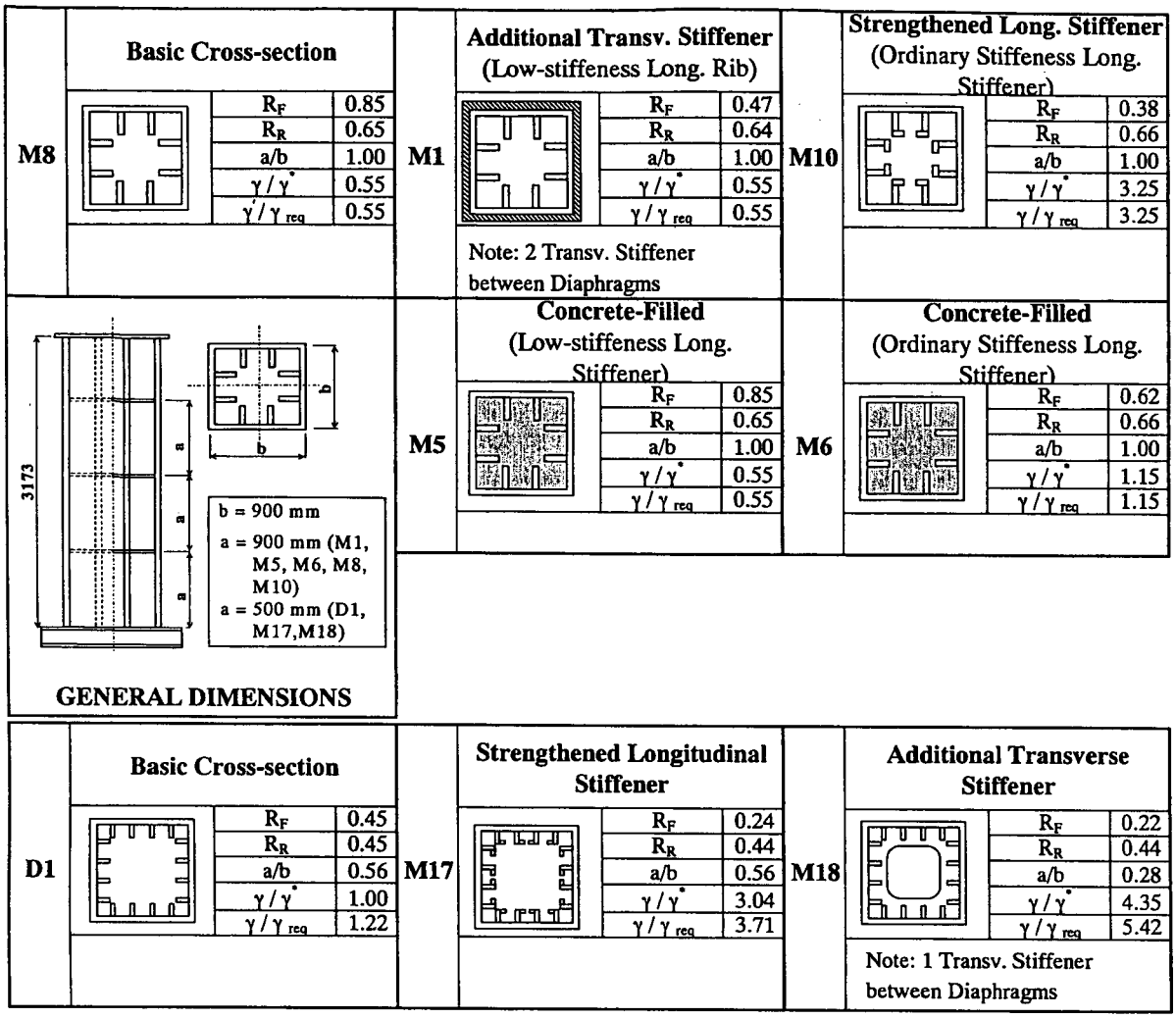


Fig. 2 Test Specimens

Fig. 3 shows the transverse stiffener retrofit and Fig. 4 shows a case of longitudinal stiffener strengthening. In the additional transverse stiffener retrofit, one transverse stiffener is added between diaphragms or transverse stiffeners. The strengthening of the longitudinal stiffener was obtained mainly by adding a flange at the top of the longitudinal stiffeners, at one of its sides, as shown in Fig. 4. This structural detail was chosen so as to keep the increase of the load carrying capacity to a minimum level and promote the improvement in the longitudinal stiffener stiffness to a possible maximum level. In addition, to avoid the lateral buckling of the eccentric cross-section resulting from the addition of a flange at one of the stiffener sides, a plate, hereforth called supporting ribs, was introduced at the stiffener mid-length, as shown in Fig.4.

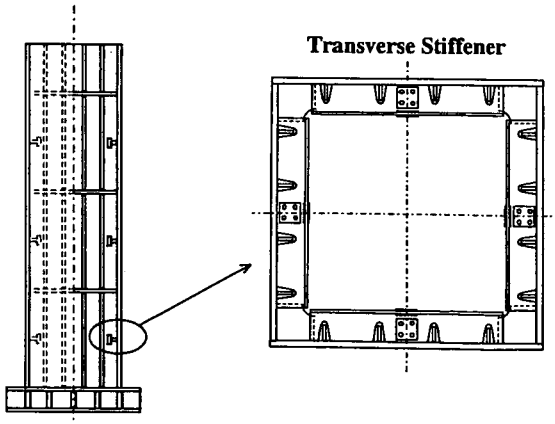


Fig. 3 Detail of Transverse Stiffener Retrofit

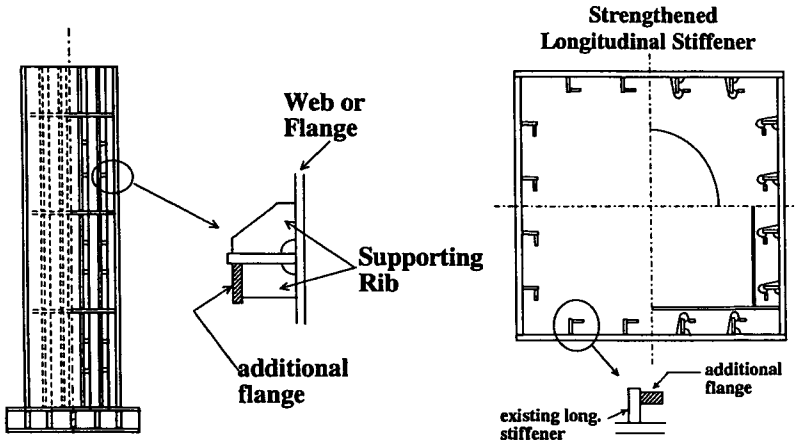


Fig. 4 Detail of Longitudinal Stiffener Strengthening Retrofit

The following specimens were tested.

(1) Retrofit for Pier buckling in the Elastic Range (R_R=0.64)

Based on piers designed according to Japanese specifications prior to 1973, in which the design method for stiffened plate was not yet clearly specified, a specimen corresponding to a low-stiffness pier type (M8), having a longitudinal stiffener stiffness ratio γ/γ_{req} (γ=stiffness of the longitudinal stiffener; γ_{req}= minimum required stiffener stiffness according to the elastic theory) of less than unity (γ/γ_{req}=0.55), was adopted as basic specimen and retrofitted with additional transverse stiffeners (M1) and strengthened longitudinal stiffeners (by adding an eccentric flange to the longitudinal stiffener plate) (M10).

(2) Pier buckling out of the Elastic Range (R_R=0.44)

Retrofit alternatives for a representative case of the recently constructed piers, were tested: one, having transverse internal stiffener retrofit (M18), and another, with strengthened longitudinal stiffeners (M17). The corresponding specimen before retrofitting is the specimen D1 of the Kozai Club.

3.2.2 Concrete Filled Specimens

A specimen with the same dimensions as that of the low-stiffness type (M8) and another, having stiffeners satisfying the current specification, that is $\gamma/\gamma_{req} \geqq 1.0$ (γ/γ_{req}=1.16), were filled in with concrete and named as M5 and M6, respectively. In order to achieve a sufficient confinement effect, the specimens were filled in to the diaphragm height. This height was determined so that the strength of the non-filled parts of the pier did not exceed the ultimate strength of the bottom section of the pier.

4. EXPERIMENTAL RESULTS

4.1 Description of the Damaged Specimens

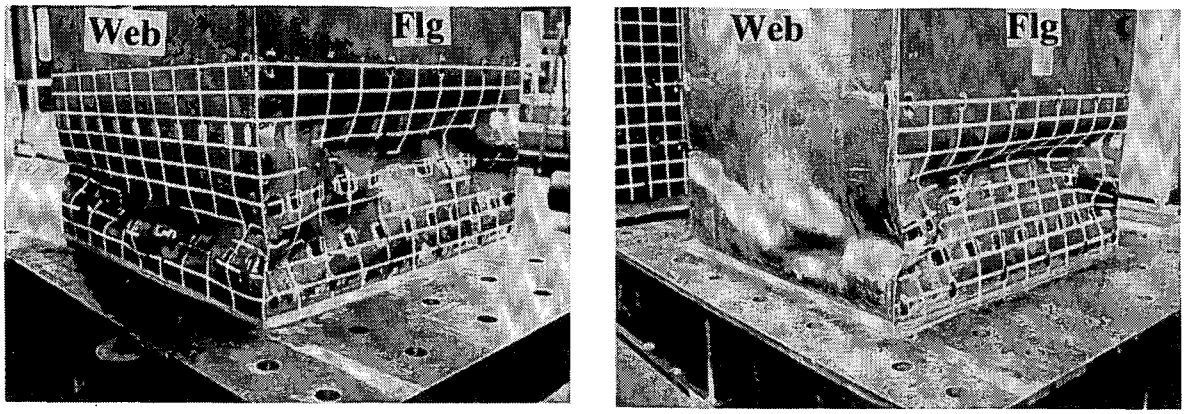
Fig. 5 shows the photographs of the specimen with strengthened longitudinal stiffener, M17, after the loading test, and a brief description of the other specimens is provided in the following lines.

The basic specimen M8 strength decreased after the global buckling of the panel between the bottom diaphragms.

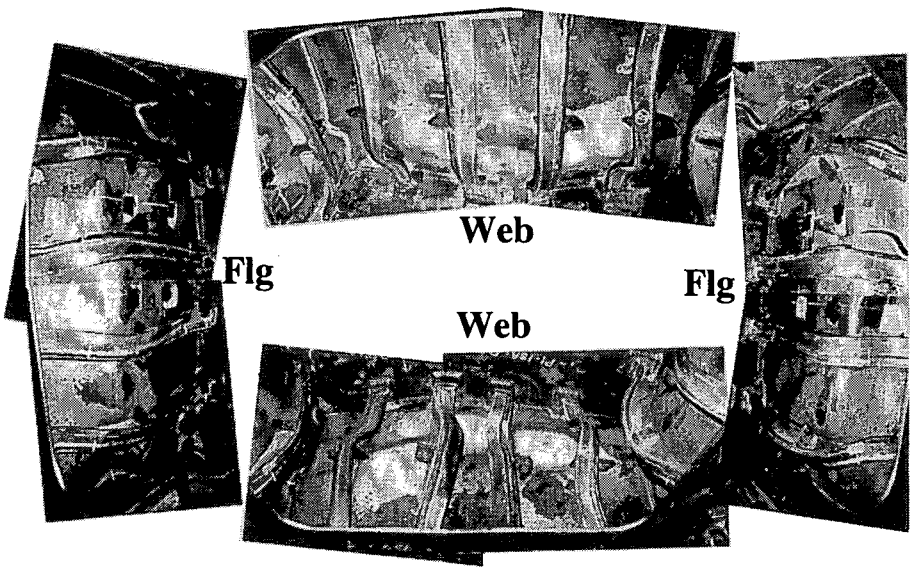
The specimen with additional transverse stiffeners (M18), due to the short distance between the transverse stiffeners, displayed a buckling mode that covered not only the bottom panel, but also at the panel just above it.

In the case of the specimen with strengthened longitudinal stiffeners (M17), due to the high stiffness of the longitudinal stiffeners, the panel between the longitudinal stiffeners buckled first.

With the increase of the deformation, a global panel buckling mode was developed. The supporting rib plates, welded in the mid-distance of the diaphragms to prevent lateral buckling of the stiffener, was effective, avoiding extreme deformations due to lateral buckling. Moreover, these supporting ribs worked as transverse stiffeners for the stiffened panel, restraining the progression of the stiffened panel buckling.



(b) External View



(b) Internal View

Fig. 5 View of the Specimen M17 after the Loading Test

As for the concrete filled specimen (M5), having modes with deformation towards the interior of the cross-section inhibited, presented higher modes of deformation towards the exterior of the cross-section. After that, the load carrying capacity decreased due to the overall exterior deformation of the stiffened plate.

4.2 Comparison of Each Specimen Hysteresis and Envelope Curves

Fig. 6 shows the hysteresis loops resulting from the cyclic loading on each specimen.

All the hysteresis loops presented concave form, characteristic of steel piers, with high energy absorption capacity. The concrete-filled specimens loops presented a behavior resembling that of a reinforced concrete pier. Transverse stiffener and longitudinal stiffener retrofit speci-

mens presented extended deformation capacity, compared with the basic specimen. The corresponding experimental results are shown in Table 1.

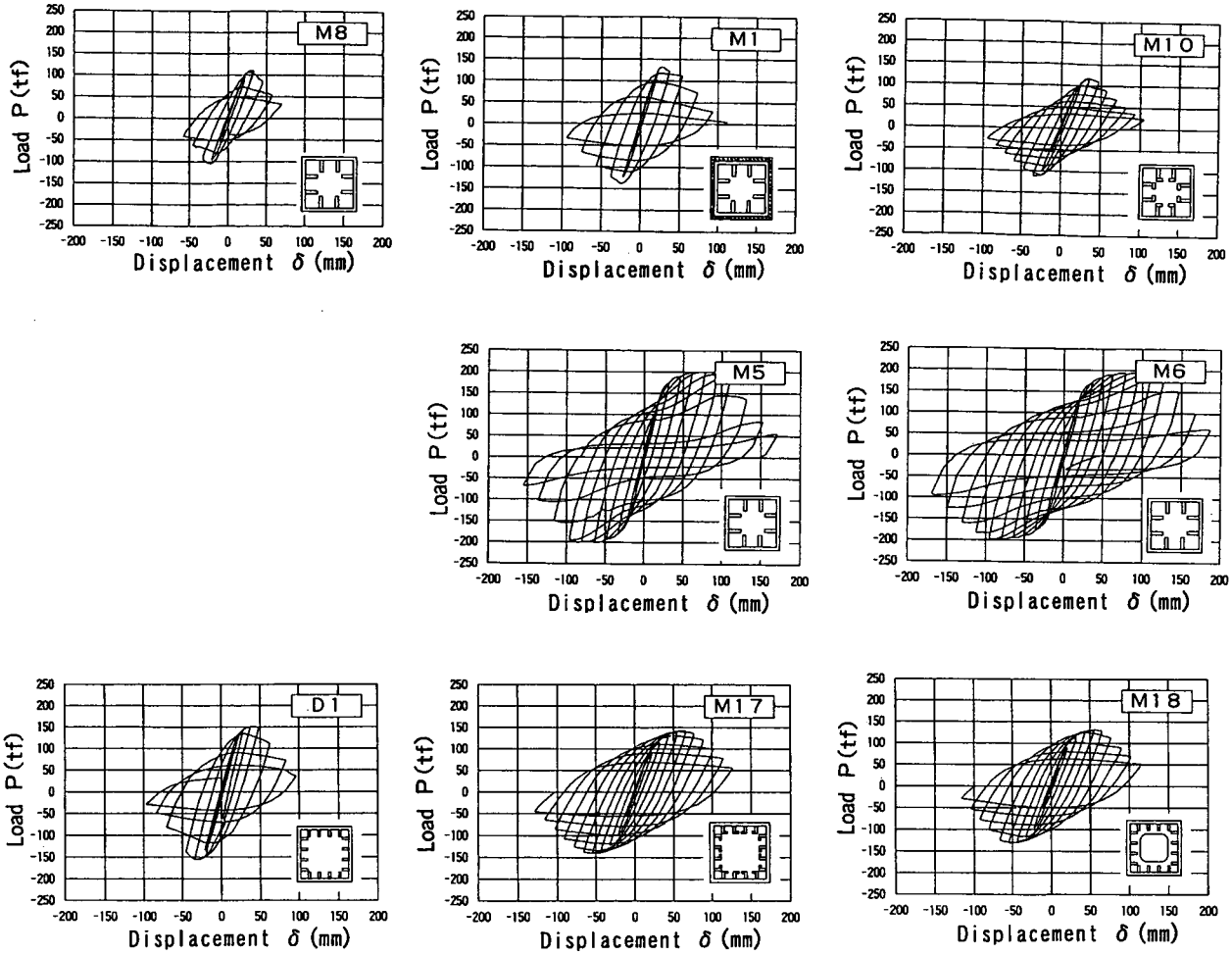


Fig. 6 Hysteresis Curves for Each Specimen

Table 1 Stiffened Panels Parameters R_F, R_R and γ/γ_{req}; δ_m/δ_y, δ_{97}/δ_y and δ_{y2}/δ_y and Maximum Load P_m/P_y

Specimen Name	R_F	R_R	γ/γ^*	γ/γ_{req}	δ_m/δ_y	δ_{97}/δ_y	δ_{y2}/δ_y	P_m/P_y
M8	0.85	0.65	0.55	0.55	1.9	2.0	2.1	1.11
M1	0.47	0.64	0.55	0.55	2.1	2.5	4.8	1.37
M10	0.38	0.66	3.25	3.25	1.9	2.4	3.1	1.15
M5	0.85	0.65	0.55	0.55	9.7	12	18.8	2.00
M6	0.62	0.66	1.15	1.16	9.2	11.6	16.8	1.78
D1	0.45	0.45	1.00	1.22	3.1	3.7	5.7	1.41
M17	0.24	0.44	3.04	3.71	3.8	4.8	7.1	1.43
M18	0.22	0.44	4.35	4.35	3.7	4.3	5.5	1.29

where δ_y= lateral displacement corresponding to the first yield or local buckling;
δ_m= lateral displacement corresponding to the maximum lateral load;
δ_{y2}= equivalent horizontal displacement at the second yield point;
δ_{97}= lateral displacement at the point where the load carrying capacity degrades to 97% of the maximum load;
P_m= maximum lateral load.

In Fig. 7, envelope curves of the retrofitted specimens, with their respective basic specimens M8 and D1 are presented. Both cases of stiffener retrofit and concrete-filled specimens showed improvement in their ductility, with concrete-filled specimens presenting higher ductility and increase in their load carrying capacity. However, considering that increase in the load carrying capacity may be harmful to the anchor bolts, which connect the pier base to the foundation, further consideration is necessary. Among the specimens with stiffeners retrofit, the case with longitudinal stiffeners has greater deformation capacity compared with transverse stiffeners which buckles out of the elastic range. Influence of the parameter R_R of the basic specimen on the effectiveness of the stiffener retrofit was also confirmed. Stiffened plate of specimen M8, in which elastic-buckling occurs, improvement of the ductility due to stiffener retrofit was relatively small.

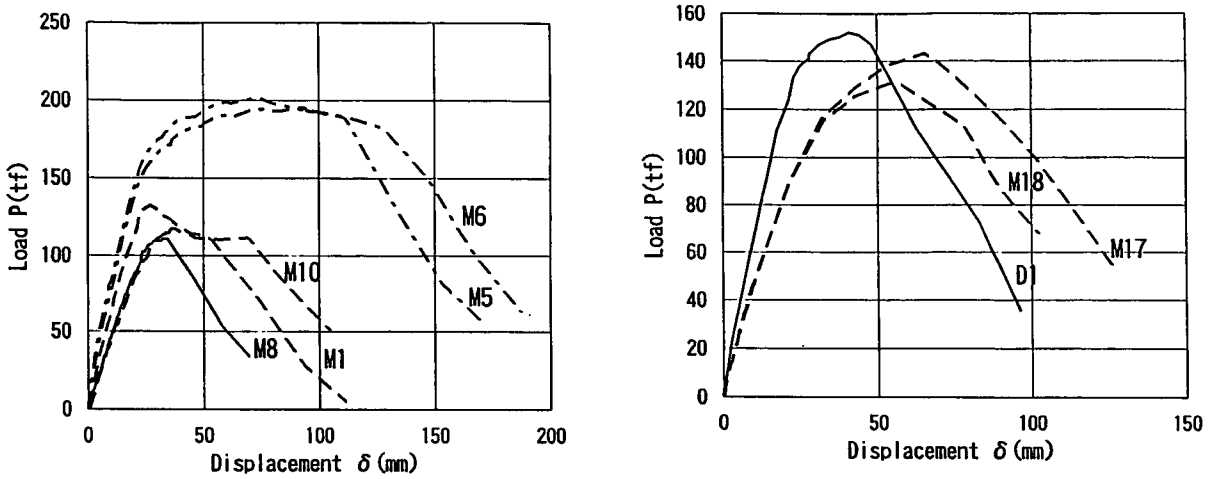


Fig. 7 Envelope of the Hysteresis Curves for Each Specimen

4.3 Relationship between δ_{97}/δ_y and R_F, P_m/P_y and R_R

Fig. 8 shows the relationship between δ_{97}/δ_y and R_F and Fig. 9, the relationship between P_m/P_y (P_m=maximum lateral load) and R_R. The figure confirms that R_F has decreased (improved) and the deformation capacity has extended due to the longitudinal stiffener strengthening,. However, it was also confirmed that in case elastic buckling occurs in the basic specimen and in case it does not occur, even with the same values of R_F, present different behaviors when considering the structural

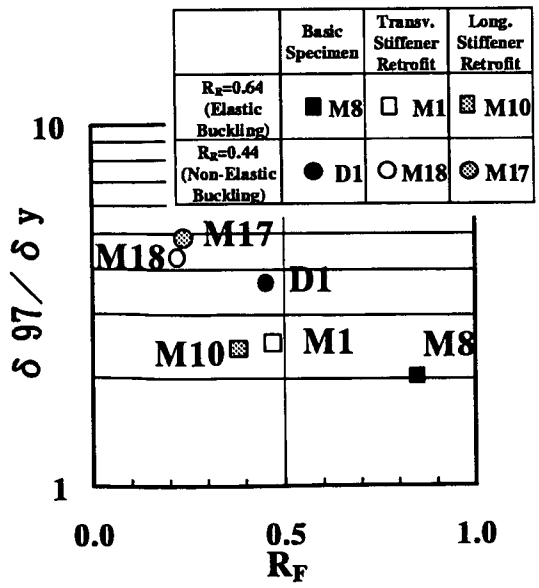


Fig. 8 Relationship between δ_{97}/δ_y and R_F

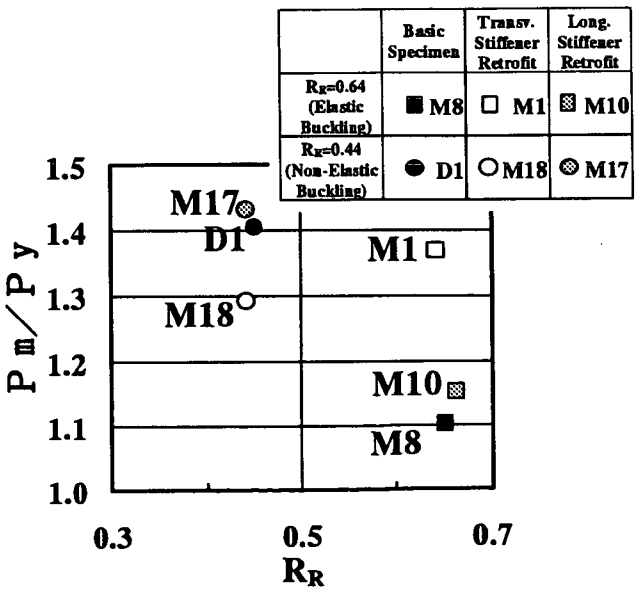


Fig. 9 Relationship between P_m/P_y and R_R.

deformation capacity. As for relationship between P_m/P_y and R_R, the values of P_m/P_y for specimen D1 and the corresponding retrofit specimens M17 and M18 ranged from about 1.3 to 1.4, and in case of the basic specimen M8, having P_m/P_y of about 1.1, with the corresponding retrofit specimens (M1, M10), these values ranged from about 1.15 to 1.37. From this it can be concluded that elastic buckling has occurred in M8.

5. CONCLUSION

As a means to investigate on the seismicity of the rectangular steel piers, a series of tests, in which cyclic loading was applied to steel pier specimens, was carried out. Concerning the case of existing piers, retrofit by additional transverse stiffeners, retrofit by strengthening longitudinal stiffener through the addition of eccentric flange plates and retrofit by concrete fill had their effectiveness confirmed. The case of strengthening longitudinal stiffeners, as a means to reduce the plate width-thickness ratio parameter R_F to improve the structural ductility was also confirmed. However in members where the elastic buckling is clearly predominant (R_R>0.6), the improvement in the ductility is small. In this case, the addition of extra longitudinal stiffeners between the existing stiffeners can be considered as necessary. Concrete fill improves the structural ductility to a great extent, but has the disadvantage of increasing the structural strength as well, being it necessary to check with the pier base anchor bolt strength.

ACKNOWLEDGMENTS

The authors would like to sincerely thank Professors Y. Fujino (University of Tokyo), T. Yoda (Waseda University) and Y. Goto (Nagoya Institute of Technology) for their valuable guidance throughout the course of the present study.

The following individuals, members of Japan Association of Steel Bridge Construction, made significant contributions to the work described in this paper: T. Okamoto (Nippon Steel, Ltd.), H. Hashimoto (Mitsubishi Heavy Industries, Ltd.) and L. H. Ichinose (Harumoto Corporation, Ltd.).

REFERENCES

[1] Tajima, et.al., "Cyclic Loading Test on Rectangular Steel Piers", Proceedings of the Annuals of Japan Society of Civil Engineering, pp.586,587, Sept. 1996. (in Japanese).

[2] Usami, et. al., "A Proposal for Check of Ultimate Earthquake Resistance of Partially Concrete Filled Steel Bridge Piers", Proceedings of Japan Society of Civil Engineering, Oct. 1995, pp.83-95. (in Japanese).

[3] Nishikawa, et. al., "Guide Specifications for Reconstruction and Repair of Highway Bridges Suffered Damage due to Hyogo-ken Nanbu Earthquake", Feb. 1995 (in Japanese).

[4] Tajima, et.al., "Cyclic Loading Test on Ductility Properties of Rectangular Steel Piers", Proceedings of the Annuals of Japan Society of Civil Engineering, pp.208,209, Sept. 1997. (in Japanese).

A Comparative Study of Elastic-Plastic Seismic Response Analysis and Pseudo-Dynamic Testing of Steel Bridge Piers

Tatsumasa Takaku[1], Sigeru Ikeda[2], Takasi Okamoto[3],
Hiroshi Matsuda[4], Hiroyoshi Noto[5], Yutaka Kawai[6]

1 Principal Eng., Steel Structure, Machinery and Construction Division, NKK Corporation, 2-1 Suehiro-chou, Tsurumi-ku, Yokohama, Japan
2 Manager, Technical Dept., Sumitomo Heavy Industries, Co., Ltd., Tokyo
3 Chief Researcher, Applied Technology Research Center, NKK Corporation, Kawasaki, Japan
4 Manager, Scientific and Technical Service Sales Dept., Japan Information Processing Service Co., Ltd., Tokyo
5 Manager, Research Laboratory, Miyaji Iron Works Co., Ltd., Tokyo
6 General Manager, Bridge and Steel Structure Engineering Dept., Kawasaki Steel Corporation, Tokyo

Abstract

This report describes a comparison of analytical simulations to the results of pseudo-dynamic tests and the results of an investigation into the applicability of simulations based on a bilinear model for the seismic design of steel bridge piers. A restoring property with a single degree of freedom model that was assumed to be bilinear agreed with hysteresis curves obtained from cyclic loading tests. Other models of the restoring property were also examined. The pseudo-dynamic tests were conducted at Nagoya University and NKK Corporation. The simulations were carried out by participating members of the Japan Association of Steel Bridge Construction (JASBC).

Introduction

Many road structures, including steel bridge piers, suffered significant damage by the 1995 Hyogo-ken Nanbu Earthquake. Since that earthquake, a number of organizations have conducted loading tests to failure to establish a reliable design method that can provide sufficient ductility for steel structures designed using the allowable stress design method. Non-linear dynamic response analysis was recognized as an effective method for designing steel bridge piers in the November 1996 revision of the Japan Highway Bridge Specifications.

The use of a highly precise method is essential for verifying the reliability of non-linear dynamic response analyses that use restoring force characteristics that are based on cyclic loading tests of a single column bridge pier. However, equipment used in seismic response testing, including shaking tables, cannot fully reproduce the response of pier members in terms of the scale factor relationship. Furthermore, testing to failure using large amplitude, seismic waveforms is difficult to perform, and equipment capable of such testing is extremely rare. For these reasons, testing that is sufficient for corroboration is difficult to achieve.

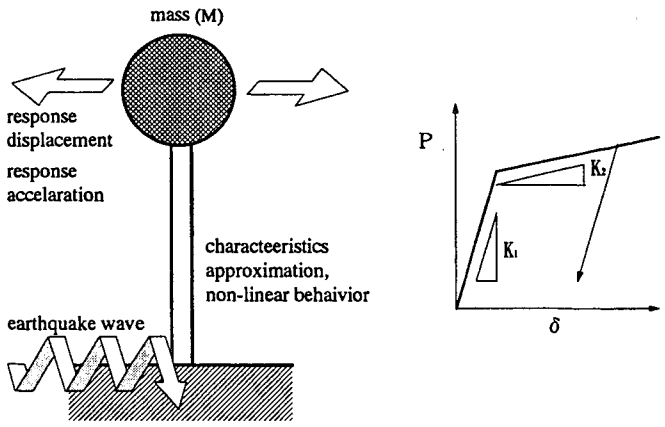


Fig-1 Non-linar simulation model of a single degree of freedom

Table-1 Bench mark test results by analysis

approximation		bi-linear model		tri-linear model	
input earthquake wave		Hyogo-ken Nanbu Earthquake			
		ground foundation class Ⅰ	ground foundation class Ⅲ	ground foundation class Ⅰ	ground foundation class Ⅲ
displacement	maximum	1.012	1.012	1.139	1.224
	minimum	0.916	0.981	0.972	0.383
	deflection	0.030	0.007	0.053	0.172
	disribution				
accelaration	maximum	1.013	1.006	1.208	1.073
	minimum	0.992	0.996	0.886	0.913
	deflection	0.004	0.002	0.075	0.030
	disribution				
reaction force	maximum	1.038	1.012	1.077	1.026
	minimum	0.967	0.995	0.974	0.917
	deflection	0.012	0.003	0.021	0.027
	disribution				
Number of analysis tests : bi-linear model : 19 tri-linear model : 16		Soft ware program : TDAPⅢ、DYNA2E、RESP、COSMOS/M、Y-DYNA/NL、Self developped program			

Table-2 Similarity law of the pseudo-dynamic test

item	dimension	for rectangular section	for circular section
length	L	S	S
mass	M	S^3	S^2
time	T	S	$\sqrt{S}$
stress	$ML^{-1}T^{-2}$	1	1
velocity	LT^{-1}	1	$\sqrt{S}$
acceleration	LT^{-2}	1/S	1
force	MLT^{-2}	S^2	S^2
rigidity (E·I)	MT^{-2}	S	S

S : Scale factor

However, several research institutes at universities and elsewhere have been conducting tests for several years in which computer calculations using differential equations and experimental measurements of the response characteristics of specimens have been performed while linked on-line. This pseudo-dynamic testing involves extending the time axis by factors of more than 100 and provides seismic inertial forces by using an actuator controller for measuring the restoration response characteristics of specimens.

This report presents the results of seismic response testing, which used equipment provided by NKK and Nagoya University, and a comparison of these results to dynamic response analyses, which were performed as a joint research project of the Public Works Research Institute (PWRI) of the Ministry of Construction, Metropolitan Expressway Public Corporation, Hanshin Expressway Public Corporation, Nagoya Expressway Public Corporation, the Kozai Club, and the JASBC. The results of a single degree of freedom dynamic response analyses were compared to those of pseudo-dynamic testing to establish how restoring force characteristics should be set for non-linear dynamic response analyses for design verification.

Benchmark Test

The analyses presented in this report were carried out individually by working groups formed by the JASBC to study the ultimate strength of steel bridge piers. Therefore, benchmark tests were carried out in advance to confirm the compatibility of the wide variety of analysis programs used.

As shown in Table 1, the results confirmed that almost no discrepancies occurred between the results of analyses performed using different programs for a single degree of freedom, bilinear model. The table also reveals that there were no significant errors caused by factors such as the integration method or the time interval used. Substantial scatter occurred in the tri-linear case because of the wide variety of setting methods used.

Structural Model

Non-Linear Dynamic Response Analysis Model

Figure 1 is a schematic diagram of the vibration model for a single degree of freedom, non-linear, dynamic response analysis. Structural members with restoring characteristics are treated as scalar spring elements. The mass, length, and other properties should be determined by using a similarity law for the pseudo-dynamic testing model.
The damping factor was set as $h = 0.05$ for the proportionally decreasing stiffness approximation.

The Pseudo-Dynamic Testing Model

Figure 2 presents a schematic of the vibration model for the pseudo-dynamic test. For this test, the restoring force was measured based on the displacement of the top of the specimen and the force of the actuator. A differential equation was solved and integrated based on the single degree of freedom vibration model.

The test was performed assuming that the scale factor for the model was 1/8 of an actual bridge pier model. The similarity law for the length, weight, time, etc., of this test is shown in

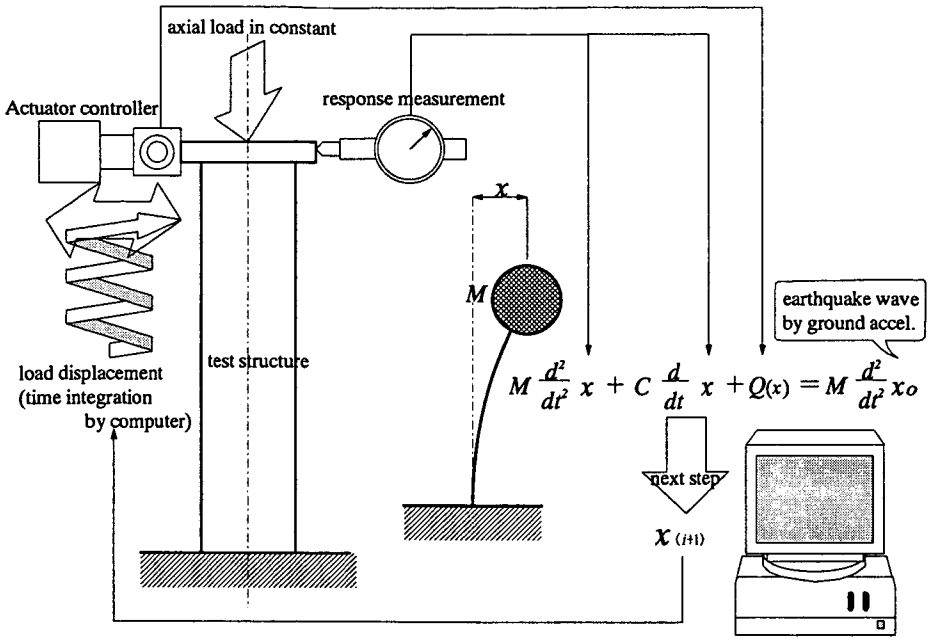


Fig-2 Schematic drawing of pseudo-dynamic test set-up

Table-3 Strucural properties of existing bridge pier model calculated based on the similarity law

		model	mass (tf·s²/cm)	yield force (tf)	yield displacement (cm)
rectangular section	series □①	R-04	3.110	910.2	8.55
		R-05	3.127	914.9	8.49
		R-06	2.331	951.6	8.73
		R-07	2.338	954.8	8.89
		R-08	3.919	1153.5	4.88
		R-09	3.916	1152.7	4.88
		R-10	3.142	919.4	8.49
		R-11	3.096	905.0	8.36
		R-12	2.363	965.1	8.94
		R-13	2.336	953.7	8.88
	series □②	R-16	2.703	652.1	5.66
		R-17	2.706	652.8	5.65
		R-18	2.717	655.4	5.66
		R-19	2.025	688.8	5.98
circular section	series ○①	P-04	2.002	584.1	6.51
		P-05	1.974	574.8	6.30
		P-06	1.458	617.9	7.03
		P-07	1.445	612.0	6.90
		P-08	2.103	613.1	4.20
		P-09	2.090	609.1	4.13
		P-10	1.876	545.1	5.94
		P-11	1.797	521.8	5.85
		P-12	1.508	639.5	7.11
		P-13	1.518	643.6	7.07
	series ○②	P-16	2.754	659.9	5.74
		P-17	2.106	741.4	6.35
		P-18	3.167	755.6	3.94
		P-19	2.806	672.8	5.80
		P-20	2.049	721.2	6.24

Table 2. Table 3 shows the weight, lateral yield load, and yield displacement of the bridge pier model based on this similarity law. The specimens included those with rectangular and circular cross sections. Each of these groups were categorized as either basic cross section 1, with low stiffened ribs, or basic cross section 2, with high stiffened ribs, because the ductility differs according to the cross section and rib type.

Earthquake Waveforms

The earthquake waveforms used for the dynamic response analysis and the pseudo-dynamic test are shown in Figure 3. Earthquake waveforms defined by the Base Isolation Design Manual and those observed during the Hyogo-ken Nanbu Earthquake were used. The waveforms were normalized with a maximum acceleration of ± 1.0[1]. Two variations for each of these waveforms were used (ground categories I and III). The amplitude of the acceleration for each of these is determined by the unit wave value multiplied by the multipliers shown in Figure 4.

Restoring Characteristics

Comparison of Restoring Characteristics

The restoring characteristics applicable to steel bridge piers include multi-linear models, such as bilinear and tri-linear models. The following analytical models were developed for defining restoring characteristics. One to several cases were analyzed for each model with suitable parameters set for each case. The results were compared to the pseudo dynamic test results to validate each of the models.

[1] Stiffness hardening type bilinear model
The restoring characteristics defined by this model are shown in Figure 4.

[2] Fully elastic-plastic type bilinear model
Analysis was performed for 3 cases, and the yield points used in the analysis were appropriately adjusted for each case.

[3] Degrading hysteresis type bilinear model
Analysis was performed for 1 case, and the degradation range was represented by a gradual gradient.

[4] Tri-linear model
Analysis was performed for 3 cases, and the third gradient was defined to be within the degradation range.

[5] E-D hysteresis model
The restoring characteristics were defined using the "damage index based on evolutionary degrading hysteresis model"[2] to establish the restoring characteristics along the displacement - load hysteresis curve. The curve was obtained prior to the pseudo dynamic test from cyclic loading of specimens with the same shape as that used for the analysis. The damage index was defined as shown below.

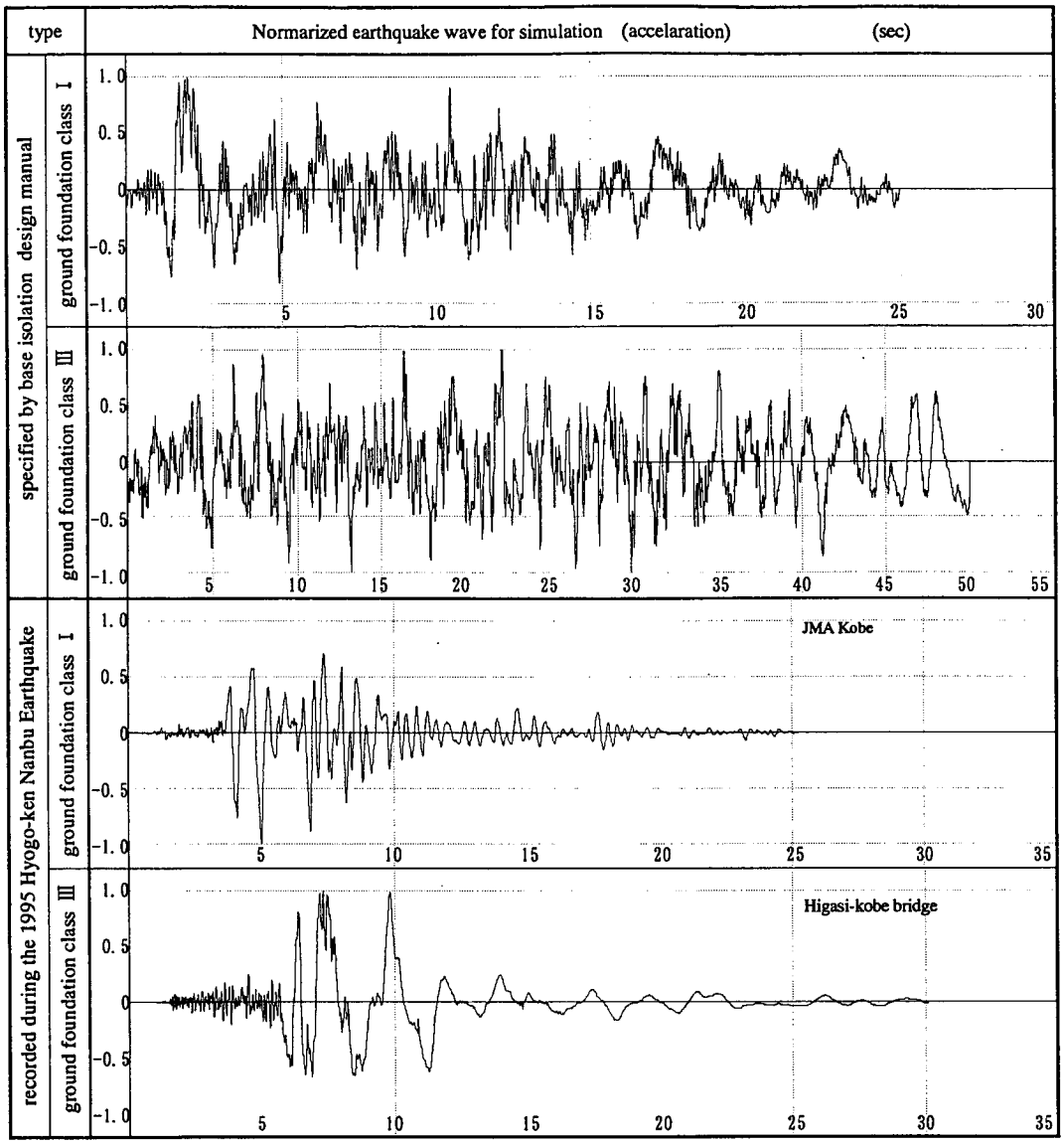


Fig-3 Normarized earthquake wave used for simulation

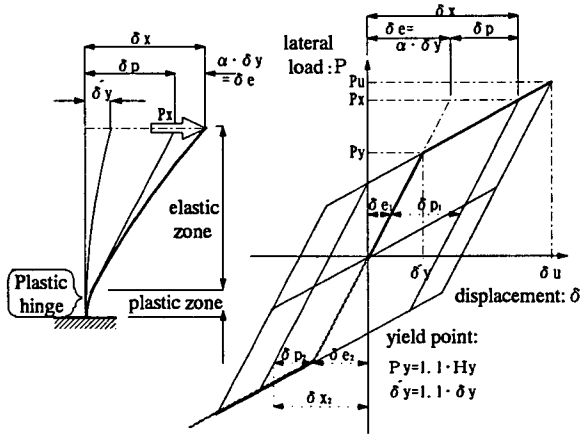


Fig-4 Hardening type bi-linear approximation of the load-displacement response

Table-4 Maxium response accelaration due to various eathquake waves on differrent ground foundations

		model	input eathquake wave		max.accelaration (gal)
			eathquake wave	ground foundat	
rectangular section	series □①	R-04	specified by base isolation design manual	class Ⅰ	360.0
		R-05			540.0
		R-06		class Ⅲ	442.9
		R-07			664.3
		R-08		class Ⅰ	360.0
		R-09			540.0
		R-10	recorded in the 1995 Hyogo -ken Nanbu Earthquake	class Ⅰ	818.0
		R-11			1227.0
		R-12		class Ⅲ	325.8
		R-13			488.8
	series □②	R-16	specified by base isolation design manual	class Ⅰ	360.0
		R-17	recorded in the 1995 Hyogo -ken Nanbu Earthquake	class Ⅰ	818.0
		R-18		class Ⅰ	1227.0
		R-19		class Ⅲ	325.8
circular section	series ○①	P-04	specified by base isolation design manual	class Ⅰ	360.0
		P-05			432.0
		P-06		class Ⅲ	442.9
		P-07			606.8
		P-08		class Ⅰ	360.0
		P-09			432.0
		P-10	recorded in the 1995 Hyogo -ken Nanbu Earthquake	class Ⅰ	818.0
		P-11			1227.0
		P-12		class Ⅲ	325.8
		P-13			488.8
	series ○②	P-16	specified by base isolation design manual	class Ⅰ	360.0
		P-17		class Ⅲ	442.9
		P-18		class Ⅰ	360.0
		P-19	recorded in the 1995 Hyogo -ken Nanbu Earthquake	class Ⅰ	818.0
		P-20		class Ⅲ	325.8

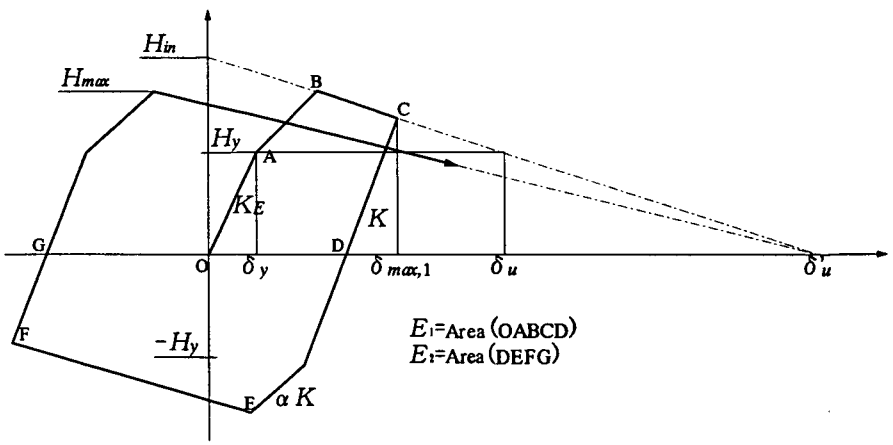


Fig-5 E-D type approximation of the hysterisis

$$D=(1-\beta)\sum_{j=1}^{N_1}\left(\frac{\delta_{\max j}-\delta y}{\delta u-\delta y}\right)^c+\beta\sum_{i=1}^{N}\left(\frac{E_i}{Hy(\delta_u-\delta y)}\right)^c$$

The degrading horizontal load and the displacement - load gradient are defined by the following formulae using this damage index for the model (Figure 5).

$H_{max} = H_{in\cdot e} — [In(H_{in}/H_y)]D$

$K = K_{E\cdot e} — [In(H_{in}/H_y)]D$

Using the four earthquake waveforms, [1] to [4] were applied to rectangular cross section specimens in the basic cross section 1 category, while [5] had a circular specimen in the basic cross section 1 category. The results are shown in Figure 8.

Stiffness Hardening Type Bilinear Restoring Characteristics

When included as part of a design method, the restoring characteristics model should provide consistent analysis results, ensure a close relationship between the design restoring characteristics of the cross section and analysis results, and allow estimation of the design restoring characteristics of the cross section required if a cross section is inadequate. It must also confirm the safety of the design while avoiding excessive safety factors.

With a stiffness hardening type bilinear model, the second gradient is not small compared to the initial gradient, unlike the other models. Moreover, variations between the results of different programs used for stiffness hardening type bilinear analyses are not as large, as shown by the results of the benchmark tests. This means that this model can satisfy the characteristics required for a design method, as described above.

This model, which is included in the commentary to the Earthquake Resistance Section of the Japan Highway Bridge Specifications as a model for designing corner stiffening structures, is expected to provide appropriate analysis results within the range of the allowable ductility factor established through static cyclic loading and other tests. This allowable ductility requirement is based on the displacement at 97% of the maximum lateral degrading load on the skeleton response curve obtained from cyclic loading tests.

Figure 6 shows a response curve setting method. Two types of skeleton curves for determining the response curve were obtained, as shown below. Each varies between the basic cross sections 1 and 2 of the rectangular and circular cross sections. These are:

[1] Curves estimated from multiple results of static cyclic load tests performed during the joint research program, and

[2] Curves obtained using the pseudo-dynamic testing facility from the results of cyclic loading tests using the same cross section.

Simulation Results

The simulation results were summarized in a format that compares them to the test results. The figures, hysteresis diagrams, and time history were compiled in reports[3].

Table-5 Summary of pseudo-dynamic test results

sect	height of model (mm)	model EQ wave (gal)	responses of pseudo-dynamic test (absolute maximum displacement → [+]) -5 0 displacement (x/ δ y) +10
rectangular section, series □① low stiffened section	1847	R_04 Manual Ⅰ 360.0	
		R_05 Manual Ⅰ 540.0	
		R_06 Manual Ⅲ 442.9	
		R_07 Manual Ⅲ 664.3	
	1396	R_08 Manual Ⅰ 360.0	
		R_09 Manual Ⅰ 540.0	11.47
	1847	R_10 Hyogo Ⅰ 818.0	
		R_11 Hyogo Ⅰ 1227.0	
		R_12 Hyogo Ⅲ 325.8	
		R_13 Hyogo Ⅲ 488.8	
series □② high stiffened section	1388	R_16 Manual Ⅰ 360.0	
		R_17 Hyogo Ⅰ 818.0	
		R_18 Hyogo Ⅰ 1227.0	
		R_19 Hyogo Ⅲ 325.8	

sect	height of model (mm)	model EQ wave (gal)	responses of pseudo-dynamic test (absolute maximum displacement → [+]) -5 0 displacement (x/ δ y) +10
circular section, series ○① thin wall section	1800	P_04 Manual Ⅰ 360.0	
		P_05 Manual Ⅰ 432.0	
		P_06 Manual Ⅲ 442.9	
		P_07 Manual Ⅲ 606.8	
	1500	P_08 Manual Ⅰ 360.0	
		P_09 Manual Ⅰ 432.0	
	1800	P_10 Hyogo Ⅰ 818.0	
		P_11 Hyogo Ⅰ 1227.0	
		P_12 Hyogo Ⅲ 325.8	
		P_13 Hyogo Ⅲ 488.8	
series ○② thick wall section	1800	P_16 Manual Ⅰ 360.0	
		P_17 Manual Ⅲ 442.9	
	1500	P_18 Manual Ⅰ 360.0	
	1800	P_19 Hyogo Ⅰ 818.0	
		P_20 Hyogo Ⅲ 325.8	

Abbreviation for EQ wave:

Manual Ⅰ :specified by base isolation design manual／ground foundation class Ⅰ
Manual Ⅲ: 〃 ／ground foundation class Ⅲ
Hyogo Ⅰ :recorded in Hyogo-ken Nanbu Earthquake／ground foundation class Ⅰ
Hyogo Ⅲ: 〃 ／ground foundation class Ⅲ

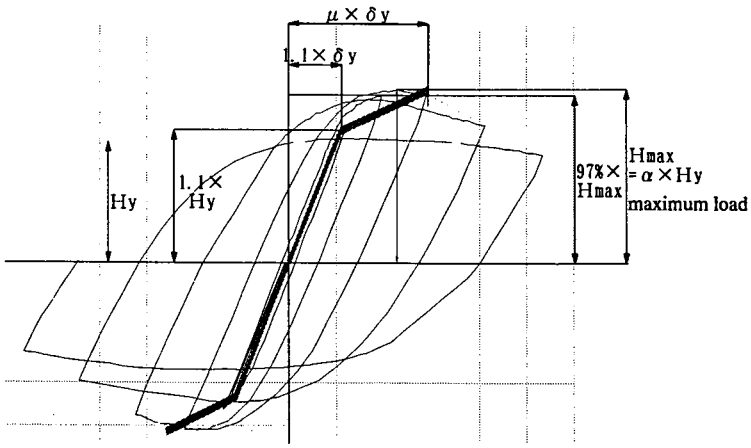


Fig-6 Response curve setting method of hardening type bi-linear approximaton

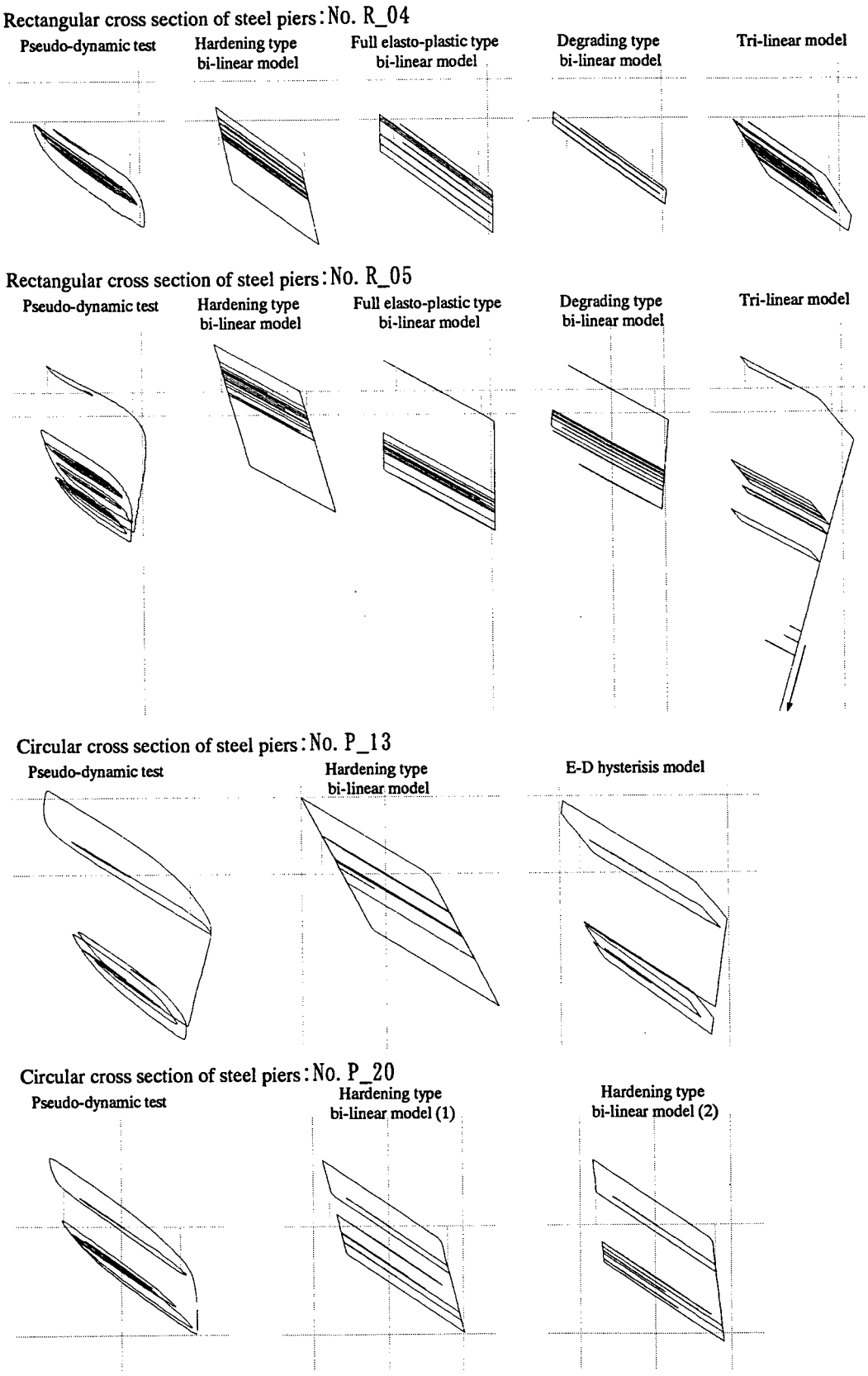


Fig-7 Hysterisis variation due to various approximation methods

Comparison of Analysis To Test Results

Table 5 presents hysteresis diagrams for the results of tests conducted to compare the corresponding dynamic response analysis results.

Figure 7 presents typical P - δ hysteresis diagrams from the analysis along with the test results. To simplify the comparison, lateral displacement is shown on the vertical axis, and lateral load on the horizontal axis.

Displacements obtained from the analysis and testing are organized and plotted based on their ratio to the allowable displacement (allowable ductility factor x yield displacement = $\mu^2 \cdot \delta y$). Figure 9 plots all the results with the test values on the horizontal axis, and the dynamic response analysis values on the vertical axis. Figure 10 plots only those results for which the ratio of the analysis result is within the range represented by the following formula.

Allowable displacement ratio:

$$\frac{|x|^A_{max}}{\mu_a \delta y} \leq 1.2$$

where, $|x|^A_{max}$ is the maximum absolute value of the displacement by analysis, and

$\mu_a \delta y$ is the allowable displacement.

In other words, Figure 10 presents the allowable displacement ratio for the limited range that can be used for design.

Observation

Comparison of analyses using various restoring characteristics to the test results led to the following findings.

(1) With a fully elastic-plastic bilinear model, only the yield point is a variable. Thus, adjusting and setting the yield point using the hysteresis curve obtained from the tests permits calculation of the maximum displacement, etc., with relatively high precision. However, it is difficult to simultaneously obtain the minimum displacement, residual displacement, etc., with high precision. By such adjustments, the maximum displacement ratio can be obtained within the range of 0.96 to 1.14 (0.96 - 1.14), and the residual displacement ratio within the range of 0.69 to 1.19 (0.97 - 1.19). (The figures in parentheses represent values within a limited range where no substantial degradation occurs.)

(2) With a degrading hysteresis, bilinear model, the maximum displacement can be calculated with the same precision as that of the fully elastic-plastic type where the degradation is represented by a gradual gradient.

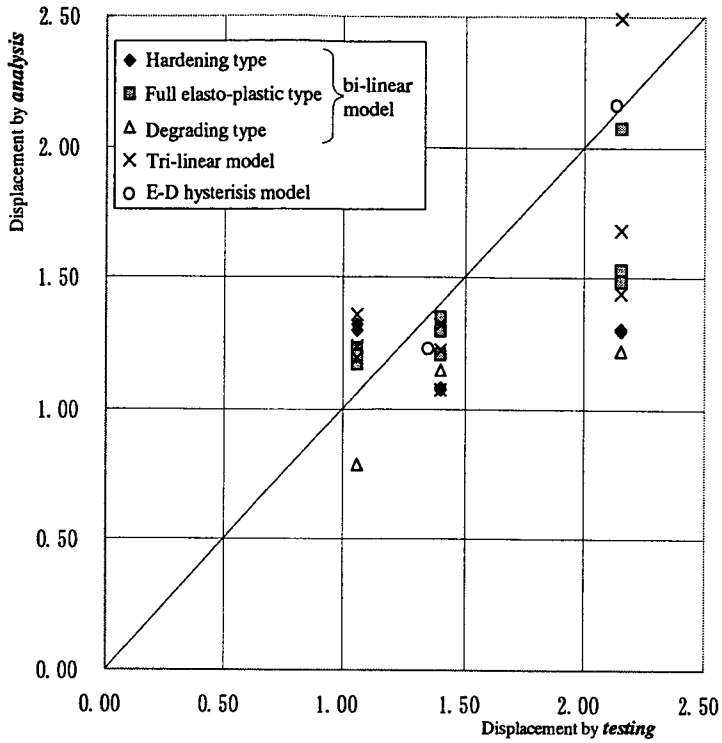


Fig-8 Maximum displacement obtained from testing and analysis for various restoring approximation methods

Explanation about axes

Displacement by *analysis* $\frac{|x|^{A}_{max}}{\mu_s \delta y}$

Displacement by *testing* $\frac{|x|^{E}_{max}}{\mu_s \delta y}$

$\|x\|^{A}_{max}$	Absolute maximum value of displacement by *analysis*
$\|x\|^{E}_{max}$	Absolute maximum value of displacement by *testing*
$\mu_s \delta y$	allowable displacement (allowable ductility factor × yield displacement)

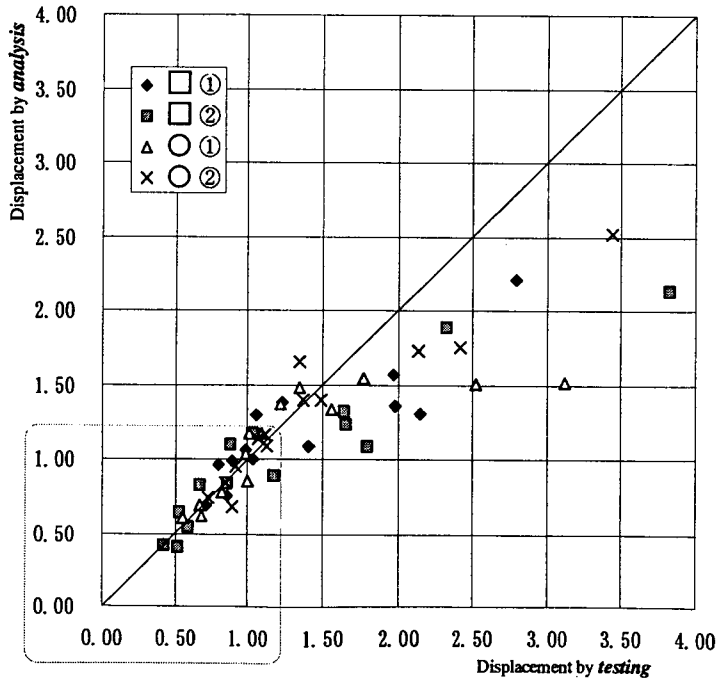


Fig-9 Maximum displacement obtained from testing and analysis for bi-liner model (1) (for all analytical values)

(3) With a standard tri-linear model, whose third gradient is treated as a bilinear degrading hysteresis type, a divergence occurs in calculations with a relatively small change in acceleration. This is attributed to the severity of the degradation gradient. The maximum displacement ratio obtained by analysis ranged from 0.67 to 1.29 (0.76 - 1.29) where there was no such divergence.
(4) With the E-D hysteresis model, the reaction - displacement relationship, etc., can be reproduced with extremely high precision based on adequate parameter settings, as shown in Figure 8. The maximum displacement ratio is within 0.92 to 1.38 (0.92).
(5) For the bilinear stiffness hardening model, the setting was determined using the yield strength of the steel specimen and the results of two cyclic loading tests, but the maximum displacement ratio shown in the figure ranges from 0.61 to 1.25 (0.76 - 1.25).
(6) These findings are limited to the maximum displacement. But, if the shape of the horizontal displacement - reaction hysteresis curve including the degradation range is considered, the reproducibility is ranked in the following order: [1] E-D hysteresis model, [2] tri-linear model, [3] fully elastic-plastic or gently degrading type bilinear model, and [4] stiffness hardening bilinear model. However, where the lateral load does not exceed the maximum load, the same settings can be used for all the model types except the fully elastic-plastic type. It is therefore difficult to determine a ranking unless the analysis models are compared.

If only the maximum displacement is considered, there is not a big difference between models where the setting of the restoring characteristics is complicated and those where it is simple. However, where the parameters related to the various restoring characteristics are determined most appropriately, the precision of the complicated ones will probably be even higher.

As stated previously, the stiffness hardening, bilinear model provides a number of benefits as a design method. Thus, the case should be considered where the non-linear properties of a beam member (as represented by M - ϕ) are defined using this model, as shown in Figure 11. For a single column bridge pier, the bending moments, curvature, rotational angle, and displacement distribution in relation to a bridge pier height should be obtained by integration in the above sequence. Requirements for designing to an ultimate state are: no degradation range and a suitable difference between the bending moments as shown by M - ϕ of the yield point and the maximum load point. A stiffness hardening bilinear model satisfies the requirements. In the case where M - ϕ is approximated by a stiffness hardening bilinear model, P - σ is not bilinear, but uniformly increasing. However, if simplified to the extreme, P - σ would be bilinear stiffness hardening. Therefore the stiffness hardening, bilinear model is the most appropriate design method.

Based on this concept, it is appropriate to define the design restoring characteristics as bilinear. The following conclusions were reached through a comparison of the dynamic response analysis using bilinear restoring characteristics to the test results.
(1) If the dynamic response analysis using the bilinear restoring stiffness hardening characteristics given in Figure 6 defines the allowable ductility factor by the maximum load point or by a slight degradation (97%), Figures 9 and 10 show only one case where the maximum displacement ratio of the analysis is 1.0 or less, while that of the measured is 1.0 or greater. Therefore, in nearly all analysis cases, the judgment will be identical to a judgment of safety in the testing. Consequently, the reliability of safety verification of the

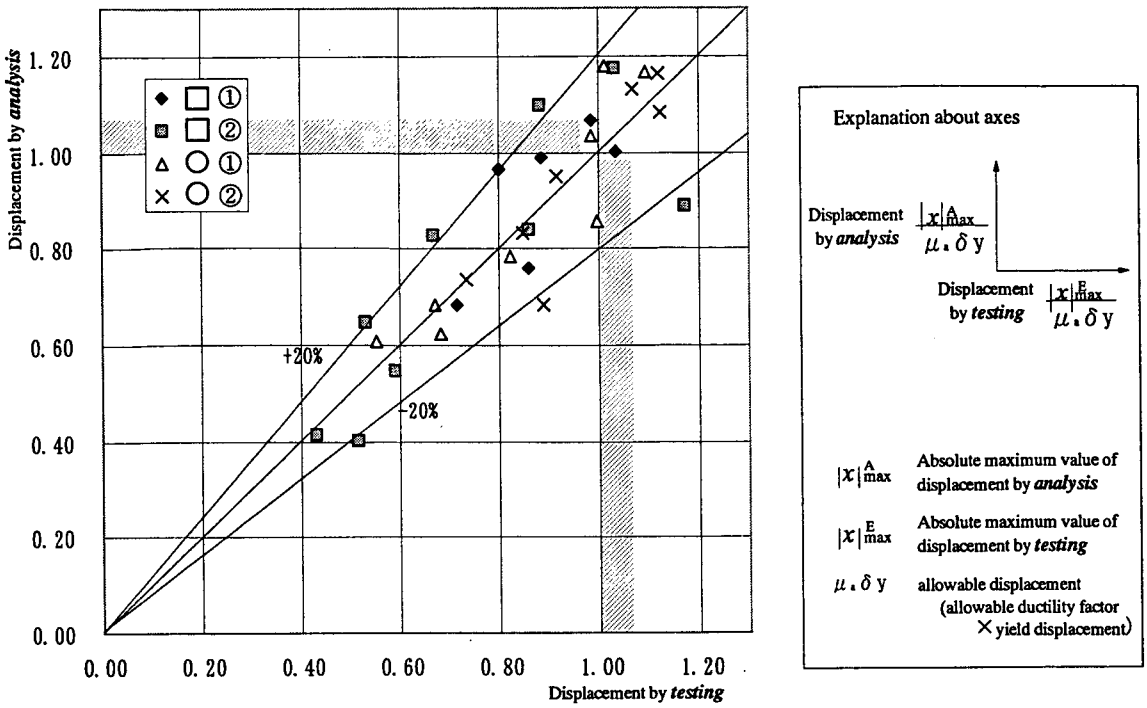


Fig-10 Maximum displacement obtained from testing and analysis for bi-liner model (2) (for analytical values selected from less than 1.2)

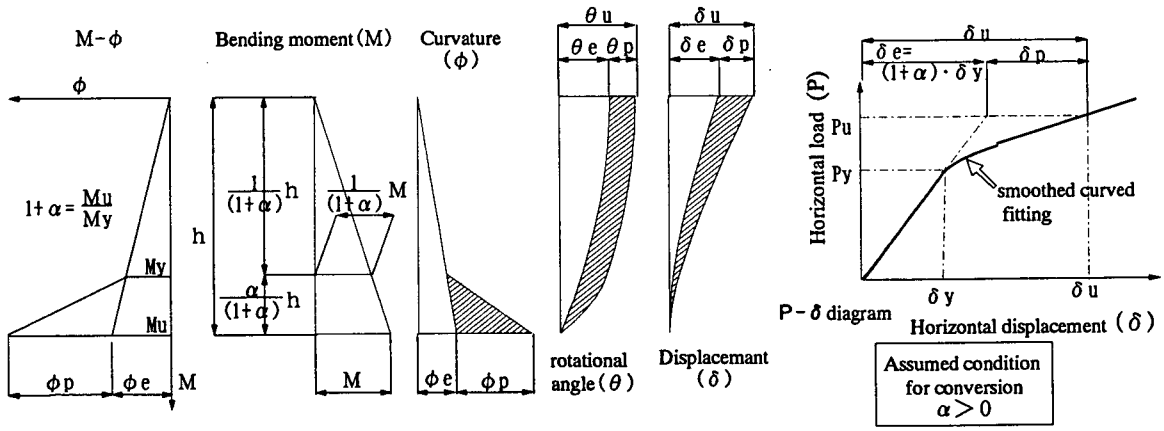


Fig-11 $P-\delta$ and $M-\phi$ relationship based on a bi-linear model

earthquake resistance based on dynamic response analysis will be generally appropriate with an error of about +/- 20% if the allowable ductility factor is not excessive.

(2) When earthquake waveforms defined by the Base Isolation Design Manual are applied to ground category III, degradation accelerates in the latter half during pseudo-dynamic testing. But, because a bilinear stiffness hardening model cannot fully reproduce the acceleration, the allowable ductility factor needs to be reduced somewhat when inputting earthquake waveforms that repeat frequently over a long period of time.

Conclusion

Various non-linear dynamic response analyses were performed to approximate the restoring characteristics, and the results were compared to the test results. In these comparisons, it was important to find a way to approximate the restoring curve obtained through integration to the hysteresis results of the testing. It was particularly difficult to simulate the degradation range. But, using a bilinear stiffness hardening model, it was not only possible to perform the analysis with relative ease, but it was also easy to verify the input structural data using the hysteresis curve. It was concluded that the hysteresis curve could be included as part of the design method within the allowable range of the ductility factor.

The mechanical properties of steel that designers of steel structures can obtain only include nominal values of the yield and ultimate strengths, the elongation, and the Charpy absorption energy, and the specified minimum strength properties of the steel material to be used. For this reason, accurate determination of the residual displacement is difficult and has not been studied sufficiently. However, much of the data presented here is summarized in a fixed format, and the hysteresis and time history are in the form of numerical data files and DXF files so that they can be retrieved when more suitable restoring curves are proposed in the future.

Acknowledgments

This research was done by working groups in the Seismic Research Program of the JASBC as part of the Joint Research Program conducted by the PWRI and other organizations. We would like to express our sincere gratitude to Professor T. Usami of Nagoya University, where the major testing work was carried out, and to participants from the PWRI and other authorities who contributed to this research project.

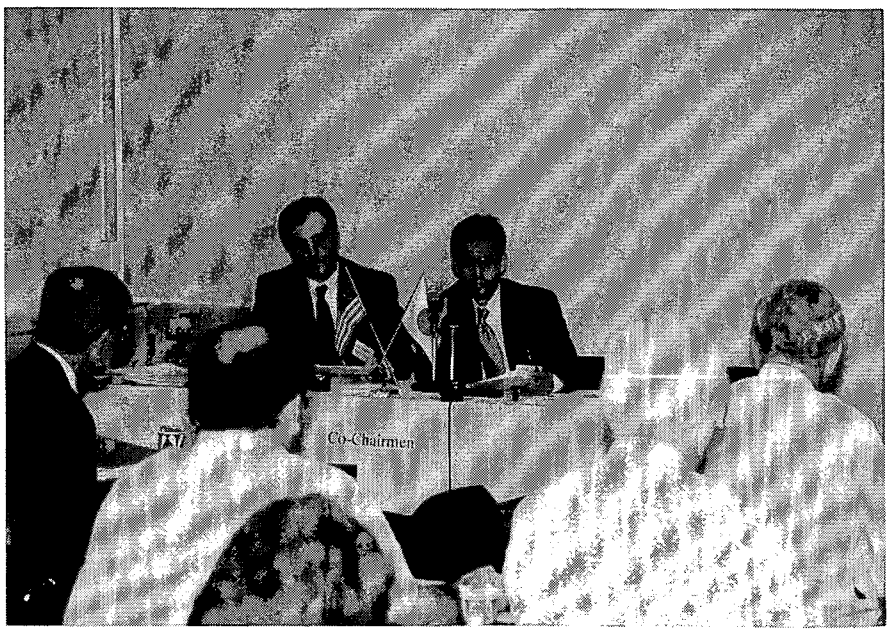
References

1. Ministry of Construction, "Base Isolation Design Manual," Civil Engineering Center, 1992,12.
2. Satish Kummar, Tsutomu Usami, "An Evolutionary -Degrading Hysteretic Model for Thin -Walled Steel Structures," Engineering Structures,1996.7.
3. Ministry of Construction, PWRI and 5 other organizations, "Ultimate Limit State Design Method of Highway Bridge Piers Under Seismic Loading," Joint Research Program Report, Vol. 7, April, 1997.

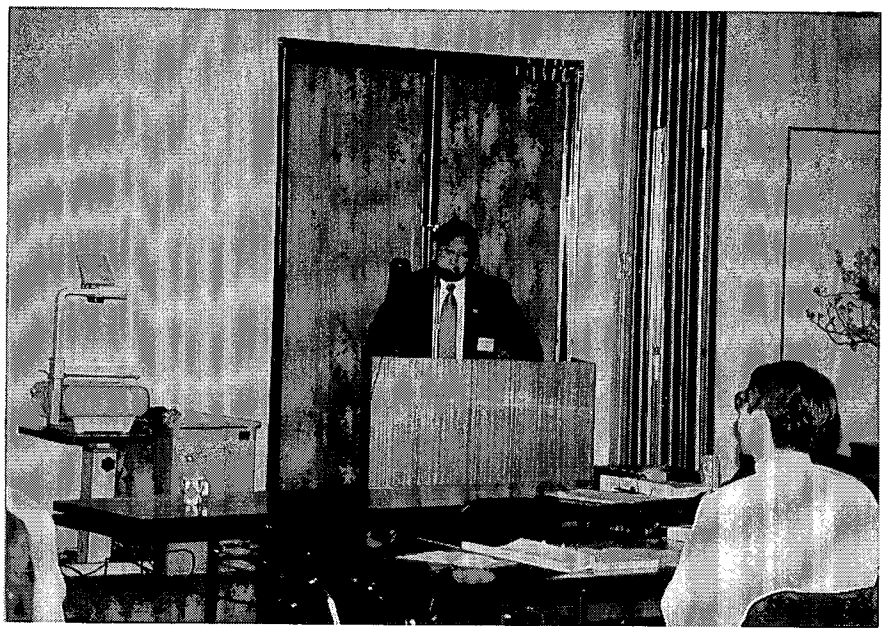
SESSION 6: MANAGEMENT (1)

(1) Network Level Comprehensive Bridge Safety Assurance and Management
(Arunprakash M. Shirole)

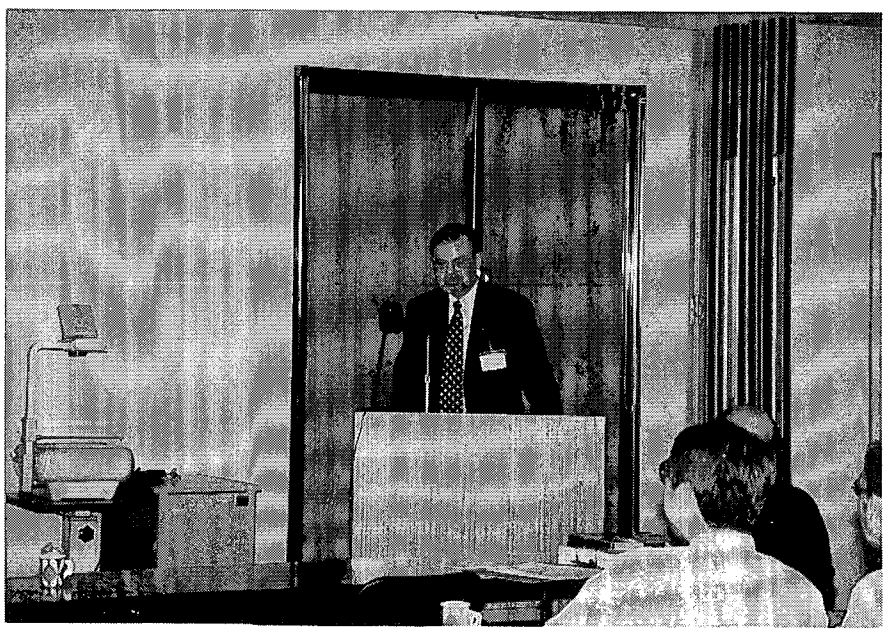
(2) Bridge Alternatives for Low Volume Roads
(F. Wayne Klaiber, Terry J. Wipf, Brent M. Phares and Jeff R. Reid)



Co-Chairmen : Jun Murakoshi, Dan Frangopol



SESSION 6 : Arunprakash Shirole



SESSION 6 : Wayne Klaiber

NETWORK LEVEL COMPREHENSIVE BRIDGE SAFETY ASSURANCE AND MANAGEMENT

Arunprakash M. Shirole', P.E.

Abstract

During the past-three decades, systematic bridge inventory inspection and management efforts were initiated by the U.S. agencies, as a result of some catastrophic bridge collapses and concerns about serious condition-deterioration of highway bridges. These efforts have been addressing the condition-related bridge safety problems. However, bridges have been known to fail not because of condition-deficiencies alone. Some existing bridges have been now known to have in-built design deficiencies that make them vulnerable to failure. This paper reviews relevant considerations and information needs, and presents a systematic approach to network-level comprehensive bridge safety assurance and management.

Introduction

The catastrophic bridge collapse at Point Pleasant, W.Va. in 1967, provided a rude awakening to bridge engineers. Since then there has been increasing concern about the serious condition deterioration of highway bridges in the United States. Agencies across the country initiated systematic bridge inventory and inspection programs that evaluate bridge component conditions. As a result repair, rehabilitation or replacement programs are developed to eliminate or reduce condition-related deficiencies that cause bridges to fail. The catastrophic bridge failures, however, are not necessarily caused because of condition-related deficiencies alone. This is because most existing bridges were not designed in anticipation of the significantly different but more realistic present day design loads and better knowledge of natural events. Certain design requirements and material characteristics once accepted as the "state-of-the-art" have been demonstrated with time and further study to be undesirable. Therefore, some existing bridges can be vulnerable to certain failure modes, such as hydraulic or seismic.

Current efforts underway in the United States have been addressing the comprehensive safety assurance that will eliminate/reduce bridge vulnerabilities to catastrophic failure. Many agencies have identified significant modes of failure to which their bridges are vulnerable and are in the process of rating their bridges according to the extent of failure vulnerability. These Vulnerability ratings alongwith condition rating will determine the priority of the needed actions and influence programming decisions in project and network level bridge management. This paper discusses relevant considerations and information needs and presents a conceptual framework for the network-level bridge safety assurance and management.

Executive Director, The National Steel Bridge Alliance, Minneapolis, MN.

Relevant Considerations and Information Needs

Project and Network-level Bridge Management: The project-level bridge management involves management of individual bridges in terms of their inspection, maintenance, repair, rehabilitation and, if needed, replacement activities. It starts with the identification of bridge needs provided by the bridge data-based that contains condition and safety related information. Once the needs are identified individual bridge work strategies, in terms of maintenance or improvement in the context of bridge life cycle, are selected and executed. With large bridge population that many agencies are responsible for, the coordination of individual bridge strategies has become necessary to accommodate continuity of traffic flow and effective use of available resources. The network-level bridge management, aims at accomplishing this objective by using the individual bridge management information to analyze collective needs of the bridge population to select cost-effective network level strategies that would improve overall bridge condition and safety, and to prioritize and optimize network-level bridge activities. Figure 1 (NYSDOT-1989) shows one bridge management system structure that clarifies the relationship between the project and network-level bridge management.

Information Needs: In order to effectively manage large bridge networks a variety of information is needed, Figure 1 indicates the general categories of such information, grouped together as the "Data Base". According to an extensive national survey and study (Shirole', Winkler and Fitzpatrick - 1993), the primary comprehensive safety assurance information considered essential pertains to bridge condition, bridge vulnerability to failure and failure vulnerability assessment. A discussion of these follows.

Bridge Condition: The systematic bridge inventory and inspection programs have been in effect in the United States for almost three decades. These programs have formalized inspection procedures and provide span-by-span bridge component condition description and extent of deterioration. Table - I indicates the typical inspection data-elements. The inspection reports provide overall condition ratings for deck, superstructure and substructure of each bridge. The ratings are in a 1 to 9, 1 to 7 or 1 to 5 (condition state) scale. This information provides the basis for determining condition-based maintenance, repair or improvement needs and priorities for needed actions.

Bridge Vulnerability to Failure: The art and science of bridge design and construction has improved with the passage of time and lessons learnt from the performance history of existing bridges. As new bridges were built with improved design and detailing practices, the existing bridges remained with what became built-in design obsolescence. The formalized bridge inspection program were not suitable, and therefore not adequate, to identify these built-in deficiencies which, in some cases, made bridges vulnerable to catastrophic failure. Current efforts in the U.S. (Shirole' and Holt, 1991) address this inadequacy. The initial step in these efforts is to identify significant modes of bridge failures based upon the frequency of incidence and potential damage that can result. For example, one agency-the New York State Department of

TABLE I: TYPICAL INSPECTION DATA ELEMENTS (SPAN BY SPAN)

BRIDGE IDENTIFICATION NUMBER

Deck Elements:
Wearing Surface
Mono Deck Surface
Curbs
Sidewalks and Fascias
Railings and Parapets
Railing Paint
Scuppers
Gratings
Median
Recommendation

Superstructure:
Structural Deck
Primary Member
Secondary Member
Paint
Joints
Recommendation

Pier:
Bearings, Anchors
Bolts and Pads
Pedestals
Top of Pier Cap or Beam
Stem Solid Pier
Cap Beam
Pier Columns
Footings
Erosion or Scour
Piles
Recommendation

Utilities:
Lighting Standards
Lighting Fixtures
Sign Structure
Utilities
Utilities Support
Recommendation

Transportation (NYSDOT) identified six failure modes to be significant for its network of about 20,000 bridges (Shirole', 1995). These failure modes listed in a prioritized order are:

1. Hydraulic
2. Overload
3. Structural Steel Detail Deficiencies
4. Collision (vehicle/vessel)
5. Structural Concrete Detail Deficiencies

and 6. Earthquake

This list was based upon the review of 1,322 bridge failures since 1950. The types and priorities of significant failure modes would very likely differ from one agency's bridge network to another and it would be necessary for every agency to have a similar prioritized list.

Bridge Vulnerability Assessment: Failure, for the purpose of vulnerability assessment is defined as any physical change of a bridge that creates a threat to public safety or the complete loss of service. To simplify the vulnerability assessment for a large population of bridges, it would be necessary to use a muti-level process (Shirole', 1995). Each level of this process will refine the list of bridges so that those structures with greater vulnerabilities can receive a more detailed evaluation. This process comprises of screening, classification and rating steps that are intended to be performed sequentially and on a priority basis. The rating step would be common to all failure modes and would provide a uniform measure of a structure's vulnerability to failure on the basis of the likelihood of a failure and the consequences should one occur. The likelihood of a failure event would provide a measure of the probability of an external load condition exceeding the structural capacity, whereas the consequences of a failure would refer to the impact of a bridge failure in terms of injury to or loss of human life or adverse economic impact. These resulting vulnerability ratings would reflect the type and urgency of corrective action needed to reduce or eliminate that specific failure vulnerability. An example of rating scale is one used by the NYSDOT (Shirole' and Holt, 1991) as shown in Figure-2.

Figure 3 presents an illustrative example of how the vulnerability assessment process is carried out to yield the steel details vulnerability ratings for a network of bridges (Shirole', 1995). The screening step consists of an inventory screen and a more refined bridge type screen. The inventory screen is a preliminary screening procedure that identifies non-metal, closed or abandoned bridges. These are assigned a vulnerably rating of 6 (not applicable). No further actions are required for these bridges. The first stage bridge type screen segregates special types of bridges that are not easily analyzed through standardized vulnerability assessment procedure and would receive special evaluation. The second stage would sort each of the remaining bridges into one of three susceptibility groups on the basis of their respective superstructure types. In the classification step the failure vulnerability of a structure is evaluated on the basis of its structural details as well as its traffic, design, deterioration, and environmental conditions. This step quantifies the potential vulnerability of a structure to steel detail deficiency failure relative to that of other bridges in the classification process and places the structure in the high, medium or low

vulnerability class. A field verification by a trained engineer may be necessary to complete the vulnerability classification step for some of these bridges. Finally, it would rate each bridge for its failure vulnerability based upon the likelihood and consequence of failure and assign it a steel details vulnerability rating of 1 through 6, one being the highest priority for action. This information would provide the basis for condition-based maintenance, repair or improvement needs and priorities for needed actions.

Conceptual Framework

The conceptual framework for network level comprehensive bridge safety assurance and management is shown in Figure 4. It would start with the inventory and condition inspection information for the bridge population. This information should consist of a description and extent of condition deterioration of deck, super and sub-structure elements in each span of the structure. The safety information should include description and extent of the built-in vulnerabilities of the structure to different modes of failure such as hydraulic, overload, steel details, collision, concrete details and earthquake. An evaluation of this condition and safety information then should result in bridge-by-bridge condition and safety improvement needs.

This list of needs would then go through an engineering review to select appropriate strategy from among replace/rehabilitate, maintain type of work activities. The resulting list would identify bridge by bridge work strategies and recommended scope of work. This list would go through cost-estimating of selected strategies on the basis of unit costs and quantities inputted by the agency. This step results in estimated bridge project by project costs, alongwith the project scope and condition as well as safety needs it satisfies. The output from this step is judged against the comprehensive safety needs and the agency goals to arrive at prioritized project lists that constitute total capital improvement and maintenance programs. The final programs are then arrived at after review of the prioritized lists against financial and any other constraints. This final program would then be assessed as to its impact on the bridge network condition and its comprehensive safety.

Conclusion

In response to the serious condition deterioration of highway bridges in the U.S. and the catastrophic bridge failures, many agencies initiated formal bridge inventory and inspection programs and started systematically addressing the management of bridges. These activities were solely based on bridge condition and condition-related safety aspects. The catastrophic bridge failures, however, are not necessarily caused because of condition-related deficiencies alone. This is because certain design requirements and material characteristics used as the "state of the art" in the design of some existing bridges have been demonstrated with time and further study to be undesirable and, therefore, unsafe. This paper has presented relevant considerations, information needs and a conceptual framework that would assure comprehensive safety and management of bridge networks.

REFERENCES

1. New York State Department of Transportation, "Bridge Management System: Concept Plan and Development Strategy," Albany, N.Y., October 1989.

2. Shirole', A.M. and R.C. Holt, "Planning for a Comprehensive Bridge Safety Assurance Program" Transportation Research Record 1290, Third Bridge Engineering Conference, Vol. 1, Bridges and Structures, Transportation Research Board, 1991, pp. 39-50.

3. Shirole', A.M., William Winkler and Michael Fitzpatrick, "Bridge Management Decision Support," Transportation Research Board Conference on Bridge Management, Austin, Texas, September 1993.

4. Shirole', A.M., "Development and Implementation of New York State's Comprehensive Bridge Safety Assurance Program," Conference Proceedings 7, Fourth International Bridge Engineering Conference, Volume 1, Transportation Research Board, 1995, pp.187-196.

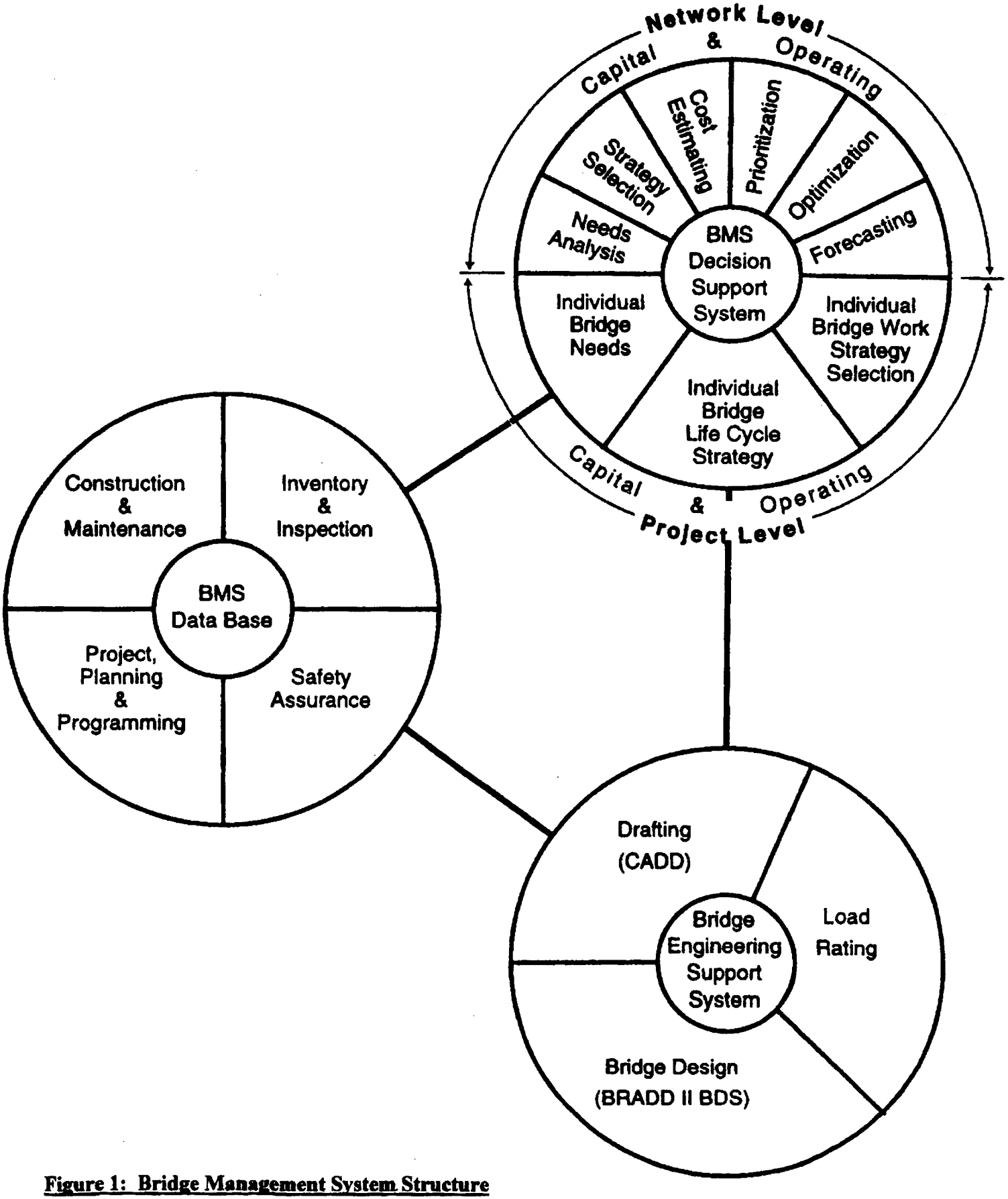


Figure 1: Bridge Management System Structure

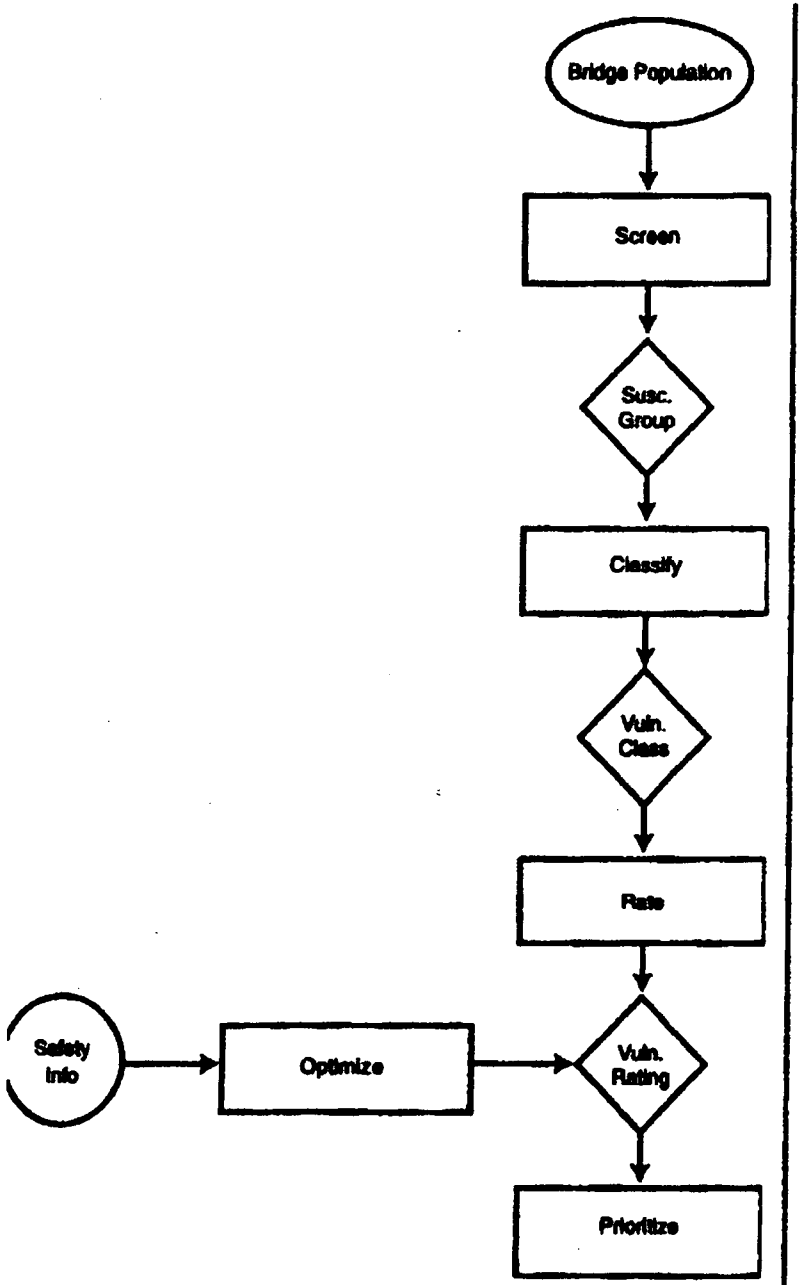
Figure 2. BRIDGE VULNERABILITY RATING CODE.

HYDRAULIC	OVERLOAD	STEEL	COLLISION	CONCRETE	EARTHQUAKE
2	3	2	3	6	5

←

INCREASING ORDER OF SIGNIFICANCE
(Based on Frequency of Occurrence)

RATING CATEGORIES
1 - HIGH PRIORITY
2 - MEDIUM PRIORITY
3 - CAPITAL PROGRAM PRIORITY
4 - INSPECTION ACTION
5 - NOT VULNERABLE
6 - NOT APPLICABLE



Step	Factors Considered	Outcome
		Steel Details Vulnerable Bridges - List
Screening for susceptibility	Inventory Screen: - Non-metal Bridges - Metal-Non-susceptible Bridges (Abandoned, closed, etc.) Susc. Screen: Special Types: Arches, Suspension, Movable, Culverts, Long Span (>500')	Susceptibility Groups: 0-3
Classifying Vulnerability	Primary Member Fatigue Vulnerability - (Super- & Sub- Structure) Fracture - Critical Details Redundancy - Load Path, Internal, Structural Fatigue Resistance, AADT, Fatigue Design Material Toughness, Distortion-induced cracking Connection - internal & external Accumulated Damage - Super- & Sub-structure: Flagged (Crack, Corrosion, other) Paint Condition Deterioration Factors (Salt-water, Industrial, Urban, Over Water, etc.) Conditioning Rating (Deck, Joints, Primary Member, Drainage, Bearings)	Vulnerability Classes: High Medium Low
Rating of Vulnerability	Likelihood: Vulnerability Class Consequence: Failure Type - Catastrophic, Partial Collapse, Damage Exposure - Traffic Volume, Functional Classification	Vulnerability Rating 1 thru 6

Figure 3: Steel Details Vulnerability Assessment

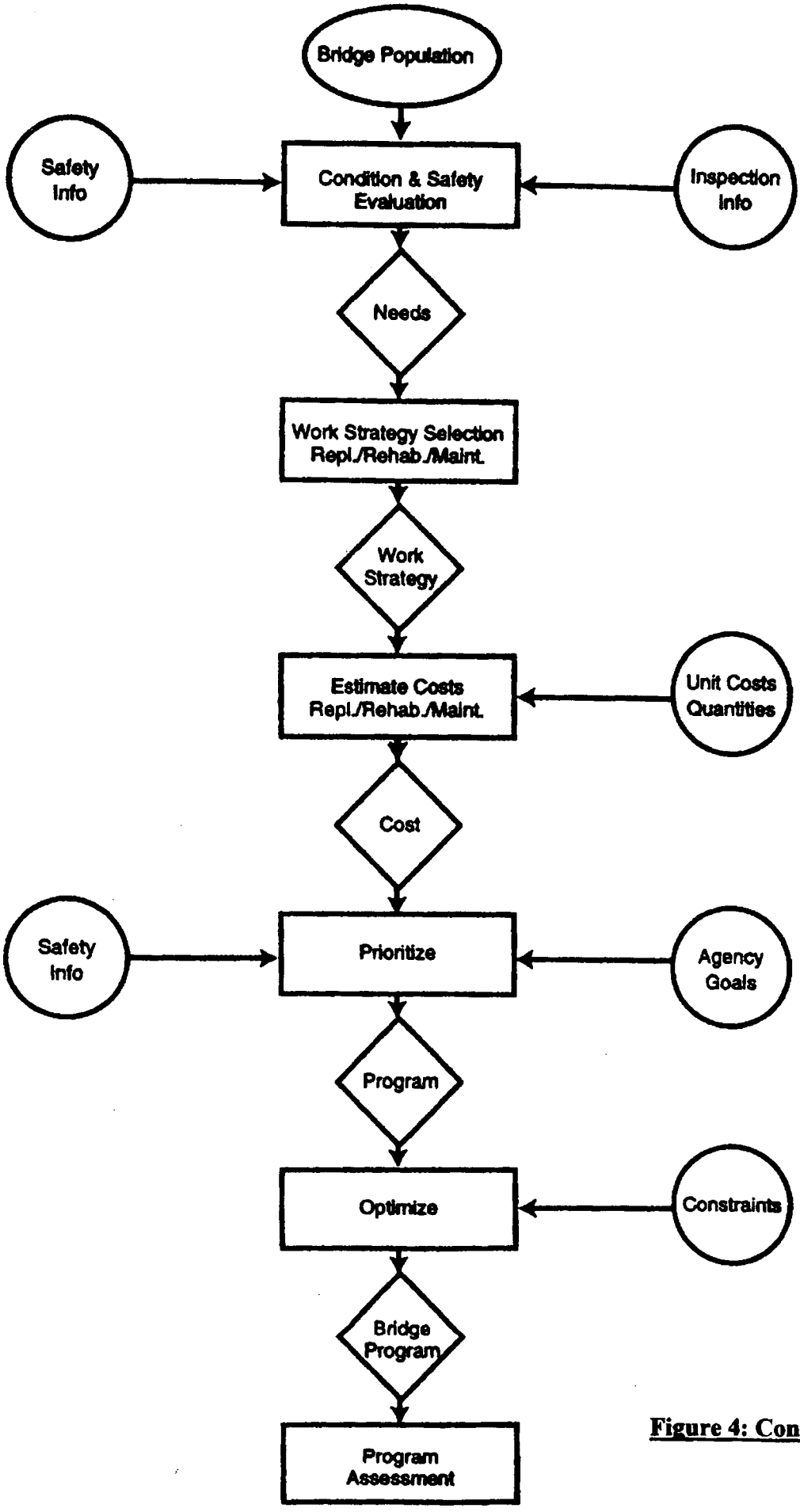


Figure 4: Conceptual Framework

BRIDGE ALTERNATIVES FOR LOW VOLUME ROADS

F. Wayne Klaiber[1], Terry J. Wipf[1], Brent M. Phares[2], Jeff R. Reid[3]

Abstract

In Iowa there are over 20,000 bridges on the secondary system. The majority of these bridges are the responsibility of the local county engineers. As county engineers have limited budgets, in many counties the engineers design and construct their own short span bridges with their own labor forces. The primary objective of this research is to perform laboratory testing on two bridge alternatives (Concept 1 and Concept 2) that counties can design and construct. Concept 1 involves the fabrication of precast units which consist of steel beams connected compositely with a concrete deck. Deck thickness is limited so that the units can be lifted and transported to the field where several of these units can be connected and the remaining portion of the deck placed. Concept 2 involves testing and modifying a system of steel beams with concrete fill between them that has been used by several Iowa counties on low water stream crossings for 20 plus years. There is no reinforcing steel in this system or connection between the steel beams and the concrete. Due to page restrictions, only Concept 1 is presented in this paper.

Introduction

This investigation involves the laboratory testing of two bridge alternatives which are being developed for use on low volume roads. Both of these alternatives are simple to construct using county crews. The alternative presented in this paper involves the fabrication of precast (PC) units consisting of steel beams (new or used) connected compositely with a concrete deck. The individual PC units can be fabricated in the maintenance garage of a given county. The precast concrete deck thickness is limited so that the PC units can be easily lifted and transported to the field where several units are placed side by side to obtain the desired width of bridge. The individual PC units are then connected and the remaining portion of the concrete deck placed. The top surface of the PC units is intentionally roughened to ensure composite action between the precast and field cast concrete.

In the experimental part of the investigation, there were the following static load tests:

- Small scale connector tests
- "Handling" strength tests of individual precast units
- Service and overload tests of a full scale model bridge

[1]Professor, Department of Civil Engineering, Iowa State University, Ames, IA.
[2]Graduate Student in Structural Engineering, Iowa State University, Ames, IA.
[3]Former Graduate Student in Structural Engineering, Iowa State University, Ames, IA.

Three finite element models (FEM's) for analyzing the bridge in various states of construction were also developed. This paper will only present results from the model bridge tests. Connectors developed, which were used in the model bridge, were tested with and without the cast-in-place (CIP) portion of the deck. Individual PC units had no problems in passing the "handling" strength tests. The PC units tested were 9.75 m (32 ft) long and 2.13 m (7 ft) wide. They were fabricated using 21W 61 steel beams with a 25.4 mm (4 in.) thick composite deck. For more details on these portions of the investigation, the reader is referred to Wipf, et al. (1997). For information on Concept 2, the reader is referred to Klaiber, et al. (1997).

Model Bridge

The model bridge was comprised of three 2.13 m (7 ft) wide PC units. Overall dimensions of the model bridge and the PC units as well as the location of the diaphragms are shown in Fig. 1. The deck thickness in the PC units (100 mm (4 in.)) was selected to minimize the weight of the individual units yet provide sufficient structural strength so that the units could be moved without damaging them. Reinforcement in the PC units was designed according to AASHTO LFD (1992) bridge deck requirements; composite action between the steel beams and the concrete was obtained using welded shear studs. The top surface of the PC units was scarified to obtain composite action with the CIP concrete that was added later. Each PC unit had 15 channel inserts on approximately .61 m (2 ft) centers along each edge so that the units could be connected to adjacent units when positioned to construct the bridge.

Figure 2 shows the bridge model after placement of the PC units; scarification of the PC concrete as well as the connection details along the two joint lines can be seen. Prior to adding additional deck reinforcement and the CIP position of the deck, the model bridge was tested varying the number of connections between the adjacent PC units. Once the number of connections required for obtaining the desired load distribution was determined, deck reinforcement (designed according to AASHTO LFD (1992)) was added and 100 mm (4 in.) of CIP concrete was cast giving the desired deck thickness of 200 mm (8 in.).

Testing of Model Bridge:

A total of 132 tests were performed on the model bridge. The breakdown of these tests is as follows: 64 on the bridge without the CIP deck, 68 on the bridge with the CIP deck; there were 128 service load tests and 4 ultimate load tests. This testing program was completed to determine the following:

- Number of connections between adjacent PC units required to obtain desired load distribution.
- Contribution of CIP in distributing live loads.
- Effect of diaphragms on load distribution.
- The behavior and strength of the system.

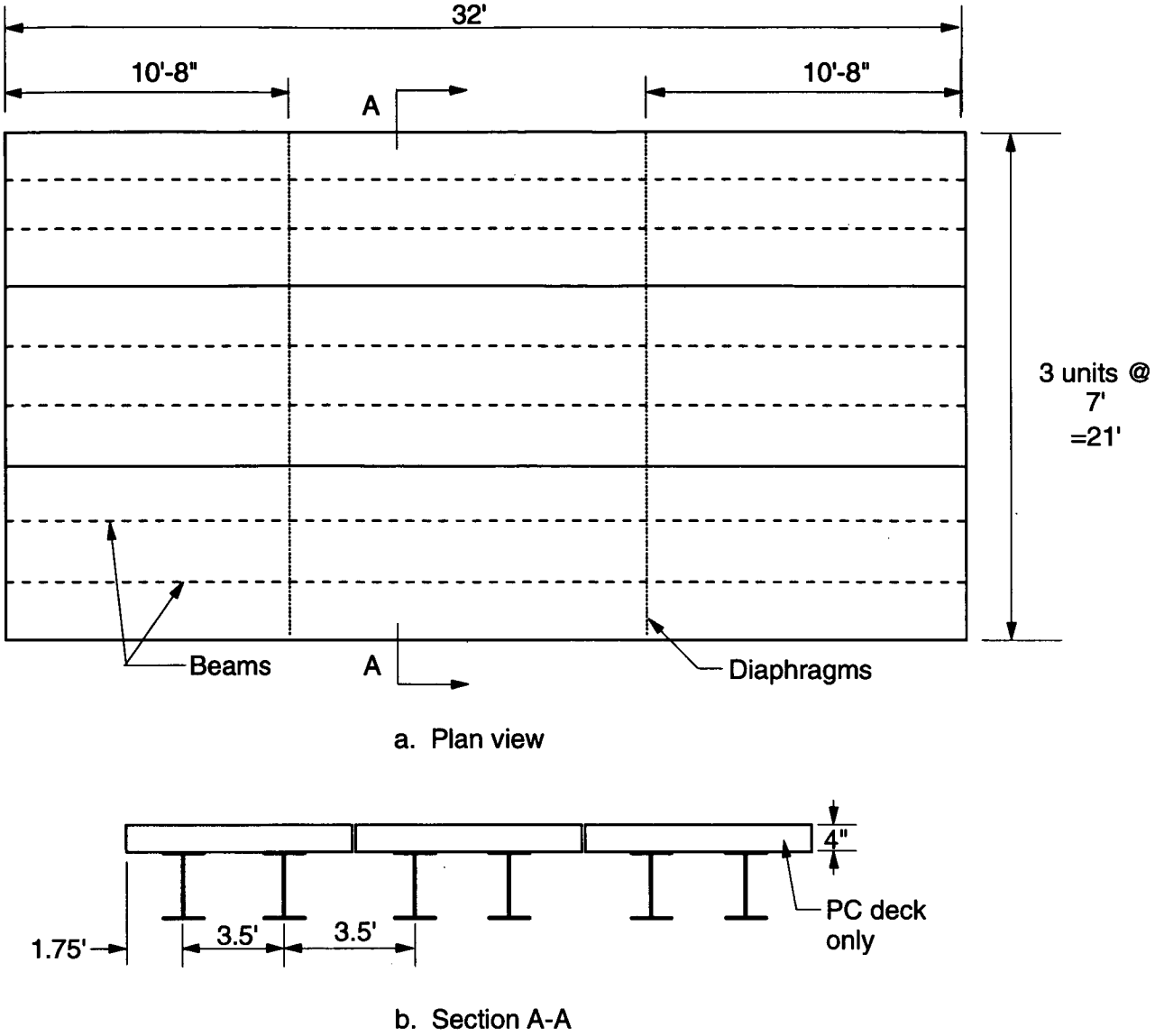


Fig. 1. Overall dimensions of model bridge.

The location of the load points used in testing the model is shown in Fig. 3. In the following discussion, load points are given a letter/number designation. For example, load point B3 indicates load was applied at transverse Sec. B and longitudinal Sec. 3. In this paper, only representative deflection data are presented. Although strains were measured in all the tests, strain data revealed the same behavior as the deflection data and thus are not presented.

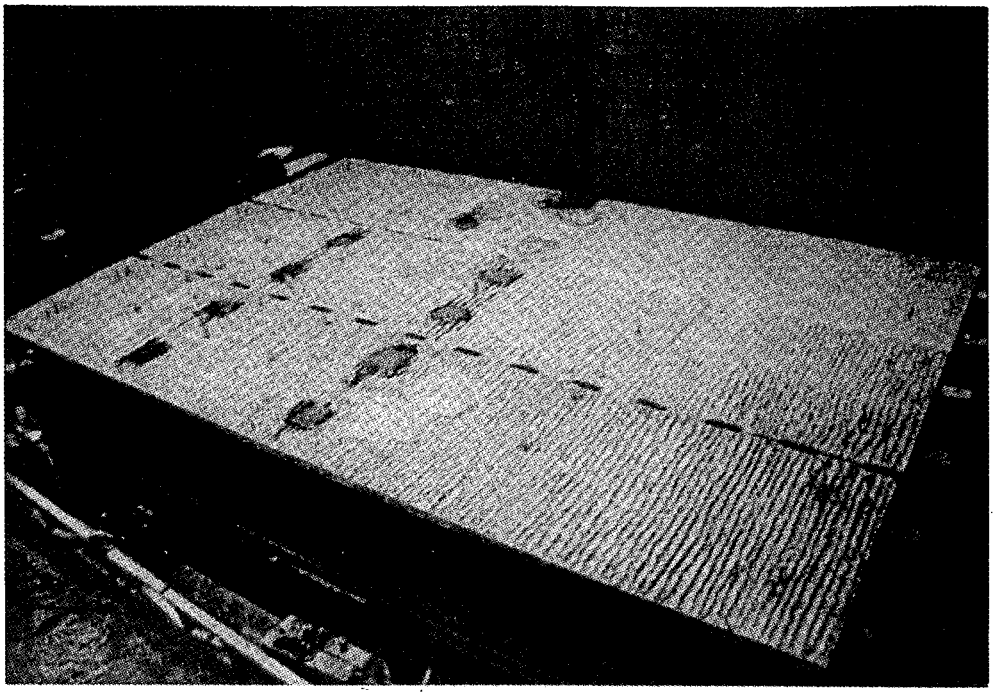


Fig. 2. Photograph of model bridge with PC units in place.

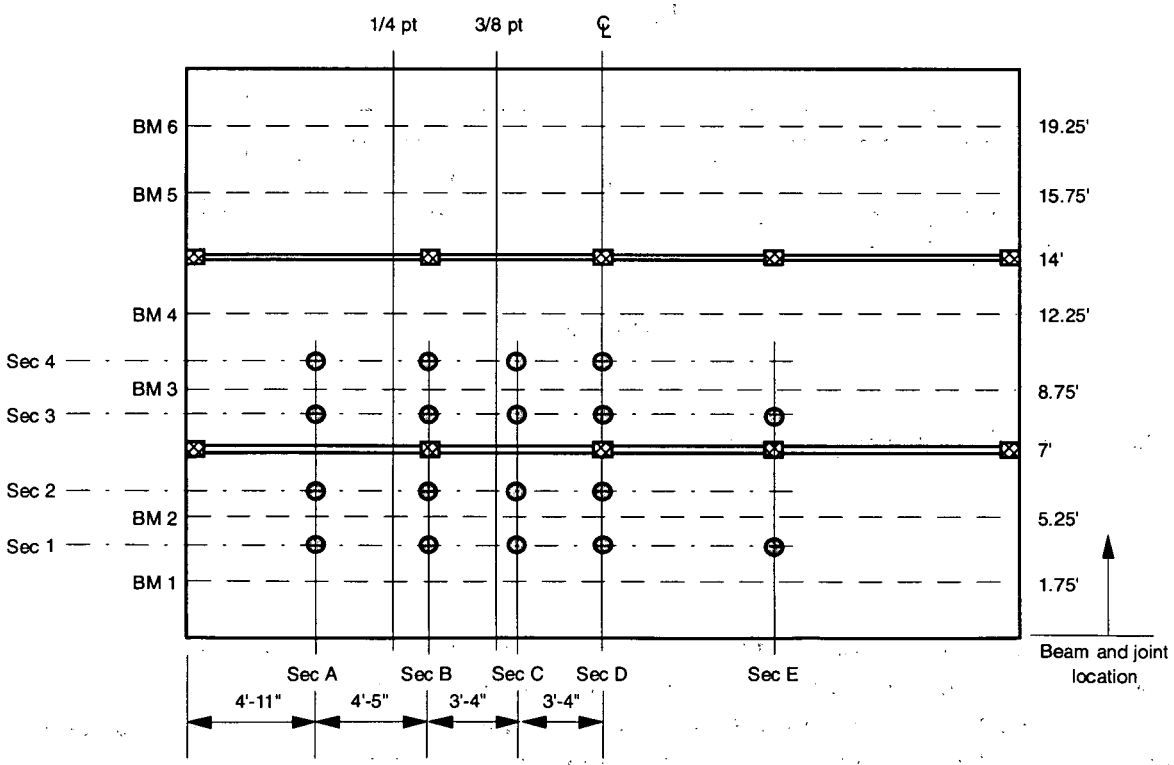


Fig. 3. Location of load points.

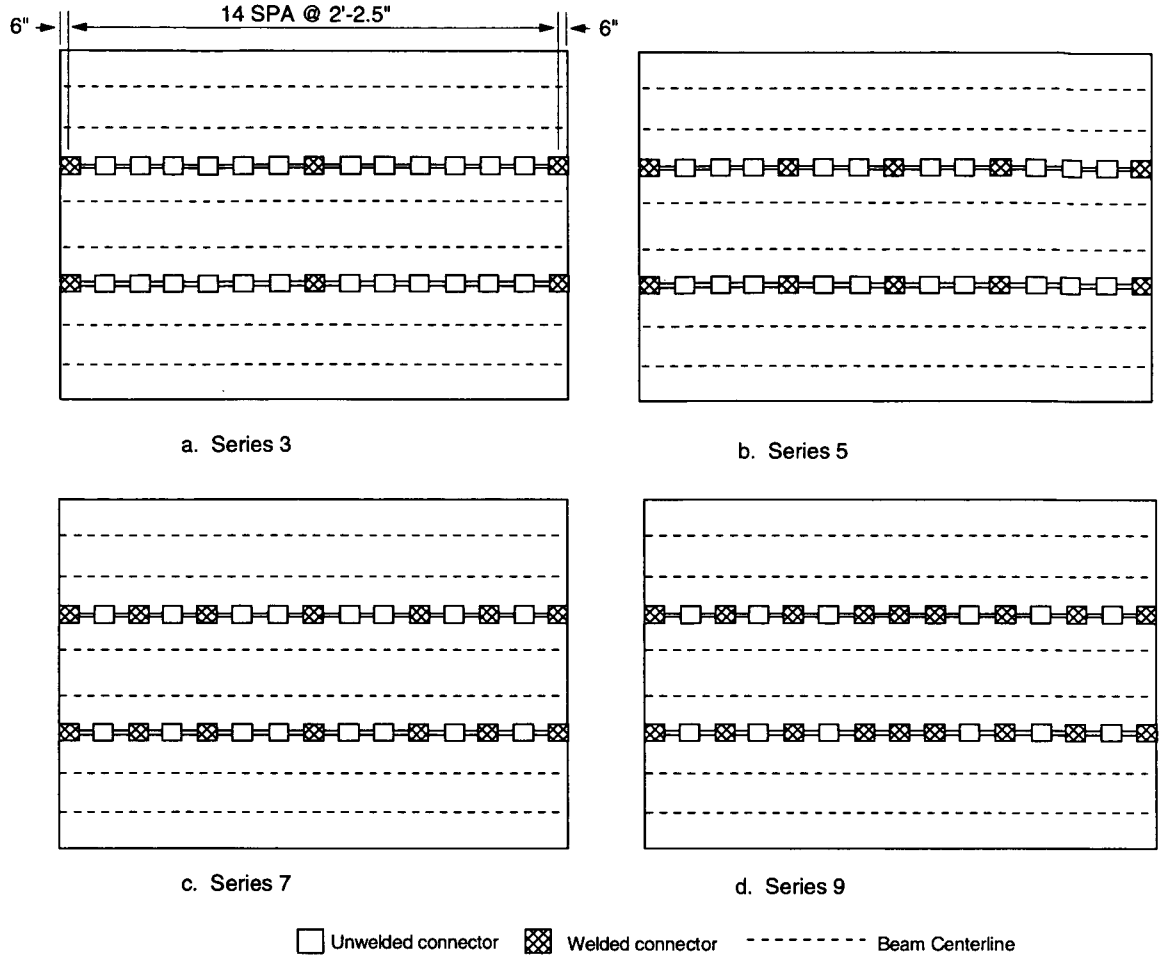


Fig. 4. Location of connections in model bridge tests.

As was previously noted, the model bridge was tested with only the connected PC units in place. Loads up to 71.1 kN (16 kips) were applied at the load points shown in Fig. 3. Four different connector arrangements (three, five, seven, and nine connectors) shown in Fig. 4 were investigated. As previously noted, there were 15 channel inserts along the edges of the PC units. To obtain a structural connection between adjacent PC units, plates were welded to the top and bottom surfaces of the channel inserts where structural connection was desired. The influence of the connectors for load being applied at Load points A1 and B4 is illustrated in Figs. 5 and 6. The key in these two figures indicates the number of connectors and the actual load being applied.

Deflections in these two figures indicate, as one would expect, the more connectors the better the lateral load distribution. As illustrated in Fig. 5, the connector arrangement has minimal influence on the deflections at the centerline (Fig. 5a) and quarter point sections (Fig. 5c). Greater differences are observed at the 3/8 point (Fig. 5b) section as a result of this section being further from the connectors. Thus, there is more differential deflection between the two PC units causing the difference in response.

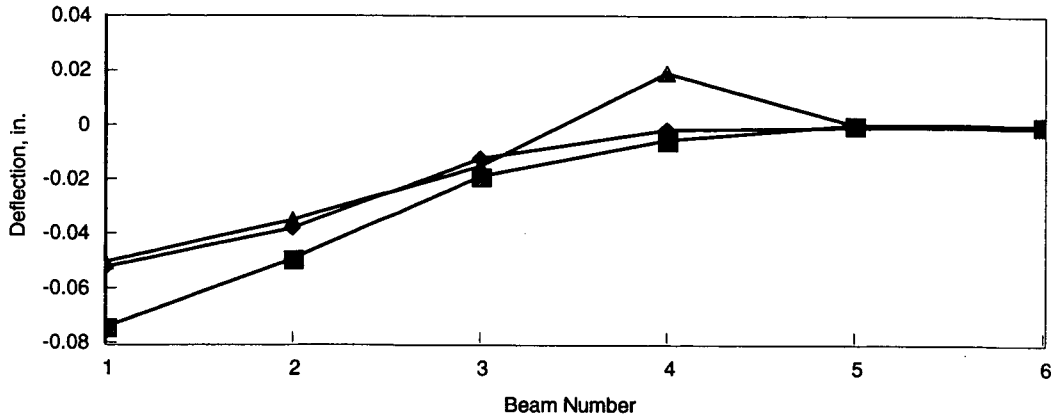
In Fig. 6, one observes the same behavior for the three, five, and seven connector schemes but a markedly different response for the nine connector scheme. The atypical deflection pattern is due to the fact that the nine connector spacing adds a connector very close to Load point B4 whereas the other connector arrangements did not. Thus, the arrangement of PC connectors influence the global as well as local behavior of the bridge system.

Review of the deflections in these figures indicates that, in general, the number of connectors has minimal effect on the resulting deflections and thus minimal effect on the lateral load distribution. An exception to this observation is illustrated in Fig. 6b where the 9 connector arrangement is seen to provide significantly better lateral load distribution.

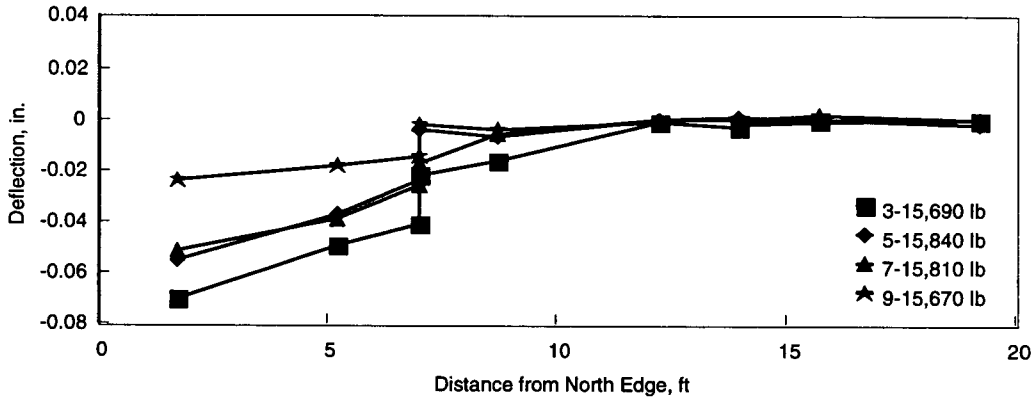
Reflective cracking in the CIP deck is dependent on controlling of differential deflection between the adjacent PC units. Data in Figs. 5 and 6 indicated that five connectors can provide the desired lateral load distribution. Reinforcement in the CIP portion of the deck will also provide lateral load distribution and provide resistance to reflective cracking. The best arrangement for eliminating reflective cracking is a combination of the two - adequate number of connectors plus a sufficiently reinforced CIP deck; data verifying this statement is presented later in this paper.

The results from these series of connector tests indicate that the five connector arrangement did improve the distribution relative to the three connector scheme. However, there was minimal improvement in lateral load distribution when the seven and nine connector arrangements were used. The small improvement with seven and nine connectors suggests it is not worth the extra cost and labor required to install them. Thus, it was decided that five connectors would provide the desired lateral load distribution for this model bridge.

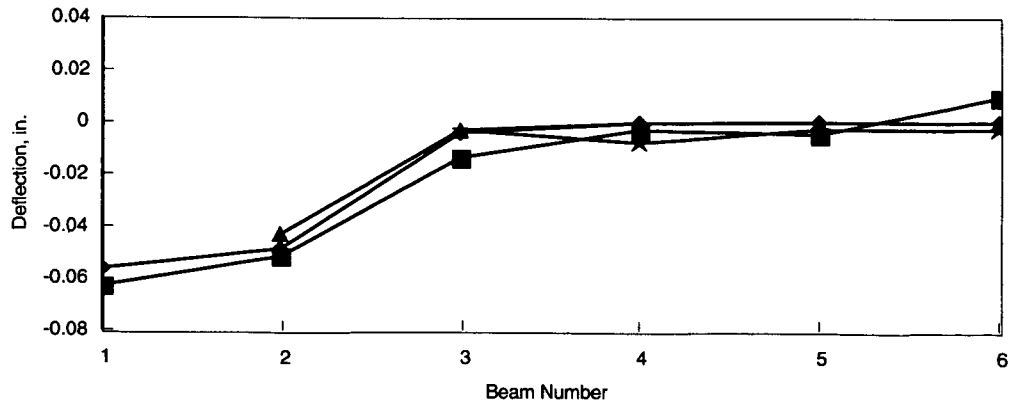
Shown in Figs. 7 and 8 are the results of testing the model bridge with and without diaphragms. As shown in Fig. 1, the diaphragms are located at approximately the 1/3 points of the span. When the diaphragms are at mid-web height of the beam webs the tests are designated as D1, and when the diaphragms are just below the concrete deck the tests are designated D2. In each of these figures, a nominal load of 71.2 kN (32 kips) has been applied to the model bridge. As in previous tests, only representative data are presented. Deflection data in these figures are from load being applied at Load points B4 (Fig. 7) and A1 (Fig. 8) which are at different distances from the diaphragms in the model bridge. As is evident in these figures, the diaphragms have minimal effect on the model bridge's behavior. Deflection curves for the two



a. Centerline

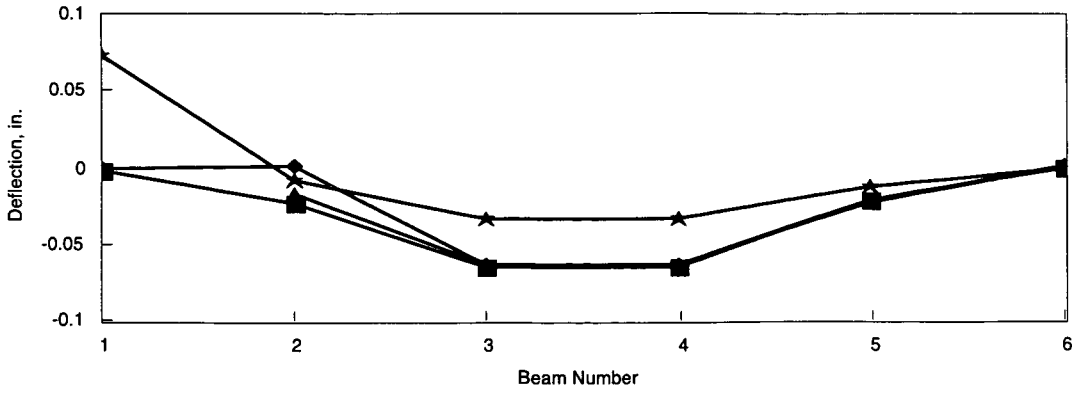


b. 3/8 point

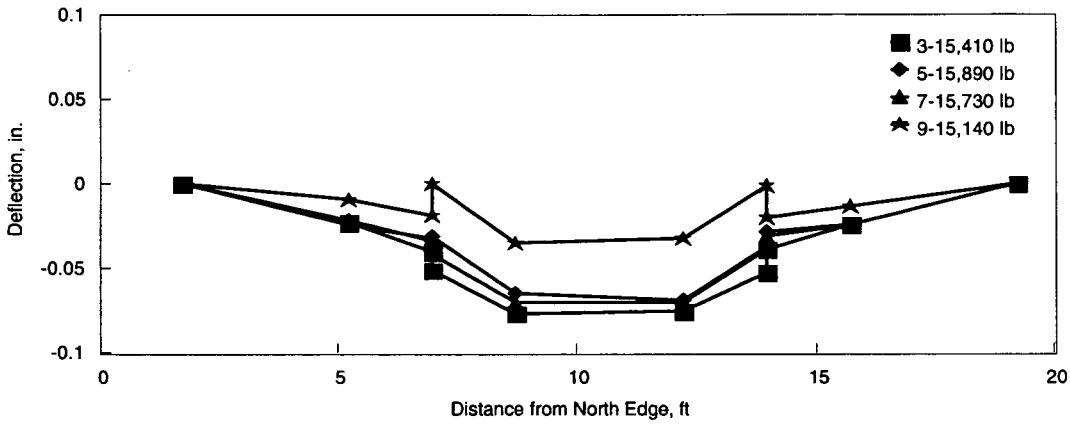


c. Quarter point

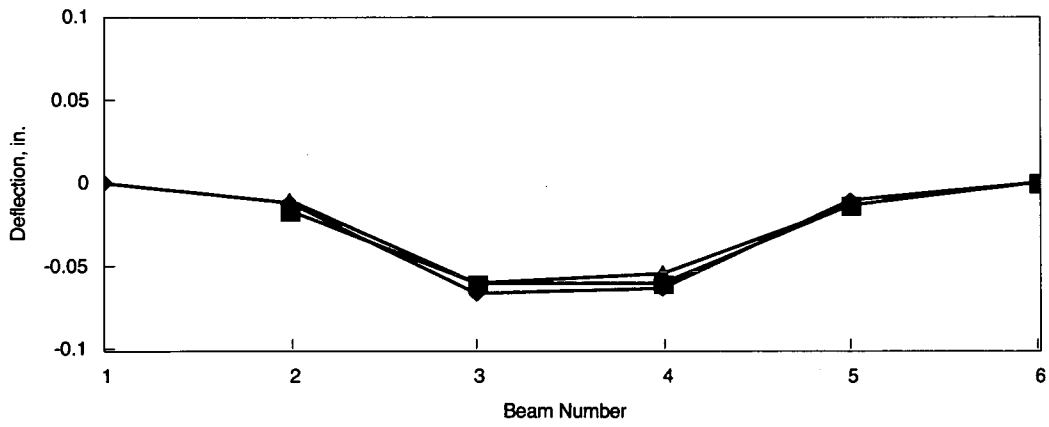
Fig. 5. Influence of connector arrangement on bridge deflections; load at A1.



a. Centerline

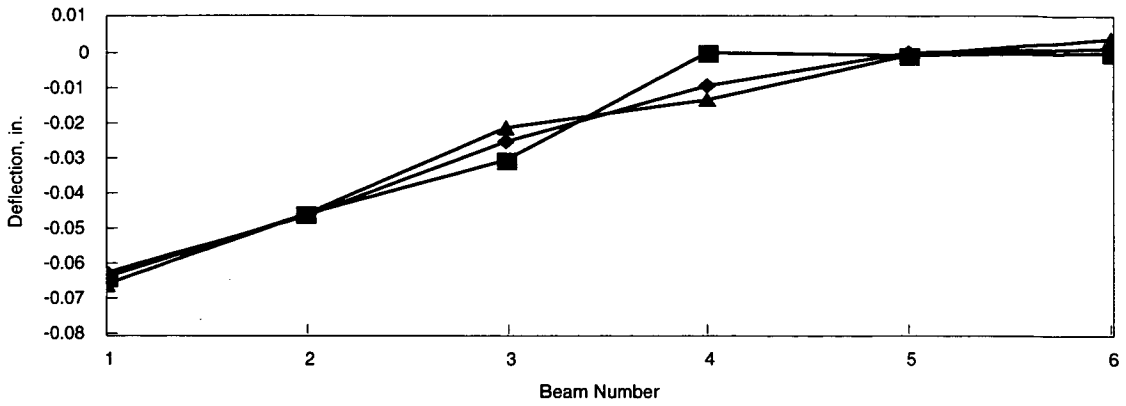


b. 3/8 point

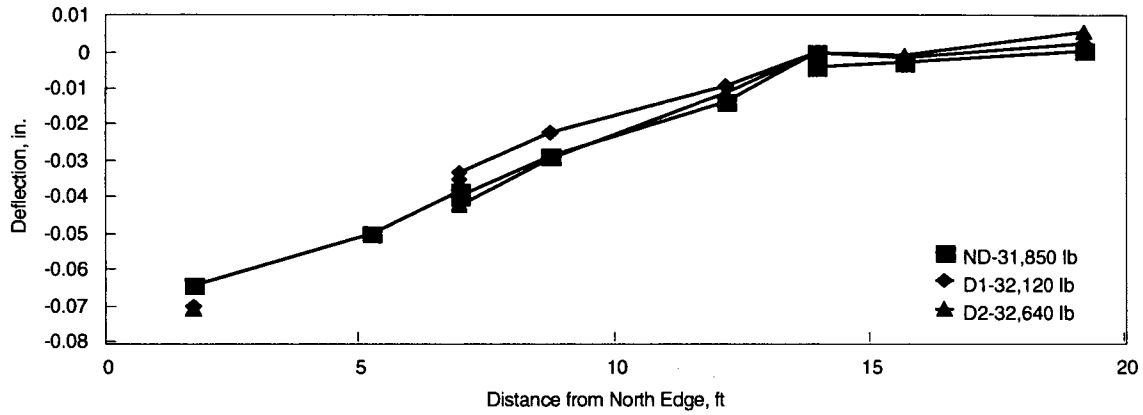


c. Quarter point

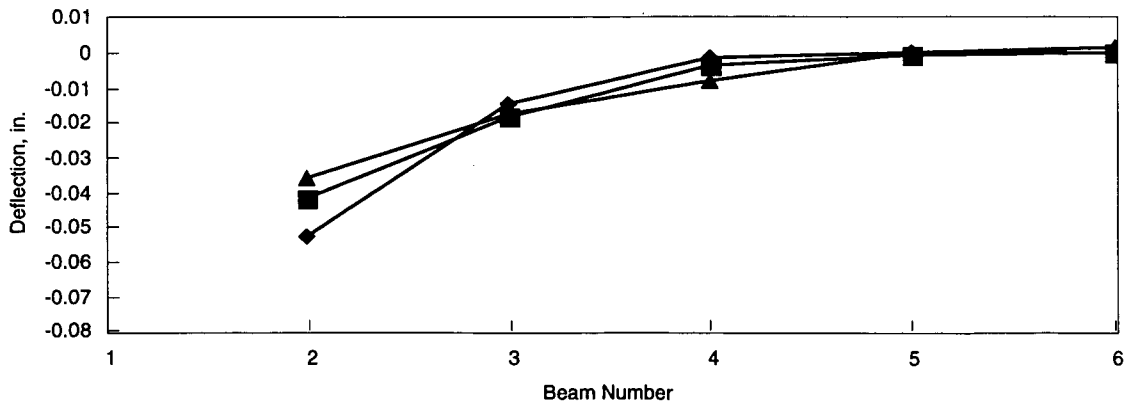
Fig. 6. Influence of connector arrangement on bridge deflections; load at B4.



a. Centerline

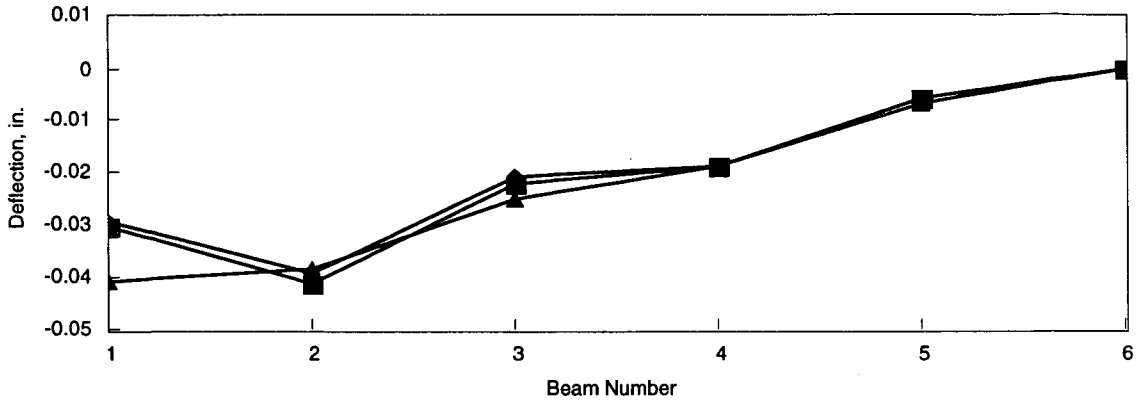


b. 3/8 point

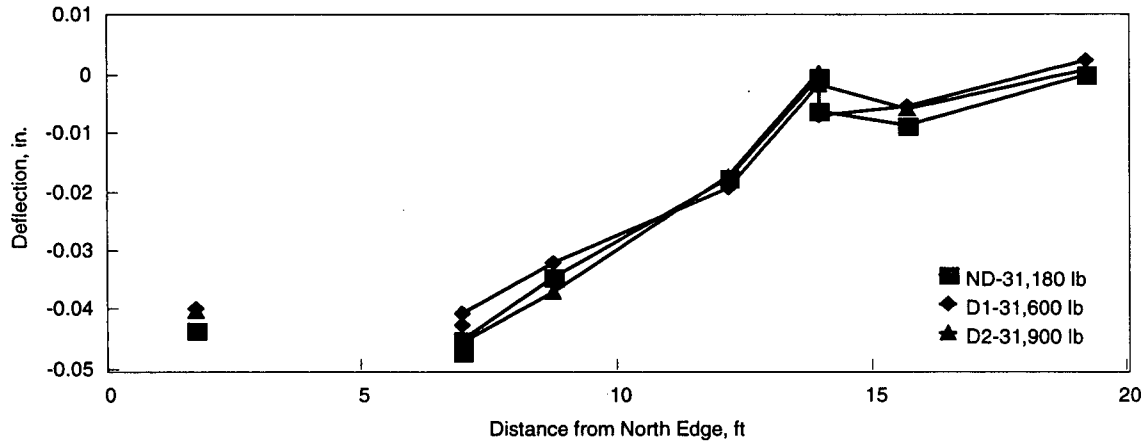


c. Quarter point

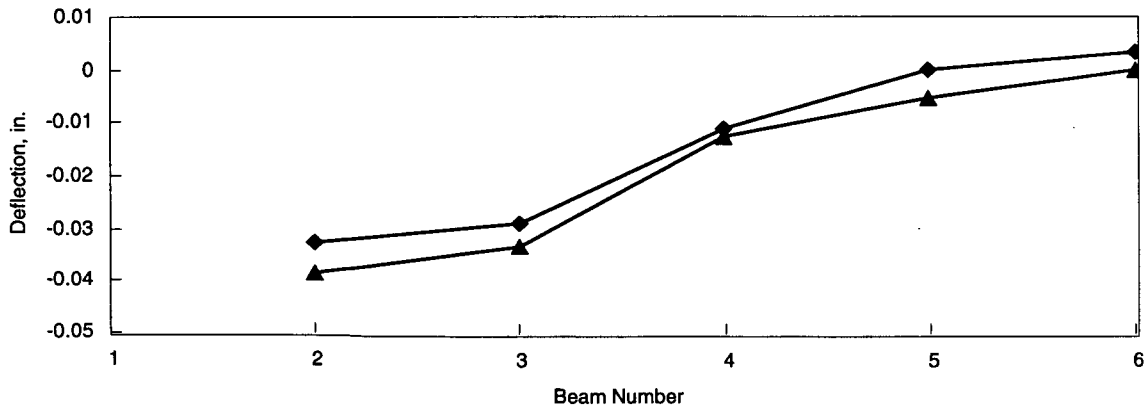
Fig. 7. Model bridge deflections with and without diaphragms; load at B4.



a. Centerline



b. 3/8 point



c. Quarter point

Fig. 8. Model bridge deflections with and without diaphragms; load at A1.

cases with diaphragms (D1 and D2) are essentially the same as the case without diaphragms (ND). The only time the diaphragms reduced the deflections was when the load was applied close to the location of the diaphragms. This slight improvement is due to the fact that the diaphragms add a degree of transverse continuity to adjacent PC units. Therefore, it is apparent that diaphragms are ineffective for load distribution.

Finite Element Models:

To predict the structural behavior of this bridge system, FEM's using ANSYS 5.1 (1992) were developed and validated with the data from the laboratory tests. Three different FEM's were developed to model the following three conditions:

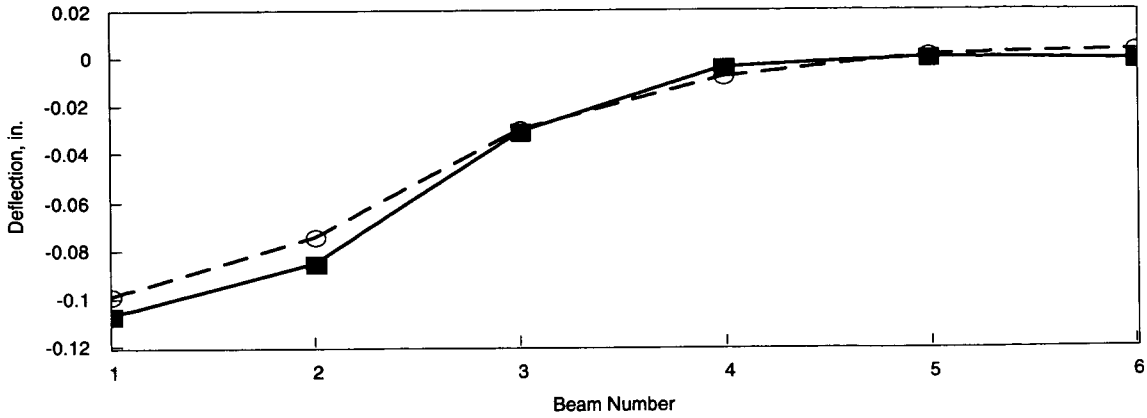
- PC units with various arrangements of connectors.
- PC units, connectors, and CIP concrete in place.
- Normal composite bridge with concrete deck placed at one time.

With these FEM's it is possible to predict the strength and behavior of the bridge system in various stages of construction and when subjected to various traffic loadings.

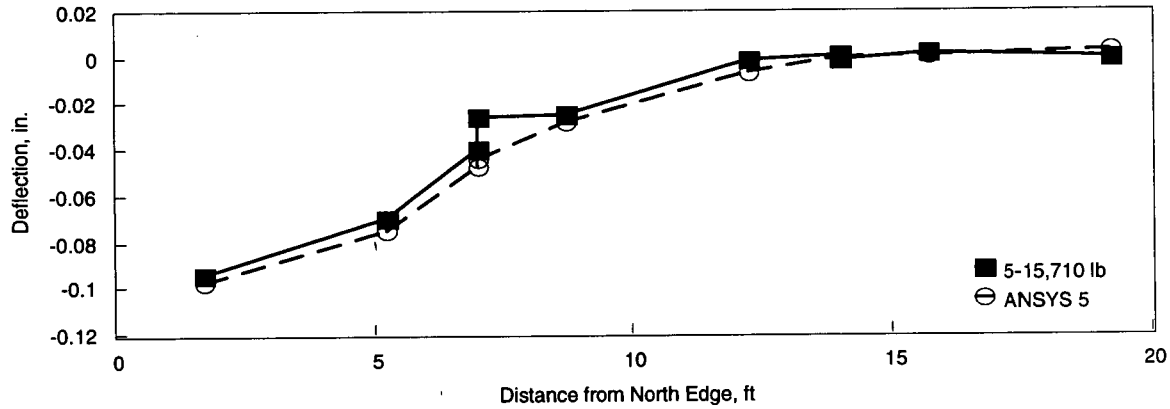
A representative sample of the analytical and experimental deflections in the PC units is shown in Fig. 9. In this figure, deflection results are presented for 71.2 kN (16 kips) being applied at Load point C1 with adjacent units being connected with five connectors (see Fig. 3b). In reviewing the theoretical and experimental deflections in Fig. 9, one observes very good agreement. The exception to this statement is at the 3/8 section (Fig. 9b) at the joint between adjacent PC units close to Load point C1. At this location, one observes larger differential displacement in the experimental deflections than in the theoretical values. The difference between the analytical and experimental results can be explained by the fact that in the analytical model, the connectors between PC units are assumed to have fixed ends. Actually they are somewhere between fixed and pinned.

In general, the analytical and experimental results are within 5-10% of each other. At a few joints between adjacent units, there is a 15% difference. The reason for this difference is connector fixity which was previously explained and the fact that although the FEM assumes that the PC units are only connected at connector locations, there is some contact at other locations as well. The contact is a function of variations in construction of the units (i.e., small variations in the widths of the PC units). Due to the randomness of the contact points, it is not possible to model this interaction. The decision to use five connectors in the bridge model was based on the experimental as well as theoretical results.

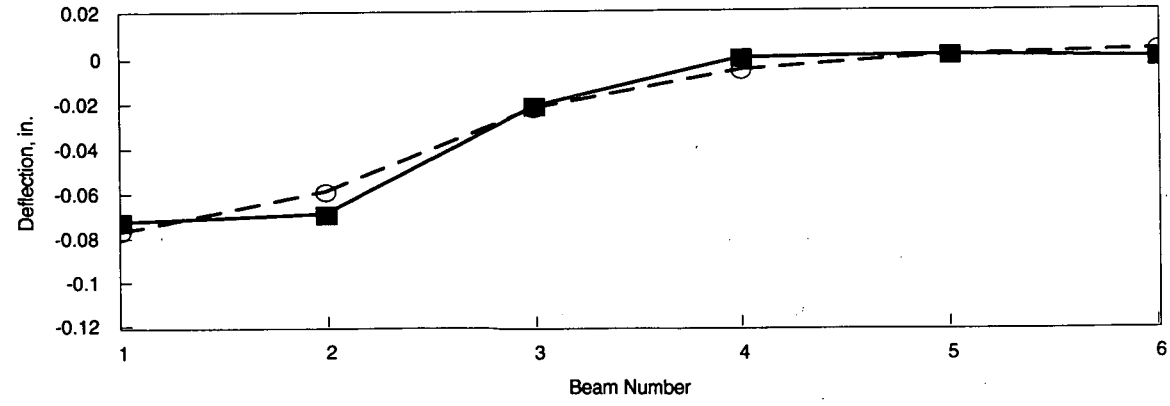
As was noted previously, a FEM was developed that predicted the behavior of a continuous transverse bridge deck with the same geometric properties as the one under investigation (Note; these results are designated "continuous"). Some of the results of these



a. Centerline



b. 3/8 point



c. Quarter point

Fig. 9. Experimental and analytical deflections in model bridge with five connectors; load at C1.

analyses are shown in Fig. 10. Deflections are presented for the load being applied at Load point C1. The two curves in Fig. 10 indicate that there is very little difference between the bridge under investigation and a continuous deck bridge. This indicates that with sufficient connection between the adjacent PC units (five connectors used in this case plus the reinforced CIP portion of deck), the bridge system can be designed by conventional bridge design procedures using current AASHTO specifications.

Conclusions

Based on the laboratory tests on the bridge model, the following observations and conclusions can be made. The majority of these conclusions have also been verified using the FEM's that were developed.

1.) The units developed and tested result in a simple-span bridge alternative for low-volume roads that is relatively easy to construct.

2.) The PC units (with their relatively thin concrete PC deck) are strong enough to resist the handling loads imposed on them during construction and transportation. Occasional "rough" handling is expected; if sufficient time is given for the PC concrete to cure, no distress should occur in the PC units from lifting, transporting, or placement.

3.) Five connectors between adjacent PC units gave the desired lateral load distribution. The use of seven or nine connectors did not change the behavior of the bridge system significantly.

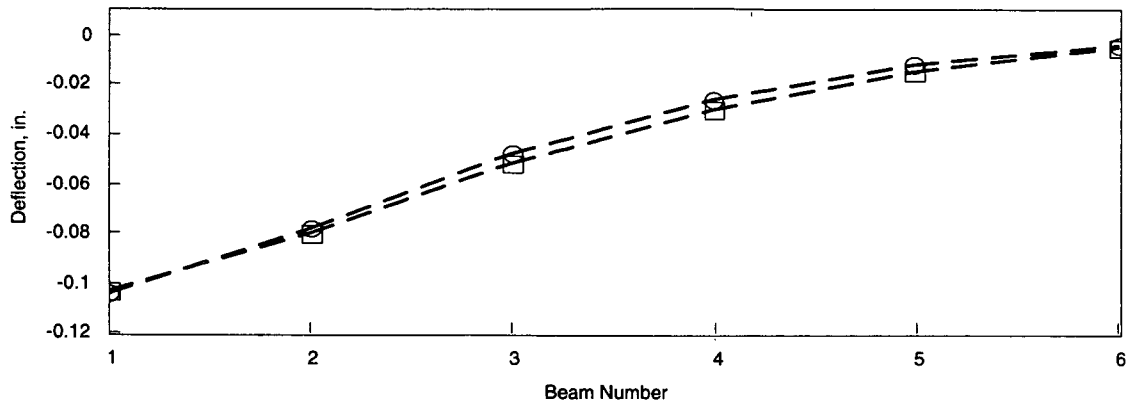
4.) The addition of the CIP deck significantly improved the load distribution characteristics of the bridge system.

5.) The combination of connectors between the PC units and reinforcement properly placed in the CIP portion of the deck should prevent reflective cracking in the system.

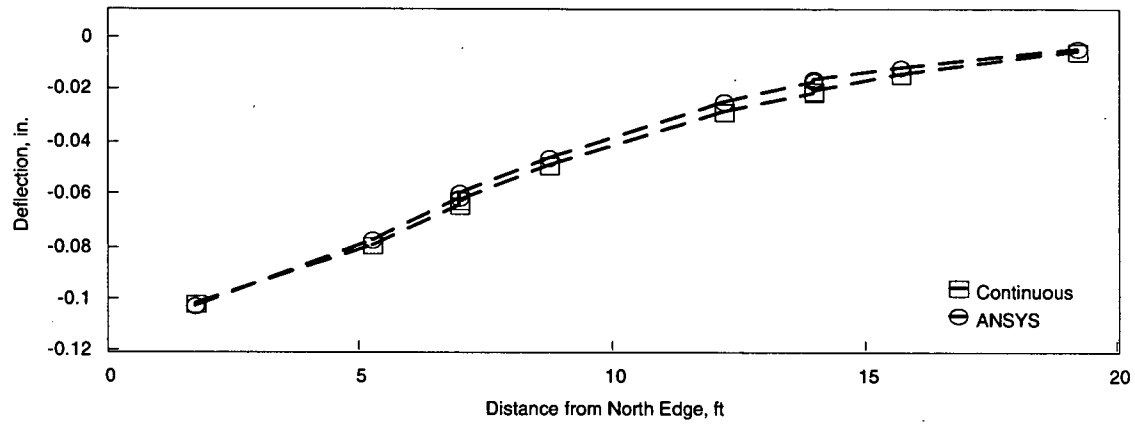
6.) The use of diaphragms did not significantly change the behavior of the model bridge. Based on this and the fact that the installation of diaphragms is very costly and labor intensive, the resulting small improvement in the behavior does not warrant their installation for lateral load distribution.

Acknowledgments

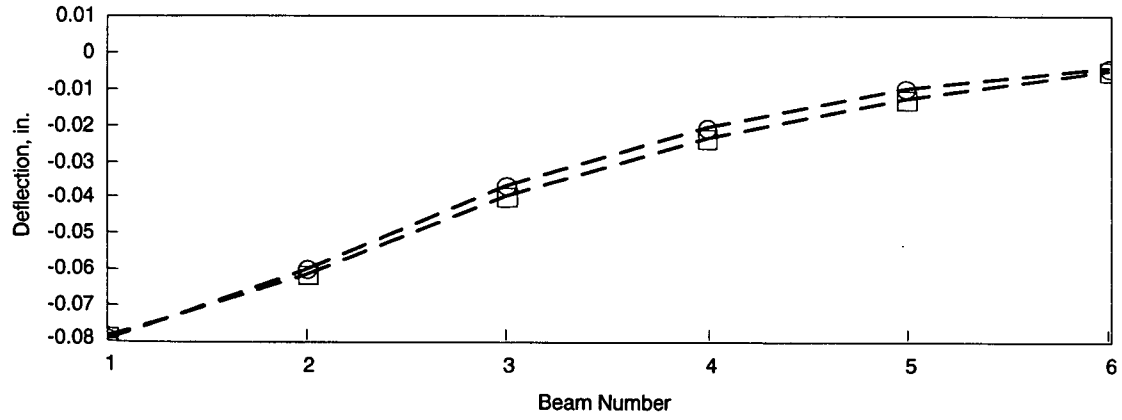
The research presented in this paper was conducted by the Bridge Engineering Center, Engineering Research Institute of Iowa State University and was funded by the Highway Research Board and the Highway Division, Iowa DOT, Ames, Iowa. The authors wish to thank numerous Iowa county engineers for their support, cooperation, and counsel. The opinions,



a. Centerline



b. 3/8 point



c. Quarter point

Fig. 10. Deflections for continuous and ANSYS models; for load at C1.

findings, and conclusions expressed herein are those of the authors and not necessarily those of the Iowa DOT or the Iowa Highway Research Board.

References

American Association of State and Highway Transportation Officials. Standard Specifications for Highway Bridges 15th Edition. Washington, D.C.: American Association of State Highway and Transportation Officials, 1992.

ANSYS User's Manual for Revision 5.1, Swanson Analysis Systems, Inc., Houston, PA. 1992.

Klaiber, F. W., T. J. Wipf, J. R. Reid, and M. J. Peterson, "Investigation of Two Bridge Alternatives for Low Volume Roads", Volume 2, Iowa DOT Final Report HR-382, ISU-ERI-Ames-97405, Engineering Research Institute, Iowa State University, April, 1997, 140 p.

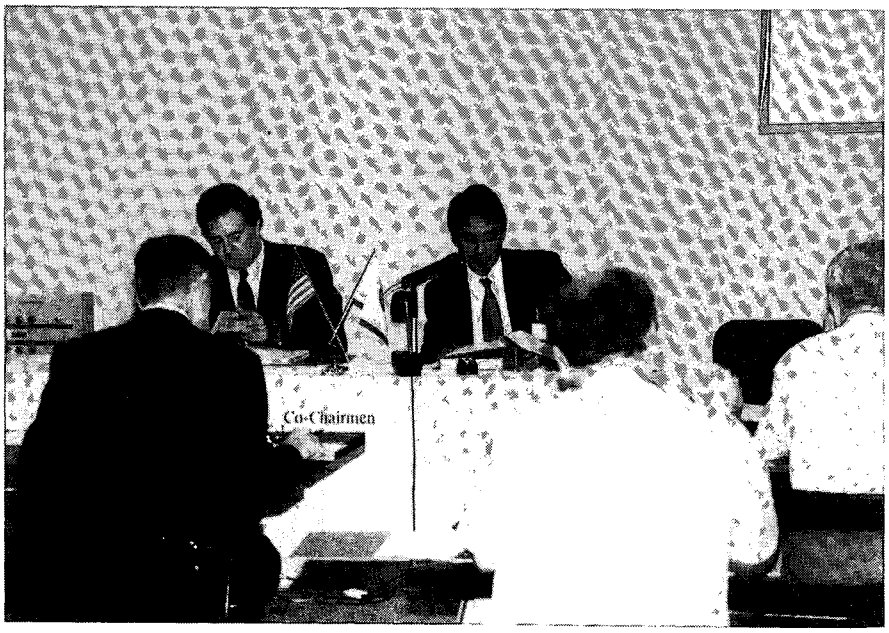
Wipf, T. J., F. W. Klaiber, and B. M. Phares, "Investigation of Two Bridge Alternatives for Low Volume Roads", Volume 1 of Iowa DOT Final Report Project HR-382, ISU-ERI-Ames-97405, Engineering Research Institute, Iowa State University, April, 1997, 138 p.

SESSION 7: MANAGEMENT (2)

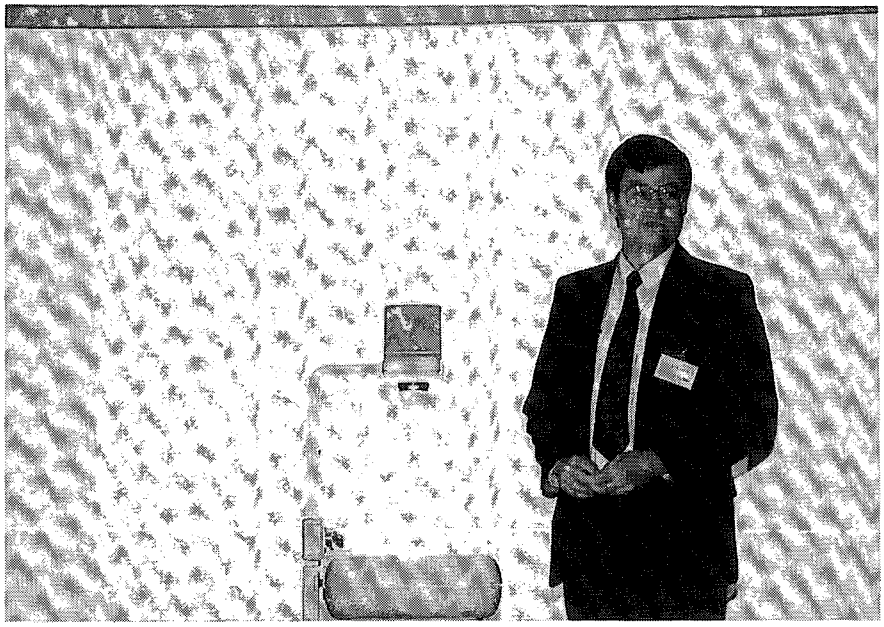
(1) Net-Capable Informatics for Instrumented Bridges
(Stuart S. Chen and Michael F. Lamanna)

(2) Development of a Bridge Management System
(H. Sato and K. Ogihara)

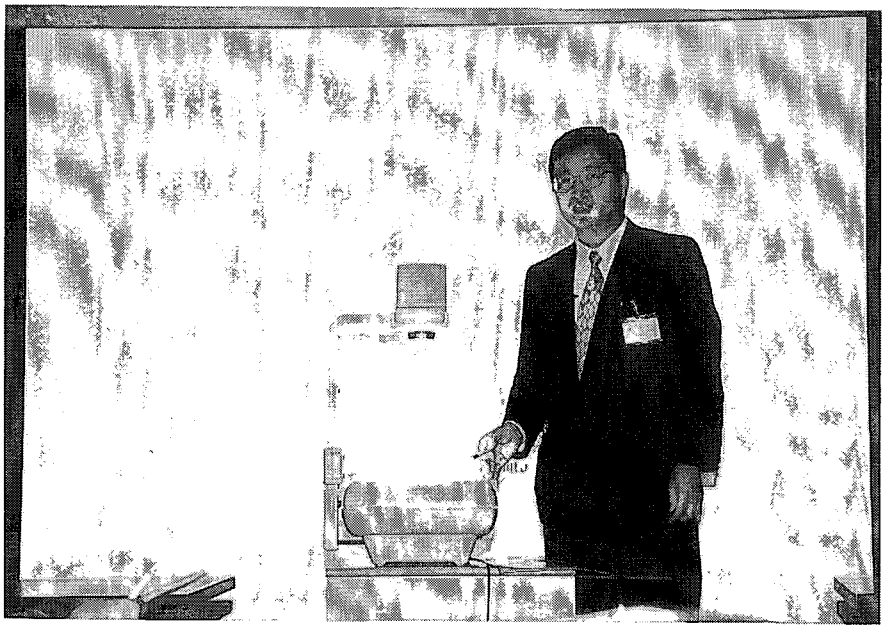
(3) Optimal Bridge Management under Uncertainty in a Life-Cycle Perspective
(Dan M. Frangopol, Allen C. Estes and Kai-Yung Lin)



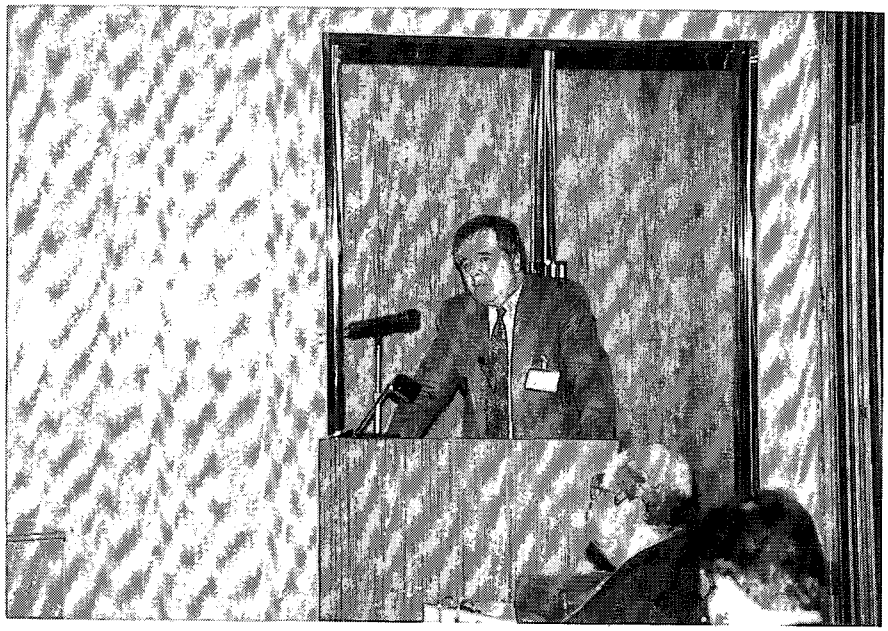
Co-Chairmen : Kazuhiro Nishikawa, Raimondo Betti



SESSION 7 : Stuart Chen



SESSION 7 : Katsuya Ogihara



SESSION 7 : Dan Frangopol

NET-CAPABLE INFORMATICS FOR INSTRUMENTED BRIDGES

STUART S. CHEN[1] AND MICHAEL F. LAMANNA[2]

1.0 Abstract

This paper addresses Health Monitoring and Condition Assessment applied to geographically dispersed civil infrastructure. The problem that is being addressed is how to do this remotely via the Internet/intranet. This system will be accessible via the Internet for the purposes of querying and obtaining data for further post-processing or for instrument control and adjustment. Much of this Internet-accessible processing can be done through the use of a programing language called JAVA[tm] and HTML documents, using the Internet/intranet paradigms. The results of this study are a framework for Network based Remote Monitoring of disperse instrumented civil infrastructures.

2.0 Introduction

This paper is organized as follows. First, various component technologies relevant to the development of an information processing environment for instrumented civil infrastructure are surveyed, with emphasis on Internet oriented aspects. Next, the information - oriented needs of both owners and users of instrumented civil infrastructure are identified. An overall framework is then proposed for combining these component technologies to provide a means of managing the information processing requirements. The use of the framework is illustrated via a case study.

2.1 Communications

The communication connection can be implemented via dedicated land lines, phone lines, wireless transmission, radio transmission [Maser, Lichenstein and Chase 1996], or an Internet based system [Ballard and Chen, 1996]. Each of these communication systems (wired, wireless and network) has its own characteristic strengths and weaknesses.

2.1.1 Internet and Intranet

An intranet differs from the Internet in that the Internet is public and global, while an intranet is private and local. Users of an intranet can have access to the Internet, but they do not have to allow the Internet to have full access to their intranet. This limiting of access is accomplished by placing a firewall between the intranet and the Internet community. Currently, there are many companies which have the hardware in place to make the move from a LAN, WAN or other network to an intranet. The only things that are needed are the appropriate software packages and protocols (IP); both of which have been developed and are being improved upon.

In an intranet, the server reduces the amount of duplicate material by providing easy access to these materials at a single location. There may be some aspects of a bridge condition

1.Associate Professor, Department of Civil Engineering, State University of New York at Buffalo, Buffalo, NY.
2.Research Assistant, Department of Civil Engineering, State University of New York at Buffalo, Buffalo, NY.

that are internal matters, like the remaining fatigue life. However, other aspects, such as current load rating and surface conditions are things that should be made known to the public. The intranet allows its users to centralize their information in a single, easy to use environment (the browser). Many browsers are available for a variety of platforms (PC, Unix, etc.). This allows each user to work on the platform they feel most comfortable with, while still maintaining the same high degree of accessibility.

2.1.2 World Wide Web

"The World Wide Web is an interactive, global, platform-neutral, hypermedia information retrieval system." [Newman et al 1996].

Since the World Wide Web uses the Internet it can go wherever the Internet goes. Furthermore, the World Wide Web is not limited to a single type of hardware architecture or operating system because it uses the Internet, which is also platform-neutral. Your web browser and the system it is connecting to speak a common language.

Web page addresses are given by a Uniform Resource Locator (URL) and are written in the HyperText Markup Language (HTML), which allows web page designers to include hyperlinks which allow users to navigate a document or even to another site. Hypertext is a non-linear method of organizing elements like words, pictures and addresses, that point to one another.

2.2 Software Development Languages

Providing fast and reliable data transfer is important, but it is not the end of the process. The appropriate software must be in place to do something with the incoming data. An appropriate "bridge" needs to be constructed using one or more programming languages.

2.2.1 Markup Languages

HyperText Markup Language (HTML) at its core is simply ASCII text with some additional information that informs a browser how the text is to be displayed. An HTML file is very similar to the file formats of early word processing and text formatting programs.

Virtual Reality Markup Language (VRML) is similar to HTML in that they both strive to provide a more "human" interface to the Internet. The main difference between VRML and HTML is that VRML creates a 3D interface to the Internet.

2.2.2 Languages for Interactivity: CGI and Java

Common Gateway Interface (CGI) is a way of interfacing external applications with information servers (e.g. http). That is, we execute a program and not just display some static information. Since the content is executable it is the equivalent of letting anyone in the Internet community run a program on your server. A CGI program can be written in any language that is executable on the system. The advantage to writing CGI scripts is that they are easier to debug, modify, and maintain than a typical compiled program. The problem is that they use system resources on the server rather than the client side.

Table 2-1: Communications Advantages and Disadvantages

Type	Advantages	Disadvantages
Dedicated Land Lines	High speed transmissions Very secure	Large installation expense Requires maintenance Limited points of access
Phone Lines	High speed transmissions Low installation cost No maintenance	Limited security Monthly and usage charges
Wireless	Low cost installation	Licensing is needed Limited range Lower speed transmission Requires maintenance
Internet	High speed transmissions Competitive installation and maintenance costs Security. Covers large geographic area	Non interactive
World Wide Web	High speed transmissions Competitive installation and maintenance costs It's Interactive Security Covers large geographic area	Requires an Internet account connection and a browser

The phenomenonal proliferation of the Java language stems from the need to have a full-fledged programming language that is executable across the World Wide Web to supplement the markup languages of HTML and VRML in a way that avoids the disadvantages of CGI. Sun Microsystems, which developed the Java language, has provided the following official statement describing the Java programming language. "Java is a simple, object-oriented, distributed, interpreted, robust, secure, architecture neutral, portable, high performance, multithreaded, and dynamic language" [JavaSoft 97]. These characteristics of the language exhibit potential for use in bridge monitoring applications.

Java is distributed, referring to the relationship between system objects. These objects can be on the local system or a remote system. Java applets and applications can both open and access

objects across the World Wide Web via URLs as easily as if they were on the local file system.

The fact that Java is interpreted allows for security and stability. This is accomplished through the linker, which checks the data coming into your machine to insure that it does not contain harmful files or files that could disrupt the computer system. Also, since the final portion is being done by a platform specific device (i.e. the user's own machine and browser), the programmer need not maintain multiple versions of a program to support different platforms.

Java is considered robust (reliable). It cannot cause a system crash since it is strongly typed and it only has access to a limited portion of computer memory. Security is important in part because the idea of downloading a binary file sight unseen does not create a feeling of comfort for most people. Even though this downloading is required for Java to function as an applet there are several safety features built into the language to safeguard the user from viruses and other malicious programs. Since Java code is first compiled into byte code, extra type information is included in it which can be used to check for potential security violations.

Java can keep track of more than one thing at a time by using threads. Each thread does not have to come to completion before another can be started or continued. The multithreading ability of Java gives it a extremely good real time behavior. In addition to the threading ability, priorities can be assigned to each thread. This tells the program whether to spend more or less time on a particular task. The priority assignment is not a static attribute. It can be changed by the program during run-time.

Since there are multiple measurands and quantities derived from them being monitored on a real instrumented bridge, using Java with dynamic priority assignment allows for multiple tasks to be performed simultaneously. For example, consider a bridge that is instrumented to do both fatigue monitoring and weigh in motion with a camera to capture the license plate number of an overweight truck. A program can be written to do both of these analyses. Each thread can be running at the same time with more priority given to the weigh in motion system when an overweight vehicle is detected to insure that the capture of the license plate on camera will not be delayed by the need to wait for the completion of a fatigue analysis.

2.2.3 Expert Systems

"An expert system is a computing system capable of representing and reasoning about some knowledge-rich domain with a view to solving problems and giving advice. It can be distinguished from other kinds of artificial intelligence programs in that:

- "It deals with subject matter of realistic complexity that normally requires a considerable amount of human expertise.
- "It must exhibit high performance in terms of speed and reliability in order to be a useful tool.
- "It must be capable of explaining and justifying solutions and recommendations in order to convince the user that its reasoning is, in fact, correct" [Jackson 1986].

Table 2-2: Language Advantages and Disadvantages

Development Language	Advantage	Disadvantage
HyperText Markup Language (HTML)	Widely used. Usable with any browser.	Not a full fledged programing language. Only 2D
Virtual Reality Markup Language (VRML)	Has 3D capability. Excellent graphics.	Requires special browsers. Not widely used.
Common Gateway Interface (CGI)	Easy to incorporate pre-existing programs. Usable with any browser. Platform Independent	Runs on server side. Slower than fully compiled languages.
Java	Runs on clients computer. Usable with any browser. Compatable with HTML and VRML Many security features. Extensive graphics capabilities. Platform Independent	Slower than fully compiled languages.

A system that cannot function well when faced with real world problems such as missing and/or unreliable data is of limited use. For example, in a real instrumented structure there is more than one member of interest that has been instrumented. It would be unacceptable for the entire system to stop functioning because one sensor is not responding. Also, for the system to be used with any significant degree of automation, it must be able to "weed out" bad data or uninteresting data. It should either continue with the data considered missing, or a reasonable value should be inferred from other valid sensor data.

2.2.4 Java Expert System Shell (JESS)

The appeal of the Internet and Java coupled with expert systems led to the development of a Java Expert System Shell (JESS) [Friedman-Hill 1997]. JESS is potentially suited for use in a monitoring system since forward chaining expert systems are believed to be useful in monitoring and control applications. JESS is an forward chaining expert system shell written entirely in Java that emulates the popular CLIPS [Riley 1997] style language.

Since JESS is written entirely in Java, it can be included in any HTML document with a properly formatted applet tag. The Java applet can be written so as to accept input parameters from the HTML document that it is included in. This will allow the same applet code to be used for a variety of different applications. The number and type of input parameters and what they do

will depend on how the applet has been written.

3.0 Informatical Framework: Requirements and Approach

3.1 Needs of owners and users

The needs of owners reflect the problems encountered in the actual implementation and maintenance of a health monitoring and condition assessment system. These will affect how data is obtained, what is done with the data, how any needed analysis is performed and what to do with the results of the analysis. All these concerns must be handled while keeping the costs low and planning for future changes and developments. These concerns may be summarized as follows:

- Repetitive post-processing of data
- Domain defined rules in conditional format
- Coverage of geographically large areas
- Flexibility and adaptability for future development
- Data handling: "What do we do with all this data?"
- Information sharing: Some of the results are needed only for internal usage while other results need to be made available to related agencies and the general public.

The needs of the users are not directly addressed in the development of the overall system. However, they have been included in the present discussion to demonstrate some of the motivating factors for the choice of component technology used to address problems associated with health monitoring and condition assessment systems. These needs may be summarized as follows and should be addressed in a cost-effective manner:

- Safety and reliability
- Timely access to important and useful information

3.2 Solutions

The following discussion addresses one of the specific problems or issues identified earlier and identify a solution to that problem.

3.2.1 Repetitive post-processing of data

The problem of repetitive post-processing of data is handled by implementing computer automation. Computers can easily perform the same task numerous times producing correct results each time. This is provided that the program the computer is running is free of bugs and errors.

3.2.2 Coverage of geographically large areas

Since the pieces of infrastructure to be monitored can cover a large geographic area the need to do the monitoring from a remote location is evident. The problem that this creates is that the data and or results must be transmitted to the off-site location where the information is needed.

What is needed is a low cost system that can provide sufficient transmission rates with the appropriate amount of security and that does not require a great deal of special licensing or attention. The World Wide Web can provide such a system through the use of secure servers, HTML and Java. The costs are competitive with phone based systems, but the best feature is that it is already in place and very reliable.

3.2.3 Domain defined rules

The domains that are suitable for health monitoring and condition assessment often use rules that are defined in English-like statements of a conditional type. This creates problems when generating conventional programs that must decide what to do in light of the current conditions. Expert systems are designed to handle problems that are best described in English-like sentences rather than mathematical equations. Therefore, the decision of when to apply which rule can be handled through the use of an expert system. Since many of the available expert system shells can also do the mathematical calculations, an expert system is ideally suited to handle the computer implementation of the domain rules.

Since the proposed system is to use the Internet to transmit data and results, the expert system shell to be used must be written in a language that the can be run through a web browser. The decision to use JESS (Java Expert System Shell) was made since it was readily available and upon further investigation was able to implement all the needed functions.

3.2.4 Flexibility and adaptability for future development

Many buildings and bridges change their roles during their lifetime. The amount of traffic that a bridge carries may change in response to population shifts. Thus, any system that is implemented to perform health monitoring and condition assessment of the infrastructure must also be able to change with these conditions. The intranet paradigm offers a simple and powerful implementation of client/server computing. It is the simplicity of the model that gives it great flexibility, versatility and cost effectiveness. The browser is a cost-effective, versatile interface to information and programs involved in the day to day operations. In addition, the intranet paradigm can support both internal and external applications, unlike groupware systems. As the information and programs change either internally or externally the browser will remain as the common interface. It is for these kinds of reasons that the Internet/intranet paradigm is considered sufficiently flexible and adaptable for civil infrastructure monitoring.

3.2.5 Data handling

The problem of dealing with the avalanche of data cannot be handled by any of the component technologies described in Section 2. The problem must be dealt with on a case by case basis so as to "weed out" uninteresting data.

3.2.6 Access to important and useful information

Both the owners and end users of instrumented infrastructure need access to the information that a health monitoring and condition assessment system provides. The type and

degree of access will depend on what the system has been designed to provide.

Owners may need to have access to the monitoring system itself, and not just the data and results that are produced [Aktan et al 1995]. This will allow them to perform the necessary system diagnostics, and adjustment of controls (e.g. sensor gain). Much of this can be done off-site, but some on-site inspection and maintenance will still have to done. For example, a diagnostic run off-site may detect that a sensor is malfunctioning and needs replacement, however an actual person will have to visit the site to make the needed repair. As of yet there has not been a system developed that has the ability to make physical corrections of this type remotely.

The type of results that are produced from the system may be for internal agency use. For example, any flags that are posted for bridges are only of use to the owner and do not need to be made public. The reason for this is that the general public is not familiar with the meaning of the flags, nor are they capable of doing anything about them. The owner will also need the ability to change some settings, like flags on a bridge, once the corrective measure has been taken. Providing this ability brings up the question of how privileges are provided.

The use of a secure server in an intranet can accomplish the setting of protections for the different user types based on a simple login procedure that uses a password. However, this is not required for all areas on the web site. There is no need to require the use of a login name and password for access to information that is to be made available to the general public. Another way of allowing a higher level of access to owners is by providing the access on the secure side of the server. For end users, the type and amount of information that is given will depend on the actual application and end users' needs. The two main outlets for information from an owning agency of instrumented infrastructure to the general public discussed in this paper are the World Wide Web and Intelligent Transportation Systems.

Since the intranet paradigm was shown to serve some of the needs of the owners and it uses the same IP protocol that the Internet does, creating web pages to provide the information that users need can be accomplished through this outlet. The web pages can be updated dynamically to reflect the up-to-the-minute conditions that are being reported.

Since this paper addresses concerns about instrumented infrastructure such as bridges and roads, it is also possible to make some information available through IVHS/ITS. Variable message boards and on-board route guidance systems can be used to provide information about delays concerning construction or incidents, as well as current weather conditions.

3.3 Combining the elemental solutions to develop the overall framework

Section 3.1 discussed the specific problems that needed to be addressed, while section 3.2 identified a component technology that was best suited to handling a specific problem. This section presents how the component technologies that were identified to address one of the specific problems are combined to form the overall system framework. The following table summarizes the previous discussion about which component technology is best suited to handle which problem.

Table 3-3: Problems and corresponding solutions

Problem	Solution
Repetitive post-processing of data	Computer automation
Domain defined rules	Expert System
Coverage of geographically large areas	Remote monitoring Internet and WWW transmission
Flexibility and adaptability for future development	Intranet paradigm
Access to important and useful information	Intranet Intelligent Transportation Systems Intelligent Vehicle Highway Systems Web pages

Two possible scenarios are envisioned for structuring the overall framework. They both use the same component technologies, but the questions of how access is provided and where the different components are placed are handled differently in the two scenarios.

3.3.1 Scenario 1: Off-site web server

As seen in Figure 3-3, in the first scenario the web server and the file server are located at the Home Office. The connection of the Remote Site to the Home Office can take place via the most appropriate data transfer method (e.g. land lines, wireless, Internet, etc.). All post processing of data will be done at the home office and the appropriate results will be made available to the appropriate parties.

For example, consider the following hypothetical situation. Suppose the sensor system at the Remote Site sends some sensor data to the Home Office after determining that the data is significant enough to warrant further processing. The Home Office server then performs the needed analysis. The results of the analysis indicate that the bridge is iced over. The Home Office then updates the IVHS/ ITS systems to warn motorists. At the same time an update is made to the owning agency's web page to indicate that travel on this route may be hazardous, to warn motorists who are planning a trip that a different route might be more appropriate. Not only are motorists notified of these conditions, but an automated call is placed to work crews indicating that de-icing crews are needed for that bridge.

The main advantage to this system is that it allows for considerable centralization. The Home Office is the center of information allowing the owner to track what type of information is accessed by what type of user. In addition, it also allows for access to the server from behind the firewall for employees, which reduces some of the access limitation complications. Users at the Home Office (employees) will not have to go through the firewall to access the server. This approach adds a little more security since it reduces the likelihood of someone being able to

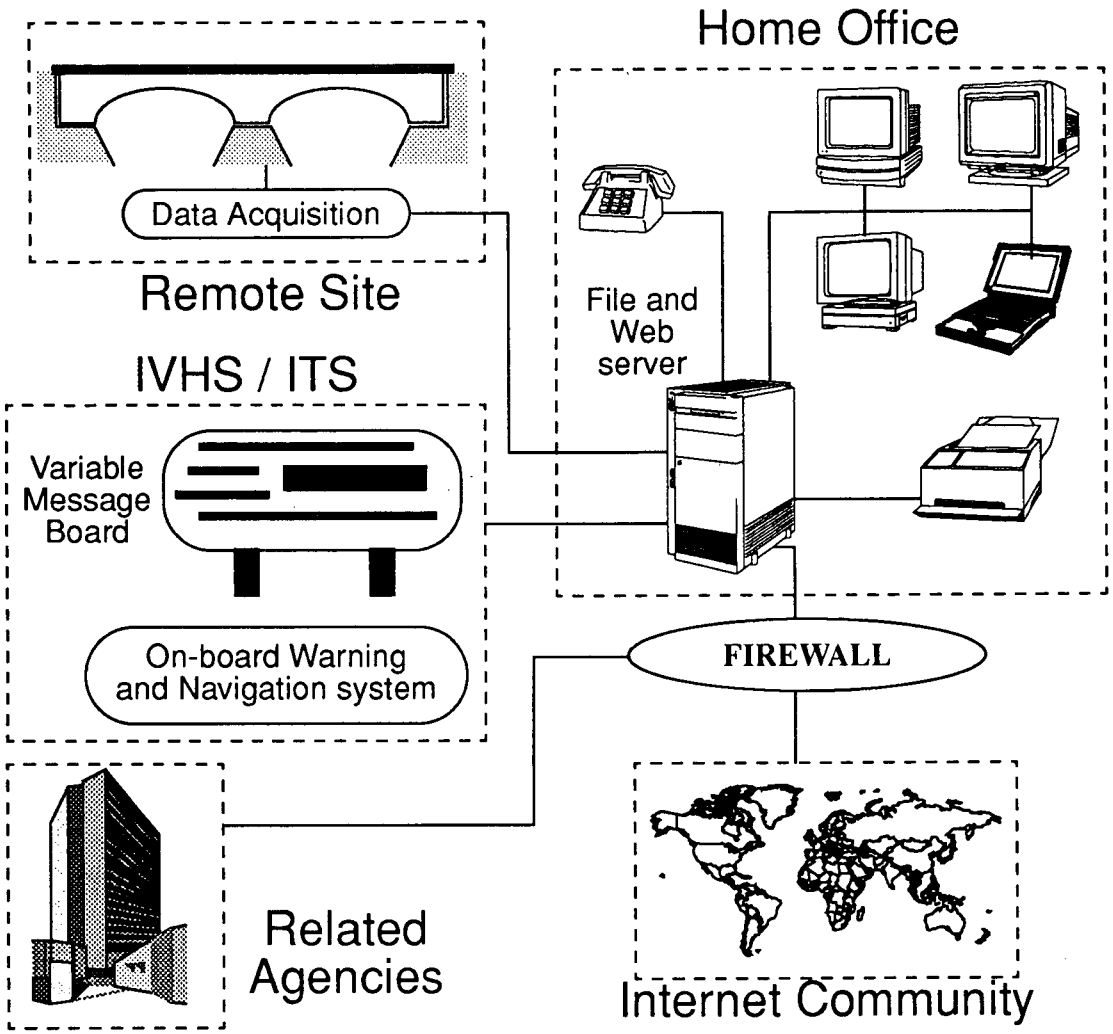


Figure 3-1. Scenario 1: Off-site web server

tamper with the system from outside the Home Office by guessing the username and password that will grant them higher access. Another advantage is that it allows for the most cost effective and suitable method of data transfer from the instrumented structure to the post-processing site.

One disadvantage is the fact that all the information is going through one computer. When multiple sites are added issues such as file size, storage space, and memory can become very important and possibly expensive. The cost of a computer, that is acting as the server, will depend on the amount of memory required and storage space needed. This problem is not as limiting, however, as it might first appear. Through the use of languages like Java the server demand can be reduced by executing the analysis program on the end user's computer and not the server. However, a large number of file requests can also place a high demand on the server.

3.3.2 Scenario 2: On-site web server

As seen in Figure 3-4, in the second scenario the web server is now located at the Remote Site and not the Home Office. The connection from the Home Office to the Remote Site should take place over the internet, with the use of a tunnel allowing control from the Home Office. Now all post-processing will take place at the Remote Site and only the information (results of an analysis) will need to be sent anywhere. While not shown, the Home Office can still run its own web server, but it would not have to carry the load of information from the Remote Site.

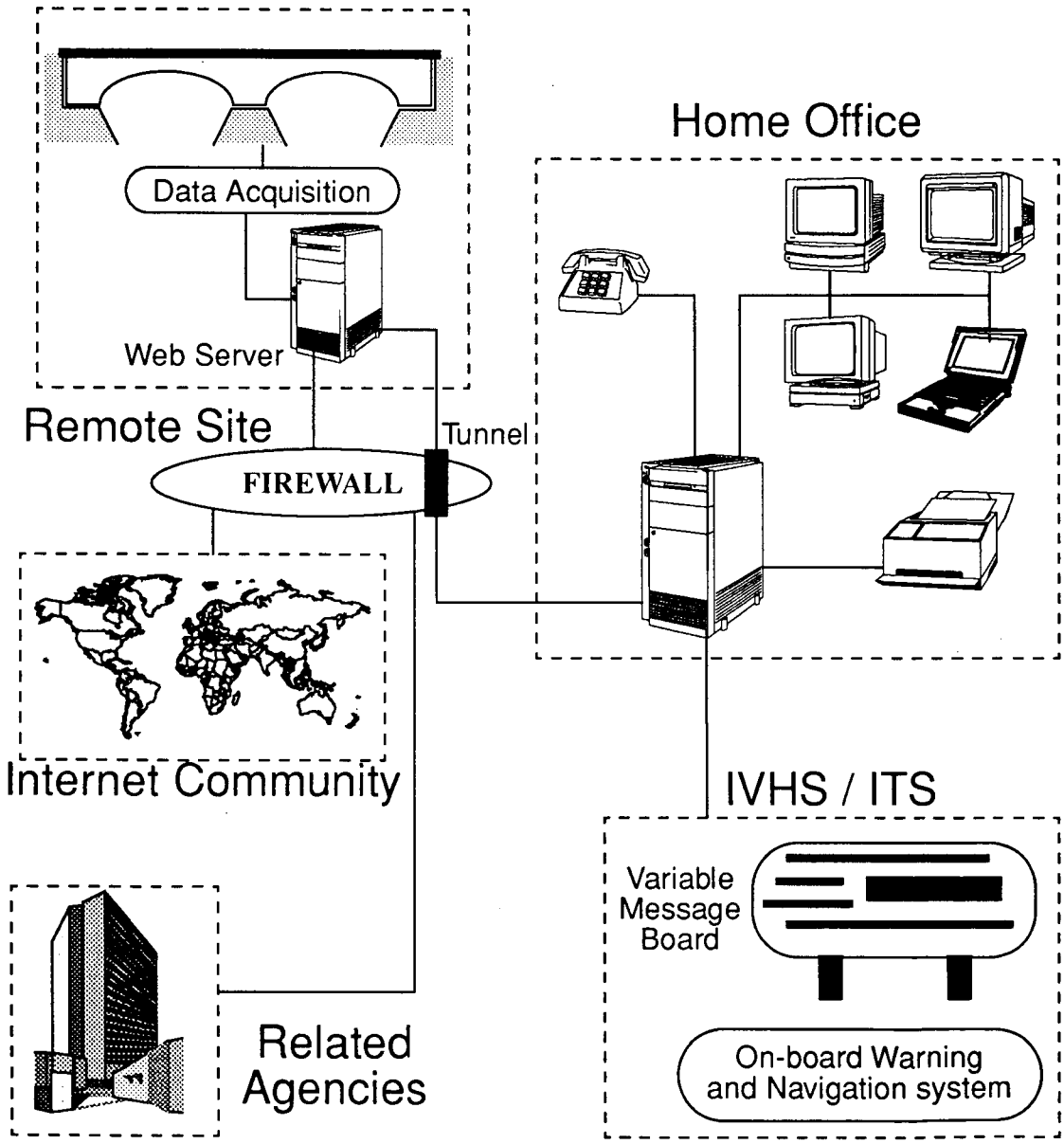


Figure 3-2. Scenario 2: On-site web server

For example, consider the same situation as before except that this time the data, that has been determined to be significant, is not sent to the Home Office. Instead, the data is post-processed at the remote site and only the results need to be sent to the Home Office. In general, this scenario will result in a significant savings on bandwidth. This time the Remote Site's computer system informs the general public and related agencies of the necessary information.

The main advantage of this system is that the load on the Home Office server is reduced. It has been assumed all along that the Home Office does more with its system than just the remote monitoring application. Therefore, a server with smaller capabilities, and smaller cost, can be used to provide for the needs of the owning agency. Another advantage of this setup is that only results are transferred. This provides significant savings on bandwidth used by transfer.

A disadvantage of this system is that it increases the number of hardware systems that have to be maintained. However, a malfunction of one system at a Remote Site is not as devastating as a malfunction of the main server at the Home Office. Another disadvantage is the fact that the problem of providing security accesses for users at the Home Office to control and adjust the system and its settings must be implemented. This will require the use of a tunnel and some web server administration. While there are several web site administrative tools available to do this, it is just one more thing that has to be done and maintained.

3.3.3 Comparison of On-site to Off-site web server scenarios

There is no "best" solution to determining which framework is the better. Table 3-3 shows a comparison of the two scenarios' strengths and weaknesses.

Table 3-4: Advantages and disadvantages of scenarios 1 and 2

Scenario	Strengths	Weaknesses
1	Only one server to configure and maintain. Information is centralized in one location. Easier high level access for owning agency	Increased demands and loads on server. Transfer of data. Large memory and storage requirements on single server. "Eggs in one basket"
2	Reduced demands and loads on server. Transfer of results only Smaller memory and storage requirements for each server.	Many separate servers to configure and maintain. Information is distributed over several locations Complicated high level access procedure for owning agency

4.0 Case Study: Surface condition detection

The danger posed by slippery or icy bridge surfaces can be reduced by providing adequate warning to motorists of these conditions. Also, improved response of plows and salters can be achieved with better detection capabilities.

Converting Domain Rules to JESS code

Consider the following sample rule for ice detection.

```
IF   the bridge-temperature is cold                AND
     the bridge-moisture-level is high
THEN the bridge-surface is icy
```

The terms cold, high, and low are vague or "fuzzy" and need to be further defined. Cold in reference to the bridge temperature is referring to the temperature at which applying salt will not melt the ice. The point at which this occurs is a function of more than just the temperature. It varies with barometric pressure and salinity. The bridge-temperature could also be warm, the temperature at which any moisture on the bridge will not freeze, or cool, the temperature range in which the possibility of freezing depends on the salinity and pressure. A preprocessor can be used to convert the incoming sensor data (temperature, barometric pressure, salinity, moisture, etc.), which is in numerical format, to the appropriate "fuzzy" terms for use in the JESS applet.

The following rules are a sample of those used to assess the current condition of the bridge surface and display the appropriate message to the user. These rules apply to the conditions that make the bridge icy regardless of the salinity. The message that is to be displayed is an example of the type of information that is intended to be sent to various types of IVHS systems, such as variable message boards and on-board navigation aids.

```
(defrule bridge-is-icy-1
  (current-phase check-bridge-surface)
  ?f1 <- (bridge-plowed not-yet)
  (bridge-temperature cold)
  (bridge-moisture high)
  =>
  (retract ?f1)
  (assert(display-message icy-1)
         (dispatch-bridge-crew plow)
         (bridge-plowed yes)))
...
(defrule display-condition-icy-1
  (current-phase update-message-board)
  (display-message icy-1)
  =>
  (printout t crlf "CAREFUL!" crlf "Bridge is ICY!"
  (printout t crlf))
```

Sample Outputs

Figure 4-3 shows a screen capture of a Netscape window. The document being displayed through Netscape is `Surface.html` which is listed in the following piece of HTML code.

```
<html>
<applet code=MyJESS width=800 height=300>
<param name="KBfilename" value="Ice.clp">
<param name="FACTSfilename" value="Ice.facts">
<param name="ButtonName" value="Recheck Surface">
</applet>
</html>
```

The file `Ice.clp` contains all the rules that were implemented in the formation of the knowledge base regarding bridge surface monitoring. The file `Ice.facts` that was used in generating the output shown in Figure 4-3 is listed below. These facts represent the results of converting the numerical data obtained by data acquisition to the form needed for processing in this knowledge base.

```
(current-phase check-bridge-surface)
(phases update-message-board)
(bridge-plowed not-yet)
(bridge-salted not-yet)
(bridge-temperature cold)
(bridge-moisture high)
(bridge-salinity low)
```

The status of the lights and the information displayed in the text area shown in Figure 4-3 are shown for the conclusion of the analysis. The analysis was run with the above facts as the initial working memory.

Summary

This paper has presented some preliminary directions for the use of the world-wide web and associated utilities as a potentially useful platform for management of geographically dispersed instrumented Civil Infrastructure such as bridges. A preliminary framework is proposed and illustrated in the context of bridge surface condition monitoring as part of an IVHS. Partial support provided by the University at Buffalo Multidisciplinary Pilot Project Program is gratefully acknowledged, as is help provided by Dr. E. Friedman-Hill of Sandia National Laboratories.

References

Aktan, A.E., Helmicki, J.J., and Hunt, V.J., "Instrumentation and Intelligence Issues in Bridge Health Monitoring", in Smart Structures and Materials 1995: Smart Systems fro Bridges, Structures, and Highways, Larryl K. Matthews, Editor, Proc. SPIE 2446, pp. 106 to 115 (1995).

Ballard, C M, and Chen, S S, "Internet Structural Monitoring System," in Ansari, F., ed., Intelligent Civil Engineering Materials and Structures, Special Publication of ASCE,1997.

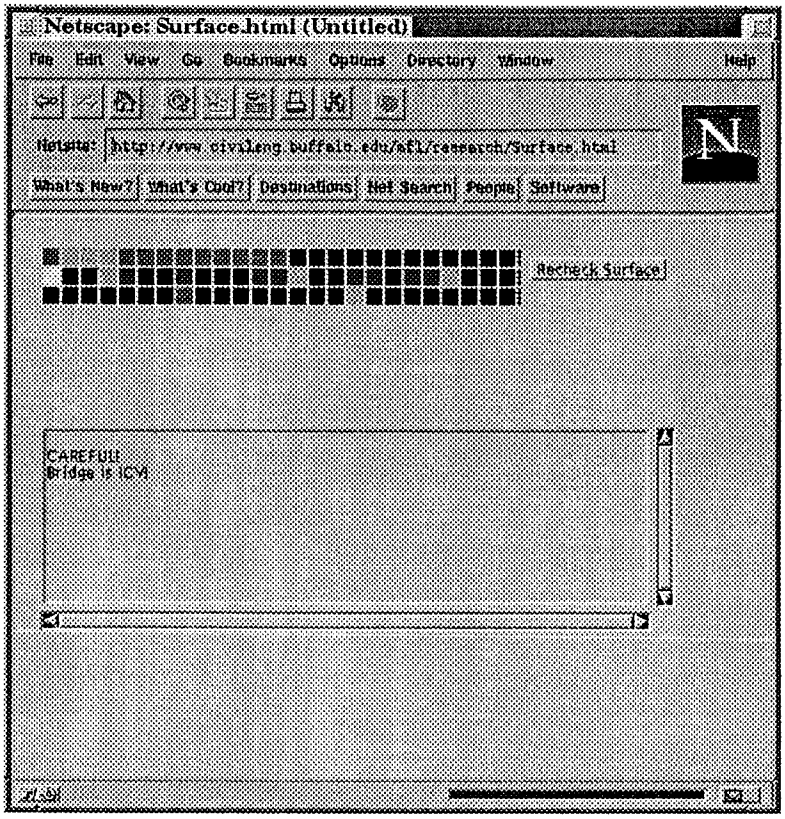


Figure 4-3. Surface Monitoring output from Netscape

Friedman-Hill, E. and Sandia National Laboratories, "The Java Expert System Shell", http://www.ca.sandia.gov/jess/README, (November 1996).

Jackson, P., *Introduction to Expert Systems*, Addison-Wesley, Reading, MA, 1986.

JavaSoft, "All About Java", http://www.javasoft.com/aboutJava/index.html (January 1997).

Maser, K., Egri, R., Lichtenstein, A., and Chase, S., "Development of a Wireless Global Bridge Evaluation and Monitoring System (WGBEMS)", in Proceedings of ASCE Structures XIV, vol. 2, April 1996, pp 734-741.

Newman, A, Ablan, J., Afergan, M., Benson, A., Blossom, E., Brintle, L., Carpenter, J., Cassady-Dorion, L., Cross, J., Greene, S., Jois, S.K., Krakow, I., Krom, K.M., Pietrowicz, M., Waks, M., Walsh, G.A., Webber, J.L., Williams, S., Wutka, M., Special Edition using Java™, QUE®, 1996.

Riley, G, "CLIPS: A tool for building Expert Systems",.http://www.jsc.nasa.gov/~clips/CLIPS.html (January 1997).

DEVELOPMENT OF A BRIDGE MANAGEMENT SYSTEM

Hiroshi SATO[1] and Katsuya OGIHARA[2]

Abstract

Japan has already highly developed and it is difficult to expect high economic growth any more. It is necessary to carry out cost-effective and systematic bridge management. In 1990, the Public Works Research Institute (PWRI) started to develop a bridge management system (BMS) to assist bridge managers and engineers. A prototype of the BMS was completed in 1995. The BMS consists of two program modules, which are the bridge condition evaluating module and the bridge rehabilitation planning module. The bridge condition evaluating module evaluated the present bridge condition from the inspection data. The bridge rehabilitation planning module optimized the bridge rehabilitation plan according to the incremental benefit cost ratio. The prototype has been tested at several work offices, and it is being improved by the test result.

1 Introduction

Japan has been improving roads and road bridges. The road stocks have been increasing in volume. There are about six hundred and fifty thousand bridges longer than 2m, about one hundred and twenty thousands of which are longer than 15 m. The road maintenance budget increases year by year. The increase ratio of the road maintenance budget is higher than that of the road construction budget. Considering such a situation, it is necessary to keep huge infrastructures good condition for long time. Here, cost-effective and systematic bridge management is required for road bridge stocks. Several countries that have much bridge stock have already developed their own bridge management systems (BMS)[1].

Inspection techniques, evaluation techniques and maintenance techniques have been improved in Japan, and manuals of those have also been improved. Here, computer, especially personal computer, has been remarkably improved and wide-spreading. Personal computer can be treated easily and a lot of data are treated and stored quickly and accurately by it. The database for road related data was developed earlier by the Ministry of Construction (MOC). Following the database, the Public Works Research Institute (PWRI) of MOC started to develop a bridge management system for personal computers in 1990 to assist bridge engineers. At first, the computer language "C" was used to develop the system under MS-DOS of Japanese version. The developing language was changed to "visual basic" according to the change of operating system from MS-DOS to MS-WINDOWS.

[1]Head, Structure Division, Structure and Bridge Department, Public Works Research Institute, Ministry of Construction

[2]Senior Research Engineer, Structure Division, ditto

2 Outline of bridge management

The bridge management is to repeat the three works, namely to inspect bridges, to evaluate the bridge condition, and to rehabilitate bridges if necessary. The BMS assists the works of evaluation and rehabilitation of bridges and make these works effective.

Ideal total bridge management system is shown in Fig.1. Though some countries, namely USA, Denmark and U.K, have already developed and applied their own BMS, Japan has not applied the whole system but the database.

MOC has developed the Ministry of Construction Highway Information Data Base System (MICHI). The data treated in the MICHI are image data such as maps, surrounding conditions, road situations, road structures, structures, supplementary facilities and so on. These data can be extracted to the BMS by several forms. Generally, the BMS is a total system including database, but PWRI's BMS is a personal computer software. The BMS treats several data, which are bridge structure data and inspection records, extracted from the database "MICHI."

2.1 Storage of inspection data

Inspection standards of MOC were united under the Bridge Inspection Manual issued by PWRI in 1988. All bridges longer than 15m has been inspected closely at ten-year intervals, which is called the close inspection. The flow chart of inspection and repair work is shown in Fig.2. The necessity of investigation or repair work depends on the deficiency rating. Condition of each part of bridges is evaluated according to the deficiency rating for each kind of defect (for example, corrosion, crack, etc.). Description of deficiency ratings is shown in Table 1. There are five deficiency ratings, namely I, II, III, IV, "O.K." In the manual, serious damage that may cause any traffic problems is ranked "deficiency rating I" by bridge inspectors. No damage is ranked as "O.K." When bridge inspectors suspect some defect as the deficiency rating I, detailed investigation or rehabilitation of the damaged bridge should be conducted immediately. Inspection data of each part of bridges have been expected to be stored in the MICHI. Basic structure of the MICHI was developed in 1990.

2.2 Bridge management system

The ultimate purpose of the BMS is to minimize the life cycle cost of bridges. The BMS developed in Japan seeks the most effective rehabilitation plan under financial constraint. The BMS uses bridge structure data and inspection data from the MICHI. The BMS consists of two program modules, which are the bridge condition evaluating module and the bridge rehabilitation planning module. The flow chart of the BMS is shown in Fig.1.

The bridge condition evaluating module evaluates the present bridge condition from the rating of bridge members. The bridge condition rating, output of the module, can be used to screen out heavily damaged bridges and scarcely damaged bridges.

The bridge rehabilitation planning module optimizes the bridge rehabilitation plan. For example, the module suggests which bridge should be rehabilitated, and how deeply the bridge should be rehabilitated under financial constraint. The standard deterioration curve is used in the bridge rehabilitation planning module.

3 Bridge condition evaluating module

In this module, rating of each part of a bridge is integrated to evaluate the rating of the whole bridge. The demerit rating of each damage is calculated from deficiency rating in the MICHI. The conversion were as follows.

1. Demerit rating d_I corresponding to deficiency rating I of each damage was decided.
2. Other demerit ratings were calculated by following equations,

$$d_{II} = d_I \times a_{II}, \quad (1)$$
$$d_{III} = d_I \times a_{III}, \quad (2)$$
$$d_{IV} = d_I \times a_{IV}. \quad (3)$$

Here, a_{II}, a_{III} and a_{IV} : reducing ratios shown in Table 2 . The ratio were decided from the comparison to those made by inspection specialists. When deficiency rating I is found, the rehabilitation work is conducted immediately. As rating I is not kept and marked in the MICHI, d_I is rarely used. d_{OK} is obviously 0.

The evaluation method of bridge condition was decided by comparing the weighted average method with the subtracting point method. The explanations of the methods are shown in Table 3 and Table 4. Even when a bridge is suffered by a heavy damage, the bridge condition rating calculated by the weighted average method is not so bad in some cases. On the other hand, when the subtracting point method is used, the method can reflect the heavy damage of a part into the bridge condition rating directly. From this reason, the subtracting point method was selected. The bridge condition rating is calculated by adding up demerit ratings of parts and subtracting total demerit ratings from 100, full mark. For example, if a bridge has no demerit rating, the condition rating is 100.

The bridge condition rating provided by this method has been compared with the rating made by inspection specialists. The results were shown in Fig.3. The rating by the BMS ranged wider than those by the inspection specialists. We found that it was very difficult to fit the ratings by BMS to those of inspection specialists because of the small number of sample data. The module should be improved using sufficient data for long time so that the module become more reliable.

4 Bridge rehabilitation planning module

First of all, the bridge rehabilitation planning module performs screening of bridges. If a bridge is in very good condition, no rehabilitation is required. For these bridges, the following procedure is not necessary.

The module makes fourteen rehabilitation plans for each bridge. Each bridge is divided into main three parts, namely floor system, main girders and substructures. Each part has three options, which are replacement, rehabilitation and no rehabilitation. The module combined these rehabilitation plans of three parts to each rehabilitation plan for a bridge. Here is a condition that, when some part is replaced, other parts upper than the replaced part must be replaced. Total number of combinations for a bridge is fourteen.

The module can accept a rehabilitation plan by manual input for each bridge. The module calculates the rehabilitation cost of each plan, and calculates the benefit of each plan. The benefit B is calculated by following equations,

$$B = C_0 - C_1 . \tag{4}$$

Here, C_0 is a present value of rehabilitation cost in the future under the condition that no rehabilitation is performed at present and the bridge is replaced t_r year after from now, and is replaced at T year intervals. C_1 is a present value of rehabilitation cost in the future under the condition that the bridge is rehabilitated at present, and it is replaced $t_r + e$ year after from now, and is replaced at T year intervals. Rehabilitation extends e years of the bridge life. Explanation of t_r, T and e is shown in Fig.4 and Fig.5. It is important to consider not only present bridge condition but also future condition. The module expects the future condition of the bridge to calculate the benefit. The standard deterioration curve is used for calculating the benefit. C_0 and C_1 can be calculated as follows.

$$C_0 = A\left[\frac{(1+i)^T}{(1+i)^T-1}\right]\left[\frac{1}{(1+i)^{t_r}}\right] , \tag{5}$$

$$C_1 = A\left[\frac{(1+i)^T}{(1+i)^T-1}\right]\left[\frac{1}{(1+i)^{t_r+e}}\right] . \tag{6}$$

Here, A is replacement cost of the bridge, i is discount rate.

The module calculates benefits and costs of all plans of all bridges. Then it lists all plans of each bridge in order of increasing cost and calculates an incremental benefit cost ratio for each plan. When the ratio is less than 1, the plan will be removed. When the list of plans in order of increasing cost does not result in incremental benefit cost ratios in descending order, the list is also arranged by removing some plans. Then new incremental benefit cost ratios will be calculated. The module ranks all plans of all bridges in descending order of the ratio. The module selects a plan according to its rank and repeats it until total cost of selected plans reaches the annual budget. Finally, the group of selected plans will be proposed.

As a result of trail use until now, there were some troubles. They are as follows:

- Standard deterioration curve was unclear according to the insufficient data.
- The estimated cost of rehabilitation by the BMS was not reliable according to the lack of sufficient rehabilitation work data.
- Some data required for the BMS were not stored in the database MICHI.

These problems are not easy to be solved. At first step of practical use, only the bridge condition evaluating module will be used mainly. The rehabilitation planning module should be used as a reference or as a sample program, which will be the most important part of the BMS in near future.

5 Conclusion

The bridge management system, that consists of the bridge condition evaluating module and the bridge rehabilitation planning module, is being developed in Japan. The first version (prototype) of the BMS was completed in 1995. At present, the BMS is in a stage of trial

use. Hearing the comments and claims of the trial users at site office, the BMS is being improved so that bridge engineers and managers can use the BMS more easily, and that the BMS will provide more reliable outputs.

To put the BMS into practical use, the BMS should be modified so that the system may select rehabilitation plans on the basis of present condition and importance of the bridge, and that the data on rehabilitation may be accumulated into the system. After operating such a simple BMS for a decade or so, we hope that we will be able to utilize more sophisticated BMS.

6 References

1.U.S. Department of Transportation, Federal highway Administration. *BRIDGE MANAGEMENT SYSTEMS*, FHWA-DP-71-01R, OCTOBER 1989.

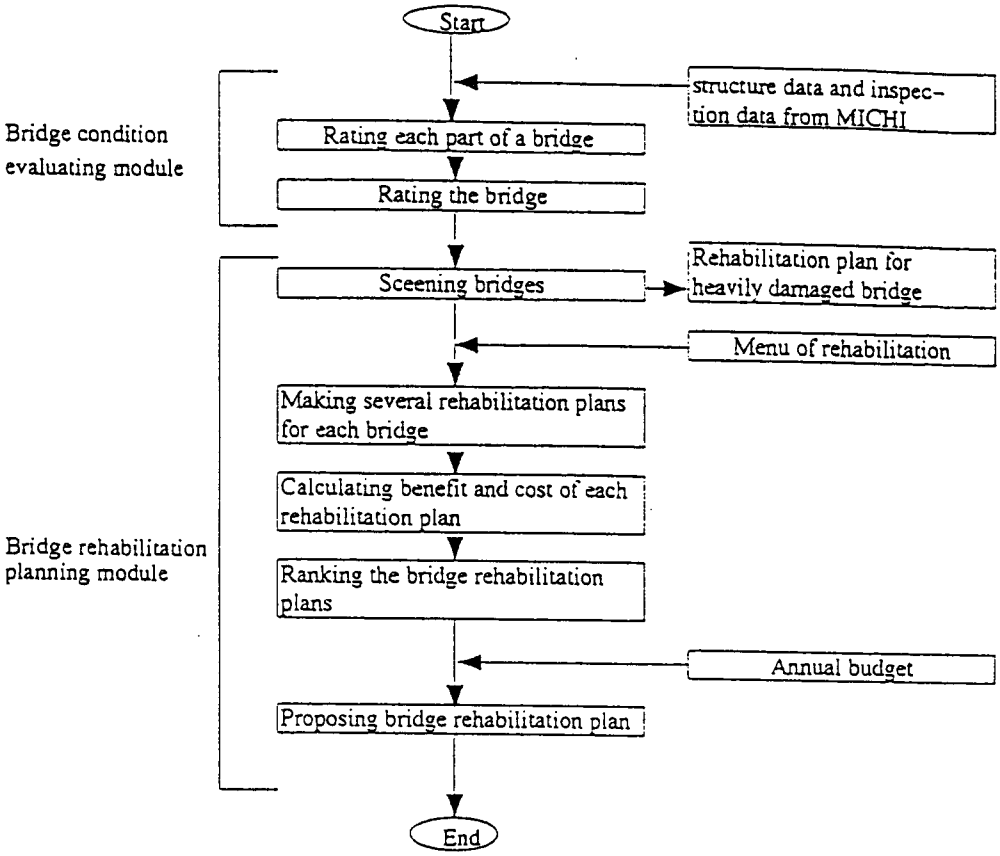


Fig. 1. Flow chart of the BMS

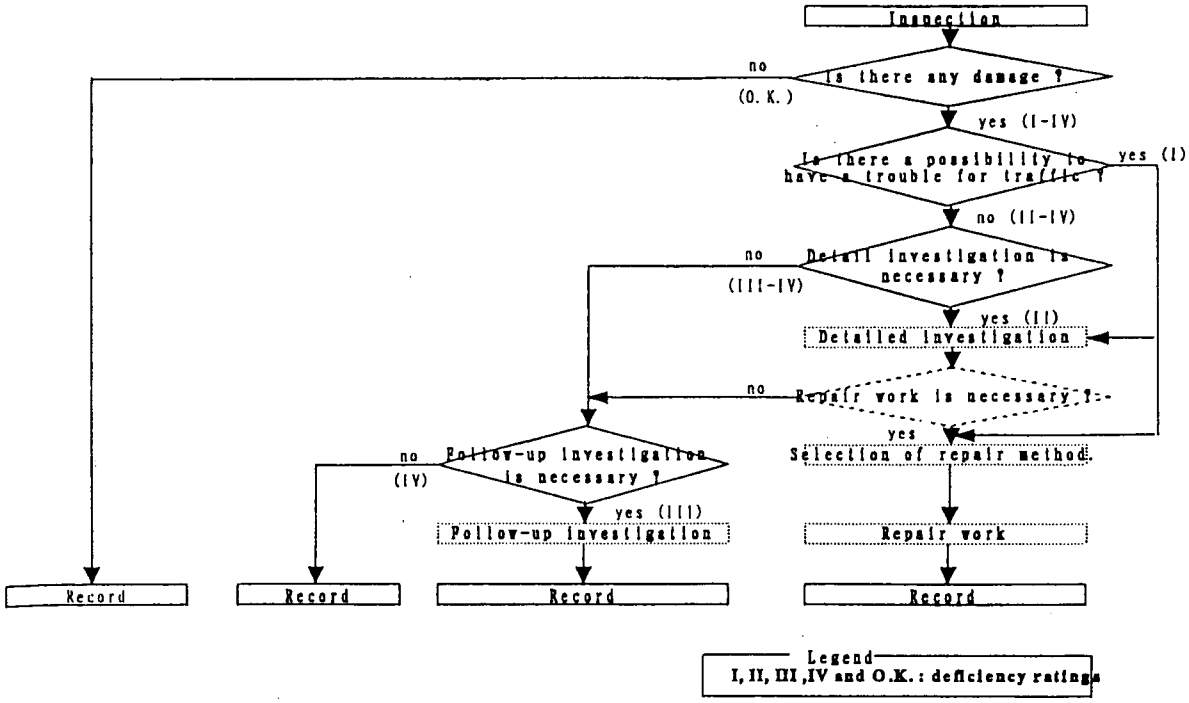
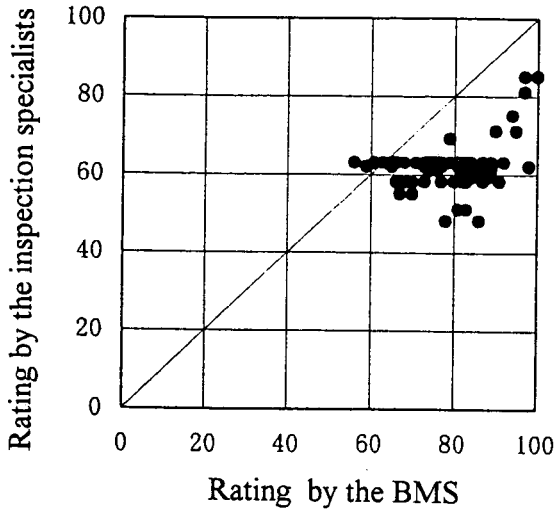
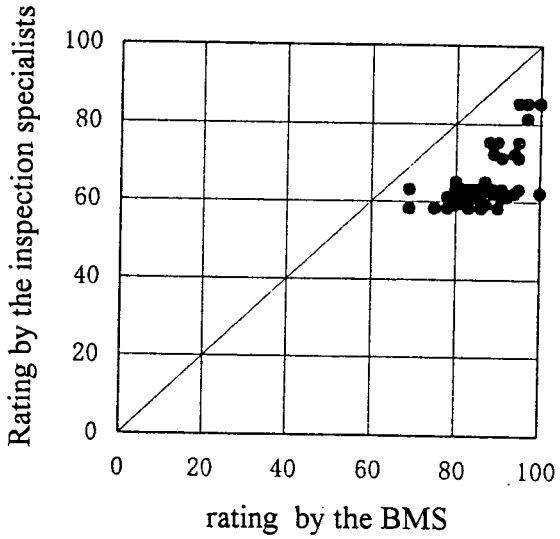


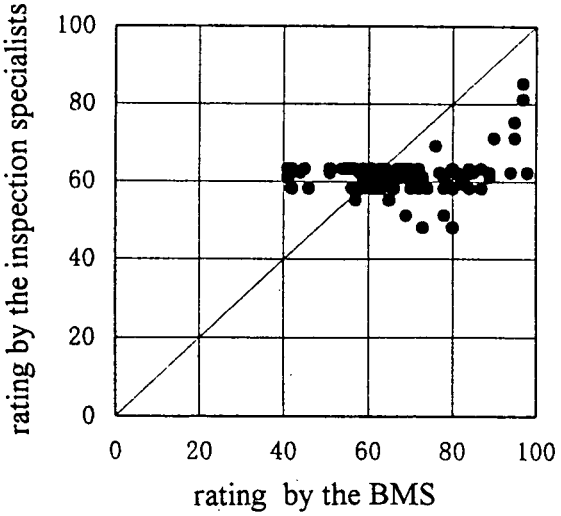
Fig. 2 Flow chart of inspection and repair work



(a) Condition rating of superstructure



(b) Condition rating of substructure



(c) Condition rating of bridge

Fig. 3 Bridge condition rating by the BMS and by inspection specialists

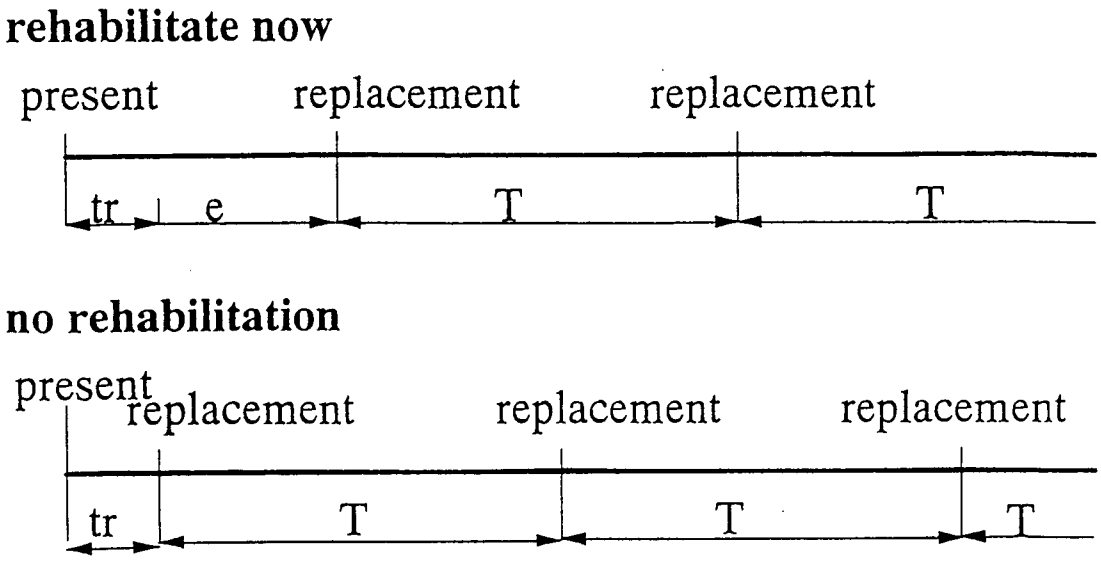


Fig. 4 Replacement cycle

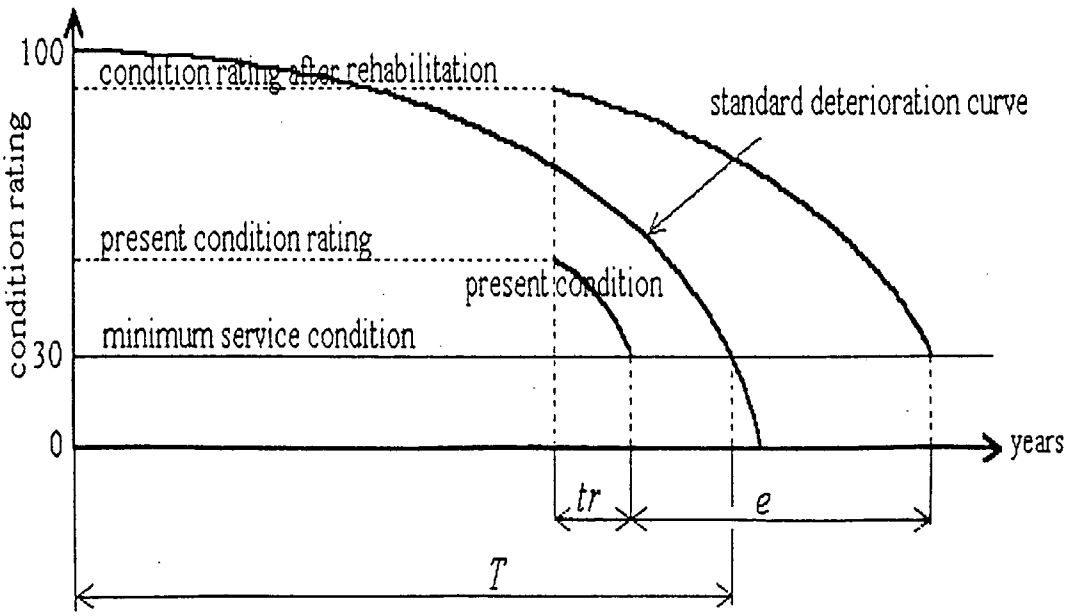


Fig. 5 Standard deterioration curve

Table 1. List of deficiency ratings of MICHI

deficiency rating	description
I	Serious damage. There is a possibility to cause a trouble for traffic.
II	Damage in large area. Detailed investigation is required. Following the investigation, necessity of immediate repair work should be evaluated.
III	Damage. Follow-up investigation is required.
IV	Slight damage. Inspection data is recorded.
O.K.	No damage.

Table 2. Reducing ratios and deficiency ratings

Deficiency rating $x =$	I	II	III	IV	O.K.
Reducing ratio $a_x =$	1	0.18	0.12	0.06	0

Table 3. Calculation sample by the weighted average method

Part	Superstructure				Substructure		
	Main girder	floor system Stringer	Crossbeam	floor plate	abutment	pier	foundation, pile
Demerit rating	36	0	12	0	0	6	0
Maximum rating	100	50	50	70	60	60	90
Weight	30	5	4	15	8	8	24
Sum of demerit ratings	36/100x30 + 0/50x5 + 12/50x4 + 0/70x15 + 0/60x8 + 6/60x8 + 0/90x24						
	= 12.6						
Bridge condition rating	100 - 12.6 = 87.4						

Table 4. Calculation sample by the subtracting point method

Part	Superstructure				Substructure		
	Main girder	floor system Stringer	Crossbeam	floor plate	abutment	pier	foundation, pile
Demerit rating	36	0	12	0	0	6	0
1st adding-up (threshold level	36 100		12 50	0 70		6 60	0 90)
2nd adding-up (threshold level	36 100			12 70		6 90	)
3rd adding-up (threshold level		48 100				6 90	)
Final adding-up (threshold level				54 100			)
Bridge condition rating	100 - 54 = 46						

OPTIMAL BRIDGE MANAGEMENT UNDER UNCERTAINTY IN A LIFE-CYCLE PERSPECTIVE

Dan M. Frangopol, [1] Allen C. Estes,[2] and Kai-Yung Lin[3]

Abstract

Efforts to develop comprehensive Bridge Management Systems (BMS) have increased significantly during the 1990s. A comprehensive bridge management system has to use powerful tools to predict the future conditions and cost of bridges in a life-cycle perspective. The goal is to provide bridge management decisions which will balance structural reliability and life-cycle cost in an optimal manner. Therefore, BMS have to rely on life-cycle engineering, reliability and optimization concepts and methods. Because these concepts and methods have a relatively short history, a commonly accepted methodology for optimal bridge management balancing structural reliability and life-cycle cost currently does not exist. In this paper, the framework of such a methodology is presented and applied to both new and existing bridges. This framework is further used to formulate an optimal lifetime non-destructive (NDE) inspection methodology based on minimum total inspection/repair cost. The proposed methodology offers the real potential for integrating economic and safety issues into optimum strategies over the design life of new bridges and over the remaining life of existing bridges.

Introduction

The United States has a multi-trillion dollar investment in civil infrastructure systems (CIS) (Zimmerman and Sparrow 1997). This huge investment has to be managed in an optimal manner. In this context, the recent introduction of life-cycle engineering based on life-cycle cost analysis constitutes an important development (Chang and Shinozuka 1996). The purpose is that management decisions about infrastructure investments (such as design of new CIS and repair, rehabilitation, replacement, and removal of existing CIS) have to result in the most efficient use of limited available resources.

Due to the fact that infrastructure decision making is typically fragmented, global optimal management solutions are far from being achieved (Zimmerman and Sparrow 1997).

[1] Professor, Department of Civil, Environmental, and Architectural Engineering, University of Colorado, Campus Box 428, Boulder, CO 80309-0428, USA

[2]Commander, 169th Engineer Battalion, Fort Leonard Wood, MO, 65473, USA; formerly, Grad. Student, Department of Civil, Environmental, and Architectural Engineering, University of Colorado, Campus Box 428, Boulder, CO 80309-0428, USA

[3]Project Manager, Chung-Shen Institute of Science and Technology, Taiwan, Republic of China; formerly, Grad. Student, Department of Civil, Environmental, and Architectural Engineering, University of Colorado, Campus Box 428, Boulder, CO 80309-0428, USA

Moreover, in spite of recent efforts, optimal management solutions for specific components of CIS such as highway bridges are typically not achieved. This paper presents a framework for an optimal bridge management under uncertainty in a life-cycle perspective. Numerical examples are also presented. Finally, research needs to successfully use the proposed approach in current bridge management practice are identified.

Goal of Bridge Management

As mentioned in Shirole (1994) "the goal of comprehensive bridge management is to determine and implement an infrastructure preservation and improvement strategy that best integrates capital and maintenance activities at the lowest possible life-cycle cost". In the United States, the 1991 Intermodal Surface Transportation Efficiency Act (ISTEA) required that life-cycle costs be considered in the design of transportation facilities such as bridges and tunnels. Furthermore, current bridge management systems such as PONTIS (Thompson 1994) and BRIDGIT (Lipkus 1994), which were developed with support from the Federal Highway Administration (FHWA) and National Cooperative Highway Research Program (NCHRP), respectively, incorporate life-cycle cost considerations. Additionally, work is in progress on a project on "Life-Cycle Cost Analysis for Bridges", sponsored by the National Cooperative Highway Research Program (NCHRP 1996). This project is aimed at developing a consistent methodology for bridge life-cycle cost analysis for use by transportation agencies.

Although there has been great progress in applications of probabilistic concepts and methods to bridge management, investigation of the optimal bridge management strategy from a life-cycle cost perspective has been very limited. A consistent methodology for bridge management based on life-cycle cost has to include all uncertainties associated with the design and evaluation processes of new and existing bridges. In addition, all components of bridge life-cycle cost, such as construction, maintenance, delay, user and capital costs have to be considered. The purpose is to achieve the best solution in a probabilistic context (i.e., minimum expected life-cycle cost). Such a methodology was developed by Frangopol and his co-workers (Estes 1997, Estes and Frangopol 1997, Estes *et al.* 1996, 1997, Frangopol and Lin 1997, Frangopol *et al.* 1997 a-c, and Lin 1995). Borrowing from these studies, this paper describes both the framework of the proposed methodology and the lifetime nondestructive evaluation inspection optimization approach. Numerical examples are also provided.

Framework

The life-cycle cost, deterioration modeling, target lifetime reliability, inspection method, inspection time interval, quality of repair, and repair time interval must all be considered when optimizing the management strategy for new or existing bridges. There is a trade-off between reliability and expected total cost. The goal of bridge management is to

optimize the life-cycle cost while ensuring that the bridge maintains an allowable (target) reliability level throughout its expected service life.

The formulation of this problem for new bridges was presented by Frangopol *et al.* (1997b, 1997c) as follows:

$$min\ C_{ET} = min\ (C_T + C_{PM} + C_{INS} + C_{REP} + C_F) \tag{1}$$

$$subject\ to \quad \beta_{life} \geq \beta^*_{life} \tag{2}$$

where C_{ET} = expected total bridge cost over its lifespan (i.e., design life); C_T = initial cost; C_{PM} = preventive maintenance cost; C_{INS} = inspection cost; C_{REP} = lifetime repair cost; and C_F = total failure cost. The preventive maintenance, inspection, repair, and failure costs are total expected expenditures during the design life of the bridge. β_{life} and β^*_{life} are the lifetime reliability index and the lifetime target reliability index, respectively.

Of course, other terms may be included in the expected total cost. For example, Chang and Shinozuka (1996) used the following expression for computing the expected life-cycle cost:

$$C_{ET} = C_1 + C_2 + C_3 + C_4 \tag{3}$$

where C_1 = planned costs and owner's costs; C_2 = user costs associated with C_1; C_3 = unplanned costs and owner's costs; and C_4 = user costs associated with C_3. In this manner, not only owner costs but also user costs are explicitly included in the optimization process. These latter costs depend on the extent of service disruption (e.g., closing bridge lanes to traffic) and are explicitly defined in Johnston *et al.* (1994) and Yanev (1994).

The formulation of optimum cost design over the remaining life of existing structures is similar to that described in Eqns. (1) and (2). The difference is that the reliability indices and all costs, except the initial cost C_T, are now related to the remaining life instead of the design life. Two numerical examples follow.

Optimal Lifetime Design of a RC Bridge. Using the optimization formulation defined by Eqns. (1) and (2), where all costs and reliability indices are given in Lin (1995), a reinforced concrete bridge was optimized for a service life of 75 years using three different corrosion rates ν (i.e., 0.0064, 0.0089, and 0.0114 $cm/year$). The value of the lifetime target reliability index β^*_{life} was assumed to be 2.0, and three different non-destructive evaluation inspection techniques A, B, and C were used. The inspection techniques have different detection capabilities. The costs associated with these inspection techniques are also different $C_A < C_B < C_C$, where C_i is the cost associated with inspection technique i.

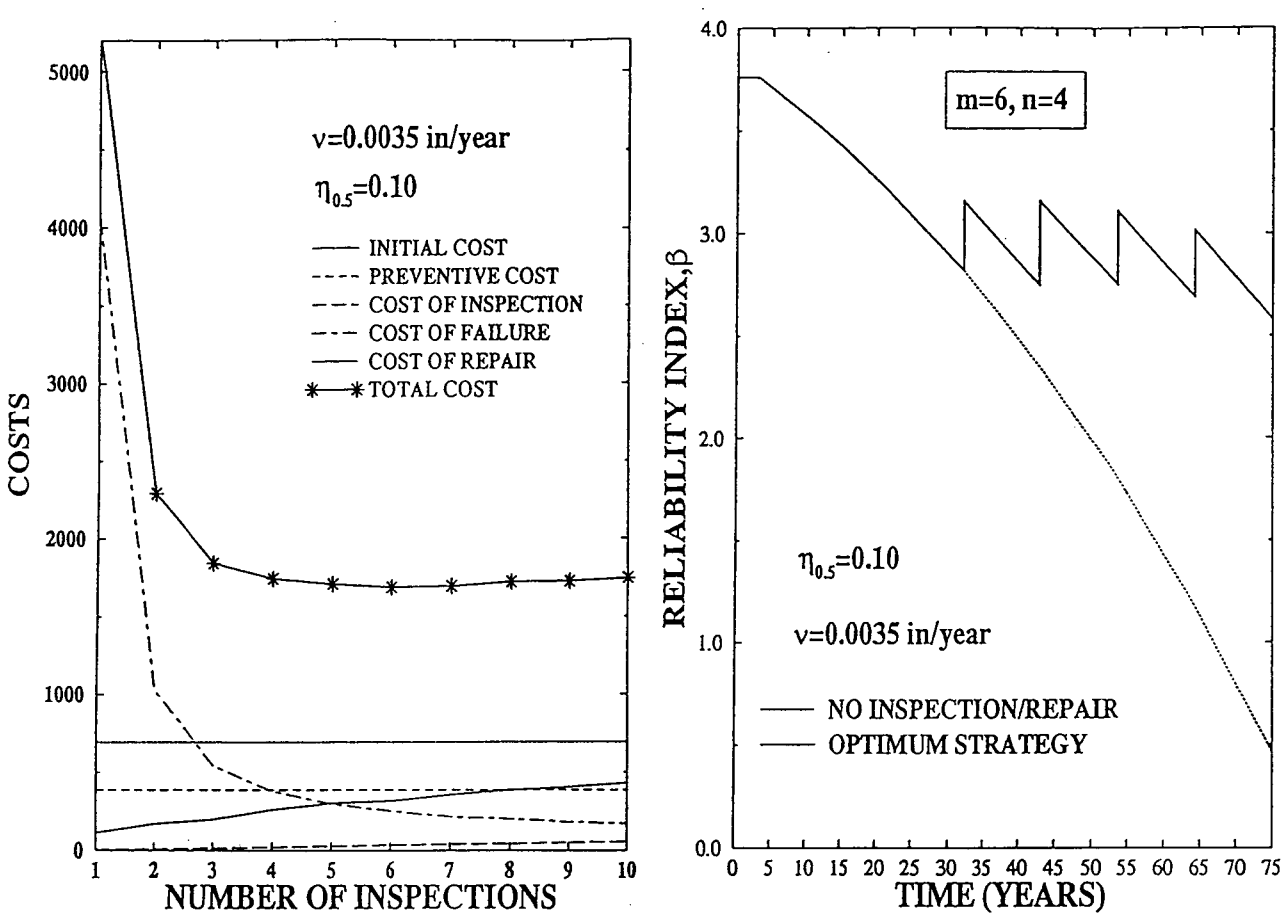
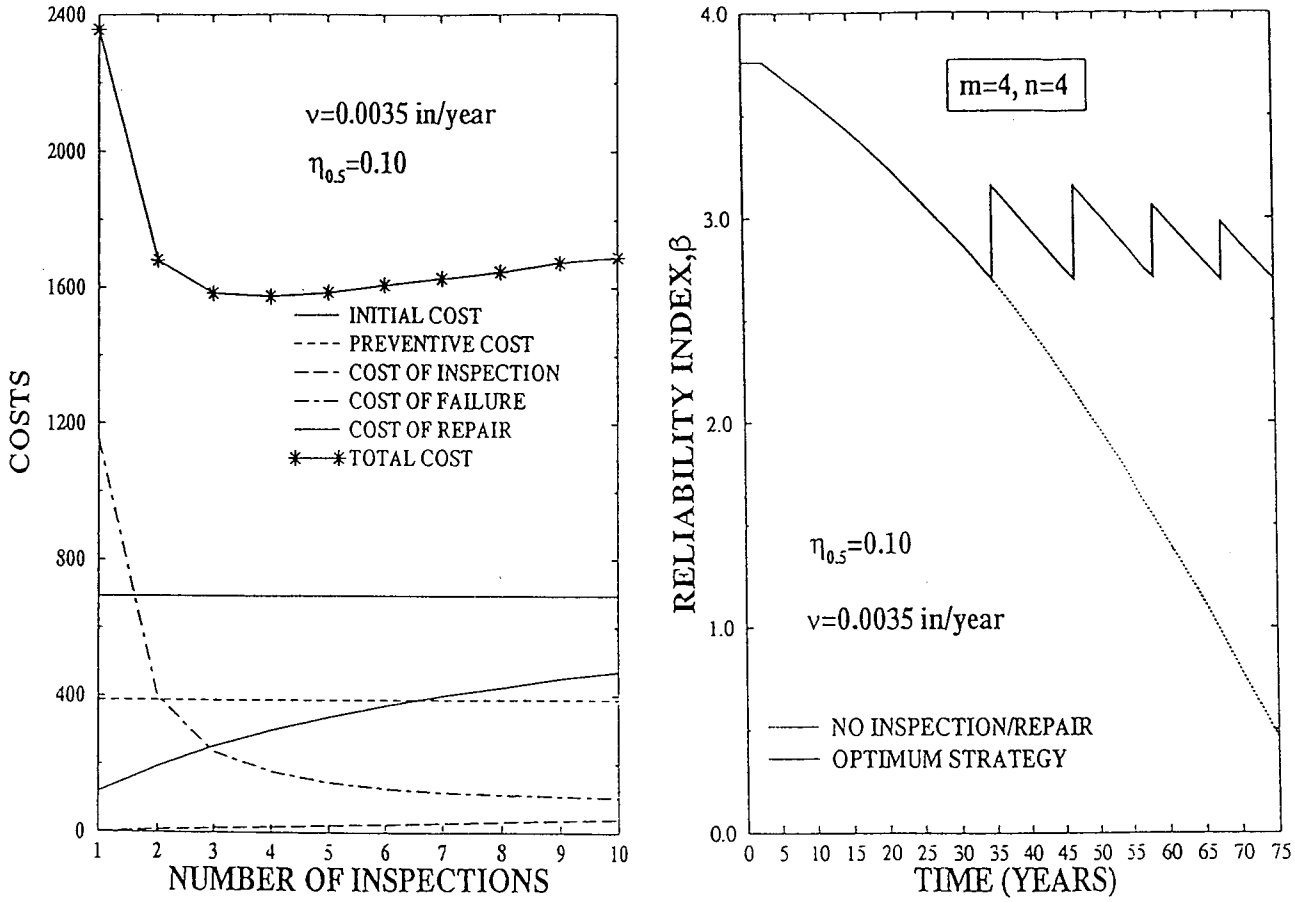


Fig. 1. Uniform Time Interval Inspections: (a) Costs vs. Number of Inspections, and (b) Optimal Inspection/Repair Strategy [Corrosion Rate ν = 0.0089 cm/year (0.0035 in/year); Inspection Method B] (Frangopol et al. 1997b).



(a) (b)

Fig. 2. Nonuniform Time Interval Inspections: (a) Costs vs. Number of Inspections, and (b) Optimal Inspection/Repair Strategy [Corrosion Rate ν = 0.0089 cm/year (0.0035 in/year); Inspection Method B] (Frangopol et al. 1997b).

The steel to concrete unit cost ratio C_s/C_c was varied from 10 to 90, and the total failure cost was assumed

$$C_F = C_f P_{f,life} = 50,000 C_c P_{f,life} \tag{4}$$

where C_f = failure cost, and $P_{f,life}$ = lifetime probability of failure.

Assuming a corrosion rate of $\nu = 0.0089$ $cm/year$ (0.0035 $in/year$), the inspection method B (median detectability = 0.10, coefficient of variation = 0.10), the steel to concrete unit cost ratio = 50, and a discount rate of 2 %, Figures 1 and 2 (Frangopol *et al.* 1997b) shows the optimum solutions for the design of a reinforced concrete bridge with an expected lifespan of 75 years. Figure 1 is associated with a uniform time interval inspection strategy and Figure 2 with a nonuniform time interval inspection strategy. As shown in these figures, if the bridge is left without any inspection/repair ($m = n = 0$, where m = number of inspections and n = number of repairs) its reliability index falls below the target level ($\beta^*_{life} = 2.0$) after about 40 years.

Comparing Figures 1 and 2 it is concluded that the optimal nonuniform time interval inspection/repair strategy (Figure 2) is more economic and requires fewer lifetime inspections than that based on a uniform time interval inspection (Figure 1). Additional results representing the sensitivity of optimal solution to changes in damage intensity, quality of inspection methods, and failure cost are presented in Frangopol *et al.* (1997b).

Lifespan Extension of an Existing Bridge. For existing bridges, there is no opportunity to optimize an initial design for expected conditions. However, as shown by Verma and Moses (1988) and Estes (1997), there is opportunity to reduce the subjective uncertainties. The formulation of the lifespan extension problem for existing bridges based on bridge system reliability and cost, and a detailed case study are presented in Estes (1997). As an example, Table 1 shows the optimum repair strategies for various lifespan extensions of a specific Colorado Bridge under corrosion attack (Estes 1997). The five repair options used and their associated 1996 costs are as follows: (a) Option 0: Do nothing → \$ 0; (b) Option 1: Replace slab → \$ 225,600; (c) Option 2: Replace exterior two girders → \$ 229,200; (d) Option 3: Replace exterior two girders and entire slab → \$ 341,800; (e) Option 4: Replace entire superstructure → \$ 487,100; and (f) Option 5: Replace entire bridge → \$ 659,900. The target system reliability index for the remaining life of the bridge is $\beta^*_{remaining\ life} = 2.0$ and the net discount rate is 2 %.

Changes in the main descriptors of the random variables considered, the system reliability model, the deterioration model, the target system reliability level, or the net discount rate can affect the results in Table 1 considerably (Estes 1997).

Table 1: **Optimal Repair Strategies for a Colorado Bridge Using a System Reliability Model Requiring Failure of Two Adjacent Girders (Estes 1997)**

Lifespan Extension (years)	Optimal Repair Strategy	Cost (1996 U.S.$)
0-50	Do nothing	0
50-70	1@50*	83,813
70-92	3@50	126,979
92-100	3@50, 1@92	163,458
100-104	1@50, 3@70	169,269
104-106	1@50, 4@70	205,588
>106	3@50, 5@92	233,685

* 1@50 indicates option 1 (replace deck) at year 50

Lifetime NDE Inspection Optimization

While most inspection information on bridges comes from visual inspections, specialized non-destructive evaluation (NDE) tests may be required to detect defects that cannot be found visually. These inspection methods could include acoustic, ultrasonic, electrical, infrared, thermographic, radar, and nuclear methods (AASHTO 1994). The NDE methods are usually employed to investigate a specific defect or type of deterioration, while the visual inspections provide a condition assessment of the entire bridge. For each relevant defect, it must be decided which inspection technique to use and how often the test needs to be conducted.

A probability-based methodology for determining the optimum lifetime inspection strategy for a deteriorating structure based on balancing reliability and cost has been proposed by Estes and Frangopol (1997). This approach which determines the optimum inspection technique, number of lifetime inspections, and the timing of those inspections is applied to an existing concrete bridge deck using the half-cell potential method.

The inspection optimization method is summarized as follows (Estes and Frangopol 1997):

- Define the structure and the criterion which constitutes failure of the structure.
- Specify how the structure deteriorates over time. Develop a deterioration model.
- Specify the inspection methods available to detect this deterioration. Quantify the detection capability and cost of these methods.

- Define the available repair options and compute their costs.
- Quantify the probability of making a repair if a defect is detected.
- Formulate the optimization problem based on the optimization criterion, failure constraints, expected life of the structure, and any other constraints that should be imposed such as minimum or maximum time intervals between inspections.
- Use an event tree to account for all of the repair/no repair decision possibilities that must be made after every inspection.
- For a discrete number of lifetime inspections, optimize the timing of these inspections for a specific inspection technique.
- Repeat the problem for other numbers of lifetime inspections and inspection techniques to develop the optimum strategy.
- Update the optimum strategy after every inspection using the new information provided from the inspection results.

Existing Concrete Bridge Deck. The approach to lifetime NDE inspection optimization previously discussed was applied to an existing concrete deck using the half-cell potential inspection method and realistic (1996 U.S. $) cost data (Estes 1997). The only repair option considered is replacement of the deck at a repair cost of C_{rep} = $225,600. The probability of making a repair is a function of the number of half-cell readings, the interpreted results of the inspection, and the bridge manager's approach to repair. Four repair approaches (*delayed*, *linear*, *proactive*, and *idealized*) as shown in Figure 3 are used. The repair approach relates the interpreted damage for the deck to the bridge manager's policy to make the repair based on past performance.

After an inspection, a decision regarding whether or not to repair the structure based on the degree of damage that was detected in the inspection must be made. The repair decision made after the first inspection affects the later decisions. As the number of inspections increases, the number of decision paths (also called branches of the event tree) increases by 2^n where n is the number of inspections.

The probability of taking any path or branch i (also denoted as $Branch_i$) is:

$$P(Branch_i) = P_{b_i} = \prod_{i=1}^{n} P_{sub_i} \tag{5}$$

where P_{sub_i} is the probability of taking any sub-branch along the path.

For each $Branch_i$ on the event tree, the expected damage to the structure given that $Branch_i$ was used (i.e., $E(Damage|Branch_i)$) is multiplied by the probability of occurrence

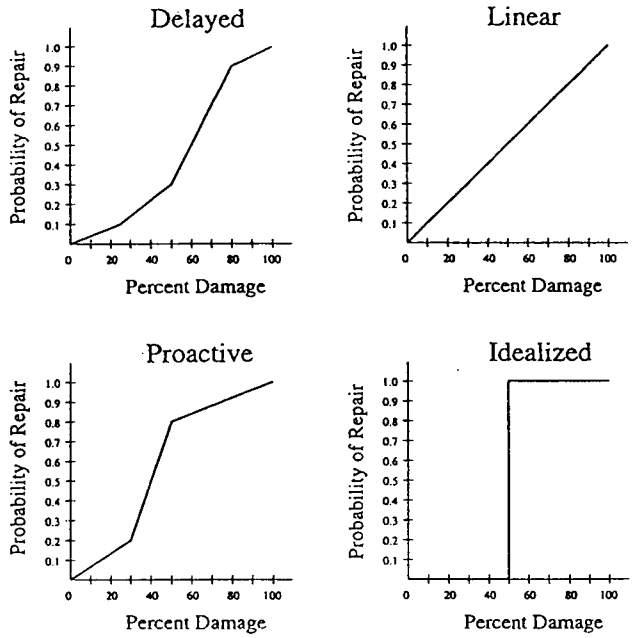


Fig. 3. Repair Policies Based on Inspection Results (Estes 1997).

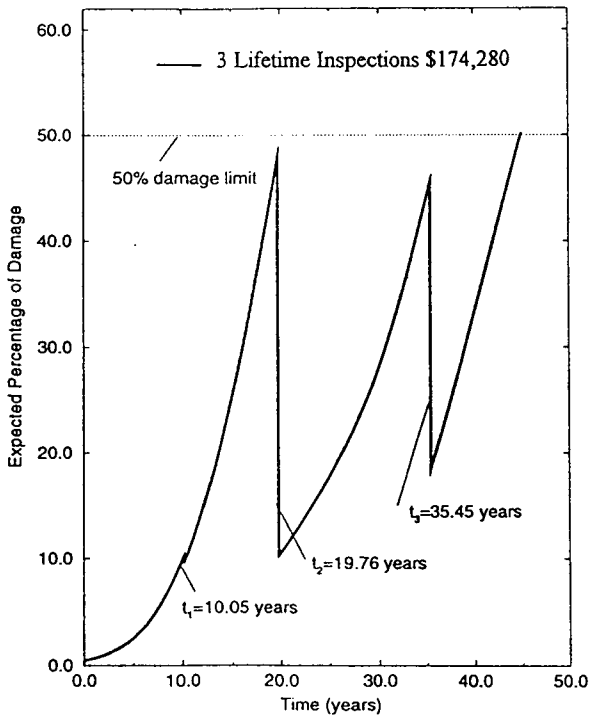


Fig. 4. Optimal Inspection/Repair Strategy for a Bridge Deck with 45 Years Service Life Based on Proactive Repair Policy Approach (Estes 1997).

of this branch P_{b_i}. The total expected damage to the structure $E(Damage)$ is equal to the sum over all branches

$$E(Damage) = \sum_{i=1}^{2^n} E(Damage|Branch_i)P_{b_i} \tag{6}$$

where n = number of lifetime inspections.

The expected value of the total cost $E(C_{tot})$ to be minimized is equal to

$$E(C_{tot}) = C_{insp_{lifetime}} + E(C_{rep}) \tag{7}$$

Assuming a discount rate $r = 2\%$, an expected service life of the bridge of 45 years, a *proactive* approach to repair (see Fig. 3), and an inspection method characterized by a cost of \$1,027 (216 half-cell potential readings spaced at 1.52 m interval on a 12.2 m by 42.1 m bridge deck), the optimum inspection strategy requires three lifetime inspections where the optimal inspection times were 10.05 years, 19.76 years, and 35.45 years. The expected total cost is \$174,280. Fig. 4 shows the expected value of damage at each inspection and the expected effect of the deck replacement. There appears to be little probability of replacing the deck after the first inspection, but a fairly high likelihood of replacement after the second and/or third inspection.

Conclusions

The life-cycle optimization approach presented herein and the additional results in Thoft-Christensen and Sorensen (1987), Mori and Ellingwood (1994), Tao *et al.* (1994), Lin (1995), Frangopol *et al.* (1997 a-c), and Estes (1997) offer a rational basis for integrating economic and safety issues into an optimal management strategy over the design life of new bridges and over the remaining life of existing bridges. Moreover, the approach can be used for finding the optimal lifespan extension of existing bridges. Reliable prediction models for lifetime performance and total cost are key elements in the optimal management of highway bridges. For this reason, research is required to develop better life-cycle models and tools to quantify the risks, costs, and benefits associated with highway bridges as well as their interrelationships in highway networks.

Acknowledgements

This material is based upon work partially supported by the National Science Foundation under Grant Nos. CMS-9319204, CMS-9506435, CMS-9522166, and CMS-9522541, and by the NATO under Grant No. CRG. 960085. This support is gratefully acknowledged. Also, the support from the U.S. Army and the Chung-Shen Institute of Technology for the second and third writer, respectively, is gratefully acknowledged. However, opinions

expressed in this paper are those of the writers and do not necessarily reflect those of the sponsors. The writers would also like to thank the Colorado Department of Transportation for providing technical support.

References

AASHTO (1994). "The Manual for Maintenance Inspection of Bridges", American Association of State Highway and Transportation Officials, Washington, D.C.

Chang, S.E., and Shinozuka, M. (1996). "Life-cycle cost analysis with natural hazard risk," *Journal of Infrastructure Systems*, ASCE, New York, 2 (3), 118-126.

Estes, A.C. (1997). *A System Reliability Approach to the Lifetime Optimization and Repair of Highway Bridges*, Ph.D. Thesis, Department of Civil, Environmental, and Architectural Engineering, University of Colorado, Boulder, Colorado.

Estes, A.C. and Frangopol, D.M. (1997). "Optimal management of bridge lifetime inspection to balance reliability and cost", *Proceedings of the 7th International Conference on Structural Faults and Repair*, (Edited by M.C. Forde), Engineering Technics Press, Edinburgh, Vol. 1, 57-65.

Estes, A.C., Frangopol, D.M., and Hearn, G. (1996). "Reliability-based optimum bridge repair strategy," *Probabilistic Mechanics & Structural Reliability* (Edited by D.M. Frangopol and M.D. Grigoriu), ASCE, New York, 372-375.

Estes, A.C., Frangopol, D.M., and Lin, K.Y. (1997). "Minimum expected life-cycle cost design of bridges," *Reliability and Optimization of Structural Systems* (Edited by D.M. Frangopol, R.B. Corotis, and R. Rackwitz), Pergamon, Oxford, 133-140.

Frangopol, D.M., and Lin, K-Y. (1997). "Reliability-based optimum design for minimum life-cycle cost" *Proceedings of the First U.S.-Japan Seminar on Structural Optimization*, Chicago, Illinois, April 13, 1996; in *Recent Advances in Structural Optimization*, (edited by D.M. Frangopol and F.Y. Cheng), ASCE, New York, 67-78.

Frangopol, D.M., Lin, K-Y., and Estes, A.C. (1997a). "Reliability of reinforced concrete girders under corrosion attack", *Journal of Structural Engineering*, ASCE, New York, 123 (3), 286-297.

Frangopol, D.M., Lin, K-Y., and Estes, A.C. (1997b). "Life-cycle cost design of deteriorating structures", *Journal of Structural Engineering*, ASCE, New York, 123 (10) (in print).

Frangopol, D.M., Estes, A.C., and Lin, K-Y. (1997c). "Optimum design for minimum expected life-cycle cost". *Proceedings of the International Symposium on Optimization and Innovative Design* (edited by H. Yamakawa, M. Yoshimura, S. Morishita and M. Arakawa), *JSME Centennial Grand Congress, Japan Society of Mechanical Engineers*, Proceedings on CD-ROM, Paper # 148, 9 pages.

Johnston, D.W., Chen, C-J., and Abed-Al-Rahim, I. (1994). "Developing user costs for bridge management systems." *Characteristics of Bridge Management Systems*, Transportation Research Circular, Number 423, National Academy Press, Washington D.C., 139-149.

Lin, K-Y. (1995). *Reliability-Based Minimum Life Cycle Cost Design of Reinforced Concrete Girder Bridges,* Ph.D. Thesis, Department of Civil, Environmental and Architectural Engineering, University of Colorado, Boulder, Colorado.

Lipkus, S.E. (1994). "BRIDGIT bridge management system software", *Characteristics of Bridge Management Systems*, Transportation Research Circular, Number 423, National Academy Press, Washington D.C., 43-54.

Mori, Y. and Ellingwood B.R. (1994). "Maintaining reliability of concrete structures I: Role of inspection/repair," *Journal of Structural Engineering*, ASCE, New York, 120 (3), 824-845.

NCHRP (1996). National Cooperative Highway Research Program, Research Project Statement, NCHRP Project 12-43, FY '96, Life-Cycle Cost Analysis for Bridges.

Shirole, A.M. (1994). "Bridge management to the year 2000 and beyond", *Characteristics of Bridge Management Systems*, Transportation Research Circular, Number 423, National Academy Press, Washington D.C., 150-153.

Tao, Z., Corotis, R.B., and Ellis, J.H. (1994). "Reliability-based bridge design and life cycle management with Markov decision processes", *Structural Safety*, Elsevier, 16 (1+2), 111-132.

Thoft-Christensen, P. and Sorensen, J.D. (1987). "Optimal strategy for inspection and repair of structural systems," *Civil Engineering Systems*, 4, 94-100.

Thompson, P.D. (1994). "Pontis", *Characteristics of Bridge Management Systems*, Transportation Research Circular, Number 423, National Academy Press, Washington D.C., 35-42.

Verma, D. and Moses, F. (1988). "Bridge reliability - evaluation vs. design." *Probabilistic Methods in Civil Engineering* (Edited by P.D. Spanos), ASCE, New York, 233-236.

Yanev, B.S. (1994). "User costs in a bridge management system." *Characteristics of Bridge Management Systems*, Transportation Research Circular, Number 423, National Academy Press, Washington D.C., 130-138.

Zimmerman, R. and Sparrow, R. (1997). "Workshop on integrated research for civil infrastructure systems", Final Report to the National Science Foundation, New York University, New York.

SESSION 8: MANAGEMENT (3)

(1) Evaluation of Bridges by Field Testing
(Andrzej S. Nowak, Sangjin Kim and Vijay Saraf)

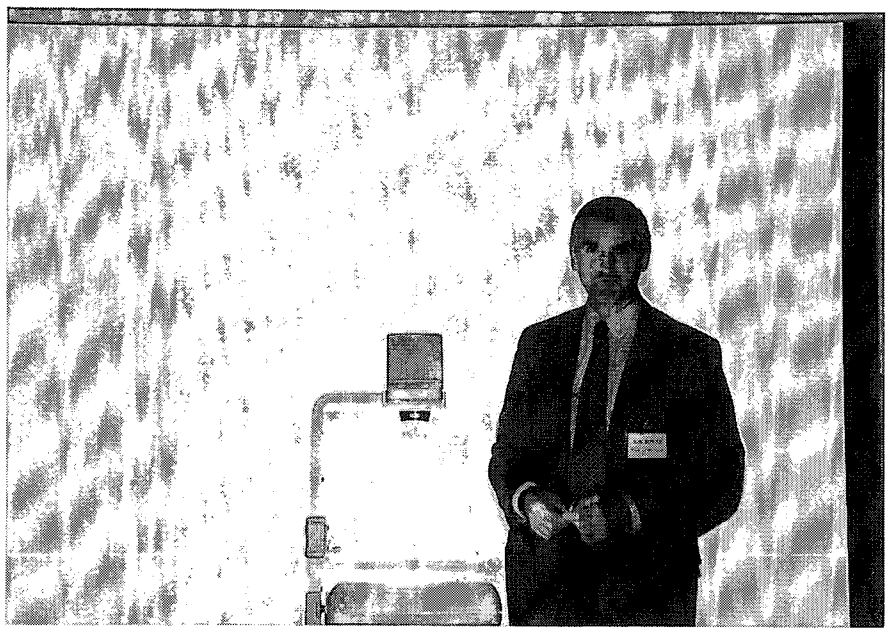
(2) Development of Survey Method for Bridge Foundations
(M. Ishida, N. Akita, A. Watanabe and J. Fukui)

(3) Detection of Concrete Bridges Using Micropower Impulse Radar and Multi-Frequency Diffraction Tomography
(Terry D. Philbin)

(4) Hydrogen Embrittlement and Deterioration Effects on Wires in Cable-Supported Bridges
(Raimondo Betti, Maciej P. Bieniek, Paul F. Duby, Alan C. West, Scott C. Barton and Garry Veermaas)



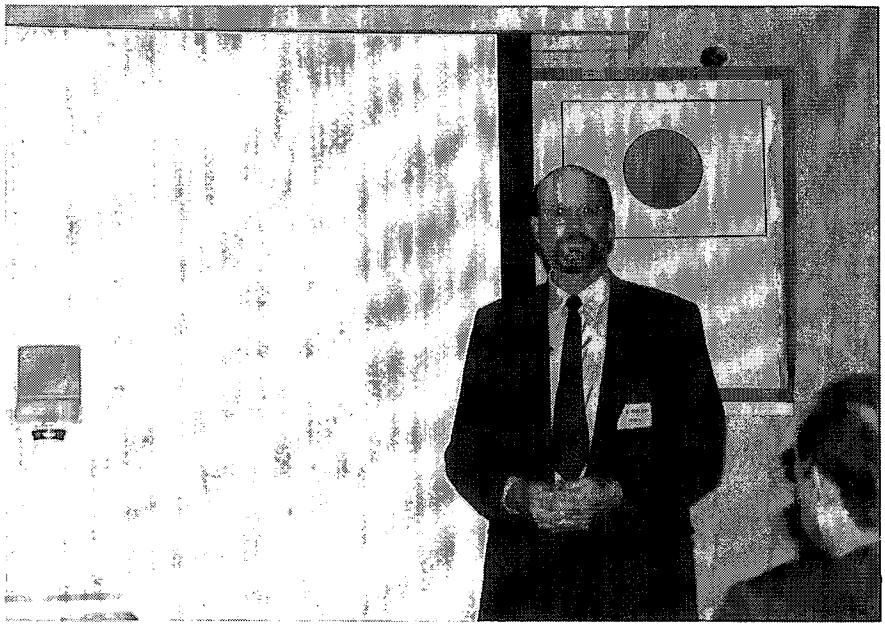
Co-Chairmen : Hiroshi Sato, Manos Maragakis



SESSION 8 : Andrzej Nowak



SESSION 8 : Masahiro Ishida



SESSION 8 : Terry Philbin



SESSION 8 : Raimondo Betti

EVALUATION OF BRIDGES BY FIELD TESTING

Andrzej S. Nowak[1], Sangjin Kim[2] and Vijay Saraf[3]

Abstract

The objective of this paper is to present examples of efficient procedures for field measurement of live load and live load effect in bridge components. The major truck parameters include gross vehicle weight (GVW), axle weights, and axle configuration (spacing). These parameters can be measured using weigh-in-motion technique, invisible to the drivers (to avoid bias). Stress spectra are important for prediction of the remaining life for bridge girders and details. Dynamic load is measured to verify the design procedures. Proof load test is performed to verify if a bridge can carry the maximum allowable load.

Introduction

Management of bridges is becoming an important problem for the owners, including State Departments of Transportation, County Road Commissions, and City Engineering Departments. Limited available resources require a rational basis for making decisions about repair, rehabilitation and replacement. The basic questions are what is the actual strength of the structure, what are the actual loads, and what is the remaining life (e.g. with regard to corrosion and/or fatigue). Field testing can often provide answers, in particular this applies to the first two questions.

Monitoring of live load is an important element of evaluation of existing bridges. There is also a need for verification of live load used for the development of a new generation of bridge design codes (Nowak 1995). It has been confirmed that truck loads are strongly site-specific. Furthermore, load effects such as bending moment, shear and/or stress are component-specific. The objective of this paper is to review some of the practical procedures used for field measurement of truck weights and strains. Field measurements can also be used to verify the dynamic loads due to moving trucks, in particular heavy vehicles. The results are presented for a representative bridge.

The load carrying capacity can be verified by proof load test. Application of a load which exceeds the legal limits can be used as a verification of the minimum required strength. Proof load level must be determined taking into account a safety factor. The procedure is demonstrated on a steel girder bridge. Selected structure was corroded and required posting for a reduced load limit. Bridge was instrumented and proof load was applied in form of military tanks. The paper describes the test methodology and the results.

---

[1]Professor, Department of Civil and Environmental Eng., University of Michigan, Ann Arbor, MI
[2]Research Associate, Dept. of Civil and Env. Eng., University of Michigan, Ann Arbor, MI
[3]Research Assistant, Dept. of Civil and Env. Eng., University of Michigan, Ann Arbor, MI

WIM Truck Weight Measurements

Truck axle weights, gross vehicle weights, and axle spacing were obtained with a bridge weigh-in-motion (WIM) system from Bridge Weighing Systems, Inc. This bridge WIM system collects strains in each lower flange of the girders and decomposes the strain time history using influence lines to determine vehicle axle weights. The strain transducers used for the system are clamped to the upper or lower surface of the bottom flange of the steel girders. All transducers are placed on the girders at the same distance from the abutment, in the middle third of a simple span. The vehicle speed, time of arrival, and lane of travel is obtained by the system through lane sensors on the roadway placed before the instrumented span of the bridge. The WIM equipment was calibrated using state weigh scale calibration trucks. The readings are verified and calibration constants are determined by running a truck with known axle loads over the bridge several times in each lane. The comparison of the results indicates that the accuracy of measurements is within 13 percent for 11-axle trucks. GVW accuracy for 5-axle trucks is within 5 percent, however, the accuracy is $\pm$ 20 percent for axle loads.

The WIM measurements were applied to seven bridges (Kim, Sokolik and Nowak 1997). The selected structures are located in Michigan. The basic parameters are listed in Table 1. Bridge location is denoted by intersection of two roads; the first symbol stands for the road carried by the bridge, and the other one indicates the road under the bridge. Spans vary from about 10 to 25 m. The traffic volume is expressed in terms of the average daily truck traffic (ADTT). The selected bridges represent typical structures. Results of GVW WIM measurements for seven bridges considered in the study are shown in Fig. 1 in a form of cummulative distribution functions on the normal probability paper.

Table 1. Parameters of Selected Bridges.

Bridge Location	Span (m)	Number of Girders	Girder Spacing (m)	Number of Lanes	ADTT (One Direction)
WY/I94	10.0	9	1.55	2	750
I94/M10	23.2	5	2.70	2	1,500
US12/I94	12.0	9	1.68	2	500
DA/M10	13.1	8	1.57	2	750
M39/M10	10.0	8	1.85	3	1,500
I94/I75	13.5	8	1.40	2	1,500
M153/M39	9.5	12	1.75	3	500

Statistics of the truck weight data Statistical data are presented in the form of histograms and cumulative distribution functions (CDFs). CDFs are used to present and compare the critical extreme values of the data. They are plotted on normal probability paper (Benjamin and Cornell, 1970). The horizontal scale is in terms of the considered truck parameter (e.g. gross vehicle weight, axle weight, lane moment or shear force). The vertical scale represents the probability of being exceeded, p. It is more convenient to plot CDF's using computer. Then, the probability of being exceeded (vertical scale) is replaced with the inverse standard normal distribution function,

$\Phi^{-1}(p)$. For example, $\Phi^{-1}(p) = 0$, corresponds to the probability of being exceeded, $p = 0.5$; $\Phi^{-1}(p) = 1$, corresponds to $p = 0.841$; and $\Phi^{-1}(p) = -1$ corresponds to $p = 0.159$; and so on.

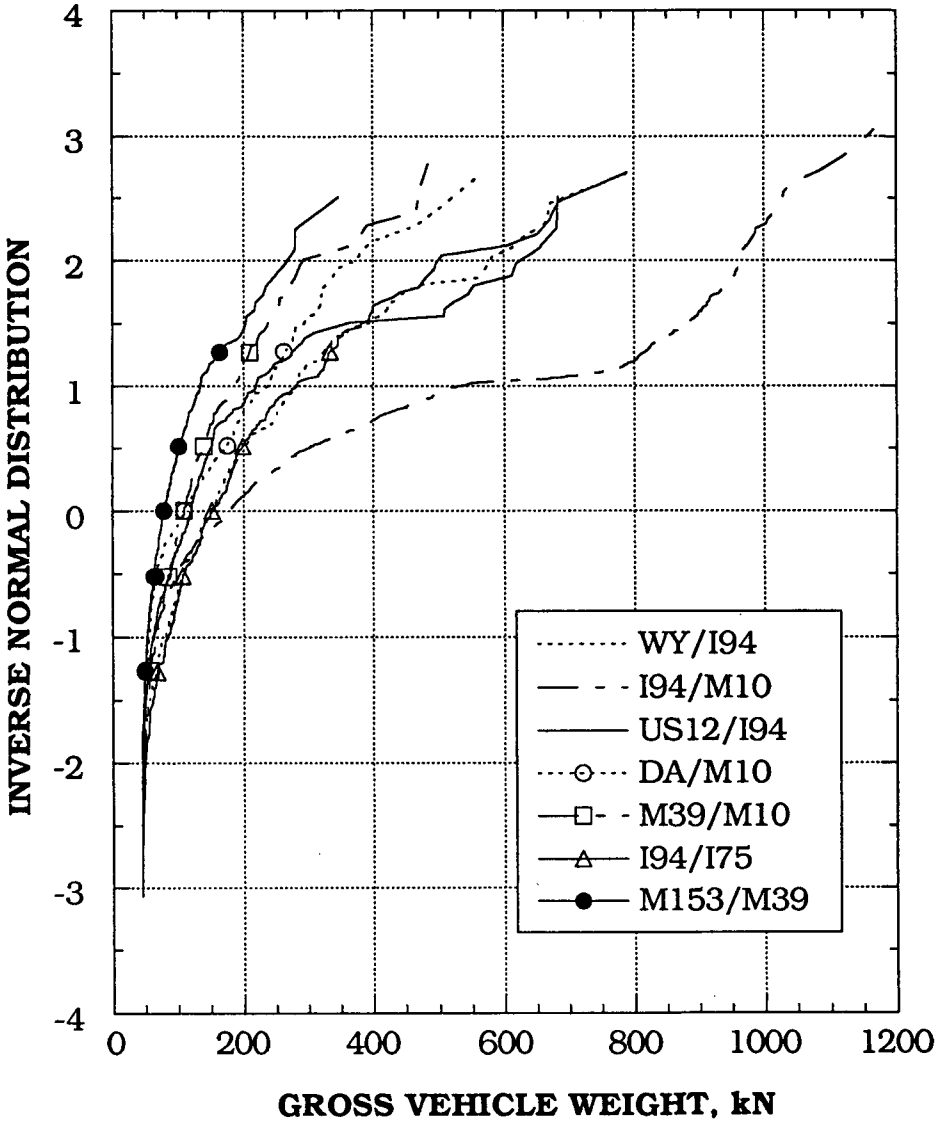


Fig. 1. CDF's of Gross vehicle Weight for the Considered Bridges.

The distribution of truck type by number of axles will typically bear a direct relationship to the GVW distribution; the larger the population of multiple axle vehicles (greater than five axles) the greater the GVW load spectra. Past research has indicated that 92% to 98% of the trucks are four and five axle vehicles. The data obtained in this study indicates that between 40% and 80% of the truck population are five axle vehicles, depending considerably on the location of the bridge. Three and four axle vehicles are often configured similarly to five axle vehicles, and when included

with five axle vehicles account for between 55% and 95% of the truck population. Between zero% and 7.4% of the trucks are eleven axle vehicles in Michigan.

Most states allow a maximum gross vehicle weight (GVW) of 355 kN where up to five axles per vehicle are permitted. The State of Michigan legal limit allows for an eleven axle truck of up to 730 kN, depending on axle configuration. There were a number of illegally loaded trucks measured during data collection at several of the sites. Maximum WIM truck weights (1192 kN) exceeded legal limits by as much as 63%.

Axle Weight Distributions

Potentially more important for bridge fatigue and pavement design are the axle weights and spacing for the trucks passing over the bridge. Fig.2 presents the distributions of the axle weights of the measured vehicles. All distributions include axles with weights greater than 22 kN.

Lane Moment and Shear Distributions

The structure is affected by load effects rather than loads. Therefore, for the measured trucks, lane moments and shears were calculated for various spans. The resulting cumulative distribution functions for span 27 m are shown in Fig. 3 for lane moment and Fig. 4 for lane shear. The calculated moments (shears) are divided by design moment (shear) specified by the new LRFD AASHTO Specification (1994). The design live load according to LRFD AASHTO is a superposition of a truck weighing 320 kN (three axles: 35 kN, 145 kN, and 145 kN spaced 4.25 m) and a uniformly distributed load of 9.3 kN/m.

Strain Data for Fatigue Load Spectra

The data was collected and recorded using Stress Measuring System (SMS) with the main unit manufactured by the SoMat Corporation. The SMS compiled stress histograms for the girders and other components. Strain transducers were attached to all girders at the lower, mid span flanges for each of the five bridges. Dynamic strain cycles were measured under normal traffic using the rainflow algorithm (Laman and Nowak 1996).

The SMS collects the strain history under normal traffic and assembles the stress cycle histogram by the rainflow method of cycle counting, and other counting methods. The data is then stored to memory and down loaded at the conclusion of the test period. The rainflow method counts the number, n, of cycles in each predetermined stress range, S_i, for a given stress history. The SMS is capable of recording up to 4 billion cycles per channel for extended periods in an unattended mode. The batteries used for this study enabled testing to continue uninterrupted for as long as three weeks.

Strain histories were collected continuously for one week periods and reduced using the rainflow algorithm. Data was collected for each girder in the bridge. The data is presented here in

the form of CDFs and represents strain cycles due to 7 days of normal traffic. For an easier interpretation of results, the CDFs are plotted on normal probability paper.

For each bridge, the CDFs are shown for strains in girders numbered from 1 (exterior, on the right-hand side looking in the direction of the traffic). The number of girders in each bridge vary from 6 to 10. The average strain is less than 50 x 10^{-6} for all girders and all bridges, however, the largest strains were observed in girders supporting the right traffic lane (girder numbers G3, G4 and G5) and nearest the left wheel of traffic in the right lane. As expected, the exterior girders of each bridge experience the lowest strain extremes in the spectrum.

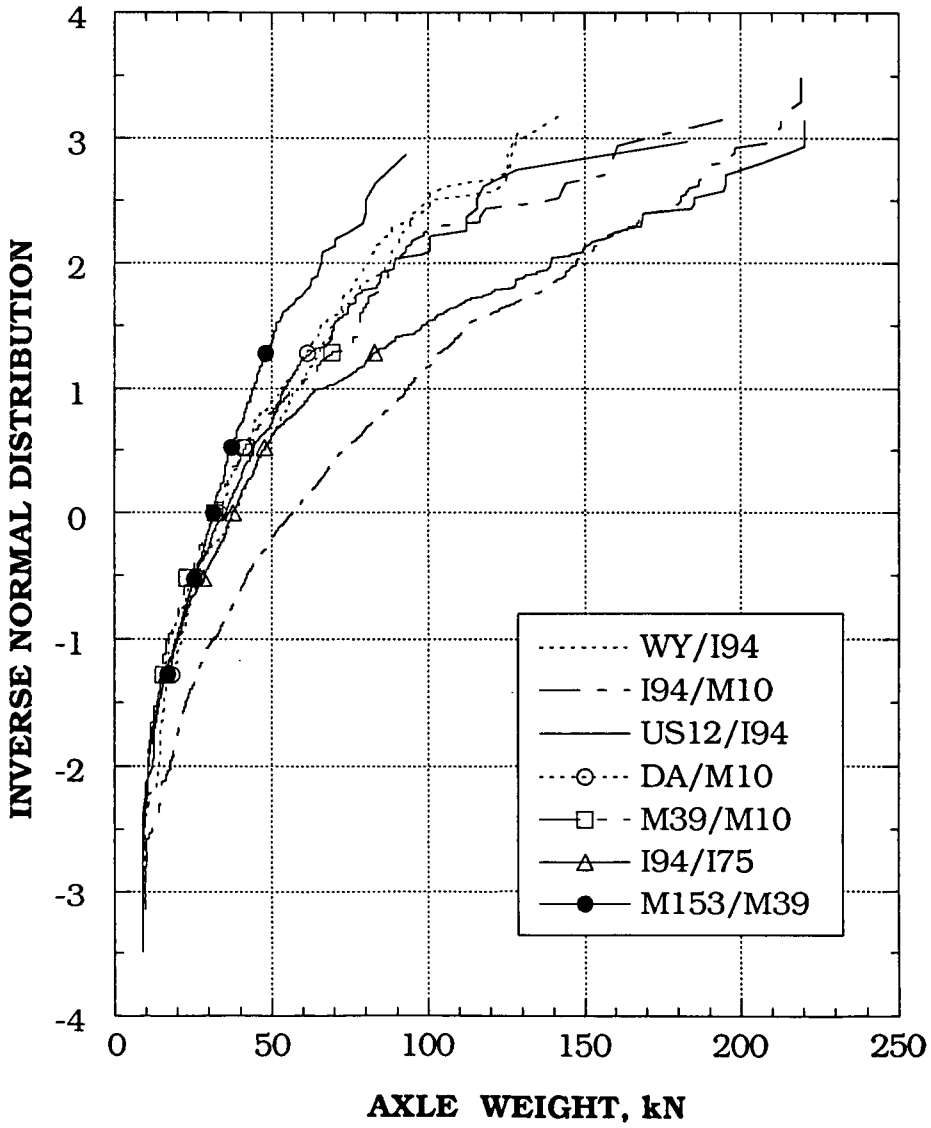


Fig. 2. CDF's of Axle Weight for the Considered Bridges.

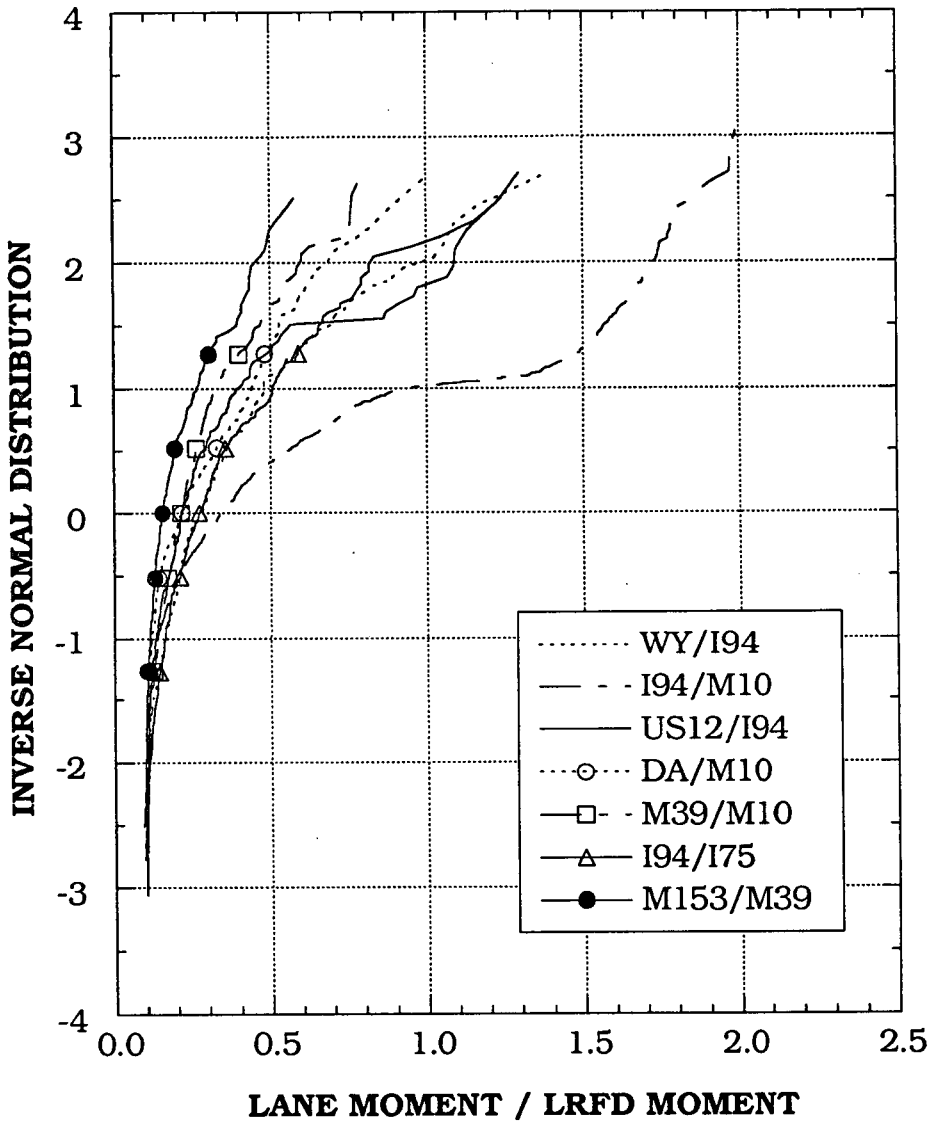


Fig. 3. CDF's of Lane Moment for the Span Length of 27 m.

As a means of comparison of fatigue live load, the equivalent stress, s_{eq}, is calculated for each girder using the following root mean cube (RMC) formula:

$$s_{eq} = \sqrt[3]{p_i^3 * S_i^3} \tag{1}$$

where S_i = midpoint of the stress interval i and p_i = the relative frequency of cycle counts for interval i. The stress, S_i, is calculated as a product of strain and modulus of elasticity of steel.

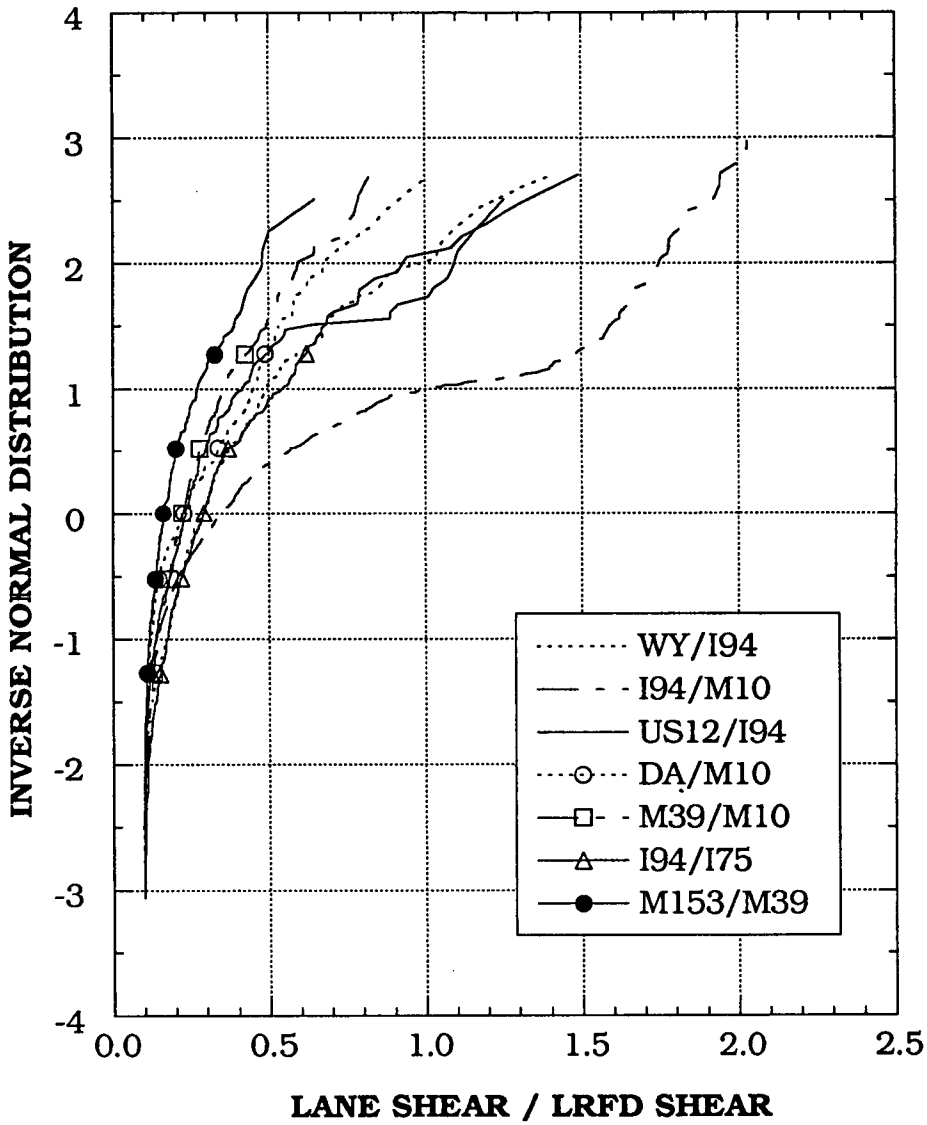


Fig. 4. CDF's of Lane Shear for the Span Length of 27 m.

Examples of the CDFs of strain cycles and the corresponding equivalent stress values are shown in Figs. 5 and 6.

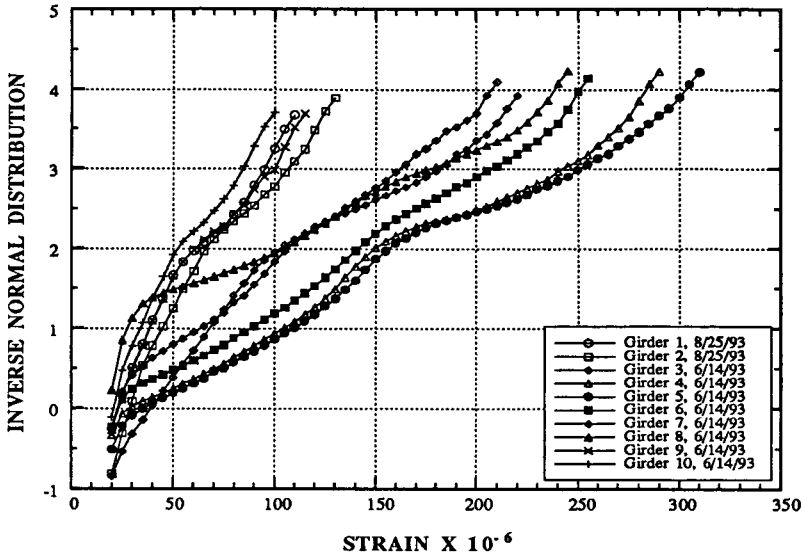


Fig. 5. Strains for Girders in Bridge I94/PR.

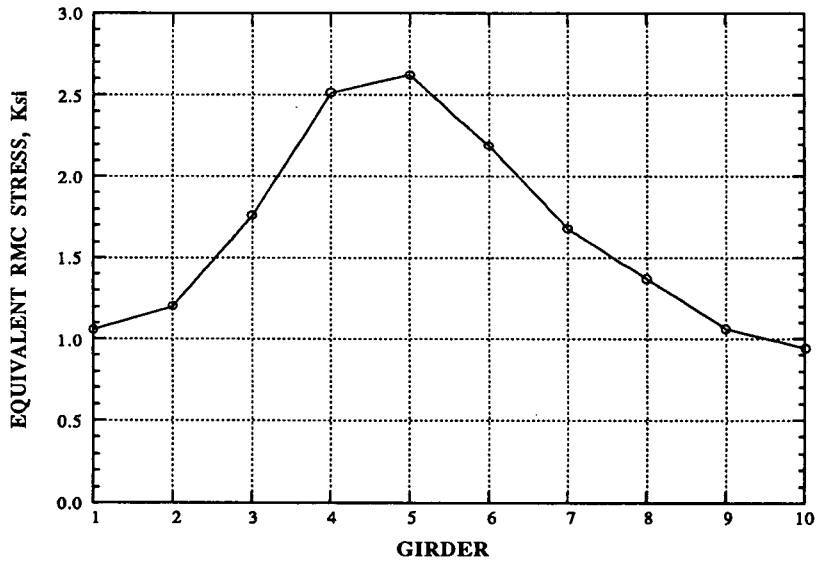


Fig. 6. Equivalent Stresses for Girders in Bridge I94/PR.

Dynamic Loads

Bridge dynamic load is defined as the ratio of dynamic to static responses. Field measurements are performed to determine the actual truck load effects and to verify the available analytical models (Hwang and Nowak 1991).

The tests are carried out on four steel girder bridges. Measurements are taken using a weigh-in-motion (WIM) system with strain transducers. For each truck passage, the dynamic response is monitored by recording strain data. The truck weight, speed, axle configuration, and lane occupancy are also determined and recorded. A numerical procedure is developed to filter and process collected data. The dynamic load factor (DLF) is determined under normal truck traffic of various load ranges and axle configurations.

The field measurements confirmed the results of analytical studies (Nassif and Nowak 1995; Kim and Nowak 1997). An example of the actual static and dynamic stresses is shown in Fig. 7. CDF of the static stress is plotted on the normal probability paper. For each value of static stress, the corresponding dynamic stress is also shown. The stress due to dynamic load is nearly constant and is dependent on truck weight. Fig. 8 show dynamic load factors as a function of static strains. Also shown in the figure is the power curve fit, which approximately represents mean values of dynamic load factors. In general, dynamic load factor decreases as the static strain increases. Therefore, the dynamic load factor is reduced for heavier trucks.

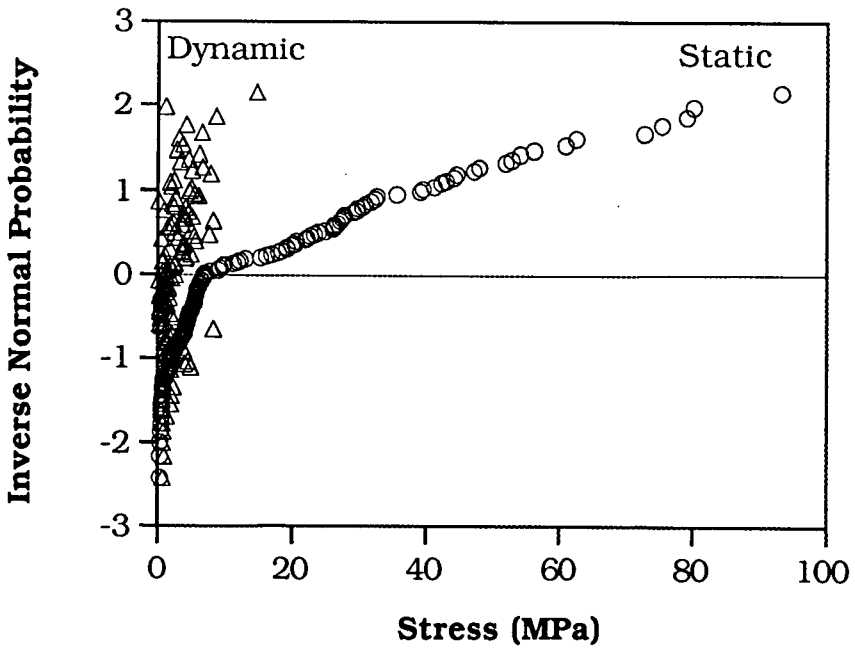


Fig. 7. Typical CDF of Static Stress and Corresponding Dynamic Stress.

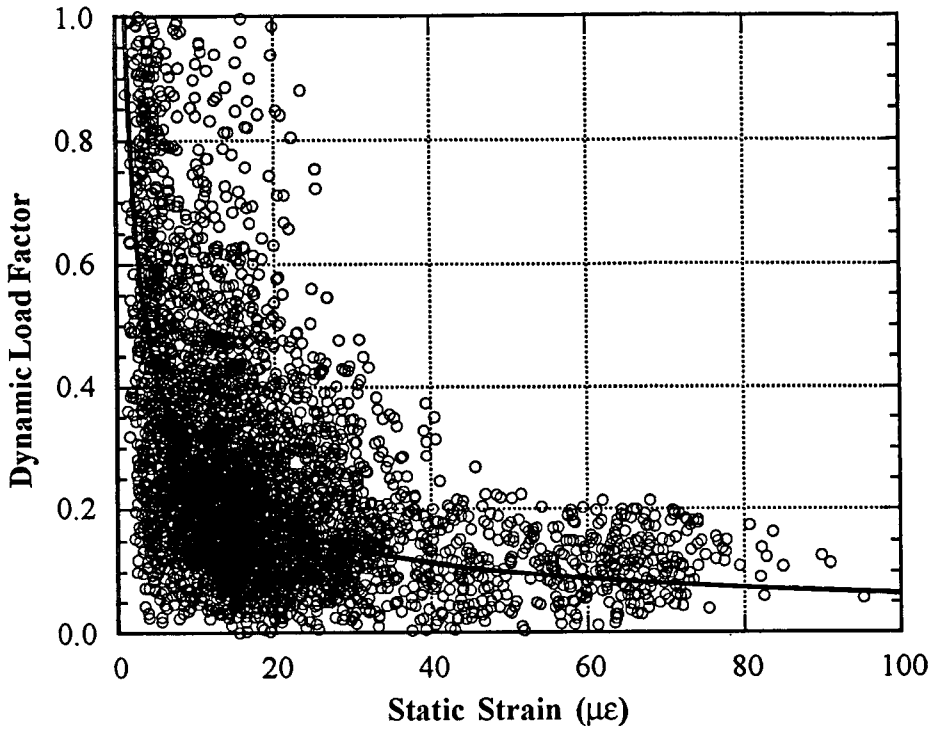


Figure 8. Dynamic Load Factor versus Static Strain.

Proof Load Test

The objective of the study was to verify the load carrying capacity of an existing steel girder bridge. The load capacity of the bridge was in question due to extensive corrosion of steel girders. Initial rating showed that the bridge had marginal operating rating factor for the 11-axle two-unit truck (77 tons), which is the heaviest vehicle allowed in Michigan. To avoid the load limit posting, it was decided to verify if the bridge is safe to carry the normal truck traffic by using a proof load test (Saraf, Sokolik and Nowak 1997).

The bridge is a simply supported steel girder bridge carrying state route M-50 over Grand River in Jackson County, Michigan. The total span length is 14.6 m. The total width is 13.8 m. It carries one lane in each direction with total ADT of 11,900. There are ten steel girders, a 165 mm thick reinforced concrete slab, 150 mm thick cast-in-place concrete wearing surface, and a 170 mm thick bituminous overlay. It was designed to behave as non-composite section. Based on the initial inspection, lower flanges of steel girders were found heavily corroded. At some locations close to mid-span, the flange thickness was reduced by as much as 60 percent. This reduces the moment capacity of steel girder by about 25 percent. There was not much corrosion in steel girders near the supports, and reinforced concrete slab was in moderate condition.

Based on the specifications in the Michigan Bridge Analysis Guide, the remaining capacity to carry live load and impact corresponding to the operating rating was determined to be 1,550 kN-m per lane. In preliminary calculations, the inventory rating factors were 0.98 and 0.53 for H15 and HS20 trucks, respectively. The operating rating factor for the 11-axle two-unit truck was 0.95. A rating factor less than 1.0 indicates that the bridge is deficient. The critical limit state for this bridge was the moment capacity at mid-span. The shear capacity was found to be adequate at all sections. These rating factors were reduced after the site inspection to include better estimates of the steel section loss. The revised inventory rating factor was 0.60 for H15 truck and operating rating factor was 0.45 for the 11-axle truck.

Since proof load testing requires careful comparison of analytical and experimental results during the testing in order to avoid accidental overload, two different types of analytical models were prepared by using the semi-continuum method developed by Jaeger and Bakht (1989). In the first model, the structural properties were taken as specified in design drawings, i.e., the slab-girder-interaction was considered to be non-composite and the effect of non-structural components was not included. For second model, the possibility of unintended composite action and contribution of non-structural members, such as parapets and railings, etc., were incorporated. For both models the supports were idealized as pin supports.

For the proof load test, a heavy load is used to test the bridge. The load is increased in several steps until the yield capacity of the bridge, or a pre-specified load limit is reached. Usually, the yield capacity of a bridge is very high. Therefore, this bridge was loaded only up to a predetermined load limit. Since, the objective of the test is to check if the bridge can carry the maximum allowable load, the applied proof load should exceed the legal load by a comfortable margin of safety. If the target proof load is successfully reached without any distress, then the resulting operating factor would be 1.0.

The target proof load was calculated using the draft report on NCHRP project no. 12-28(13) A (Lichtenstein 1993), by multiplying the maximum legal load by a factor of safety of 1.4. It was further multiplied by an impact factor. According to the AASHTO Specifications (1996), the impact factor would be 1.29. However, for this bridge, it was taken to be 1.10, because the dynamic experiments conducted by Nassif and Nowak (1995) showed that the multi-axle vehicles with heavy loads exhibit much smaller impact. Also, it was decided to load one lane at a time. Therefore, the target load was increased by 15 percent to account for unloaded adjacent lanes.

The required proof load was calculated to be an 11-axle two-unit truck with gross vehicle weight of 1,210 kN. In previous studies by other researchers (Juntunen and Isola, 1995), concrete barrier blocks were placed on a flat bed truck to load the bridge. Each block weighs about 22 kN. Therefore, for this study the required number of blocks would be so large that it would not be possible to safely fit all of them on one truck. Therefore, a different scheme had to be prepared. Since the moment capacity at mid-span was found to be critical in preliminary calculations, it was decided to apply a load that would cause the equivalent proof load moment.

The innovative idea was to use M-60 military tanks on flat-bed trailers to achieve a very high target proof load level. Each tank weighs over 490 kN. This load is distributed over a small track of 4.5 m. Two such tanks were required to test this bridge. These tanks were provided by the Michigan National Guard. Only the four rear axles of each trailer were used to load the bridge. Each tank was placed on a flat bed trailer, such that the load on rear tandem axles was maximum. Both tanks had the same total weight. However, the configuration of the trailers was different. Therefore, the resulting axle loads were different.

For first load step, the tank on military trailer was placed close to support, to start with small mid-span moment. Then, the mid-span moment was increased gradually in several steps by moving the trailer towards mid-span. For third load case, the trailer was placed so that it caused maximum mid-span moment. For the fourth load case, the second trailer was positioned on the bridge, to further increase the moment. Load was also moved to three different transverse load positions. They were called upstream, center and downstream, depending on their location with respect to the flow of the river underneath, i.e. in upstream load position the trailers were placed close to the upstream railing.

Results of the test were closely monitored for any sign of distress. Several strain transducers were placed on steel girders close to mid-span and quarter-points. These transducers are reusable and clamped to the lower flanges of girders. Deflections at mid-point of all interior girders were measured using LVDT's. Deflections at quarter-points of selected girders were also measured. After placing the trailers in each load position, the data from each instrument was collected using a portable data acquisition system. The real time response of selected transducers was also monitored at all stages of testing. The data from LVDT's and strain transducers was collected by a portable SCXI-1200 data acquisition system. The system consists of a four slot SCXI-1000 chassis, one SCXI-1200 data acquisition card and two SCXI-1100 multiplexers. Each multiplexer can handle up to 32 channels of input data. The current system is capable of handling 64 channels of strain or deflection inputs. Up to 32 additional channels can be added if required. A portable field computer is used to store, process and display the data on site.

During the test a maximum mid-span moment of 2,120 kN-m was applied, which is over 2.6 times the moment caused by the HS20 design truck. The target proof load level was successfully reached without any noticeable distress. Therefore, the operating rating factor for an 11-axle two-unit truck is 1.0, after the test. Fig. 9 shows the stresses at mid-span of girders for upstream loading.

The maximum stress of 19.4 MPa was observed during experiments, for girder no. 3. It is less than 0.1 of the yield strength of steel. Also, for all girders, the stress increased linearly with increasing lane moment, and similar behavior was observed for center and upstream load cases. This indicates the extra safety reserve in the structure. The predicted maximum analytical stresses were 29 Mpa and 48 MPa for composite and non-composite models, respectively. It shows that the composite action between concrete slab and steel girders is present even at loads several times larger than the design load. The non-structural members also contributed to the overall flexural

strength of the structure. Lateral distributions of girder deflections at mid-span is shown in Fig. 10. Although several diaphragms were severely deteriorated, the actual load sharing between girders is more uniform than analytically predicted. Following the test, the bridge was opened for normal traffic without any load posting.

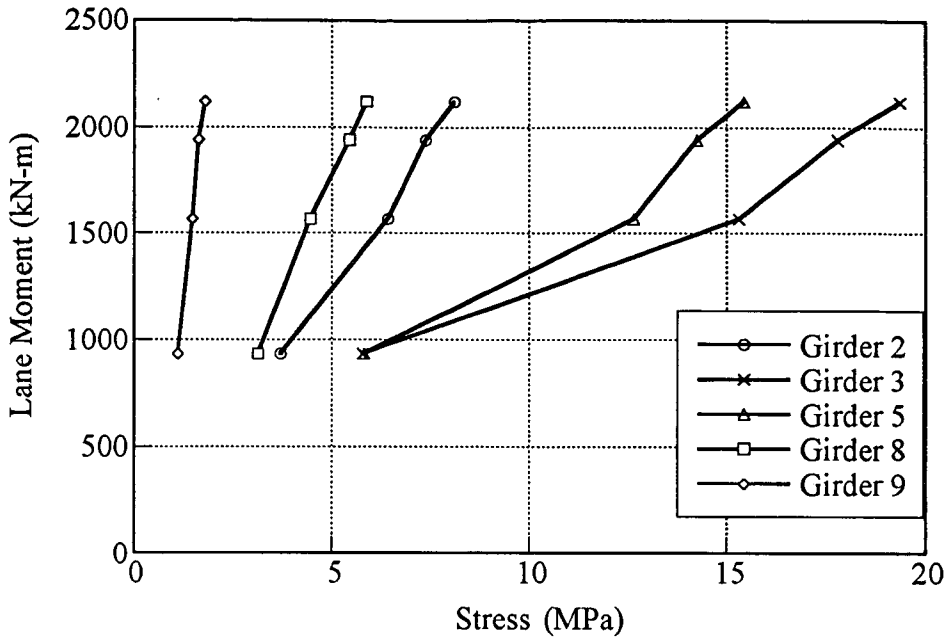


Fig. 9. Example of Stresses at Mid-Span.

Conclusions

On the basis of WIM measurements, site-specific load spectra are presented for several bridge sites. Component stress spectra are presented for girders in the form of CDFs and the equivalent stresses are calculated for comparison. Site-specific statistics required for fatigue analysis based on current models are presented. Strains are measured to determine component-specific load spectra.

The truck load spectra for bridges are strongly site-specific. Bridges located on major routes between large industrial metropolitan areas will experience the highest extreme loads. Routes where vehicles are able to circumvent stationary weigh stations will have very high extreme loads. Bridges not on a major route, that are very near a weigh station, or that are within a metropolitan area experience much lower extreme loads.

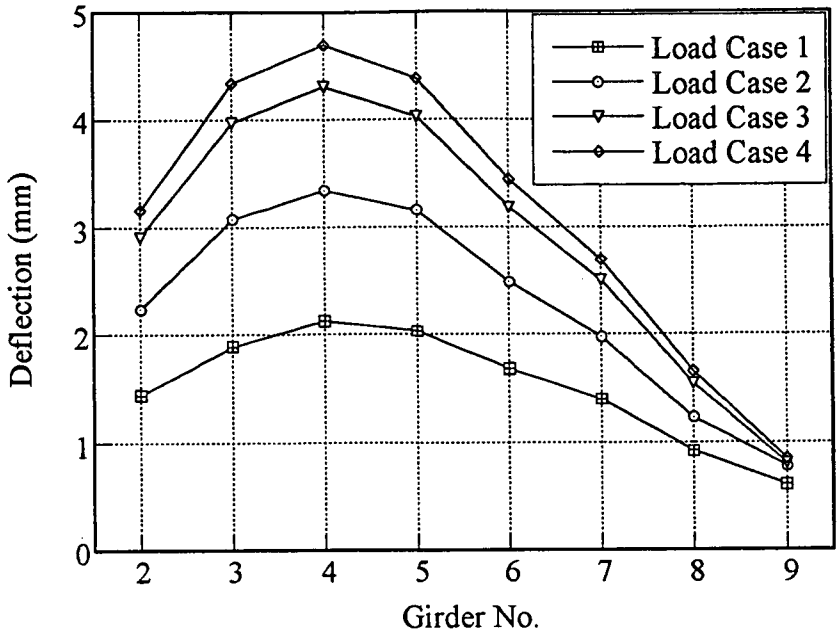


Fig. 10. Example of Lateral Distribution of Deflections at Mid-Span.

Live load stress spectra are strongly component-specific. Each component experiences a very different distribution of strain cycle ranges. The girder that is nearest the left wheel track of vehicles traveling in the right lane experiences the highest stresses in the stress spectra and decreases as a function of the distance from this location. This information can be useful to target bridge inspection efforts to the critical members.

The stress due to dynamic load is nearly constant and is dependent on truck weight. In general, dynamic load factor decreases as the static strain increases. Therefore, the dynamic load factor is reduced for heavier trucks.

The proof load tests required relatively greater effort, but it provided immediate answers about the load carrying capacity. As a result, the bridge was found to be safe to operate under normal traffic.

Acknowledgments

The research presented in this paper has been partially sponsored by the Michigan Department of Transportation, the Great Lakes Center for Truck Transit Research, National Science Foundation, IDEA Transportation Research Board, and the University of Michigan, which is gratefully acknowledged. Thanks are due to former doctoral students at the University of Michigan: Hani Nassif, and Jeff Laman.

References

"AASHTO LRFD Bridge Design Specifications," (1994), American Association of State and Transportation Officials, Washington, D.C.

"AASHTO Standard Specifications for Bridge Design", (1996) American Association of State Highway and Transportation Officials, Washington, DC.

Benjamin, J.R. and Cornell, C.A., (1970), Probability, Statistics and Decision for Civil Engineers, McGraw-Hill, New York.

Hwang, E-S. and Nowak, A.S., (1991), "Simulation of Dynamic Load for Bridges," ASCE Journal of Structural Engineering, Vol. 117, No. 5, pp. 1413-1434.

Jaeger, L.G., and B. Bakht, (1989), "Bridge Analysis by Microcomputer". McGraw-Hill Book Company, New York.

Juntunen, D.A., and M.C. Isola, (1995), "Proof Load Test of R01 of 61131 M-37 over CSX Railroad, South of Bailey. Michigan". Michigan Department of Transportation. Lansing, MI.

Kim, S-J. and Nowak, A.S., (1997), "Load Distribution and Impact Factors for I-Girder Bridges", ASCE Journal of Bridge Engineering, Vol. 2, No. 3, pp. 97-104.

Kim, S-J., Sokolik, A.F., and Nowak, A.S., (1997), "Measurement of Truck Load on Bridges in the Detroit Area", Transportation Research Record, No.1541, pp. 58-63.

Laman, J.A., and Nowak, A.S., (1996), "Fatigue Load Models for Girder Bridges", ASCE Journal of Structural Engineering, Vol. 122, No. 7, pp. 726-733.

Lichtenstein, A. G. (1993), "Bridge Rating Through Nondestructive Load Testing". NCHRP Report No. 12-28(13) A.

"Michigan Bridge Analysis Guide", (1983), Michigan Department of Transportation, Lansing, MI.

Nassif, H. and Nowak, A.S., (1995), "Dynamic Load Spectra for Girder Bridges", Transportation Research Record, No. 1476, pp. 69-83.

Nowak, A.S., (1995), "Calibration of LRFD Bridge Code", ASCE Journal of Structural Engineering, Vol. 121, No. 8, pp. 1245-1251.

Saraf, V., Sokolik, A.F., and Nowak, A.S., (1997), "Proof Load Testing of Highway Bridges", Transportation Research Record, No.1541, pp. 51-57.

Development of Survey Method for Bridge Foundations

Masahiro Ishida[1], Naoki Akita[2], Akisada Watanabe[3], Jiro Fukui[4]

Abstract

In Japan, there are many bridges that their foundation types or their foundation dimensions are unknown, because there is hardly design drawing of old bridges. On the other hand, it is difficult to survey that there is a damage in a foundation after an earthquake. Therefore, Public Works Research Institute is developing 1) method of survey of unknown foundations, and 2) method of survey of damage of foundations.

1. Introduction

After the Hyogo ken Nanbu Earthquake, database of seismic resistance based on bridge dimensions has been preparing to make emergency transportation network. But types or dimensions of many bridge foundations are unknown, because there is hardly design drawing of old bridges.

On the other hand, many bridge foundations were surveyed of their damage by means of Bore-Hole Camera after the earthquake. But this method is expensive and takes much time.

Public Works Research Institute has been started collaboration research, "Research for survey method of bridge foundations", with Public Works Research Center, Hanshin Expressway Public Corporation, and 12 private companies from 1996.

The objects of this research are as follows.

1) Development of survey method for bridge types and dimensions of unknown foundations.
2) Development of survey method for damages of bridge foundations after an earthquake.

2. Survey and counter measures for foundations after Hyogo-ken Nanbu Earthquake

Many bridge piers were damaged by the Hyogo-ken Nanbu Earthquake. Minor damaged bridge piers were repaired or reinforced, and major damaged bridge piers

1) Researcher, Foundation Engineering Division, Public Works Research Institute, Ministry of Construction, Japan
2) Assistant Researcher, Ditto
3) Researcher, Ditto
4) Head, Ditto

were reconstructed. But bridge foundations were reused.

Some foundations of highway bridges were excavated under the footings and the pile tops were sawn to survey the damages. There are some cracks in the pile.

Loading tests were performed to check that the damaged foundations could be reused. The test could execute in low force and low deformation. The stiffness was smaller than that of calculation of non damaged foundation in low deformation level. But the calculation of considering the pile damage is similar to that of non damaged foundations in high deformation level. This foundation was judged reused.

Many foundations were surveyed using bore-hole camera or pile integrity test. Loading test shows that the cracks in piles have small influence to the stability of foundations, but filling cement were injected into cracks using holes of bore hole camera.

3. Survey method for foundations

New survey method for foundations is developing now, including 6 methods as follows.

1) Bore Hole Camera
2) Integrity Test
3) Radar
4) Acoustic Emission
5) Magnetic Survey
6) Impact Vibration Test

As shown in **Figure-1**, the common specimen which has damaged RC piles was made to verify applicability of these methods.

Outlines, past results, applicability and problems of these methods are shown as follows.

3.1 Bore Hole Camera

Bore Hole Camera has been used for survey of cracks in rocks. After the Hyogo-ken Nanbu Earthquake, many bridge foundations were surveyed by this method.

Bore Hole Camera is inserted in the core boring of a pile and show the cracks. The camera takes a video of full circumference of pile using prism as shown in **Figure-2** and this video is restored to exterior figure as shown in **Photo-1**.

This is the most reliable method to survey cracks in the piles. But the affair is pointed out that this camera shows thicker cracks than actual, because the cracks are damaged during digging of bore hole. The point of digging boring is not clear when there is no drawing of the foundation. It is difficult to survey hollow piles. It takes much money and time to survey deep pile. So, this method should be used with other methods.

The suitable rotation velocity of bit, the suitable type of bit and the suitable velocity of digging should be defined to prevent damage of the cracks.

3.2 Integrity Test (IT)

IT was originally developed for management of site execution of cast in place

piles. As shown in **Figure-3**, pile top is hit by hammer. An elastic wave in the pile changes at the changing point of pile section. The soundness of piles is verified by measuring of elastic wave.

IT shows the damage of pile, shown in **Figure-4**. This result is almost the same with that of Bore Hole Camera. This method has good applicability to survey the damage of piles. But the evaluation of damage level is not established. If the damage is found, the extent of damage should be surveyed by Bore Hole Camera.

The judgement criteria that the pile should be surveyed by other methods has to established.

3.3 Radar

Bore Hole Radar is inserted in the boring of ground near the pile, as shown in **Figure-5**. This method is divided into 2 types. One is called "one hole method", transmission and receive antenna is inserted in one hole, and it catch the reflection wave. Second one is called "two hole method", transmission antenna and receive antenna are inserted in different holes, and it catch penetration wave.

This method can survey the pile position or the pile length, using diagonal boring as shown in **Figure-6**. But this method cannot use in the ground which has salty ground water, because the wave is attenuated. As using lower frequency, the longer reach distance but lower precision.

The suitable wave frequency to survey foundations should be determined.

3.4 Acoustic Emission (AE)

Some AE sensors are inserted in the ground boring near the pile, as shown in **Figure-7**. Sensors catch the AE wave from existing cracks when the pile was loaded. The position of cracks can be determined, as shown in **Figure-8**. The results of AE method are almost same with that of Bore Hole Camera.

After the Hyogo ken Nanbu Earthquake, some foundations of buildings were surveyed by AE method. The foundation was loaded by power shovel as shown in **Figure-9**.

It should be determined how long measuring time is required to find the pile is sound.

3.5 Magnetic survey

A magnetic sensor is inserted in the ground boring near the pile. It catches the change of magnetic field due to steel pipe pile or reinforcing bar in a concrete pile, as shown in **Figure-10**.

As same as radar, pile point or pile length can be surveyed using diagonal boring. Strength of magnetic field can show which the pile is steel pile or concrete pile. But the distance from sensor to pile cannot be found.

It should be determined how long measuring distance and its precision.

3.6 Impact vibration test

Vibration of pier is measured in this method as shown in **Figure-11**. Soundness of the pier or the foundation is checked based on the natural frequency.

This method has been used to check the soundness of piers or foundations under scouring for mainly railroad bridges. Normal frequency for railroad bridges is defined, which is based on the results measured about 1,000 railroad bridges. When the measured frequency is different from normal one, the bridge has something trouble. Japan Railway Group has a plan that all sound piers will be surveyed by this methods to compare the frequency with that of the piers after earthquake.

This method is useful to check general soundness of piers including foundation, ground and body. Unknown foundation type can be determined.

To use for highway bridges, it should be confirmed that normal frequency of highway bridges isn't different from that of railway bridges.

4. Conclusions

Each method has been executing to common specimen in PWRI. Each method has suitable situation to survey. Foundations should be surveyed by using combination of some methods.

It is difficult for general engineers to judge the result of these method now. We will improve these methods and write survey manual for general engineers to use them.

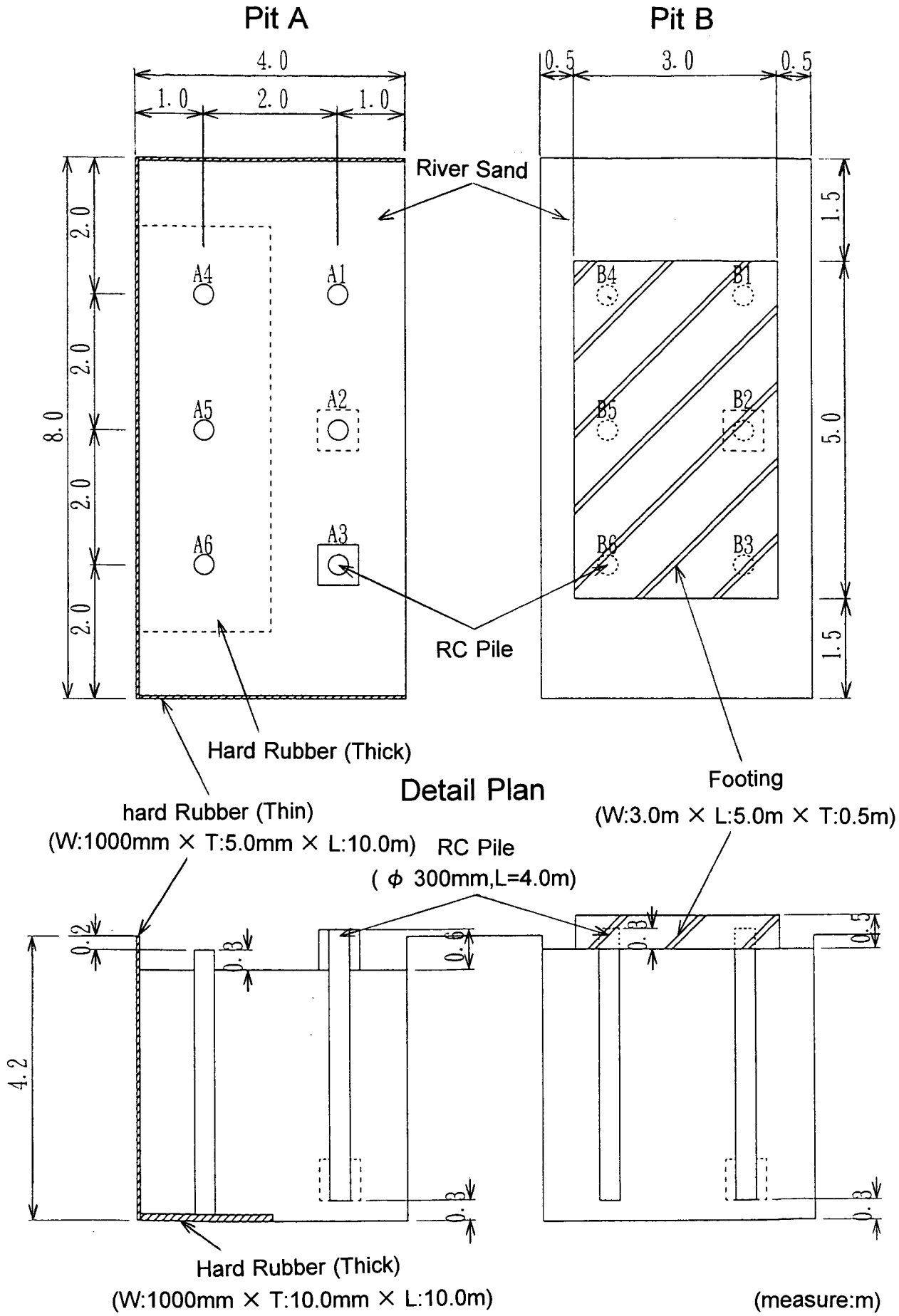


Figure-1.1 Set Up Location of Test Pile

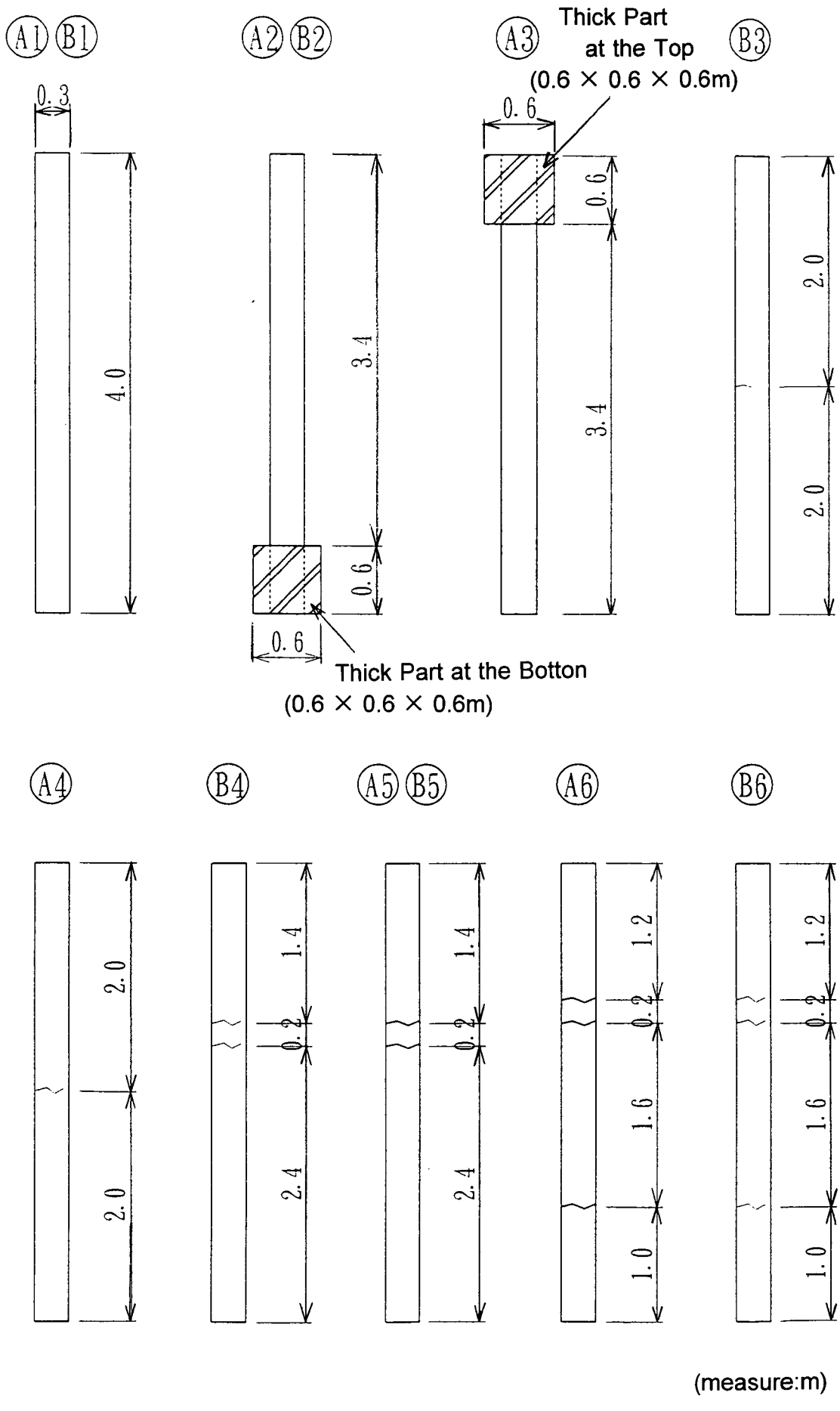


Figure-1.2 Shape of Test Pile

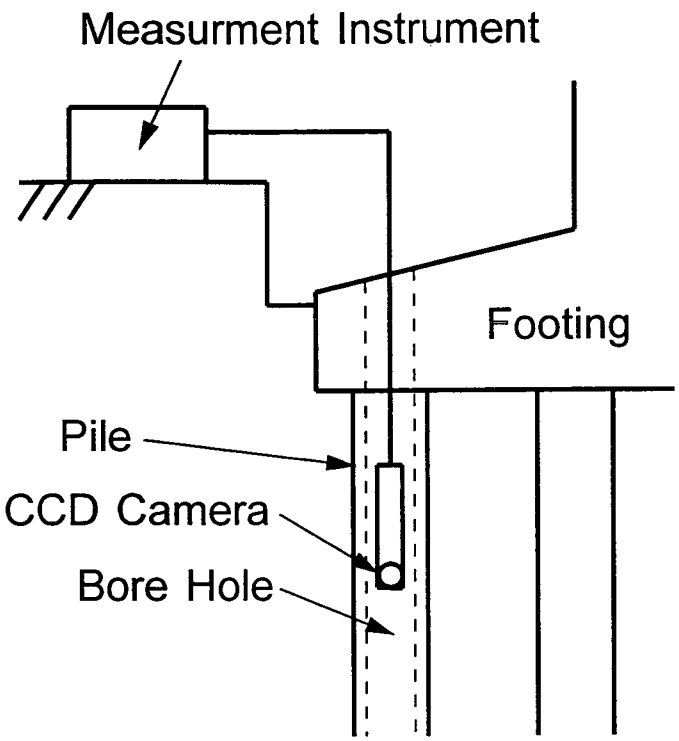
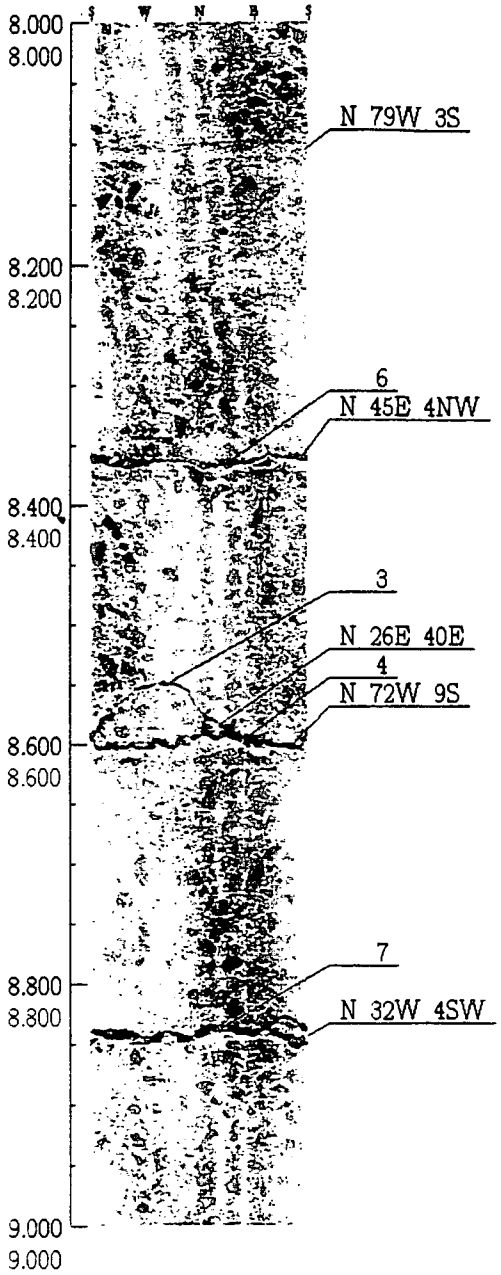


Figure-2 Summary of Bore Hole Camera



Picture-1 Result of Pile Damage by Using Bore Hole Camera

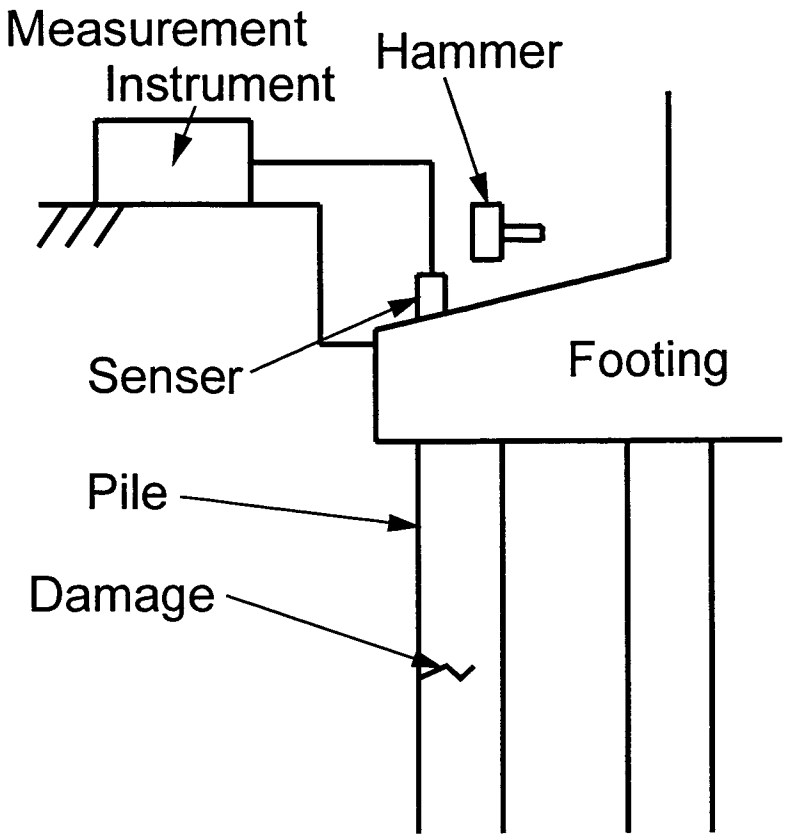
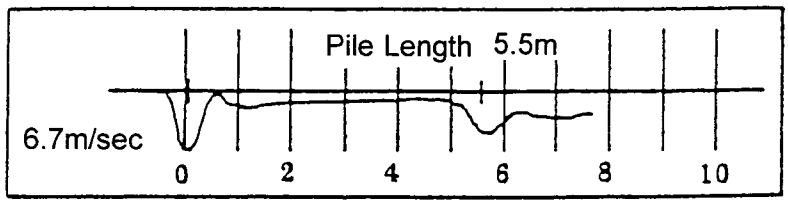
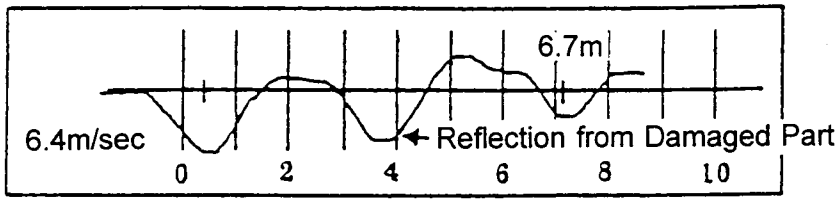


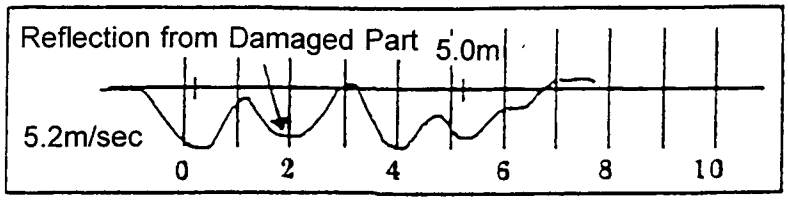
Figure-3 Summary of Integrity Test



(1) Wave Shape of Sound Pile



(2) Wave Shape of Damaged Pile



(3) Wave Shape of Damaged Pile

Figure-4 Wave Shape of Integrity Test

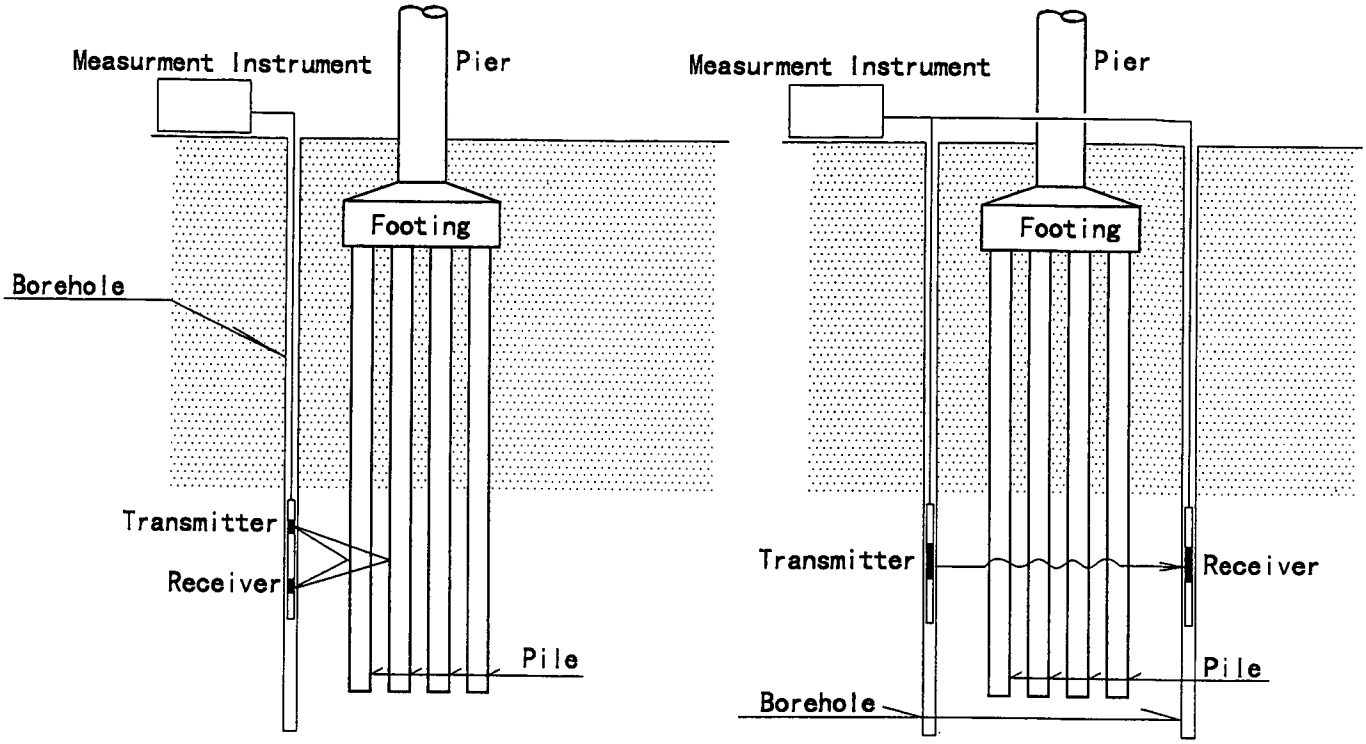
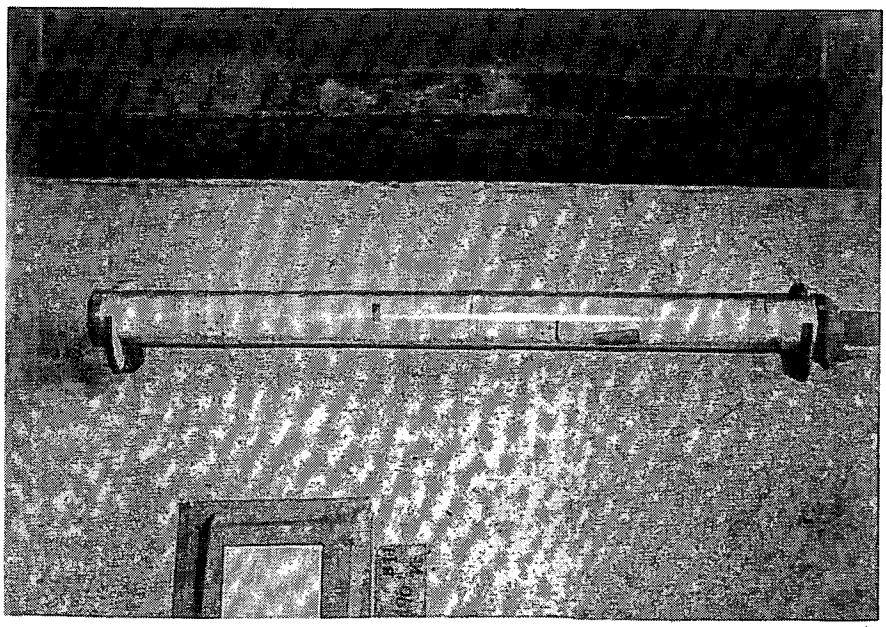
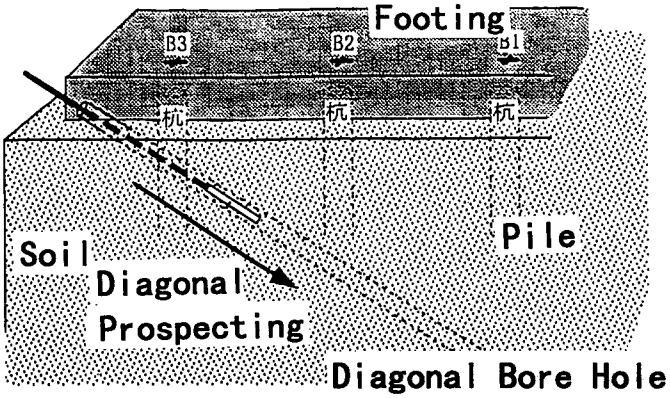
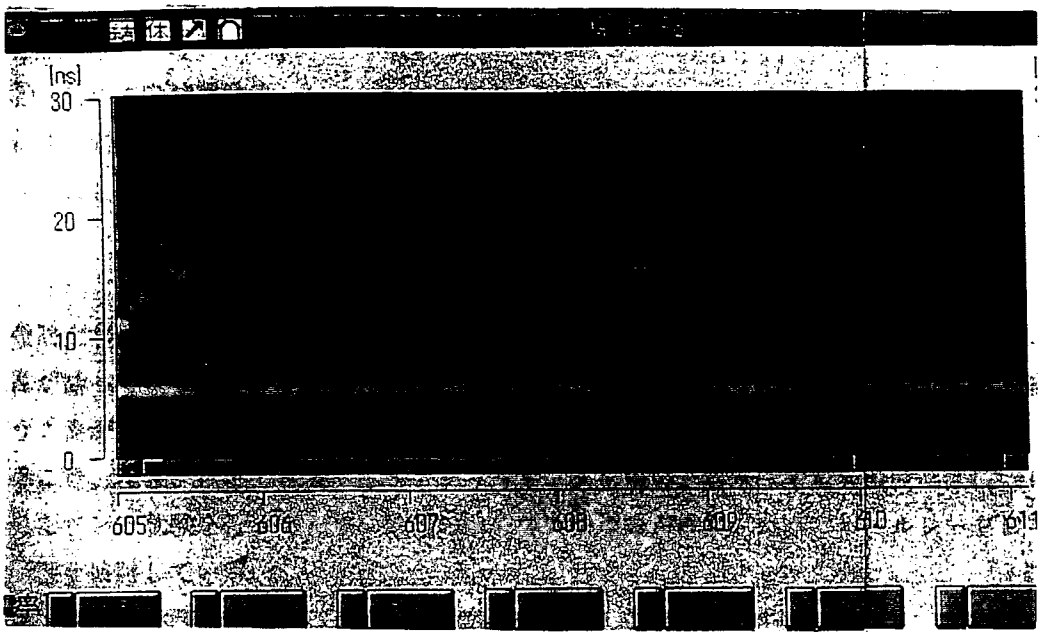


Figure-5 Summary of Borehole Radar

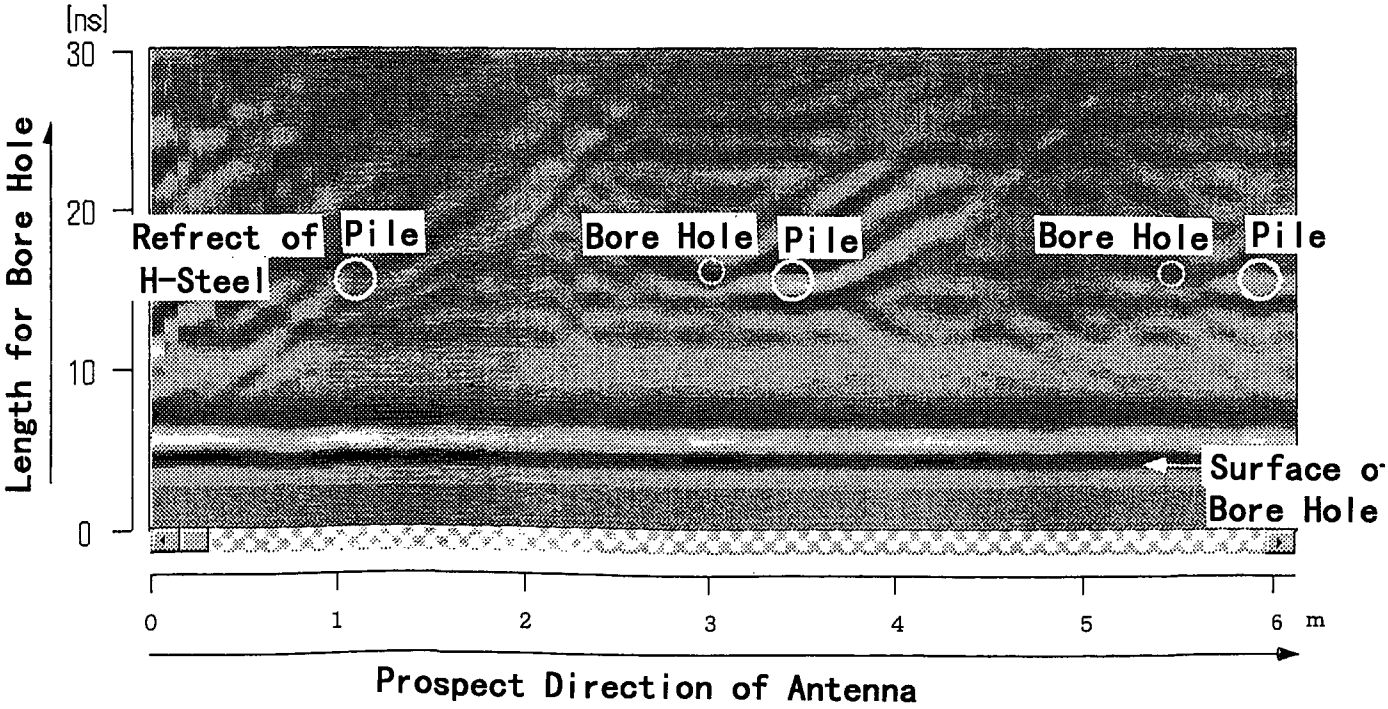


Picture－2 Radar





Picture of Radar



Figure－6 Results of Bore Hole Radar Test

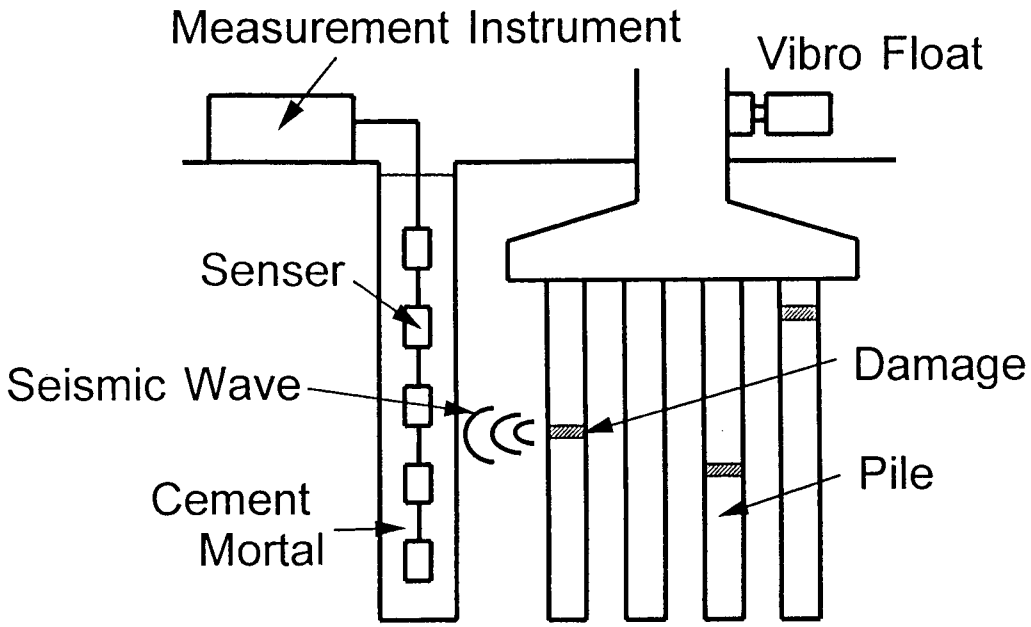
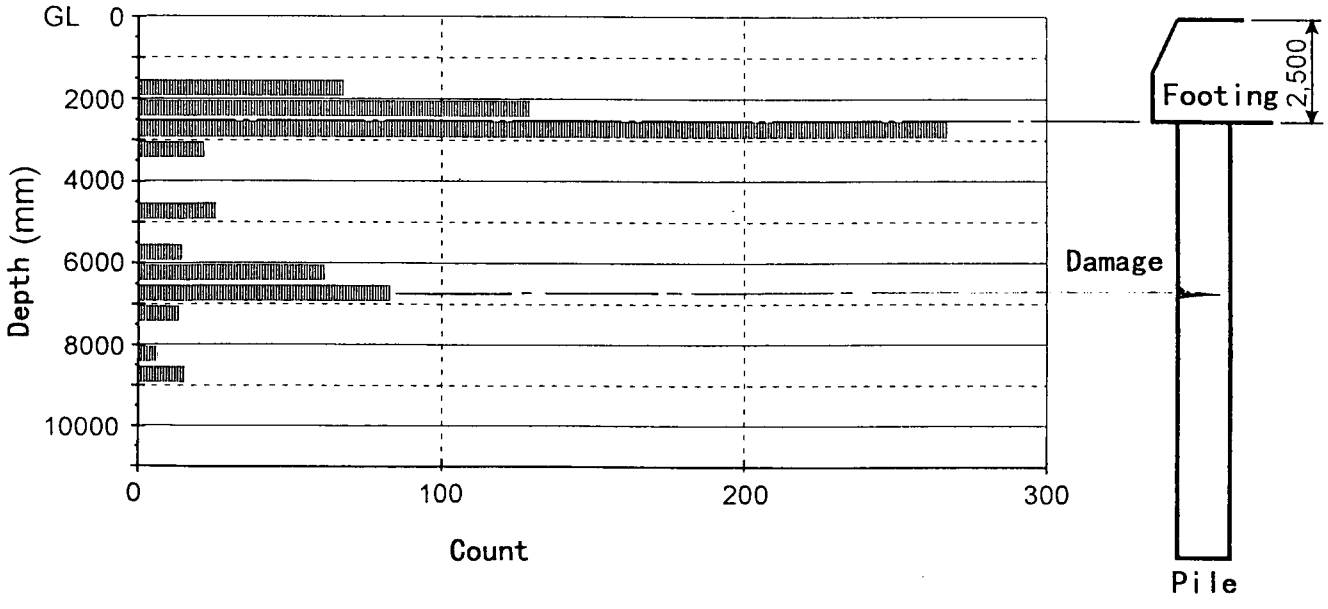


Figure-7 Summary of Acoustic Emission



Figure－8 Results of Acourstic Emission Test

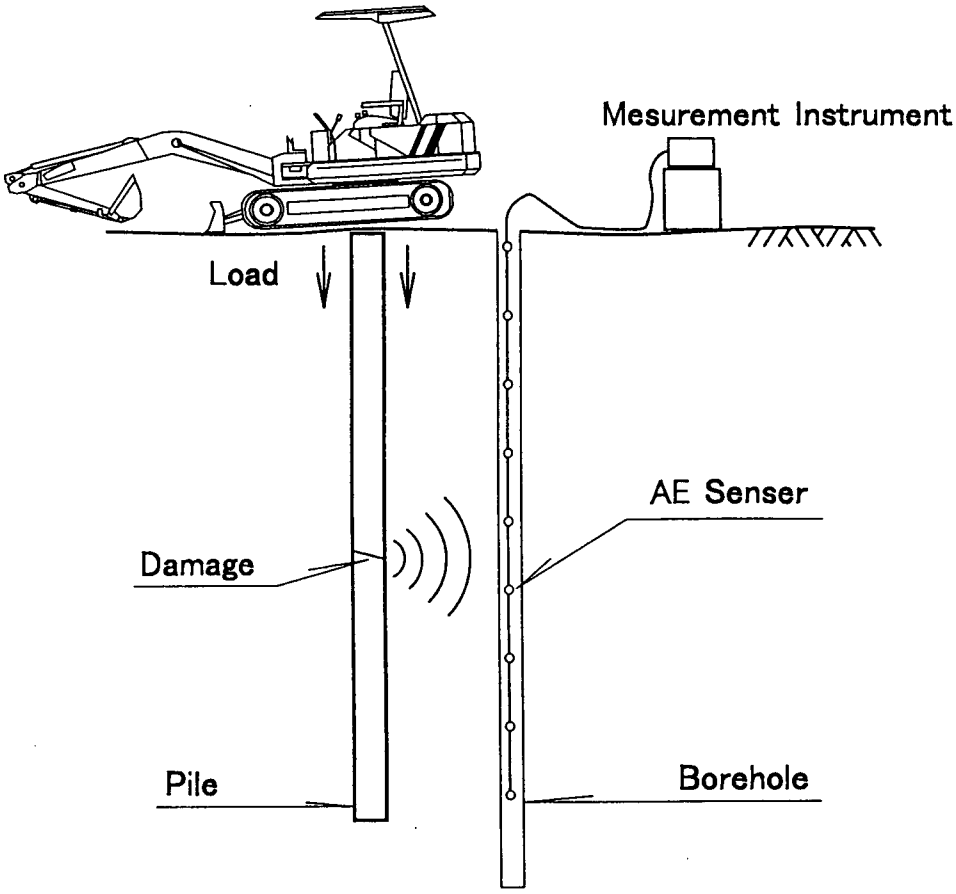
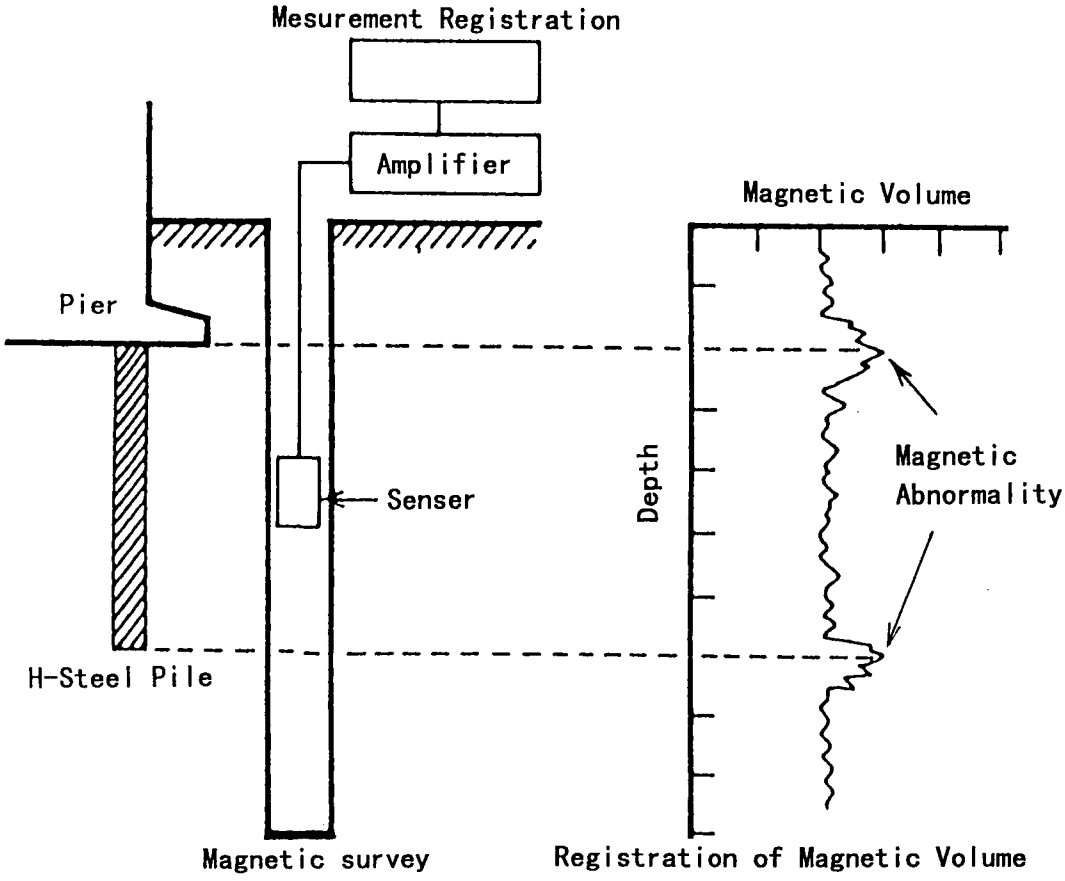


Figure-9 Situation of Shaking Pile



Figure－１０　Summary of Magnetic Survey

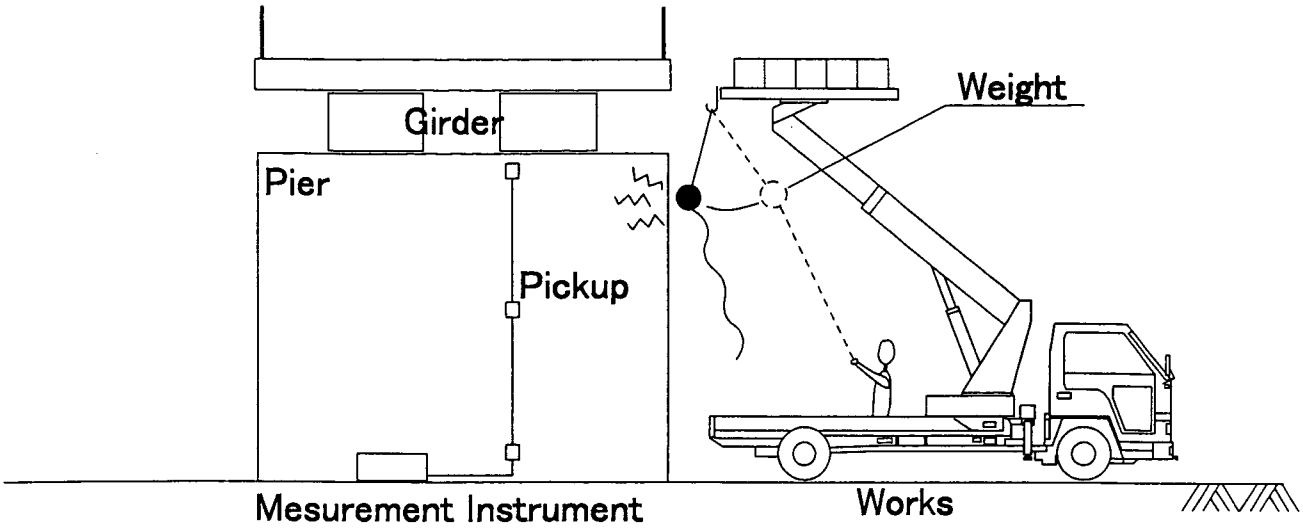


Figure-11 Situation of Impact Vibration Test

HERMES: DETECTION OF CONCRETE BRIDGES USING MICROPOWER IMPULSE RADAR AND MULTI-FREQUENCY DIFFRACTION TOMOGRAPHY

Terry D. Philbin[1]

Abstract

The inspection of concrete bridges decks for deterioration is commonly a low tech process that is complicated by several factors. The presence of inspectors on the deck can cause safety problems for the inspectors and the traveling public alike. Lane closures that provide safety to the inspectors are not only expensive, they can create congestion problems. Asphalt overlays frequently hide the surface of the deck from inspectors. Since bridge inspectors can only provide data on what they see or determine with other techniques, there is a need to provide them with tools to safely, rapidly, and accurately assess the level of deterioration to the bridge decks. The FHWA is currently funding research into micro-impulse radar as a solution to these problems. This paper provides a short discussion on what micro-impulse radar is, and presents the results of its first field application to bridge deck inspection.

[1] Regional Structural Engineer, United States Department of Transportation

The Problem

Monitoring the deterioration of bridge decks is an important element of the overall bridge management process. Bridge decks are subject to the direct effects of traffic, weather, and deicing chemicals used in winter road maintenance. This environment makes decks one of the most likely elements to require maintenance, repair, or rehabilitation in the life of the bridge, yet their inspection is often difficult and sometimes dangerous. In the United States there are 583,317 highway bridges over 6.1 meters long. Of these, 371,655 have concrete decks. Of the 371,655 bridges with concrete decks, 137,221 have asphalt overlays[2].

The typical deterioration of a bridge deck begins with the attainment, at the top mat of reinforcing steel, of an adequate level of moisture and chloride ions to initiate corrosion. The byproducts of corrosion occupy a greater volume than the base metal. This tendency to increase in volume places the concrete in tension and eventually leads to delaminations in the concrete. Additional corrosion and the effects of traffic and weather cause the unification of isolated delaminations into larger areas and to the eventual spalling of concrete from the surface of the bridge deck. Any of the described steps on the continuum of deterioration can be difficult to detect when an asphalt overlay is placed on the bridge deck.

In order to properly model the deterioration of bridge decks through their lifespan, their gradual deterioration must be divided into easily observed condition states (distress definitions).

The bridge management software Pontis is widely used in the United States. The condition state language used in Pontis for concrete decks is listed below[3].

> **Condition State 1**: The surface of the deck has no repaired areas and there are no spalls/delaminations in the deck surface.
>
> **Condition State 2**: Repaired areas and/or spalls/delaminations exist in the deck surface. The combined area of distressed area is 2% or less of the deck area.
>
> **Condition State 3**: Repaired areas and/or spalls/delaminations exist in the deck surface. The combined area of distressed area is 10% or less of the deck area.
>
> **Condition State 4**: Repaired areas and/or spalls/delaminations exist in the deck surface. The combined area of distressed area is more than 10% but less than 25% of the deck area.
>
> **Condition State 5**: Repaired areas and/or spalls/delaminations exist. The combined area of distress is more than 25% of the deck area.

It is seen that three specific items of deterioration are tracked; repaired areas, spalls, and delaminations. Each of these has its problems with either their definition or inspection. For example:

There is currently some disagreement among Pontis users as to whether all repaired areas should be considered deterioration;

An asphalt overlay can make spalls, which are normally easily detected, invisible to the inspector;

Delaminations cannot be detected through a visual inspection so some external means must be used to enhance the inspector's abilities.

One method commonly used to detect delaminations is the chain drag (Figure 1).

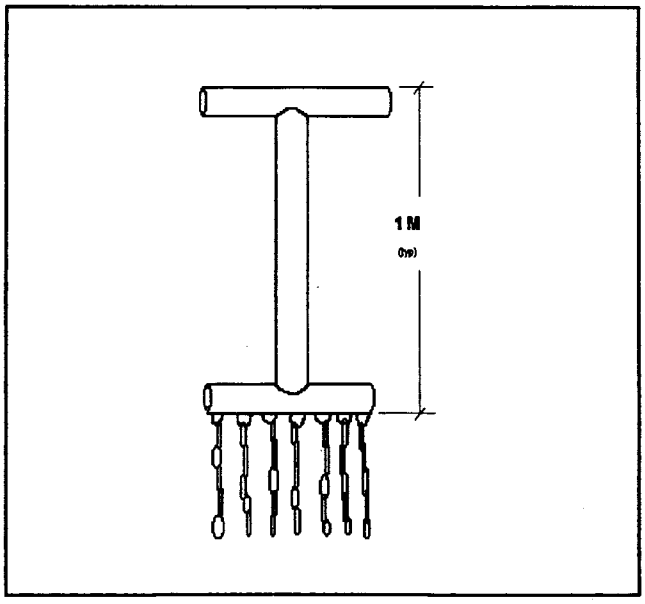


Figure 1

A common type of chain drag is made up of a tubular frame supporting short lengths of metal chain. The chain is dragged over the surface of the deck and a change in the pitch (tone) of the chain on the deck serves as an indication of a delamination.

This procedure has several shortcomings, not the least of which is that the inspector must be within arms reach of all portions of the deck during the inspection, often during heavy traffic. To counter this problem traffic control can be used, but it creates a substantial expense and often causes traffic congestion at the structure under inspection.

A tool that would determine the quality of bridge deck patches, the quantity of delaminations and spalls, and be able to accomplish these tasks at or near traffic speeds would be a major benefit to the inspection process and to the bridge management system in general.

The Solution

The Federal Highway Administration (FHWA) is currently funding research and development of a new system (HERMES) which combines micropower impulse radar (MIR) with powerful data acquisition and image processing systems for the inspection of concrete bridge decks. The objective of this research is to have a system that is able to penetrate asphalt overlays to detect flaws in concrete deck patches and quantify delaminations and spalls, while traveling at near highway speed.

MIR is a low power pulsed radar that was developed at the Lawrence Livermore National Labs based on data gathering needs that came to light during experiments using the LLNL's 100-trillion-watt Nova laser. MIR emits much shorter pulses than most radars and can be built out of a small number of off the shelf electronic components. The MIR has been coupled with powerful data acquisition and imaging software and hardware to provide both real-time visualization of raw data and, after processing, two and three dimensional representations of chosen sections of the bridge deck. In early laboratory tests, the radar was able to detect delaminations of approximately 3 cm.

In the spring of 1997, two prototype systems were tested in the field on actual bridges. These bridges had some areas covered with asphalt overlays and, in those areas where the overlay was not present, displayed significant deterioration on the surface of the deck. One prototype system consists of a single pair of antennae (transmit/receive) that are mechanically driven on a robotic cart. After the cart advances a small distance longitudinally, the antennae are scanned transversely across the bridge deck. This process is very accurate, but it has the disadvantage of being quite slow and requiring traffic control to route traffic around the lane under investigation. This prototype provided images of not only the mats of reinforcing steel, but construction flaws that were not anticipated (Figure 2).

The full-scale (Figure 3) system has a 128 antennae; 64 pairs of transmitting and receiving antennae on an eight by eight array (Figure 4). This model will scan an approximate two meter width of the bridge deck by triggering the individual antennae, rather than by physically moving one antenna pair across the deck. It is hoped that through this process, high-resolution data can be acquired at near traffic speeds.

As shown in figure 2, detailed representations of the reinforcing steel, bridge joints, and voids in the concrete were developed by the HERMES system. Cores were taken at various locations in the deck to verify the findings of the radar and as shown in the figure, a strong correlation was found between the images produced and voids found in the deck.

The full-scale system had only 48 of the 64 antenna pairs operational at the time of the test, and processed images are not yet available. Improvements have been made to the imaging software since the time of the field trial, as have improvements to the antenna array. A detailed report on the overall findings of this trial has not been produced.

At present, operation of the prototypes are beyond the capabilities of the average bridge inspector. Detailed knowledge of the software and the calibration procedure are required. It should be recognised that this apparatus is still in the prototype stage. Future enhancements are expected to make the operation much simpler.

It is possible that future refinements to the Hermes system will lead to automatic mapping and quantifying of delaminations and spalls. It is also possible that treating deck patches as any other part of the deck will lead to the elimination of patches from the bridge deck condition state language used in bridge management.

The Hermes system holds promise to more accurately acquire, quantify, and present the state of deterioration of individual bridge decks. It also promises to do this with less disruption to traffic, and in a safer fashion.

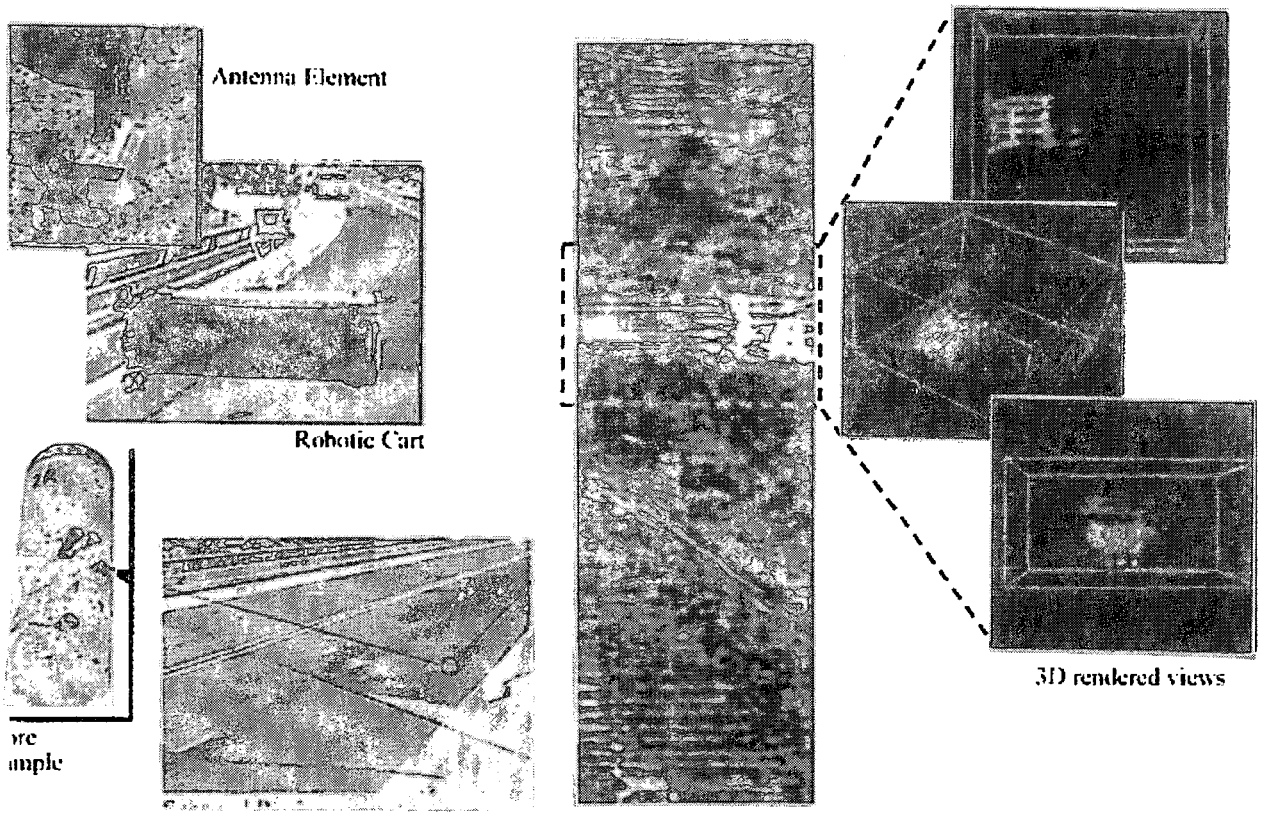


Figure 2



Figure 3

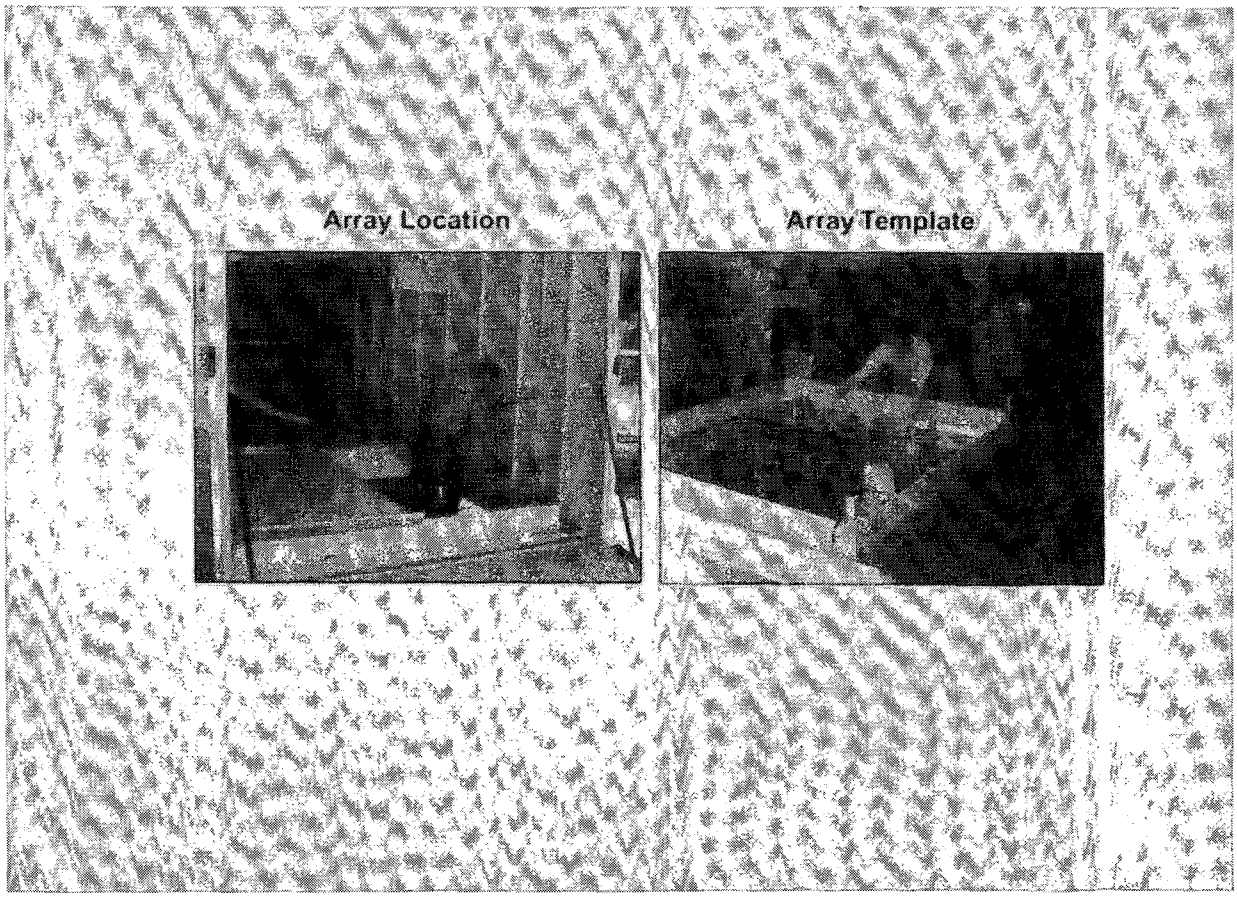


Figure 4

1. Regional Structural Engineer
FHWA Region 8
555 Zang St. Room 400 HES-08
Lakewood, Colorado, USA 80228

2. Data from the National Bridge Inventory August 19, 1997
FHWA Bridge Division HNG-33
Office of Engineering
400 7th Street, S.W.
Washington, D.C. USA 20590

3. Pontis Version 2.0 Users Manual
Appendix 1. Condition State Definitions.

Bibliography

Advanced Ground Penetrating Radar: John P. Warhus, Jeffrey Mast, Erik M. Johansson, Scott D. Nelson; Lawrence Livermore National Laboratory; Electronics Engineering Department; P.O. Box 808, L-153; Livermore, California, 94551.
(http://www-dsed.llnl.gov/documents/em/gpirhardware.html)

Three-dimensional ground penetrating radar imaging using multi-frequency diffraction tomography: Jeffrey E. Mast and Erik M. Johansson; Lawrence Livermore National Laboratory; P.O. Box 808, L-153; Livermore, CA 94550
(http://www-dsed.llnl.gov/documents/imaging/jemspie94.html)

Three-dimensional ground penetrating radar imaging using synthetic aperture time-domain focusing; Erik M. Johansson and Jeffrey E. Mast; Lawrence Livermore National Laboratory; P.O. Box 808, L-153; Livermore, CA 94550
(http://www-dsed.llnl.gov/documents/imaging/emjspie94.html)

Imaging Radar for Bridge Deck Inspection: John Warhus, Jeffrey Mast, Scott Nelson; University of California; Lawrence Livermore National Laboratory; Electronics Engineering Department; Livermore, California 94550
(http://www-lasers.llnl.gov/lasers/idp/mir/files/warhus_spie/spiepaper.html)

HYDROGEN EMBRITTLEMENT AND DETERIORATION EFFECTS ON WIRES IN CABLE-SUPPORTED BRIDGES

Raimondo Betti[1], Maciej P. Bieniek[1], Paul F. Duby[2], Alan C. West[2], Scott C. Barton[2], Garry Veermaas[1]

Abstract

This paper summarizes the findings of inspections of suspension bridge cables in the New York metropolitan area and presents the preliminary results of a research project, currently ongoing at Columbia University, on the corrosion deterioration and hydrogen embrittlement of low-carbon high-strength bridge wires. Such wires are widely used in cables, suspenders and stays of suspension and cable-stayed bridges as well as in prestressing strands of prestressed concrete bridges. Although the conditions of the New York bridge cables are generally satisfactory, especially considering their age (between 60 to 120 years old), some effects of environmental degradation are evident. For bridge wires, the deterioration process manifests itself, in addition to the loss of material, in a number of phenomena referred to as stress corrosion, corrosion cracking, corrosion fatigue, hydrogen embrittlement, etc. Results from studies at Columbia University show that a corrosive environment drastically reduces wire ductility, leading to virtually brittle fractures. Accelerated corrosion tests on galvanized wires are currently under investigation, focusing on the interaction between corrosion processes, hydrogen embrittlement and mechanical stresses.

Introduction

Today, the United States is facing the difficult problem of rebuilding its infrastructure system, a system that has been allowed to deteriorate because of inadequate investment in maintenance and life extension technology. Many bridges in this country are structurally deficient: in the New York metropolitan area, 56% of the bridges are rated in poor conditions (less than 4.5 on a 1-7 scale).

In bridges, the primary cause of deterioration is represented by corrosion of steel. However, while basic research on corrosion of structural and various specialty steels has been extensively performed over the past 30-40 years, the corrosion process and the associated strength deterioration of high-strength bridge wires have received only scant attention, mainly from bridge designers and engineers[1]. While the effect of corrosion of ordinary steel is mainly represented by the loss of material and the ensuing reduction of cross-sections of members, the corrosion process in high-strength wires is a much more complicated process, resulting from various

[1] Department of Civil Engineering and Engineering Mechanics, Columbia University, New York, NY, 10027.

[2] Department of Chemical Engineering, Columbia University, New York, NY, 10027.

electrochemical processes and their interaction with mechanical stresses. In addition to the reduction of cross-sectional area, a number of phenomena such as stress corrosion, corrosion cracking, hydrogen assisted cracking, corrosion fatigue and hydrogen embrittlement develop and they appear to have a more detrimental effect on the strength reduction of the wire than the reduction of the wire's cross-sectional area.

The safety of existing cable-supported bridges is closely related to the problem of environmental deterioration of wires. Today, because of the lack of knowledge on deterioration of high-strength bridge wires, engineers formulate their judgement on available field observations and on extrapolation of laboratory results. However, these field observations and laboratory results are linked to specific structures rather than to basic research, creating a scattering of results that is difficult to generalize. After inspection and evaluation of bridge cables, engineers have only two reliable points on the cable deterioration curve: 1) the as-built condition (from original drawings and specifications), and 2) the actual condition. Their difficult task consists in making the right decision on the extrapolation of the deterioration curve over the next century, accounting for the (estimated) progressive rate of deterioration and for the rehabilitation measures applied to the bridge.

In the design of new suspension bridges, it is customary to consider a safety factor, with respect to the ultimate strength, of about 2.5, with a new trend to further reduction to about 2. However, such low safety factors totally ignore the effects of wire deterioration under service conditions and could be quite disastrous for the future life of the bridge. In addition, in the current design practice, the effects of residual stresses associated with the wire manufacturing process are completely neglected. Such stresses could reach up to 35-40% of the ultimate wire strength so that neglecting such effects induces an additional reduction of the cable safety factor. Bridges built in the U.S. at the end of the 19th century and at the beginning of 20th century were designed using a safety factor greater than 4 and they will last longer than the originally anticipated life span of 70 years. However, inspections of the main cables in suspension bridges have revealed: 1) there is water penetration inside the cable, with water pH as low as 4, 2) there is corrosion of zinc coating in the form of zinc hydroxide, followed by corrosion of steel, which could show quite substantial losses of cross section, 3) there are broken wires within the cables, wires that, from laboratory tests, present significant loss of ductility and reduced fatigue strength [2,3,4]. Fracture surfaces of all wires broken in service and in many laboratory specimens confirm the presence of corrosion/hydrogen assisted cracking and/or hydrogen embrittlement, with an hydrogen concentration in steel up to 12 ppm. All these factors contribute to a drastic reduction of the cable strength and, consequently, of the bridge safety factor.

To address such a complex problem, a series of tests has been planned and is currently under investigation at Columbia University. The focus is on cold-drawn wires of carbon steel, with a carbon content of about 0.8%, galvanized and ungalvanized, of 5 mm diameter and tensile strength of 1600 to 1900 MPa. Wires have been provided by Williamsport Wirerope Inc.. Tests for hydrogen embrittlement are also being performed on a seven wire strand, for applications in stays and prestressing cables.

Electrochemical Processes In Stressed Wires

The environmental deterioration of bridge wires is a result of electrochemical processes and their interaction with mechanical stresses. Although atmospheric air is the most common environment, aqueous solutions, including natural water, atmospheric moisture, and rain, as well as man-made solutions, are the environments most frequently associated with degradation problems. The wire degradation manifests itself in two different forms: corrosion and hydrogen embrittlement.

With the term corrosion, we indicate the loss of metal due to electromechanical processes. In these processes, material is lost from the corroding element (anodic element) and is deposited on the other (cathodic) element. Thus, in such a type of corrosion process, electroplating of the cathodic element is developed. In a different process, which is called wet or aqueous oxidation and is mainly responsible for the corrosion deterioration of bridge wires, the lost material, in the form of iron ions, develops a new compound, iron hydroxide ($Fe(OH)_3$), commonly called rust.

In bridge wires, various forms of material deterioration have been associated with the word corrosion. They are the following: surface corrosion, corrosion pitting, intergranular and crevice corrosion, stress corrosion and corrosion fatigue. The main loss of metal occurs by uniform surface corrosion. In galvanized bridge wires, the protective zinc coating corrodes first, forming zinc hydroxide (white rust). Then, once the zinc coating has been corroded, then steel corrosion takes place. The steel corrosion process can occur quite rapidly and the loss of material associated with such a phenomena can drastically reduce the cross section of the bridge wire. Laboratory tests have shown that a moderate amount of surface corrosion has a relatively small effect on the wire static strength and ductility.

If the anodic zone on a wire is spread over a large surface or if the anodic and cathodic zones shift along the wire, the surface corrosion is quite uniform. It may happen that a small corrosive zone stays in one location leading to the formation of corrosive pits on the wire surface. With the term corrosion pitting, we define an extremely localized corrosive attack. Simply stated, pitting is the type of localized corrosion that produces pits, that is, sites of corrosion attack that are relatively small compared with the overall exposed surface. If appreciable attack is confined to a relatively small fixed area of wire acting as anode, the resultant pits are considered deep. If the area of attack is relatively large but not so deep, the pits are called shallow. Depth of pitting is usually expressed in terms of pitting factor: this is the ratio of deepest metal penetration to average metal penetration as determined by the weight loss of the specimen. A pitting factor of unity represents uniform corrosion.

Intergranular corrosion takes place when the corrosion rate of the grain-boundary areas of the metal is greater than that of the grain interior. This difference in corrosion rate is generally the result of differences in composition between the grain boundaries and the interior. In this way, the crystal grain boundaries in the steel tend to become anodic with respect to the interior and so corrosion penetrates along the grain boundaries. The presence of narrow openings

or spaces (gaps) between metal-to-metal or nonmetal-to-metal components may give rise to localized corrosion at these sites. Similarly, unintentional crevices such as cracks, seams and other metallurgical defects could serve as sites for corrosion initiation. This phenomenon is known as Crevice Corrosion. In an existing crack or crevice, corrosion occurs at the tip of the crack (anodic region) and penetrates into the wire.

Stress-corrosion cracking is a term that is used to describe service failures in engineering materials that occur by slow environmentally induced crack propagation. The observed crack propagation is the result of the combined and synergistic interaction of mechanical stress and corrosion reactions. Parts of the steel wire subjected to stress becomes anodic with respect to other, unstressed, areas of the wire. Hence, the portion of wire with higher stresses is then subjected to corrosion. In this degradation process, the residual stresses, due to wire manufacturing (cold drawing and zinc coating), play a key role. Today, the conventional method of stress calculation in a wire due to axial load and bending is based on the classical elastic rod theory. In this approach, the residual stresses in the wire and the effect of interaction between the residual and applied stresses (which may lead to local plastic strains in the wire material) are ignored. More importantly, stress-corrosion cracking is also associated with the fact that crack tips in a wire under tension are subject to high stress concentration. This causes corrosion process to attack the crack tip zone and, thus, to accelerate the crack growth.

Corrosion fatigue occurs in metal as a results of the combined action of a cyclic stress and a corrosive environment. Corrosion fatigue is dependent on the interaction among loading, environmental and metallurgical factors. This interaction increases the rate of growth of transversal cracks in wire under tension. In fact, for a given metal, the fatigue strength (or the fatigue life at a given maximum stress value) generally decreases in the presence of an aggressive environment. Corrosion fatigue cracks are always initiated at the surface unless there are near-surface defects that act as stress concentration sites and facilitate subsurface crack initiation. The, cyclic stresses breaks the protective oxides at the tip of a crack, exposing clean metal. Exposed clean metal is then attacked by corrosion that weakens its tip zone and facilitate further crack growth during the next cycle. Although corrosion fatigue phenomena are diverse, crack growth rate is influenced by the following variables: stress intensity factor, load frequency, stress ratio, aqueous environment electrode potential, environment and metallurgical variables.

Another important process in wire degradation is represented by hydrogen embrittlement. In contrast to most forms of corrosion, hydrogen embrittlement generally occurs in service when the part is being protected from corrosion or when corrosion on the part is absent, that is, when a high-strength steel is cathodically protected. The corrosion is usually taking place elsewhere (at the anode), but atomic hydrogen is being generated at the surface of the steel (cathode) by the dissolution of water. These hydrogen atoms diffuse in the interior of the wire and weaken the interatomic bond of the wire metal. The penetration and movement of hydrogen within the wire are towards zones of high tensile stress, e.g. at crack tips in wires under tension. As for the corrosion process, hydrogen effect enhances the grow of cracks under sustained stress (or stress increasing at a very slow rate) or under cyclic stress. In fact, slowly increasing tensile or cyclic

stress facilitate the hydrogen penetration by breaking the protective oxides at the crack tip and exposing new clean metal surface. From this consideration, it is clear the existence of a stress rate that makes this phenomenon of hydrogen embrittlement more pronounced: this is the rate of stress that is slow enough to allow for the hydrogen to weaken the metal, but also fast enough to prevent the formation of protective oxides at the crack tip.

In acid environment, such as acid rain or polluted water, the bare steel wire becomes cathodic relative to zinc and is the site of hydrogen evolution. Investigation of fractured wires extracted from bridge cables and wires tested for tensile strength in the laboratory shortly after their extraction from a cable reveal the presence of hydrogen in steel with concentrations occasionally reaching 12 to 25 ppm. While such hydrogen concentrations are known to cause embrittlement of other high-strength steels, the degree of hydrogen embrittlement of the bridge wire due to hydrogen attack is unknown.

Accelerated Corrosion Tests

A series of accelerated corrosion tests on new bridge wires is currently ongoing at the Robert A. W. Carleton Strength of Material Laboratory of the Department of Civil Engineering and Engineering Mechanics at Columbia University. New coiled galvanized and ungalvanized wires are pretensioned in appropriately designed testing fixtures and placed in an accelerated corrosion chamber (fig. 1). These fixtures are designed to keep the specimen at a constant elongation. The level of applied tension to the wire specimens ranges from 0 to 22.25 KN (5000 lb) corresponding to a stress level of about 70% of the ultimate tensile strength. The purpose of having different levels of applied stresses at the wires is to investigate possible effects of stress level on the corrosion rate. Loaded and unloaded wires have been kept in the corrosion chamber (see fig. 1) for extended periods of time, ranging from one to several weeks.

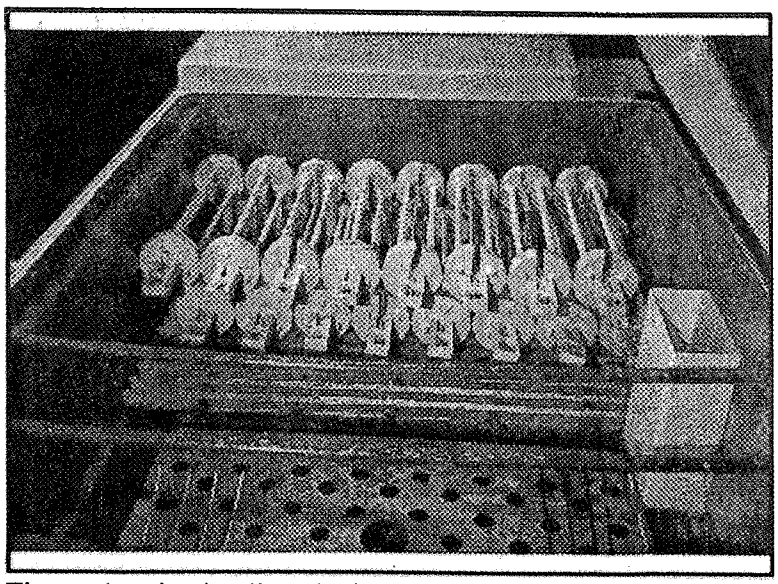


Figure 1: wire loading devices in corrosion chamber

ASTM cyclic, acidified salt tests have been run [5,6]. For all experiments, the temperature of the chamber is maintained at 49°C. A six-hour wet-dry cycle has been appropriately designed. It consists of:

1) 0.75 hours of salt spray,
2) 2.0 hours of dry-air purge
3) 3.25 hours of high-humidity air.

The cycle is repeated continuously until all specimens have been withdrawn from the chamber for mechanical testing. The salt spray, made from distilled water, is adjusted to a pH of 3.0 by addition of acetic acid. Such a testing environment recreates wires conditions which are very similar to the real environment on the bridge. The salt concentration of NaCl has been set at either 5 weight percent (for the highly corrosive spray) or 0.05 weight percent for the more mild conditions. For the high-humidity-air portion of the cycle, air is humidified by bubbling it through a water-saturation tower.

The results of this series of tests show that the protective zinc coating in galvanized wires seems to be extremely effective in inhibiting the corrosion process in the steel wire. Even in the highly corrosive environment, the galvanized coating deteriorates but no changes in the mechanical properties of the wires are manifested. In ungalvanized wires, however, the corrosion effects are quite drastic. Mass loss measurements as a function of the exposure time to a corrosive environment clearly show that the mass loss is quite dependent from the NaCl content. For the case of highly corrosive environment (5.0 wt.% NaCl), the reduction in cross-sectional area increases quite rapidly from 3% after 2 days to almost 70% in 14 days. A much lower reduction of cross-section is obtained for the case of lower NaCl content (about 6% mass loss in a three week experiment). It is interesting to notice that, even though there has been a drastic reduction in cross-sectional area in ungalvanized wires, no deterioration of the mechanical properties of steel was noted.

In planning such tests, it is very important that the accelerated tests is able to reproduce in the wire samples the effects of many years (30-40 years) of service conditions in the bridge cable. Therefore, an accelerated corrosion test that simulates, for example, a 40-year condition of the wire in four weeks should attempt to not only match the general corrosion rate (i.e. the loss in cross-sectional area of the wire) but also the hydrogen content in the wire. For this reason, since the protective zinc coating has been proven to be quite effective in the corrosion protection of steel wires, a second set of tests has been planned so to enhance the effects of hydrogen embrittlement in the case of galvanized wires. An inch-long segment of zinc coating has been removed by dipping the wires in a solution of HCl. These wires will be referenced as "damaged galvanized wires". These "damaged" wires have then been loaded in the tension fixtures and placed in the corrosion chamber. The exposed bare steel, in contact with zinc and acqueous vapor, will form a galvanic cell and hydrogen will evolve on the surface of the wire. This process is supposed to change the mechanical strength and ductility of the wire. From a visual inspection of the wires subjected to a three week experiment in a mildly corrosive environment, the zinc protective coating is now badly corroded in the vicinity of the exposed area. A large portion of the wire is now covered with a distinctive layer of "white rust" (zinc hydroxide), resulting from the corrosion of the zinc. The exposed bare steel portion of the wire presents steel corrosion with the same cross-section reduction as the ungalvanized wires.

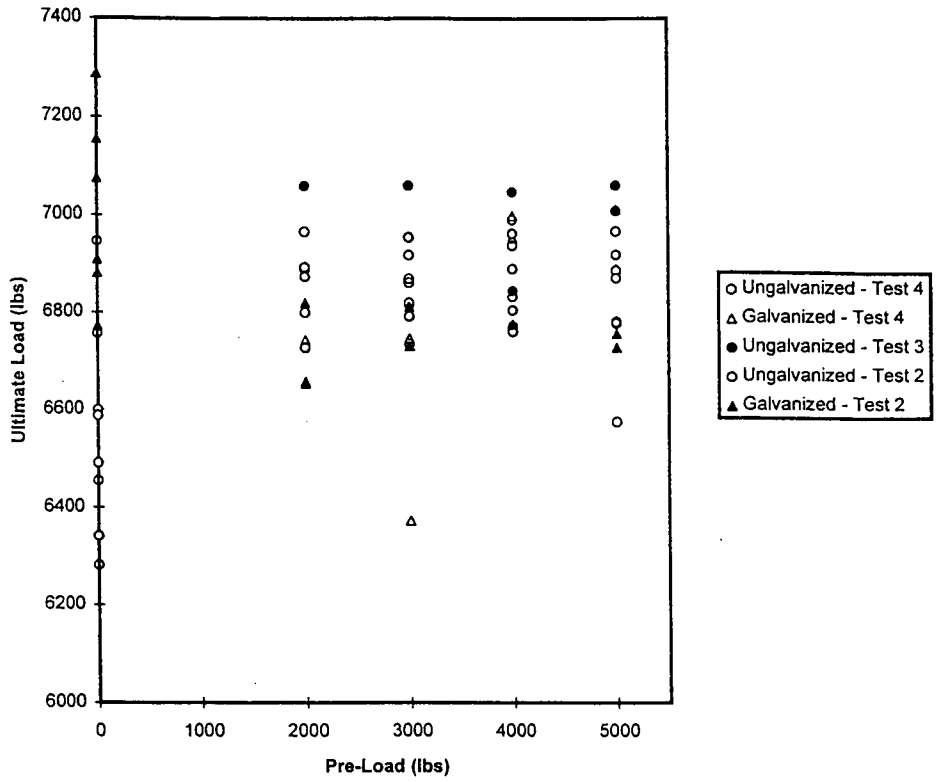


Figure 2: Effects of pre-load on corrosion rate

Ultimate Strength Tests

Interesting observations can be obtained from the analysis of the results. First, it seems that there is no sign of any effect of the level of stress on the corrosion rate. Figure 2 shows that the value of the ultimate strength of the wires subjected to a 0.05 weight % NaCl corrosive environment are distributed over a range between 27.6 kN (6200 lbs) to 32.5 kN (7300 lbs). This distribution does not seem to be dependent on the preload in the wire. Both galvanized and ungalvanized wires show a reduction of ultimate strength that seems to be associated only with the reduction in cross sectional area. For the galvanized wire samples, the ultimate strength changes from a value of 32.507 kN (uncorroded) to 30.523 kN (corroded), which correspond approximately to a reduction of 6.1% of the cross-sectional area. The standard deviation of the corroded specimens population is double compared with that of the uncorroded specimens (0.706 kN vs. 0.314 kN), due to the fact that internal local defects in the material microstructure are emphasized by the corrosion process.

The most important result obtained from this series of tests is represented by the drastic reduction of ductility in galvanized wires with bare steel exposed to the corrosive environment. This confirms the results obtained from previous tests on wires removed from existing bridges conducted at Columbia University. Figure 3 shows the load-strain curve for an uncorroded

galvanized wire (fig. 3a) and for a galvanized wire after a three-week test (fig. 3b). The ultimate strain reduces from 7% (uncorroded) to below 3% (corroded), considering a gage length of 25.4 cm. (10 in.). The surface fractures of the wire specimens are stepped or rectangular with no necking, showing the characteristics of brittle fracture. This embrittlement is definitely caused by atomic hydrogen being generated at the surface of the exposed steel by the dissolution of water during the corrosion of the galvanized coating. These hydrogen atoms diffuse in the interior of the wire and weaken the interatomic bond of the wire metal. The amount of these effects is dependent on the time of exposure of the specimen to the aggressive environment. An identical behavior, with an elongation reduction of the same amount, was also found in testing wire samples obtained from real bridge cables after 30-40 years of service.

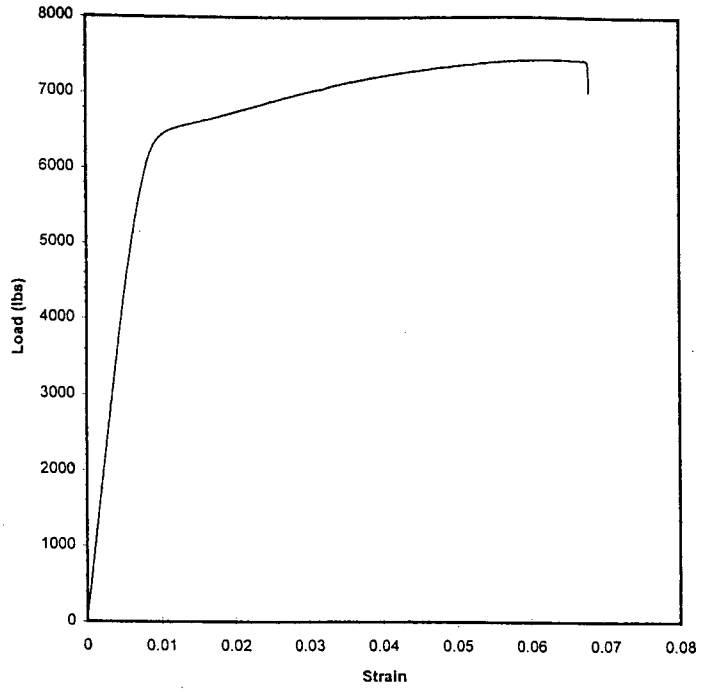
The ductility reduction effect in bridge wires, induced by hydrogen embrittlement, represents a key point in the determination of the remaining strength of existing cable systems. In fact, the assumption of sufficient wire ductility, assumption that would allow all the wires to yield to the same total elongation and weaken wires to continue to carry load at their tensile strength until the entire cable breaks at once, is not conservative and a "brittle" cable model should be considered.

Conclusions

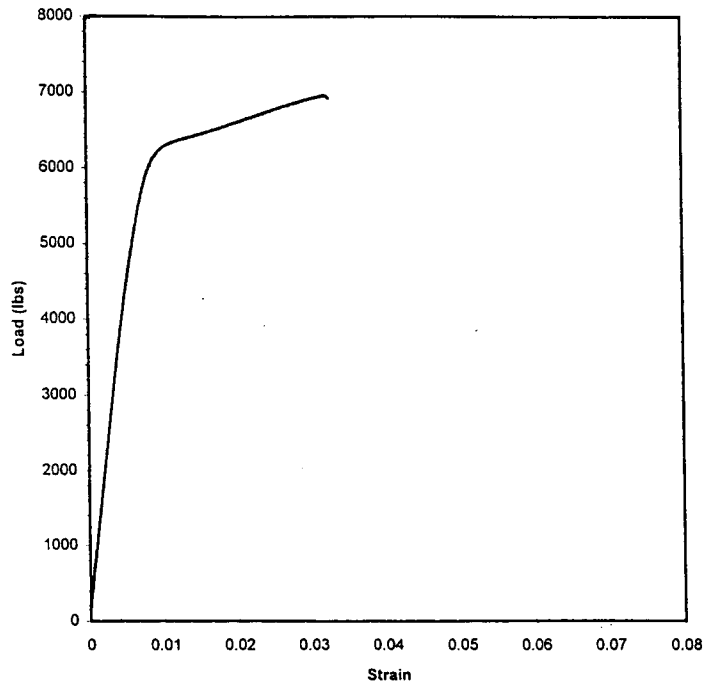
In this paper, a series of tests on corrosion and hydrogen embrittlement effects in cold-drawn high strength bridge wires, currently under investigation at Columbia University, has been presented. The preliminary outcomes of these tests confirm the importance of such effects on the ultimate strength of such wires and emphasize the need for further studies.

Acknowledgements

This research study is sponsored by the National Science Foundation under the research grant CMS-9532082.



(a)



(b)

Figure 3: Load-Strain curves for uncorroded (a) and corroded (b) galvanized bridge wires.

References

1. Stahl, F.L. and Gagnon, C.P.:"*Cable Corrosion in Bridges and Other Structures*", ASCE Press, 1996.
2. Silano, L.G. (Editor):"*Bridge Inspection and Rehabilitation*", J. Wiley & Sons, 1993.
3. Bieniek, M.P.:"Suspension Bridges: Design for Durability", Proceedings *Infrastructures '91*, The Hong Kong University of Science and Technology, 1991.
4. Bieniek, M.P.:"Safety and Aging of Cables of Suspension Bridges", Proceedings of *4th International Conference on Structural Failure, Product Liability and Technical Insurance*, Vienna, 1992.
5. ASTM Method B117:"Standard Practice for Operating Salt Spray (Fog) Testing Apparatus", *Annual Book of ASTM Standards*, ASTM, Philadelphia.
6. ASTM Method G85-94:"Standard Practice for Modified Salt Spray (Fog) Testing", *Annual Book of ASTM Standards*, ASTM, Philadelphia.

SESSION 9: ADVANCED MATERIALS

(1) The Use of High Performance Materials in Virginia's Bridges
(Malcolm T. Kerley and Jose P. Gomez)

(2) Test Methods and Long-Behavior of Polymer Composites for Bridge Structures
(A. Zureick)

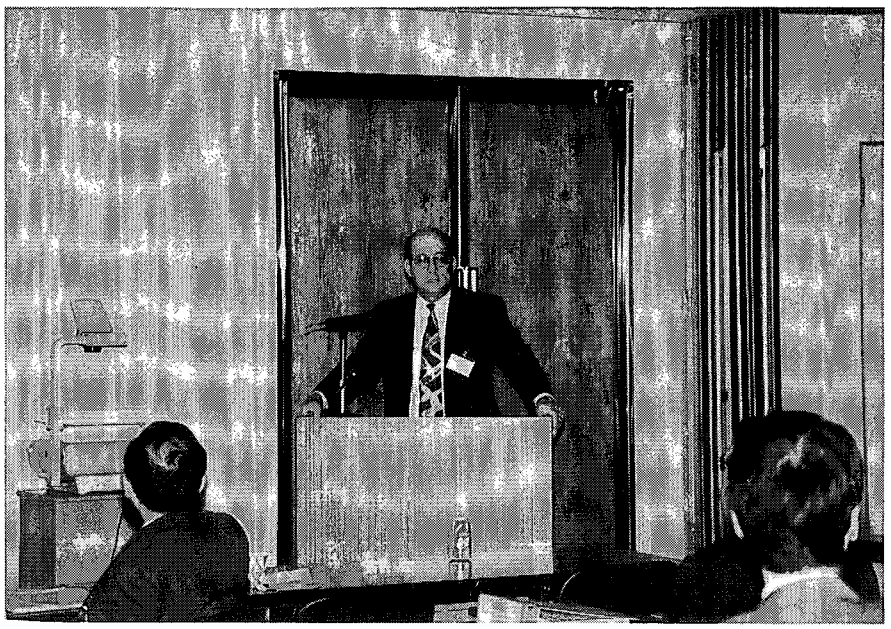
(3) Experimental Study on Strengthening Effect of High-Modulus Carbon Fiber Sheet on Damaged Concrete Deck Slab
(T. Hoshijima, H. Sakai, H. Otaguro and S. Matsui)

(4) Preliminary Evaluation of an Aluminum Bridge Deck Design for Highway Bridges
(Adam Matteo, Peter Massarelli, Jose Gomez, William Wright and James Cooper)

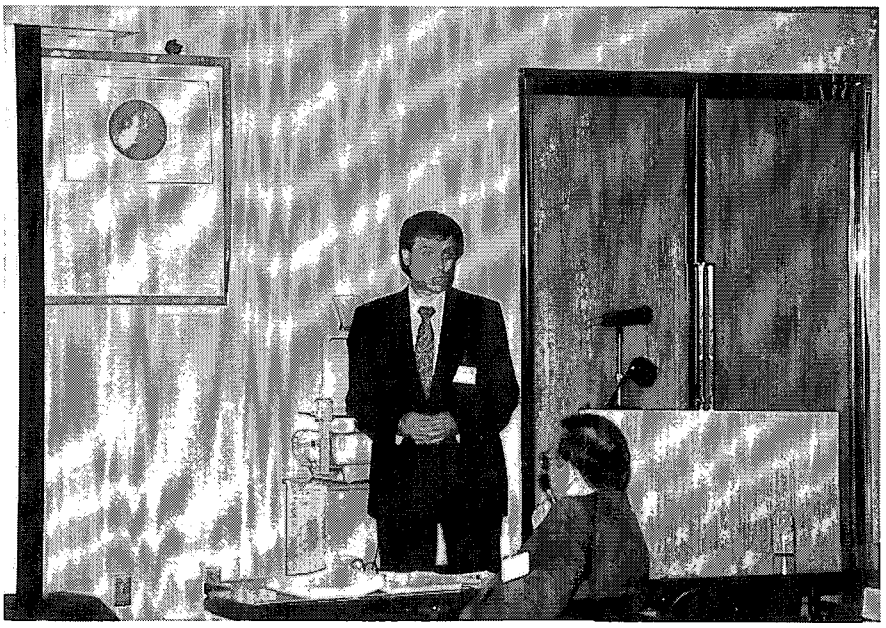
(5) The Design and Construction of Composite-Material Bridges in Delaware
(Dennis R. Mertz, John W. Gillespie,Jr. and William A. Edberg)



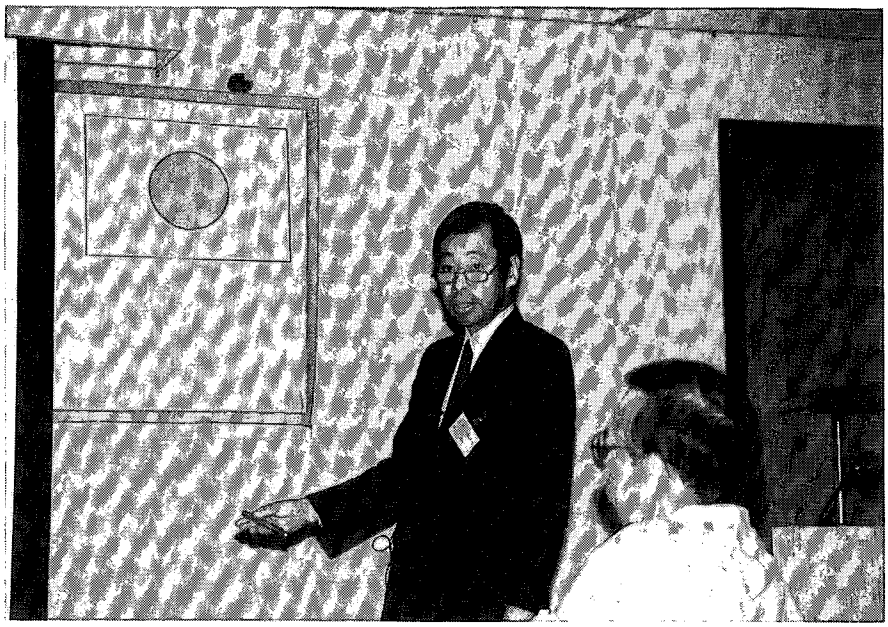
Co-Chairmen : Jun Murakoshi, Wayne Klaiber



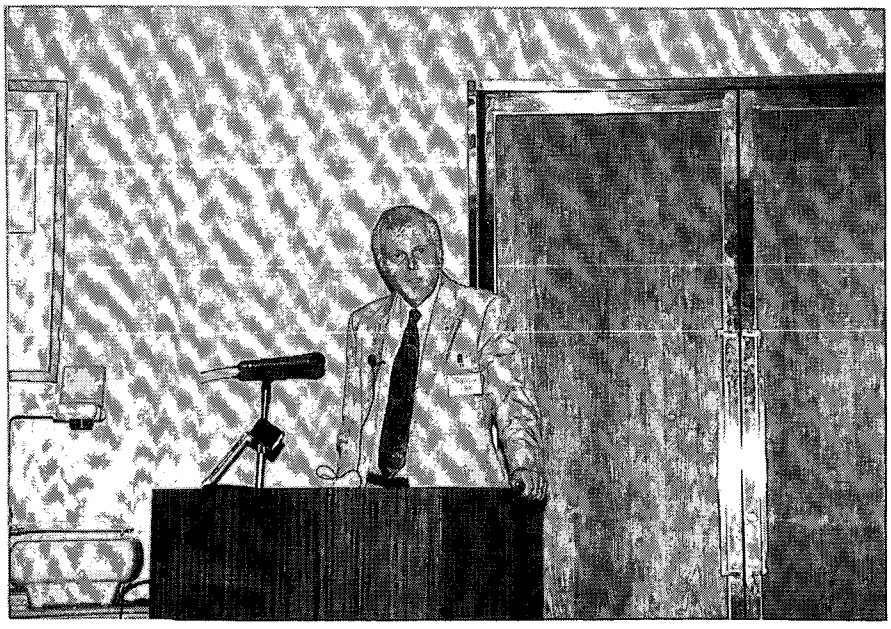
SESSION 9 : Malcolm Kerley



SESSION 9 : Abdul Zureick



SESSION 9 : Tokitaro Hoshijima



SESSION 9 : James Cooper



SESSION 9 : Dennis Mertz

THE USE OF HIGH PERFORMANCE MATERIALS IN VIRGINIA'S BRIDGES

Malcolm T. Kerley, P.E.[a] and Jose P. Gomez[b]

ABSTRACT

This paper summarizes the Virginia Department of Transportation's efforts in the use of high performance materials in its bridge structures. The goals are to seek longer design lifes in new construction, to improve existing structures to extend their service lives, and to reduce maintenance and user costs resulting from repair and rehabilitation requirements. To date, the Department has focused on the use of high performance concrete in both substructure and superstructure applications, an innovative aluminum deck system, and composite materials.

OVERVIEW

High Performance Concrete

Over the years, hydraulic cement concrete (HCC) has been successfully used in bridge structures. However, many concrete structures have exhibited premature failure requiring costly repairs. Increased traffic and vehicle loads and severe exposures have put more demand on these structures. Limited resources also demand longer service life, prompting the new AASHTO Load and Resistance Factor Design (LRFD) Specification to require a 75-year service life.

When concrete is exposed to the environment, many destructive forces start acting on it and can cause premature failure. The four major types of distress in bridge structures are corrosion of the reinforcement, alkali-silica reactivity, freeze-thaw damage, and sulfate resistance.[1] In each case, water and solutions penetrating into concrete initiate the distress. Corrosion is the most common and costliest distress and has been accelerated by the increase in the use of deicing salts containing chlorides. For longevity, harmful solutions should be kept away from concretes, and this can be achieved by using low-permeability concretes.[2] Such concretes can be categorized as high-performance concrete (HPC), since HPC is expected to provide enhanced workability, durability, strength, and/or dimensional stability.[3] In Virginia, and other parts of the country where cycles of freezing and thawing take place, concretes exposed to the environment must also have the proper air-void system.

To achieve low permeability, pozzolans and slag are used and the water-cementitious material ratio (W/CM) is kept below 0.45.[4] Pozzolanic material and slag generally improve the ultimate strength of conventional portland cement concrete. Sometimes, ultimate strengths higher than those attained by using pozzolans and slag in ordinary mixtures are needed, especially in prestressed beams. In such applications, W/CM is reduced to very low values of about 0.30 or below.[5] These modifications result in high compressive strengths that together

[a] State Structure and Bridge Engineer, Virginia Department of Transportation, 1401 East Broad Street, Richmond, Virginia 23219
[b] Research Scientist, Virginia Transportation Research Council, 530 Edgemont Road, Charlottesville, Virginia 22903

with low permeability result in more economical structures, initially by reducing construction costs through increased span lengths and the use of fewer beams and, in the long term, by reducing maintenance costs through increased durability.[6,7]

For the 1995-97 construction season, VDOT selected seven HPC bridge structures, as shown in Table 1. The new low permeability specification was planned for five. The first two bridges given in Table 1 are complete. The first bridge had the low-permeability requirement for all the concrete. The beams of the seventh bridge will have a compressive strength of 69 Mpa (10,000 psi) and will contain 15-mm (0.6 in) strands.

Table 1. Bridges with High-Performance Concrete

#	Location	L(m)	No. Spans	Span L (m)	Beam Type	Bms/ Span	Bm Str. MPa	Low Perm.
1	Rte. 40	97.5	4	24.4	IV	5	55	Yes
2	Rte. 629	365.8	12	30.5	IV	5	55	No
3	Telegraph Rd.	55.5	2	27.7	Steel			Yes
4	Rte. 10	654.4	22	27/30	IV	5	55	No
5	Rte. 250	16	1	16	II	20	48	Yes
6	Second Str.	27	1	27	IV	6	48	Yes
7	Virginia Ave.	45.1	2	22.6	III	5	69	Yes

The first HPC bridge in Virginia, with both low permeability and high strength in the prestressed beams, was constructed in 1995 on Rte. 40 over the Falling River in Campbell County. The prestressed beams of the first two bridges were fabricated with a release strength of 41 MPa (6,000 psi) and a 28-day strength of 55 MPa (8,000 psi). All of the concrete placed in this structure met the permeability requirement. Mixture proportions and the requirements for air content and strength for the prestressed beams and cast-in-place substructure and deck concretes are given in Table 2. The coarse and fine aggregates were crushed limestone. In the substructure and deck, the coarse aggregate was crushed arch marble, and the fine aggregate natural sand.

A total of 20 AASHTO Type IV beams were placed with a compressive strength of 55 MPa (8,000 psi) instead of 28 AASHTO Type IV beams with a strength of 41 MPa (6,000 psi). VDOT generally uses a minimum 28-day design strength of 35 MPa (5,000 psi), and strengths as high as 41 MPa (6,000 psi) have been specified. The bridge construction costs per square meter

of deck surface was $527, less than the 1994 average cost of $624 for 34 bridges in the federal-aid highway system in Virginia.

Table 2. Mixture Proportions and Requirements for the First and Second Bridge

Item	First Bridge			Second Bridge
	Beam	Substructure	Deck	Beam
Portland Cement (kg/m^3)	446	209	195	303
Silica Fume (kg/m^3)	31	---	---	---
Slag (kg/m^3)	---	139	195	202
Coarse Aggr. (kg/m^3)	994	1056	1052	1157
Coarse Aggr. Size	#67	#57	#57	#68
Fine Aggr. (kg/m^3)	846	772	696	586
W/CM	0.32	0.44	0.40	0.33
Air (%)	5.5±1.5	6±2	6.5±1.5	5.5±1.5
28-d design str. (MPa)	55	21	28	55

In the second bridge, on Rte. 629 over the Mattaponi River, only the beams were specified to be HPC. AASHTO Type IV beams were used with a compressive strength of 55 MPa (8,000 psi) instead of an equal number of larger AASHTO Type V beams with a strength of 41 MPa (6,000 psi). Sixty beams were cast, and all were steam cured. The mixture proportions are given in Table 2. Cementitious material was finely ground Type II cement and slag. The coarse aggregate was crushed granite. The fine aggregate was natural sand. Based on a single cylinder from each of the 60 batches, the average strength at release was 45.1 MPa (6,500 psi), with a standard deviation of 4.0 MPa (580 psi), and 61.4 MPa (8,900 psi), with a standard deviation of 3.2 MPa (460 psi) at 28 days. Extra cylinders were available from two batches and were tested for permeability. The values, as an average of two specimens, were 323 and 536 coulombs at 6 weeks. The bridge construction cost per square meter of deck surface was $511.

The bridge carrying Virginia Avenue over the Clinch River in Richlands, Virginia is currently under construction. This structure has two 22.6-m (74 ft) spans, designed to be continuous for live load, and has high strength, low permeability concrete in all its components, details of which are shown in Table 3. The prestressed beams were designed with a concrete strength of 69 MPa (10,000 psi) and 15 mm (0.6 in) prestressing strands, at a 51 mm (2 in)

spacing. The use of the larger prestressing strands allowed for an increase in the prestressing force, thereby fully utilizing the high-strength concrete as well as avoiding steel congestion by reducing the number of strands required. Selected beams have been instrumented to monitor internal concrete

Table 3. Specification details of the Richlands Bridge.

Element	Compressive Strength Mpa (psi)	Chloride Permeability Coulombs
Beams	69 (10,000)	1,500
Deck	41 (6,000)	2,500
Substructure	21 (3,000)	3,500

temperatures, internal concrete strains, long term deflections, strand transfer length, and strand end slip. The goals of this long term monitoring are:

1. investigate the accuracy of the prestress loss calculations done for these beams
2. compare the measured transfer lengths of the beams to the recommended equations in the literature

The prestress loss and the subsequent camber and deflection calculations were done according to the AASHTO *Standard Specifications for Highway Bridges*[8] which do not include provisions for the use of HPC.

Aluminum

The Reynolds Metal Company (Reynolds) has developed an aluminum bridge deck system which has been installed on Route 58 in Mecklenburg County, Virginia. Aluminum has been recognized as a high performance material by the AASHTO Subcommittee for Bridges and Structures for use in bridges. It offers several advantages when used in bridge decks, such as a higher strength to weight ratio and improved corrosion resistance. Traditional reinforced concrete bridge decks weigh approximately 5.7 kPa (120 pounds per square foot), while aluminum decks weigh between 0.9 and 1.2 kPa (18 and 25 pounds per square foot). A bridge that has been determined to be structurally deficient and thus posted for a certain maximum load could benefit from an aluminum deck which may increase its live load capacity by decreasing the dead load of the structure. It has been estimated that a posted bridge with an aluminum deck retrofit could be upgraded by 30 to 40 percent. Furthermore, the time required to install an aluminum deck system will be much shorter than for conventional construction. Aluminum deck panels can be fabricated off-site and then shipped and placed very rapidly, reducing the costs associated with traffic control as well as user costs associated with delays and detours. Maintenance costs may also be reduced, because of aluminum's high corrosion resistance.

The deck is comprised of extruded multi-void shapes which are welded together at the sides to form a voided, or cellular deck. The aluminum alloy is 6063-T6, which has a minimum tensile yield strength of 172.4 MPa (25 ksi) and a minimum tensile ultimate strength of 206.8

MPa (30 ksi). The webs of each extrusion intersect the flanges to create a truss. After welding, the webs of adjacent extrusions act together to extend the truss, thereby creating a deck with substantial strength in the direction transverse to the extruded direction. The decks are shop-coated with a 9.53 mm (3/8 inch) nominal thickness epoxy-based wearing surface. The weight of the aluminum portion of the deck is about 0.96 kPa (20 lb/ft^2), and the wearing surface adds another 0.24 to 0.29 kPa (5 to 6 lb/ft^2). The decks could be fabricated in panels as large as can be shipped, which for highway shipments is about 4.3 m (14 feet) wide by 36.6 m (120 feet) long.

Two basic extruded shapes have been investigated, each of which has been designed to resist AASHTO HS-20 loading: a two-void shape, shown in Figure 1(a); and a three-void shape, which is shown in Figure 1(b). The two-void shape is lighter in weight, but the local bending stresses in the three-void shape are significantly lower, making it a more favorable choice. The two-void shape is being used on the superstructure replacement of the Route 58 bridge. Future decks will probably employ the three-void shape which is currently being tested.

The deck is nearly isotropic rather than fully isotropic because the rigidity in the extruded direction is about 15% greater than in the direction transverse to the extrusion. Thus , the preferred orientation of the extrusions is parallel to the girders. This helps both the strength and the fabricability of the deck. The orientation of the extrusions enhances the allowable stress capacity of the top fiber of the aluminum deck, which is subjected to System I (longitudinal bending) stresses resulting from the composite action with the underlying girders. The longitudinal orientation also allows for accommodation of roadway crowns and skewed supports. However, even in the transverse direction the deck possesses rigidity similar to a typical 203 mm (8 in) concrete slabs in use today. Torsional stiffness of the deck is also comparable to that of a typical 203 mm (8 in) concrete slab.

Several methods of compositely connecting a steel beam or girder with an isotropic aluminum deck are available. Each of the methods provides distinct advantages. One method allows for shop attachment of the deck and girders. An aluminum plate, welded to the bottom of the deck, is bolted with galvanized A325 bolts directly to the top flange of the coated steel beam. Other attachment methods are field-based and involve filling the connection area between the

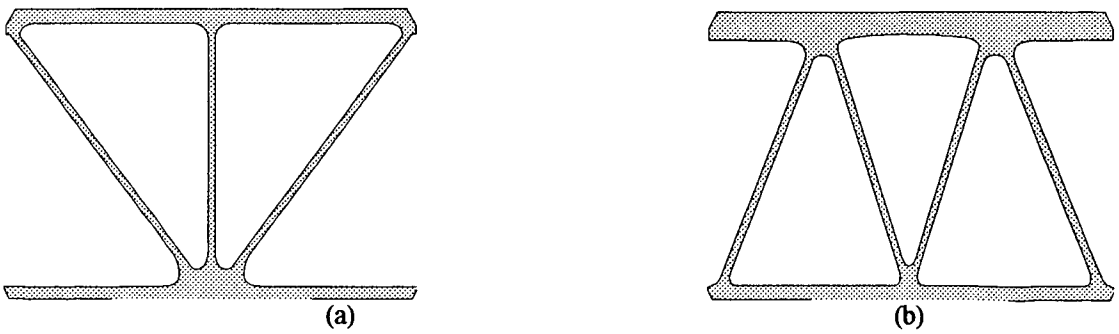


Figure 1. Schematic illustrations of two aluminum extruded shapes: (a) two-void design and (b) three void design.

Table 4. Elastic load case configurations.

Load Case	Description
1	Simply-supported on four sides with all supports located 152 mm (6 inches) from the panel edges. A single load patch was applied to the center of the panel.
2	Simply-supported on the two 3.66 m (12 foot) sides and simply-supported on one of the 2.74 m (9 foot) sides with all supports located 152 mm from the panel edges. Freely constrained on the second 2.74 m side. A single load patch was applied to the center of the panel.
3	Simply-supported on the two 2.74 m sides with all supports located 152 mm from the panel edges. Freely constrained on the two 3.66 m sides. A single load patch was applied to the center of the panel.
4	Clamped through 152 mm of one of the 3.66 m sides and simply-supported along the length 1.52 m (5 feet) from the fixed edge. Freely constrained on the second 3.66 m side and on the two 2.74 m sides. A single load patch was applied so that its center was 0.31 m (1 foot) from the edge of the unconstrained long side.
5	Clamped through 152 mm of one of the 2.74 m sides and simply-supported along the width 2.13 m (7 feet) from the fixed edge. Freely constrained on the second 2.74 m side and on the two 3.66 m sides. A single load patch was applied so that its center was 0.31 m from the edge of the unconstrained short side.
7	Simply-supported on the two 3.66 m sides with all supports located 152 mm from the panel edges. Freely constrained on the two 2.74 m sides. A single load patch was applied to the center of the panel.

deck panel and shear studs on top of the girder with grout.

The Virginia Transportation Research Council, with support from the Federal Highway Administration, has initiated a three part study to evaluate the aluminum deck system. The first phase involved structural testing and evaluation of a 2.74 m x 3.66 m (9 feet x 12 feet) deck panel. The structural testing was conducted at the Federal Highway Administration (FHWA) Turner-Fairbank Research Center's Structures Laboratory. Several tests were conducted in which the panel was loaded to its design limit and with various support conditions. A final test to failure was conducted. The second phase involves a series of static and dynamic load tests on the completed Route 58 structure. The third phase will focus on the long term durability of the deck system

The laboratory panel was subjected to seven distinct elastic load case tests and two ultimate load case tests. Six of the seven elastic load tests involved a single load patch, and their support conditions are given in Table 4. The support conditions of the sixth elastic load case were identical to that of Load Case 7; however, two load patches were applied to the panel. The center of each patch was located 0.91 m (3 feet) from the center of the panel along its width. Figure 2 shows schematic drawings of Load Cases 1, 6, and 7.

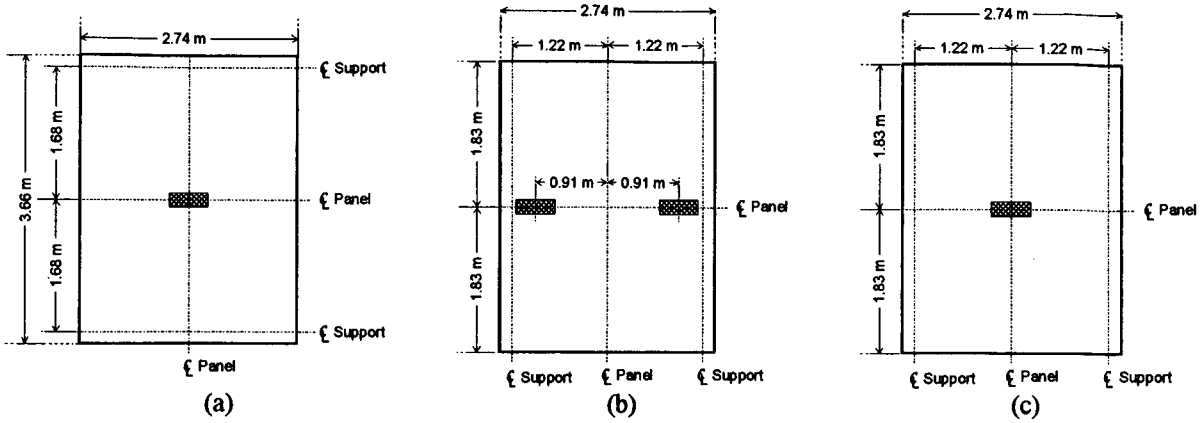


Figure 2. Schematic illustrations of constraints and load patch placement for (a) Load Case 3, (b) Load Case 6, and (c) Load Case7.

Each of the load patches were 508 mm (20 inches) in length and 216 mm (8.5 inches) wide to coincide with the AASHTO LRFD Bridge Design Specifications. All of the load patches were oriented with their shorter side parallel to the longitudinal axis of the deck panel (as shown in Figure 2). The elastic tests were conducted with an applied load of up to approximately 102 kN (23 kips). The photograph in Figure 3 shows the panel being tested under one load/constraint configuration.

Strain gauge rosettes were oriented at the top and bottom of the panel along the transverse and longitudinal center lines. Deflection gauges were placed on the bottom of the panel. For Load Cases 1 to 3, 6, and 7, deflections were measured along the longitudinal and transverse center lines. For Load Case 4, deflection gages were placed along the transverse center line and at the unconstrained long edge, and for Load Case 5 the gages were oriented

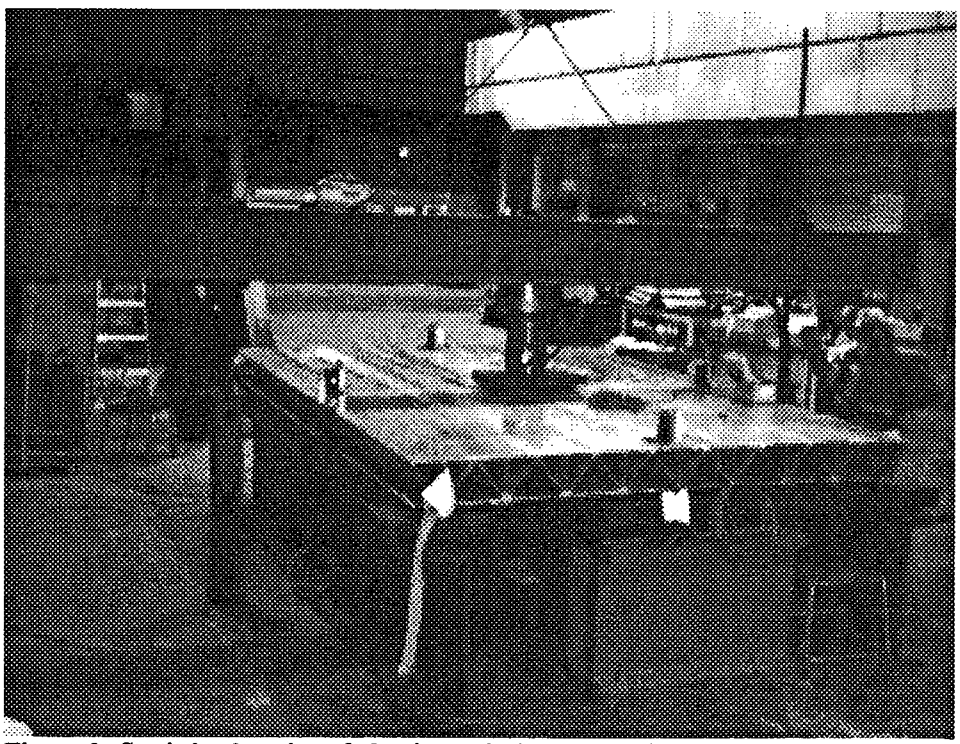
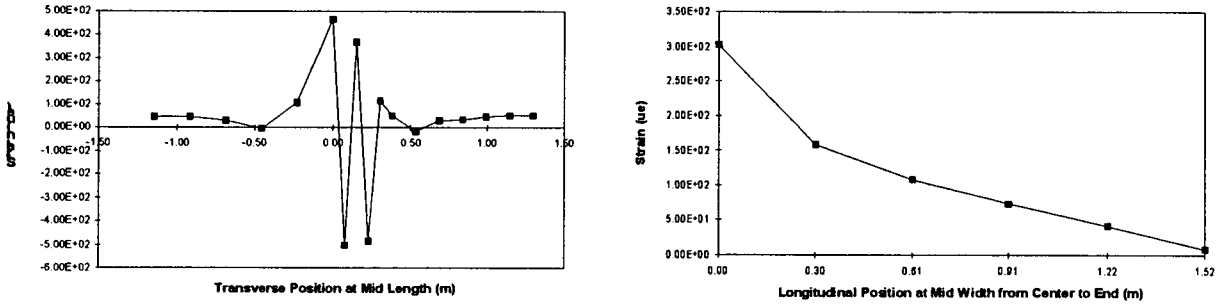


Figure 3. Static load testing of aluminum deck panel section.

along the longitudinal center line and at the unconstrained short edge.

The greatest deflections were measured for Load Cases 4 and 5 which employed the clamped constraints. These deflections occurred at the midpoint of the free edges and were -13.92mm (-0.548 inches) and -11.99 mm (-0.472 inches), respectively. Of the simply-supported scenarios, Load Case 3 had the greatest measured deflection of -2.87 mm (-0.113 inches). Each of the other load cases had maximum measured deflections below 2.54 mm (0.1 inches); however, no deflection data was recorded for Load Case 2.

The strain data suggest that local bending effects occurred under the load patch. Excessive tensile strain measurements on the top of the panel at the location of the load may be explained by the occurrence of transverse bending between the vertical and diagonal inner truss members of the panel. For example,Figure 4(a) shows the transverse strains across the width of the panel top at mid length for Load Case 3, and Figure 4(b) shows the longitudinal strains along



(a) (b)

Figure 4. Strains measured during Load Case 3: a) Transverse strains at top of panel at mid length and b) Longitudinal strains at bottom of panel at mid width.

the length of the panel from center to end for the same load case. These strains were measured under an applied load of 102.3 kN (23 kips). It can be seen from these figures that the local tensile strains at the top of the panel are actually greater than the global tensile stresses on the panel bottom . Table 5 shows the ratio of maximum global tensile strain (bottom of panel) to maximum local tensile strain (top of the panel) for all load cases other than those with a cantilever configuration. It can be seen that in each of these cases the local bending strains are of greater magnitude than the global bending strains.

Table 5. Ratio of maximum local to global strains for each elastic load case.

Load Case	Load (kN)	Local Tensile Strain (ue)	Global Tensile Strain (ue)	Ratio of Local to Global strain (ue)
1	102.3	372	224	1.66
2	102.3	369	230	1.60
3	102.3	464	302	1.54
6	102.3	284	183	1.55
7	97.9	314	207	1.52

After completing the elastic tests described above, the panel was tested to failure. The same loading configuration for Load Case 7 was used to perform the initial overload test. The panel was continuously loaded to 556 kN (125 kips). Then the test was paused for apparatus readjustments. The test was then continued, and the panel was loaded to 823 kN (185 kips). At an applied load of 832 kN (187 kips), local buckling under the load patch occurred. At 881 kN (198 kips), "punching" failure occurred under the load patch. Figure 5 shows the longitudinal strain on the bottom of the panel at its center and the transverse strain on the top of the panel at the center (under the load patch). This shows that the ratio of local to bending strain increases as

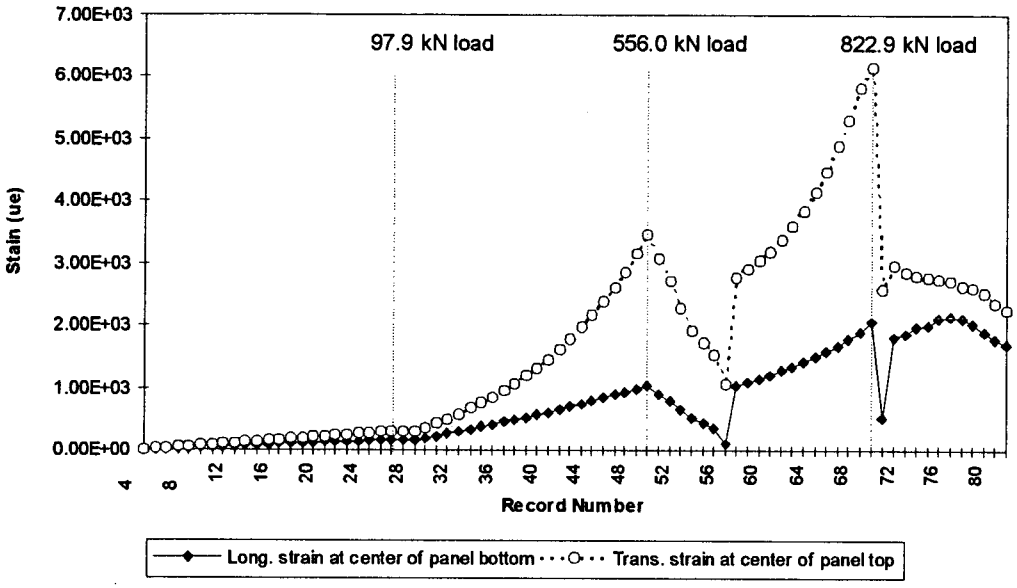


Figure 5. Transverse strains at center of panel top and longitudinal strains at center of panel bottom during ultimate load test.

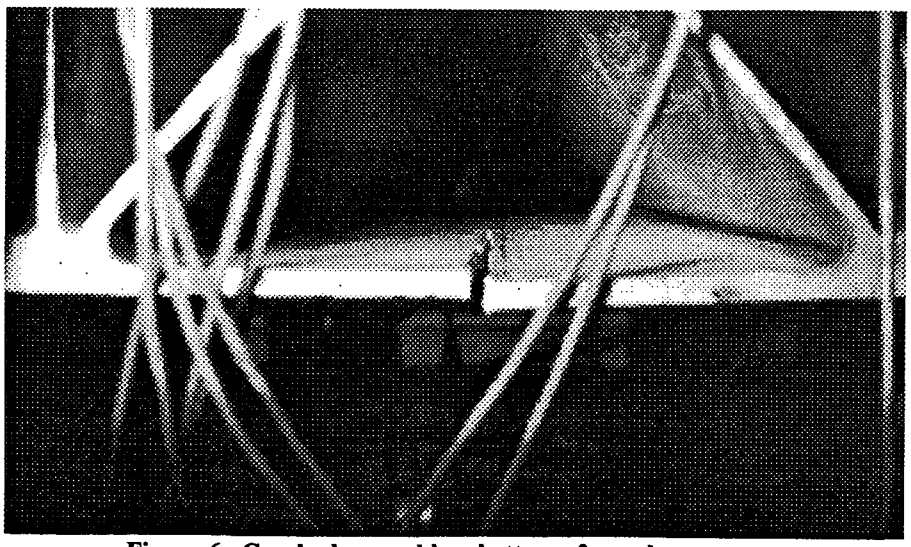


Figure 6. Crack along weld on bottom of panel.

the applied load approaches its ultimate value. At 185 kips, this ratio had risen to a value of 2.995. Consequently, the strains due to the local bending effect controlled the first failure mode.

Another test was run using two load patches oriented along the longitudinal axis with their centers 635 mm (25 inches) from the center of the panel. Equivalent loads were applied to each of the patches in 22.24 kN (5 kip) increments. At a combined load of 1441 kN (324 kips), total weld failure occurred at the bottom of the panel, as shown in Figure 6.

Composite Materials

The Tom's Creek Bridge, located in Blacksburg, Virginia, is owned and maintained by the Town of Blacksburg. Recent inspections of the bridge have revealed significant section loss in several of the steel stringers. It is expected that the road will be widened within the next 10 years. Thus, the bridge will be replaced. Until that time, the town is looking for a short term fix. The Town agreed to replace the bridge with an experimental bridge structure designed with beams made entirely from composite materials.

Researchers at Virginia Tech, in conjunction with Morrison Molded Fiber Glass (MMFG) of Bristol, Virginia, have identified a pultruded composite beam that structurally meets the needs of the repair. The beam, developed by MMFG & Georgia Tech, is a small scale prototype of a potential beam that would meet the AASHTO standards for future bridge construction (Figure 7). This new concept in composite structural design was developed under the National Institute of Standards and Technology's Advanced Technology Program. This is one of the first applications of composite materials as the primary load-carrying element for a bridge subjected to vehicular traffic in the United States.

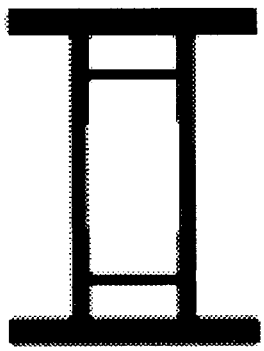


Figure 7. Composite Beam Cross Section.

Composite materials, produced from polymer resins and high strength fibers, have the potential to be effective construction materials because of their corrosion resistance and high strength-to-weight ratio. However, very little data exist on the synergistic effects of vehicular loads and actual environmental conditions, factors which cannot be duplicated in the laboratory. A team of civil engineers, chemists, and composite material engineers from Virginia Tech, the

Virginia Transportation Research Council, and the Structure and Bridge Division of the Virginia Department of Transportation have collaborated to develop a testing protocol to examine the durability of composite materials in actual field conditions.

The Town Engineer of Blacksburg agreed to use these innovative, all-composite material beams in the replacement of the Tom's Creek Bridge, provided an engineer of record completed the structural design. The Structure and Bridge Division for the Virginia Department of Transportation agreed to provide this service.

A field test of the Tom's Creek Bridge will be conducted with a vehicle of known weight. The bridge will be instrumented with various transducers and subjected to static and dynamic loading with a vehicle of known weight.
The goals of this project are as follows:

1. To establish a baseline of behavior of this innovative structure under known live loads for comparison with future load tests to assess its long-term structural adequacy.
2. To compare to load tests previously conducted on the structure in the Structures Laboratory at Virginia Tech.
3. To establish a response/behavior benchmark to calibrate a finite element model. The finite element model, once calibrated with actual response data, will be used to predict overload behavior and possible failure modes. The finite element model has been developed by researchers at Virginia Tech.

CONCLUSIONS

High Performance Concrete

Air-entrained HPCs with very low permeability values have been achieved with the use of a pozzolan or slag at W/CM below 0.45. Additionally, workable air-entrained HPCs with high early strength (exceeding 41 MPa {6,000 psi} at release) and ultimate strength with very low permeability (exceeding 55 MPa {8,000 psi} at 28 days) have been successfully made on a production basis. Higher early and ultimate strengths (exceeding 55 MPa {8,000 psi} at release and exceeding 69 MPa {10,000 psi}at 28 days) were produced using locally available materials for test beams. Proper temperature management is essential to achieve high early and ultimate strengths.

Aluminum

The first phase of this project involved elastic and ultimate load testing of a 6063-T6 aluminum two-void design deck panel section. The panel was tested under seven distinct elastic load cases using an applied load designed to simulate an AASHTO HS-20 loading. Tensile strains caused by localized bending under the applied load were detected. These strains were frequently greater in magnitude than the maximum tensile strains due to global bending.

Maximum tensile strains recorded during the elastic testing corresponded to stresses less than 15 percent of the material yield stress. Overload testing was also performed. The first local failure mode occurred at 881 kN (198 kips). This failure occurred under the load patch in a region exhibiting relatively high strain due to localized bending effects. Strains in the vicinity of this region at failure were measured at approximately 6000 ue. A second load patch was applied to lessen the local buckling effects and final failure occurred at the center weld on the bottom of the panel at a combined load of 1441 kN (324 kips).

The second phase of this project involves a series of static and dynamic load tests on the completed Route 58 structure. The construction has been completed and load testing was conducted in July, 1997. The third phase will focus on the long term durability of the deck system. In the Fall of 1997, full-scale fatigue testing of a three-void design deck panel will be conducted at Virginia Polytechnic Institute in Blacksburg, VA.

Composite Materials

The Tom's Bridge was replaced and traffic allowed to return in one week. Prior to field installation, the entire bridge structure was built in the Structures Laboratory at Virginia Tech and subjected to a series of load tests. Additionally, a single composite beam was tested to failure. Results of these tests will be forthcoming in another publication. Long term monitoring of the structure has begun. The field test will be conducted in late summer, thus results were not available for this publication.

ACKNOWLEDGEMENTS

Studies reported here were conducted by the Virginia Transportation Research Council of the Virginia Department of Transportation, and Virginia Tech and sponsored by the Federal Highway Administration. The authors wish to acknowledge the Reynolds Metal Company for the development of their innovative deck system. The authors wish to acknowledge the efforts of researchers at Virginia Tech in the successful construction of the Tom's Creek Bridge. The authors are also grateful to the technical staff at the Turner-Fairbank structures lab for their test setup and instrumentation efforts. The opinions, findings, and conclusions expressed in this paper are those of the authors and not necessarily those of the sponsoring agency.

REFERENCES

1. Ozyildirim, C. 1993. Durability of Concrete Bridges in Virginia. *ASCE Structures XI Proceedings: Structural Engineering in Natural Hazards Mitigation.* American Society of Civil Engineers, New York, pp. 996-1001.

2. Ozyildirim, C. 1993. High-Performance Concrete for Transportation Structures. *Concrete International*, Vol. 15, No. 1, pp. 19-26.

3. Zia, P., Leming, M. L., Ahmad, S. H., Schemmel, J. J., Elliott, R. P., and Naaman, A. E. 1993. *Mechanical Behavior of High Performance Concretes. Volume 1. Summary Report.* SHRP-C-361. Strategic Highway Research Program, Washington D. C.

4. Ozyildirim, C. 1994. Resistance to Penetration of Chlorides into Concrete Containing Latex, Fly Ash, Slag, and Silica Fume. *ACI SP-145, Durability of Concret.,* American Concrete Institute, pp. 503-518.

5. Ozyildirim, C., Gomez J., and Elnahal, M. 1996. High Performance Concrete Applications in Bridge Structures in Virginia. *ASCE Proceedings: Worldwide Advances in Structural Concrete and Masonry.* American Society of Civil Engineers, New York, pp. 153-163

6. Lane, S. N., and Podolny, W. 1993. The Federal Outlook for High Strength Concrete Bridges. *PCI Journal,* Vol. 38, No. 3.

7. Bruce, R. N., Russell, H. G., Roller, J. J., and Martin, B. T. 1994. *Feasibility Evaluation of Utilizing High-Strength Concrete in Design and Construction of Highway Bridge Structures.* LA-FHWA-94-282. Louisiana Transportation Research Center, Baton Rouge.

8. *Standard Specifications for Highway Bridges, Fifteenth Edition,* 1992, American Association of State Highway and Transportation Officials, Inc., Washington, D.C.

TEST METHODS AND LONG-TERM BEHAVIOR OF POLYMER COMPOSITES FOR BRIDGE STRUCTURES

A. Zureick[1]

Abstract

This paper outlines some highlights of an investigation aimed toward the development of an accelerated test methods for determining the long-term behavior of fiber-reinforced polymer composite structures. The work included the development of new destructive and non-destructive test methods for examining the engineering properties of civil engineering polymeric composite materials as well as the generation of short- and long-term design data for composites subjected to a variety of mechanical and environmental loading conditions.

Introduction

In 1993, The Federal Highway Administration embarked on a research program aimed toward the development of accelerated test methods for determining the long-term behavior of fiber-reinforced polymer (FRP) composites for bridges; the purpose of the study is to provide future researchers with test methods acceptable to the highway bridge design community to examine the behavior of such materials and structures so that design criteria can be developed.

Because of the considerable interest in using polymeric composites for new construction and also for the rehabilitation of existing structures, it was deemed necessary to devote the attention to:

1- Test methods for the mechanical loading of stand-alone FRP composite material structures; this included creep, fatigue and impact and non-destructive tests. The effects of temperature and moisture fluctuations that do not cause irreversible material degradation were also considered.

2- Test methods for the mechanical characterization of FRP/concrete hybrid structural materials to examine the mechanism of interaction between FRP reinforcement and concrete for both prestressed and non-prestressed systems.

3- Test methods for the environmental loading of stand-alone FRP materials and FRP/concrete hybrid materials where the concern was with irreversible material degradation, damage and deterioration in the presence of adverse exposure and environmental conditions.

[1] School of Civil & Environmental Engineering, Georgia Institute of Technology, Atlanta, GA 30332.

Brevity precludes a complete presentation of the results obtained from all the aforementioned tasks. Thus, only selective tasks pertaining to the first of the above three categories will be presented

Test Methods

Destructive Test Methods: Destructive test methods were developed for the determination of the in-plane properties of composites. These test methods were based upon current ASTM Standards (ASTM D3039, ASTM D341, and ASTM D5379) that required many modifications to better represent the inhomogeneous materials at hand. These modifications varied in degree with most effort being devoted to the determination of the in-plane shear properties. The newly developed in-plane shear test adopts a specimen whose basic geometry and loading system are shown in Figure 1. The overall length of the specimen is 20.3 cm (8.0 in.) and the height is 3.81 cm (1.5 in.). The outside loads, P_e, are 15.2 cm (6.0 in.) and the inside loads, P_i, are 5.08 cm (2.0 in.) apart. Loading pads of 2.54 cm (1.0 in.) locally distribute the applied forces. This specimen and loading system are very similar to those devised by Iosipescu (1967) for producing a region of essentially pure shear in the central notch region.

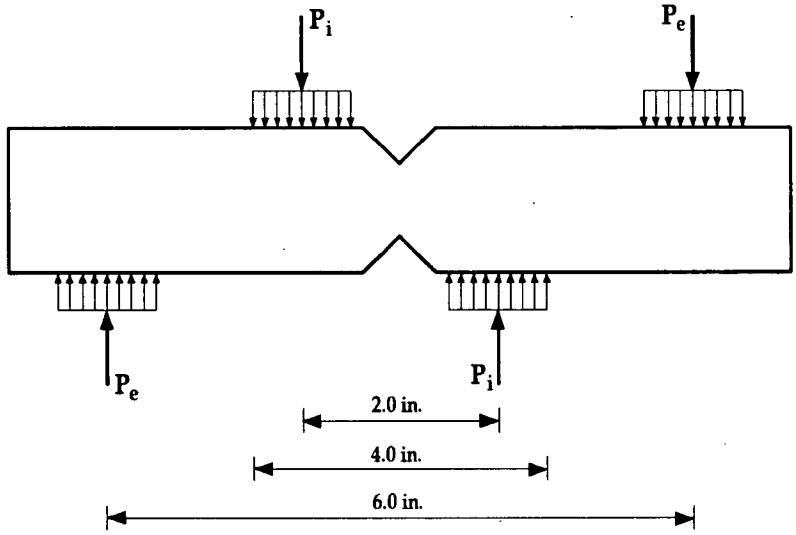


Figure 1: Specimen loading application system

This specimen and test configuration were used in a series of experiments (Zureick et al. 1997) to study the shear stresses in the various principal planes of pultruded plate material. Electrical

resistance strain gages were used. The results showed very low extensional strains compared to shear strains, especially in the plane of the plate with the fibers horizontal in the specimen.

The loading system and the size of the specimen are different from those used in the ASTM shear test. The size in the specimen plane is twice as large as that of the ASTM specimen. The larger size is chosen to reduce the effect of the inherent heterogeneity of the material (Wang and Zureick 1995). This is evident in the roving spacing, which is somewhat variable, and which is of the order of 1.5 mm (0.06 in.). (The distance between the notches is 2.54 cm (1.0 in.), but is only about twice as much in the ASTM specimen.). Furthermore, the test retains the specific load application locations used by Iosipescu (1967), compared to the flat platen used on the upper and lower specimen surfaces in the ASTM test. A typical shear stress-strain diagram resulting from this new test is shown in Figure 2.

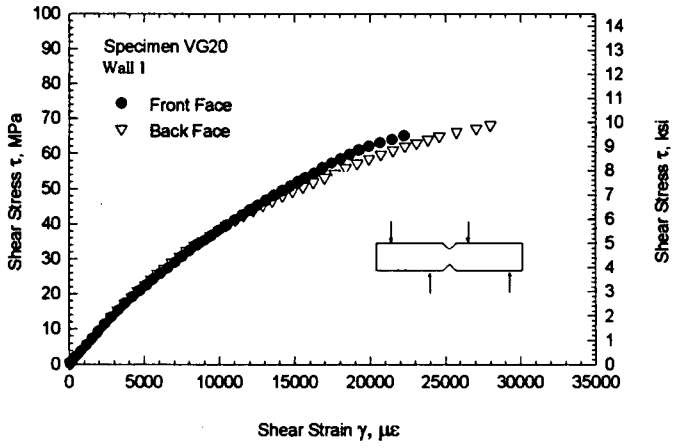


Figure 2: Typical In-Plane Shear Stress-Strain Response of FRP Materials

Nondestructive Test Methods: Under this part of the experimental investigation, new nondestructive techniques were developed to estimate the engineering constants of pultruded specimens using ultrasonic methodologies (Littles, Jacobs, and Zureick 1995; Jacobs, Littles, and Zureick 1996a, 1996b). These ultrasonic methods have several advantages over mechanical tests: all of the engineering constants are measured for a single specimen; the measurements are made over a "local" volume of material, so it is possible to evaluate small specimens (i.e., the transverse

dimension of a 101.6 mm. by 101.6 mm angle). Due to the finite size of strain gages (approximately 0.125 in^2), the actual strain values recorded in mechanical tests are from a small area of the composite material. However, the strain experienced by this finite location is influenced by the surrounding material, (since the entire specimen is being loaded) resulting in more of an average value. The ultrasonic wave speeds are only influenced by the material through which the wave passes; these ultrasonic techniques provide much more of a local measurement. Another benefit of the local measurements is that spatial variations within a specimen can be observed. Further, these ultrasonic techniques do not destroy the specimen, so there is the potential for in-service monitoring of components or tracking time-dependent material properties in long term tests.

First, an ultrasonic immersion technique is applied to measure the phase velocities of ultrasonic waves that travel through the FRP specimens. These phase velocities are then used to calculate the components of the stiffness matrix. The engineering constants, which are the preferred material constants for structural design, are then calculated from the components of the stiffness matrix. The validity and accuracy of these values is determined through comparisons with the results from mechanical tests. The immersion technique is also used to ascertain the degree of spatial variation of this material; engineering constants are measured at several locations parallel to, and perpendicular to, the pultrusion (fiber) direction.

There are several limitations to ultrasonic immersion techniques, the most significant of which is that the specimen must be immersed in a water tank. As a result, it is impractical to use this immersion technique to monitor large components. Further, due to significant variation in one of the elastic constants obtained using the immersion technique, another relationship between this constant and an ultrasonic wave speed is sought. Therefore, a second ultrasonic technique is developed. This technique uses surface acoustic wave speeds for material characterization. These surface acoustic waves are generated and detected optically with a Q-switched, pulse laser and a heterodyne interferometer, respectively. A third technique, which also uses surface acoustic waves, is developed that measures all five of the independent elastic constants of a transversely isotropic material, when access to only one side of the specimen is available. Surface acoustic wave methods have great potential for applications where immersion is impractical; this research was a vital step toward the development of a technique for the "in-service" monitoring of polymeric composite structural components.

Long-Term Design Data

The long-term design data generated under this research program included the in-plane uniaxial strengths and moduli of pultruded composite materials under various mechanical and environmental loading conditions. Only the conclusion related to the compression creep test results will be presented in this paper.

The prediction of the long-term behavior of the longitudinal modulus was based on a series of compression coupon tests subjected to three different stress levels for time duration up to 10,000 hours. The three stress levels corresponded to approximately 20%, 40%, and 60% of the short-term compressive strength. All experiments were conducted in dead-weight lever-arm creep fixtures developed to apply compression loads to the coupons. The fixtures were constructed from structural steel with pillow block roller bearings functioning as the fulcrum. The lever-arm was designed to magnify the load applied to the specimens by a factor of 10. Each fixture is capable of loading three coupons simultaneously at a desired constant load. A set of cages was constructed for each fixture to transfer the tensile load applied by the lever arm to each coupon as compression. Strain gages were attached to each coupon and data were recorded at specified time increments ranging from one minute to two weeks for the entire duration of the experiment.

Based upon the experimental results obtained from this creep experiment and from others (Holmes and Rahman 1980, Daniali 1991, Mosallam and Bank 1991, Bank and Mosallam 1992, Mottram, 1993, Scott, Lai, , and Zureick 1995, McClure and Mohammadi 1995) the following practical power law creep model (Findley 1944, Findley and Khosla 1956) is proposed for the design of E-glass/vinylester pultruded structures:

$$E(t) = \phi_t E_o \qquad (1)$$

Where ϕ_t is a time-dependent reduction factor given by

$$\phi_t = \frac{1}{1 + \frac{10}{\beta} t^{0.25}} \qquad (2)$$

In the above equations, t is the time in years and $\beta = \frac{E_t}{E_o}$ is a time-dependent parameter that can be found in general for any polymeric composite material using Findley's power law from creep tests of only 1,000 hours in duration. For a class of composite materials for which the composition of the resin system is similar to that of the Derakane 411, values of β are generally less than 80. Figure 3 shows the reduction in the longitudinal modulus as a function of time for the case in which $\beta = 60$. For t = 10, 25, 50, and 75 years, the estimated reduction in the longitudinal modulus will approximately be 23%, 27% , 30%, and 33% respectively.

AKNOWLEDGEMENT

This work is supported by the Federal Highway Administration under Contract No. DTFH61-93-C-0012. Mr. Eric Munley serves as Program Director. The author would like to thank Drs. J. Littles, Jr., L. Jacobs, D. Berghaus and D. Scott for their continuous input to the development of this program. This paper was originally published at the US-Canada-Europe

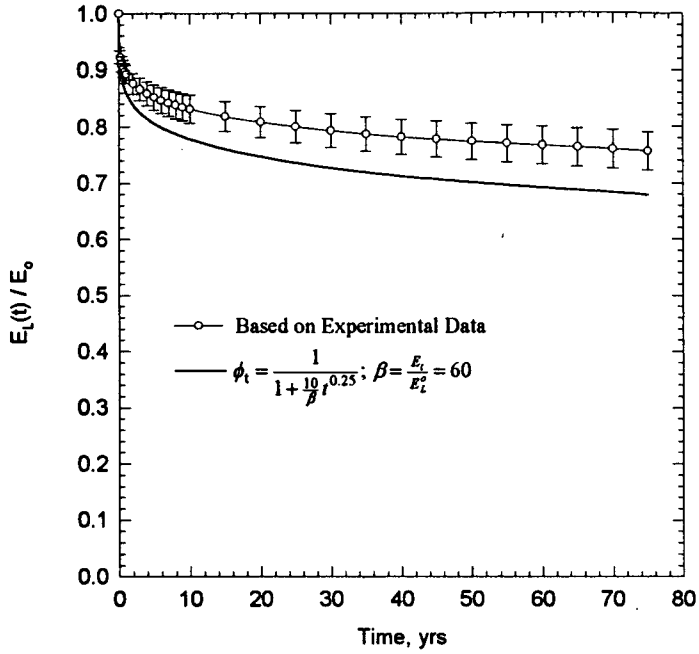


Figure 3: Time-reduction coefficient ϕ_t vs. time

References

Bank, L.C., and Mosallam, A.S. (1992), "Creep and Failure of a Full Size Fiber Reinforced Plastic Pultruded Frame," *Composites Engineering*, Vol. 2, No. 3, pp. 213-227.

Daniali, S. (1991). "Short-Term and Long-Term Behavior of Two Types of Reinforced Plastic Beams," 46th Annual Conference, Composites Institute, February 1991, pages. 13-A-1 through 5.

Findley, W.N. (1944), "Creep Characteristics of Plastics", 1944 Symposium on Plastics, ASTM.

Findley, W.N., and Khosla, G. (1956), "An Equation for Tension Creep of Three Unfilled Thermoplastics", *SPE Journal*, December, pp. 20-25.

Holmes, M., and Rahman, T.A. (1980), "Creep Behavior of Glass Reinforced Plastic Box Beams," *Composites*, No. 4, 1980, pages 797-802.

Iosipescu, Nicolae (1967). " New Accurate Procedure for Single Shear Testing of Metals," Journal of Materials, Vol. 2, No. 3, September, pages. 537-566.

Jacobs, L.J, Littles, J. and Zureick, A. (1996a). "Ultrasonic Characterization of FRP Composites for Bridge Applications," ASCE 11th Engineering Mechanics Conference, Fort Laderdale, Florida, May 19-22, 1996.

Jacobs, L.J, Littles, J. and Zureick, A. (1996b). "Ultrasonic Characterization of FRP Composites for Bridge Applications," ASCE 11th Engineering Mechanics Conference, Fort Laderdale, Florida, May 19-22, 1996.

Littles, J.W.; Jacobs, L.J. and Zureick, A.H. (1995). "Development of Nondestructive Evaluation Techniques for the Characterization of FRP Components," ASCE Structures Congress 1995, Boston, Massachusetts, April 3-5.

McClure, G., and Mohammadi, Y. (1995), "Compression Creep of Pultruded E-Glass-Reinforced-Plastic Angles", *Journal of Materials in Civil Engineering*, Vol. 7, No. 4, pages 269-276.

Wang, Y., and Zureick, A.H. (1994) "Characterization of the Longitudinal Tensile Behavior of Pultruded I-Shape Structural Members Using Coupon Specimens," *Composite Structures*, No. 29, pp. 463-472.

Mosallam, A.S., and Bank, L.C. (1991), "Creep and Recovery of a Pultruded FRP Frame", Advanced Composite Materials in Civil Engineering Structures, ASCE, Edited by S. Iyer and R. Sen, pages 24-35.

Mottram, J.T. (1993), "Short and long-term structural properties of pultruded beam assemblies fabricated using adhesive bonding," *Composite Structures*, March, pages 387-395.

Scott, D., Lai, J., and Zureick, A. (1995), "Creep Behavior of Fiber-Reinforced Polymeric Composites: A Review of the Technical Literature," *Journal of Reinforced Plastics and Composites,* Vol. 14, June, pp. 588-617.

Zureick, A. Berghaus, D., Cho, B. and Javidinejad, A. (1997). "The In-plane Shear Properties of Pultruded Composite Materials," Georgia Institute of Technology.

Experimental Study on Strengthening Effect of High-Modulus Carbon Fiber Sheet on Damaged Concrete Deck Slab

Tokitaro Hoshijima [1] , Hiromichi Sakai [2] , Hirofumi Otaguro [3] , Shigeyuki Matsui [4]

Abstract

A series of wheel trucking fatigue test was conducted on the intentionally-damaged reinforced concrete slab of highway bridges by changing the elastic modulus of carbon fiber sheet to confirm the durability improvement effect by carbon fiber sheet.

As a result of this experiment, it was found that the strengthening effect for the fatigue fracture was greatly improved by restricting the cracked surface movement by carbon fiber sheet bonding and restriction of the deck slab deformation due to the improvement of rigidity in section. And the durability improvement effect was higher in the test specimen with the carbon fiber sheet of higher elastic modulus.

1. Introduction

In Japan, the damage of the road bridge reinforced concrete deck slab (hereafter called "deck slab") has become a problem from the middle of 1960's, and then the study and examination have been done for the clarification of deck slab damage mechanism and the countermeasures against damage.

The deck slab damage mechanism results from the alternate shearing force and twisting moment acting on the distributing bar section caused by vehicle running and generates the penetrating crack in the axial direction of bridge, thus, permitting the load distributing action to be reduced in the axial direction of bridge and the main bar section becoming like beam among the penetrating cracks to be fractured by shearing force.

The complication in its process causes such a fracture to be called " Fatigue phenomenon " in a broad sense.

The following major methods established for strengthening the deck slab have been adopted.

① Stringer increasing method
② Steel plate attaching method
③ Slab thickness increasing method

There are many examples that these methods covered the damage perfectly, however, such a trouble occurred again. There is still room for improvement to establish the reliability on the complicated damage mechanism of deck slab. [1)]

1 General Manager,Mitsubishi Chemical Corporation
2 Dr.Eng.,Deputy General Manager,Mitsubishi Chemical Corporation
3 Assistant Manager,Mitsubishi Chemical Corporation
4 Dr.Eng.,Prof. of Civil Engineering., Osaka University

In this situation, the carbon fiber sheet bonding method attracts public attention as a deck slab strengthening method and necessitates a basic study. [2)]

In this study, the wheel load travelling fatigue test was executed on a reinforced deck slab by changing the elastic modulus of carbon fiber sheet (hereafter called " CFS ") to confirm the strengthening effect by CFS.

2. Content of experiment

2 - 1 Shape of test specimen

Fig. 1 shows the section and bar arrangement of the deck slab used for this experiment. The test specimen is of width 200cm (in the direction of main reinforcing bar) × length 300cm (in the direction of distributing bar) × thickness 18cm and has haunch at both longitudinal end supports.

All reinforcing bars are of D16. In the lower tension side, the main reinforcing bar was arranged at the interval of 10cm and the distributing bar was arranged at the interval of 12.5cm. In the upper compression side, the reinforcing bar was arranged at the interval twice as much as the lower tension side.

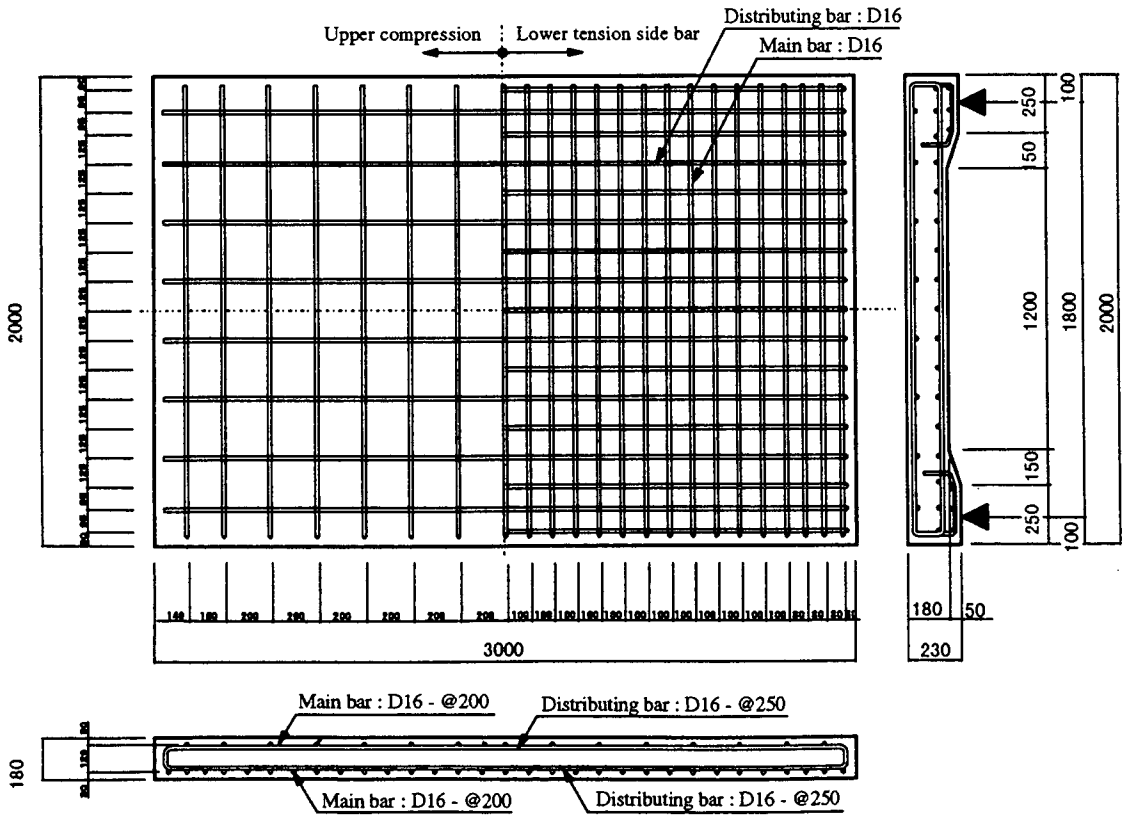


Fig. 1 Shape and bar arrangement of test specimen

2 - 2 Materials for experiment

Table - 1 Shows its physical properties. The reinforcing bar is of SD295.

Table - 1 Physical properties of reinforcing bar

Size	Yield point (N/mm ^{2})	Tensile strength (N/mm ^{2})	Elongation (%)
D16	365	524	22

The ready mixed concrete of 24 N/mm ^{2} (Specific design strength) was used. Table - 2 and Table - 3 show mix proportion and the physical properties, respectively. For Table - 3, curing was done as follows :

Test specimen of 28 days age :

Water curing in 20 ℃ .

Test specimen of 282 days age :

Air curing at the same condition as the storage of deck slab test specimen.

Table - 2 Concrete mix proportion

W/C (%)	s/a (%)	Unit (kg/m ^{3})				
		Water	Cement	Fine aggregate	Coarse aggregate	Admixture
55.0	44.9	172	313	786	1010	0.626

Table - 3 Physical properties of concrete Average of n=3

Age (days)	Compressive strength (N/mm ^{2})	Statically longitudinal Young's modulus (N/mm ^{2})
28	28.0	—
282	30.3	2.26×10^4

All materials used for bonding CFS are of epoxy-based resin. Table - 4 shows the type and quantity of resins. Putty was used for filling pin holes.

Table - 5 shows the physical properties of CFS.

Table - 4 Resins used for bonding CFS

Brand name	Quantity (kg/m ^{2})	Viscosity (mPa·s)
Primer	0.25	300
Putty	As needed	N/A
Bonding resin	0.60	3500

Table - 5 Physical properties of CFS

Brand name	Thickness (mm)	Tensile strength (N/mm ^{2})	Tensile Young's modulus (N/mm ^{2})
GM	0.167	3930	2.3×10^5
HM1	0.143	3000	4.7×10^5
HM2	0.143	2970	6.5×10^5

The physical properties of CFS show the test value as a hardened body.

2 - 3 Type of test specimens

Table - 6 shows the kind of test specimens. Four test specimens were manufactured for the test, that is, one unstrengthened and three strengthened concrete slab by bonding CFS in the direction of main bar, of distributing bar and every layer, respectively.

Table - 6 Kind of test specimens

Test specimen	The kind and method of reinforcement		
S - U	Not strengthened		
S - GM	Strengthened with CFS	GM	In the direction of main bar
S - HM1		HM1	In the direction of distributed bar
S - HM2		HM2	Every layer

2 - 4 Bonding CFS

Fig. 2 shows the process of bonding CFS. After inducing crack by preloading at the wheel load travelling test, the load was temporarily removed and the work for bonding CFS was done at the state of additional bonding to realize an execution in the actual deck slab under dead load (self weight). Any repair such as resin injection into crack was not done.

As shown in Fig. 3, CFS was bonded first in the direction of main bar and afterward in the direction of distributing bar. CFS was bonded to the haunch in the direction of main bar and to the bed end in the direction of distributing bar with each bonding area of 150cm × 300cm. The open area for mounting a crack measuring gauge was also strengthened by CFS having same width as the opening at both sides as shown in Fig. 4. Then, the strengthening sheet was bonded along the sheet length of 20cm beyond the open end.

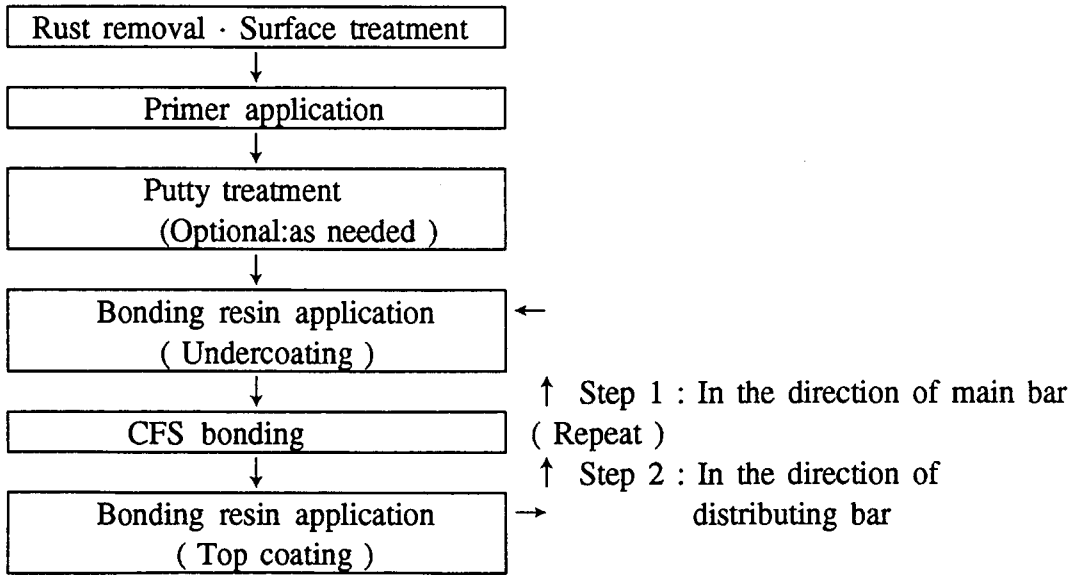


Fig. 2 CFS bonding process

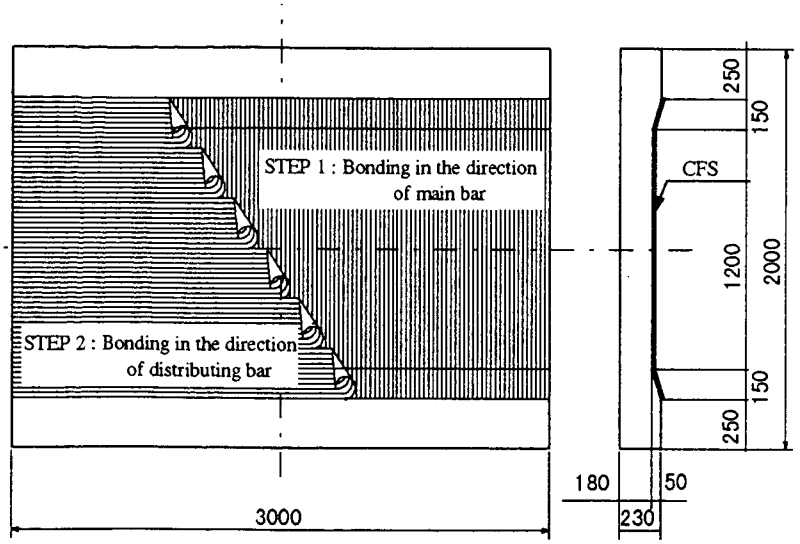


Fig. 3 CFS bonding situation

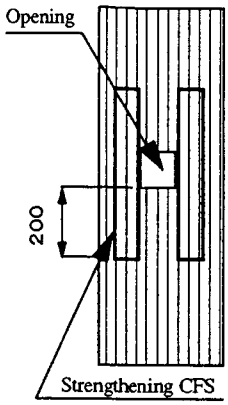


Fig. 4 Specifications for opening reinforcement

2 - 5 Experimental method

(1) Wheel trucking machine

The testing device is for simulating a wheel trucking machine acting directly on a deck slab. Fig. 5 shows the outline of the testing machine.

The testing machine is composed of the chassis running by applying load on the test specimen and the railway on which the chassis is reciprocated by motor rotation.

Table - 7 shows the features of the testing machine.

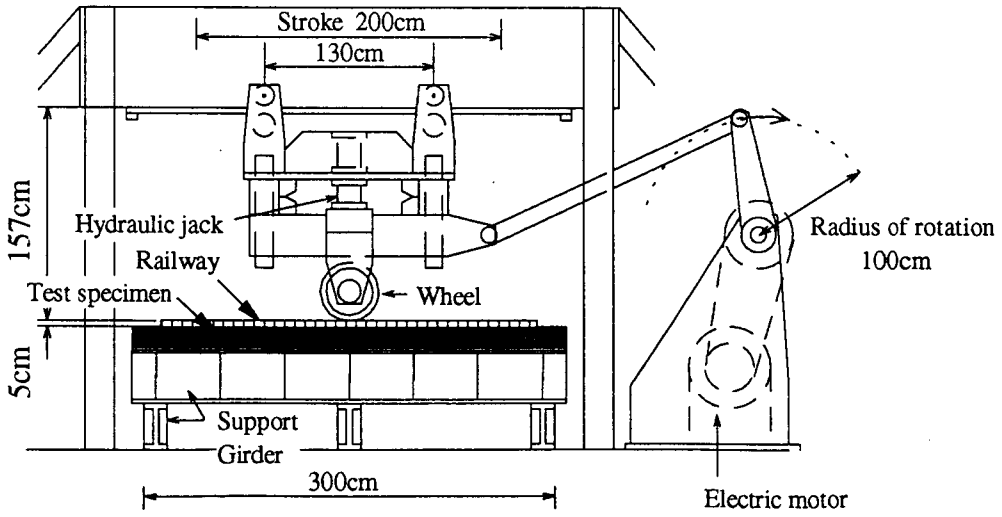


Fig. 5 Outline of testing machine

Table - 7 Features of testing machine

Loading capacity	100 ~ 300 KN
Range of load trucking	± 100cm from the center of deck slab
Trucking speed	112 m/min. (28 reciprocations / min.)
Diameter and width of wheel	50cm and 30cm

(2) Method of supporting test specimen

The test specimen is supported so that two longer sides are supported simply and two other sides are supported elastically by transverse girders.

Furthermore rising prevention device is mounted at four corners of deck slab to prevent the deck slab from rising on account of the wheel load trucking test.

(3) Track

The track as shown in Fig. 6 was adopted to realize the area load due to an actual tire running, because an iron wheel was used as the wheel of testing machine. To shift the load by ensuring a constant loading area, many blocks of same size were arranged on the top of deck slab and the travelling load was given to the deck slab through the blocks. The block size was of 12 × 30 × 5cm reduced to 60% of each side of the wheel loading area (50 × 20cm) required by the Road Bridge Regulation. Nineteen (19) blocks were arranged to get a caterpillar form having the clearance of 5mm among blocks. An iron plate of 10mm thick was placed on these blocks to keep the smoothness of wheel travelling surface and in addition, a plywood was placed between deck slab and block, and between block and steel plate, respectively to relieve an impact and to prevent friction on the top of deck slab.

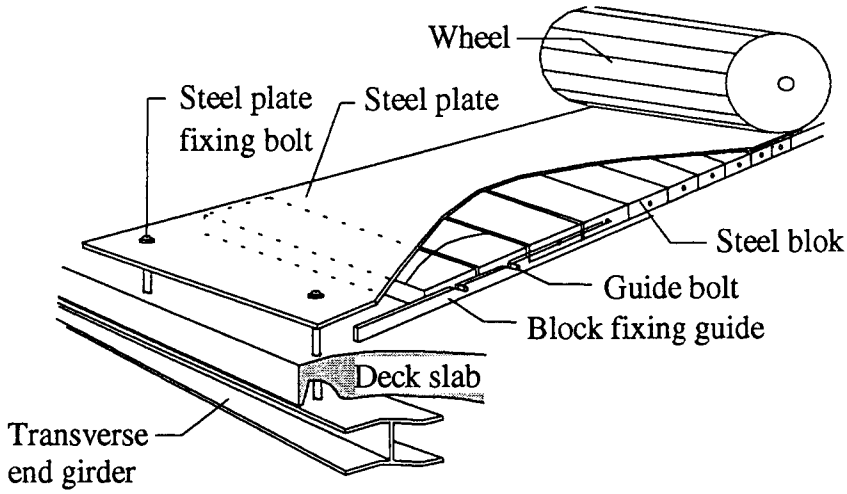


Fig. 6 Outline of track

(4) Loading condition

In the case of assuming the live load equivalent to TL-25, one axial load of near wheel is designed by 100KN. However, the experiment load was based on 180KN in consideration of an addition to the impact and traffic volume. From the actual measurement result that maximum wheel load of an overloaded vehicle on actual bridge was 150KN, the wheel load in this experiment is considered equivalent to the fatigue condition when an overloaded vehicle is running always

① Preliminary loading : Cracks were caused to concrete slabs for CFS test by 50,000 times running test of wheel load of 180KN at the unstrengthened state.

② Actual loading : It was decided as a standard that after strengthening the test specimen with CFS and executing the 100,000 times running test at the wheel load 150KN, the

900,000 times running test was to be done by increasing the wheel load level to 180KN and when the test specimen was not fractured, the 1,000,000 times running test was to be done by increasing the wheel load to 210KN.

For the unstrengthened test specimen, the 500,000 times running test was done at the wheel load 150KN and then the wheel load was increased up to 180KN till it fractured.

(5) Measuring method

Table - 8 shows the measurement items and Fig. 7 shows the measurement positions. Statical measurement was done by stopping the testing machine temporarily and applying the wheel load to the center of deck slab after every required running times. While, dynamic measurement was done during wheel running and the data for five seconds during (five seconds) was measured every 1/100 second.

Table - 8 Measurement items

Measurement items		Measurement method
Statical measurement	Deflection	Displacement meters, electric output type
	CFS surface strain	1 axis - 3 wire strain gauge
	Reinforcing bar strain	
Dynamic measurement	CFS surface strain	1 axis - 3 wire strain gauge
	Reinforcing bar strain	
	Creasing movement	π gauge, 3 - way gauge

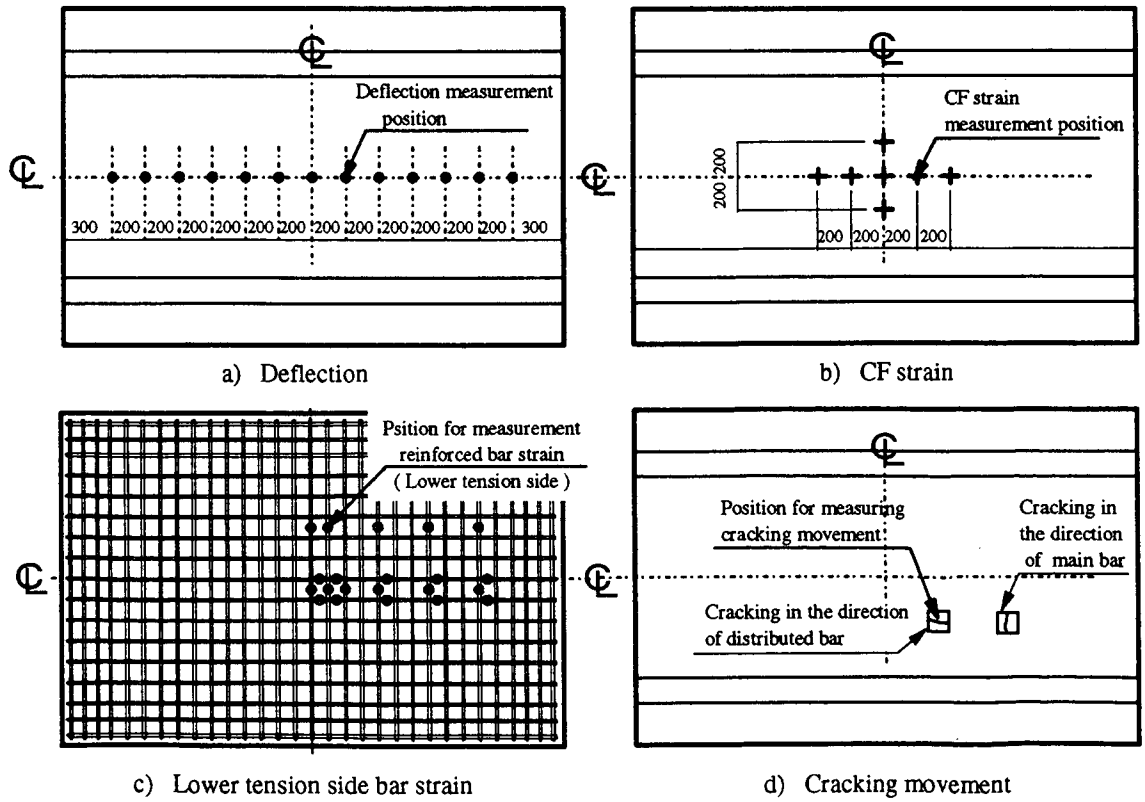


Fig. 7 Measurement position

3. Experimental results

3 - 1 Preliminary loading

Fig. 8 shows the example of cracking occurrence at the lower surface of deck slab caused by preliminary loading. Creasing occurred in two straight directions (hexagonal pattern) on the lower surface of deck slab on account of the preliminary loading (180KN × 50,000 times running).

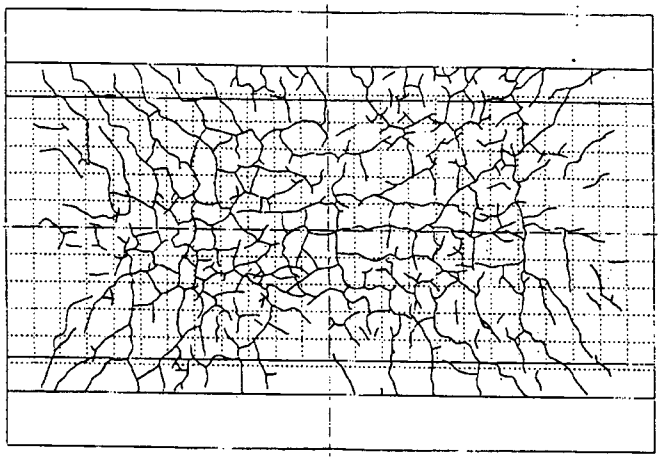


Fig. 8 Crack pattern due to preliminary loading (example)

3 - 2 Wheel trucking times

Table - 9 shows the loading condition and the form of fracture. The extension of fatigue life was confirmed by the CFS strengthening in spite of slight variation of in the running times due to the testing machine condition.

Also, the difference in the fatigue life was found according to the type of CFS strengthening. And the fatigue life of the test specimen strengthened by the high elastic modulus CFS was longer. Furthermore, the strengthened HM2 did not reach the final fracture.

Table - 9 Loading condition and form of fracture

Test specimen	Preliminary loading 180kN →	Actual loading 150kN →	Actual loading 180kN →	Actual loading 210kN	Form of Fracture
S - U		50,000 times	230,000 times		Punching and shearing fracture
S - GM	50,000 times	120,000 times	954,000 times		Do.
S - HM1	50,000 times	100,000 times	978,000 times	158,000 times	Do.
S - HM2	50,000 times	100,000 times	810,000 times	140,000 times	Not fractured

3 - 3 Deflection

Fig. 9 shows the relation between the times of running and the live load deflection in the center of deck slab.

Comparing with the unstrengthened test specimen, the CFS strengthened test specimen had smaller deflection. In the trucking test after strengthening the test specimen with CFS, the strengthened test specimen S - GM represented the tendency of increasing the deflection gradually, while both the test specimens S - HM1 and S - HM2 strengthened with the CFS of high elastic modulus minimized an increase of deflection and the deflection being always at smaller level.

The times of running were applied to the test specimens as follows :

Unstrengthened (S - U) ····· Approx. 200,000 times
Strengthened GM (S - GM) ····· Approx. 950,000 times
Strengthened HM1(S - HM1)···· Approx.1,200,000times (210KN)

After the above times, the deflection were increased suddenly and caused fracture.

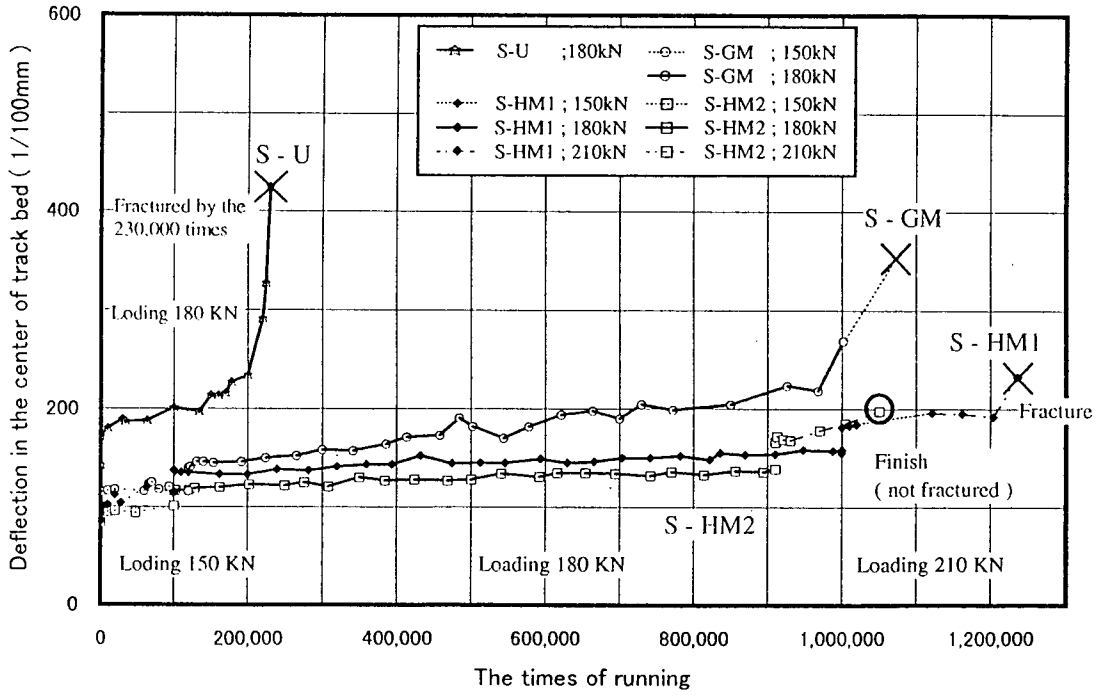


Fig. 9 The relation between the times of wheel running and the live load deflection in the center of deck slab

3 - 4 Relationship between the strains of rebar and CFS

Fig.10 & 11 show the typical change in the tensile strains of tension main bar and CFS in the center of deck slab due to static loading, respectively.

Maximum strain of each reinforcing bar was as follows :

Approx. 750 μ in the unstrengthened test specimen.
Approx. 550 μ in the CFS strengthened test specimen.

Comparing with the unstrengthened test specimen, the CFS strengthened test specimen was

changed with smaller value in the reinforcing bar strain.
There was a tendency that the larger CFS elastic modulus reduced the reinforcing bar strain. An increase of the reinforcing bar strain due to the times of running was slow with the same tendency as deflection.

The CFS strain represented the same tendency as deflection and then the CFS strain of the strengthened test specimen GM was increased gradually.
At this time, maximum strain of CFS was approx. 1000 μ .

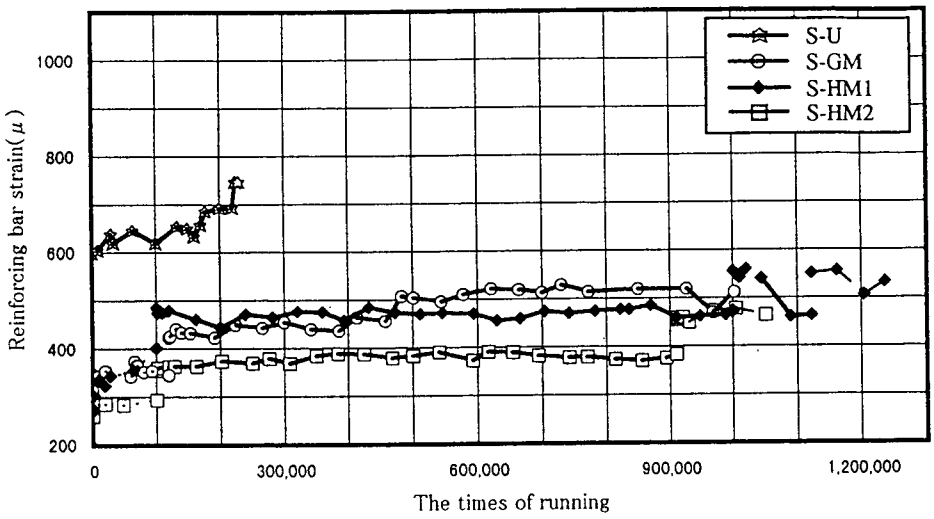


Fig. 10 Tension side main bar strain

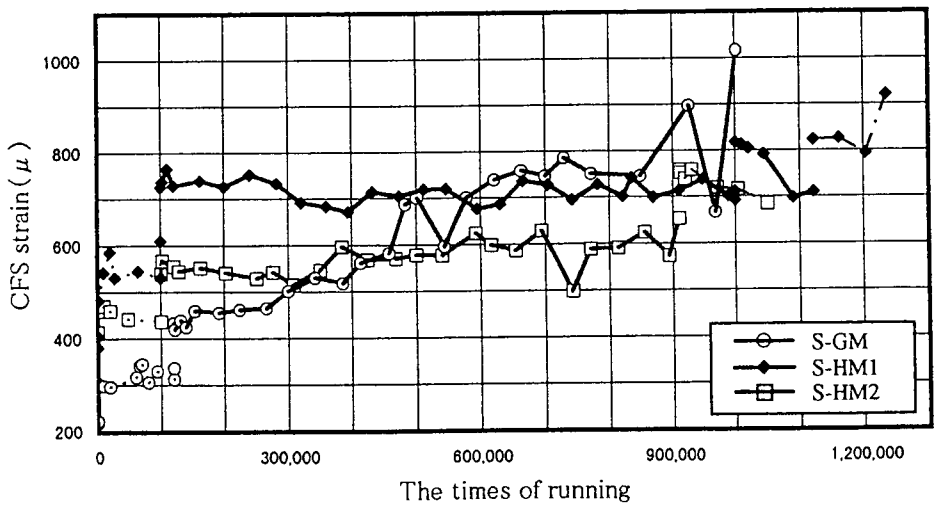


Fig. 11 CFS surface strain

3 - 5 Cracking width

Fig. 12 shows the cracking width variation due to dynamic measurement.
The cracking width in the direction of distributing bar (right angle to main bar) is larger than that in the direction of main bar (right angle to distributing bar).

The cracking width of unstrengthened test specimen was increased suddenly in hexagonal pattern. From this results, it can be guessed that the cracking increased its width and caused the cracked surface to become at the state of slit.

It is represented that the cracking width of CFS strengthened test specimen was at the state of gradual increase and the restriction effect due to CFS was being kept.

Especially, it is considered that both the strengthened test specimens HM1 and HM2 was small in the cracking width enlargement and the slitting caused by the abrasion of the cracked surface was small.

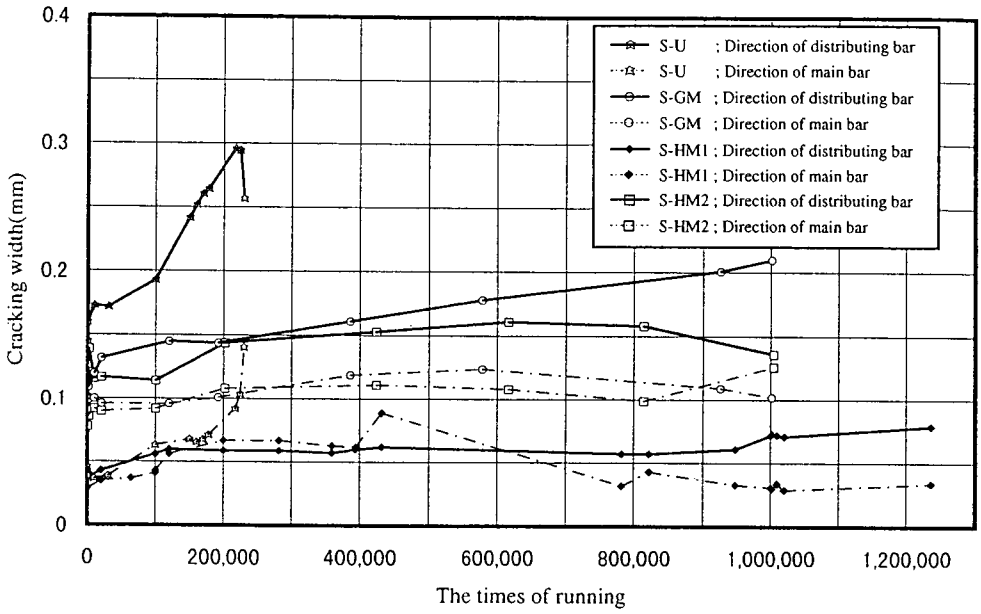
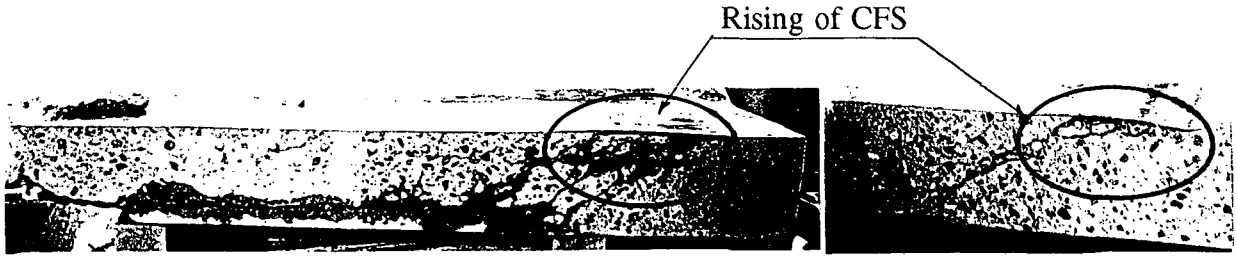


Fig. 12 Cracking width variation

3 - 6 The state of fracture

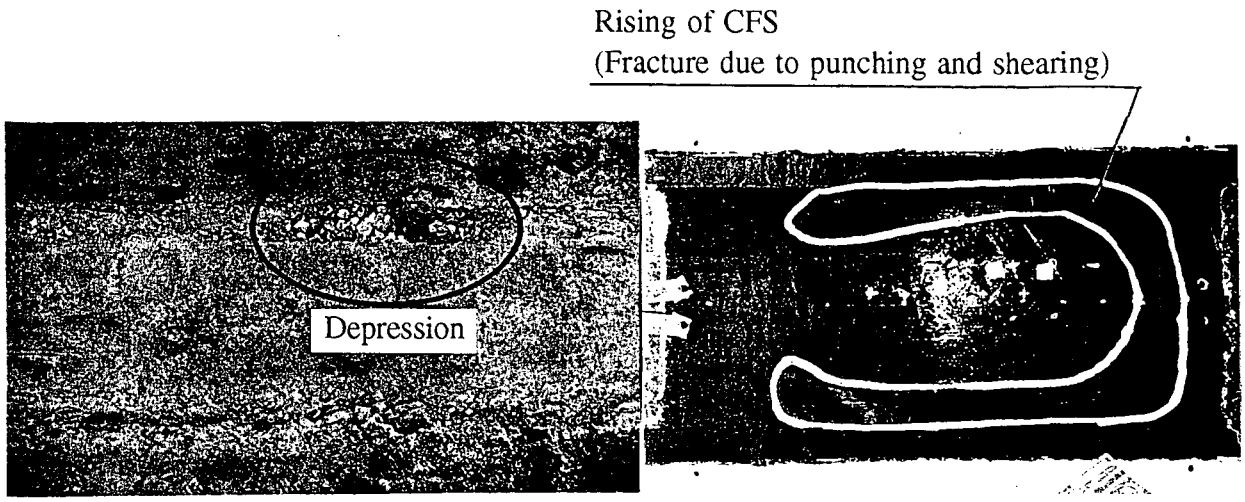
Fig. 13 shows the cross sections of the test specimen (in the center of deck slab after fracture)and Fig. 14 shows the top and bottom surfaces of CFS at that time. The test specimen was fractured entirely by the upper concrete depression immediately below track, and the punching and shearing based on the track.

In the punched portion of CFS, local rising occurred without the damage and peeling of CFS, and the CFS was fractured in the form of holding the lower concrete spalling.



Direction of distributing bar Direction of main bar

Fig. 13 State of cutting the test specimen



Top surface Bottom surface

Fig. 14 State of the top and bottom surface

4. Consideration

It was found from the experimental result that as shown in Fig. 15, the deflection of the fractured test specimen had a tendency of increasing suddenly and causing fracture when the deflection due to the live load in the center of deck slab reached the value of 2.0 ~ 2.2mm.

The fatigue life was estimated by assuming this point as the fatigue life of deck slab and obtaining the times of fatigue reaching the displacement 2mm at 180KN running from the transition of the live load deflection in the center of deck slab.

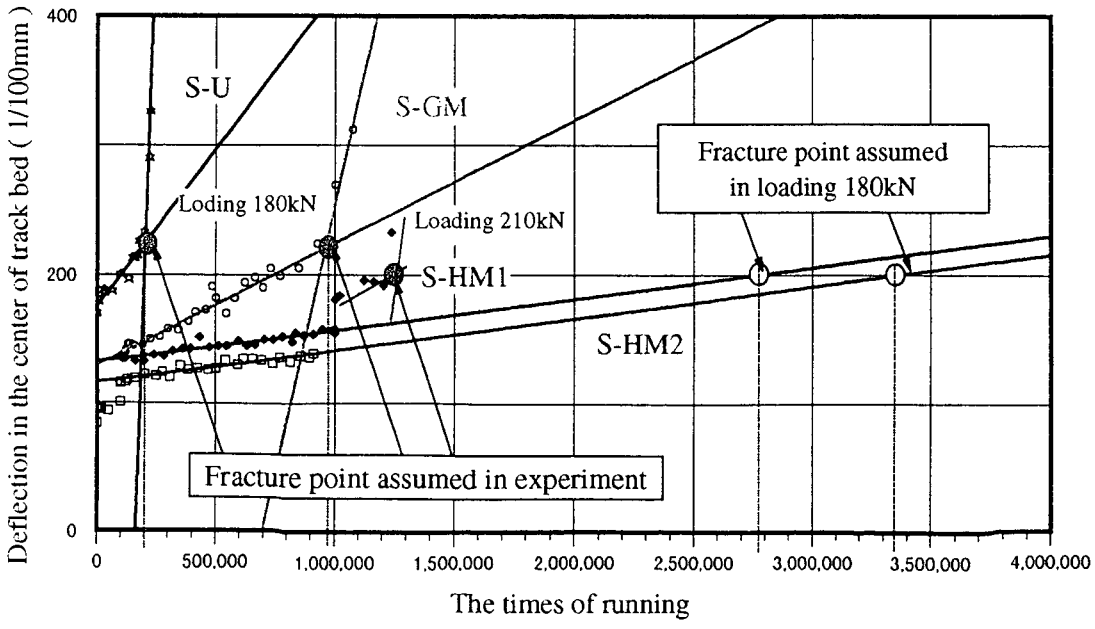


Fig. 15 Fatigue life estimated from the live load deflection in the center of deck slab

As this experiment depended upon the loading condition of every test specimen, the times of an equivalent repeated running was calculated by the loading condition of 180KN in accordance with the following formula (1) to simulated the loading condition. [3), 4)]

Table - 10 shows the fatigue life estimated by this method for each test specimen.

The times of running in Fig. 15 and Table - 10 include the times of running in the preliminary loading before CFS strengthened.

The times of an equivalent repeated running due to random load.

$$Neg = \Sigma (Pi / Po)^{m} \times ni \quad \cdots\cdots\cdots\cdots (1)$$

where,

Neg : The times of an equivalent repeated running converted to the base load Po.

Pi : Random load (KN)

Po : Base load (KN)

ni : The times of running due to random load

m : Coefficient 1/K, K=0.07835

Punching and shearing resisting force (Psx) of unstrengthened test specimen.

$$Psx = 2B (\tau \max \cdot Xm + \sigma \max \cdot Cm)$$

where,

B : Effective width of beam (cm)

$B = b + 2dd$

Xm : Depth of neutral axis in main bar section (cm)

Cm : Covering height of main bar (cm)

τ max : Max. shearing stress of concrete (N/mm^2)

$\tau \max = 0.252 \sigma ck - 0.000246 \sigma ck^2$

σ max : Max. tensile stress of concrete (N/mm^2)

$\sigma \max = 0.583 \sigma ck^{2/3}$

σ ck : Compressive strength of concrete (N/mm^2)

b : Length of the side of deck slab in the distributing bar direction (cm)

dd : Effective height of distributing bar (cm)

Table - 10 Fatigue life estimated in each test specimen
(at the state of 180KN running)

Test specimen	Shearing resisting force Psx	The times of an equivalent repeated running	Fatigue life estimated from deflection curve	The ratio of CFS strengthening effect
S - U	308 KN	234,880	200,000	1
S - GM		1,026,446	960,000	4.3 ~ 4.8
S - HM1		2,167,812	2,770,000	9.2 ~ 13.8
S - HM2		*1,871,072	3,360,000	>7.9 ~ 16.8

*The test specimen HM2 did not be fractured.

It is assumed that higher elastic modulus of strengthening CFS is more effective for extending fatigue life and the life of deck slab after strengthening with CFS would be extended 4 ~ 16 times.

5. Conclusion

The following conclusions were drawn from the wheel trucking experiment on the deck slab strengthened from below by the CFS with different elastic modulus.

(1) Bonding CFS below the damaged deck slab for strengthening improved the rigidity of section together with the restriction of cracked surface movement with smaller deflection and then reduced the degrading speed of deck slab remarkably.

(2) The use of the CFS with higher elastic modulus was more effective in restricting the deck slab deflection and in extending the fatigue life.

(3) CFS strengthening of one layer in both main bar direction and distributing bar direction made the fatigue life longer 4.8 times (strengthened GM) to 16.8 times (strengthened HM).

(4) The ultimate fracture properties of test specimen represented the fracture due to punching and shearing, however, no peeling of CFS was found. This means the effect of preventing concrete from spalling after fracture.

In future, we intend to add the study on the effect of improving the punching and shearing resisting force affected by the outermost restricting effect to fix the quantity for estimating the fatigue life due to the wheel load travelling on the deck slab strengthened with CFS.

[Acknowledgment]

The authors thank for the cooperation from the members in the Chemical Engineering Co. and students of Civil Engineering class of the Department of Engineering Osaka University, and from Mr. Tatsuo Ando and Mr. Shinichi Aibe, Mitsubishi Chemical Corporation.

[References]

1) Y.Maeda,S.matsui and I.Shimada : Deterioration and Repairing of Reinforced Concrete Slabs of Highway Bridges in Japan - Ⅲ - Inspection and Repairing Cracked Slabs - , Osaka,Technology Rept. of The Osaka Univ. Vol 31,No.1599.Japan,1980

2) N.Mori,F.Wakashita,S.Matsui and K.Nishikawa : Reinforcing Effect of Carbon Fiber Sheet on Damaged Bridge Slab, Bridge and Foundation 1995 - 3,pp25 ~ 32

3) Y.Maeda and S.Matsui : Punching Shear Load Equation of Reinforced Concrete Slab, Tokyo,Proc.of JSCE No.348,Japan,1984,pp133 ~ 141

4) Hanshin Expressway Corporation et al.
Cracking damage and durability on road bridge reinforced concrete deck slab. Dec, 1991

PRELIMINARY EVALUATION OF AN ALUMINUM BRIDGE DECK DESIGN FOR HIGHWAY BRIDGES

Adam Matteo,[1] Peter Massarelli,[2] Jose Gomez,[3] William Wright,[4] and James Cooper[5]

ABSTRACT

The Reynolds Metal Company has developed an aluminum bridge deck system which is currently being installed on Route 58 in Mecklenburg County, Virginia. Aluminum has been recognized as a high performance material by the AASHTO Subcommittee for Bridges and Structures for use in bridges. It offers several advantages when used in bridge decks, such as a higher strength to weight ratio and improved corrosion resistance. Traditional reinforced concrete bridge decks weigh approximately 5.7 kPa (120 pounds per square foot), while aluminum decks weigh between 0.9 and 1.2 kPa (18 and 25 pounds per square foot). A bridge that has been determined to be structurally deficient and thus posted for a certain maximum load could benefit from an aluminum deck which may increase its live load capacity by decreasing the dead load of the structure. It has been estimated that a posted bridge with an aluminum deck retrofit could be upgraded by 30 to 40 percent. Furthermore, the time required to install an aluminum deck system will be much shorter than for conventional construction. Aluminum deck panels can be fabricated off-site and then shipped and placed very rapidly, reducing the costs associated with traffic control as well as user costs associated with delays and detours. Maintenance costs may also be reduced, because of aluminum's high corrosion resistance.

INTRODUCTION

The vast majority of highway bridge decks in service today are constructed of reinforced concrete. While this material system is versatile and relatively inexpensive, its primary disadvantages are evident in commonly occurring serviceability problems. Over time, water and road salts penetrate the decks, corroding the steel reinforcement, expanding the steel and eventually spalling the deck. Furthermore, concrete decks are heavy, usually weighing over 4.8 kPa (100 lb/ft^2), and the formwork they require may be time consuming to construct. With these limitations on concrete, it can be seen that there exists a need for a corrosion-resistant, lightweight, and easily installed deck for highway bridges.

For the past two years Reynolds Metals Company (Reynolds) has been actively developing an aluminum deck system for highway bridges. Reynolds started its program by examining and purchasing the most deteriorated portions of an aluminum orthotropic deck being removed from the Smithfield Bridge in Pittsburgh, PA in 1994. Forensic analysis showed that an

---

[1] Research Engineer, Reynolds Metal Company, Richmond, VA
[2] Faculty Research Associate, Dept. of Civil Engineering, University of Virginia, Charlottesville, VA
[3] Research Scientist, Virginia Transportation Research Council, Charlottesville, VA
[4] Structural Research Engineer, Structures Division, Turner-Fairbank Research Center, FHWA
[5] Chief, Structures Division, Turner-Fairbank Research Center, FHWA

overly flexible deck plate, inadequate surfacing, and less than optimal alloy selection in some locations were sources of problems. However, it was readily apparent that, despite these shortcomings, the uncoated metal withstood the harsh environment with minimal degradation over 28 years. Also, with the exception of some localized fatigue cracks, the structural integrity of the metal remained sound.

Utilizing the analysis of the Smithfield Bridge deck, a new deck was designed which is nearly isotropic -- rather than orthotropic. By making the deck essentially isotropic -- possessing similar strength and stiffness characteristics in the two primary directions -- significant advantages are realized. The deck may now be oriented in either direction, and when the deck is used in conjunction with longitudinal girders, a greater effective width of the deck can participate in bending between girders.

The new aluminum deck is comprised entirely of extrusions welded together at the sides, providing continuity in the top and bottom flanges. After welding, the webs of the extruded parts form repeating triangles, creating trusses perpendicular to the extruded direction. The extrusions generally run longitudinally (parallel to the girders and traffic flow). The completed proprietary deck is connected securely to the underlying girders so that composite action is developed between the deck and the girders. The difference in thermal expansion coefficients between steel and aluminum induces stresses in both elements which are accounted for in the design. The decks could be fabricated in panels as large as can be shipped, which for highway shipments is about 4.3 m (14 feet) wide by 36.6 m (120 feet) long. The decks are shop-coated with a 9.53 mm (3/8 inch) nominal thickness epoxy-based wearing surface.

The first installation of this system is currently taking place on Route 58 in Mecklenburg County, VA. The Virginia Transportation Research Council, with support from the Federal Highway Administration, has initiated a three part study to evaluate the aluminum deck system. The first phase involved structural testing and evaluation of a 2.74 m x 3.66 m (9 feet x 12 feet) deck panel. The structural testing was conducted at the Federal Highway Administration (FHWA) Turner-Fairbank Research Center's Structures Laboratory. Several tests were conducted in which the panel was loaded to its design limit and with various support conditions. A final test to failure was conducted. The second phase involves a series of static and dynamic load tests on the completed Route 58 structure. The third phase will focus on the long term durability of the deck system.

DECK SYSTEM DESIGN

Component Extrusions

The deck is comprised of extruded multi-void shapes which are welded together at the sides to form a voided, or cellular deck. The webs of each extrusion intersect the flanges to create a truss. After welding, the webs of adjacent extrusions act together to extend the truss, thereby creating a deck with substantial strength in the direction transverse to the extruded direction. Two basic extruded shapes have been investigated, each of which has been designed to resist AASHTO HS-20 loading: a two-void shape, shown in Figure 1(a); and a three-void

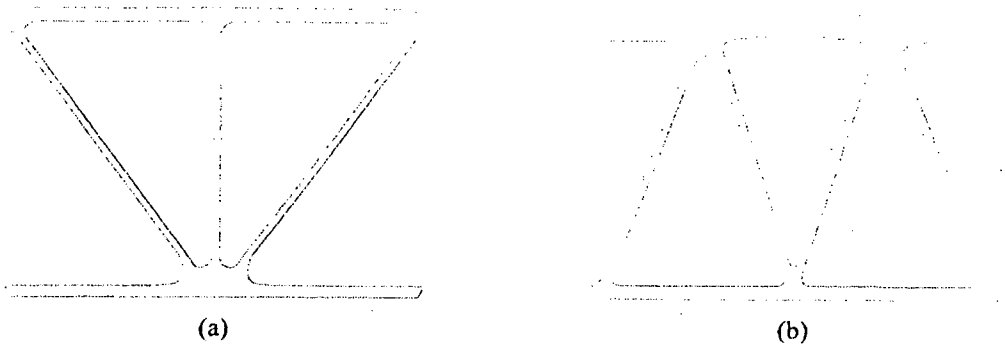


Figure 1. Schematic illustrations of two aluminum extruded shapes: (a) two-void design and (b) three void design.

shape, which is shown in Figure 1(b). The two-void shape is lighter in weight, but the local bending stresses in the three-void shape are significantly lower, making it a more favorable choice. The two-void shape is being used on the superstructure replacement of the Route 58 east bound lane of the Little Buffalo Creek Bridge near Clarksville, VA. Future decks will probably employ the three-void shape which is currently being tested.

As mentioned above, the preferred orientation of the extrusions is parallel to the girders. This helps both the strength and the fabricability of the deck. The orientation of the extrusions enhances the allowable stress capacity of the top fiber of the aluminum deck, which is subjected to System I (longitudinal bending) stresses resulting from the composite action with the underlying girders. The longitudinal orientation also allows for accommodation of roadway crowns and skewed supports.

Since the deck has very similar stiffness characteristics in each of the two primary directions its System II (transverse bending) behavior between girders is not unlike that of a concrete slab. The AASHTO Standard Specifications for Highway Bridges, as well as the new AASHTO LRFD Bridge Design Specifications suggest modeling System II behavior using a "strip method" whereby the equivalent strip, or the effective length of deck acting in flexure can be calculated for a given structural system and girder spacing. This method is based on work performed by Westergaard (1930) and others at the University of Illinois in the 1930's and extended by Wassef at Modjeski and Masters (1994).

Physical Properties

The deck is nearly isotropic rather than fully isotropic because the rigidity in the extruded direction is about 15% greater than in the direction transverse to the extrusion. However, even in the transverse direction the deck possesses rigidity similar to most 203 mm (8 inch) concrete slabs in use today. Torsional stiffness of the deck is also comparable to that of an 203 mm (8 inch) concrete slab. The weight of the aluminum portion of the deck is about 0.96 kPa (20 lb/ft^2), and the wearing surface adds another 0.24 to 0.29 kPa (5 to 6 lb/ft^2). The deck is fabricated from 6063-T6 aluminum, which has a minimum tensile yield strength of 172.4 MPa (25 ksi) and a minimum tensile ultimate strength of 206.8 MPa (30 ksi).

Composite Action

The aluminum bridge deck as utilized acts in full composite action with underlying girders, much like concrete, providing increased section modulus and moment of inertia of the combined section as well as greater redundancy. Shear engagement devices (usually headed studs) are designed in the same manner as for concrete decks, accounting for maximum anticipated interface shear. An aluminum deck, when connected to a particular steel girder, will provide a smaller composite section modulus than would be provided by a normal strength 203 mm (8 inch) concrete slab. However, since the allowable extreme fiber stresses in aluminum exceed those of concrete, aluminum/steel sections generally provide greater bending resistance. The benefits of composite aluminum deck/steel girder sections are summarized below:

a) *Reduced Girder Weight:* For any given depth, a composite section using an aluminum deck and steel girder usually requires less steel than would be required with a normal strength 203 mm (8 inch) concrete deck. The reduction in the amount of steel required can be attributed to both the reduced dead load of the combined section (which greatly reduces maximum bending and shear stresses) and to the fact that the steel girder need not support the dead load of an uncured concrete deck. A parametric study of simple span structures utilizing aluminum decks with steel girders has shown that a substantial steel material savings, perhaps as high as 40%, can be realized over a comparable concrete deck/steel girder section. If height reduction is more critical than material savings in the steel (as might be the case in a superstructure replacement for an existing bridge), then for an equivalent weight, a reduced overall section depth can be realized.

b) *Strength in Tension:* Aluminum has excellent tensile strength, so the deck provides substantial bending strength over intermediate supports in areas of negative bending. This contrasts with concrete, which has poor tensile strength, and so must rely solely on reinforcement to carry longitudinal tensile stresses in negative bending regions.

Several methods of compositely connecting a steel beam or girder with an isotropic aluminum deck are available. Each of the methods provides distinct advantages. One method allows for shop attachment of the deck and girders. An aluminum plate, welded to the bottom of the deck, is bolted with galvanized A325 bolts directly to the top flange of the locally coated steel beam. Other attachment methods are field-based and involve filling the connection area between the deck panel and shear studs on top of the girder with grout.

Design for each of these details must account for interface shear resulting from dead and live load. However, since the thermal expansion coefficient of aluminum is roughly twice that of steel, a thermal component of the interface shear must be added to the calculation. Full-scale static and fatigue tests were run on a field-based composite connection with favorable results. The connection generally created a full bond between the deck and the stringers, providing close to predicted longitudinal bending stresses. Furthermore, two panels subjected to cyclical loading showed little or no degradation of strength after almost 4 million cycles at loads which produced maximum service load interface shears.

Fatigue Strength

The deck extrusion was designed to minimize flexibility of the top plate of the deck to ensure longevity of the shop-applied wearing surface and to reduce fatigue stresses in the longitudinal welds of the top plate. The AASHTO LRFD specifications require a design load representing a truck with a tire pressure of 861.8 kPa (125 psi). This high design load creates localized stresses (System III) which are additive to System I and System II stresses. The extrusion geometry has been selected to adequately sustain the fatigue effects of this loading.

The first step in examining the deck's fatigue strength is to categorize the connection details. It is clear that the base metal of the extrusion should be classified as a Category A detail. However, the longitudinal inter-extrusion weld in the top flange does not closely resemble any of the standard fatigue categories shown in the AASHTO specifications. For this reason, fatigue testing of a candidate top flange weld connection was conducted. Preliminary results show that "runout" (the stress range at which an infinite number of cycles can be applied without inducing cracks) will usually occur when the constant amplitude stress range is less than 93.1 MPa (13.5 ksi). These data are consistent with results which might be expected for a Category A or Category B detail.

The fatigue resistance allowed by the AASHTO LRFD Bridge Design Specification varies according to detail category and the anticipated number of load cycles. The critical fatigue stresses are those which act orthogonally to the weld. The basic extrusion design minimizes these stresses in the weld, allowing the deck system to meet the stringent AASHTO LRFD fatigue design criteria for high traffic and interstate highway usage.

STRUCTURAL TESTING OF PANEL UNDER STATIC LOADING

A study is underway comparing the System II stresses predicted by the Westergaard model with stresses determined through finite element analysis. The finite element analysis utilized 300,000 solid (brick) elements to model a 2.74 m x 3.66 m (9 feet x12 feet) simply supported panel with two planes of geometric and load symmetry. Symmetry allowed a larger number of elements, and thus a tighter element mesh. Preliminary results show a favorable correlation between the two analytical methods. A test of a 2.74 m x 3.66 m (9 feet x12 feet) panel was conducted at FHWA's Turner-Fairbank Structures Laboratory in December, 1996. The data generated during the test will be compared to the finite element analysis and the strip method analysis. The intent of the testing was to collect data which will assist in the development of a predictive model for quantifying System II bending stresses in future applications of the deck.

Elastic Behavior

The panel was subjected to seven distinct elastic load case tests and two ultimate load case tests. Six of the seven elastic load tests involved a single load patch, and their support conditions are given in Table 1. The support conditions of the sixth elastic load case were identical to that of Load Case 7; however, two load patches were applied to the panel. The center

Table 1. Elastic load case configurations.

Load Case	Description
1	Simply-supported on four sides with all supports located 152 mm (6 inches) from the panel edges. A single load patch was applied to the center of the panel.
2	Simply-supported on the two 3.66 m (12 foot) sides and simply-supported on one of the 2.74 m (9 foot) sides with all supports located 152 mm from the panel edges. Freely constrained on the second 2.74 m side. A single load patch was applied to the center of the panel.
3	Simply-supported on the two 2.74 m sides with all supports located 152 mm from the panel edges. Freely constrained on the two 3.66 m sides. A single load patch was applied to the center of the panel.
4	Clamped through 152 mm of one of the 3.66 m sides and simply-supported along the length 1.52 m (5 feet) from the fixed edge. Freely constrained on the second 3.66 m side and on the two 2.74 m sides. A single load patch was applied so that its center was 0.31 m (1 foot) from the edge of the unconstrained long side.
5	Clamped through 152 mm of one of the 2.74 m sides and simply-supported along the width 2.13 m (7 feet) from the fixed edge. Freely constrained on the second 2.74 m side and on the two 3.66 m sides. A single load patch was applied so that its center was 0.31 m from the edge of the unconstrained short side.
7	Simply-supported on the two 3.66 m sides with all supports located 152 mm from the panel edges. Freely constrained on the two 2.74 m sides. A single load patch was applied to the center of the panel.

of each patch was located 0.91 m (3 feet) from the center of the panel along its width. Figure 2 shows schematic drawings of Load Cases 1, 6, and 7.

Each of the load patches were 508 mm (20 inches) in length and 216 mm (8.5 inches) wide to coincide with the AASHTO LRFD Bridge Design Specifications. All of the load patches were oriented with their shorter side parallel to the longitudinal axis of the deck panel (as shown in Figure 2). The elastic tests were conducted with an applied load of up to approximately 102 kN (23 kips). The photograph in Figure 3 shows the panel being tested under one load/constraint configuration.

Strain gauge rosettes were oriented at the top and bottom of the panel along the transverse and longitudinal center lines. Deflection gauges were placed on the bottom of the panel. For Load Cases 1 to 3, 6, and 7, deflections were measured along the longitudinal and transverse center lines. For Load Case 4, deflection gages were placed along the transverse center line and at the unconstrained long edge, and for Load Case 5 the gages were oriented along the longitudinal center line and at the unconstrained short edge.

Results

The greatest deflections were measured for Load Cases 4 and 5 which employed the clamped constraints. These deflections occurred at the midpoint of the free edges and were -13.92mm (-0.548 inches) and -11.99 mm (-0.472 inches), respectively. Of the simply-supported

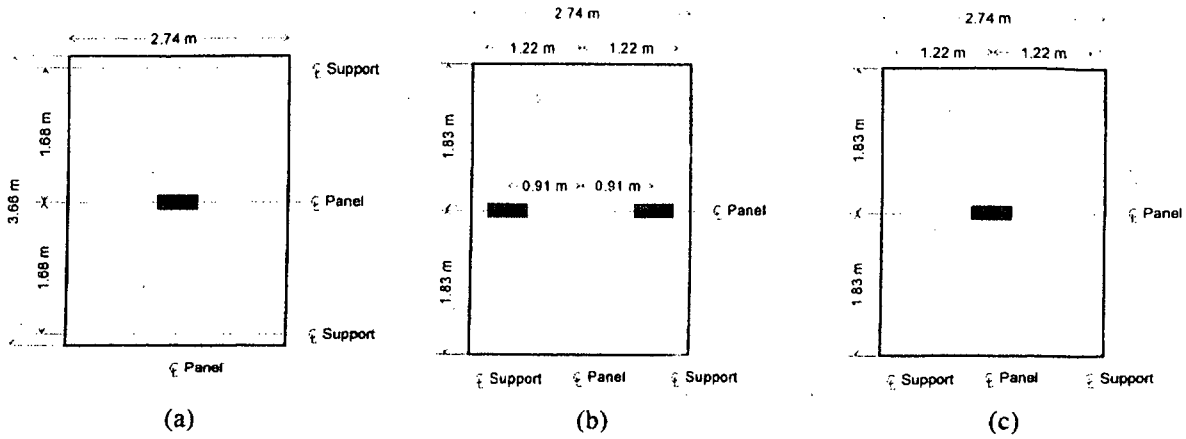


Figure 2. Schematic illustrations of constraints and load patch placement for (a) Load Case 3, (b) Load Case 6, and (c) Load Case 7.

scenarios, Load Case 3 had the greatest measured deflection of -2.87 mm (-0.113 inches). Each of the other load cases had maximum measured deflections below 2.54 mm (0.1 inches); however, no deflection data was recorded for Load Case 2.

The strain data suggest that local bending effects occurred under the load patch. Excessive tensile strain measurements on the top of the panel at the location of the load may be explained by the occurrence of transverse bending between the vertical and diagonal inner truss members of the panel. For example, Figure 4(a) shows the transverse strains across the width of the panel top at mid length for Load Case 3, and Figure 4(b) shows the longitudinal strains along

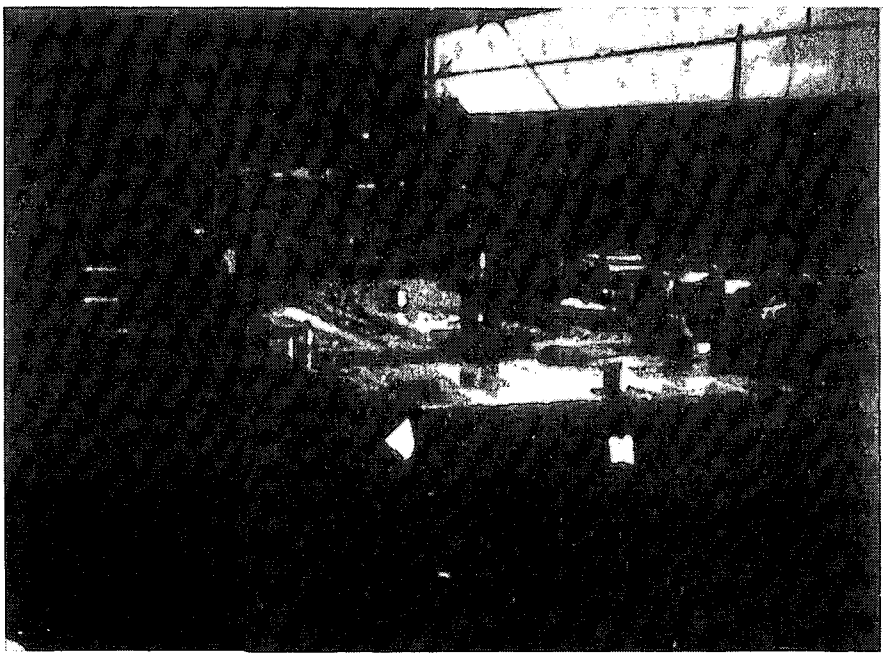
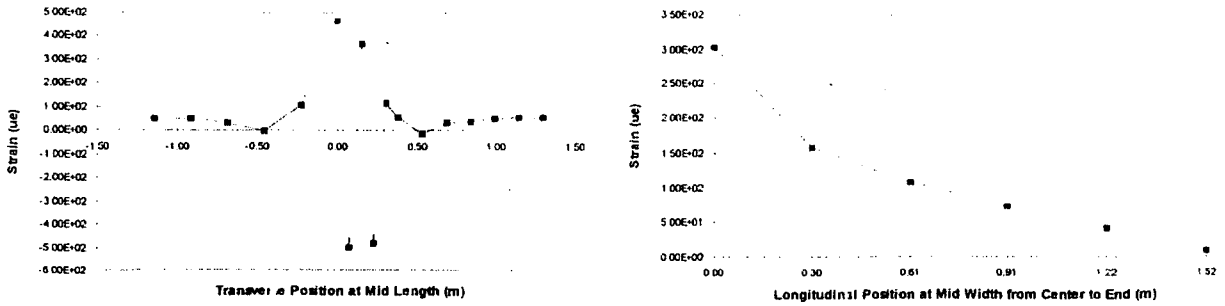


Figure 3. Static load testing of aluminum deck panel section.



(a) (b)

Figure 4. Strains measured during Load Case 3: a) Transverse strains at top of panel at mid length and b) Longitudinal strains at bottom of panel at mid width.

the length of the panel from center to end for the same load case. These strains were measured under an applied load of 102.3 kN (23 kips). It can be seen from these figures that the local tensile strains at the top of the panel are actually greater than the global tensile stresses on the panel bottom. Table 2 shows the ratio of maximum global tensile strain (bottom of panel) to maximum local tensile strain (top of the panel) for all load cases other than those with a cantilever configuration. It can be seen that in each of these cases the local bending strains are of greater magnitude than the global bending strains.

Ultimate Load Test

After completing the elastic tests described above, the panel was tested to failure. The same loading configuration for Load Case 7 was used to perform the initial overload test. The panel was continuously loaded to 556 kN (125 kips). Then the test was paused for apparatus readjustments. The test was then continued, and the panel was loaded to 823 kN (185 kips). At an applied load of 832 kN (187 kips), local buckling under the load patch occurred. At 881 kN (198 kips), "punching" failure occurred under the load patch. Figure 5 shows the longitudinal strain on the bottom of the panel at its center and the transverse strain on the top of the panel at the center (under the load patch). This shows that the ratio of local to bending strain increases as the applied load approaches its ultimate value. At 185 kips, this ratio had risen to a value of 2.995. Consequently, the strains due to the local bending effect controlled the first failure mode.

Table 2. Ratio of maximum local to global strains for each elastic load case.

Load Case	Load (kN)	Local Tensile Strain (ue)	Global Tensile Strain (ue)	Ratio of Local to Global strain (ue)
1	102.3	372	224	1.66
2	102.3	369	230	1.60
3	102.3	464	302	1.54
6	102.3	284	183	1.55
7	97.9	314	207	1.52

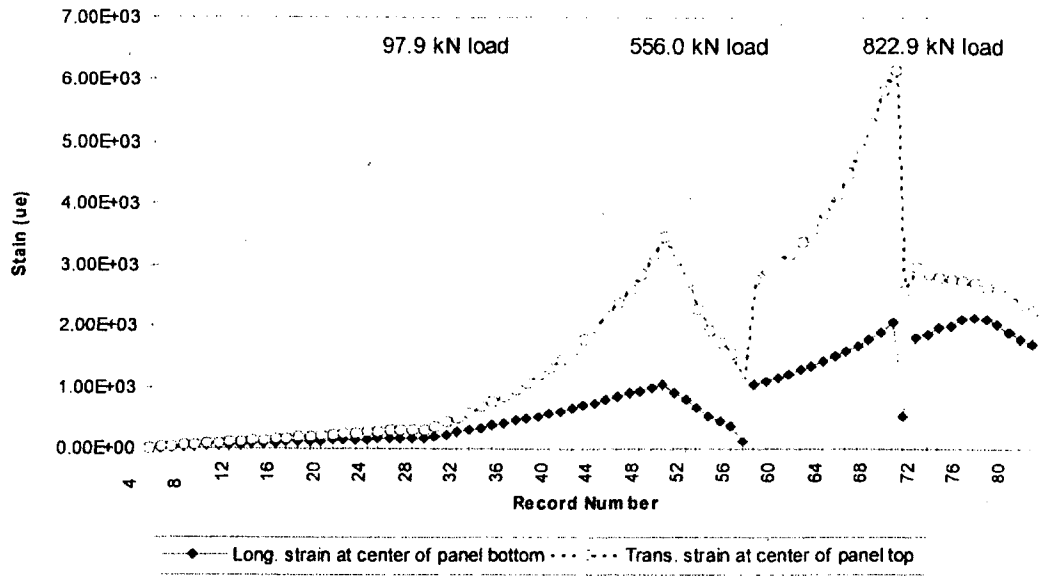


Figure 5. Transverse strains at center of panel top and longitudinal strains at center of panel bottom during ultimate load test.

Another test was run using two load patches oriented along the longitudinal axis with their centers 635 mm (25 inches) from the center of the panel. Equivalent loads were applied to each of the patches in 22.24 kN (5 kip) increments. At a combined load of 1441 kN (324 kips), total weld failure occurred at the bottom of the panel, as shown in Figure 6.

CONCLUSIONS

The first phase of this project involved elastic and ultimate load testing of an 6063-T6 aluminum two-void design deck panel section. The panel was tested under seven distinct elastic load cases using an applied load designed to simulate an AASHTO HS-20 loading. Tensile

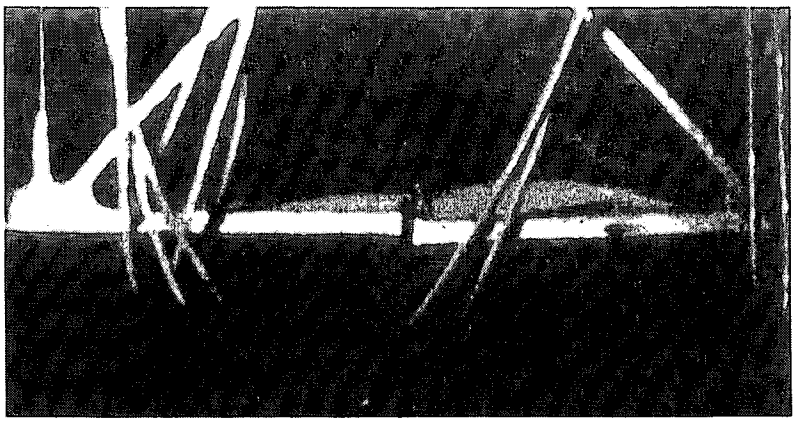


Figure 6. Crack along weld on bottom of panel.

strains caused by localized bending under the applied load were detected. These strains were frequently greater in magnitude than the maximum tensile strains due to global bending. Maximum tensile strains recorded during the elastic testing corresponded to stresses less than 15 percent of the material yield stress.

Overload testing was also performed. The first local failure mode occurred at 881 kN (198 kips). This failure occurred under the load patch in a region exhibiting relatively high strain due to localized bending effects. Strains in the vicinity of this region at failure were measured at approximately 6000 ue. A second load patch was applied to lessen the local buckling effects and final failure occurred at the center weld on the bottom of the panel at a combined load of 1441 kN (324 kips).

The deck panel extrusion component design used in the tests reported in this paper has been revised. A three-void design (shown in Figure 1b) was developed to alleviate these local bending effects.

The second phase of this project involves a series of static and dynamic load tests on the completed Route 58 structure. This structure is currently being constructed, and testing is expected to commence in early May, 1997. The third phase will focus on the long term durability of the deck system. In the Fall of 1997, full-scale fatigue testing of a three-void design deck panel will be conducted at Virginia Polytechnic Institute in Blacksburg, VA.

ACKNOWLEDGMENTS

The authors wish to acknowledge the Reynolds Metal Company for the development of this innovative deck system. Reynolds has conducted an extensive design development and testing program to ensure the success of its deck and wearing surface. The authors are also grateful to the technical staff at the Turner-Fairbank structures lab for their test setup and instrumentation efforts.

REFERENCES

Westergaard, H.M., "Computation of Stresses in Bridge Slabs Due To Wheel Loads", *Public Roads*, March, 1930.

Modjeski and Masters Internal Calculations to Develop Design Effective Widths in The LRFD Bridge Design Specification,1994.

THE DESIGN AND CONSTRUCTION OF COMPOSITE-MATERIAL BRIDGES IN DELAWARE

Dennis R. Mertz[1], John W. Gillespie, Jr.[2] and William A. Edberg[3]

Abstract

An incremental approach to the introduction of composite-materials into the bridge design and construction industry is being implemented in the State of Delaware. A series of three traditional-material bridges, of increasing complexity and risk, are in the process of being replaced with bridges of composite materials fabricated by Hardcore DuPont Composites. In addition, technology is being transferred to the Delaware Department of Transportation, allowing them to design, construct, maintain and operate such composite-material bridges at the completion of the projects.

Approach to Design and Construction

Revolutionary innovation in the bridge construction industry is very difficult due to the momentum represented by the institutions and existing cultures of the industry. In order to implement the introduction of composite materials into the bridge construction industry, an incremental approach to the design and construction of composite-material bridges is being taken in the State of Delaware. The approach begins with relatively modest bridges with controlled or limited traffic, growing into an on-system bridge with significant truck traffic. In addition to the grow in apparent risk, so too the complexity of the geometry and structural requirements of the bridges grow. The progress of the construction of the series of bridges assumes success at each step along the way.

Projects' Participants

Participants in the three-bridge replacement effort are the University of Delaware (UD) and the Delaware Department of Transportation (DelDOT) through their Delaware Transportation Institute (DTI), the Delaware River and Bay Authority (DRBA), the Federal Highway Administration (FHWA), the US Department of Defense, Hardcore DuPont Composites, LLC and J. Muller International.

---

[1] Associate Professor, Department of Civil & Environmental Engineering, University of Delaware, Newark, DE.
[2] Technical Director, Center for Composite Materials, University of Delaware, Newark, DE.
[3] Research Assistant, Department of Civil & Environmental Engineering, University of Delaware, Newark, DE.

Common Feature

The common composite-material feature shared by all three bridges is a fiberglass "honeycomb"-like bridge deck manufactured by Hardcore DuPont Composites. A typical deck is seen in cross section in Figure 1. The material characterization was made at the University of

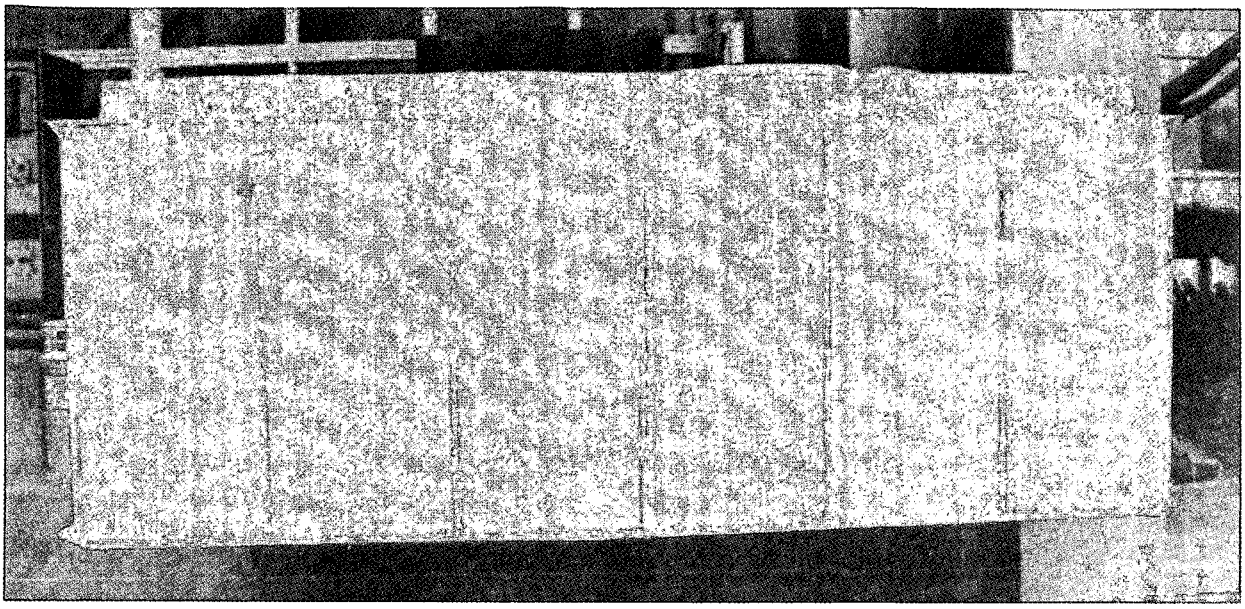


Figure 1 Typical Composite-Material Bridge Deck Cross Section

Delaware's Center for Composite Materials (CCM) with design criteria developed by the University's Department of Civil & Environmental Engineering.

The specific component materials used in this deck are a quasi-isotropic E-glass stitched fabric produced by Brunswick Technologies, Inc. labeled as QM6408 and a vinyl ester resin produced by Dow labeled as 411-PC100. The SCRIMP fabrication process is used by Hardcore Dupont Composites to produce the composite portion of the structure as a continuous piece, as opposed to fabricating plates and then joining the plates by secondary bonding to form the structure. The deck section is basically formed by laying fabric to form the bottom face sheet, placing the core material, laying the top face sheet, and then using the SCRIMP process to infuse resin into the component. The core was formed for this bridge by wrapping individual foam cells with the QM6408 fabric and placing those cells together to form a "web core" construction, the resulting cross section is shown in Figure 1. The QM6408 fabric is composed of five layers of E-glass which are then stitched together through the thickness. The first four layers consists of continuous strand rovings of E-glass oriented at 0/90/+45/-45, the nominal weights in oz/yd^2 for each layer are 26/16/12/12, respectively. The last layer is a matt consisting of 50-mm (2 in.) binderless chop strand E-glass with a weight of 6.75 oz/yd^2. The stitching yarn is a polyester.

Design Considerations

The bridges are being designed to meet the performance requirements implicit to the AASHTO *LRFD Bridge Design Specifications* (AASHTO 1994), even though such materials are not explicitly included in the specifications. The *LRFD Specifications* require the consideration of four limit states: (1) the service, (2) fatigue-and-fracture, (3) strength, and (4) extreme-event limit states. Glass fiber-reinforced polymer bridges will be governed by the service limit state, which specifies that the live-load deflection of the bridge not exceed the span length divided by 800 or 1000, for bridges with and without sidewalks, respectively. With the bridge's cross section proportioned to satisfy the service limit states, the calculated stresses associated with the strength and fatigue-and-fracture limit states are insignificant in comparison with stress limitations based upon a 75-year service life (Mertz and Kulicki 1997).

The Magazine Ditch Bridge

The first bridge to be replaced is owned by the DRBA and is called the Magazine Ditch Bridge. As can be seen in Figure 2, the bridge is on the grounds of the DRBA's Delaware Memorial Bridge Twin Spans, twin suspension bridges spanning the Delaware Bay between Delaware and New Jersey. The Magazine Ditch Bridge is a private bridge and only carries the

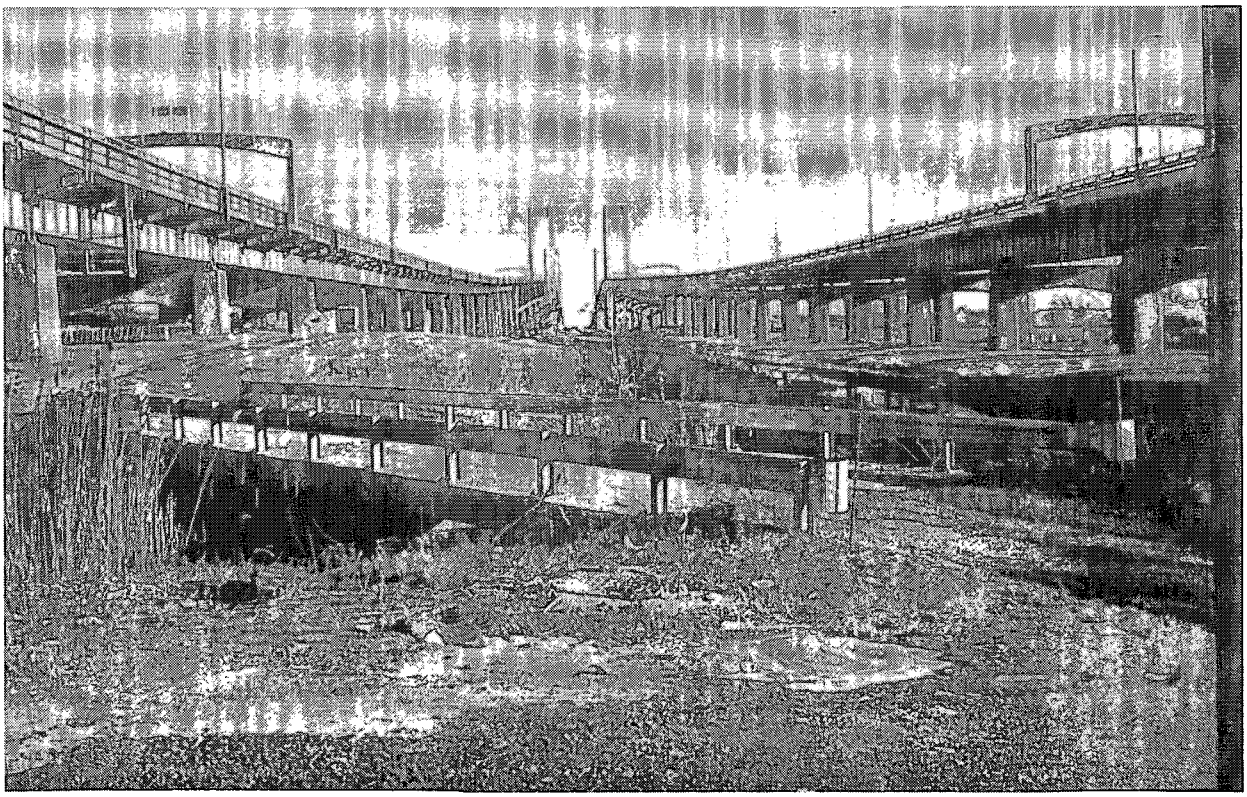


Figure 2 Original Magazine Ditch Bridge



Figure 3 Magazine Ditch Bridge Test Specimen in UD Structures Laboratory

DRBA's maintenance vehicles from their storage yard and de-icing agent storage area to the suspension bridges and back. The bridge is not open to the general public. Further, the bridge represents a redundant traffic pattern. By virtue of crossing only a ditch, traffic can be routed the long way around the ditch if the bridge needs to be closed for experimentation.

The new Magazine Ditch bridge is a 21.3-m (70-ft) long simple span consisting of a 6.1-m (20-ft) wide composite-material bridge deck spanning between two post-tensioned concrete edge girders. The bridge was designed by J. Muller International, utilizing their channel-bridge technology (HITEC 1996), and the concept tested by the University of Delaware. The test setup for a full-scale cross section of the Magazine Ditch Bridge is shown in Figure 3. The entire bridge deck (6.1 m (20 ft) by 21.3 m (70 ft) by 460 mm (18 in.)) was fabricated by Hardcore DuPont Composites in one single piece. This presented unique fabrication challenges, but the problem of deck joints was delayed for the next bridge replacement.

The replacement bridge includes a 50-mm (2-in.) wearing surface of latex-modified concrete, to not only protect the top face sheet of the polymer deck but also to help meet the service limit-state deflection criteria. The wearing surface is not required for the strength limit

state, only for the service limit state. This philosophy is entirely consistent with the *LRFD Specifications*, as applied to the stiffness of bridge railings.

At the time of this writing, the bridge is undergoing experimental bridge rating by the University of Delaware and will be opened to DRBA truck traffic immediately thereafter. The erection of the bridge replacement is shown in Figure 4. In the figure, the composite deck



Figure 4 Erection of Magazine Ditch Bridge

section is being lowered onto the two concrete channel-bridge edge girders. Epoxy adheres the stepped edges of the composite deck to the edge girders. Additionally, bolts are provided to control pressure during curing of the joint.

Bridge No. 1-351

Bridge No. 1-351 is located along Business Route 896 in New Castle County, Delaware and is owned by DelDOT. The existing bridge is shown in Figure 5. Unlike the Magazine Ditch

Bridge, Bridge No. 1-351 is on the public system, yet it has very little truck traffic (an estimated two million cycles over 75 years) and is again redundant in that Route 896 provides a very nearby detour should the bridge require closing for future experimentation.

The existing bridge is a 9.1-m (30-ft) simple-span adjacent prestressed concrete box-



Figure 5 DelDOT Bridge No. 1-351

beam bridge, which has experienced severe deterioration due to the corrosion of its prestressing strands. The planned replacement is a 7.9-m (26-ft) wide, 9.1-m (30-ft) long, 610-mm (2-ft) thick composite-material slab bridge designed by DelDOT with assistance by the University of Delaware. The bridge is being designed as two transportable pieces, 4.0-m (13-ft) by 9.1-m (30-ft), connected by a longitudinal joint.

The joint, running longitudinally down the centerline of the bridge, is designed to be a redundant joint. Splice plates will be adhered to the top and bottom face sheets. If the adhesive bond between the vertical surfaces of the two deck sections was to fail, the splice plates are sufficient to carry all required loads at the strength limit state, and vice versa. In either case, it is anticipated that deflections in excess of the service limit state would signal the owner that the joint requires attention. Again, in either case, the structural integrity of the bridge is not compromised.

Since the determination of the crash-worthiness of a composite-material bridge parapet, or a concrete New Jersey-type barrier-to-composite material deck connection, was beyond the scope of this bridge project; a separate, structurally independent bridge railing was designed by DelDOT. A typical compression seal will be installed between the independent bridge railing and the composite-material slab superstructure.

The bridge is to be constructed during the 1998 construction season. Prior to construction, all of the design elements will have been validated including full-scale laboratory fatigue specimens which will have experienced more than the necessary two million cycles required for a 75-year life at this bridge site.

Bridge No. 12

DRBA Bridge No. 12 (also known as DelDOT Bridge No. 1-666) carries US Route 13 over the approaches to the Delaware Memorial Bridge Twin-Spans and Interstate 295. Figure 6 is a photograph of Bridge No.2. Truck traffic is very significant on this bridge with an estimate

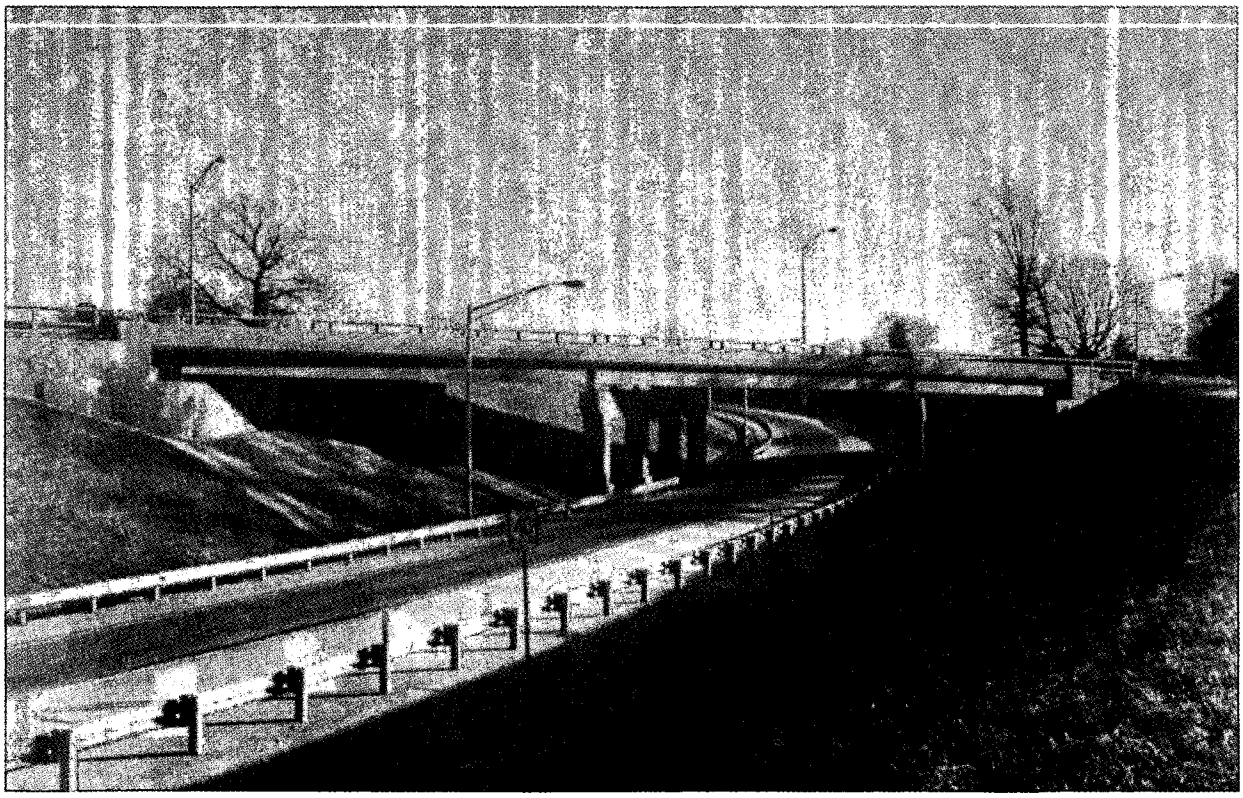


Figure 6 DRBA Bridge No. 12

average daily truck traffic of over 2500 trucks per day. The bridge is three-spans continuous and carries two through traffic lanes and an on-ramp. The geometry is complicated by horizontal

curvature and super-elevation. The geometry potentially requires both transverse and longitudinal joints.

The existing bridge has a veritcal clearance problem. In order to improve vertical clearance without altering the grade of either the highway over or under the bridge, the channel-bridge concept proven at the Magazine Ditch was chosen for this site. Further, speed of erection is of utmost concern to the DRBA. Unlike free bridge owners, the DRBA can easily estimate their loss in revenue if the replacement of Bridge No. 12 requires closure or traffic restriction of their Delaware Memorial Bridge. Thus, the potential increased cost of the composite-material bridge, over a bridge of traditional materials, can be offset by savings in lost toll revenue.

Bridge No. 12 is being designed by J. Muller International with the concept validated by the University of Delaware and is anticipated to be constructed during the 1999 construction season. By late 1999, fatigue testing at the University should demonstrate adequate fatigue life for this high-traffic volume application with 100 million truck cycles necessary over the 75-year life of the bridge.

Summary

The process of designing and constructing composite-material highway bridges is underway in the State of Delaware. An incremental approach to this implementation of innovative technology is assuring that the change in culture required for successful introduction of these materials into the civil infrastructure is accomplished. The entire effort is intended to transfer technology from the University and advanced industries of the State of Delaware to the bridge design and construction community.

Acknowledgments

The design and construction of the Magazine Ditch Bridge was funded by the DRBA. The monitoring of the completed bridge is being funded by the FHWA. The design and construction of Bridge No. 1-351 is being funded by DelDOT in conjunction with the FHWA, and administered through the DTI. Its subsequent monitoring is also being funded by the FHWA. Finally, the design and construction of Bridge No. 12 is being funded by the US Department of Defense's DARPA and the DRBA.

References

American Association of State Highway and Transportation Officials (AASHTO), *AASHTO LRFD Bridge Design Specifications*, First Edition, Washington, D. C., 1994.

Highway Innovative Technology Evaluation Center (HITEC), *Evaluation Findings: The Segmental Concrete Channel Bridge System*, HITEC 96-01, Washington, D.C., March 1996.

Mertz, D. R., and Kulicki, J. M., *THE APPLICATION OF THE AASHTO LRFD BRIDGE DESIGN SPECIFICATIONS TO COMPOSITE-MATERIAL BRIDGES*, Preceedings of the US-Canada-Europe Workshop on Bridge Engineering, Zurich, Switzerlad, July 1997, pp. 178-184.

SESSION 10: SEISMIC ISSUES (5)

(1) Compressive Behavior of Concrete Stub Columns Confined by Carbon Fiber Composite Jackets
(Y. Xiao and H. Wu)

(2) Design Considerations on the Retrofit of RC Columns with CFRP Sheet
(F. Hakamada)

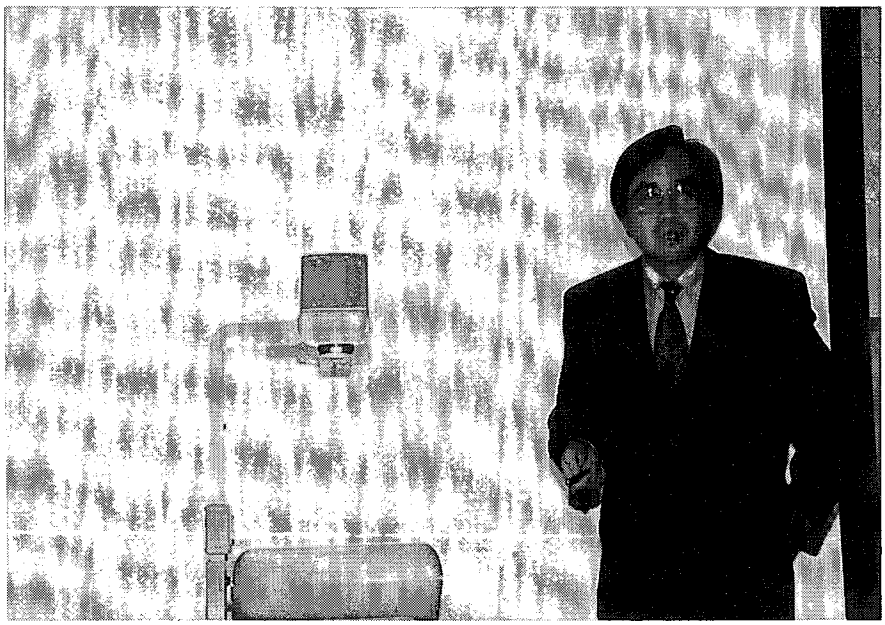
(3) California's Program for the Use of Composite Materials for Seismic Retrofit
(Thomas Post and Mohsen Sultan)

(4) Evaluation of Foundations on the Hanshin Expressway Kobe Route Damaged by the Great Hanshin Earthquake
(H.Hayashi, K. Kosa, Y. Kimura and H. Kitahara)

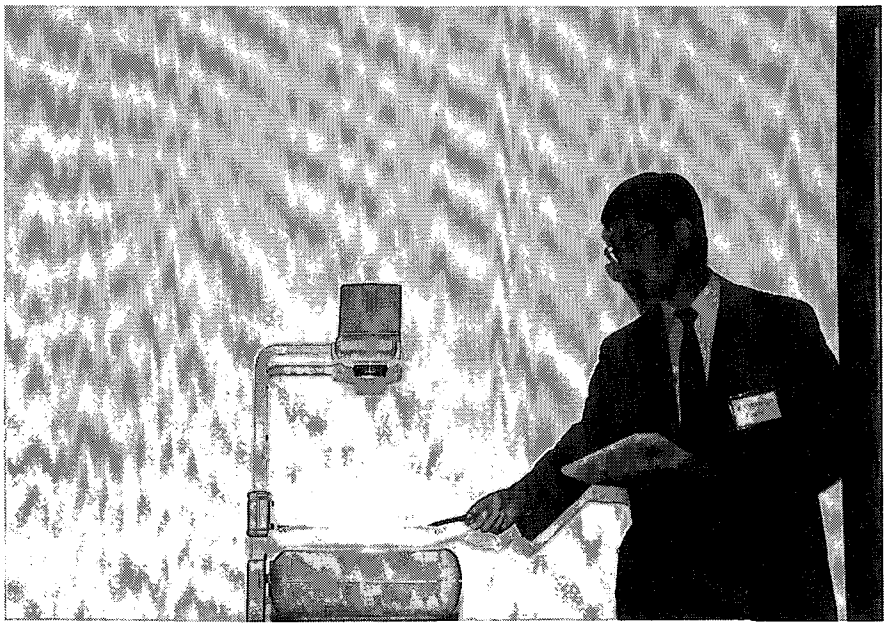
(5) Retrofitting of Railway Bridges
(E. Manos Maragakis, Bruce M.Douglas, Qingbin Chen and Ray Zelinski)



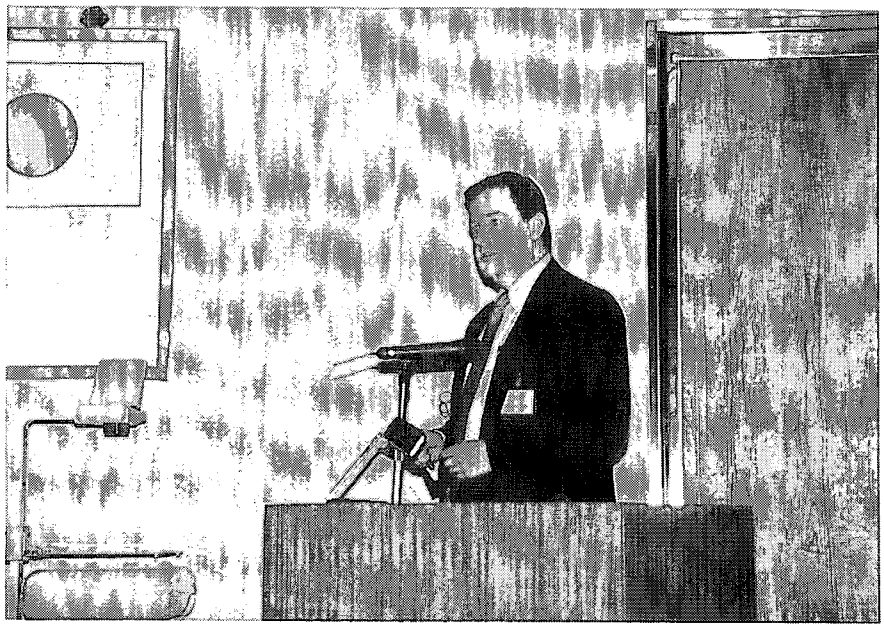
Co-Chairmen : Toru Terayama, Dennis Mertz



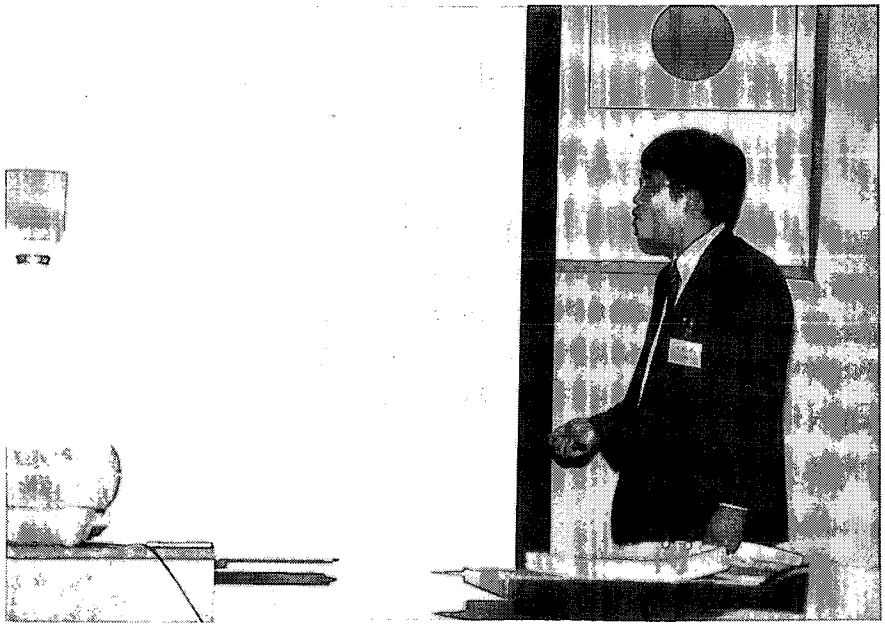
SESSION 10 : Yan Xiao



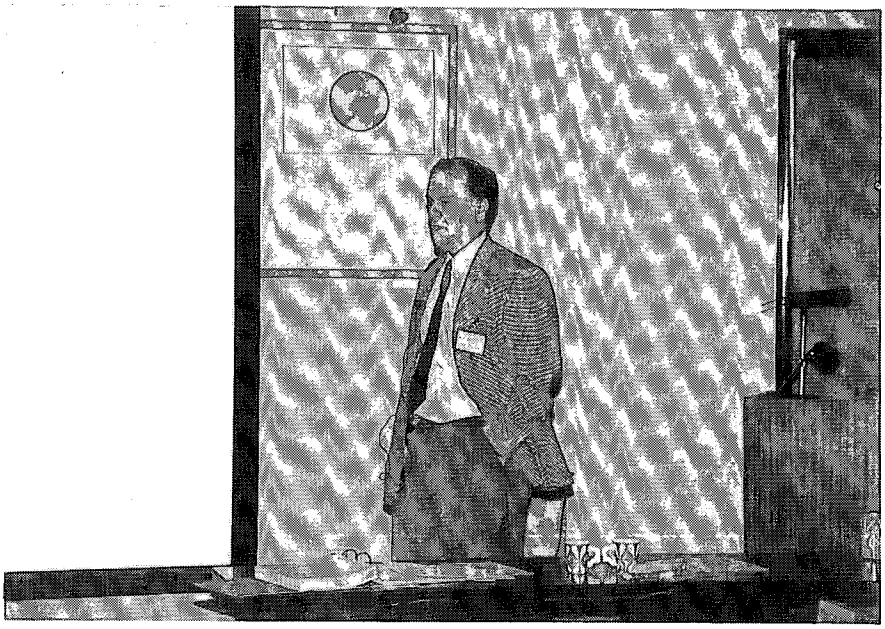
SESSION 10 : Fumio Hakamada



SESSION 10 : Thomas Post



SESSION 10 : Kenji Kosa



SESSION 10 : Manos Maragakis

COMPRESSIVE BEHAVIOR OF CONCRETE STUB COLUMNS CONFINED BY CARBON FIBER COMPOSITE JACKETS

Y. Xiao [1] and H. Wu [2]

ABSTRACT

This paper describes the experimental results from an on going comprehensive research program to study the fundamental stress strain behavior of concrete confined in various types of advanced composite jackets. More than 200 concrete stub columns with composite jackets are currently being tested under axial compression. Experimental parameters include plain concrete strength, types of composites as well as jacket thickness. This paper discusses the test results on concrete stub columns with carbon fiber sheet reinforced composite jacketing.

INTRODUCTION

Advanced composite materials have been recently applied to bridge column retrofit. The general expectations from composite retrofit systems include light weight, high stiffness or strength to weight ratios, etc. Several composite jacketing systems have been developed and validated in laboratory or field conditions. Matsuda et al. [1990] tested a system for bridge pier retrofit using unidirectional carbon fiber sheets wrapped longitudinally and transversely in the potential plastic hinge region or in the region of main bar cut-off. The carbon fiber sheets were bonded to the concrete surface using epoxy resin. Another composite wrapping system using E-glass fiber, which is much more economical than carbon fiber, has been experimentally studied by Priestley and Seible [1991, 1993]. Priestley et.al.'s test results on 40% scale bridge piers wrapped with the glass fiber composite jacketing demonstrated significant improvement of seismic performance with increased strength and ductility. Priestley and Seible also developed a full design package for seismic retrofit of existing columns using different retrofit jacketing systems. Saadatmanesh, et.al. [1994] have proposed a wrapping technique using glass fiber composite straps for column retrofit. Seible et al. [1995] have experimentally validated a carbon fiber retrofit system, which utilizes an automated machine to wrap carbon bundles to form a continuous jacket. Successful field construction demonstration is also reported by Seible et al. [1995]. These composite retrofit measures can be categorized as in-situ fabricated jacketing which involves hand or automated machine placement of epoxy saturated glass or carbon fabrics

[1] Assistant Professor of Civil Engineering, University of Southern California, Los Angeles, CA.;
[2] Graduate Research Assistant, University of Southern California, Los Angles, CA.

on the surface of existing concrete. An in-situ fabricated jacket can match the shape of the existing column. However, due to the fact of in-situ fabrication, these systems may need special attention to the job-site quality control and curing of the composite jackets. Xiao et al. [1996, 1997] have investigated a prefabricated composite jacketing system for retrofitting reinforced concrete columns. The prefabricated jacketing system is expected to have superior constructability in terms of the quality control and the speed of installation.

Despite of the successful applications of various composite jacketing systems in retrofitting laboratory models as well as prototype bridge columns, research into the fundamental interaction mechanisms between the composite jackets and the confined concrete is still limited. Although several stress strain models have been proposed and calibrated against several individual jacketing systems [Picher et al. 1996; Hosotani et al. 1996; Mirmiran et al. 1997], they are not yet calibrated for general use due to the lack of sufficient data, thus, in many cases of structural retrofit design, engineers are relying on the models developed based on test results of concrete confined in transverse reinforcing steel.

This paper presents the experimental results on stress - strain behavior of concrete stub columns confined in carbon fiber reinforced composite jacket and discusses issues related to the modeling of stress - strain relationships. Note that throughout the paper, compression is defined as positive while tension is defined as negative for forces, stresses and deformations.

EXPERIMENTAL PROGRAM

Specimens

A total of 36 standard concrete cylinders with the diameter of 152 mm (6 in.) and the height of 300 mm (about 12 in.) have been tested under axial compression. The main experimental parameters include unconfined concrete strength, thickness of in-situ fabricated carbon fiber composite jackets. Table-1 summarizes the testing matrix.

For each type of composite jacket system, three batches of concrete representing lower, medium and higher strength concrete were prepared. Concrete mix design proportions are shown in Table-2. The maximum size of the coarse aggregates was about 13 mm (about 0.5 in.). The target strengths at 28 days for the lower, medium and higher strength concrete were 27.6 MPa (4 ksi), 37.9 MPa (5.5 ksi) and 48.2 MPa (7 ksi), respectively. The actual concrete strength at testing ages about 60 to 80 days after casting was slightly higher than the mix design target strength. For each batch of concrete, 12 cylinders were made using the standard procedure. The specimens were cured in a close-can condition at room temperature. Three cylinders from each batch were tested without jacket to provide control data for the unconfined concrete, and nine others were wrapped with composite jackets at three different types of thickness. For each combination of testing parameters, three identical specimens were fabricated and tested. The ends of the concrete cylinders were capped with high strength sulfur.

Composite Jackets

The jacket system investigated involves hand layout of uni-direction carbon fiber sheets on epoxy saturated surfaces. The installed jackets had a fiber orientation configured along the circumferential direction. A thin layer of primer epoxy was first applied to the concrete surface. After the primer epoxy on concrete surface was cured at the ambient temperature for several hours, the carbon fiber sheets were installed. For each layer of carbon fiber sheets, two plies of epoxy, one on the cylinder surface prior to installing the sheet and the other on top of the installed sheet were applied using paint brushes to fully saturate the layers with epoxy. The extra epoxy for each layer was squeezed out using a flat plastic edge. After the required layers of the sheet were installed, the carbon fiber reinforced composite jacket was cured in the ambient condition.

The mechanical properties including the modulus and the tensile strength of the composite jackets were obtained through tensile testing of flat coupons with fibers configured uni-directionally along the coupon axis. The tensile coupons were made at the same time and condition along with the jackets. Table-3 summarizes the mechanical properties.

Confinement Modulus and Confinement Strength

Besides the material properties of concrete, there are two significant factors affecting the performance of confined concrete. They can be defined as confinement modulus and confinement strength (Xiao et al. 1990). Based on the cylindrical coordinate system shown in Fig.1, the confinement modulus, C_j, can be as the ratio of the increments of confinement stress, Δf_r, and radial (transverse) strain, $\Delta\varepsilon_r$,

$$C_j = -\frac{\Delta f_r}{\Delta \varepsilon_r} \tag{1}$$

where, the "-" sigh represents the passive confinement.

Using the equilibrium condition and the deformation compatibility condition in the cross section, the following two equations can be established,

$$f_r = -\frac{2t_j}{D} f_{j\theta} \tag{2}$$

$$\varepsilon_r = \varepsilon_{j\theta} \tag{3}$$

where, t_j is the thickness of the jacket; D is the diameter of the concrete cylindrical column; $f_{j\theta}$ and $\varepsilon_{j\theta}$ are the circumferential stress and strains of jacket, respectively. Using equations (2) and (3), the confinement modulus can be expressed as,

$$C_j = \frac{2t_j}{D}\frac{\Delta f_{j\theta}}{\Delta \varepsilon_{j\theta}} \tag{4}$$

Since the composite jacket is essentially a linear elastic material, $\Delta f_{j\theta}/\Delta \varepsilon_{r\theta}$ can be assumed to be equal to tensile modulus of E_j. Thus, a constant confinement modulus based on the thickness of jacket, diameter of column and jacket modulus can be defined.

$$C_j = \frac{2t_j}{D}E_j \tag{5}$$

Based on the tensile coupon test results, the confinement modulus is found as 525 MPa, 1,050 MPa and 1,580 MPa for the jackets with one, two and three plies (layers), respectively.

On the other hand, the confinement strength limit, f_{ru}, is determined by the ultimate strength of the jacket, f_{ju}, given by,

$$f_{ru} = -\frac{2t_j}{D}f_{ju} \tag{6}$$

or using ultimate strain, ε_{ju},

$$f_{ru} = -C_j\varepsilon_{ju} \tag{7}$$

Test Methods

As shown in Fig.2, all the specimens were tested using the SATEC One Million Pounds Compression Machine at the Structural Laboratory of USC. This unique equipment has sufficient capacity and stiffness, required for conducting such tests. The extremely high stiffness of the test frame makes it possible to measure the falling branch, if any, of concrete stub columns. The machine is also equipped with a sophisticated computer control and data acquisition system.

The instrumentation included the applied axial load, P, axial deformation of concrete, transverse and axial strains of the jacket. As shown in Fig.2, in order to avoid the influences due to the possible imperfect contacts as well as the end confinement due to the friction between the ends of the specimen, the axial deformations of the specimen were measured for the middle portion with a gauge length of 1502 mm (about 6 in.), using a specially designed device composed of linear bearings and linear potentiometers. The jacket strains were measured using electrical resistance gauges with a gauge length of 30 mm (1.18 in.).

Calculation of Concrete Stresses and Strains

The axial strain of concrete, ε_z, is determined based on the linear potentiometer measurements. The jacket axial and circumferential strains, ε_{jz}, $\varepsilon_{j\theta}$, are directly measured. The

concrete transverse (radial and circumferential) strains, ε_{cr}, $\varepsilon_{c\theta}$, are obtained using the deformation compatibility condition in the column cross section.

$$\varepsilon_{cr} = \varepsilon_{c\theta} = \varepsilon_r = \varepsilon_{j\theta} \tag{8}$$

The transverse (radial and circumferential) stresses of confined concrete, f_{cr}, $f_{c\theta}$, are obtained using the equilibrium condition between the confined concrete core and the jacket, and the above equation (8),

$$f_{cr} = f_{c\theta} = f_r = -\frac{2t_j}{D} f_{j\theta} = -C_j \varepsilon_{j\theta} \tag{9}$$

The axial stress of confined concrete, f_{cz}, are calculated using the equilibrium condition in the column axial direction with ignoring the jacket axial stress, thus,

$$f_{cz} = \frac{P}{A_c} \tag{10}$$

where, A_c is the sectional area of concrete core.

EXPERIMENTAL RESULTS AND DISCUSSIONS

Axial Stress - Strain Relationships

Axial stress vs. axial and transverse strains of confined concrete are shown in Fig.3 (a) to (c) for specimens with different unconfined concrete strength. The axial stress strain relationships obtained for unconfined concrete stub columns are also shown in Fig.3. As shown in Fig.3, the initial portions of stress strain responses of confined concrete essentially followed the curves of unconfined concrete. After exceeding the unconfined concrete strength, the axial stress - axial strain as well as axial stress - transverse strain relationships of most specimens softened slightly and eventually exhibited an almost linear behavior until the sudden failure due to the rupture of carbon fiber composite jackets. Such near linear behavior of concrete confined in elastic materials have been noticed in existing studies (Xiao 1989; Xiao et al. 1991; Hosotani et al. 1996; Mirmiran et al. 1997]. For the three specimens of high strength concrete confined by one-layer jacket and one specimen with medium strength concrete confined by one-layer jacket, although the peak stress exceeded the unconfined concrete strength, the post peak behavior exhibited a sudden drop. Even for the specimens with a descending stress strain response, the post peak stress eventually stabilized at a lower stress level until the rupture of the jacket.

The failure corresponding to the rupture of carbon fiber jacket was very explosive. For some specimens, the rupture of jacket was accompanied by slight delamination between the layers. The recorded jacket strains corresponding to the failure ranged from 0.007 to 0.015, which were about 50% to 80% of the rupture strains obtained for the tensile coupons. The reduced rupture

strains of the jackets probably reflected the differences of the quality controls for flat coupons and the jackets, dynamic development of concrete cracks, etc. The concrete ultimate axial strains corresponding to failure varied widely from 0.005 to 0.03, with a tendency of increase for specimens with lower strength and more jacket layers.

Axial - Transverse Strain Responses

Typical relationships for axial and transverse strains are shown in Fig.4 for the three specimens with medium strength concrete and 3 layers of carbon fiber composite jacket. As shown in Fig.4, the initial slopes of the axial strain and transverse strain relationships are very close to dashed line corresponding to a slope value of 0.18, which represents the typical initial Poisson's ratio for concrete. As the axial strain increases, the ratio between the transverse strain and axial strain increases, indicating the acceleration of the dilation of the concrete. The curves appear to eventually converge into a linear line, which can be expressed as,

$$\varepsilon_r = \varepsilon'_{ro} - \nu' \varepsilon_{cz} \tag{11}$$

where, ε'_{ro} is the intersection of the linear line at zero axial strain; and ν' is the slop value of the line. For all the 27 specimens with jackets, ε'_{ro} and ν' were calculated. Based on the test results, ε'_{ro} had an average value of about -0.00047. It was recognized that the value of slope, ν', increases for higher concrete strength, f'_{co}, and lower confinement modulus, C_j, and can be given by the following equation obtained from regression analysis.

$$\nu' = 7\left(\frac{f'_{co}}{C_j}\right)^{0.8} \tag{12}$$

Note that the value of ν' approaches to zero when C_j becomes infinity. This is consistent with experimental observations for concrete with significantly large confinement modulus [Bazant et al. 1986; Xiao 1989, 1991]. Comparison of equation (12) and all the test data is shown in Fig.5. The calculated value of 0.40 based on equation (12) is also shown in Fig.4 for the specimens with f'_{co}=43.8 MPa and C_j=1,580 MPa.

Axial Stress - Confinement Stress Responses

As an example, the axial stress - confinement stress relationships for the specimens with medium concrete strength and 3-layer carbon composite jacket are depicted in Fig.6. The stresses in Fig.6 are shown as the ratios of stresses divided by unconfined concrete strength, f'_{co}. The initial slopes of the curves are very close to the dashed line with a slope of k_o=166, which was calculated based on the following equation (12).

$$k_o = \frac{E_c}{C_j \nu_o} \tag{13}$$

where, E_c is the elastic modulus of unconfined concrete, taken as $4{,}733\sqrt{f'_{co}}$; ν_o is the initial Poisson's ratio, taken as 0.18.

As shown in Fig.6, after the axial stresses exceed the unconfined concrete strength, the curves tend to converge into linear lines with much smaller slopes than the initial behaviors. The final linear portion of the axial and confinement stress relationships can be expressed by the following equation,

$$\frac{f_{cz}}{f'_{co}} = \alpha + k\frac{f_r}{f'_{co}} \tag{14}$$

where, α and k represent the intersection with vertical axis and slope of the linear line, respectively. If taking α=1.0, k=4.1, the above equation becomes the well known Richart's failure criterion [Rechart et al. 1929]. The values of α for all the specimens vary around an average value of 1.10. Based on the regression analysis for all the specimens with setting the ultimate value of k to be 4.1 corresponding to infinite C_j, the following equation was obtained.

$$k = 4.1 - 0.75\frac{f'^2_{co}}{C_j} \tag{15}$$

Fig.7 shows the correlation of equation (15) with test data. Note that the small or negative values for k corresponding to small values of C_j/f'^2_{co} were obtained for the final linear portions in the axial stress and confinement stress relationships rather than the points at peak axial stresses. The test data indicated that a boundary of $C_j/f'^2_{co} \approx 0.3$ exists to distinguish the performances with or without descending axial stresses.

Bilinear Simulations for Stress - Strain Relationships of Confined Concrete

Based on the test results and theoretical equations between the four mechanical variables of confined concrete, ε_{cz}, ε_r, f_{cz},, and f_r, it is suggested to use the following two sets of linear equations to describe the mechanical natures of initial and final performances of concrete confined by composite jacket.

For initial performance,

$$f_{cz} = E_c\varepsilon_{cz} \tag{16a}$$

$$\varepsilon_r = -\nu_o\varepsilon_{cz} \tag{16b}$$

$$f_r = -C_j\varepsilon_r \tag{16c}$$

For final performance,

$$f_{cz} = \alpha f'_{co} + k f_r \tag{17a}$$

$$\varepsilon_r = \varepsilon'_{ro} - \nu'_o \varepsilon_{cz} \tag{17b}$$

$$f_r = -C_j \varepsilon_r \tag{17c}$$

The ultimate condition of the confined concrete can be determined by substituting the ultimate rupture strain of jacket into equation (17). Based on the test results, it is conservatively suggested to use the 50% of the rupture strain measured for flat tensile coupon samples of carbon fiber composites.

The simple bilinear simulations based on equations (16) and (17) were performed for the test results conducted by Hosotani et al. (1996), as compared in Fig.8(a) and (b). As shown in Fig.8, the bilinear equations describe the trends of Hosotani et al.'s test data reasonably well.

CONCLUSIONS AND SUMMARIES

(i) Significant increase in strength and ductility of concrete can be achieved by carbon fiber composite jacketing.
(ii) As the parameters to describe the confinement effectiveness, the confinement modulus and the confinement strength of the composite jacketing have been defined.
(iii) Besides the material properties such as concrete strength, the performance of the confined concrete is dominated by the confinement modulus.
(iv) The ultimate condition of the confined concrete is determined by the rupture of the composite jacket. The rupture strain of the jacket is much lower than the rupture strain obtained for flat tensile coupon samples.
(v) The final stress strain performances of confined concrete with carbon fiber composite jacketing exhibit a linear behavior. Equations to define the relationships between the mechanical variables of the confined concrete are proposed.
(vi) The proposed equations together with the equations for elastic behavior of unconfined concrete are suggested to provide the simple bilinear simulation to the mechanical behavior of confined concrete.

ACKNOWLEDGMENTS

The study described in this paper was conducted as one phase of the California Department of Transportation (Caltrans) evaluation program for various composite jacketing systems. The tests on concrete stub columns confined by carbon fiber reinforced composite jackets were

funded by Master Builders, Inc. The authors would like to thank Caltrans engineers Mr. L.H. Sheng and Mr. M. Sultan for their valuable inputs. Special thanks are due to Dr. H. Kliger, Technical Representative of Tonen Corporation in US, for his helps and valuable technical inputs related to the carbon fiber system tested in this study. Comments and conclusions described in this paper are solely those of the authors and do not necessarily reflect the views of Caltrans or the funding agency.

REFERENCES

Bazant, Z.P.; Bishop, F.C. and Chang, T.P., (1986), "Confined Compression Tests of Cement Paste and Concrete up to 300 ksi," ACI Journal, V.83, July-August, pp. 553-560.

Hosotani, M., Kawashima, K., and Hoshikuma, J., (1996), "Seismic Retrofit of Reinforced Concrete Bridge Piers by Carbon Fiber Sheets," *Proc., 3rd US-Japan Workshop of Seismic Retrofit of Bridges*, ISSN 0368-5878, Technical Memorandum of PWRI, No. 3481.

Matsuda, T.; Sato, H.; Fujiwara, H.; and Higashira, N., (1990), "Effect of Carbon Fiber Reinforcement as a Strengthening Measure for Reinforced Concrete Bridge Piers," *Proceedings of the First U.S.-Japan Workshop on Seismic Retrofit of Bridges*, Public Works Research Institute, Ministry of Construction, Tsukuba Science City, Japan, December 17-18.

Mirmiran, A., and Shahawy, M., (1997), "Behavior of Concrete Columns Confined by Fiber Composites," *ASCE Journal of Structural Engineering*, Vol. 123, No.5, 583-590.

Picher, F., Rochette, P., and Labossiere, P. (1996), "Confinement of Concrete Cylinders with CFRP," *Porc., 1st Int. Conf. Composites in Infrastructure*, H. Saadatmanesh and M.R. Ehsani, eds., University of Arizona, Tucson, Ariz., 829-841.

Priestley, M.J.N.; and Seible, F., (1991), "Seismic Assessment and Retrofit of Bridges," Edited by M.J.N. Priestley and F. Seible, University of California at San Diego, *Structural Systems Research Project*, Report No. SSRP-91/03, July, 418p.

Rechart, F.E.; Brantzaeg, A.; and Brown, R.L., (1929), "The failure of Plain and Spirally Reinforced Concrete in Compression," Bulletin No. 185, Engineering Experiment Station, University of Illinois, Urbana, November.

Saadatmanesh, H.; Ehsani, M.R.; and Li, M.W. (1994), "Strength and Ductility of Concrete Columns Externally Reinforced with Fiber Composite Straps," *ACI Structural Journal*, July-August Issue, pp.434.

Seible, F. and Priestley, M.J.N., (1993), "Retrofit of Rectangular Flexural Columns with Composite Fiber Jackets," California Department of Transportation, *Proceedings of the Second Annual Seismic Research Workshop*, Sacramento, March 16-18.

Seible, F.; Hegemier, G.A.; and Innamorato, D., (1995), "Developments in Bridge Column Jacketing Using Advance Composites," *Proceedings of the National Seismic Conference on Bridges and Highways*, Federal Highway Administration and California Department of Transportation, San Diego, California, December 10-13.

Xiao, Y., (1989), "Experimental Study and Analytical Modeling of Triaxial Behavior of Confined Concrete," Ph.D. Thesis, Kyushu University, Japan.

Xiao, Y.; Tomii, M.; and Sakino, K., (1991), "Triaxial Compressive Behavior of Confined Concrete," *Concrete Research and Technology*, Japan Concrete Institute, Vol.2, No.1, January, pp.1-14.

Xiao, Y.; Martin, G.R.; Yin, Z.; and Ma, R., (1996), "Seismic Retrofit of Existing Reinforced Concrete Bridge Columns Using A Prefabricated Composite Jacketing System," *Proceedings of the First International Conference on Composite in Infrastructure*, Tucson, Arizona, January 15-17, pp.903-916.

Xiao, Y. and Ma, R., (1997) "Seismic Retrofit of RC Circular Columns Using Prefabricated Composite Jacketing," *ASCE Structural Journal*, October.

Table-1 Test Matrix

Type of Jacket	Concrete Strength	Jacket Layers	Specimen Numbers
Carbon fiber sheet reinforced composite jacket	Lower	Plain concrete	3 specimens each
		1-layer	
		2-layer	
		3-layer	
	Medium	Plain concrete	
		1-layer	
		2-layer	
		3-layer	
	Higher	Plain concrete	
		1-layer	
		2-layer	
		3-layer	

Table-2 Mix Proportion of Concrete

Series	Target f'_{co} (MPa)	W/C	Water (kg/m^3)	Cement (kg/m^3)	Fine Aggregates (kg/m^3)	Coarse Aggregates (kg/m^3)
L	27.6	0.68	196	288	1087	853
M	37.9	0.48	196	408	986	853
H	48.2	0.38	197	515	857	853

Table-3 Mechanical Properties Based on Carbon Fiber Composite Tensile Coupon Tests

Type of Jacket	Thickness/Ply (mm)	Modulus E_j (MPa)	Modulus E_j (kN/cm)	Strength f_{ju} (MPa)	Strength f_{ju} (kN/cm)
Carbon (FTS C1-30)	0.381	1.1×10^5	259	1,577	6.01

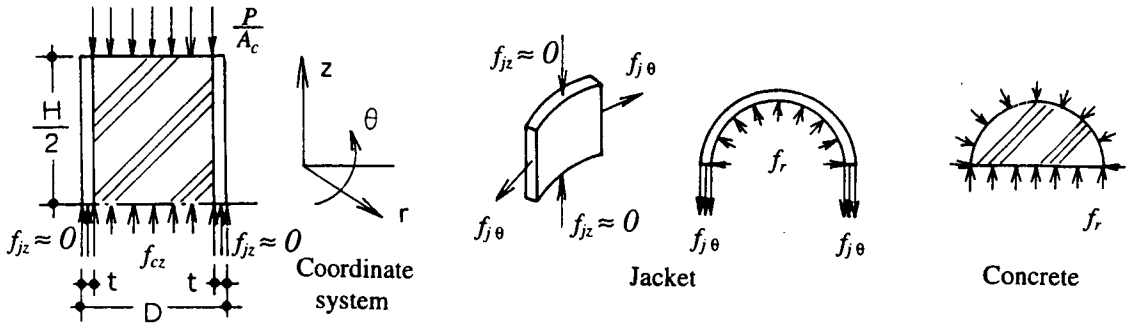


Fig.1 Definition of Mechanical Variables

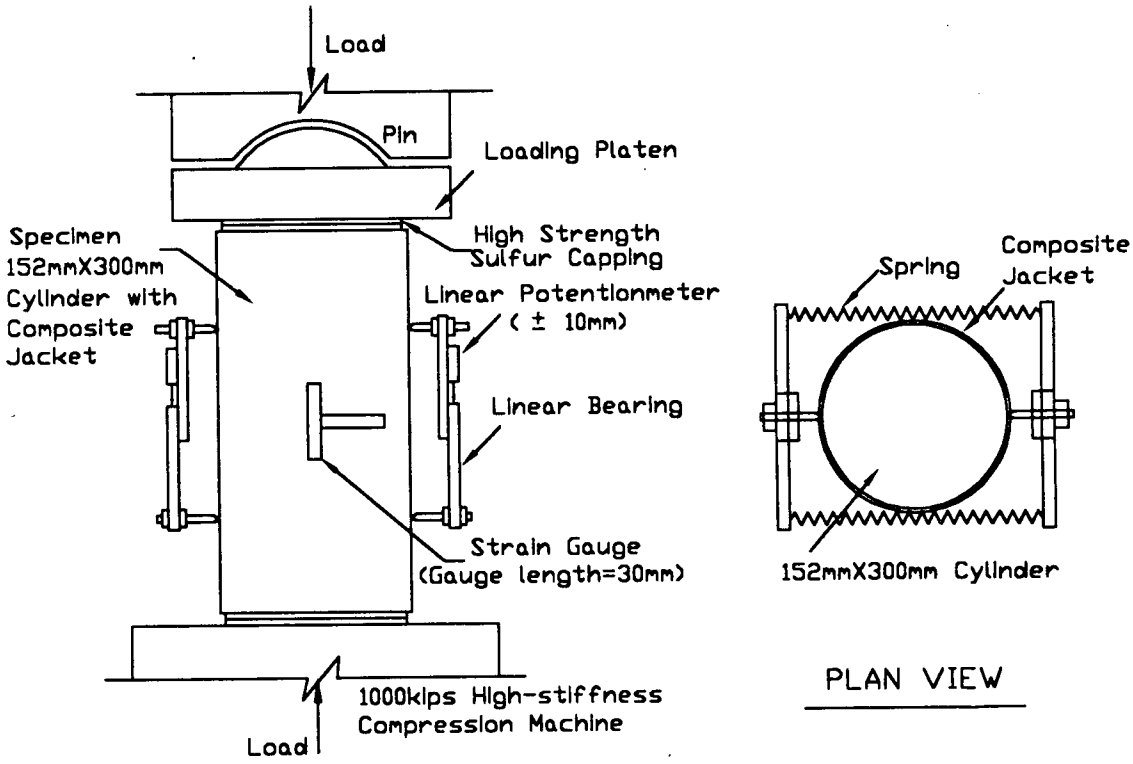
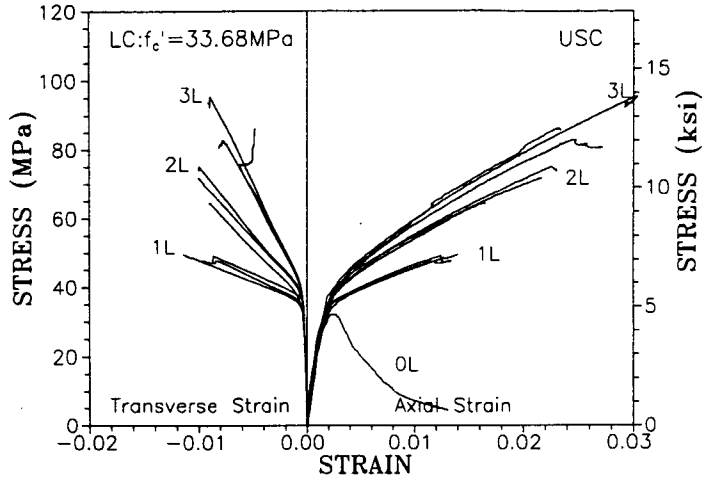
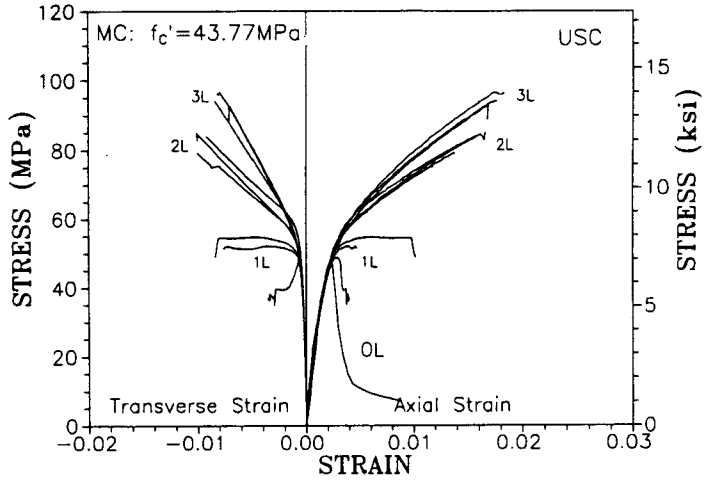


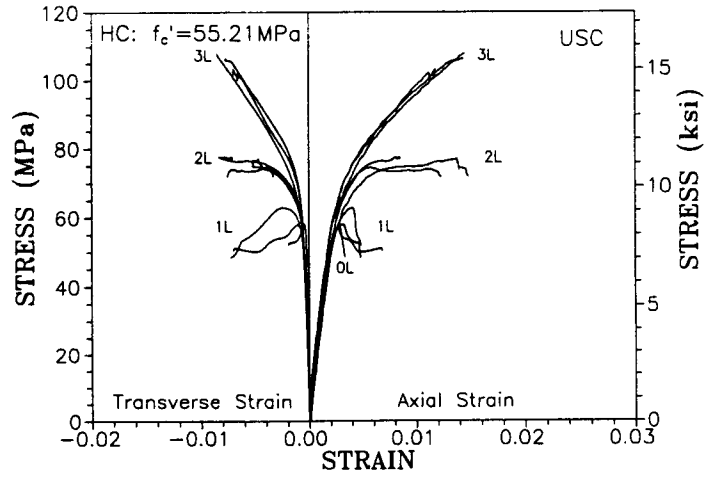
Fig.2 Test and Instrumentation Configurations



(a) Lower-Strength Specimens



(b) Medium-Strength Specimens



(c) Higher-Strength Specimens

Fig.3 Axial Stress - Strain Relationships for Concrete with Carbon Fiber Composite Jackets

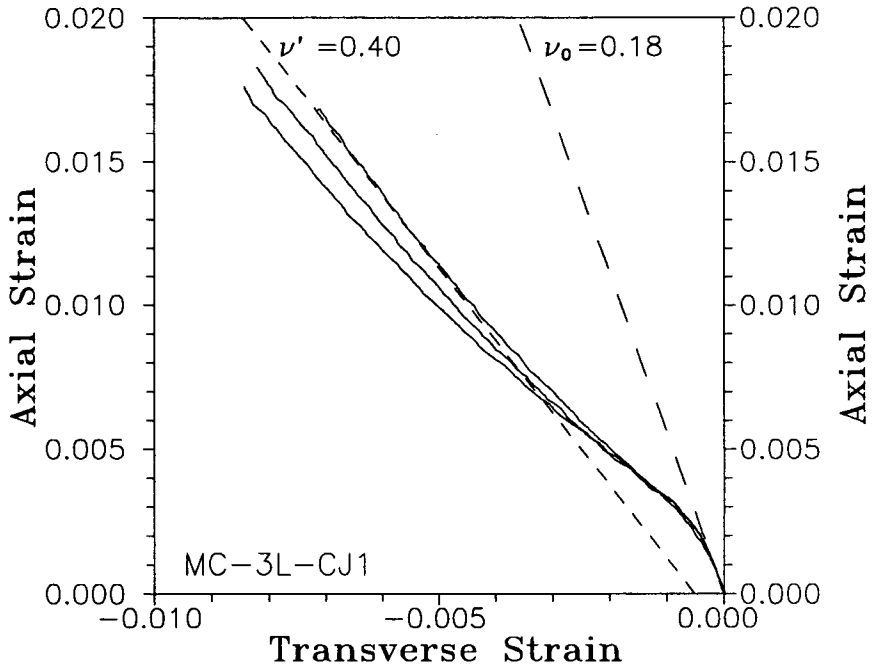


Fig.4 Typical Axial - Transverse Strain Responses

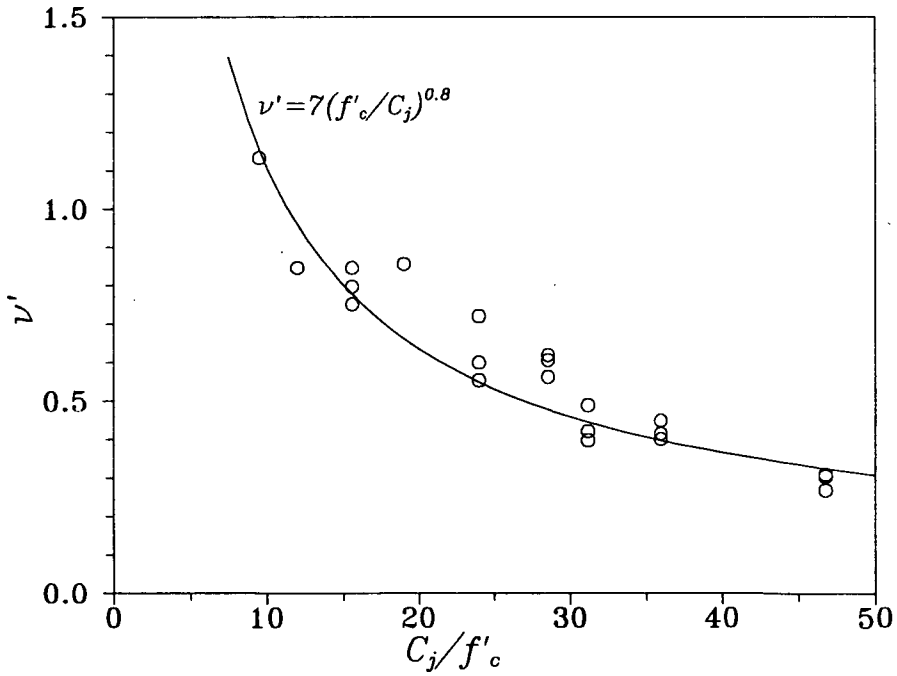


Fig.5 Test Data and Regression Equation for Coefficient ν' Between Axial and Transverse Strains of Confined Concrete

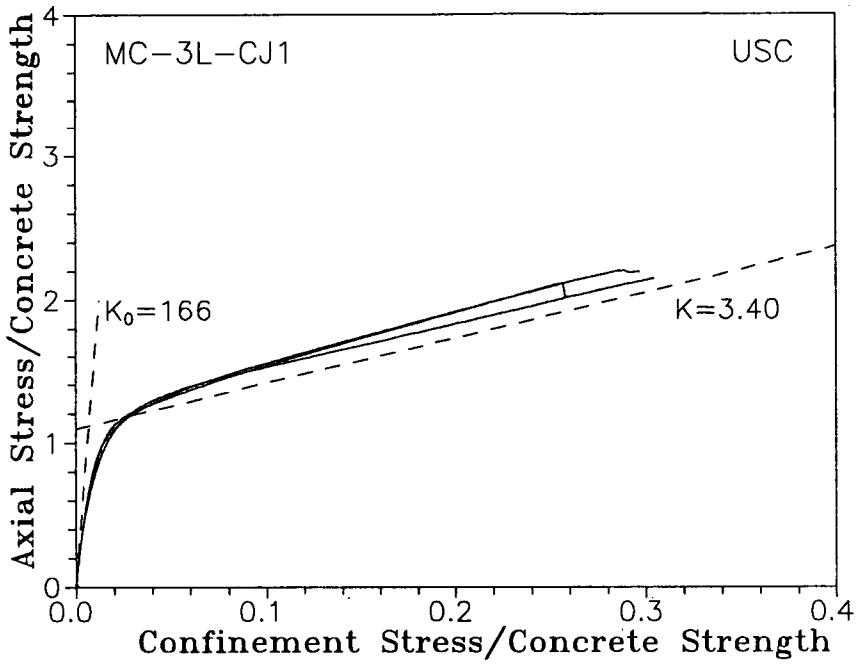


Fig.6 Typical Axial - Confinement Stress Responses

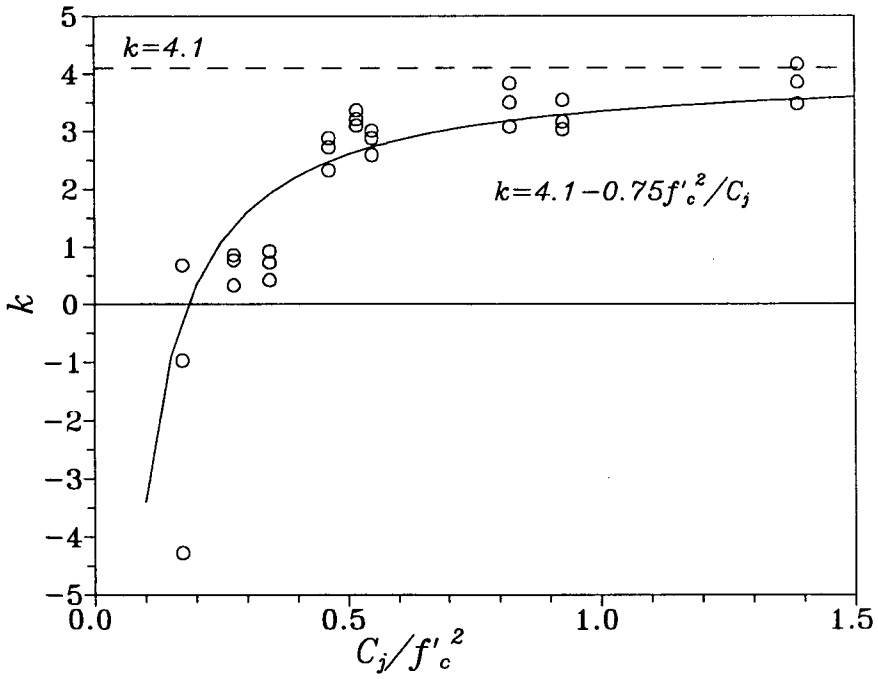
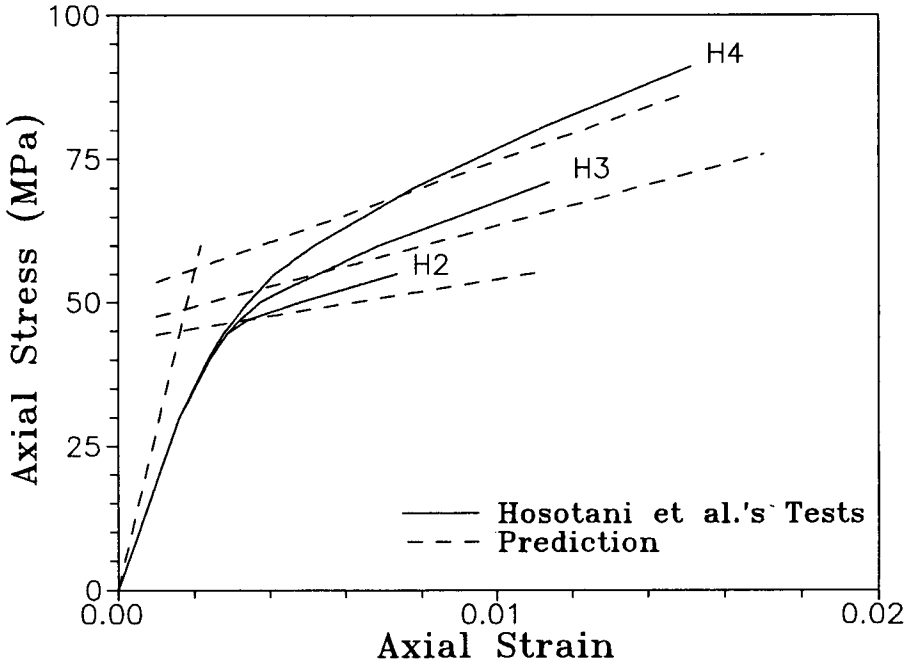
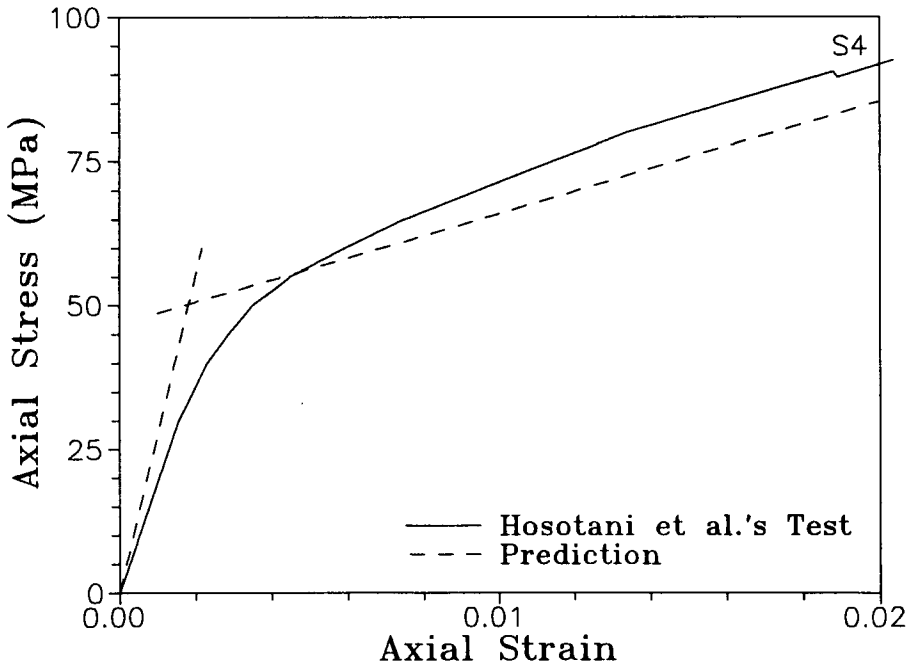


Fig.7 Test Data and Regression Equation For Final Confinement Coefficient *k*



(a) Specimens with High Modulus Carbon Fiber Jackets



(b) Specimen with Regular Modulus Carbon Fiber Jacket

Fig.8 Bilinear Simulation of Hosotani et al.'s Test Results

The 13th U.S. - Japan Bridge Engineering Workshop
Tsukuba, Japan, October 2-3, 1997

DESIGN CONSIDERATIONS ON THE RETROFIT OF RC COLUMNS WITH CFRP SHEET

Fumio HAKAMADA

Structural Engineer, Hanshin Expressway Public Corporation

ABSTRACT

Experiments on RC cantilever columns retrofitted with Carbon Fiber Reinforced Plastic (CFRP) sheet have shown good structural performance during severe earthquakes as shown in the previous report. Analysis was carried out so that characteristics could be evaluated quantitatively and applied in practice. In the design consideration several concepts such as second balanced failure, reinforcement-dominant or concrete-dominant failure were introduced. An equation and design value were proposed to evaluate the equivalent tie reinforcement of CFRP sheet.

INTRODUCTION

Since the Kobe Earthquake, there has been an urgent need to retrofit bridge columns of urban highway networks such as the Hanshin Expressway in Osaka and the Metropolitan Expressway in Tokyo. Design guidelines were prepared by the Ministry of Construction, a financial framework was put in place and the resulting program is to be completed by Fiscal Year 1998.

Table 1 shows number of columns to be retrofitted on the Hanshin Expressway, together with financial figures. Besides the retrofit, reconstruction work covers 1,270 columns on the Kobe line. Of the total of 7,504 existing columns on the Hanshin network, 6,083 are to be rehabilitated. Because all columns must meet the current seismic code requirements, the retrofit covers most columns in operation.

Table 1 Numbers of Columns retrofitted on the Hanshin Expressway

	Retrofit
Concrete	3,979
Steel	834
Total	4,813
Cost	132 b¥.

The retrofitting of superstructure components such as bearings, restrainers and girder connections is in progress. Other than several exceptional columns near embankments on reclaimed land, there are not many such substructures in need of retrofitting on the Hanshin Expressway.

Because of land use under highways, the retrofit design method is primarily by steel jacketing, which is in contrast to the Japan Highway Authority and other governmental sections, where concrete jackets are preferred for economic reasons. But where space is even more limited, CFRP jacketing has been proposed, and its structural performance has been validated through several investigations as reported previously[1]. In this paper, design considerations are covered briefly with respect to practical applications, noting that the use of CFRP is limited to where working constraints exist which hinder other construction methods. The Hanshin Expressway proposed a design guideline of CFRP retrofit method, the contents of which are covered here.

PREVIOUS STUDIES

In previous reports 1) and 2) the authors introduced the use of CFRP on the RC columns of highway bridges. The tests were performed by cyclic loading as shown in **Figure 1**. The salient points of the studies are:

1) Objectives cover round and rectangular cross-sections.
2) Objectives of retrofitting are enhancement of shear capacity, ductility and moment strength. Columns of an in-situ model are also included as a comparison.
3) The round casing of rectangular columns is included.
4) Experiment sites and subsequent model scales are different.

Round, rectangular and cylindrically-cased columns are depicted in **Figure 2**.

Experiments revealed increases in shear strength and ductility. Test specimen specifications are listed in **Table 2** and shown in **Figure 3**. Details of the moment strength enhancement of a base are shown in **Figures 4** (a) & (b) for S21M and D21M, respectively. The material test results are listed in **Table 3**.

CFRP sheet was placed circumferentially around a column to enhance shear reinforcement or to increase ductility. In the cases of specimens S21K and D20K, where casing was applied to rectangular columns, the improvement in ductility was significant. On the other hand, to increase moment strength, CFRP sheet was attached in the axial direction, except for the plastic hinge zone, where a minimum of steel plate was inserted between the axial CFRP and footing. Specimen D21M is one case where improved moment strength was obtained, although practical application of the method would not be straightforward.

DESIGN CONSIDERATIONS

When structures are exposed to a severe earthquake, they must exhibit an elastic plastic response sufficient to reduce the loading. Load reduction is achieved by the structure behaving inelastically within a sound hysteresis loop, so absorbing kinematic energy. The ductility index is a widely-used measure of the load reduction.

Although no terminology is used for the "load reduction factor" in the current code, the reduction factor R can be interpreted as

$$R = \sqrt{2 \times \mu - 1} \geqq 1$$

where μ is the displacement ductility, defined as the ratio of ultimate over yield displacement.

In the design process, it is necessary to evaluate the ultimate displacement and confirm that it is in good agreement with experimental results.

When analyzing the test results, it was assumed that the strain is distributed on a plane during deformation. Characteristic points in the interaction curve, shown in **Figure 5**, are assumed as follows.

Point 1 is the case where uni-axial compression is applied. Because the stress-strain curve has a peak as shown in **Figure 6** [3], the strain of the concrete is less than maximum (ecc<ecu).

2 is the boundary above which no tension is observed in the section.

3 is the boundary above which no yield of reinforcement is observed. This is a point of "balanced failure" where the concrete fiber reaches ecu and steel reinforcement reaches the steel yield strain, ey. In the ultimate design method, this point is less significant than point 5 below.

4 is where the section reaches its maximum bending strength.

5 is the boundary below which concrete does not reach ecu. Because they reach the ultimate strain, eyu, steel reinforcements dominate the section, and improvement of ecu by confinement is no longer effective. Normally 5 appears when the axial force is negative (tension), but when confinement prevails it may appear at positive axial force as a result of increasing ecu. In comparison with point 3, this point is referred to as "second balanced failure".

6 is the case of a beam where no axial force is applied. It does not necessarily indicate that the phenomena appear in numerical order. In columns built before the 1980 specifications, tie reinforcements are sparse compared with today, so there are many cases where point 5 is given when equilibrium axial forces are negative (tension).

7 is the boundary below which no compression exists in the section.

8 is pure tension, if the section is symmetric, given that strain is ey in the bilinear model case, where the symbols are defined in **Figure 6** or otherwise explained in the text.

Figure 7 shows the corresponding strain distribution. States 1 through 5 are **concrete-dominant** sections, where additional confinement of a section is effective. States 5 through 8 are **steel-dominant** sections, where additional reinforcement is effective.

Suppose the axial load at second balanced failure is Nb2. It can be classified according to the axial load N in equilibrium as:

1) N≥Nb2 Failure mode is concrete crushing, buckling of axial reinforcement or rupture of tie reinforcement.

2) N<Nb2 Failure mode is tensile disruption of steel reinforcement.

Note that "disruption of steel reinforcement" does not necessarily mean that of the rupture test. In the case of such cyclic loading, rupture is accelerated by low cycle fatigue failure. Therefore it is assumed the rupture strain will be less than that in the static rupture test.

In addition, the section can be classified into two, according to the vulnerability to the cause of failure. When shear reinforcement is inadequate, the section exhibits shear failure in Plane 1 shown in **Figure 8**, and it is called the **shear-dominant** section. When the shear capacity is sufficient compared with the moment strength, the failure mode is bending in Plane 2, perpendicular to the direction of the loading, and the section is said to be **bending-dominant**.

In summary, any RC column can be classified as in **Figure 9** and due consideration has to be made in the design process. From this observation, it can be stated that the failure mode is decided

neither by the horizontal load intensity nor load history, but it is inherent in the configuration of the cross-section and its applied axial load.

BASIS OF CALCULATIONS

The ultimate state is defined as follows in this paper. It is assumed to be absolute maximum response throughout an experiment. The ultimate displacement is where the envelope of the response reaches 80% of the maximum.

The stress-strain relationship of confined concrete follows those shown in **Figure 6** [3], where concrete strength and ultimate strain increase significantly with the number of tie reinforcements. The confinement of round and rectangular cross-sections differs, and the confinement of round cross-sections can be evaluated more effectively than that of rectangular cross-sections. The ultimate strain of concrete ecu was assumed to be not less than 0.005, however small the number of tie reinforcements in the analysis.

When calculating the shear capacity of a section, it is known that the design method underestimates practice except for plastic hinge zone, therefore it follows the method of Ref. 4), where shear comprises concrete, tie and axial forces. For simplicity of calculation, deformation calculation also follows Ref. 4), where plastic rotation is assumed in the plastic hinge region. Throughout the analysis the plastic hinge region for calculation purposes was assumed to be 0.5D, where D is the depth of the section. The cover concrete was not treated separately from core concrete, because the simulated in-situ RC column had too few tie reinforcements to cause separation between them, and when wrapped in CFRP the cover concrete can be treated as a part of the core concrete.

COMPARATIVE STUDIES OF ANALYSIS AND EXPERIMENT

(1) Ultimate Concrete Strength and Ultimate Load

It is known that the concrete strength is improved as a result of confinement by tie reinforcements. But the effect on ultimate load and displacement is not well understood. Analysis of a round cross-section was carried out for this study.

Taking C21 as an example of investigating the ultimate load and displacement, its four stress-strain curves are shown in **Figure 10**. Curve No.1 is the norm as shown in Ref. 3); No. 2 is the case when post peak decay was neglected; No.3 is when maximum strain was suspended at its peak, ecu = ecc; and No. 4 is the case with no confinement.

The interaction curves for axial load and bending moment are shown in **Figure 11**. The load capacity is compared in **Figure 12**. Because in the single column the axial load, 77 tons, is less than 10% of the axial load capacity of the column, the concrete strength enhancement has little effect on the load reaction, therefore the maximum load response does not change over the various configurations of stress-strain curves, whatever strength the concrete has.

On the other hand, the ultimate displacement improves significantly as also shown in **Figure 12** as a result of the increase in the ultimate strain of the concrete. The maximum displacement is not affected by the concrete stress-strain curve as long as the final concrete strain is identical.

(2) Equivalent design value for CFRP strength: 23,000 or 35,000 kgf/cm^2?

It was difficult to determine which specific value of CFRP to use for the design calculation. CFRP is a strong material that can sustain about 44,000 kgf/cm^2. The design value had to be selected so that it would be in good agreement with experimental results.

The first choice was the nominal strength of the fiber, 35,000 kgf/cm^2. A second, reduced value of 23,000 kgf/cm^2, 2/3 of the first, was selected and compared with experimental results.

Figure 13 is the result of the comparison. The specimen No. are identified in **Figure 14**. It must be taken into account that:

1) Testing of specimen S41 was not completed, because after the concrete crush was observed, it was decided to try different retrofit method by making use of the damaged specimen. Therefore it can be assumed that the final displacement of the experiment would be larger. The repaired one is to be named S21K.

2) Specimens S00, C00 and D00 were not retrofitted, so they were unaffected by differences due to CFRP.

3) Specimens C21M, D20K and D21M were the cases that the CFRP did not rupture. In other words when CFRP rupture does not take place, significant improvement of ductility can be achieved. From the viewpoint of the current design objective, since the change errs on the conservative side, no further interpretation was made here.

Though the experimental results vary depending on whether the sections are round or rectangular, cased or uncased; whether the design objectives are aimed at shear enhancement or moment strength enhancement; or whether in-situ specimens are included or not, the fact that the discrepancy between experimental and analytical results is not large is useful in itself. The results are especially close for the case where the strength fy=35,000 kgf/cm^2. When fy=23,000 kgf/cm^2 is used, results tend well on the side of safety.

(3) Ultimate strength

Figure 15 is a comparison of ultimate strength. The specimens are also identified in **Figure 16**. Compared with ultimate displacement, the difference in CFRP strength is negligible, and good agreement between experiment and analysis can be achieved. Note that in specimens C21M and S21M no strength increase was achieved in the experiment because the cohesion between the steel plate and CFRP was so weak that bond slippage took place in the loading process. Note also that analysis is identical to that of the experiment on D21M, therefore the mechanism of moment strength enhancement was achieved.

As well as the comparison of ultimate state, a yield state comparison was made but because the measurement was so sensitive and the deformation inside the footing could not be ignored, a generalized observation was not achieved.

(4) CFRP experiments in general

CFRP experiments have been performed by several organizations including Japan Railways, the Japan Railway Research Institute, the Japan Highway Authority and Osaka University. Although details of each experiment were not known, their interim reports were studied, and similar analysis were repeated to compare experiment with analysis, to confirm the above

principles. The material strengths were used as far as they were known in the analysis.

Figures 17, 18 and **19** show the displacement, load, displacement ratio and tie bar ratio ρ. Several experiments cover the shear failure model, but most of them are excluded from consideration since it was only intended to observe bending failure under cyclic loading. From **Figure 18**, the analysis coincides with experiments of load response. Analysis of the ultimate displacements shown in **Figure 17** indicates that they are well within the safety margin. **Figure 19** plots analysis/experiment ratios of the displacement against the tie bar volume ratio ρ. It may be stated that the experiments show the value of ρ having a range of about $\rho < 3\%$ when CF design stress is 23,000 kgf/cm^2.

The discussion so far is confined to CFRP retrofit. Because the concept cannot be limited to only CFRP, a comparative study of experiment and analysis was made in a general test. Similar results were observed, though the tie bar ratio was modest.

(5) Program

The computer programs used in the various investigations were open to public scrutiny during their development, and revised from time to time. As well as being capable of analyzing the required data, programs were designed to have simple, flexible input formats and graphically-oriented output. Use was made of existing software for aspects such as graphic output where possible.

TENTATIVE DESIGN GUIDELINE FOR CFRP RETROFIT

It is a general rule that, once a design method is formulated, design and construction guidelines are prepared to transfer knowledge. After these major investigations, Hanshin Expressway began to formulate guidelines. Though some problems are still unsolved, as long as the material is reliable and there are cases where it is difficult to apply conventional methods, it is unreasonable not to consider the use of CFRP, and so tentative guidelines have been prepared. 5)

A brief outline of the contents follows.

1) Scope

The usage of CFRP sheet is limited to where conventional retrofitting methods are not possible because of site constraints. In cases of even more restricted sites, an alternative analytical design method, Design 2, is introduced other than conventional design method, Design 1.

2) Material

The design value for CFRP sheet is 23,000 kgf/cm2.

3) Design 1

For a rectangular section, the designer can choose a rectangular or cylinder casing method according to site constraints. A method to evaluate tie reinforcement in view of concrete confinement and shear reinforcement is formulated. Once the CFRP sheet is replaced by an equivalent tie, the following method follows routine design procedures.

In the guidelines, the equivalent areas of CFRP as tie reinforcements are stated. The tie reinforcement including CFRP can be treated as an equivalent volume of existing tie reinforcement on an equivalent strength basis for the purpose of confinement and shear. The equivalent area can

be treated differently for each purpose and superimposed on a base model with section $B \times D$:

3-1) For the constitutive equation for stress and strain of confined concrete

Suppose that the carbon fiber sheet has thickness t, number of layers n and yield strength f_{cf}, while the tie reinforcement for a base model with area A_h has tie spacing s, yield strength f_{yh} and core width b_f. Then,

$$A_h = \mathrm{n} \times \mathrm{s} \times \mathrm{t} \times \frac{b_f}{B} \times \frac{f_{cf}}{f_{yh}}$$

In the case of carbon fiber sheet with a tube of diameter D_{tube},

$$A_h = \mathrm{n} \times \mathrm{s} \times \mathrm{t} \times \frac{b_f}{D_{tube}} \times \frac{f_{cf}}{f_{yh}}$$

The tie reinforcement ratio is calculated as $\rho = \dfrac{4 \times A_h}{s \times b_f}$

3-2) For the shear capacity, contribution of two legs,

$$A_v = 2 \times A_h$$

For a carbon fiber sheet with core depth d_w,

$$A_v = 2 \times \mathrm{n} \times \mathrm{s} \times \mathrm{t} \times \frac{D}{d_w} \times \frac{f_{cf}}{f_{yh}}$$

In the case of a carbon fiber sheet with tube of diameter D_{tube},

$$A_v = 2 \times \mathrm{n} \times \mathrm{s} \times \mathrm{t} \times \frac{D_{tube}}{d_w} \times \frac{f_{cf}}{f_{yh}}$$

4) Design 2

An analytical method is proposed, where a partial retrofit is included and shear strength capacity is evaluated as in Ref. 4, though the application of this approach is limited. A proposed method of bending enhancement is introduced.

5) Construction

To ensure accurate construction verified by experiment, field inspection items were listed. Development length, surface roughing, minimum number of sheet layers, surface coating, weather conditions and so forth are introduced. Because epoxy resin is sensitive to the construction method and has much effect on the final structural behavior, checklists are made so that a field engineer can make correct use of the appropriate material. A design list format is also attached to collect data.

SUMMARY

1) The concept of "second balanced failure" was introduced as the boundary of a control section.

2) The bending failure of a column was classified into concrete-dominant and

reinforcement-dominant sections.

3) A comparison between experimental & analysis results was made which achieved good correlation of ultimate load, together with a reasonable estimation of ultimate displacement when the CFRP strength is 35,000 kgf/cm^2, plus a conservative estimation when the strength is 23,000 kgf/cm^2. Experiments made by organizations other than Hanshin Expressway show similar results but with larger scatter.

4) A design method, where the CFRP is substituted by tie bars of equivalent strength which are added to the existing tie bars for the purposes of calculation, is assumed to be appropriate for practical applications.

5) Tentative design guidelines were prepared and applied into practice.

REFERENCES

1) Hakamada, F., Maekawa, Y. J., Hoshikuma : Experimental Study Concerning Retrofit of RC Column by CFRP Sheet, The 3rd US-Japan WS on Seismic Retrofit of Bridges Osaka City, Japan, December 10-11, 1996
2) Hakamada, F.: Experimental Study on Retrofit of RC Column using CFRP Sheet, Third International Symposium on Non-Metallic (FRP) Reinforcement for Concrete Structures, Sapporo, October 1997. (In Press)
3) Design Specification of Highway Bridge in Japan, Ministry of Construction, December 1996 (in Japanese)
4) Priestley, M.J.N., Seible, F., Y.H. Chai: Design Guidelines for Assessment Retrofit and Repair of Bridges for Seismic Performance, University of California San Diego, August 1992
5) Tentative Design Guidelines for Retrofit of RC Column by CFRP Sheet, Hanshin Expressway Public Corporation, May 1997 (in Japanese)

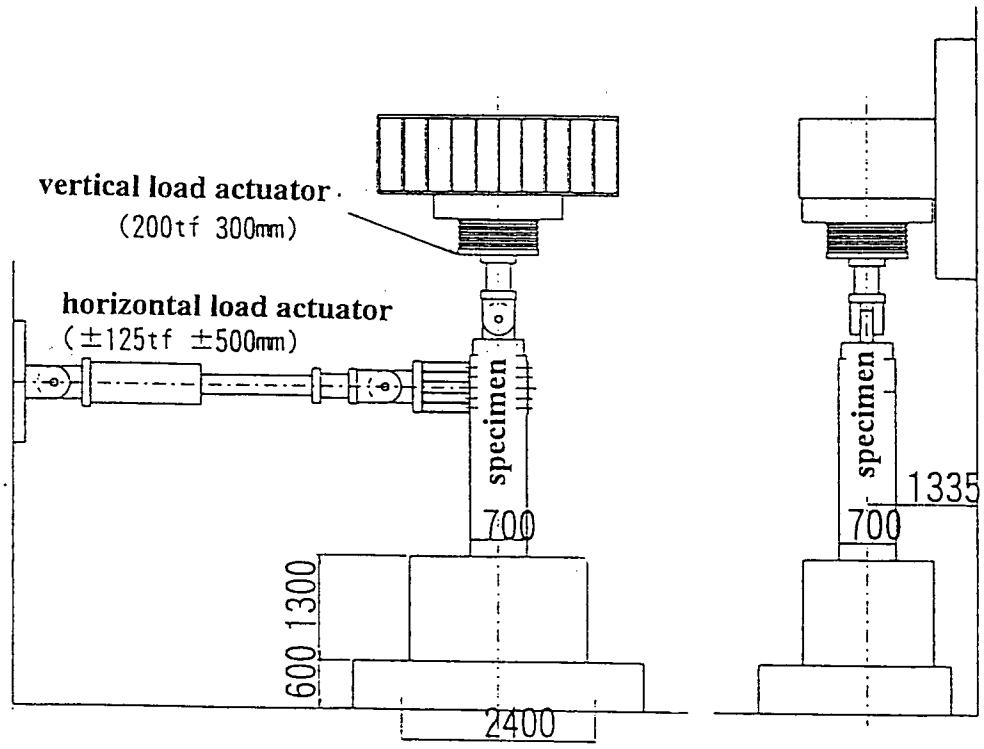
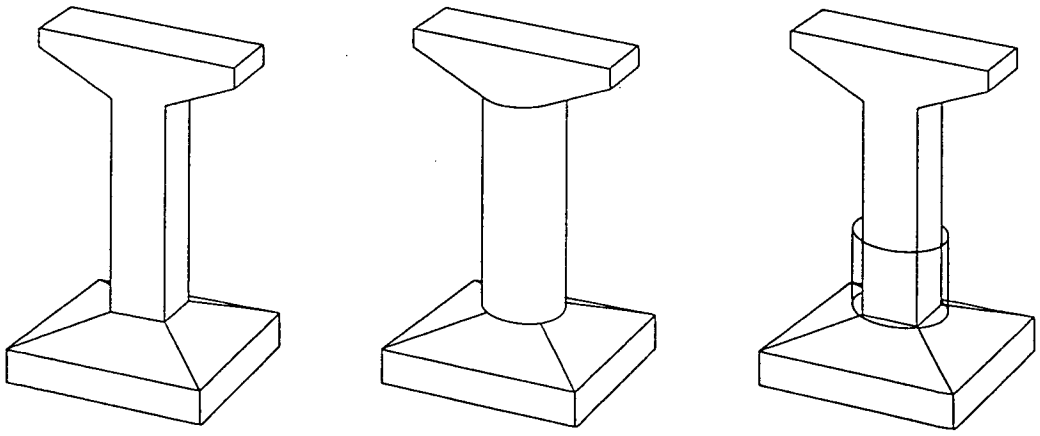


Figure 1 Test method



(a) Rectangular (b) Round (c) Cylinder casing

Figure 2 Three types of column

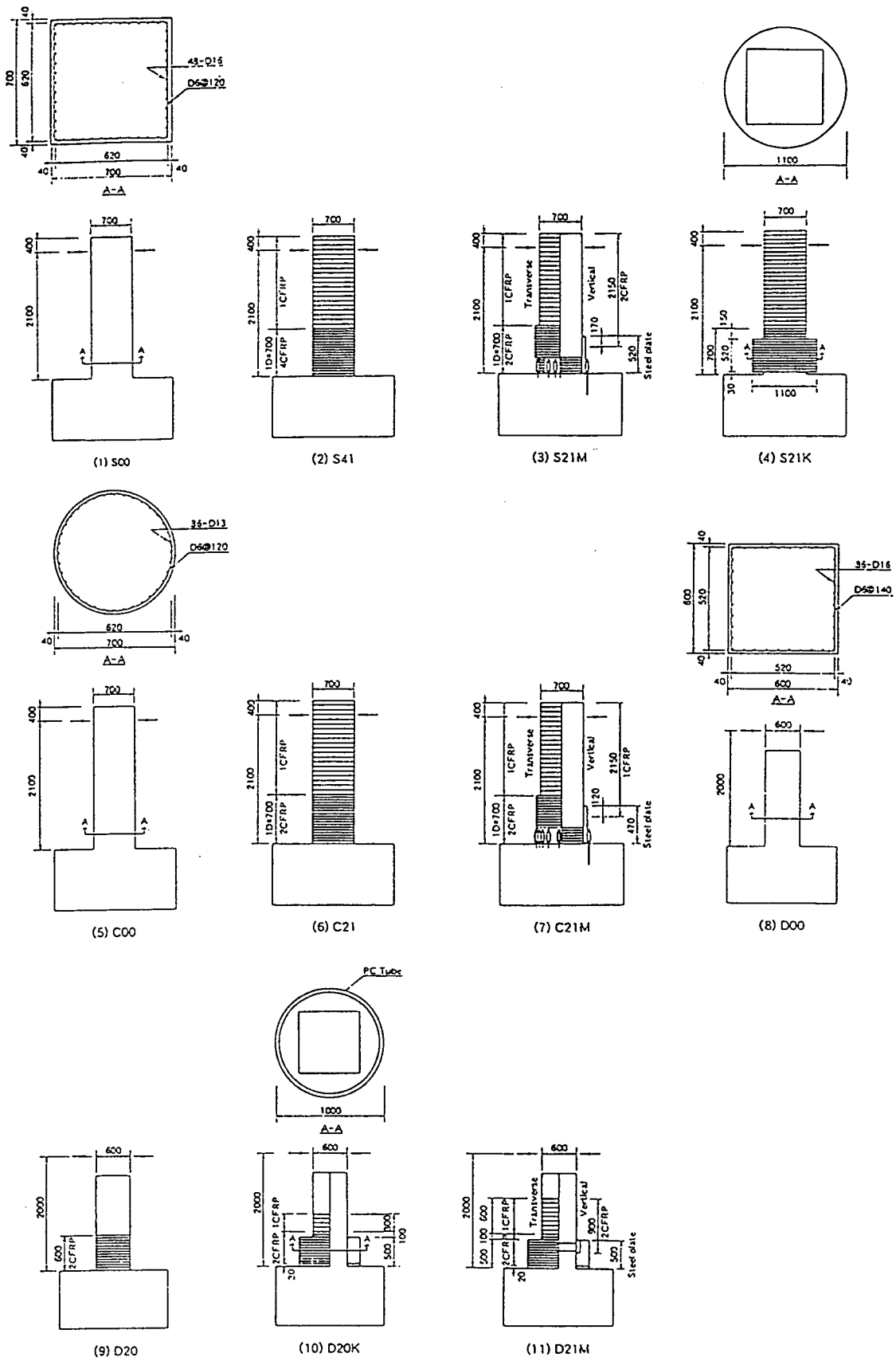
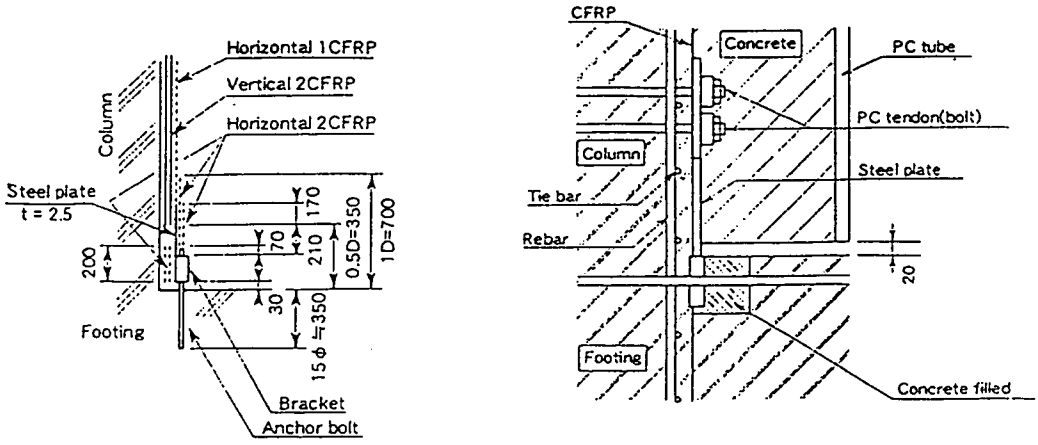


Figure 3 Shape of specimens



(a) S21M (b) D21M

Figure 4 Detail at base

Table 2 List of specimens

Symbol	Cross section	Size	Height of the applied load	Tie	Ductility enhancement	Main rebar	Moment strength enhancement
S00	□	700×700	2100	D6@120	---	48-D16	---
S41	□	700×700	2100	D6@120	4 layers of CFRP in D, 1 in the rest	48-D16	---
S21M	□	700×700	2100	D6@120	2 layers of CFRP in D, 1 in the rest	48-D16	4 steel plates with t=2.3mm in D, 2 layer of CFRP in the rest
S21K	□	700×700	2100	D6@120	2 layers of CFRP in D with casing, 1 in the rest	48-D16	---
C00	○	φ 700	2100	D6@120	---	36-D13	---
C21	○	φ 700	2100	D6@120	2 layers of CFRP in D, 1 in the rest	36-D13	---
C21M	○	φ 700	2100	D6@120	2 layers of CFRP in D, 1 in the rest	36-D13	2 steel plates with t=1.6mm in D, 1 layer of CFRP in the rest
D00	□	600×600	2000	D6@140	---	36-D16	---
D20	□	600×600	2000	D6@140	2 layers of CFRP in D	36-D16	---
D20K	□	600×600	2000	D6@140	2 layers of CFRP in D with casing	36-D16	---
D21M	□	600×600	2000	D6@140	2 layers of CFRP in D with casing, 1 in the rest	36-D16	2 steel plates with t=2.3mm in D, 2 layer of CFRP in the rest

Note: D is the depth of the section

Table 3 Material test

(a) Steel

Material		Symbol	Unit	Yield	Ultimate
Rebar	D16	SD295	kgf/cm^2	3,701	5,481
	D13	SD295		3,746	5,206
	D6	SD295		3,379	5,285
Steel plate	t=2.3mm	SS400		2,261	3,470
	t=1.6mm	SS400		2,598	3,676

(b) Concrete

Unit	Strength	Remark
kgf/cm^2	295	S00
	268	S41,S21K
	266	S21M
	336	C00
	294	C21
	324	C21M
	336	D00
	309	D20
	334	D20K
	322	D21M

(c) CFRP

Combination	Size	Unit	Value	Failure mode
CFRP	t=0.0167 mm, b=12.5 mm	kgf/cm^2	44,690	
CFRP-CFRP	b=25 mm, L=12.5 mm		12,470	Boundary
	b=25 mm, L=25 mm		24,800	Boundary
	b=25 mm, L=150 mm		38,476	CFRP
	b=25 mm, L=200 mm		38,353	CFRP
CFRP-steel plate	b=25 mm, L=12.5 mm		103	Boundary
	b=25 mm, L=25 mm		77	Boundary
	b=25 mm, L=150 mm		27	Boundary
CFRP-concrete	b=50 mm, L=200 mm		24	Concrete
Peeling test	40 mm × 40 mm		34	Concrete

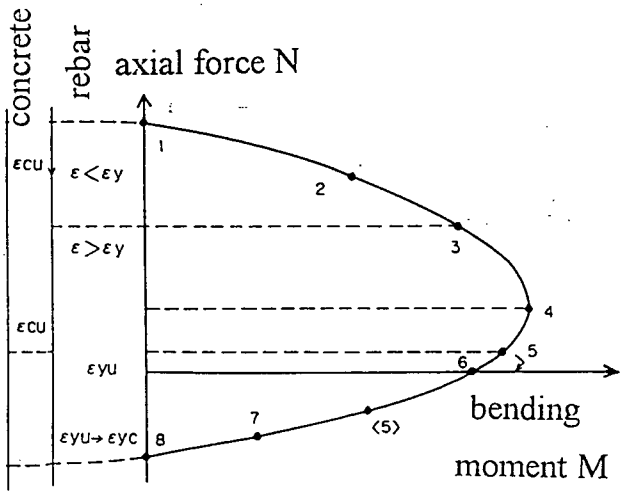


Figure 5 Characteristic points

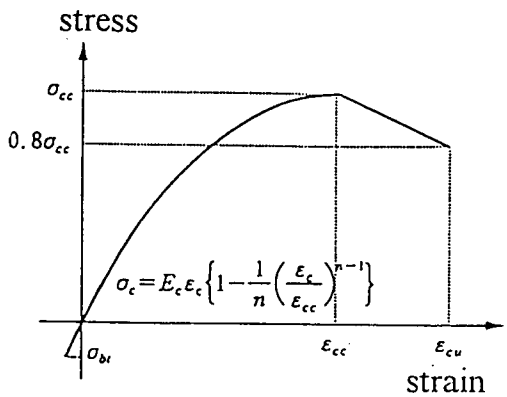


Figure 6 Stress strain curve

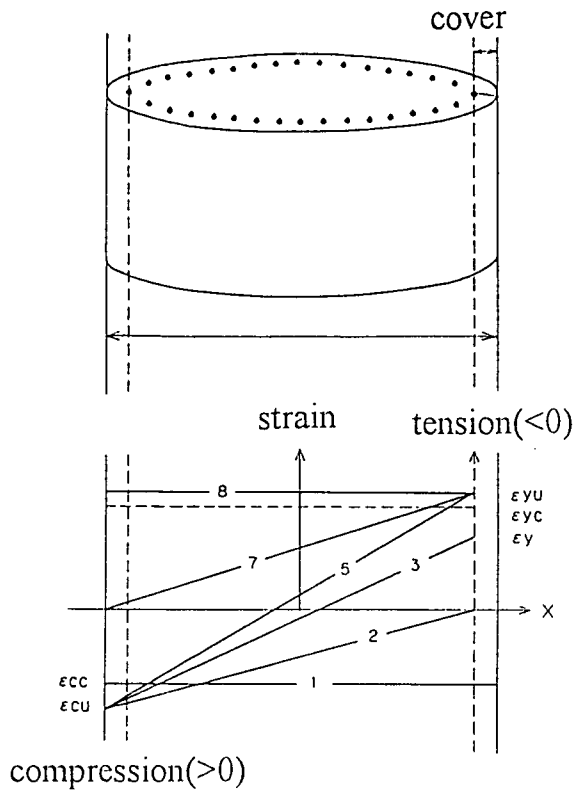


Figure 7 Strain distributions

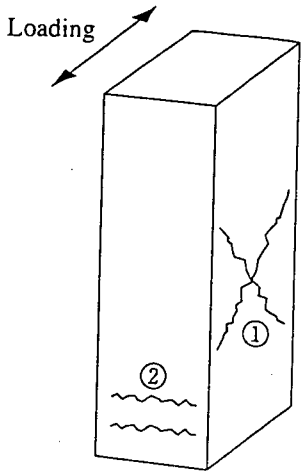


Figure 8 Load direction and failure plane

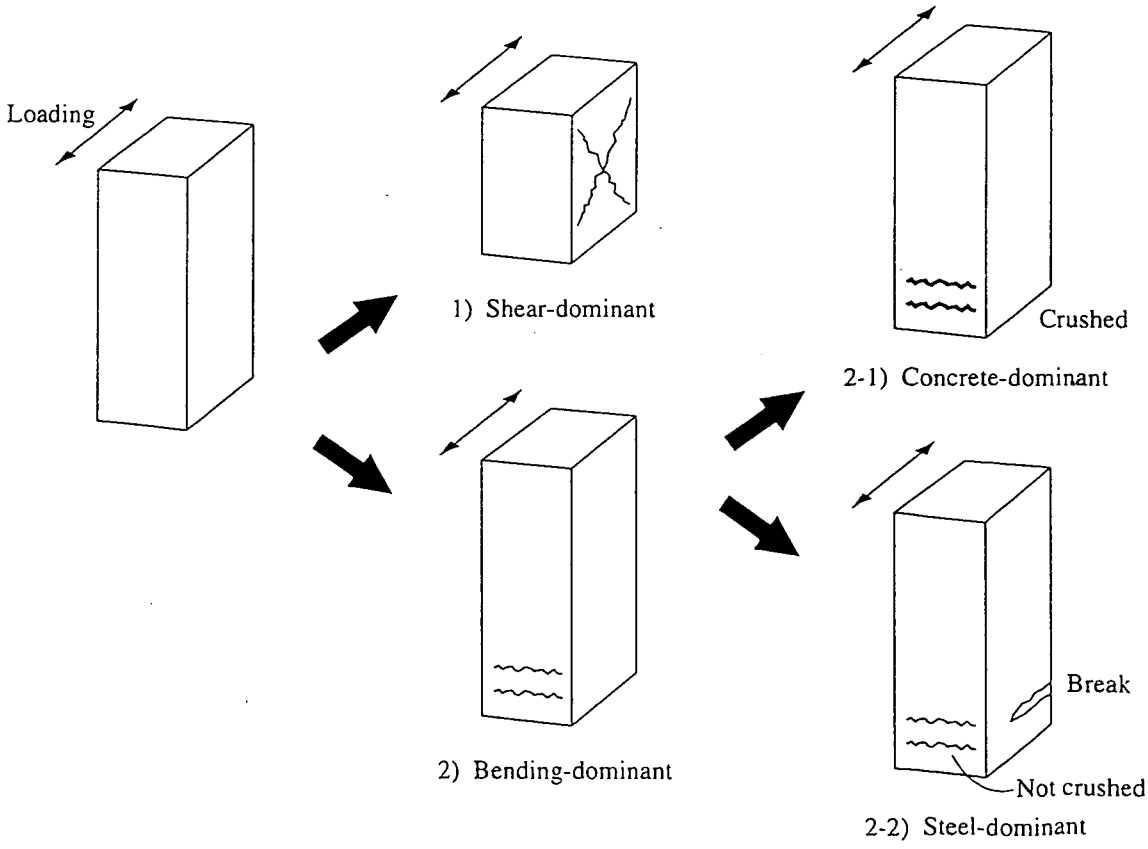


Figure 9 Illustrated classification of RC failure

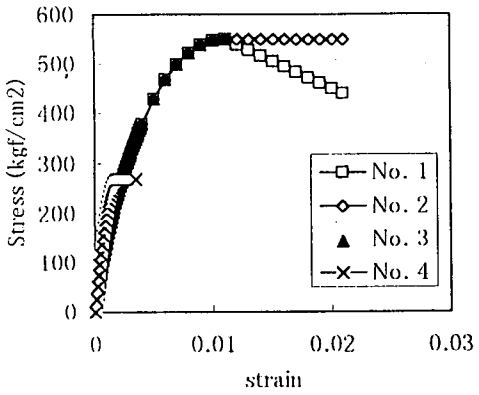


Figure 10 Four stress strain relations

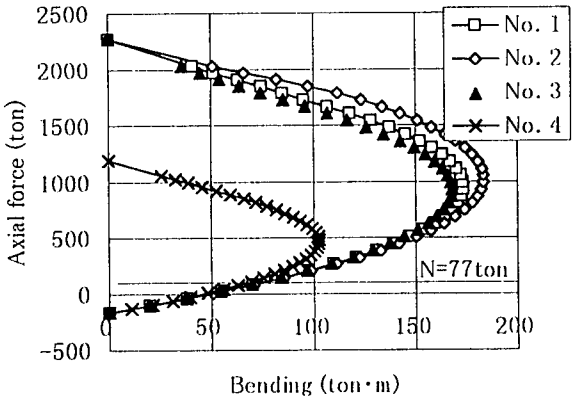


Figure 11 Interaction curve

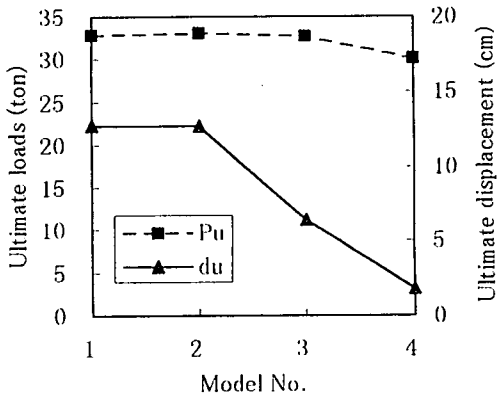


Figure 12 Ultimate states

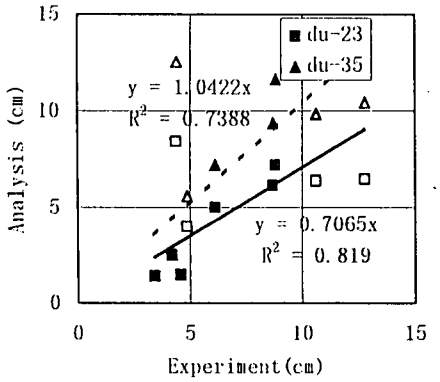


Figure 13 Comparison of maximum displacement by CF=23,000 and 35,000

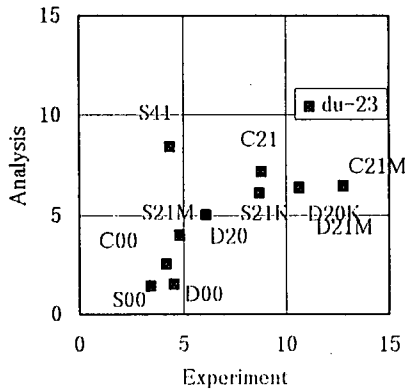


Figure 14 Identification of specimens

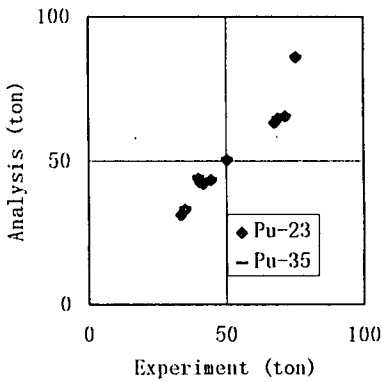


Figure 15 Comparison of maximum load

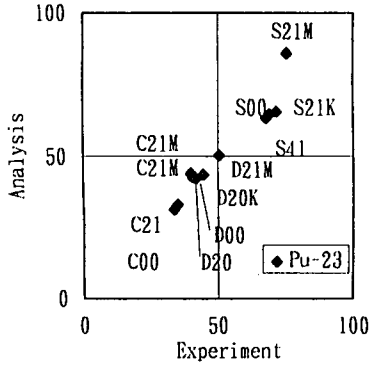


Figure 16 Identification of specimens

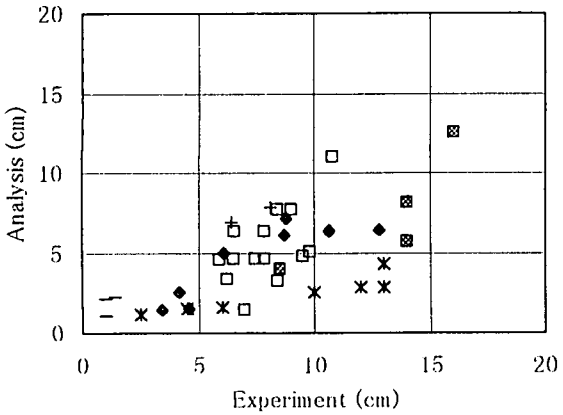


Figure 17 Maximum displacement

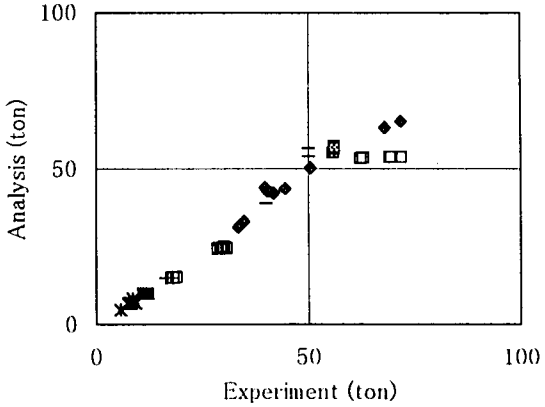


Figure 18 Maximum loads

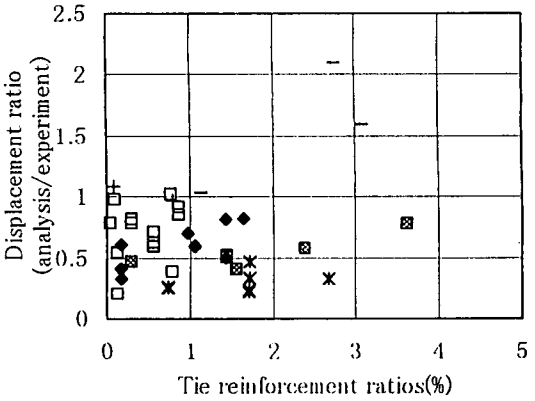


Figure 19 Displacement ratio and tie reinforcement ratio

California's Program for the Use of Composite Materials for Seismic Retrofit

by
Thomas Post, P.E., J.D.
and
Mohsen Sultan, P.E.

California Department of Transportation
Engineering Service Center
Office of Earthquake Engineering
Sacramento, California

Summary

The California Department of Transportation (Caltrans) has been involved over the last several years in the development of advanced composite materials for both repair and retrofit of existing structures and for new bridge construction. To date, most of our experience with composites has been with the retrofitting of existing highway bridge columns to improve their ductility during a seismic event. Large scale testing of epoxy/glass fiber and epoxy/carbon fiber column casing systems has taken place at different universities in California. These tests have demonstrated that composite materials can compete with steel column casings for seismic retrofit projects. Field applications have been performed and quality control and evaluation programs have been started.

Background

The 1971 Sylmar Earthquake in Southern California was the watershed event for seismic design of highway bridges in the United States. Prior to that event, seismic loadings were dealt with by assuming they were a lateral load equivalent to a percentage of the dead load. Sylmar indicated that the loadings can be substantially higher and that improved structural details were needed not only for added strength but also to provide increased ductility.

The typical highway structure in today's California inventory consists mainly of concrete box girder structures as it did also in the 1970's. The increased efforts in developing better analytical tools as well as improved reinforcing details which rose out of the Sylmar Earthquake have led to more reliable structures being built. However, there was also a need to improve the existing structures and raise their resistance to seismic damage. Thus began a retrofit program to enhance the seismic survivability of highway structures.

The first phase targeted superstructure hinges. Prior to 1971, the typical California highway bridge hinge did not have the resisting elements needed to keep large earthquake displacements from unseating the supported span and leading to a collapse mechanism. Therefore, the retrofit program for hinges was to add steel restrainer cables inside the cells of the box girders or on either side of the girder webs in the case of steel girder structures.

The second phase of the retrofit program involved improving the performance of the substructure elements, mainly the columns and foundations. Typically, the retrofit for a concrete column is to place a steel casing around the outside of column, as the column reinforcement details prior to 1971 provided little in the way of ductility. The main reinforcing bars were tied together with #4 bars at a spacing of 12 inches. While this did provide some shear resistance and confinement for the column, its primary intent was to facilitate the hoisting of the column cage into place. It certainly did not give the ductile behavior associated with a continuous spiral of rebar placed around the main bars.

Additionally, the main column bars typically were not continuous into the footing. Starter bars extended out of the footing to which the main column bars were then lap spliced. This lap splice, combined with little confinement capacity would lead to the pulling apart of the lap splice during severe shaking. In the case of bridges with only a single column in each bent, the formation of a hinge at the columns base could lead to collapse.

The steel casing helps to provide the confinement and shear capacity lacking in the pre-1971 columns. Based primarily on research originated in New Zealand, the steel casing acts as a pressure vessel and confines the column during the violent shaking from an earthquake. Thus, the load carrying capacity of the column is maintained and a collapse is avoided. The casing is typically composed of two steel plate shells placed around the column and the welded together.

The foundations would also require retrofitting as they had been designed for gravity loads and not for the uplift potential associated with seismic loadings. In those footings deficiencies include a lack of reinforcing steel at the top of the footing and very light reinforcement in the piles. Therefore, additional piles would typically be placed around the perimeter of the existing footing and a top mat of reinforcement placed atop the existing footing with new concrete cast over the new elements.

Composite Column Strengthening Systems

As stated above, the typical column encasement system used steel plate. Reinforced concrete was used in some applications where increasing the stiffness of the overall system was desired or where aesthetic treatment needed to be matched.

The advantage of these traditional civil engineering materials is that they are well known to civil engineers. The design strengths, allowable stresses and deformations have quite a

bit of research and documentation. Basically, we feel comfortable with these materials. However, they are not without their disadvantages. Both structural steel and reinforced concrete are subject to corrosion. Thus, regular maintenance is necessary to insure performance. This is especially true in the case of structural steel where it not only would not have a concrete cover but would also have lengthy welds which a particularly subject to corrosion and require close inspection during construction. Additionally, erection of the steel shells requires heavy lifting equipment. This can be an issue when there is not much available space around the site or when the column is adjacent to traffic and would require closure of traffic lanes to achieve the pick and placement. Typically, the construction placement determines the thickness of the steel plate. That is, in many cases, the buckling potential determines the jacket thickness rather the column shear or confinement needs.

Composite manufacturers began to seriously consider applications in the civil infrastructure market in the early 1990's. While several manufacturers had been making use of composites for markets other than the Defense industry, the downturn in military spending in the United States prompted the large manufacturers who concentrated on aerospace application of composites to pursue new markets. Infrastructure applications seemed like a good choice. Composites were first considered by Caltrans in 1992 when the Hexcel-Fyfe system was proposed by it's developer as an alternative to steel casings. Currently, four systems are approved by Caltrans for use on highway bridges and are described below. However, it is likely that the list will grow as additional systems complete the evaluation program.

The Fyfe system utilized essentially a glass fabric which is wetted through an epoxy resin bath on site. Once wetted through, the composite is then taken up on a hand carried roller which a worker uses to place it on the column. Another worker follows behind to smooth the composite and squeeze out air and excess resin. The composite is wound onto the column in a helical, overlapping pattern as many times as necessary to achieve the design thickness of the jacket. The workers move up the column on scaffolding. The composite utilizes an ambient cure epoxy.

The advantages of this system are that it is simple and it does not require heavy lifting equipment. It is particularly attractive for locations where space is very tight. Also, the material amount used is closer to just what is needed for the column needs.

The disadvantages are that there is not as much real time data for these materials in this application as there is for steel or concrete. Additionally, it may be difficult to get all of the air bubbles squeezed out from between the layers of composite. These voids could lead to the composite delaminating. There is also concern about glass fiber degradation if they are exposed to alkalines.

Another system, which followed soon after the Fyfe system, was developed by Xxsys Corporation. This system utilizes an epoxy pre-impregnated carbon fiber tow which is mechanically wrapped onto the column. The casing is then heated with ovens that snap in place around the column to cure the composite. Like the Fyfe system, the Xxsys system is

also a continuous reinforcement. However, because of carbon's higher Young's Modulus, the carbon jackets can be significantly thinner than those made from glass.

Advantages of this system include good control of jacket thickness as the system is computer controlled to lay the tow up and down the column. Additionally, jacket thickness can be verified. A strip of copper foil is adhered to the column prior to wrapping and the jacket thickness confirmed by use of an eddy current. Also, the epoxy is an elevated temperature cure so its durability may be better than that of an ambient cure epoxy.

Disadvantages of this system are that it requires specially trained personnel for operation and that for carbon, impact resistance can be an issue. As with the Fyfe system, this system also lacks the long term application data of steel or concrete.

Caltrans has also approved the use of two other composite casing systems. Both utilize sections formed on a mandrel which matches the curvature of the column on which they will be placed and both feature glass as the fiber. The Hardcore-DuPont system is composed of semi-circular segments resembling the steel shell sections used in retrofitting except they are much thinner. The matrix material used with this system is a vinyl ester and the segments are formed by a resin transfer molding method under shop control. The first two segments are glued onto the column and subsequent segments are glued to the previous shells with their seams rotated 90 degrees to provide lap splicing. The process is repeated until the design thickness is achieved.

The other system is the Snap-Tite system which is formed on a mandrel and have a cut down one side so it can be pulled apart and fitted onto the column. Subsequent sections are fitted over each other with their seams rotated 180 degrees from the previous segment's to provide lap. The Snap-Tite system uses a polyester resin matrix.

The advantage of these two systems is that they lend themselves to repeatability particularly on large jobs with similar column sizes and they are fairly easy to install. The disadvantage is that these systems are not continuous and for bursting or confinement resistance the systems place a premium on glued lap splices which may present a durability concern.

Testing Program

With the number of parties interested in proposing composite column casing systems, it was important for Caltrans to establish a formal evaluation program for allowing the use of these systems on the state highway system. One of the largest concerns in evaluating these systems was the bridge engineer's unfamiliarity with these materials. Therefore, we put together an evaluation team with varied backgrounds. Caltrans has teamed with the Aerospace Corporation of El Segundo, California for their expertise in composite materials and their properties, The Society for the Advancement of Material and Process Engineering (SAMPE) for coordination with the composite material industry, and the

Federal Highway Administration (FHWA) for coordination with other states and programs around the country and for their leadership in infrastructure research. These players teamed with Caltrans bridge and materials engineers to develop the evaluation program consisting of structural and material testing and construction details and specifications.

Structural Testing

Under this specific program, the structural testing is being performed by the University of California, Irvine. However, we have tried to be careful to not omit competent data from other institutions. The structural testing consists of large scale (about ½ scale) columns tested to failure, or as close to failure as possible, under cyclic loading with a series of test required for each column shape (typically circular or rectangular) for which the manufacturer seeks system approval. For example, if the manufacturer would like his system to be approved for use on circular columns he needs to perform the following tests:

1. As-built (unretrofitted) shear test for circular column
2. As-built (unretrofitted) column base lap splice test for circular column
3. Retrofitted shear test for circular column subject to double bending load
4. Retrofitted lap splice test for circular column subject to single bending load

If the manufacturer wished to have his system qualify for use on rectangular columns he would need to repeat the above tests with rectangular test specimens.

The retrofitted test columns must satisfy the following criteria:

1. Minimum confinement stress of 300 psi in the lap splice or plastic hinge zone
2. Maximum material elongation of 0.001 inch/inch in the lap splice zone and 0.004 inch/inch in the plastic hinge zone
3. Minimum confinement stress of 150 psi and material elongation of 0.004 inch/inch must be maintained elsewhere in the column with an appropriate transition
4. A displacement ductility in the range of 8 to 12 should be achieved

Material Testing

With the expertise of the Aerospace Corporation, Caltrans is performing environmental durability qualification tests. Here, test panels of the composites are subjected to different elements to determine any adverse reaction. Degradation of mechanical and physical properties is being monitored following exposure to various conditions with durations up to 10,000 hours. The exposures include 100% humidity at 100°F, immersion in salt water, immersion in alkaline solution, exposure to ultraviolet light, dry heat at 140°F, a freeze-thaw test, and immersion in diesel fuel.

The effects of the test are being quantified in terms of panel mass, tensile modulus, tensile strength, interlaminar shear strength, failure strain, and glass transition temperature. Measurements are made at exposure intervals of 1,000 hours, 3,000 hours, and 10,000 hours.

Qualification Program Summary

The following briefly summarizes the tasks used to qualify different systems as composite column casings for use on California highways.

Task 1: Analytical Verification

Objective: Conduct analytical modeling of selected tests. Help develop a simplified method of design for composite casings.

Deliverable: Internal stress analysis of selected tests and critical flaw size estimation.

Task 2: Composite Properties Characterization

Objective: Develop specific requirements for the manufacture and testing of composite casings.

Deliverable: Recommended manufacturing and testing methods

Task 3: Scale Test Column Verification

Objective: Determine the quality of the wrap on the test specimens and determine non-destructive testing techniques.

Deliverable: Non-destructive evaluation maps of columns both before and after testing. Comparison of test results to analytical models.

Task 4: Quality Assurance

Objective: Establish a plan to assure composite column casings meet performance requirements.

Deliverables: Define standard testing procedures and minimum requirements to assure quality.

Task 5: Non-Destructive Evaluation

Objective: Document column assessment techniques.

Deliverables: Document most effective techniques and demonstrate on specimens.

Task 6: System Evaluation

Objective: develop a cost comparison model between composites and steel casings.

Deliverables: Estimates of labor and material costs and life-cycle costs.

Task 7: Database Organization and Project Management

Objective: Establish a database for tasks one through six. Manage tasks one through six.

Deliverables: Cost and schedule reports. Data from previous tasks.

References

Roberts, J. E., "Composite Construction in California Bridge Seismic Retrofitting" US-Japan Workshop on Seismic Systems for Bridges, Hawaii, July, 1997

Sultan, M, "Evaluating Advanced Composites for Applications in Transportation Structures - a Model Public-Private Partnership"

Evaluation of Foundations on the Hanshin Expressway Kobe Route Damaged by the Great Hanshin Earthquake

Hidenao Hayashi [1] Kenji Kosa [2]
Yoshitomi Kimura [3] Hideki Kitahara [4]

1) Chief Engineer, Hanshin Expressway Public Corporation, Osaka
2) Senior Engineer, Hanshin Expressway Public Corporation, Osaka
3) PWRI, Ministry of Construction, Tsukuba
4) Chodai Engineering, Inc., Osaka

ABSTRACT

The Great Hanshin Earthquake in January 1995 gave tremendous damage to the structures of Hanshin Expressway. Especially, damage was disastrous on the Kobe route that runs in the Hyogo prefectural area, where girders fell off and piers collapsed or tilted. Due to such extensive damage, it was feared that the foundations of those bridges might also be affected. To investigate the severity of damage, typical foundations were selected from the affected area and their level of integrity was evaluated using a borehole camera. Then, the relationship between the damage level of piles and their ultimate strength was investigated analytically.

Also, as a result of seismic retrofit, another fear came out that the piles might not have enough strength to support strength-increased retrofitted piers above them. Hence, an investigation was carried out to identify if the pile foundations still retain sufficient ultimate lateral strength. Piles were added when some foundations were found insufficient in strength. Results of these investigations carried out on the pile foundations of the Kobe Route are presented in this report.

1. Investigation of damage level

1.1 Types of foundations

The types of foundations existing on the Kobe route and their numbers are shown in Table 1. 84% of the entire foundations of the Kobe route are pile foundations, and 92% of them are cast-in-place pile type. Caisson foundations are mostly employed at the intersection with rivers. Spread foundations are used in the western area of the route where the ground condition is good.

1.2 Determination of damage level

The damage to the foundations was investigated by core drilling and the use of a borehole

camera. As to the cast-in-place piles, a total of 122 piles were chosen for investigation from 855 piles based on a combination of possible affecting factors such as the position and the arrangement of piles. A core of ϕ 66 mm was drilled on those piles from the ground surface and the inside condition was pictured by a borehole camera inserted into the hole. The number of damaged piles grouped according to the damage rank shown in Table 2 is given in Table 3. The results of this investigation are summarized as follows:

① The majority of piles were ranked as damage level d (minor damage) or no damage, though some were ranked as damage level c (slightly serious than d).

② Cracks were mainly concentrated around the pile head, and cracks around the pile mid-section were mostly minor cracks.

③ The crack width was 2 - 3 mm at the biggest. Therefore, the effect of those cracks on the strength of the pile was very small.

From these findings, it can be said that damage level of the cast-in-place pile foundations on the Kobe route was small.

The same procedure was applied to the investigation of six caisson foundations chosen out of 44 existing on the Kobe route. Though damages were found on those foundations, they were also very minor.

The damage level of precast piles was investigated by the impact method because their diameter (400 mm) was too small to employ other methods. 48 precast piles were selected for investigation from 74 piles on the Kobe route. By the hammering of the upper face of the footing, an elastic wave was introduced into the pile and the reflected wave was measured using an accelerometer. No abnormal reflected waves were found in the measured results. Accordingly, it is judged that the precast piles of the Kobe route sustained minor damage or no damage.

Regarding the spread foundations, 12 foundations were selected from 133 and investigated directly by excavating soil up to the surface of the footing, but damage such as a crack was not found. Then, slightly tilted piers were investigated using a fiber scope if there exists a gap below the footing. No cracks were observed and thus it is confirmed that the spread foundations of the Kobe route retained integrity.

2. Investigation using the borehole test results

2.1 Geology

Using the borehole test results shown above, the relation between the damage of piles and the geological structure or other local factors is investigated analytically. The geological structure along the Kobe route and the inspection sites where a borehole camera was positioned are shown in Fig. 1. The severely damaged bridge section on the Kobe route was the section between the River Muko in Nishinomiya City and Tukimiyama in western Kobe, about 28 km section. This section is grouped into five geological areas: starting from the east side, the alluvial lowland, the borderland between the hilly area and the alluvial lowland, the former coastal area, the alluvial

lowland, and the hilly area. When the alluvial layer where foundations are built is focused, its thickness changed around the River Sumiyoshi in eastern Kobe. On the east side of the river, the alluvial layer composed mainly of sandy soil spreads at a thickness of 15 ~ 20 m, whereas on the west side of the river the thickness is generally less than 10 m. The pile damage investigation was conducted in almost all areas in this section, except the 4 km-long western end area of the route where spread foundations are used. At first the entire depth of the pile was investigated, but after it was found that cracks were few in the lower part of the pile, only the upper half of the pile was investigated. Analysis was done, as shown in Fig. 1, by dividing the target section into five geological areas and also by dividing the alluvial layer into four zones at every 5 m depth from Zone I (depth: below 5 m) to Zone IV (depth: over 15 m).

2.2 Results of investigation

2.2.1 Relation between geological area and crack distribution

The average number of cracks found on the piles in the range up to 10 m deep from the pile head is shown in Fig. 2. It is seen in this figure that the average number of cracks is larger in areas 1 and 3 than the number in areas 2, 4, 5. The average number of cracks except hair cracks (smaller than 1 mm) is also shown in the figure. In Area 2, cracks over 1 mm wide are relatively many, whereas in Area 4 all cracks are hair cracks, indicating that crack width varies by areas. Next, the crack distribution in the depth direction is given in Fig. 3. In all areas, cracks occurred mainly in the upper part of the pile, and especially cracks over 1 mm wide were concentrated in the pile upper section within 2 m from the pile head. From the fact that damage was primarily found around the pile head, it is presumed that the dominating damage mode was the bending mode. The distribution of damage in the depth direction varies, though slightly, by areas. In Area 2 and 3, cracks were concentrated around the 'shallow' section within 2 m from the pile head, whereas in Area 1 cracks were decreased gradually as the depth increases, and in Area 4 hair cracks were distributed partially in the range of 8 m ~ 12m from the pile head, although the majority of them are found around the upper part of the pile.

2.2.2 Relation between geological layer and crack distribution

The relation between geological layer and crack distribution on the piles was investigated. The weak ground along the Kobe route is the alluvial layer between the ground surface and the diluvial layer. The investigation focused the relation between the depth of the alluvial layer and the number of cracks on the piles existing in that depth. The results are shown in Fig. 4. In this figure, it is seen that the number of cracks is increased dramatically in the alluvial layer below 11 m. Using the result of Area 1 in Fig. 3, the relation between the depth of geological layer and crack distribution was obtained and shown in Fig. 5. When geological layer III (depth of the alluvial layer: 10 ~ 15 m) and geological layer IV (depth of the layer: over 15 m) , both rich in

data, are compared, it is seen that cracks are concentrated in the range above 4 m in geological layer III, whereas in geological layer IV cracks are partially distributed in the range between 8 ~ 14 m. This indicates that cracks occurred at a different depth by the thickness of the alluvial layer.

Cracks also occurred at the boundary of the alluvial layer and the diluvial layer. However, their width was like that of hair cracks and hence they were assumed to give little effect to the strength of the piles.

3. Analysis of damaged foundations for integrity assessment

3.1 Analytical method

Nonlinear analysis based on the 'Reference (draft) for the application of "Specifications for the Retrofit of Bridges Damaged by the Great Hanshin (Kobe) Earthquake"' [1] was employed for the assessment of pile integrity.

The analytical model is briefly explained below:

① The horizontal strength of a pile foundation and its behavior during severe deformation can, as shown in Fig. 6, be analyzed by replacing the pile foundation with a rigid frame structure supported by a ground spring and considering this to be nonlinear.

② The resistance properties in the vertical direction of the pile were considered to be elasto-plastic form, with the pile axial direction spring constant K_{VE} considered to be the initial gradient, and the ultimate bearing capacity P_{NU} and the ultimate pull-out bearing capacity P_{TU} treated as the upper limit values.

③ Horizontal ground resistance was estimated by modelling as a bilinear model of the kind shown in Fig. 6 (c). The effectiveness of this analysis method was confirmed by the results of horizontal loading tests.

④ The points of inflection in the bending moment-curvature relationship when bending moment acts on the concrete pile are usually treated as the cracking state (C), the state when the reinforcing bars begin to yield (Y), and the ultimate state of the section (U). The analytical model was a trilinear model linking these points found for a circular steel reinforced concrete cross section with the axial direction N and subjected to the bending moment M (Fig. 6 (d)).

⑤ The direction for investigation was the direction perpendicular to the bridge axis, because damage to the pier is larger and earthquake motion was bigger in that direction.

⑥ Derive the ultimate lateral strength of the pier. The check method was the method shown in the specifications for retrofit, but 1.0 was chosen as the ductility factor because the shear strength was used as the strength for assessment.

⑦ The cracking strength of the piles was taken when all the piles reached the crack state. The bending strength of the piles was taken when all the piles reached the yield state or when the reaction force at the pile head has reached the design tensile strength.

In the calculation of passive earth pressure in front of the pile, the weight of soil between

the footing bottom and the ground surface was considered as the load imposed on the pile.

In the calculation of the relationship between bending moment vs. curvature of the pile body, the axial force was made to be zero (0) in the piles on the pull-out side from the center of the pile group, and in the piles on the tensile side the value derived by dividing the dead load (the total of reaction force by the superstructure, weight of the pier body, weight of the footing, and weight of soil imposed on the footing) by the number of piles, was used as the axial force. In the current analysis, axial force of the piles was assumed to remain constant at the initial value given as above.

3.2 Results of analysis

3.2.1 Strength and damage level of piers

The relationship between damage level of the piers and analytical results for shear strength of the piers is given in Fig. 7. The abscissa of this figure in the value defined as the resistance coefficient. This value was derived this way: in the results of damage factor analysis of the piers conducted separately, a good agreement was found between the damage level and the shear strength (elastic response acceleration) of the piers, and the boundary between rank B and ranks C & D was around 500 gal; therefore, assuming this intensity as the elastic response acceleration and assuming 0.5W as the acting external force, the value derived by dividing the shear strength of the pier (Su) by the 1/2 of the equivalent weight (0.5W) was defined as the resistance coefficient. The ordinate is the ratio of each damage rank (starting from the most severe damage, As and A, B, C, D) . Given in () in Fig.7 is the number of piers classified into that damage rank.

It is seen in this figure that piers of severe damage (damage rank A and As, and B) mainly exist in the pier group with a low resistance coefficient and do not exist in the pier group with resistance coefficient over 0.9.

Qualitatively, it can be said that piers with relatively large damage exist mainly in the ratio group with a low resistance coefficient.

3.2.2 Strength and damage level of piles

The relationship between the damage level determined by the use of a borehole camera and the strength of piles derived from nonlinear analysis is shown in Fig. 8 and Fig. 9.

The abscissas of Fig. 8 and Fig. 9 are the values derived by dividing P_y by 0.5W and P_c by 0.5W, respectively, and defined as the resistance coefficient. P_y is the yield strength of the pile and P_c is the cracking strength of the pile, both derived from the nonlinear analysis.

0.5W is half of the equivalent weight and it is assumed as the acting external force in the same way as done in 3.2.1.

The ordinate shows the ratio of each damage group (c1, c2, d1, d2). These damaged piles were grouped by the careful examination of the number of cracks and their width. The figure

shown in () is the number of piers belonging to a given group.

In Fig. 8, it is seen that the pile foundations ranked as relatively severely damaged belong mainly to the group with a low resistance coefficient. This shows that a good relationship exists between the resistance coefficient and the damage level of piles. For example, piles with major damage (damage rank C) are not found among piles with resistance coefficient over 3.0. However, resistance coefficient 3.0 (three times the strength of reinforcement yielding) is the load level that would not cause the reinforcement yielding analytically. Also, from the fact that the crack width was a few millimeters at the biggest, the damage may be the level of cracking on the piles by analysis.

Then, the damage of the piles and the load imposed on them up to causing cracks are compared in Fig. 9. In this figure, piles with major damage (damage rank C) were not found in the piles with resistance coefficient over 1.0. However, no clear relationship was found between the resistance coefficient and the damage level.

From these figures, it can be said that there is a tendency that pile foundations ranked as relatively large damage exist mainly in the group with a low resistance coefficient. As the resistance coefficient, yield strength (P_y) is better to be used than cracking strength (P_c) because the former corresponds well with the damage level.

From the above, it can be concluded that an agreement exists between the damage level of piles and the analytical value for reinforcement yielding, though there is a slight doubt in terms of resistance coefficient.

3.2.3 Relationship between resistance coefficient and damage level of piles and piers

The relationship between the resistance coefficient and the damage level of piers and piles is shown in Fig. 10.

In Fig. 10, areas A, B, C, D are separated at 0.8 in the resistance coefficient of the pier and at 2.0 in the resistance coefficient of the pile. Of the four areas, the damages of piles and piers in areas A and D are given in Fig. 11. One of the separating values, resistance coefficient of the pier, 0.8, is the value derived from the boundary value (elastic response acceleration: 400 gal) that can divide damage levels of the piers between A and As vs. B, C, D. The other separating value, the resistance coefficient of the pile, 2.0, is the value averaging the resistance coefficients of the piles.

As seen in Fig. 11, 64% of the piers in Area D are those ranked as minor damage or not damaged in both the column and the pile. Piers in this area did not suffer much because both columns and piles had higher resistance coefficients. In Area A, though the resistance coefficients of columns and piles were low, it was only 8% of them that suffered large damage. Hence, no clear difference is seen in the results of Area A and Area D. Therefore, it is difficult to determine from these results that a relationship exists between the resistance coefficient and the damage level pf piles and piers.

However, the ratio of piers whose columns were assessed to have large damage is 36% in

Area D, but it is 52% in Area A, indicating a tendency of increase. Similarly, the ratio of piers whose piles were assessed to have relatively large damage is 9% in Area D, but it is 18% in Area A, which also indicates a tendency of increase. From these facts, it is possible to say that a tendency exists qualitatively between the resistance coefficient and the damage level, though a relatively large scatter is seen.

4. Investigation for the reinforcement of pile foundation

4.1 Preliminary investigation

In a retrofit work, many piers have gained an increase in both bearing capacity and strength to have enough ductility to withstand large earthquakes. However, as a result of those retrofit, another fear came out that the pile foundations under those piers might not have enough strength to support those retrofitted piers. Therefore, an investigation was conducted to identify a need for pile reinforcement.

To apply preliminary reinforcement design, to obtain a tendency in the strength of pile foundations, and then to find piers in need of detailed investigation, 50 piers were selected from about 850 piers on the Kobe route

Those 50 piers were selected from single-column piers with pile foundations, considering such factors as the pile arrangement and the number of piles.

The factors that give effect to the bearing capacity of piles are the number of piles, the diameter of the pile, the reinforcement ratio of the pile and coefficient of ground reaction.

Among those factors, the diameter of the pile and the coefficient of ground reaction were excluded because the former is the same in all piles and the latter does not make much difference by areas.

Fig. 12 is a graph depicting the preliminary design results obtained from the 50 piers. The ordinate is the reinforcement amount in the axial direction per one pile. The abscissa is the horizontal force imposed on one pile that is derived by dividing the ultimate lateral strength of the column by the number of piles.

As shown in the figure by the solid line, the relationship between the bearing capacity of the piles and that of the piers is divisible at a certain angle by the reinforcement amount of the pile and the horizontal force imposed on the pile.

Thus, it is clearly depicted in the graph that a pile with a lower reinforcement amount is weak when subjected to the same horizontal force, and when its reinforcement amount is the same a pile that has received a larger horizontal force is weak.

4.2 Investigation of affecting factors based on the design data for column reinforcement

Using the results derived above, check was carried out on the ultimate strength of 100 columns that had completed reinforcement design based on the "Design Procedure for Retrofit

(draft)" compiled by our Corporation. The results of the check are graphed in Fig. 13 using the reinforcement ratio of the pile for the ordinate and the bearing capacity of the pier divided by the cross sectional area of the piles for the abscissa.

In this graph, it is possible to draw a line to indicate piles which do not have the required bearing capacity. Hence, bridges potentially exposed to over 80tf/m^2 in the bearing capacity of the pier divided by the cross-sectional area of the piles, were selected for check by nonlinear analysis to see if they satisfy the required bearing capacity of the piles.

4.3 Results of the check

Of all pile foundations on the Kobe route, 357 foundations were checked by the deformation method and the nonlinear analysis. Fig. 14 is a plot showing the results of the check. The ordinate is the reinforcement ratio in the axial direction of the pile and the abscissa is the horizontal force imposed on the pile derived by dividing the ultimate lateral strength of the column by the cross sectional area of the piles.

Of 357 foundations, five foundations (Kobe P446, 447, 452, 479, 521) were found to lack in strength in the final check by nonlinear analysis and hence in need of reinforcement. They are confined in a small area and all of them restricted in the direction of building a footing because they are located at the intersection of busy roads on the ground level, which may be the reason they were found weak.

5. CONCLUSIONS

Based on the investigation, the following conclusions can be drawn:

① Damage to the bridge foundations of the Earthquake-affected Hanshin Expressway Kobe Route was investigated by a borehole camera. As a result of investigation, it was found that damage to bridge foundations was small, with minor cracks occurring locally.

② Regarding cracks on the piles, they were mainly concentrated in the upper part of the pile, and few existed in the deeper part.

③ A relationship was found between the damage level of piles and their resistance coefficient derived by dividing the strength of columns and pile foundations by acting external force.

④ From the fear that piles might not have enough strength to support the strength-increased retrofitted piers above them, an investigation was carried out to identify if some piles are in need of reinforcement. Cat-in-place piles whose ultimate lateral strength divided by the number of piles were over 80 tf/m^2 were found to lack in strength and deformation capacity and hence need to be reinforced.

REFERENCES

1) References for the Adoption of "Specifications for the Retrofit of Piers Damaged by the Great Hanshin (Kobe) Earthquake" (draft), Road Association of Japan, June 1995.

Table 1 Number of foundations according types

	Types of foundations				Total
	spread foundation	caisson foundation	Pile foundation		
			cast-in-place piles	precast piles	
Piers existed	133 (12%)	44 (4%)	865 (77%)	74 (7%)	1106 (100%)
Piers investigated	12	6	122	(48)	140 (48)

Table 2 Damage rank of pile foundation

Damage rank	Definition
a	Large lateral movement as well as large settlement
b	Large lateral movement , or some flexural cracks on piles
c	Small flexural cracks on piles
d	No damage or minor damage

Table 3 Damage level of pile foundations (piers)

Damage rank	a	b	c	d	Total
Number of damaged piers	(0%) 0	(0%) 0	(16%) 19	(84%) 103	(100%) 122

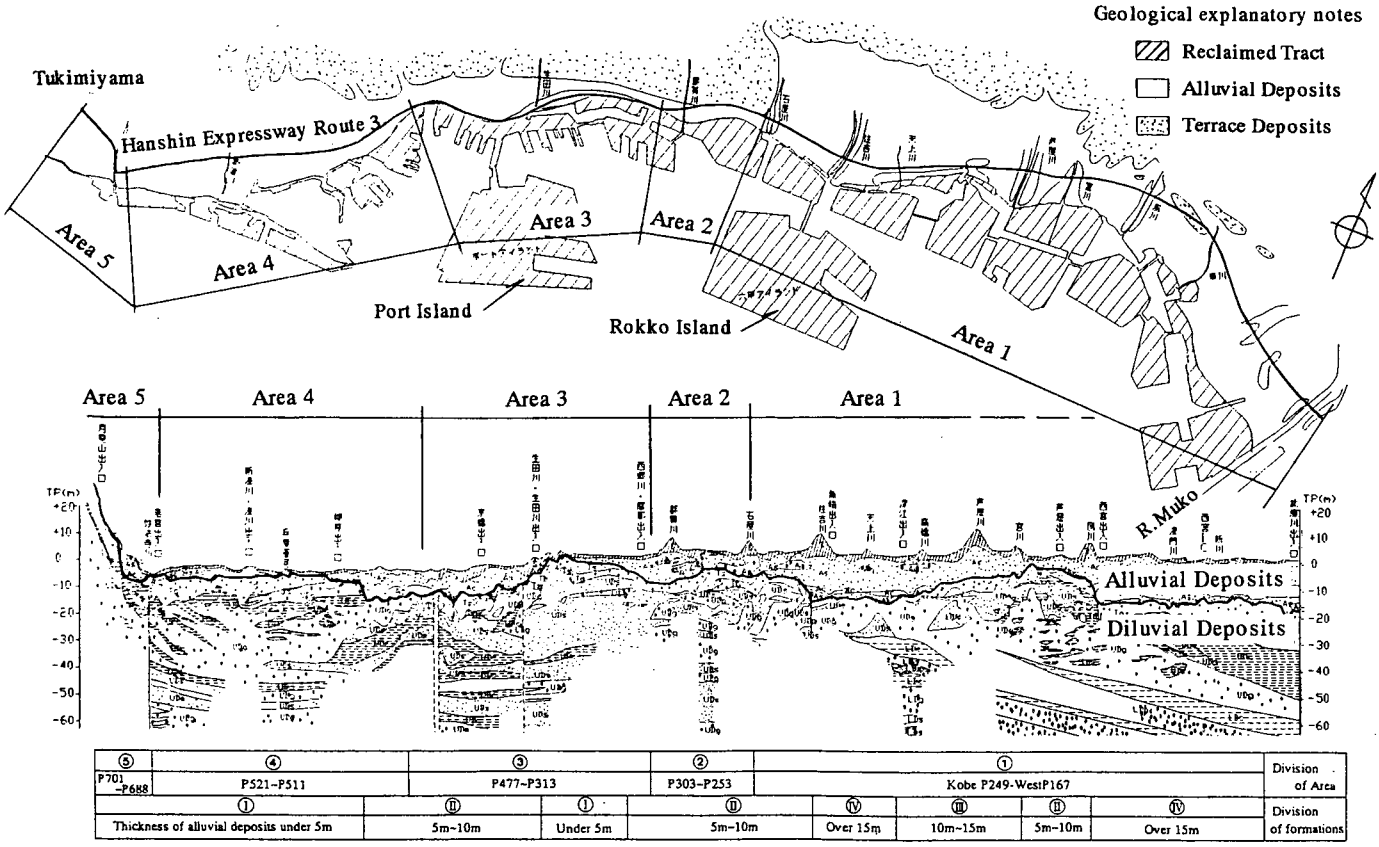


Fig.1 Formations around Hanshin Expressway Route 3(Kobe Route) and Division of area

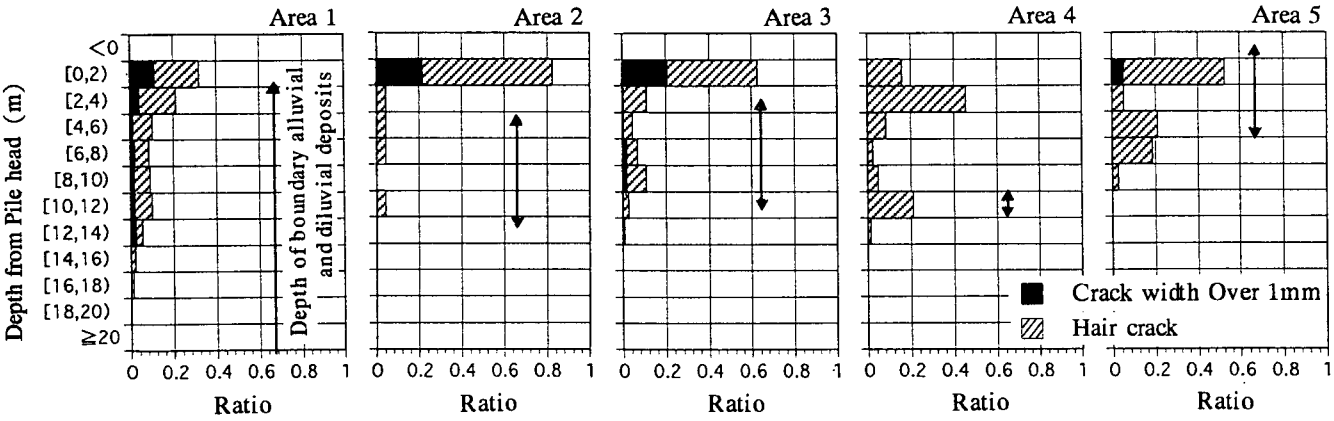


Fig.3 Distribution of cracks depth

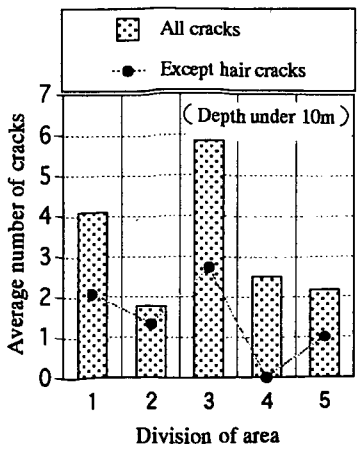


Fig.2 Average number of cracks at the different region

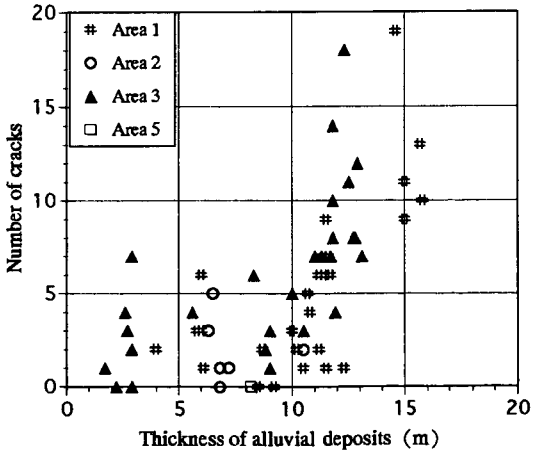


Fig.4 Thickness of alluvial deposits and number of cracks

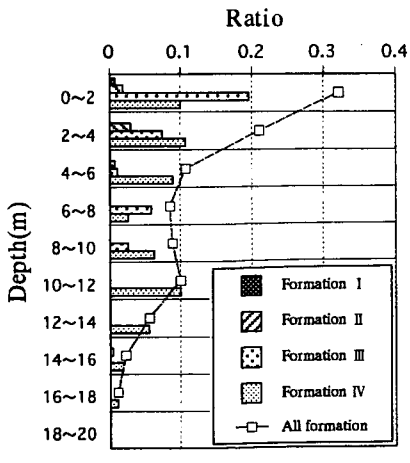
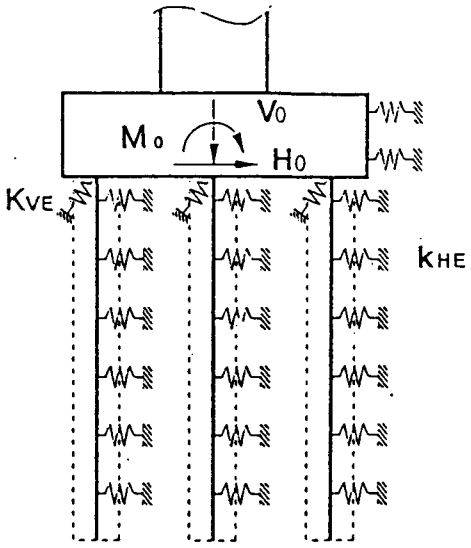
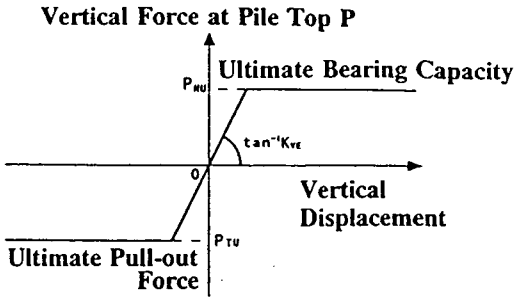


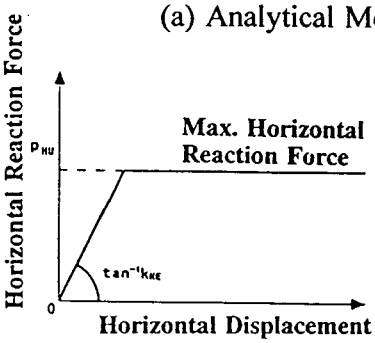
Fig.5 Division of formations and distribution of cracks(Area 1)



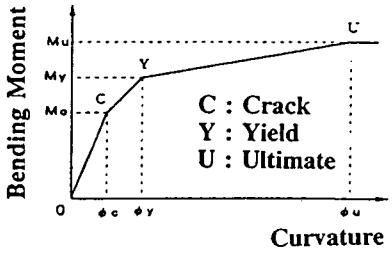
(a) Analytical Model



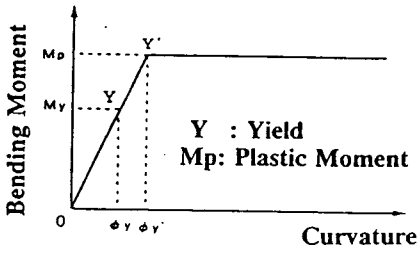
(b)Vertical Force vs. Vertical Displacement Relation



(c) Horizontal Force vs. Horizontal Displacement Relation



(d) Moment vs. Curvature Relation of Reinforced Concrete Piles



(e) Moment vs. Curvature Relation of Steel Pipe Piles

Fig. 6 Analytical models of pile foundations

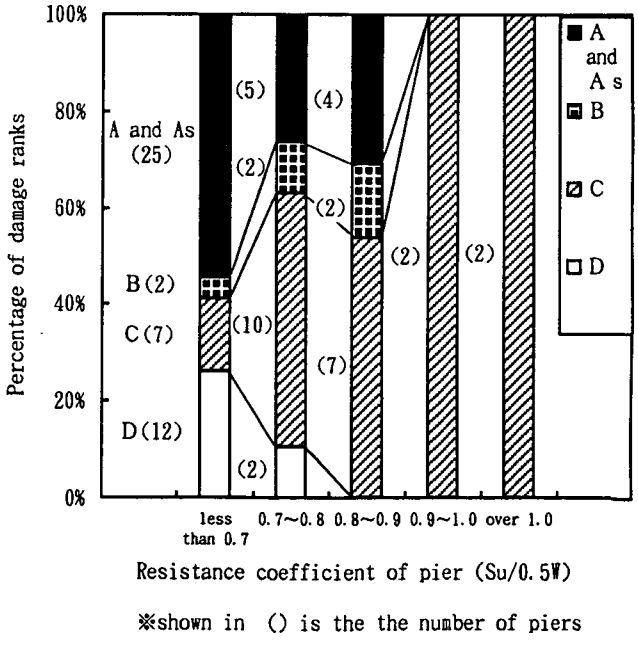


Fig. 7 Relationship between resistance coefficient and damage rank of piers

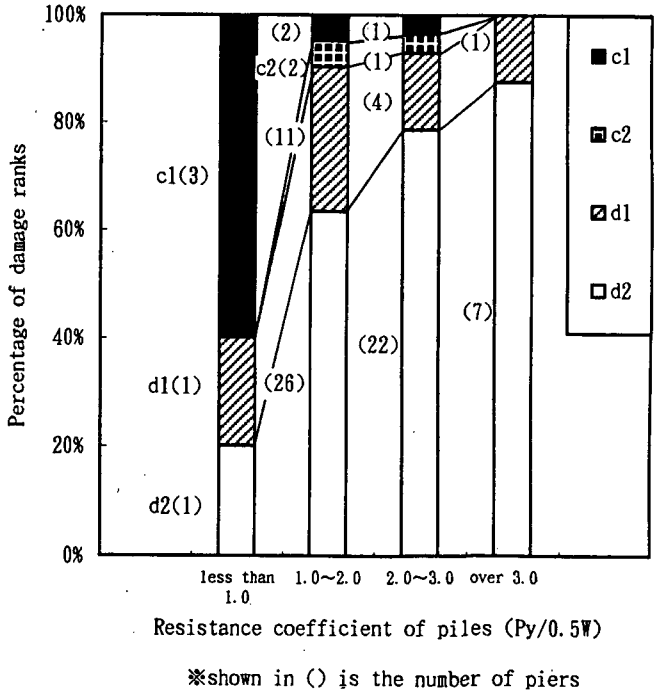
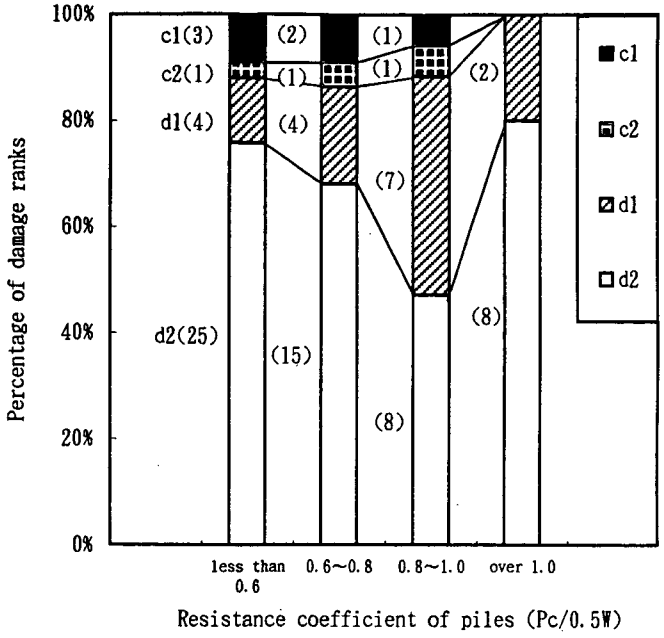


Fig. 8 Relationship between resistance coefficient and damage rank of piles



※shown in () is the number of piers

Fig. 9 Relationship between resistance coefficient and damage rank of piles

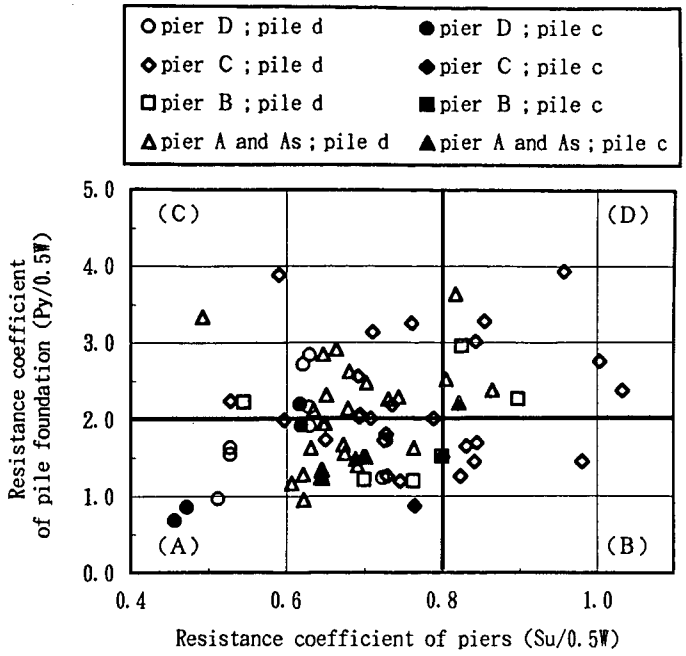


Fig. 10 Relationship between resistance coefficient and damage rank of piers and piles

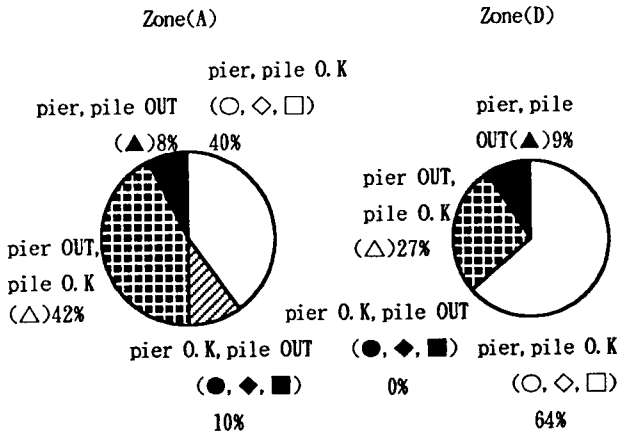


Fig. 11 Damage of piers in areas A and D

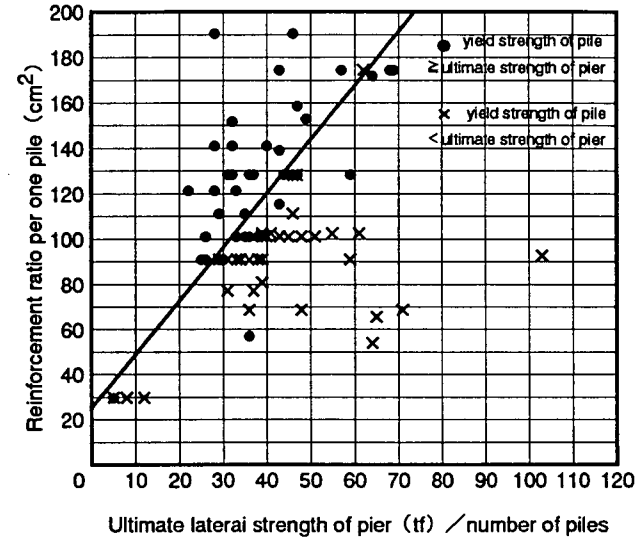


Fig. 12 Results of preliminary design

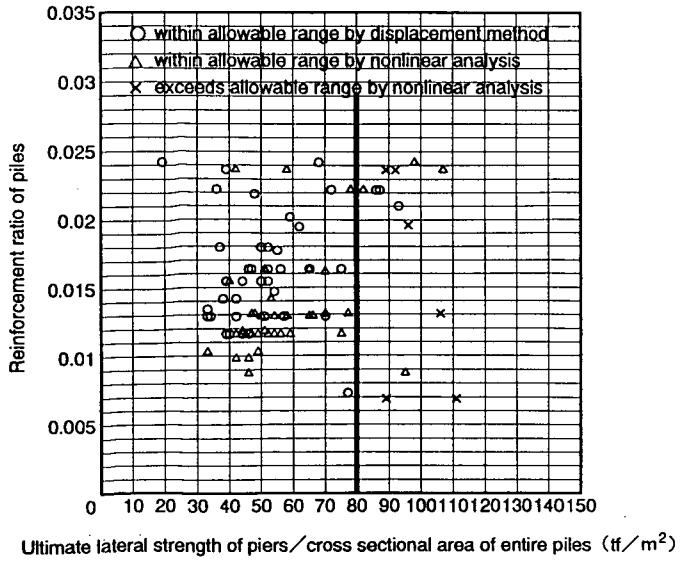


Fig. 13 Results of checking for 100 piers

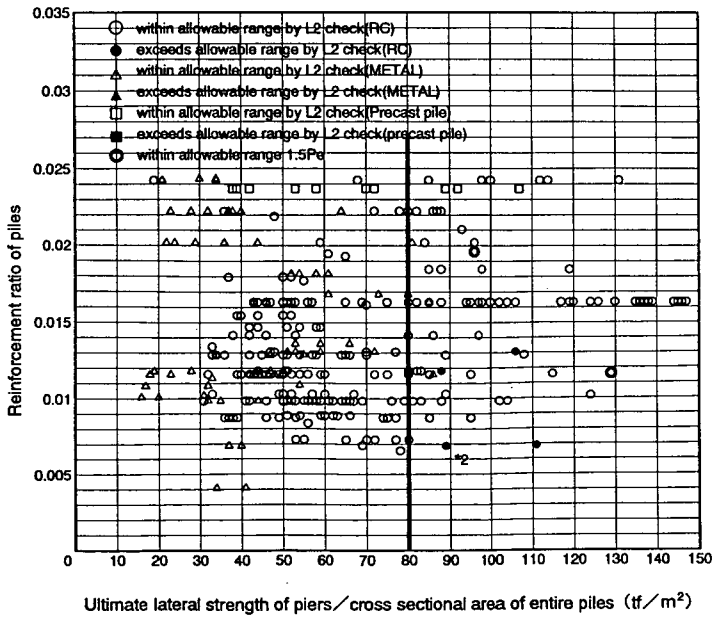


Fig.14 Results of checking

RETROFITTING OF RAILWAY BRIDGES

E. "Manos" Maragakis[1], Bruce M. Douglas[2], Qingbin Chen[3] and Ray Zelinski[4]

ABSTRACT

Full scale ultimate load tests of the Strawberry Park Bridge were conducted in March 1995. This was a two span 148' (45m) long ballasted railway bridge, typical of many railway bridges around the country. The bridge was located in Los Angeles and it was scheduled for removal in spring 1995. The main objective of these experiments was to identify the extent to which the unique railway bridge components, consisting of the rails, ties, ballast and ballast pan, help strengthen it during a seismic event. It was found that railway elements increased significantly the ultimate capacity of the bridge. The results of these tests had a major impact on the implementation of retrofitting techniques on railway bridges in the state of California.

INTRODUCTION

During the last two decades, significant research has been conducted to investigate the seismic response of highway bridges and to address their seismic retrofitting requirements. This research has included several experimental and analytical studies. During the same time, no significant studies have been performed to identify the dynamic properties of railway bridges, their ultimate strength and their response under earthquake excitations. One important difference between comparable simple highway and railway bridges is that, in the case of railway bridges, the rail tracks, the ties, the ballast and the ballast pan provide a strong connection between the bridge structure and the adjacent roadbed. The presence of the rails could provide a significant benefit in terms of providing additional restraint and a mechanism for transferring seismic loads to the roadbed. Thus, the structural elements of the railway bridges could be relieved from the demand to carry all of the seismic load.

The California Department of Transportation (Caltrans), has funded a study to perform a full scale failure test of the deck - abutment connections of the Strawberry Park Underpass. This bridge, was scheduled for demolition and replacement in spring 1995 (it was replaced in April 1995), and thus presented an excellent candidate for a failure test. The objective of this study was to quantify the beneficial effects of the railway elements on the ultimate capacity of the bridge. Its results were to be used in the Caltrans retrofitting program of railway bridges.

---

[1]Professor and Chair, Civil Eng. Dpt., Univ. Of Nevada, Reno
[2]Professor, Civil Eng. Dpt., Univ. Of Nevada, Reno
[3]PhD Candidate, Civil Eng. Dpt., Univ. Of Nevada, Reno
[4]Design Engineer, California Department of Transportation

Full scale ambient or forced vibration tests have been used extensively in the past to determine the dynamic characteristics of either buildings or highway bridges [1-9]. In the case of the forced vibration tests, the structures have been excited by using either a dynamic shaker [5, 6, 7, 8] or by the quick release method [2, 3, 4].

The objective of this paper is to describe the failure tests and their impact on the retrofitting program of railway bridges in the state of California. During the tests, the tracks were cut, the ballast was removed and the ballast pan was cut at the west abutment of the bridge, while the east abutment was left intact. Then, the bridge was pushed to failure at both ends and comparison of the failure loads allowed for an assessment of the role of the tracks, the ballast and the ballast pan on the ultimate capacity of the abutment connections of the bridge. Details about these tests, as well as about a series of resonance tests which were performed on the same bridge but are not described in this paper, are provided in [10, 11]

LOCATION AND DESCRIPTION OF THE BRIDGE

The Strawberry Park Underpass was a two-span simply supported ballasted railroad bridge across the Harbor Freeway in the City of Los Angeles, California. The bridge measured 148'3" (45.2 m) long by 18'0" (5.5 m) wide and had a steel deck girder superstructure with a concrete substructure. It was designed in 1959 by Caltrans. The superstructure consisted of two adjacent built-up girders measuring 18' center to center connected by W 18 x 60 floor beams spaced at 2-ft (61 cm) longitudinally and covered by a 0.5-in (13 mm) thick low alloy steel plate (ballast pan), which contained the ballast. The substructure consisted of a two-column bent approximately 23' (7 m) high with a single 2' x 4' x 13' (0.61 m x 1.22 m x 3.96 m) bent cap. The columns were monolithically connected to a single 2.5' x 27' x 2.6' (0.76 m x 8.23 m x 0.79 m) concrete spread footing. The abutments were the high seat type with steel rocker bearings; the connecting wingwalls were cast monolithically in the longitudinal direction and nonmonolithically in the transverse direction. Figures 1, 2, and 3 show respectively a plan view, an elevation view, and the abutment bearings of the bridge.

DESCRIPTION OF THE ULTIMATE LOAD TESTS

To prepare the bridge for the ultimate load tests, the tracks were cut at the center of the bridge over the pier and at the west abutment. The tracks on the west half of the bridge were completely removed to about a distance of 25 feet (7.6 m) to the outside the west abutment. Then the ballast was completely removed from the centerline of the bridge and at the west abutment to expose the ballast pan at both locations. The ballast pan was cut through so that the west span of the bridge was supported only by its bearings at the central pier and the abutment (Fig. 4). This was done to minimize the transfer of lateral forces to the central pier when the bridge was pushed laterally at the west abutment. The only remaining lateral force resisting mechanism for a transverse load at the central abutment was that of the pin ended bearings at the central pier, which provided some minor resistance. This was unavoidable because the safety of the traveling public below

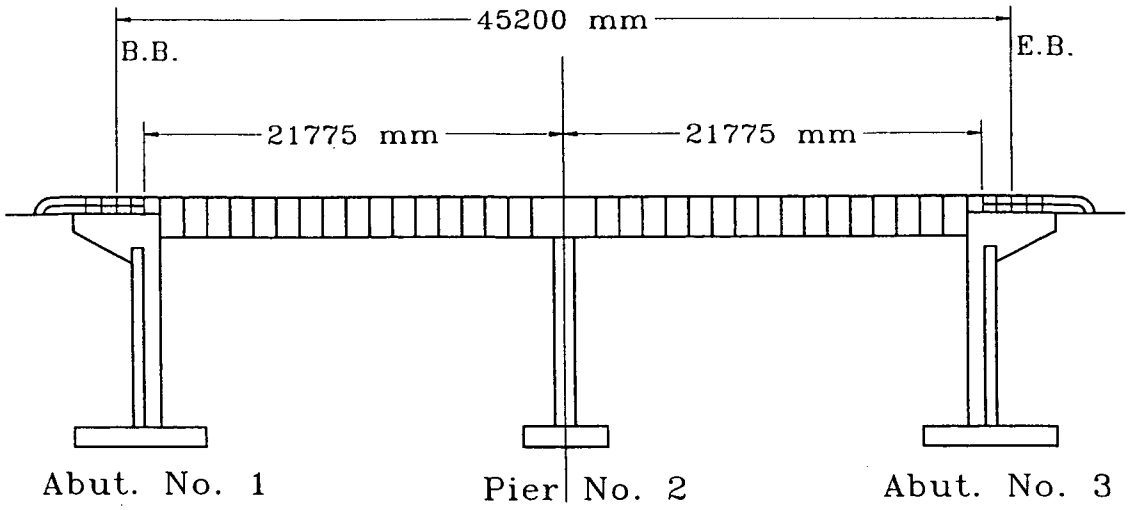


Fig. 1 Elevation of the Bridge

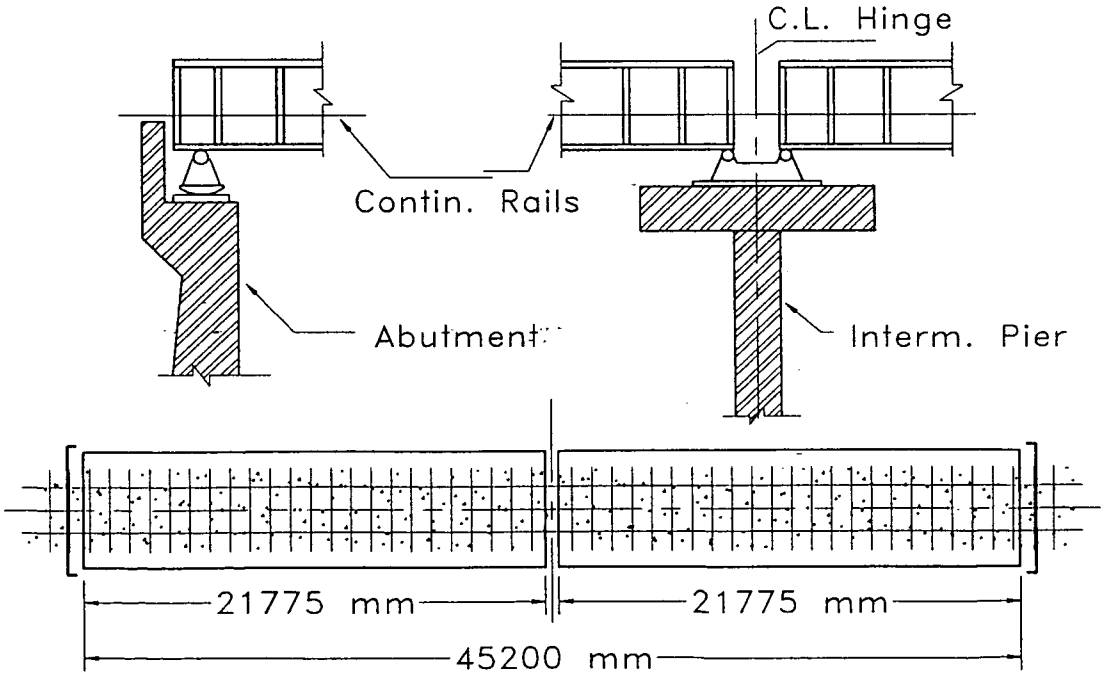


Fig. 2 Plan view of the Bridge

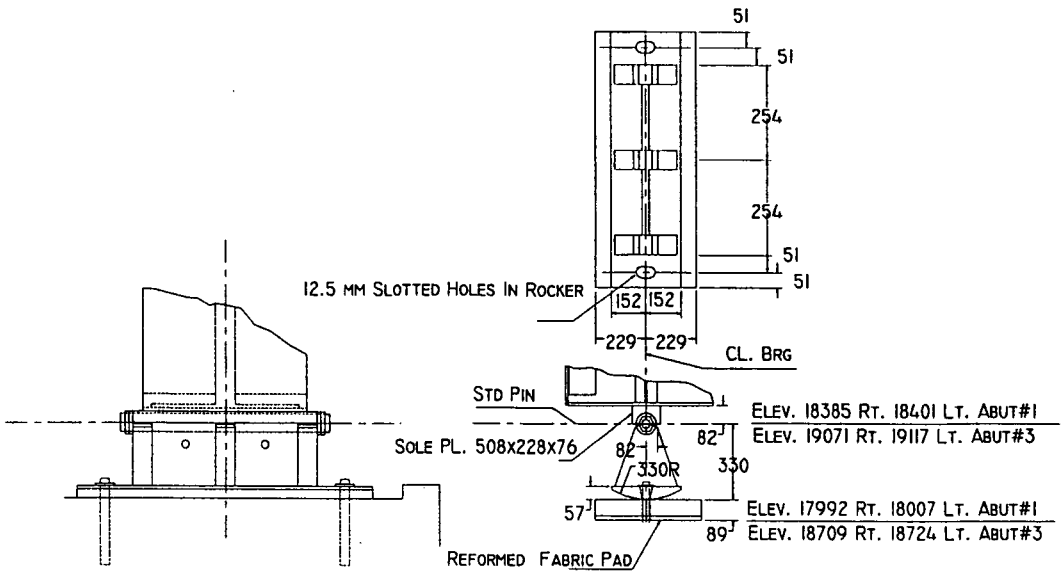


Fig. 3 Abutment Bearings

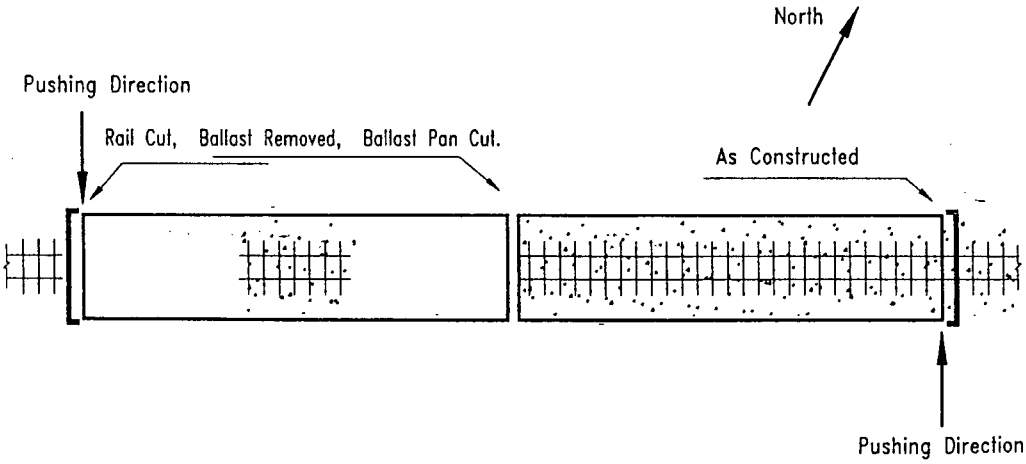


Fig. 4 Bridge Preparation for Failure Tests

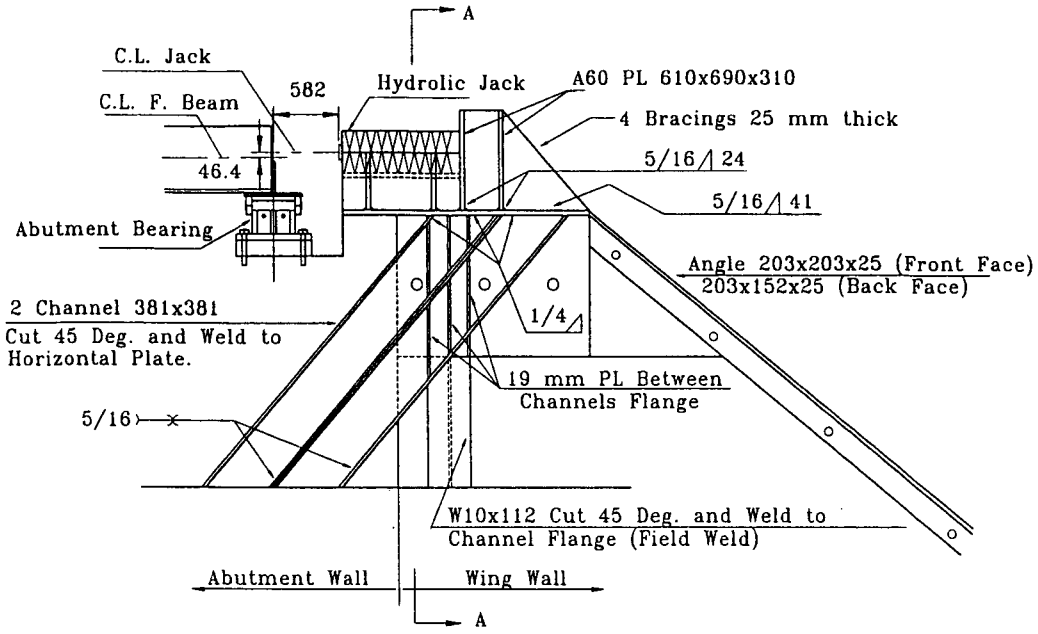


Fig. 5 Elevation of Reaction Frame

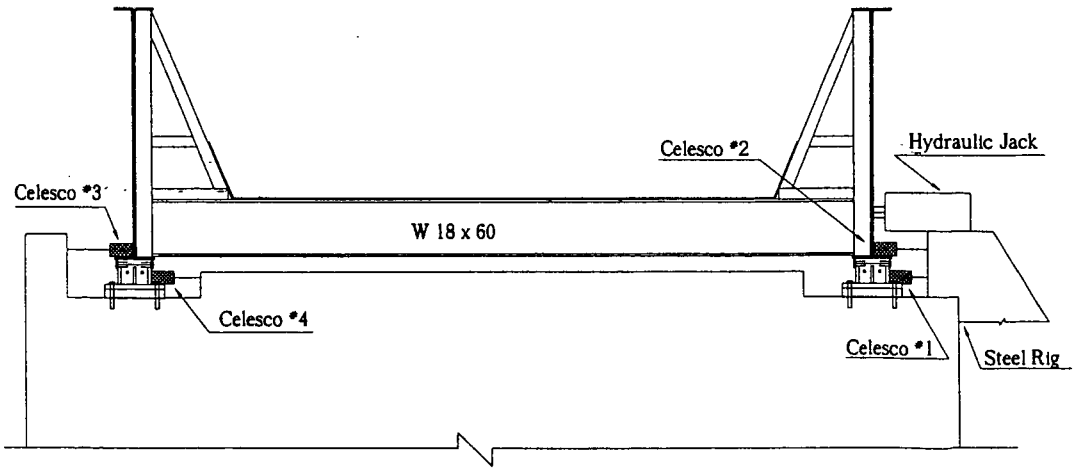


Fig. 6 Instrumentation of West Abutment

demanded that the bearing welds be left undisturbed. The east abutment was left in its "as built" condition with the ties, rails, ballast, and ballast pan intact. This set up resulted in two different types of bridge-abutment connections: one, at the east abutment, of a railway bridge with rails, ballast pan and ballast and another, at the west abutment, with these elements missing and the bridge deck being supported on bridge bearings, like a highway bridge. This allowed for a comparison of bridge-abutment connections, between highway and railway bridges.

To apply the lateral force to the bridge directly over the bearings at the abutments, a load spreader was developed to deliver the loads in compression directly to at least two of the floor beams. A 400-kip (200 ton or 1780 kN) 18-in (46 cm) stroke jack made by Enerpac was used to apply the loads. To react these loads, two identical reaction rigs were constructed and installed at the abutments and wing walls (Fig. 4). The elevation view of this reaction rig is shown in Fig. 5. Four Celesco potentiometer displacement transducers were installed at the abutments of the bridge to measure the lateral displacements. At the west abutment, transducers 1 and 4 measured the lateral displacement of the bottom rocker flange while transducers 2 and 3 measured the lateral displacement of the bottom flanges of the plate girders (Fig. 6). At the east abutment, the arrangement was the same except that the number 4 transducer measured the displacement of the south rail relative to the concrete abutment wall (Fig. 7). A Magadec data acquisition system recorded the displacement responses and the force level of the jack, obtained from a pressure transducer. The jack force was obtained by multiplying the pressure times the area of the cylinder.

RESULTS OF THE FAILURE TESTS

Figure 8 shows the force deformation curve for the west abutment, which was fully free with the bridge sitting cleanly on the bearings. At point A, the first bearing tiedown bolt broke; this was the north bolt on the north bearing. At B, the south bolt at the north bearing assembly broke. At C and D, the remaining bolts on the south bearing assembly broke. For displacements greater than those associated with the breaking of bolt D, the bridge simply slid on the abutment since all the tiedown bolts had broken. This was mainly a friction resistance. The lower set of dashed lines represents the secant stiffness up to the horizontal line which, in turn, represents a lower bound resistance force. The upper set of dashed lines represents the initial elastic stiffness up to the upper dashed line. The upper dashed line was drawn so that the area under the actual load resistance curve and the upper set of dashed lines have equal area or equal energy absorption. The ultimate load for the west abutment was 285 kips (1270 kN), while the lower bound resistance load was 120 kips (534 kN). Similar curves were obtained for the remaining channels of the west abutment.

Figure 9 illustrates the displacements at the west abutment as a function of time during the tests for all four channels. Notice that Channels 1 and 4, which measured the slip of the bottom rocker bearing flange at the north and south bearings, track fairly close together. Channels 2 and 3, which measured the lateral displacement of the bottom flanges of the

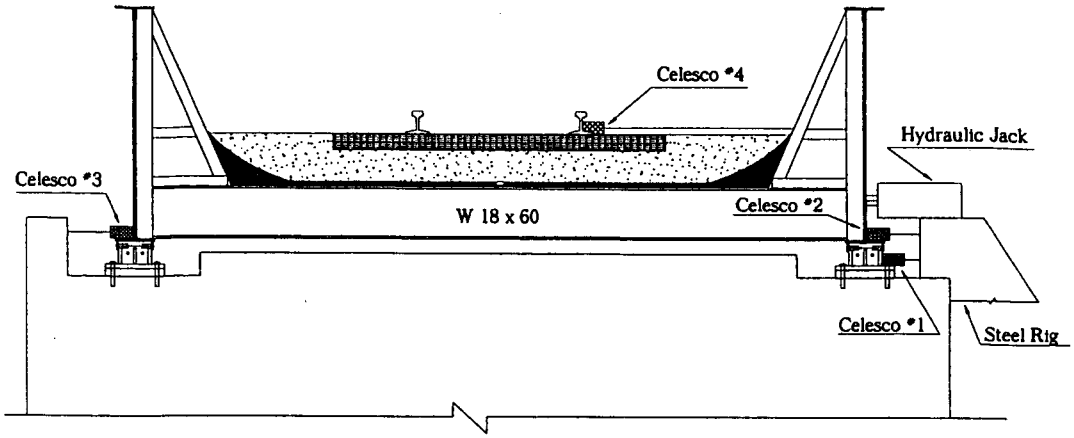


Fig. 7 Instrumentation of East Abutment

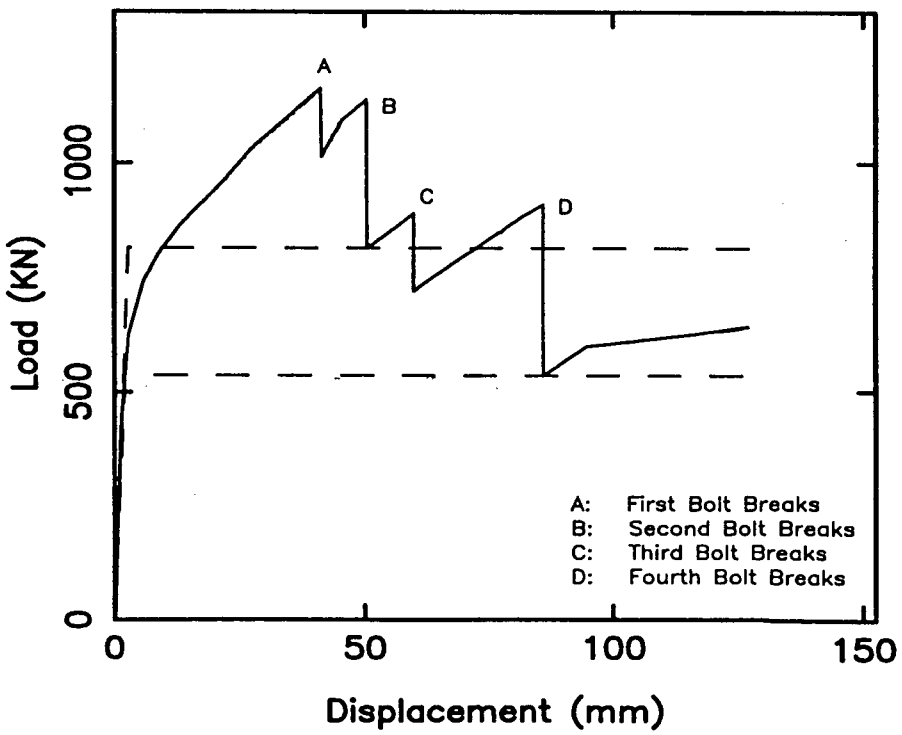


Fig. 8 Load - Displacement Curve at the West Abutment, Celesco #1

north and south plate girders, also track fairly well together, with the displacements of the bottom flanges being larger than those of the rocker flange. This is the expected result since the load was delivered above the bottom flange.

Figure 10 shows a typical failure mechanism of the bearing at the west abutment. The failure surface is at the interface between the bottom of the bearing and the concrete. The bearing moved about two inches (5 cm) in the transverse direction and lifted up by about 3/4 in (1.9 cm) at its north end before the first bolt broke in tension.

Figure 11 depicts the displacements of the south rocker flange at the east abutment. In this case, the east abutment was in the "as built" condition. In this figure, A represents the point where the first bearing tiedown bolt broke. The load dropped to that point below point B. After this, the load was increased to point B where the bearing pin nut broke explosively. At this point, the bottom of the rocker flange rebounded about ½ inch (13 mm) with the load falling to the lower bound dashed line in the figure. Because this nut had broken, no further load was transmitted through the south bearing as the top of the rocker bearing simply slid along the rocker pin.

Figure 12 shows the full load displacement curve measured on the girder bottom flange. Point A represents the breaking of the first tiedown bolt mentioned above. Point B represents the explosive breaking of the rocker pin nut with the load falling to the lower bound line. As the displacement increased with further application of load, bolts 2 and 3 broke at the north bearing. The meanings of the upper and lower sets of dashed lines in this figure are the same as those for Fig. 8. The ultimate load at the east abutment is 385 kips (1710 kN), while the lower bound load is 215 kips (956 kN).

CONCLUSIONS OF THE FAILURE TESTS

Figure 13 contains the load displacement curves for the east and west abutments superimposed for Channel 2, which measured the displacement of the bottom flange nearest the point of loading. It can be seen that the ultimate load at the "as built" end is substantially larger than that of the "free" end. This is also true of the lower bound resistance values. It is also interesting to note that the load displacement curves at both ends, up to a load of about 160 kips (712 kN), are essentially the same for both the "free" and the "as built" ends. This load value of 160 kips is coincidentally also the dead load reaction of the bridge at the abutments. x it is believed, that this is about the yield point of the system; proof of this awaits cyclic testing.

The mechanism for the increased resistance at the "as built" end is explained by the presence of the ballast pan, ballast, ties and rails. A significant contribution to the increased strength is due to the ballast pan plate, which engaged a slot in the abutment back wall to allow the ballast pan to pass through the abutment. As the ballast pan engages the edge of the back wall, it becomes an additional structural resisting element which begins to crumple and yield. As this is taking place, the concrete of the abutment back wall spalls absorbing additional energy.

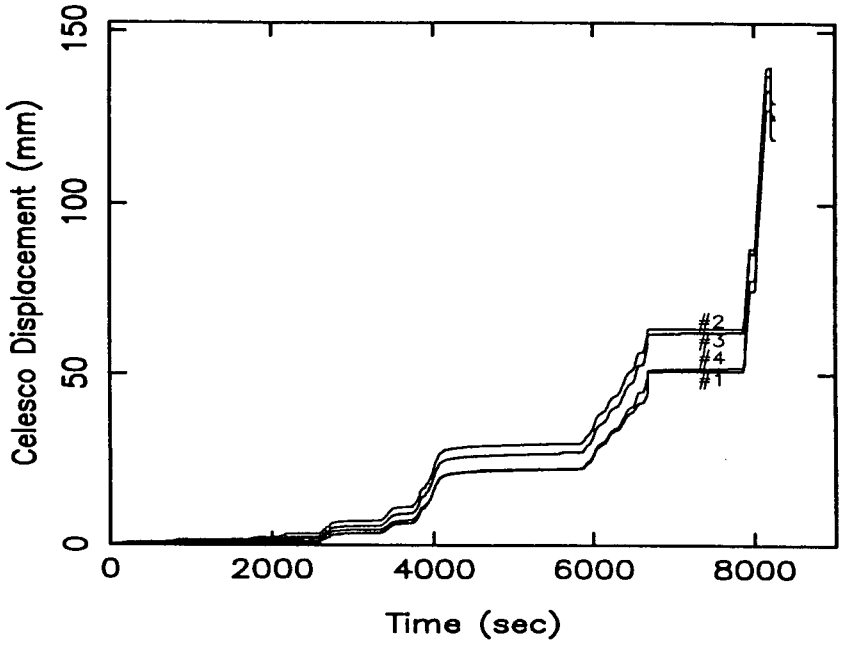


Fig. 9 Displacement Time Histories at West Abutment

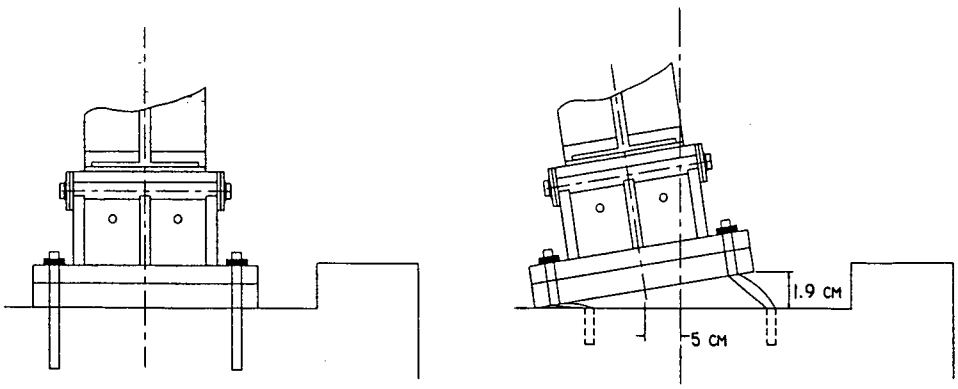


Fig. 10 Failure of Bearing at West Abutment

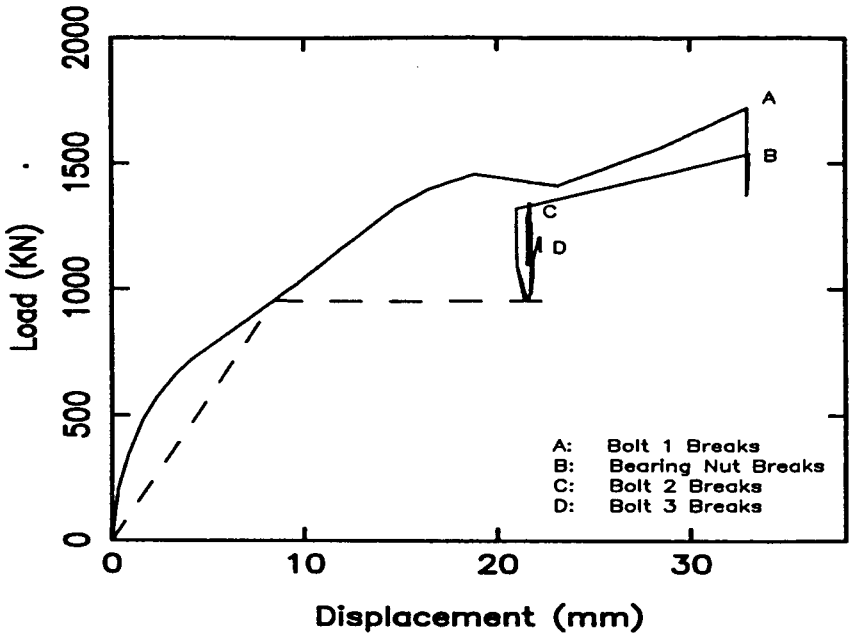


Fig. 11 Load -displacement Curve at East Abutment, Celesco #1

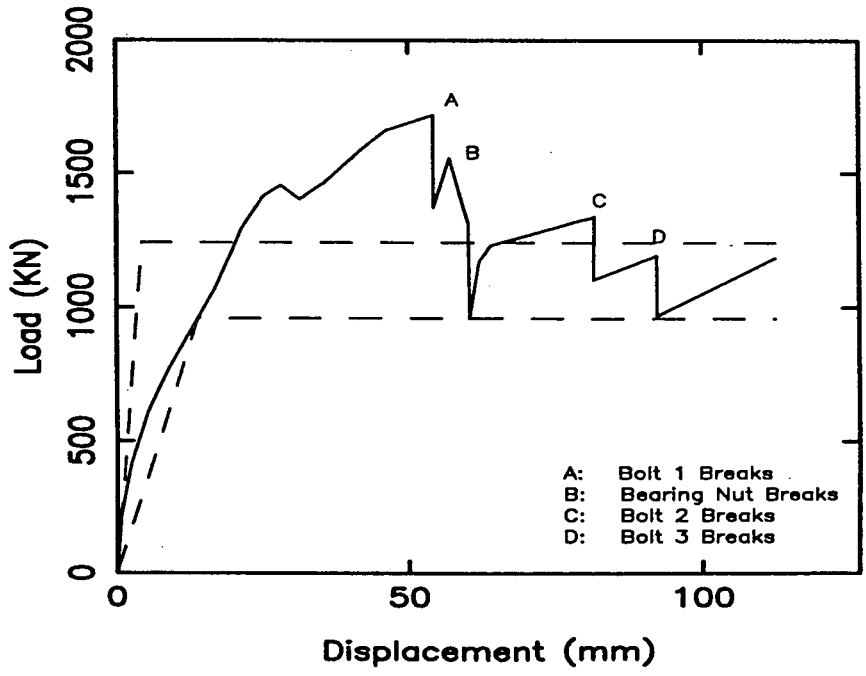


Figure 12 Load - Displacement Curve at East Abutment, Celesco #2

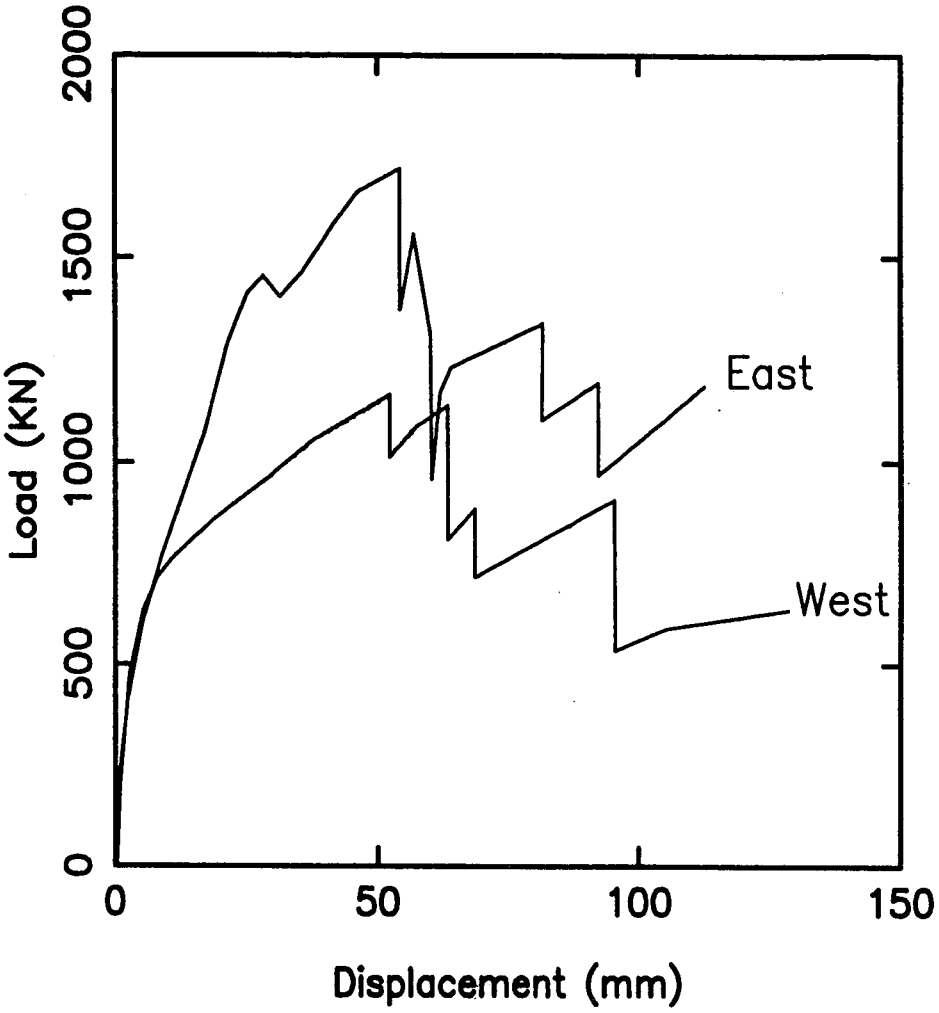


Fig. 13 Comparison of Load -Displacement Curves at the East and West Abutments, Celesco #2

In order to insure that existing bridges of this type can achieve their full ultimate strength, they could be retrofitted by replacing the bearing pin nut. The nut failed on the 3-inch diameter (76.2mm) bearing pin in this test because it had only five threads engaged. This was an insufficient number to develop a failure in the tiedown bolts. The pins and nuts could be replaced so that the full strength of the bearing tiedown bolts can be developed. At the east end of the bridge, one of the tiedown bolts was not allowed to break due to the premature failure of the bearing pin nut.

Table 1: Summary Table of Ultimate Load Tests

Type of Load	West End "Free"	East End "As Built"
Ultimate Load	285 kip (1270 kN)d	385 kip (1710 kN)
Ultimate Load as Ration of Dead Load Reaction	1.78	2.41
Lower Bound Resistance	120 kip (534 kN)	215 kip (965 kN)
Lower Bound Resistance as Ratio of Dead Load Reaction	0.75	1.34
Note: Dead Load Reaction is 160 kip (712kN)		

Table 1 presents the principal numerical results. At the free end, the ultimate load defined by the breaking of the first tiedown bolt is 1.78 times the dead load reaction at the "free" end, while it is 2.41 times the dead load reaction at the "as built" end. It would take a fairly considerable earthquake to achieve these levels of lateral load. The lower bound resistance at the "free" end is 0.75 times the dead load reaction, while at the " as built"' end, it is 1.34 times the dead load reaction. Again, these also represent a considerable resistance to lateral loads.

IMPACT OF THE TESTS ON THE CALTRANS RETROFITTING PROGRAM

The tests described in this paper were completed in April 1995. There were 51 underpasses in California listed in the September 1995 retrofit status. The preliminary cost estimate for those bridges was $8.28-million. As a result of applying the test results, which at that time were preliminary, some candidate retrofit bridges were deleted from the program, while others had retrofit schemes downscoped, some significantly. Because of the urgency of the retrofitting program at that point, not all the bridges were scrutinized

using the test results. Only a sampling of railroad bridges was used to apply the results of this test at that time. However, it was estimated that, based on that sampling, a 25% reduction in retrofit cost was realized. This reduction equals to $2.07-million savings.

An example of a retrofitted railway bridge, in which the results of the tests were used, is the Loveridge Road Underpass. This is a railroad bridge which crosses State Highway 4, near Pittsburgh, in Contra Costa County, California and it is similar to the Strawberry Park Underpass, which was tested to failure.

The final retrofit scheme for this structure, was to widen the abutment bearing seats. Seat widenings are generally inexpensive retrofits as compared to usual column and footing retrofits. This retrofit scheme, is a prime example of the reduced level of retrofit needed for railroad underpasses as a result of the Strawberry Park testing. This bridge is located at a site where peak rock acceleration is estimated to be 0.6g, with a depth of alluvium greater than 150 feet. For a stiff structure, such as the Loveridge Road Underpass, the maximum spectral acceleration is approximately 1.0g. Prior to the tests described in this paper, the Caltrans dynamic modeling procedures would not have considered rail/ballast/ ballast pan/tie continuity at the abutments. Furthermore, the frictional springs, representing fused bearings, would have been considered to be relatively weak. The results of these modeling assumptions would have produced relatively large displacements. Retrofitting strategy would have included one or more of the following techniques: (I) massive keys at the abutments, (ii) large capacity restrainers at abutments and bent, (iii) casing the columns and retrofitting foundations, and, (iv) all of the above. Those type of installations become costly, often interfere with bearing inspections, can impair existing horizontal and vertical clearings and require disruptive and costly lane closures during construction activities.

ACKNOWLEDGMENTS

These tests were funded by the California Department of Transportation (Caltrans). This financial support is gratefully acknowledged. The participation and comments received from researchers and engineers of the Association of American Railroads is appreciated. The cooperation of the railroads during the preparation and performance of the tests is also acknowledged.

REFERENCES

1. "A Guide for the Field Testing of Bridges" American Society of Civil Engineers, Committee on Safety of Bridges, New York, 1980.

2. Douglas, B. M., Maragakis, E. A., and Bhabananda N., " Static Deformations of Bridges from Quick-Release Dynamic Experiments", ASCE Journal of Structural Engineering, Vol. 116, No.8, August 1990, pp. 2201-2213.

3. Richardson, J. A., "Dynamic Response Analysis of the Dominion Road Bridge Test

Data", PhD. Thesis, University of Nevada, Reno, December, 1988.

4. Douglas, B. M., Drown, C., D., and Gordon M., L., "Experimental Dynamics of Highway Bridges", Proceedings of the Second Specialty Conference on Dynamic Response of Structures: Experimentation, Observation, Prediction and Control, Jan.1981, Atlanta, Georgia.

5. Guy, J., and Favillier, M., "Parameter Estimation from Full-Scale Cyclic Testing", Proceedings of the Second Specialty Conference on Dynamic Response of Structures: Experimentation, Observation, Prediction and Control, Jan.1981, Atlanta, Georgia.

6. Pardoen, G. C., Car, A.J., and Moss, P. J., "Bridge Modal Identification Problems", Proceedings of the Second Specialty Conference on Dynamic Response of Structures: Experimentation, Observation, Prediction and Control, Jan.1981, Atlanta, Georgia.

7. Foutch, D. A., "A Study of the Vibrational Characteristics of Two Multistory Buildings" Report No. EERL 76-03, California Institute of Technology, Pasadena, California.

8. Foutch, D. A., Housner, G., W., and Jennings, P. C., "Dynamic Responses of Six Multistory Buildings during the San Fernando Earthquake", Report No. EERL 75-02, California Institute of Technology, Pasadena, California.

9. Wilson, J. C., "A Study of Seismic Response of a Cable-Stayed Bridge", Proceedings on the Second Workshop on Bridge Engineering Research in Progress, pp. 55-58, Oct 1990, Reno, Nevada.

10. Maragakis, E., Douglas, B. M., and Sandirasegaram, U., "Full- Scale Field Resonance Tests of a Railway Bridge", Report No. CCEER 97-01, University of Nevada, Reno, May 1997.

11. Maragakis, E., Douglas, B., Chen, Q., "Full-Scale Field Capacity Tests of a Railway Bridge", A Report to the California Department of Transportation, Report No. CCEER-97-1, University of Nevada, Reno, May 1997.

SESSION 11: WIND

(1) Development of Expert System for Wind Resistant Design of Highway Bridges
(H. Sato and T. Mabuchi)

(2) Wind Characteristics for Structural Design in Osaka City
(Y. Inoshita and T. Yokota)

(3) Very Long Suspension Bridges Using the Temporary Mass Method
(S. Nakazaki and H. Yamaguchi)

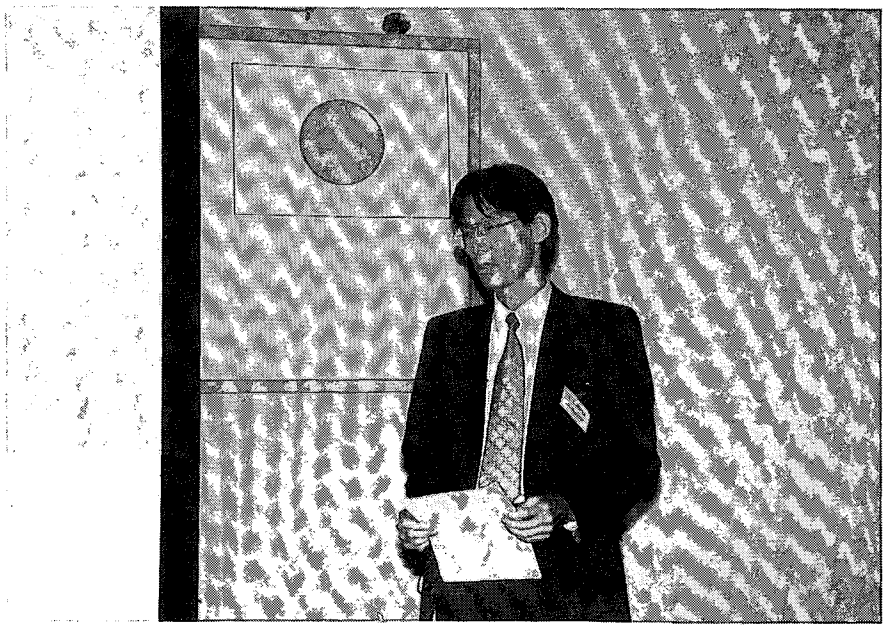
(4) On Aerodynamic Stability of a Suspension Bridge with Box Girder during Erection Stage
(R. Toriumi and M. Takeguchi)



Co-Chairmen : Hiroshi Sato, Andrzej Nowak



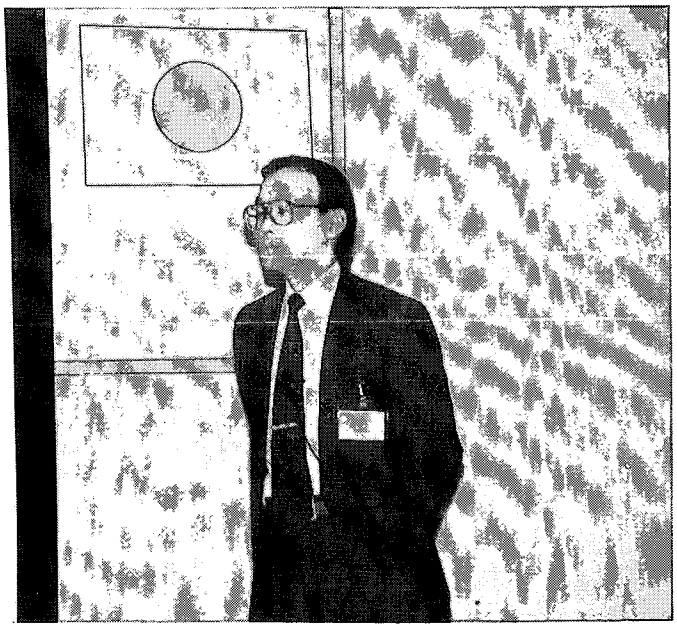
SESSION 11 : Toshiaki Mabuchi



SESSION 11 : Tetsuya Yokota



SESSION 11 : Shunzo Nakazaki



SESSION 11 : Ryuichi Toriumi

Development of Expert System for Wind Resistant Design of Highway Bridges

Hiroshi Sato[1], Toshiaki Mabuchi[2]

SUMMARY

The Wind Resistant Design Manual for Highway Bridges was published in 1991. Considering the recent progress of personal computers, the Wind Resistant Design Manual for Highway Bridges is now being converted to the Expert System so that bridge engineers can make wind resistant design more easily. In this paper, some of the features of the Manual are outlined first, then follows development of the Expert System Prototype for wind resistant design of highway bridges.

1. INTRODUCTION

The new Wind Resistant Design Manual for Highway Bridges was published in 1991. The main features of the Manual are as follows.

a. The basic wind speeds of the whole country are provided.

b. The design wind speed and the properties of wind turbulence can be obtained considering the altitude of structure and the terrain around the structure.

c. The critical wind speed for flutter and galloping can be estimated by simple formulae as well as by wind tunnel testing.

d. The amplitude of vortex-induced vibrations can be estimated by simple formulae as well as by wind tunnel testing. The effect of turbulence on vortex-induced vibrations is incorporated.

e. The method of verification of flutter, galloping and vortex-induced vibrations are provided.

f. The guideline of wind resistant design for bridge members and for bridges at their erection stages are described.

g. The standard wind tunnel testing methods are described.

For general engineers, it is difficult to follow wind engineering, which is interdisciplinary science including meteorology, statistics, structure dynamics fluid dynamics and so on. Considering the recent progress of personal computers, the wind resistant design manual for highway bridges is now being converted to the Expert System, written in dialogue styles on personal computer, so that bridge engineers can make wind resistant design more easily.

In this paper, some of the features of the Manual are outlined first, then follows development of the Expert System Prototype for wind resistant design of highway bridges.

---

1) Dr. of Eng. , Head, Structure Division, Structure and Bridge Department, Public Works Research Institute, Ministry of Construction, Japan

2) Ms. of Eng. , Research Engineer , ditto

2. THE WIND RESISTANT DESIGN MANUAL FOR HIGHWAY BRIDGES

2.1 Procedure of Wind Resistant Design Using the Wind Resistant Design Manual

The procedure of wind resistant design using the Manual is shown in **Fig. 1**. The wind properties (basic wind speed, design wind speed, turbulence intensity etc.) are decided first. The design wind load is calculated, and the static design of the bridge is made. This procedure is the same as the existing wind resistant design method.

At this stage, where major dimensions of the bridge are determined, wind-induced vibrations to be studied further are chosen considering the design wind speed, the deck width and the span length of the bridge. For bridges with short span length, no study on wind-induced vibration is required.

For other bridges, wind-induced vibrations specified above should be predicted using the formulae provided in the Manual. Then the wind-induced vibrations are evaluated. The formulae were established considering past wind tunnel test results. Since the formulae are expressed by means of only a few parameters, the prediction error of the formulae is not negligibly small. Therefore, the formulae are established, so that their prediction may become safer. It means that evaluation 'good' based on the formulae is almost always 'good', however, evaluation 'no good' based on the formulae is not always 'no good' because of the safety margin of the formulae. In case that the evaluation based on the formulae turns out to be 'no good', the bridge engineer can modify the design or he can predict wind-induced vibrations by means of wind tunnel testing. The evaluation based on wind tunnel testing has priority over that based on the formulae.

2.2 Contents

The contents of the Manual are as follows.

1. GENERAL REMARKS
2. GUIDELINE OF WIND RESISTANT DESIGN
3. DESIGN WIND LOAD
4. WIND PROPERTIES USED IN DESIGN
   (Basic Wind Speed, Design Wind Speed, Intensity of Turbulence, etc.)
5. WIND-INDUCED VIBRATIONS OF BRIDGE DECK
   (Prediction, Evaluation, Method of Alleviation, Flutter,
   Galloping, Vortex-Induced Vibrations, Gust Responses)
6. WIND-INDUCED VIBRATIONS OF TOWERS AND BRIDGE MEMBERS
7. WIND RESISTANT DESIGN AT ERECTION STAGES
8. WIND TUNNEL TESTING METHODS

2.3 Wind Properties Used in Design

Wind properties are modeled fundamentally according to Davenport [1978,1982], namely, lower mean wind speed but higher turbulence in rough terrain and low altitude, and higher mean wind speed but lower turbulence in smooth terrain and high altitude. The terrains are classified into four, namely rough sea (Terrain I), open farmland (Terrain II), suburbs (Terrain III) and city

centers (Terrain Ⅳ).

2.3.1 Basic wind speed U_{10}

The basic wind speed U_{10} is defined as the mean wind speed over open farmland (Terrain Ⅱ) at an elevation of 10m, averaged over a period of 10 minutes. Using the meteorological data at weather stations in Japan, extreme wind speeds were estimated. The probability that the annual maximum mean wind speed exceeds the basic wind speed is 40% in a 50-year period. The basic wind speeds were classified into 4 categories, namely 30m/s, 35m/s, 40m/s and 45m/s. It is shown in **Fig. 2**.

2.3.2 Design wind speed U_d

The design wind speed for dynamic design can be obtained from the following formula.

$$U_d = U_{10} E_1 \quad (1)$$

where, U_d : design wind speed.

U_{10} : basic wind speed.

E_1 : correction factor for altitude and terrains

The model of design wind speed profiles is shown in **Fig. 3**.

2.3.3 Turbulence properties

Typical values for turbulence properties such as turbulence intensities and power spectral density functions are provided in the Manual. Turbulence intensity Iu is shown in **Fig. 4**.

2.4 Design Wind Load

The design wind load for static design P_d can be obtained from the following formula.

$$P_d = 0.5 \rho U_d^2 C_d A_n G \quad (2)$$

where, P_d : design wind load

ρ : air density

C_d : drag coefficient

A_n : projected area

G : gust factor

In the Manual, as well as the Specification, the typical values for C_d are applied according to the type of bridge and members. Design wind speed U_d for static design wind load is 40m/s. Gust factor G was determined so that the shear force or bending moment induced by the design wind load may become equivalent to those estimated by the gust response analysis. In the specification, 1.9 is used for gust factor G.

2.5 Wind-Induced Vibration to be Examined

According to the types of a bridge, main span length L, deck width B and design wind speed U_d ,the type of wind-induced vibration be studied further are specified. The method of specification is shown in **Table 1**. The criteria in the table are simplified versions of what

follows. The specified wind-induced vibrations should be predicted either by the formulae provided or by wind tunnel test. The predicted vibrations should be evaluated according to the provision of the Manual.

2.6 Prediction of Wind-Induced Vibrations by the Formulae

Wind-induced vibrations of bridges can be classified into flutter, galloping, vortex-induced vibrations and gust responses. Their distinctive features are shown in **Table 2**.

2.6.1 Flutter

Reduced critical wind speeds for flutter of solid deck are shown in **Fig. 5**. It seems that the reduced critical wind speed increases with deck width to depth ratio (B/d). Lowest reduced critical wind speed is about 2.5. As for truss deck, the critical wind speed varies much with minor difference of configuration of truss and floor deck. But the reduced critical wind speed is higher than 2.5. The formula for the prediction of the critical wind speed of flutter is as follows.

$$U_{cf}=2.5f_{\theta}\ B \tag{3}$$

where, U_{cf} : critical wind speed for flutter

f_{θ} : natural frequency of the 1st torsional mode.

B : deck width

2.6.2 Galloping

Galloping may take place for solid deck whose deck width to depth ratio (B/d) is relatively small. The critical wind speed for galloping U_{cg} is very high when B/d is over 5. **Fig.6** suggests that U_{cg} changes with angle of attack and with mass-damping parameter. Considering that the reduced mass m_r of concrete desk is about 400/(B/d), U_{cg} for concrete deck is found to be high enough. Considering that m_r of steel deck is about 200/(B/d), U_{cg} for steel deck is found to be at least $4f_h$ B and $8f_h$ B for angle of attack 3° and 0° , respectively.

The formula for the prediction of the critical wind speed of galloping is as follows.

$$U_{cg}=8f_h\ B \text{ ; when angle of attack is almost 0 deg.} \tag{4}$$

$$U_{cg}=4f_h\ B \text{ ; when angle of attack is positive.} \tag{5}$$

where, U_{cg} : critical wind speed for galloping

f_h : natural frequency of the 1st bending mode.

Sinusoidal wave form observed in smooth flow changes into random form in turbulent flow. It was found that onset velocity for negative damping, which causes galloping, increases remarkably in turbulent flow (Narita et al [1987]). It suggests that U_{cg} will be high enough when turbulence intensity is high enough.

2.6.3 Vortex-induced vibrations

Vortex-induced vibrations may take place for solid deck. The amplitude decreases with mass or mass moment of inertia and structural damping. The amplitude is very sensitive to the

geometrical configuration, however, the amplitude decreases with deck width to depth ratio (B/d)(**Fig.7**). On the other hand, the variation of reduced wind speed for the occurrence of vortex-induced vibrations is smaller than that of the amplitude.

In the turbulent flow, the amplitude becomes smaller than that in smooth flow. This effect becomes more significant in high turbulence intensity and for cross section of large B/d.

The formulae for the prediction of the critical wind speed and amplitude of vortex-induced vibrations are as follows.

$$U_{cv} = \begin{cases} 2.0\, f_h B & \cdots\cdots \text{ bending} \\ 1.33\, f_\theta B & \cdots\cdots \text{ torsion} \end{cases} \quad (6)$$

$$h_c = E_h \cdot E_{th} \cdot \rho B^3 / (m_r\ \delta) \quad \cdots\cdots\cdots \text{ bending (h/B)} \quad (7)$$

$$\theta_c = E_\theta \cdot E_{t\theta} \cdot \rho B^4 / (I_{pr}\ \delta) \quad \cdots\cdots \text{ torsion (deg.)} \quad (8)$$

where, U_{cv} : wind speed for the maximum amplitude of vortex-induced vibration

$E_h = 0.065\, \beta_{ds} / (B/d)$

$E_\theta = 17.16\ \beta_{ds} / (B/d)^3$

h_c θ_c : corrected maximum amplitude of vortex-induced vibration

E_{th}, $E_{t\theta}$: correction factor for the effect of turbulence (**Table 3**)

β_{ds} : correction factor for sectional shape

m_r, I_{pr} : reduced mass or reduced mass moment of inertia

δ_h, δ_θ : logarithmic decrement

2.7 Prediction of Wind Induced Vibrations by the Wind Tunnel Testing

Wind tunnel testing increases the reliability of wind resistant design of bridges. Since the prediction of wind-induced vibrations based on the formulae may often provide safer value, there is a fair chance that wind tunnel study provides economical design.

As mentioned above, turbulence has a significant effects on wind-induced vibrations. Therefore, standard wind tunnel testing methods in turbulent flow (full aeroelastic model test, taut-strip model test) were described in the Manual as well as conventional testing methods (spring-mounted rigid model test, measurement of steady aerodynamic forces).

2.8 Evaluation of Wind-Induced Vibrations

2.8.1 Flutter and galloping

The following inequalities should be satisfied,

$$U_{cf} > U_r \quad \cdots\cdots \text{ Flutter} \quad (9)$$

$$U_{cg} > U_r \quad \cdots\cdots \text{ Galloping} \quad (10)$$

$$U_r = U_d E_{r1} E_{r2} \quad (11)$$

where, U_r : reference wind speed for flutter and galloping

E_{r1} : correction factor for the effect of gust

E_{r2} : safety factor(1.2)

2.8.2 Vortex-induced vibrations

The following inequality should be satisfied.

$$U_{cv} > U_d \quad (12)$$

In case that $U_{cv} < U_d$, the amplitude Ac should be examined in viewpoint of safety of the bridge, fatigue and serviceability.

2.9 Others

Besides the wind resistant design method of bridge deck mentioned above, the Manual describes the design methods for structural members such as towers and cables, and the design methods for bridges at their erection stages.

3. DEVELOPMENT OF EXPERT SYSTEM

3.1 Necessity of Expert System for Wind Resistant Design of Highway Bridges

The Wind Resistant Design Manual for Highway Bridges was published in 1991. In Japan bridge engineers can make wind resistant design according to the Manual. But for general bridge engineers, it is still difficult to understand wind engineering, which is interdisciplinary science including meteorology, statistics, structural dynamics, fluid dynamics and so on. The technical terms about wind resistant design are not familiar to bridge engineers.

Personal computers have made remarkable progress recently. By using computers we can calculate immediately formulae and display figures and pictures. Program language on personal computer has been also improved in a variety of ways so that we can express most of things. It has become easier to develop expert system.

Considering the recent progress of personal computers, the Wind Resistant Design Manual for Highway Bridges is now being converted to the Expert System. The system is written in dialogue styles on personal computer, so that bridge engineers can make wind resistant design more easily (**Fig. 8**).

3.2 Development of the Prototype Expert System

This prototype expert system is written in Visual C++ and Visual Basic on personal computer.

Five items are shown in the first screen (**Fig. 9**). Namely, Static Wind Load, Wind Resistant Design of Girder, Wind Resistant Design of Tower and Members, Wind Resistant Design at Erection Stage and Wind Tunnel Test.

In Wind Resistant Design of Girder, basic data of bridge can be inputted to screen (**Fig. 10**.) Then expert system will judge necessity of further study on wind effects according to the manual (**Fig. 11**). If further study is necessary, expert system will move to next screen (**Fig. 12**). Finally results of wind resistant design will be displayed like **Fig. 13**.

The technical terms about wind resistant design are not familiar to bridge engineers. Expert system can immediately show explanation through Help Function (**Fig. 14**). Calculation can be also conducted immediately in the system (**Fig. 15**).

3.3 Future Plan

In order to develop more useful expert system, the following functions should be included.

a. Simple prediction method for wind-induced vibration of towers and cables.
b. Calculation programs for natural frequencies, gust response, and flutter speed.

4. CONCLUSION

Based on the Wind Resistant Design Manual for Highway Bridges, Prototype Expert System for Wind Resistant Design of Highway Bridges is being developed on personal computer. Bridge engineers can make wind resistant design more easily.

REFERENCES

Davenport, A.G. 1978, "Wind structure and wind climate", Safety of Structures under Dynamic Loading. Trondheim, TAPIR, V.1, pp. 209-256.

Davenport, A.G. 1982, "The interaction of wind and structures", Engineering Meteorology, Amsterdam, Elservier, pp. 527-572.

Narita, N., Yokoyama, K., Sato, H. and Nakagami, Y. 1987, "Aerodynamic characteristics of continuous box girder bridges relevant to their vibrations in wind", Seventh International Conference on Wind Engineering, Aachen, V. 4, pp. 283-292.

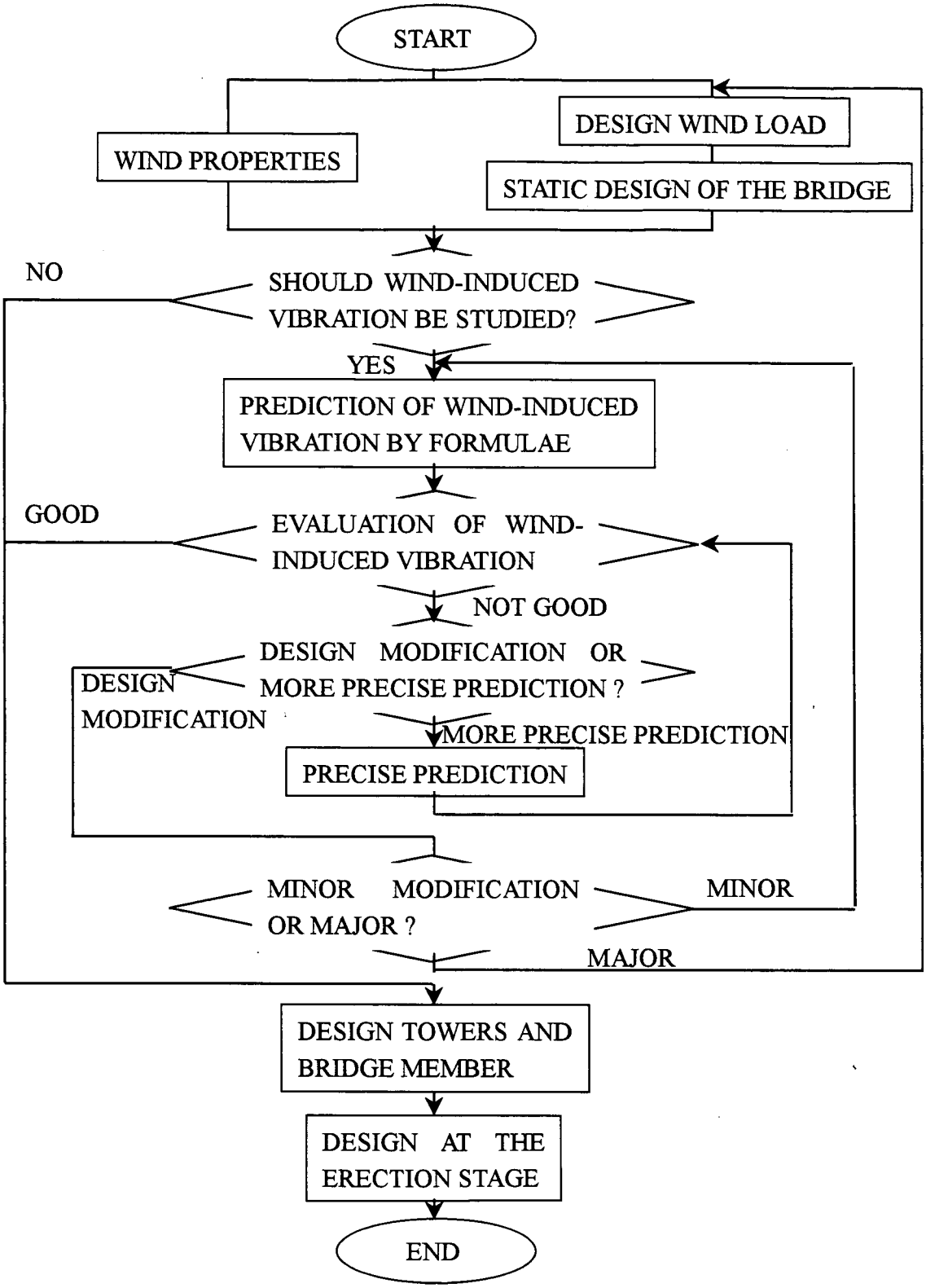


Fig. 1 Procedure of wind resistant design using the Manual

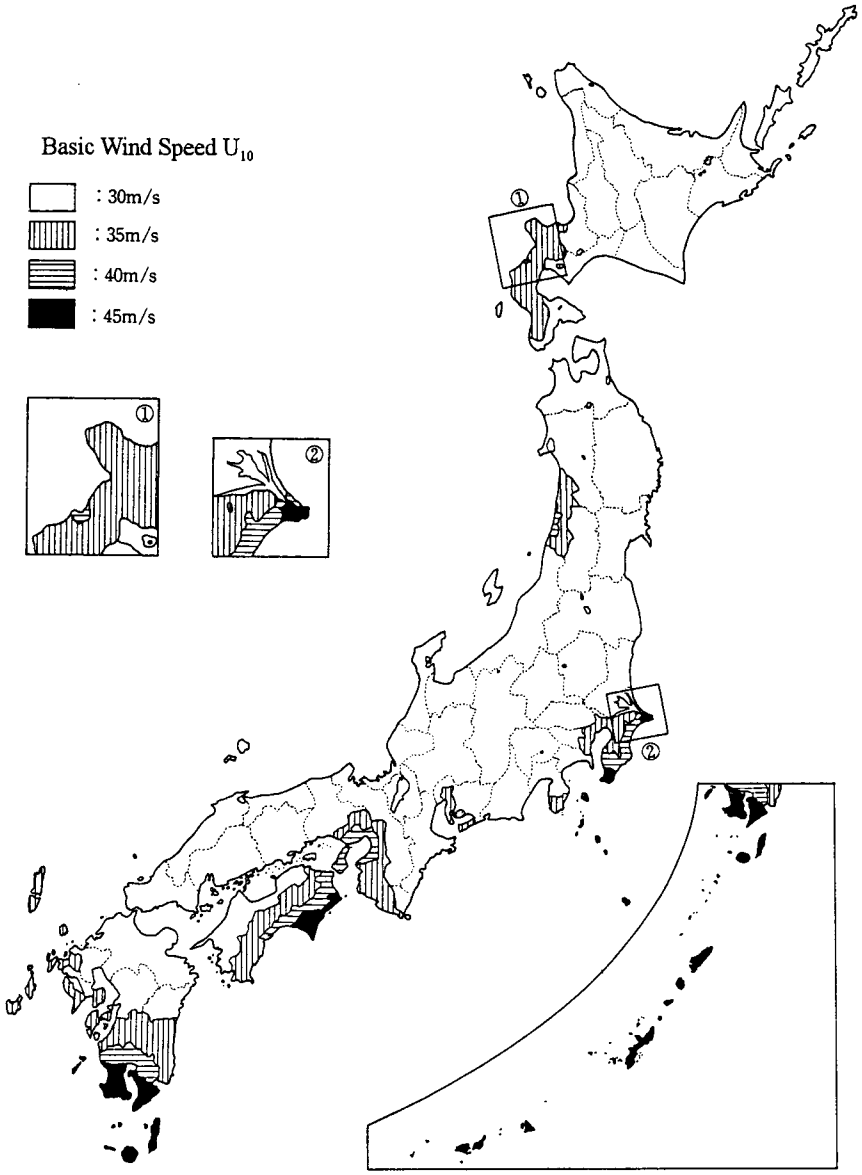


Fig. 2 Basic wind speed

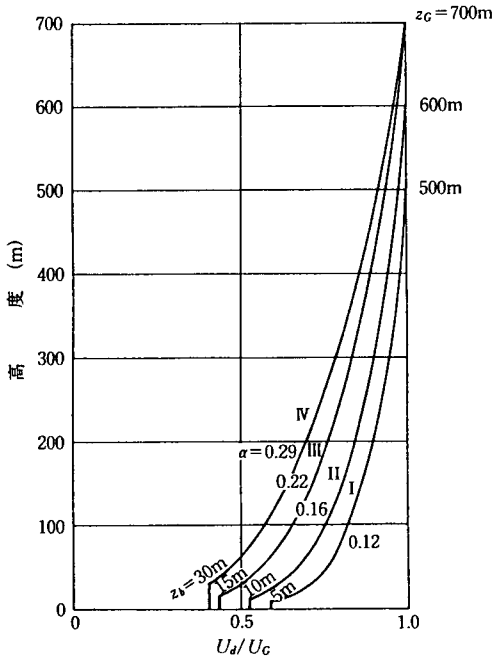


Fig. 3 Model of Design Wind Speed Profiles

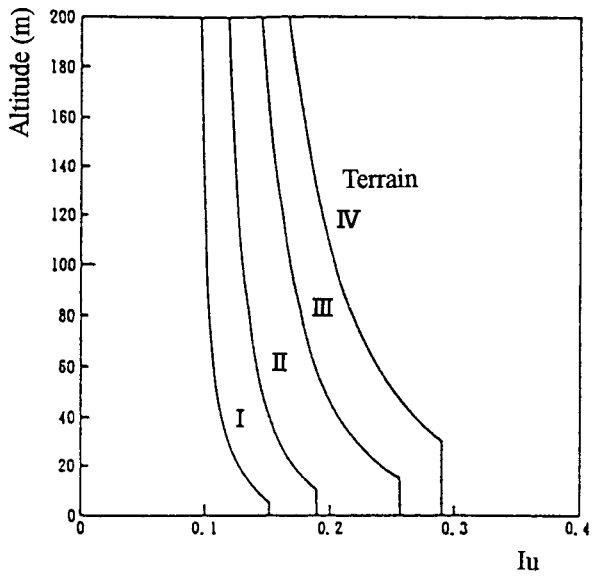


Fig. 4 Turbulence Intensity

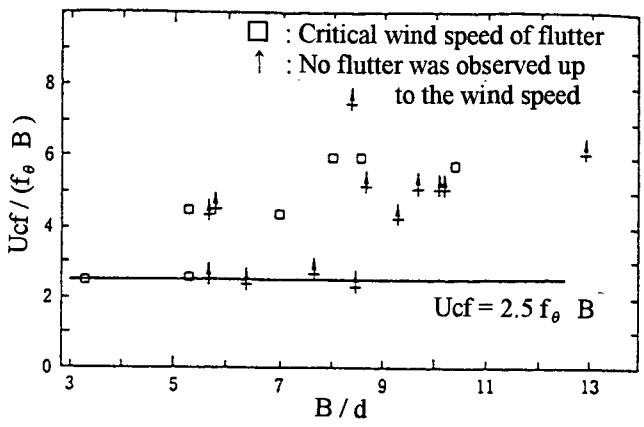
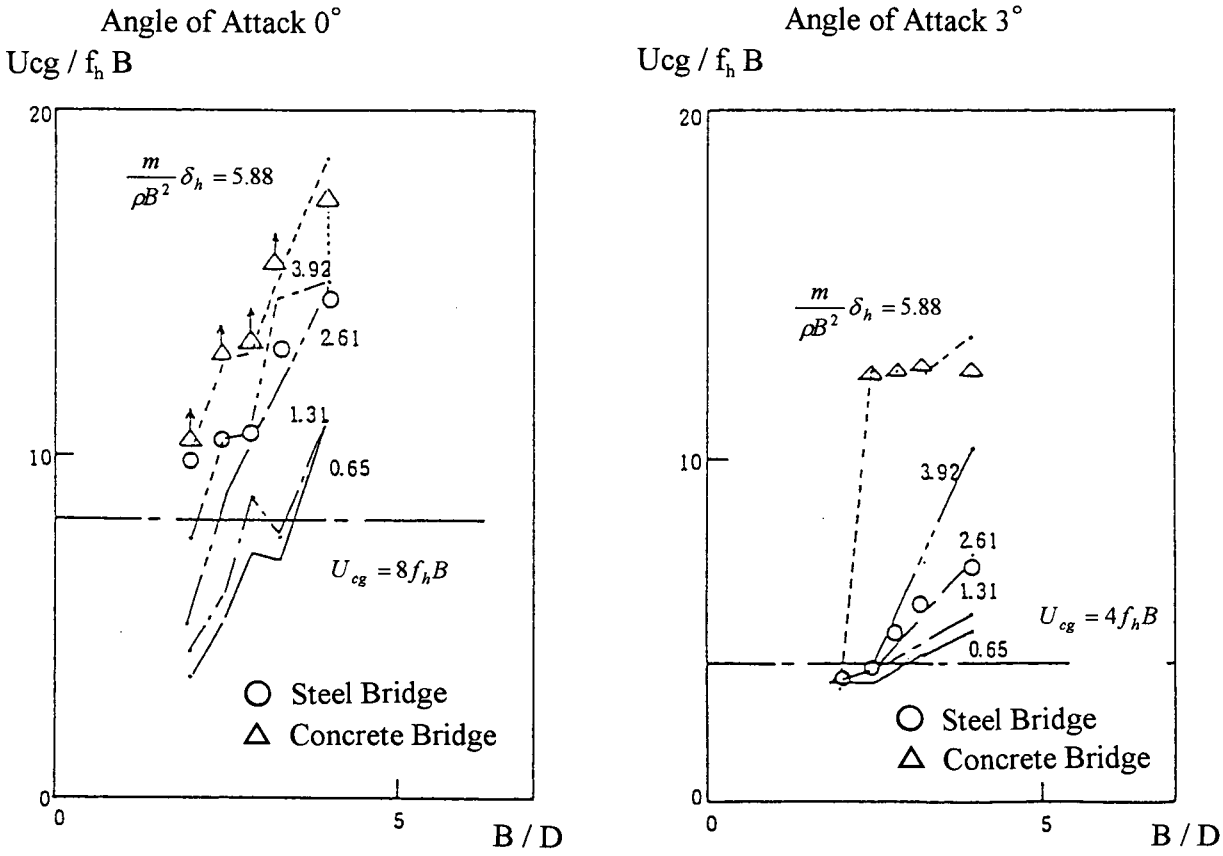


Fig. 5 Reduced critical wind speed for flutter of solid deck



numbers in figure : mass-damping parameter

Fig. 6 Reduced critical wind speed for galloping of solid deck

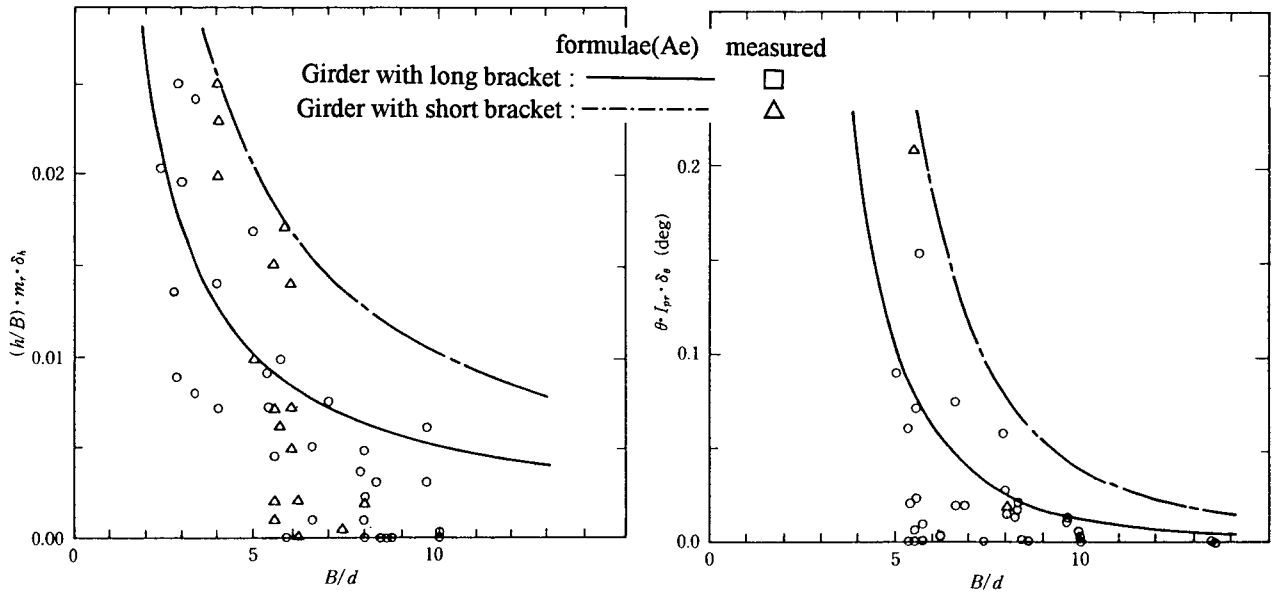


Fig. 7(a) Amplitude of vortex induced bending vibration

Fig. 7(b) Amplitude of vortex induced torsional vibration

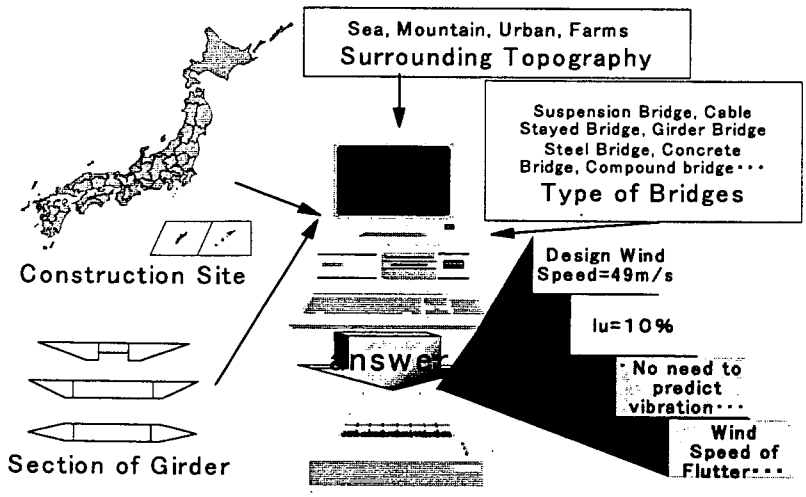


Fig. 8 Outline of Expert System for Wind Resistant design of Highway Bridges

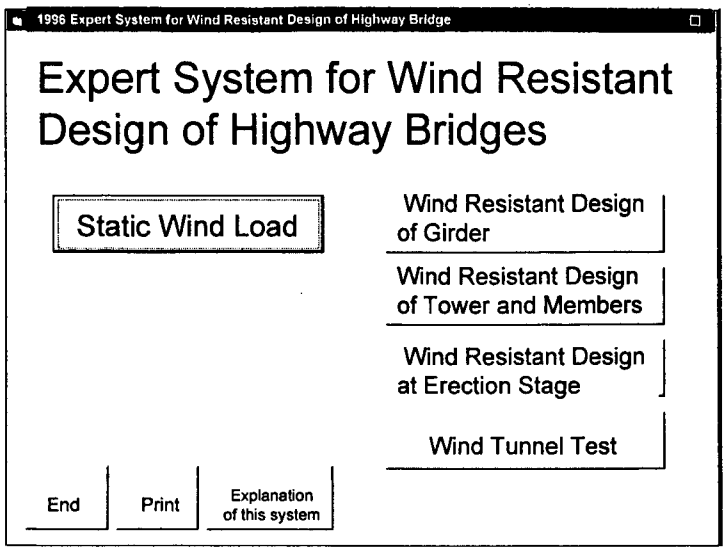


Fig. 9 Opening Screen of Expert System

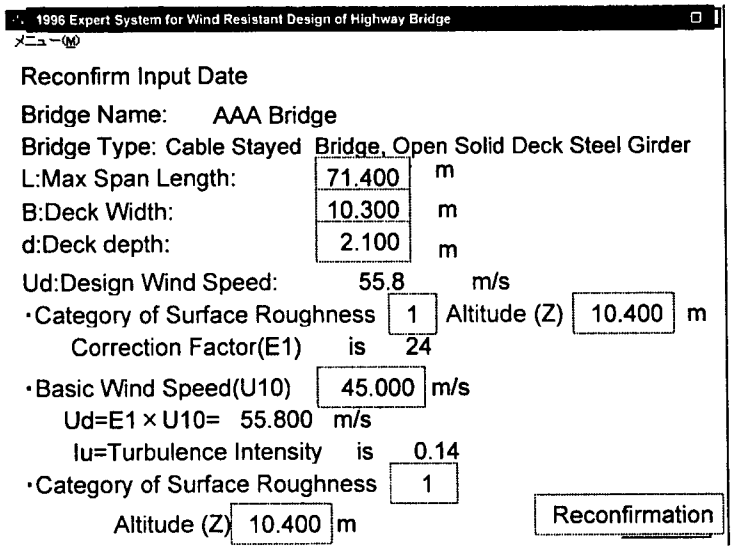


Fig. 10 Wind Resistant Design of Girder

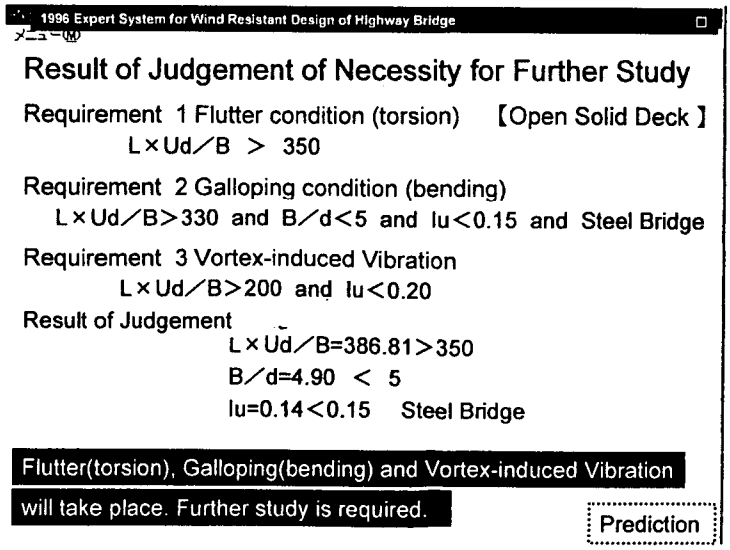


Fig. 11 Judgement of Necessity for Wind Resistant Design

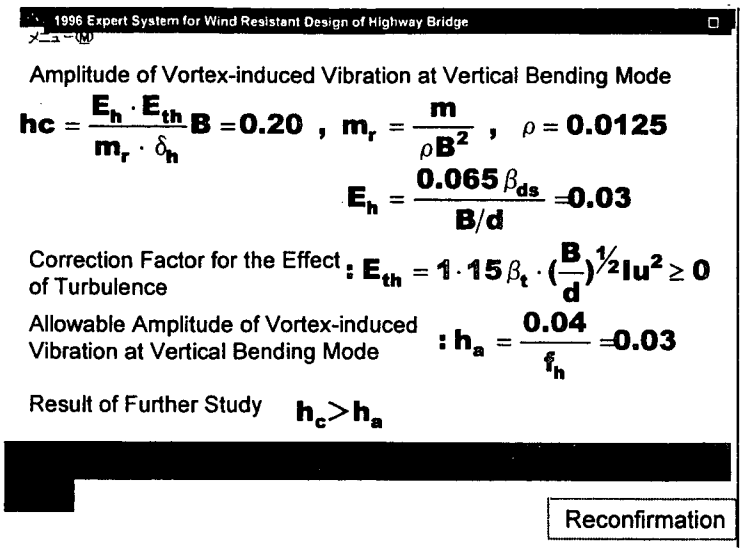


Fig. 12 Prediction of Vortex-induced Bending Vibration by Amplitude

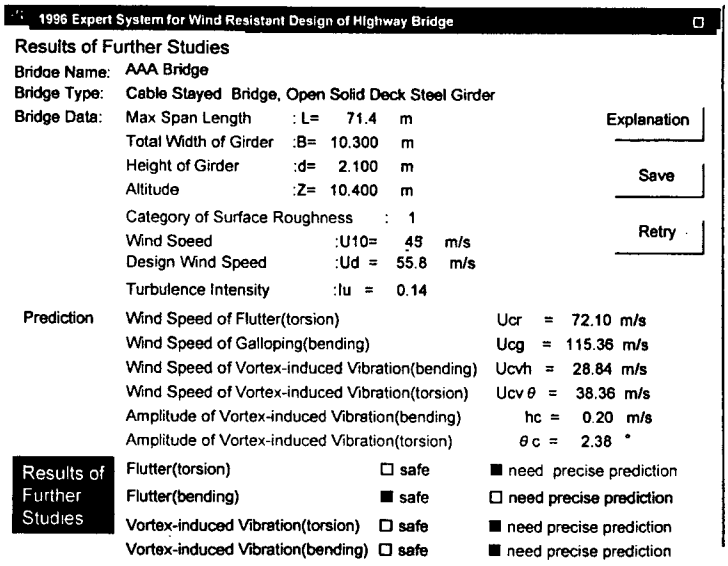


Fig. 13 Results of Wind Resistant Design

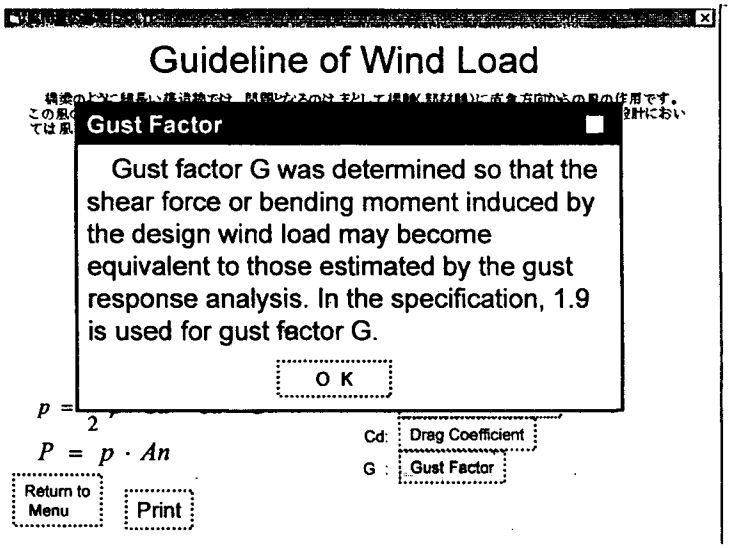


Fig. 14 Help Function

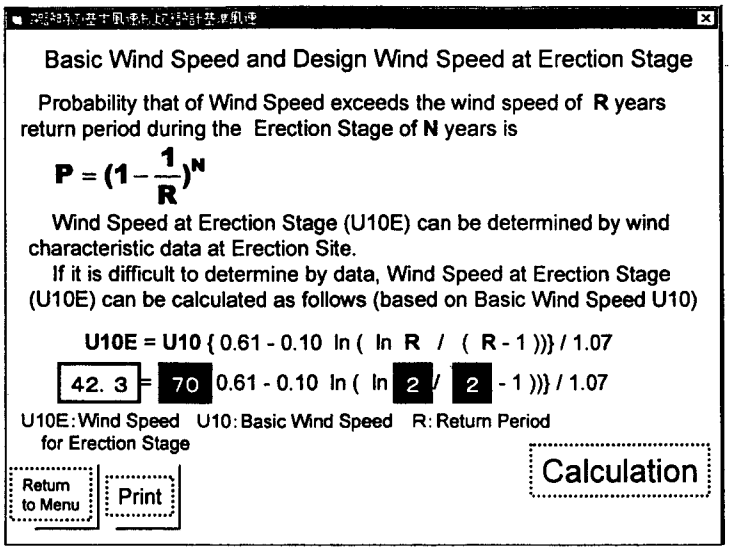


Fig. 15 Calculation Function

Table 1 type of wind-induced vibration to be studied further

Bridge Deck	Criteria	Wind-induced vibration to be expected
Truss Deck for Cable-stayed or Suspension Bridge	If L Ud／B＞350	then Flutter
Open Solid Deck for Cable-Stayed or Suspension Bridge	L Ud／B＞200 and Iu＜0.20 L Ud／B＞330, B／d＜5, Iu＜0.15 and steel deck L Ud／B＞350	Vortex-induced Vibration Galloping Flutter
Closed Solid Deck for Cable-Stayed or Suspension Bridge	L Ud／B＞200 and Iu＜0.20 L Ud／B＞330, B／d＜5, Iu＜0.15 and steel deck L Ud／B＞520	Vortex-induced Vibration Galloping Flutter
Steel Girder Bridge	L Ud／B＞200 and Iu＜0.20 L Ud／B＞330, B／d＜5, and Iu＜0.15	Vortex-induced Vibration Galloping

Where L : main span length　　Ud :design wind speed
B :bridge deck width　　D :bridge deck depth

Table 2 Distinctive features of wind-induced vibrations

	Vibration mode	Wave form	Onset Wind Speed	Amplitude
Flutter	torsion torsion and bending	sinusoidal	high	destructively large
Galloping	bending	sinusoidal	high	destructively large
Vortex-induced Vibration	bending torsion	sinusoidal	relatively low	limited
Gust Response	bending torsion	random	----------	increase with wind speed

Table 3(a) Et(for bending)

Iu / B/d	Except for hexagonal section										Hexagonal section
	0.11	0.12	0.13	0.14	0.15	0.16	0.17	0.18	0.19	0.20	
2<B/d≦ 3	0.7				0.5	0.4		0.3	0.2	0.1	1
3<B/d≦ 4		0.6		0.5	0.4	0.3	0.2	0.1			
4<B/d≦ 5				0.4	0.3	0.2	0.1				
5<B/d≦ 6		0.5									
6<B/d≦ 7			0.4	0.3	0.2	0.1					
7<B/d≦ 8					0.1		0				
8<B/d≦ 9		0.4	0.3	0.2							
9<B/d≦10											
10<B/d≦11			0.2	0.1							

Table 3(b) Et(for bending)

Iu / B/d	Except for hexagonal section										Hexagonal section
	0.11	0.12	0.13	0.14	0.15	0.16	0.17	0.18	0.19	0.20	
2<B/d≦ 3	0.7	0.6	0.5	0.4	0.3	0.2	0.1				1
3<B/d≦ 4	0.6	0.5	0.4	0.3	0.2	0.1					
4<B/d≦ 5	0.5	0.4	0.3	0.2	0.1						
5<B/d≦ 6				0.1							
6<B/d≦ 7	0.4	0.3	0.2								
7<B/d≦ 8			0.1			0					
8<B/d≦ 9		0.2									
9<B/d≦10	0.3										
10<B/d≦11		0.1									

Wind Characteristics for Structural Design in Osaka City

by

Yasutomo Inoshita[1], Tetsuya Yokota[2]

ABSTRACT

Wind characteristics for structural designs in urban area are very important to make them safe and economical. Therefore Osaka Municipal Government has been making efforts to collect wind data near construction sites of longer span bridges over these decades. This paper describes the analytical results and data on wind characteristics in Osaka City. Typhoon winds are also discussed by categorizing two basic types. This study is only preliminary however some clues are indicated for this unknown field.

1. INTRODUCTION

In the design of civil engineering structures (e.g., bridges and bridge piers), the determination of wind load is extremely important. It is particularly necessary to take careful attitude to avoid a disastrous accident when the scale of structures is large and their rigidity is relatively small. However, at present bridge designs are conducted in accordance with Specifications for Highway Bridges for bridges with their center spans of less than 200m. It gives the same value to a basic design speed (i.e., V_{10} = 40m/sec) around Japan. Also, for bridges 200m or longer, a Wind Resistance Design Manual has been issued in 1990 and it gives the basic design wind speed for each area multiplied by a correction coefficient (i.e., factor) relating to roughness of the surface around each surrounding terrain. However, this is nothing more than fairly macro-level regulation, more micro-level rules are necessary in order to promote safe and economical design of structures.

We have conducted wind observations to the degree possible at the erection site, and have worked to reflect the results of the wind observations in design during the construction of comparatively longer span bridges with their central spans of more than 200m in Osaka City. For this reason, we have collected a considerable amount of wind observation records.

In this paper, an attempt has been done to evaluate the wind environment in Osaka City by using these wind observation data. Some considerations will be also given to evaluate the wind loads in Osaka City.

2. EVALUATION METHODS OF WIND ENVIRONMENT

In various design specifications[(1), (2)], the methods employed for estimating wind characteristics such as wind speed and intensity of turbulence are based on the basic wind speed and terrain

1 Staff Officer of Bridges Dept., Public Works Bureau, Osaka Municipal Government

2 Staff Officer of Elevated Crossing Dept., Public Works Bureau, Osaka Municipal Government

surface roughness in the local area. Even if, the wind observations are conducted at the construction site in some cases they tend to be comparatively short-term. Therefore, the estimations of only wind direction, speed and intensity of turbulence are reliable. However the prediction of extreme wind speeds is generally unreliable. The comparison of the results of the wind observations in Osaka City was made and the inter-relation of them has been explored.

2.1 Expression of wind characteristics

The following items are generally used to express wind characteristics for wind-resistance design :

1) Wind speed (e.g.,10 minute average, N-year wind)
2) Intensity of turbulence
3) Scale of turbulence
4) Spectrum of turbulence
5) Spatial correlation of turbulence

The Weibull parameters indicated by the following Eq. (1) can be obtained even from comparatively short-term observation and N-year wind (i.e., N-year mean recurrence interval wind) is also obtained by the method of Gomes & Vickery as shown later.

$$f(V) = \frac{k}{c} \cdot \left(\frac{V}{c}\right)^{k-1} \cdot \exp\left\{-\left(\frac{V}{c}\right)^{k}\right\} \quad \text{---------- (1)}$$

Where,

c = Scale parameter (m/s)
k = Shape parameter
V = 10 minute average wind speed (m/s) (i.e., wind speed hereafter)

Furthermore, intensity of turbulence will be discussed later.

2.2 Terrain roughness parameters

Parameters which express terrain surface roughness are given below[3), (4), (5), (6)].

1) Roughness categories: This is the most widely used in many wind codes. With this method, terrain surface roughness is classified into a number of discrete categories, and wind speed distribution, turbulence distribution and other factors are indicated for each category. Although the method is easily applicable to general investigations, there are cases where the terrain overlaps different categories in a complex way, and the decision on the appropriate category must be made based on user's experience.
2) Roughness length (Z_0) : Compared with the above roughness categories, this parameter is a continuous quantity which facilitates detailed investigation, and correspondences with various wind characteristics have been developed to a fair extent via ESDU etc. However, just as with roughness categories, experience is needed for judgment.
3) Volume density (γ) : Objective information different from 1) and 2) above is determined from the volume and other factors relating to buildings in urban areas etc., and comparatively vigorous correspondences have been made by finding relationships with wind speed distribution and the above roughness length.

In this study, roughness length given by ESDU will be applied for its convenient use as continuous gradation.

2.3 Effects of height

The following height-correlation-relationships have been hypothesized using ESDU concerning with wind speed profile and intensity of turbulence.

1) Wind speed profile

In general, wind profile is expressed using the "power-law" or the "logarithmic-law", here the following logarithmic-law by ESDU will be used for the correction of wind speed.

$$U(z) = U_{10} \times \frac{\ln\left(\frac{z-d}{z_0}\right)}{\ln\left(\frac{10-d}{z_0}\right)} \quad \text{---------- (2)}$$

Where,

U (z) = wind speed at height z

U_{10} = Average wind speed at height 10m

z_0 = Roughness length

d = Zero-plane displacement (d = 0.0 is supported here)

2) Intensity of turbulence

The height distribution of intensity of turbulence is assumed using the following formulas.

$$\begin{aligned} F_u &= [0.867 + 0.556\log_{10}\tilde{Z} - 0.246(\log_{10}\tilde{Z})^2] \cdot \lambda \\ \lambda &= \begin{cases} 1.0 & z_0 \le 0.02m \\ 0.76 / z_0^{0.07} & 0.02m \le z_0 \le 1.0m \\ 0.76 & 1.0m \le z_0 \end{cases} \\ I_u &= \sigma_u / U(z) = F_u / \ln(\tilde{Z} / z_0) \end{aligned} \quad \text{---------- (3)}$$

Where, $\tilde{Z} = z - d$

2.4 The method of Gomes & Vickery

Gomes & Vickery proposed a method to estimate extreme values by fitting the extreme wind speed distribution to the Fisher-Tippett I type indicated by the following formula. They used the Weibull parameters (i.e., c and k) and standard deviation σ_u of the average wind speed distribution [7].

$$P(V) = \exp\{-\exp(V - U_R)\} \quad \text{---------- (4)}$$

Where,

P (V) : cumulative distribution function

V : wind speed

U_R : R-year wind speed given by Eq. (5)

$$U_R = U_1 + \frac{1}{a} \cdot \ln(R) \quad \text{---------- (5)}$$

Where,

$$U_1 = c \cdot \{\ln(N)\}^{1/k},\ \frac{1}{a} = \frac{c}{k} \cdot \{\ln(N)\}^{\frac{1}{k}-1}$$

$$N = 2\pi\nu_u \cdot \beta_u \cdot \frac{k \cdot \sigma_u}{c},\ \nu_u = 675,\ \beta_u = 0.36$$

In areas where extremely strong wind such as typhoons or cyclones etc. will attack, correction is usually done by using a typhoon coefficient[8] or cyclone factor[9] for the above estimated values.

2.5 Wind characteristics in Osaka Area

In conventional design codes, the extreme wind speed for FFW (Free Friction Wind): which is not affected by the surface terrain roughness has been given and it is nothing to do with the wind direction.

In contrast to this Osaka area is surrounded by large-scale topographic features as shown in Fig. 1. The Rokko Mountains is located to the Northwest, the Kongo and Ikoma Mountains are to the East and the Izumi Mountains is to the South. It is well known that Osaka City has strong winds from the direction of Yodo River course and also from the Kitan and the Akashi Straits. Then it is obvious that the extreme wind speed for FFW depends on the wind direction.

2.6 Wind speed estimation of each direction

Osaka City is a relatively flat area, however it also contains a complex mixture of various types of land utilization (e.g., high and low rise urban districts, agricultural land and rivers etc.). Osaka District Meteorological Observatory has comparatively long-term observation data then useful application of them were considered. Fig. 2 shows the procedure to determine the extreme wind speed for each direction based on the terrain surface roughness around the observation point. The outline is summarized below.

1) The Weibull parameters for each direction which are given by the wind speed data of the Osaka District Meteorological Observatory is corrected according to the terrain surface roughness of each direction around the observation points. Then estimation of the Weibull parameters for FFW is obtained. The estimation of extreme wind speed for FFW is calculated by the method of Gomes & Vickery.
2) The estimation of FFW is used to estimate the extreme wind speed of the wind observation points near the bridge sites. Wind profile correction based on the terrain surface roughness around the observation points is done and the results are compared with the short-term observation data.

3. WIND CHARACTERISTICS OF OSAKA CITY

Wind observations have been made at Osaka District Meteorological Observatory and Port and Harbor Bureau of Osaka City in addition to erection sites for comparatively long span bridges. The following results were obtained (Fig. 3).

1) Osaka District Meteorological Observatory

The Osaka District Meteorological Observatory has long-term wind speed records and it is surrounded by the amount of high-rise buildings constructed in recent years.

2) Sugahara Shirokita Bridge

The Sugahara Shirokita Bridge is a bridge crossing Yodo River in Osaka City. Many low rise

buildings can be seen in the area in directions other than the river course. The directionality of the intensity of turbulence is distinguishing feature here.

3) Konohana Bridge

The Konohana Bridge is a bridge crossing to the northern port of Osaka facing Osaka Bay. This is a comparatively new district of reclaimed land and is an open area dotted with low-rise buildings.

4) Nakajima Shinbashi Bridge

This bridge is located at the mouth of the Nakajima River, which marks the border between Osaka City and Amagasaki City. The surrounding area is a zone with seaside factories and many medium-rise factories have been constructed there.

5) Port and Harbor Bureau of Osaka City

Since 1970 in Osaka City, continuous wind observation has been conducted on the rooftop of the Port and Harbor Bureau of Osaka City, which is a harbor construction facing Osaka Bay. The analysis was conducted on the data from 1990 to 1992 in this study. The locations of each observation point are shown in Fig. 3. The observation content for each observation point is summarized in Table 1. The use of the observation equipment has not necessarily been standardized due to the fact that these observations were executed in different time and by different groups. The data were analyzed without calibration. Weibull parameters were extracted by assuming a Weibull distribution for the wind speed of each wind direction.

Wind roses in Table 2 show the dominant wind directions in Osaka City. The configuration of the wind roses look like 8:10 of a clock and its long minute hand indicates the direction of Yodo River course and its short hour hand coincides with the direction of Osaka Bay.

Weibull parameters of each observation point are also shown in Table 2.

The measured intensities of turbulence are shown there and those of horizontal direction (i.e., I_u) are much larger than those of vertical direction (i.e., I_v).

The 100-year wind speed of 16 wind directions are obtained using Weibull parameters as shown in Table 2. The direction of strong wind tends to be south in Osaka City.

The average wind speed and Weibull parameter (c) coincide with each other at Nakajima Shinbashi Bridge as shown Fig. 4. The intensity of turbulence (i.e., I_u) is proportional to the reverse of Weibull parameter (c) as shown Fig. 5.

These results can be summarized as follows:

(a) At all the observation points, the dominant winds blow from northeast running along the Yodo River, and the other dominant ones are west winds blowing from the Osaka Bay side. These winds are not typhoon but seasonal winds.

(b) The direction west of Osaka City lies on the sea, therefore the intensity of turbulence of west wind is small. This tendency can be confirmed by the observation results of Nakajima Shinbashi Bridge (Figs. 4, 5).

(c) The strong correlation between the Weibull parameter (c), and the average wind speed and turbulence intensity can be confirmed by the same observation records (Figs. 4, 5).

(d) The magnitude of 100-year wind is large in the south in addition to west and northeast directions where wind occurrence frequency is high.

From the above observation results, it has been confirmed that the characteristics of wind in the Osaka City depend on the wind direction and careful attention should be paid in application of wind design codes.

4. CHARACTERISTICS OF WIND OF TYPHOONS

The relationship among atmospheric pressure, wind direction, wind speed and occurrence time and so on have been explored for the wind observed in typhoons in Osaka.

4.1 Characteristics of wind in typhoons of Osaka

The characteristics of wind in typhoons in Osaka were studied by using the data[10),(11)] mainly in the Table 3 and Fig. 6. Typhoons which attacked Osaka or which gave significant effect by strong winds or rain to Osaka can be classified into two basic types: those passing on the west side of Osaka and those passing on the east. Their characteristics are shown in Table 4. In cases where the typhoon passed Osaka on the west side, the wind direction changed in a clockwise fashion, from NE or NNE to SW or WSW. Furthermore, the maximum wind speed occurred after a delay from the time of minimum atmospheric pressure occurrence. In cases where the typhoon passed Osaka on the east side, the wind directions before and after passing were almost the same as in west side passage, however the wind direction changed in a counter-clockwise fashion. The wind directions before passage of the typhoon (NE or NNE) and after passage (SW or WSW) match the dominant wind direction seen in the wind rose of Osaka District Meteorological Observatory. The wind directions before and after typhoon approach are obviously affected by the topography of Osaka district.

4.2 Atmospheric pressure, maximum wind speed and high tide during typhoons

Fig. 7 shows the relationship of minimum atmospheric pressure and maximum wind speed in Osaka during a typhoon. Even if the minimum atmospheric pressure in Osaka was the same, the wind speed during passage on the west side was somewhat higher. It has been well known that wind speeds are higher on the east side of the typhoon center because the wind direction due to the typhoon and the course direction of the typhoon coincide. Fig. 8 shows the relationship between distance from Osaka to the typhoon center and the delay time from occurrence of minimum atmospheric pressure to that of maximum wind speed. If the distance between a typhoon center and Osaka City became larger, the delay time increased. East side passage had a shorter delay time than west side passage. If the center of the typhoon is 150km or more away, the variation of the data becomes large and the trends are not clear. Fig. 9 shows the relationship between distance from Osaka to the typhoon center, and the delay time from occurrence of minimum atmospheric pressure to that of high tide. Delay time increased as the distance between a typhoon center and Osaka City became larger in two basic types. Different trends are recognized when the typhoon center is 150km or farther from Osaka.

5. CONCLUSION

The followings are the main results of this study.

1) The NNE/NE and WSW/W wind directions are dominant in wind roses of all observation points in Osaka City and the effects of large-scale topography are conspicuous for the wind along course of Yodo River and wind from Osaka Bay.
2) The preceding wind directions are almost the same wind ones of before and after typhoon approach and it may be hypothesized that wind directions during typhoons are also affected by topography.

3) The Weibull parameters c has the strong correlation with observed wind speed.
4) The values of the intensity of turbulence(e.g., I_u=10-50% and Iw=5-30%) are much affected by the terrain surface roughness.
5) The 100-year wind speed of Osaka City is large in the south in addition to ENE and WNW direction.
6) When a typhoon passes on the west side of Osaka, the maximum wind speed is often recorded in the south direction immediately after the typhoon approaches closest. This fact coincides with the above mentioned 100-year wind.

Incidentally we are working to make "wind environmental map" in Osaka City to utilize above results. The draft of it is being examined and we would like to show it at next occasion.

ACKNOWLEDGMENT

Authors express their sincere appreciation to the members of committee of Urban Wind Load (Chairman: N.Shiraishi Professor Emeritus of Kyoto University). The members of the committee are as follows :
Yoshinori Nagai (Osaka Municipal Government), Masahiro Kamei (Osaka Chikagai Co., Ltd.), Mutsuji Kawakami (Osaka City Road Corp.), Osamu Aketa (Sogo Engineering Consultants Inc.), Tohru Saito (Mitsubishi Heavy Industries, Ltd.), Hiroshi Tanaka (Hitachi Zosen Corp.), Masao Hosomi (Komai Tekko Inc.), Akihiro Honda (Mitsubishi Heavy Industries, Ltd.)

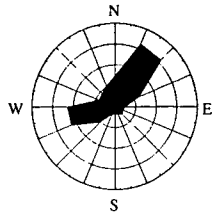
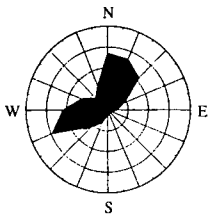
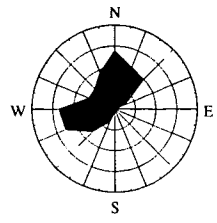
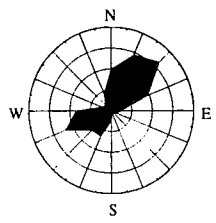
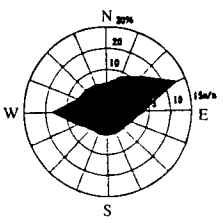
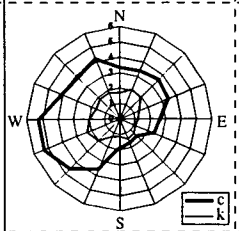
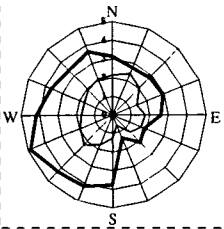
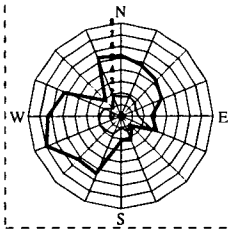
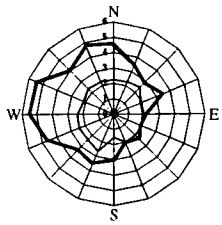
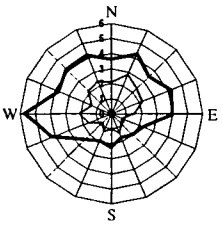
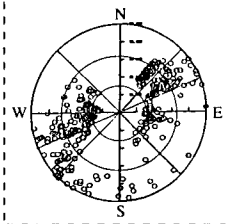
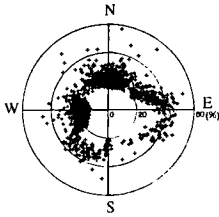
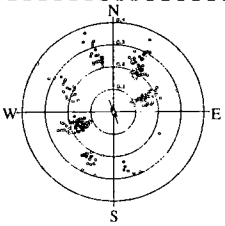
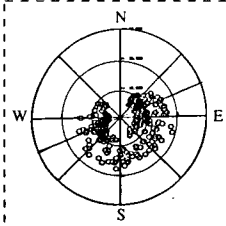
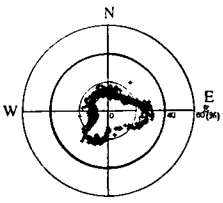
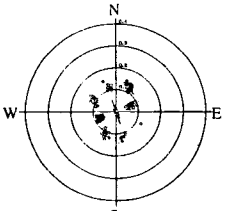
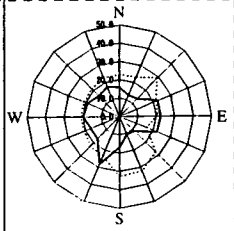
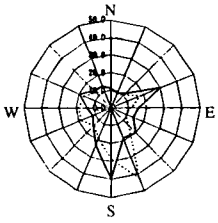
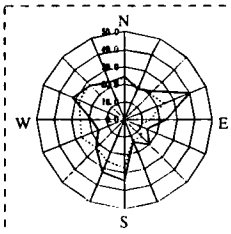
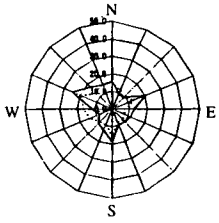
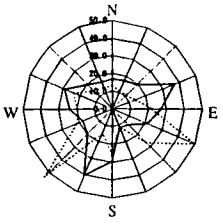
REFERENCES

(1) Wind Resistant Design Manual for Highway Bridge, Japan Road Association,1990 (in Japanese)
(2) Architectural Load Guide and Explanation (in Japanese)
(3) Engineering Science Data Unit
(4) Maruyama T., "Concerning Roughness Form in Urban Areas," Journal of Wind Engineering, Japan Association for Wind Engineering, No. 57,1993 (in Japanese)
(5) Simiu,E. and Scanlan,R.H., "*Wind Effects on Structures*", John Wiley & Sons, Second Edition
(6) Cook,J.N. "*The Designer's Guide to Wind Loading of Building Structures Part 1*", Butterworths, 1985
(7) Gomes, L. and Vickery, B.J., "On the prediction of extreme wind speeds from the present distribution," Journal of Industrial Aerodynamics,2 (1997), pp.21-36
(8) Matsumoto,M et. al., "Research on Safety of Bridge Structures against Strong Wind," Proceedings of the 10th Wind Engineering Symposium, 1988. (in Japanese)
(9) Pham, L., Holmes, J.D. and Leicester R.H., "Safety Indices for Wind Loading in Australia", Proc. of APSOWE, 1985
(10) Osaka City Port and Harbor Bureau, "*Construction Records for the Port of Osaka*," 1971.3 (in Japanese)
(11) Kinki Disaster Prevention Weather Association, "*Recent 40 years of Typhoons in Kinki District*", 1985.8 (in Japanese)

Table 1 Wind Observation Content

	Sugahara Shirokita Bridge		Nakajima Shinbashi Bridge	Konohana Bridge	Port and Harbor Bureau of Osaka City	Osaka D.M. Observation
Equipment	Ultra-sonic	Ultra-sonic	Ultra-sonic	Ultra-sonic	Vane type	Vane type
Type	KE-500P	DA 310	DA 300	TK G1 B	PK-250A	FF-6
Resolution	0.03m/s	0.005m.s	0.005m/s			
Start Time	1988/8	1988/8	1992/1	1993/10 ~	1985/7 ~	1982/7
Hight of Measurement	OP+17.9	OP+17.9	OP+17.9	OP+44.0	OP+38.8	94.2m
The Max. Instantaneous Wind Speed	◎	◎	◎	◎	◎	△
Wind Speed	◎	◎	◎	◎	◎	◎
Wind Direction	◎	◎	◎	◎	◎	◎
Angle of Attack	—	◎	◎	◎	—	—
Gust Factor	—	◎	◎	◎	—	—
Intensity of Turbulence	—	◎	◎	◎	—	—
Measurement Time	—	—	Every 3 hours	Every hour	Every hour	Every hour
Trigger Level	10m/s ~	10m/s ~	10m/s ~	5m/s ~	—	—

Table 2 Observation data & results of analysis

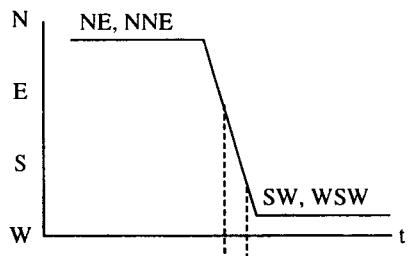
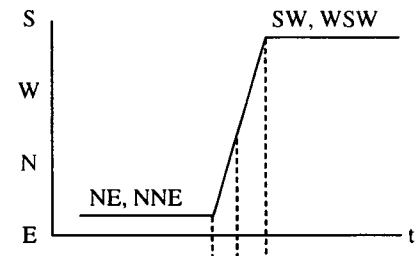
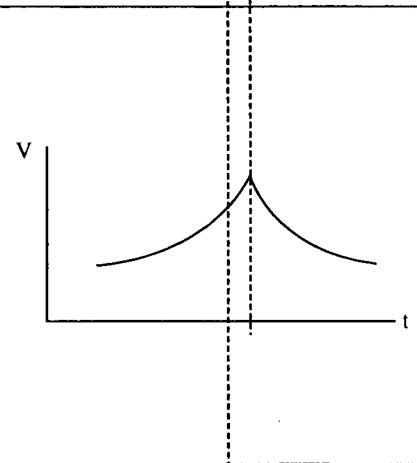
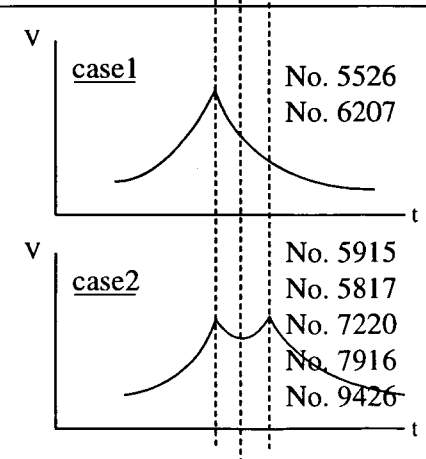
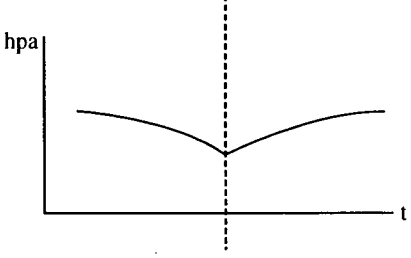
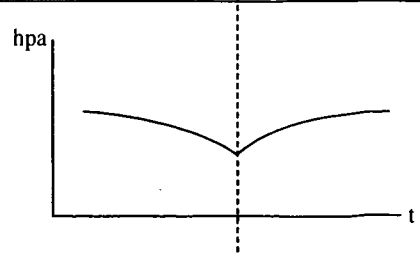
	Osaka D.M. Observatory	Port and Harbor Bureau of Osaka City	Konohana Bridge	Nakajima Shinbashi Bridge	Sugahara Shirokita Bridge
Wind Rose					
Weibull (c, k)					
Lu	—	—			
Iw	—	—			
100-years wind					

• N. B.) —— Estimation from Weibull parameters ---------- Estimation from Observation data

Table 3 Investigated Typhoons

Date	Name of Typhoons	Min. Atmospheric Pressure (hpa)	Average Max. Wind Speed (m/s)	Max.Ins. Wind Speed (m/s)	Tidal Height (m)	Distance from Center of Typhoon (km)	Typhoon's Passing Side of Osaka
1911.6.19		978	19.5		2.45		
1912.9.23		953	25.9	37	3.1		
1913.10.3		995	25.4				E
1917.8.3		995	14		2.51		
1920.8.4		985	16.8				E
1921.9.26		972	25		2.7		
1925.8.17		980	15.9		2.65		
1929.8.15		988	14.5		2.44		
1930.8.1		996	7				
1933.9.4		986	18.6		2.58		E
1933.10.20	Yashimamaru	986	13		2.64		W
1934.9.21	Muroto	954	over 40	about 60	4.19		W
1935.8.11		986	4.2		2.7		W
1935.8.29		985	13.8	21.6			E
1936.10.3		988	8.8		2.75		W
1937.9.11		985	14.5	22.8	2.7		W
1938.9.5		985	13.2	19	2.66		W
1941.8.15	4114	885	11				W
1942.8.27	4216	999	6.7	9.8	2.4		W
1942.9.21	4222	992	7.5	9.8	2.4		
1944.8.7	4411	995	15.5	21.4	2.09		
1944.9.17	4416	986	18.6	21.8	2.8		
1944.10.7	4420	978	9.5	14.8			E
1945.9.18	Makurazaki	980	19	22.5	3.2	215	W
1945.10.11	Akune	996	10.4	15.5	2.6	172	W
1949.6.21	Della	998	5.7	12.1			W
1950.9.3	Jane	970	28.1	44.7	3.85	43	W
1951.10.15	Ruth	981	15.7	24	2.95	204	W
1952.6.23	Dinah	992	13.5	21.9		140	E
1953.9.25	5313	977	22	28.9	2.62	107	E
1954.8.19	5405	981	9.6	15.7	2.43	21	W
1954.9.18	5414	990	13		2.49	172	E
1954.9.26	Tohyamaru	988	16.9	26.3	2.76	182	W
1956.8.17	5609	991	14.5		2.51		W
1956.9.10	5612		11		2.66		W
1956.9.27	5615	993	13	15.9		161	E
1957.6.27	5705	999	14.4	22.8	2.58		
1957.9.7	5710	997	11.7		2.54	97	W
1958.8.28	5817	985	17.9	23.9	2.39	17	E
1959.9.26	Isewan	956	19.9	27.8	2.54	43	E
1960.8.29	6016	992	11.8		2.8	150	W
1961.9.16	No.2 Muroto	937	33.3	50.6	4.12	32	W
1964.9.25	6420	987	19	31.7	3.72	64	W
1965.9.10	6523	976	17.3	33.1	3.19	54	W
1965.9.17	6524	979	14.7	29.5	2.09	133	E

Table 4 Wind Characteristics of Typhoon in Osaka

	Passing on the West of Osaka	Passing on the East of Osaka
Name of Typhoon	Muroto Jane(5028) No. 2 Muroto(6118) No. 6420 No. 6523 No. 7506	No. 5526 No. 5817 Isewan (5915) No. 6207 No. 7220 No. 7916 No. 9426
Wind Direction before Pass	NE or NNE	NE or NNE
Wind Direction after Pass	SW or WSW	SW or WSW
Change of Wind Direction	Clockwise	Anti– Clockwise
Wind Direction		
Wind Speed		
Atmospheric Pressure		

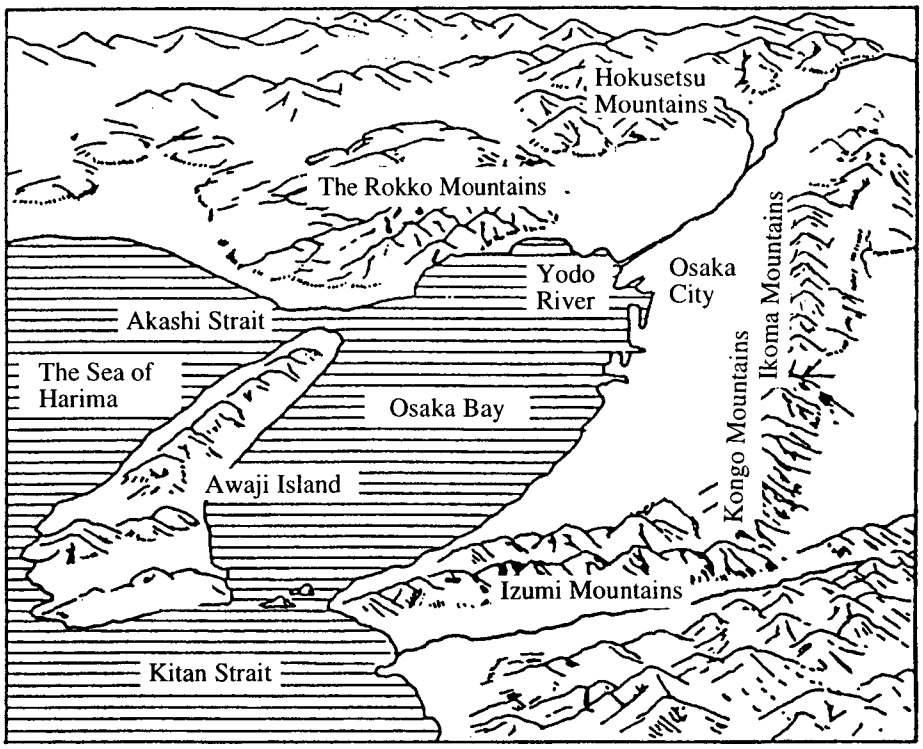


Fig. 1 Geographical Features around Osaka City

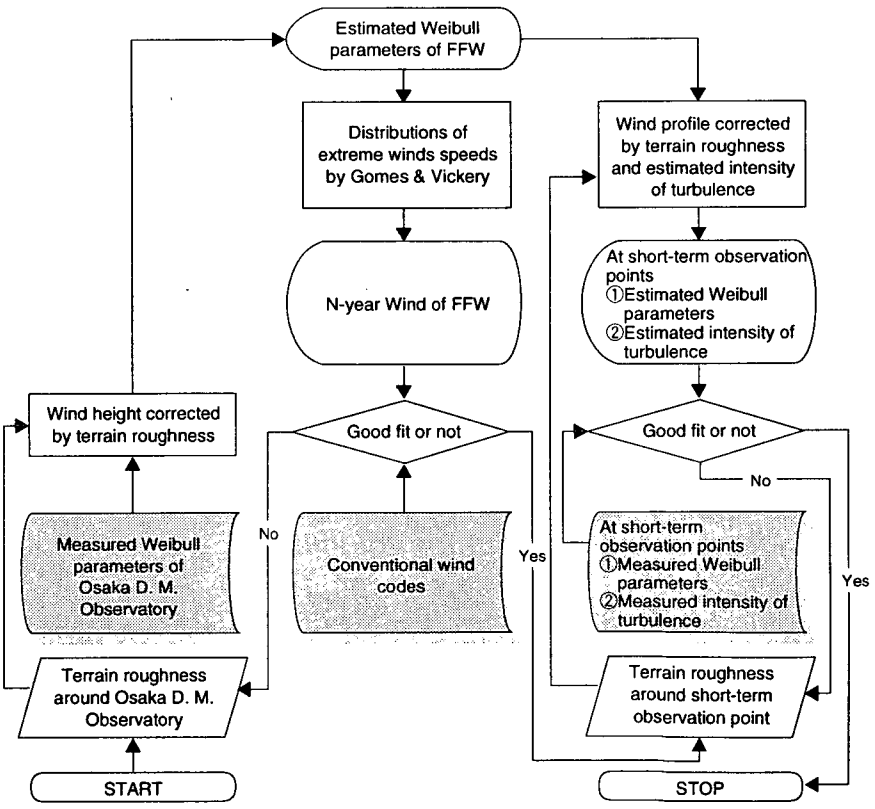


Fig. 2 Flowchart for Estimation of Extreme Wind Speed

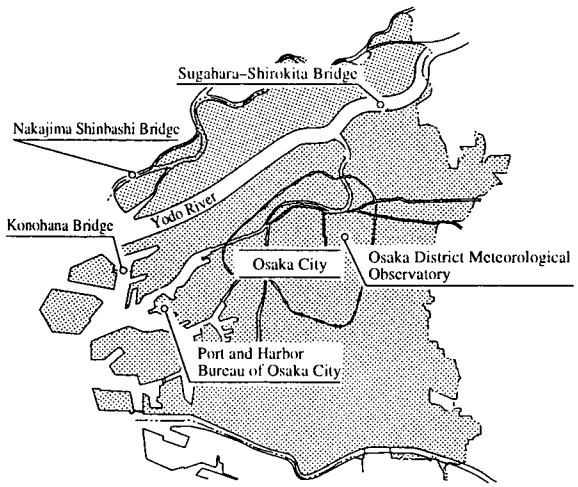


Fig. 3 Locations of wind observation points

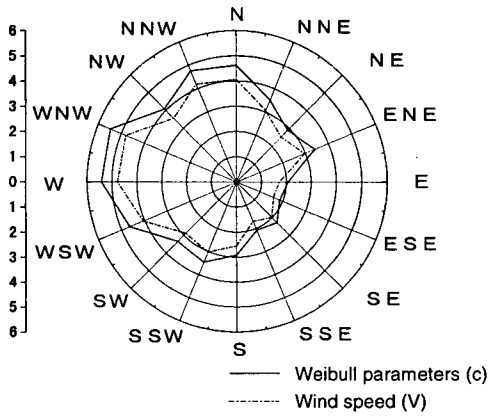


Fig. 4 Relationship between Average Wind Speed and Weibull Parameter (c) at Nakajima Shinbashi Bridge

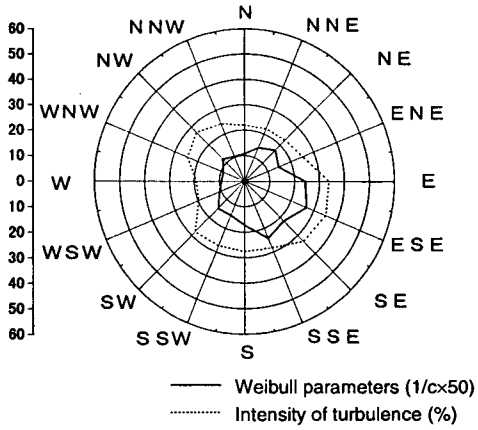


Fig. 5 Relationship between Intensity of Turbulence and Weibull Parameter (1/c × 50) at Nakajima Shinbashi Bridge

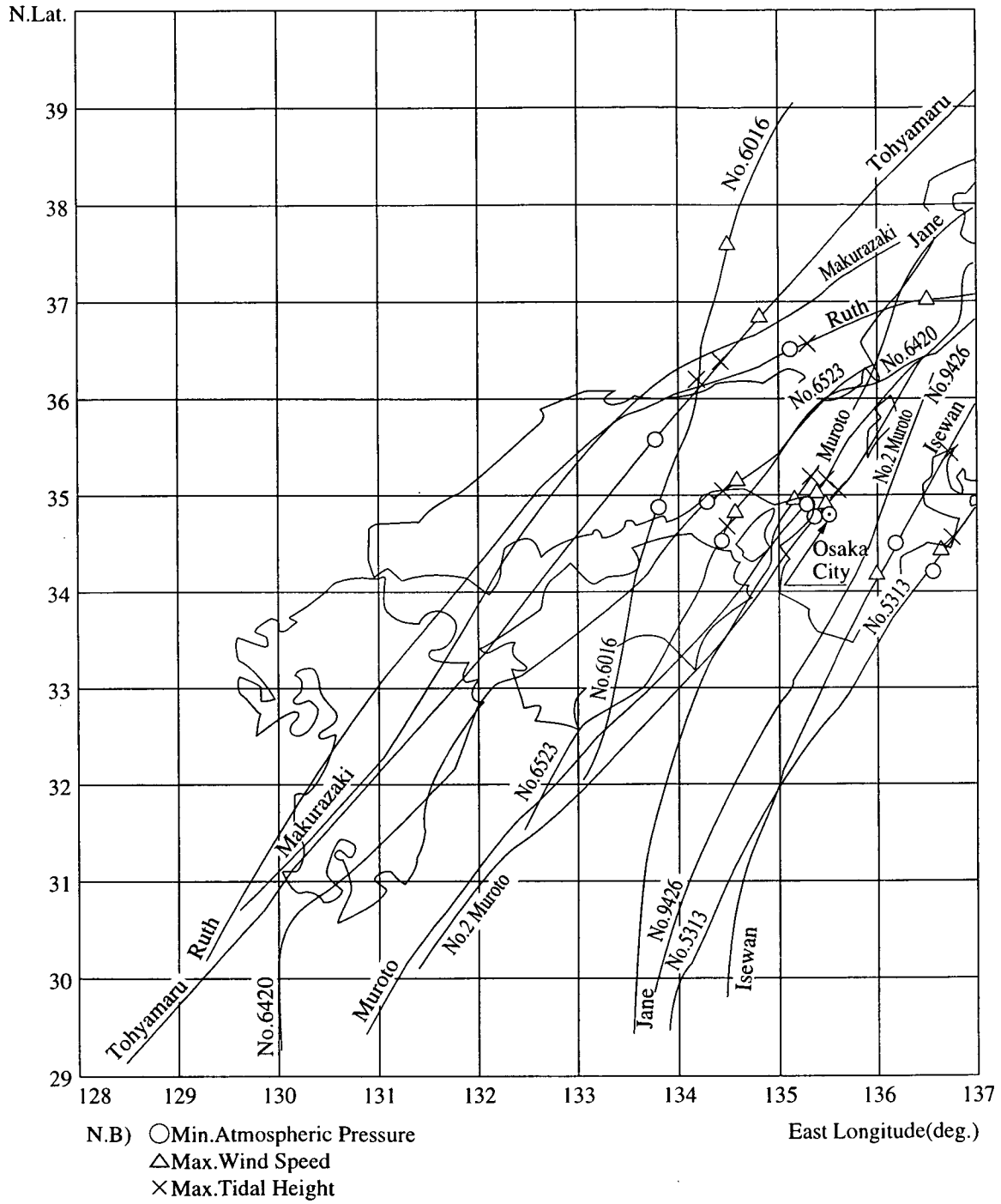


Fig. 6 Typhoon Courses & Their Locations of The Extreme Values Recorded in Osaka Bay

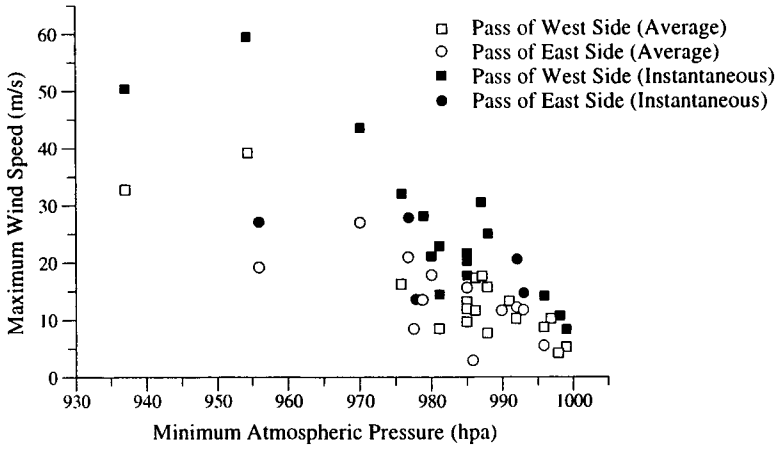


Fig. 7 The Relationship between Minimum Atmospheric Pressure and Maximum Wind Speed

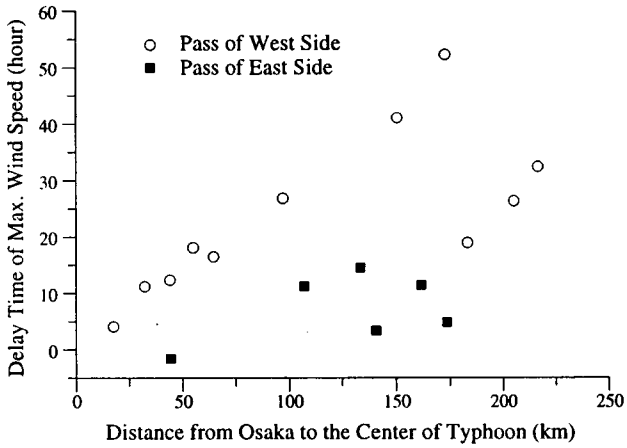


Fig. 8 The Relationship between Distance from Osaka to the Typhoon and the Delay Time from Occurrence of Min. Atmospheric Pressure to That of Max. Wind Speed

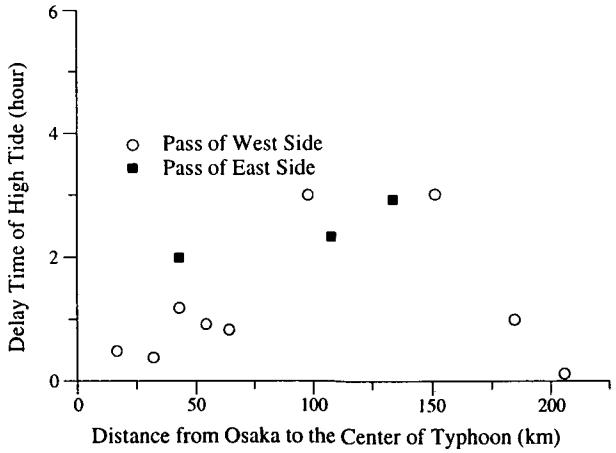


Fig. 9 The Relationship between Distance from Osaka to the Typhoon Center and the Delay Time from Occurrence of Min. Atmospheric Pressure to That of High Tide

Very Long Suspension Bridges Using the Temporary Mass Method

by

Shunzo NAKAZAKI [1] , Hiroki YAMAGUCHI [2]

Summary

This is a structural method to increase the aerodynamic stability by adding a mass temporarily into the box girder of a suspension bridge against a storm. First of all, studies were conducted to determine the most effective longitudinal position for such a mass to improve the aerodynamic stability. Roughly designed suspension bridges were accomplished by this method. This method shows the same effect as other structural methods, and reduces much structural material in comparison with the conventional design method. The characteristics of this method is a simple operation to increase the aerodynamic stability. For this study, the extended Bleich theory and a numerical integration method were used.

1. Introduction

Super long suspension bridges with more than 2000m span length are being planned in the world. If the conventional design method is used in order to achieve the required aerodynamic stability, the construction cost of such suspension bridges will be prohibitively expensive. Therefore, some new design methods (ex. mono-duo cable system and cross hanger system [1], active control system [2] and so on) are being developed. But, for example, the reference [2] describes that the slotted box girder enhances the critical wind speed by approximately 38%, but at the expense of a 36% increase in the use of structural steel. For the newly proposed system, it is necessary to consider the total cost, including the entire system.

This paper deals with the design method to enhance the aerodynamic stability by adding a mass such as the sea water temporarily into the girder of a suspension bridge during a storm. This method is expected to give the suspension bridge the mass effect, the increase of cable stiffness and the mode control, and consequently enhances the aerodynamic stability.

Studies were conducted to determine the most effective longitudinal position for such a mass to improve the aerodynamic stability. This added mass method, then, was used to design a super long suspension bridge, and it was compared with the conventional design method.

For this study, the extended Bleich theory and a numerical integration method were employed.

---

1) Manager and Engineer , Kawada Industries,Inc. ,

2) Professor , Department of Civil and Environmental Engineering , Saitama University

2. Conditions studied

2.1 Case studies of super long suspension bridges

Three suspension bridges with center span of 2000m, 2500m, and 3000m were investigated in order to study the relation between the span length and the mass effect (Fig.1).

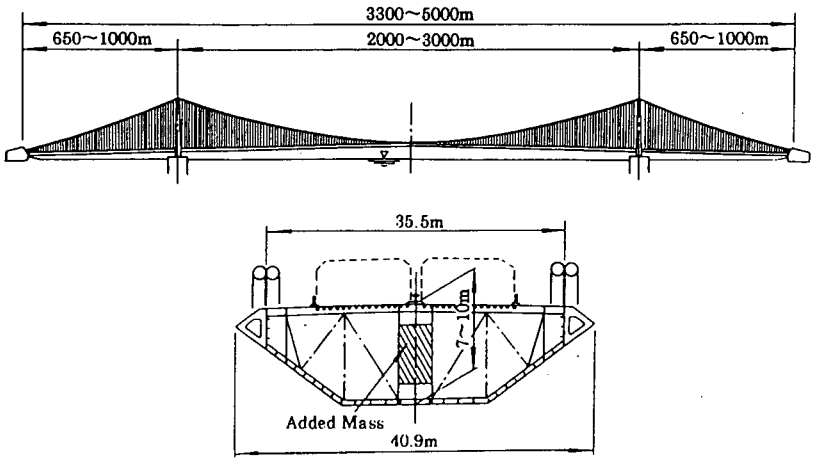


Fig.1. Super long suspension bridge

In Fig.1, the mass such as the sea water was added at the center of box girder section, so that the added mass hardly change the polar moment of inertia and the torsional frequency.

The following conditions were assumed.

1) The Theodorsen's unsteady aerodynamic force was acting on the girder.
2) The required critical wind speed of the coupled flutter was 85m/s.

2.2 Flutter analysis method

For flutter analysis, two theoretically different analysis methods were used.

(1) The extended Bleich theory

This theory belongs to the modal technique. A suspension bridge is analyzed as a continuous structure, so that the flutter analysis is easily carried out. Therefore, this theory may be suitable for the parametric study.

Natural frequency and modes are calculated by the Ritz's method. And in flutter analysis, although Bleich used only one mode for each of vertical and torsional mode [3], present study used four modes for vertical mode and one mode for torsional mode. Those are the reasons why vertical modes may become more complex and torsional modes may be unchangeable by the added mass.

(2) A numerical integration method [4]

A suspension bridge is modeled as a space frame in this method as shown in Fig.2.

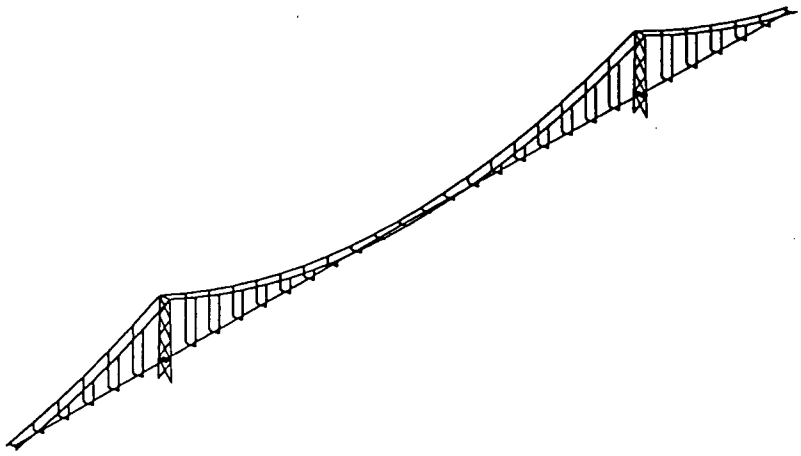


Fig.2. Model for a numerical integration method

The governing equation for this method is expressed as

$$\left([M]-[M^*]\right)\{\ddot{y}\}+\left([C]-[C^*]\right)\{\dot{y}\}+\left([K]-[K^*]\right)\{y\}=0 \cdots\cdots\cdots(1)$$

where M, C and K are the mass, damping, and stiffness matrix,
and $\{y\}$, $\{\dot{y}\}$ and $\{\ddot{y}\}$ are the displacement, velocity, and acceleration vector, respectively.

In equation (1), terms with an asterisk * represent the real part of Theodorsen's air forces as complex quantities. Equation (1) expresses the damped free vibration problem. Its solution is determined from the response due to the initial displacement. The Willson's θ method was used as the method of integration.

3. Selection of the longitudinal position for added mass

3.1 Preliminary selection

(1) Loading cases

Seventeen cases shown in Fig.3 were analyzed to determine the most effective position for the added mass from the aerodynamic stability point of view. Case-0 has no added mass. Cases-1~9 have 0~100% mass length at the center span and the full mass length at both side spans. Cases-10~17 are the same conditions as Cases-2~9 without the mass at the side spans.

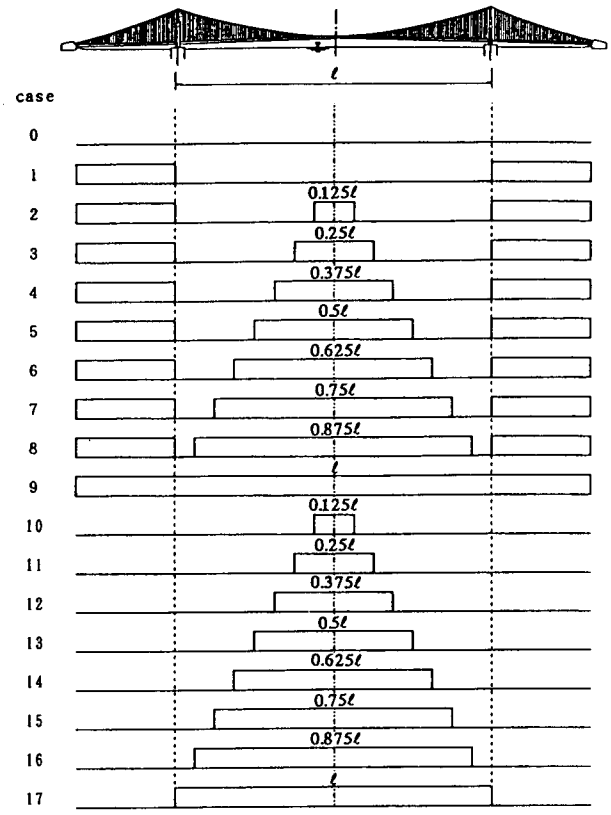


Fig.3. Added mass loading cases

(2) Mass intensity

In analyzing the critical wind speed, the same mass intensity distributions were used for all cases of a given suspension bridge. First, the mass intensity was determined in which the maximum stress of the main cable in Case-9, a uniformly distributed mass for the entire length of the bridge, was nearly equal to the allowable stress.

Although the allowable stress of the main cable is 82kgf/mm^2 in normal condition, the elastic limit of the cable material 107kgf/mm^2, which represents a storm condition was used. Even, the 107kgf/mm^2 is much smaller than 123kgf/mm^2 which is obtained by increasing the allowable stress in a storm by a factor of 1.5 [5]. Fig.4 shows the stress in the main cable for the 17 cases shown in Fig.3 for the three different span suspension bridges.

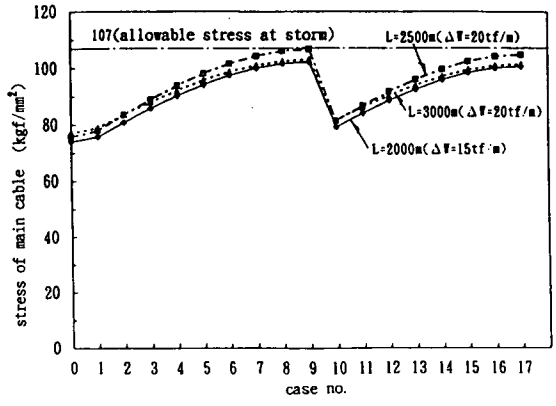


Fig.4. Stress of main cable at each loading case

From Fig.4, the mass intensities of 15tf/m,20tf/m and 20tf/m were determined for 2000m, 2500m and 3000m length suspension bridge, respectively.

(3) Critical wind speed

The critical wind speeds of coupled-flutter for the 17 cases shown in Fig.3 were analyzed with the above mass intensities. In the analysis of the flutter of a bridge, the extended Bleich theory and a numerical integration method were employed, as stated above. All cases were analyzed by the former, and some selected cases were analyzed by the latter method (Fig.5).

From Fig.5, the following trends are found.

① Results of both analytical methods show good agreement.

② The maximum increase of the critical wind speed due to the added mass is approximately 6 to 7m/s.

③ The changes from the critical wind speed of Case-4 to that of Case-9, and similarly from that of Case-11 to that of Case-17 are relatively small.

④ Case-4 and 5 and Cases-10 through 13 are configurations with better locations for the added mass, because they have higher critical wind speeds and less mass than the others.

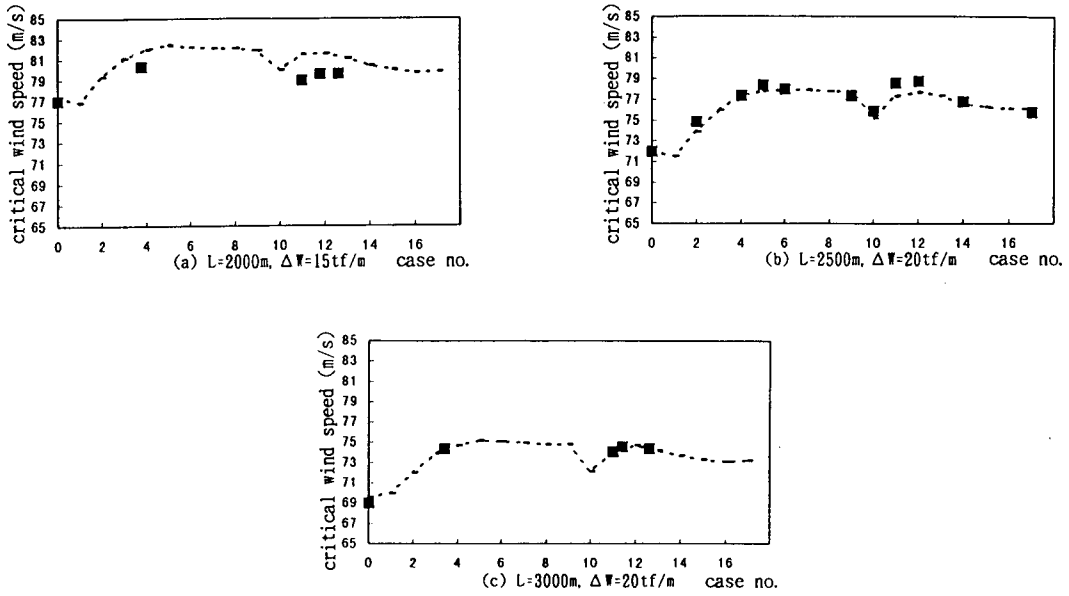


Fig.5. Critical wind speed at each loading case

3.2 Final selection

Fig.4 shows that the mass intensity for Cases-4 and 5, and Cases-10 through 13 can be increased because the stresses in the main cable in these cases are much lower than the allowable stress. Then, the effect of increased added mass on the critical wind speed was investigated, and the stress in main cables was studied (Fig.6). As an analysis method, a numerical integration method was used. Reviewing Fig.6, the following results can be noted.

(1) The increase of added mass doesn't always increase the critical wind speed. For example, the critical wind speed of Case-4 and 5 for L=2500m trends to decrease from 20tf/m.

(2) It seems that Case-11(25% of center span) is the best configuration, because it has the highest aerodynamic stability and rather low stresses in main cable.

Based on the results shown in Fig.6, Case-11 was selected and the mass intensities of

38tf/m,30tf/m and 40tf/m were determined for 2000m, 2500m and 3000m suspension bridges, respectively.

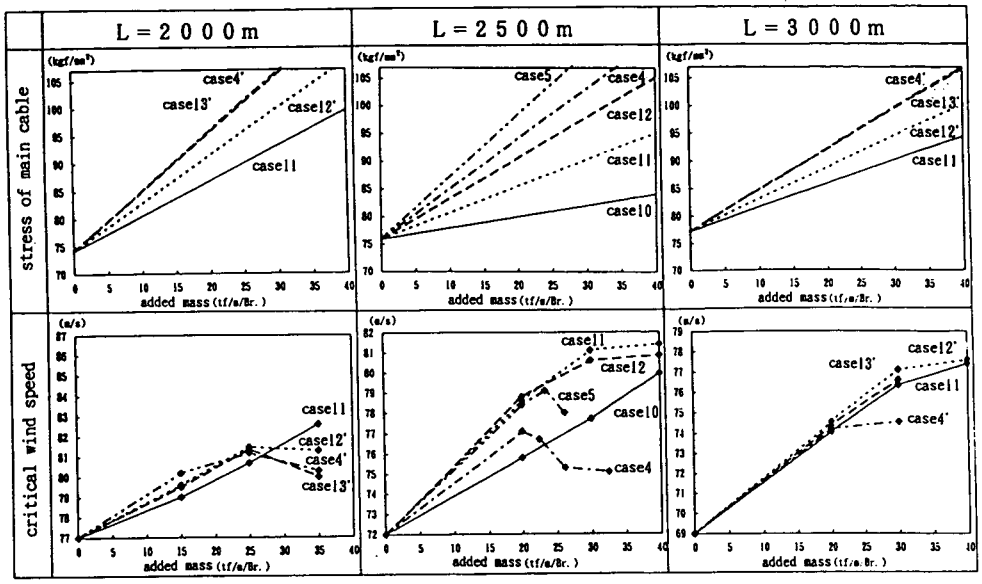


Fig.6. The effects of added mass on the main cable stress and the critical wind speed

4. Preliminary design

After determining the position and the mass intensity, a rough design of the conventional type suspension bridge was made, then the suspension bridge with the added mass was designed in order to find the economic consequences of the added mass method.

Table1 summarizes the results of designs investigated. From Table1, the following characteristics can be obtained.

① Total steel weight of suspended structure of the added mass type are fewer than the conventional type by 9%, 12% and 11% for 2000m, 2500m and 3000m suspension bridges.

② The maximum cable stress of the added mass type is 98kgf/mm^2. This value is smaller than 107kgf/mm^2 which was determined as the allowable stress. This is the reason why the temporary mass is partially loaded at the girder of center span.

Table1. A summary of preliminary design

Items		L=2000m		L=2500m		L=3000m	
		Conventional	Added Mass	Conventional	Added Mass	Conventional	Added Mass
Added Mass		------	38	------	30	------	40
Unit Dead Load	Cable	12.9	12.1	20.5	18.5	30.8	28.0
	Girder	18.2	16.4	21.9	18.8	25.1	21.8
	Pavement, etc.	7.0	7.0	7.0	7.0	7.0	7.0
	Total	38.1	35.5	49.4	44.3	62.9	56.8
Ratio of Steel Weight		1.00	0.91	1.00	0.88	1.00	0.89
Section Properties	Cable Area Ac	1.7	1.4	1.9	1.5	2.1	1.7
	Girder Ix	15.3	13.1	26.4	20.8	40.2	32.4
	Girder Iy	202.4	173.7	245.5	194.6	282.0	228.1
	Girder J	35.5	28.4	61.7	44.5	92.7	69.5
Cable Stress(kgf/mm^2)		75	98	77	91	78	93
Critical Wind Speed(m/s)		86.7	85.2	86.8	85.4	86.9	85.2

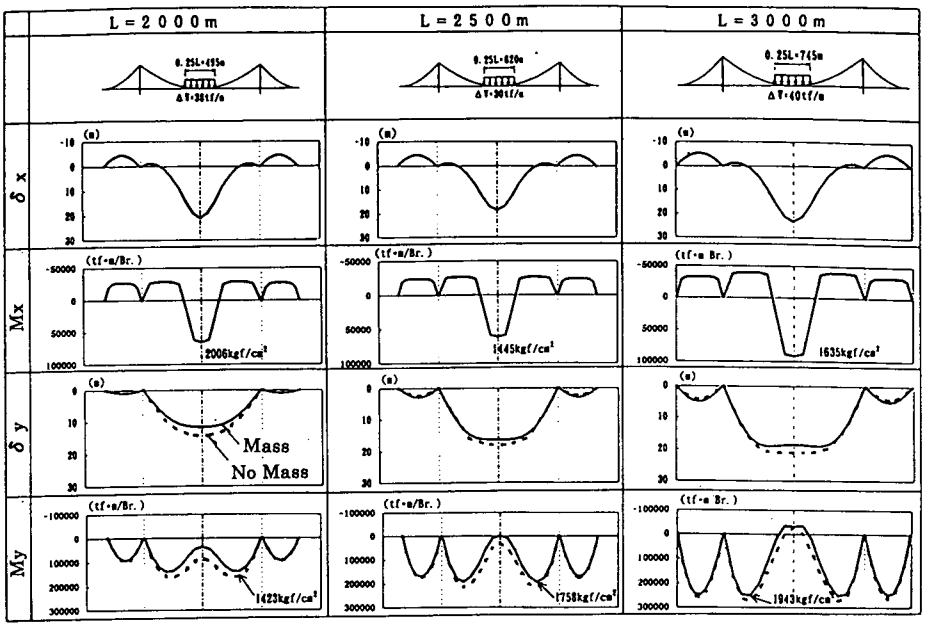
(Unit ; tf/m/Br., m^2/Br., m^4/Br.)

Fig.7 shows results of static analysis where solid lines show the added mass type and dotted lines show the conventional type.

From Fig.7, the following observations can be made.

① The maximum deflection due to the added mass is about 20m at the center span. But, since suspension bridges are planned to have 1~1.5% longitudinal slope, such deflections are almost canceled. In case of lateral displacement due to static wind, the added mass type is smaller than the conventional type, because of the added mass.

② The added mass causes high stress at the center of span as well as deflection. But, fortunately, since the maximum stress due to wind load are caused at L/4 of the center span, superposed stress doesn't show an excessive stress.



δ : Deflection, M : Bending moment, x : Vertical, y : Lateral

Fig.7. Deflection and bending moment of stiffening girder

5. Application to a divergence type suspension bridge

So far, the discussion was focused on the temporary mass added to the center of box girder. As an application of the temporary mass, it is proposed to add the temporary mass to both sides of a divergence type suspension bridge (Fig.8).

The divergence wind speed, U_D is expressed as

$$U_D = w_t\, r\sqrt{\mu} \quad \cdots\cdots\cdots\cdots (2)$$

where w_t, r, μ are torsion frequency, radius of gyration of deck and cable, and relative density(= $m / \pi\rho_A b^2$, m: mass, ρ_A : air density, b: half of deck width).

The increase of r or μ enhances the divergence wind speed, U_D. But the increase of r means the enlargement of the bridge. Accordingly, the increase of μ due to the temporary mass may be more economical.

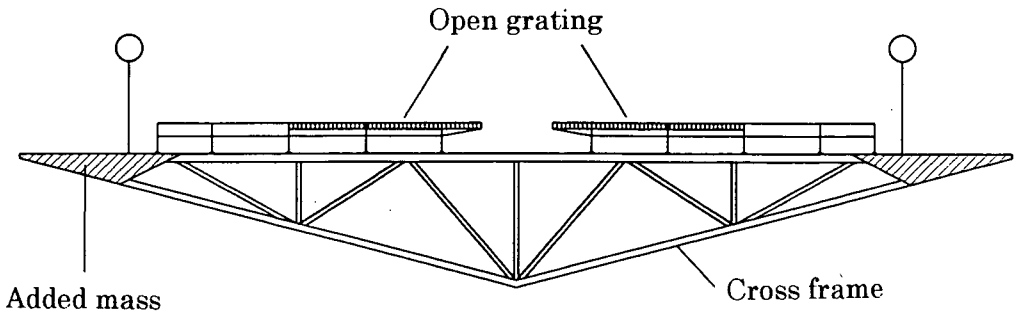


Fig.8. Added mass for a divergence type suspension bridge

Conclusion

1) The middle 25% part of the center span is the most effective position of the mass from the aerodynamic stability point of view.
2) This method increases the wind stability increase about 6~9m/s for a given condition.
3) This method reduces the steel weight of a suspended structure approximately 9~12%, compared with the conventional method.

This method can also be applied to a divergence type suspension bridge.

References

[1] M.A.Astiz and E.Y.Andersen : On wind stability of very long spans in connection with a bridge across the Strait of Gibraltar, Strait crossing, J.Krokeborg(Ed.), Balkema, 1990, pp.257-264.
[2] K.H.Ostenfeld : Innovative structural systems for the Gibraltal strait crossing project, IASS-CSCE International Congress, Toronto, July, 1992, pp.231-242.
[3] Bleich,et al. : The mathematical theory of vibration suspension bridges, Dept. of U.S.Gov.Print Office, 1950.
[4] A.J.Bell and D.M.Brotton : A numerical integration method for the determination of flutter speeds, Int.J.Mech.Sci.15, 1973, pp.473-483.
[5] Honshu-Shikoku Bridge Authority : Wind resistant design code for the Akashi Kaikyo Bridge, 1990.

On Aerodynamic Stability of a Suspension Bridge with Box Girder during Erection Stage

R. Toriumi and M. Takeguchi

Honshu Shikoku Bridge Authority, Design Dept., 1 st. Design Dept.

ABSTRACT

The 2nd. Kurushima Bridges is a suspension bridge with box girder whose center span length is 1,020m. As for the girder erection, at first, girder block for the center of the span is set in place, and then girder is extended toward towers. Aerodynamic stability during girder erection is studied through wind tunnel test using full bridge model as well as section model, and flutter analysis. As the result, it was found that flutter analysis could evaluate aerodynamic stability of such structure in this case. And interaction between cat walk and girder, bending stiffness of hungers were found to affect the flutter characteristics.

1. Introduction

The 2nd. Kurushima Bridges is a suspension bridge with box girder which has the center span length of 1,020m. This bridge is under construction as one of the bridge in the Onomichi-Imabari Route of the Honshu-Shikoku Bridges. As for the girder erection method, prefabricated block of the girder is transferred to the site on barge, lifted up directly from the barge, and fixed to the hanger. At first, girder block for the center of the span is set in place, and then girder is extended toward towers. During the girder erection work, the structural system is completely different form that of completed bridge. Therefore, aerodynamic stability during girder erection is one of the important item to be checked. This report outlines the study conducted to evaluate the aerodynamic characteristics of the Kurushima Bridge during girder erection work through wind tunnel test using full bridge model as well as section model, and flutter analysis.

2. Kurushima Bridge

General Information

The Kurushima Bridges are composed of three suspension bridges, namely the 1st Kurushima Bridge whose center span is 600m, the 2nd Kurushima Bridge whose center span is 1,020m, and the 3 rd. Kurushima Bridge whose center span is 1,030m, and they are connected each other at commonly used anchorages (Fig.1). The Bridges are under construction as a part of the Onomichi-Imabari route (west route) of the Honshu-Shikoku Bridges. For the girder of the bridges, box girder is employed. The height of the girder is 2.3m for the 1st Kurushima Bridge, and 4.5m for 2nd and 3rd Kurushima bridges.

Girder Erection Procedure

As for the girder erection of the Kurushima Bridges, prefabricated girder blocks are transferred to the site on barge, lifted up by lifting crane placed on the main cable, and fixed to the hanger. At first, girder block for the center of the center span is set in place. And then, the girder is extended toward the towers block by block. During girder erection work ,between the girder blocks are connected by temporally hinge system at the deck (Fig.2).

3. Aerodynamic Stability during Girder Erection

In the three kurushima bridge, aerodynamic stability of the 2nd kurushima bridge during girder erection was studied. In the various erection stages depend on girder length erected, aerodynamic stability of erection stage which has 180m long girder in reported in this paper.

To evaluate the aerodynamic characteristics of the Kurushima bridge during girder erection, wind tunnel test using full bridge model as well as section model were conducted. Also, flutter analysis was conducted to understand the experimental results.

3.1 Full Bridge Model Wind Tunnel Test

3.1.1 Full Bridge Model

As the structural system during girder erection is 3 dimensional system, full bridge model was used for the wind tunnel test(Fig.3, Photo.1). Geometric scale of the model was 1/60. In the model, cat walk(scaffold at the cable which are set during construction work) were modeled where the girder and cable is close and aerodynamic interaction was expected. At the other area, cables were modeled by piano wire and cylindrical weight to simulate drag force acting on the cable.

Dynamic characteristics of the model is shown in Table-1. The natural frequencies of the model measured showed good coherency with required number. Natural vibrational modes shown in Fig.4 also is close to analytical results. As shown in the Table-1, the structural damping for each mode is close to or smaller than the target number, 0.02 in logarithmic decrement.

3.1.2 Static Displacement

Wind tunnel test was conducted in smooth flow. The angle of attack was 0-degree, and +3-degree(α =0,+3 degree). Fig.5,6 shows the static dispacement of the girder due to wind load. Vertical displacement is very small at the end of the girder in comparison with that at the center of the girder. On the contrary, horizontal displacement and torsional displacement are almost constant along bridge axis. And, horizpontal displacement is very large.

3.1.3 Flutter Wind Speed

The measured flutter on set wind speed(flutter wind speed) are shown in Table-2. The case α =+3 degree results lower flutter wind speed than the case of α =0 degree. In the case of α =+3 degree, relation between wind speed and natural frequencies,

apparent logarithmic decrements in Fig.7 and 8.

No significant change in the natural frequencies with wind speed was observed. As for damping of 1st symmetric torsional mode, it becomes negative when wind speed exceed 8.7 m/s, and flutter occurred. Damping of no other natural mode decrease with wind speed. Vibrational mode of flutter (Fig.9) shows coupling between torsional vibration and vertical bending vibration.

3.2 Flutter Analysis

3.2.1 Analysis Method

Flutter analysis was conducted by modal analysis method (Ref.1). In the analysis, lower 30 modes were used. Unsteady aerodynamic forces were expressed as follows.

Lift:

$$L=\pi \rho B^3 \omega^2 \{(C_{L\eta R}+ i C_{L\eta i}\} \frac{\eta}{B} + \{(C_{L\theta R}+ i C_{L\theta i}\} \theta$$

Moment:

$$M=\pi \rho B^4 \omega^2 \{(C_{L\eta R}+ i C_{L\eta i}\} \frac{\eta}{B} + \{(C_{L\theta R}+ i C_{L\theta i}\} \theta$$

where ρ :air density B:deck width ω :anguler frequency
η , θ :vertical and torsional displacement
$C_{L\eta R}, C_{L\eta i}, C_{L\theta R}, C_{L\theta i}, C_{L\eta R}, C_{L\eta i}, C_{L\theta R}, C_{L\theta i}$:
coefficients for unsteady aerodynamic forces

Coefficient of unsteady aerodynamic force used in the analysis were measured through section model wind tunnel test. The model used to measure the unsteady aerodynamic force has model of cat walk rigidly connected to the model of girder.

Other analytical condition are summarized in the Table-3.

3.2.2 Effect of Cat Walk

In order to evaluate the effect of cat walk, spring-mounted section model test was conducted. In the test, vertical distance between girder and cat walk was varied by cases. The test result is shown in Fig.10. The effect of cat walk is significant, and in this case, flutter wind speed increase when cat walk is placed.

In the full model, the distance between girder and cable is form 50 mm at the center to 100 mm at the end of the girder. Therefore, unsteady aerodynamic forces were measured using model which has cable and cat walk model 57mm away from girder which is average distance between cable and girder of the full model.

3.2.3 Effect of Hunger Bending Stiffness

In the model, hungers were made of stainless strand. Usually, hungers were long enough that effect of bending stiffness of hunger is small and negrigible. However, at the center of the center span, hungers were short, and the effect of the bending stiffness of the hunger is not negrigible. At the early stage of the girder erection when the length of girder

is short, average length of hunger is short, and bending stiffness of the hunger was expected to affect the vibrational characteristics.

In order to examin the effecrt of bending stiffenss of hunger, flutter analysis using nalural modes culculated consigering bending stiffenss of hunger was conducted.

The result of the analysis is shown in Table-4. Due to the effect of bending stiffness of hungers, equivalent mass of torsional narural mode was increased. As the result, flutter wind speed was increased by 30%.

It is considered that mode shape of torsional mode was changed because of the effect of the bending stiffness of hungers. The component of horizontal vibration of cable in torsional mode was increased, and equivalent mass was increased (Fig.11). As the result, flutter wind speed was increased.

3.2.4 Effect of Static Displacement by Wind Force

As mentioned above, static displacement of the girder due to wind force is large. It was expected that due to the static displacement affect the structural characteristics, and aerodynamic characteristics.

Two types of effect were expected. One is the effect of torsional displacement which change angle of attack. However, in this case, as the measured torsional displacement is small, this effect is expected to be small, and not studied.

The other one is that vibrational characteristics were changed because structural system was changed due to static displacement. In order to examine this effect of static displacement, flutter analysis using natural mode where static diaplacement was considered, was conducted as well as analysis using natural modes where static displacement was not considered.

The result of the analysis is shown in Table-4. In this case, the effect of ststic displacement increase the flutter wind speed. In Fig.12, relation between apparent damping and wind speed is shown. The effect of ststic displacement slightly increase the damping.

3.2.5 Comparison with test result

As the result of flutter analysis, flutter wind speed are shown in the Table-2 with test result. When, the effect of bending stiffness of hunger and static deformation are not considered (case-1), the flutter wind speed from analysis is much smaller than that from experiment. When the effect of bending stiffness of hunger and static deformation are considered (case-2,3), flutter wind speed was increased, and the agreement with test result becomes fairly well. Therefore, it is considered that flutter analysis can be used for evaluateion of aerodynamic stability of the Kurushima Bridge under girder erectionstage.

4. Conclusion

Aerosynamic stability of the Kurishima Bridge was studied through wind tunnel test using full bridge model as well as section model test and flutter analysis. As the result of comparison between flutter wind speed from wind tunnel test and flutter analysis, it was found that flutter analysis can be used for such type of structure. Through some aparetric study in flutter analysis, it was found that interaction between cat walk and girder, bending stiffness of the hunger, static deformation affect the flutter characteristics.

Ref.1: T. Miyata, K.Tada, H. Sato, H. Katsuchi and Y. Hikami : New Findings of Coupled-Flutter in Full Model Wind Tunnel Tests on the Akashi Kaikyo Bridge, Proceeding of the Deauville Conference: Cable-Stayed and Suspension Bridges, pp163-170, Deauville, France, 1994

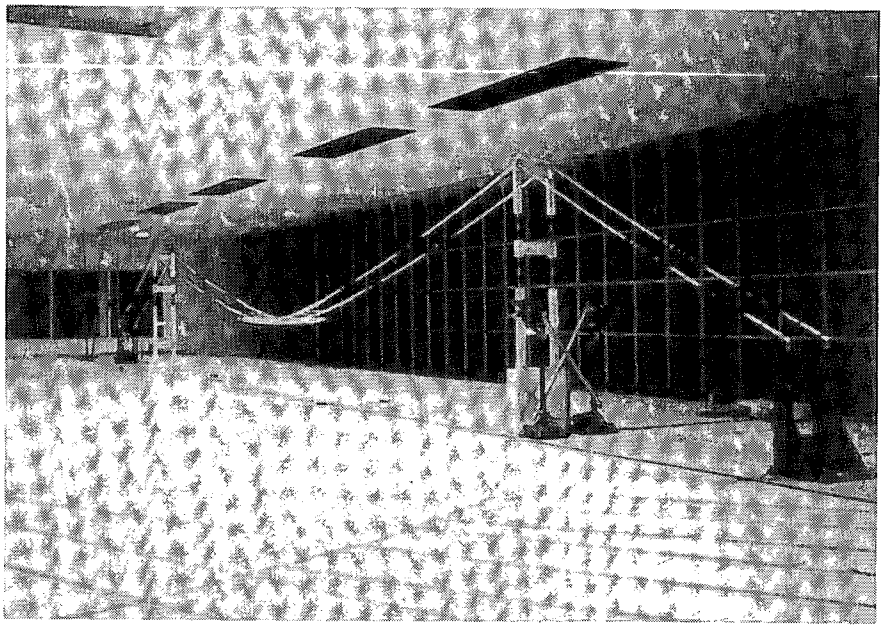


Photo-1 Full Model of 2nd. Kurushima Bridge during Girder Erection

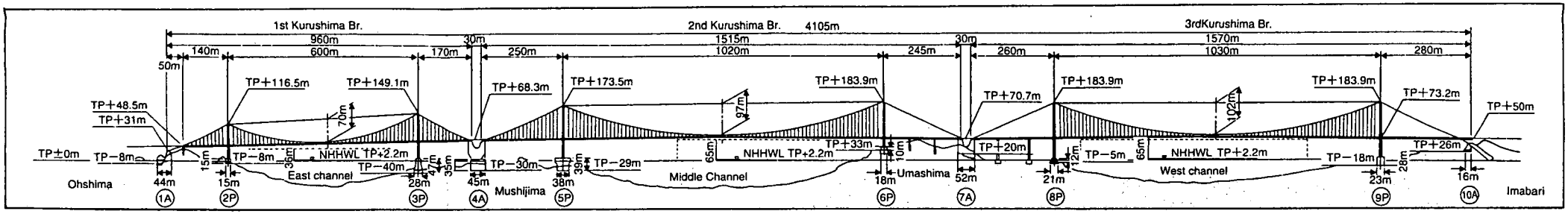
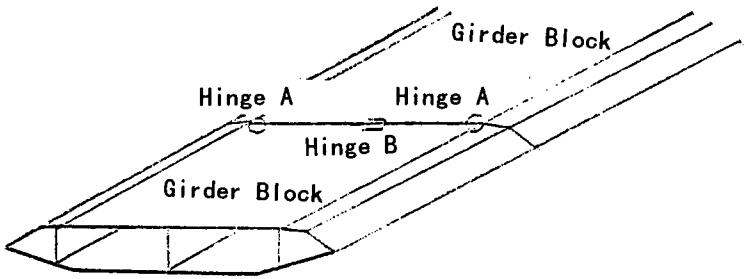


Fig.-1 Kurushima Bridges



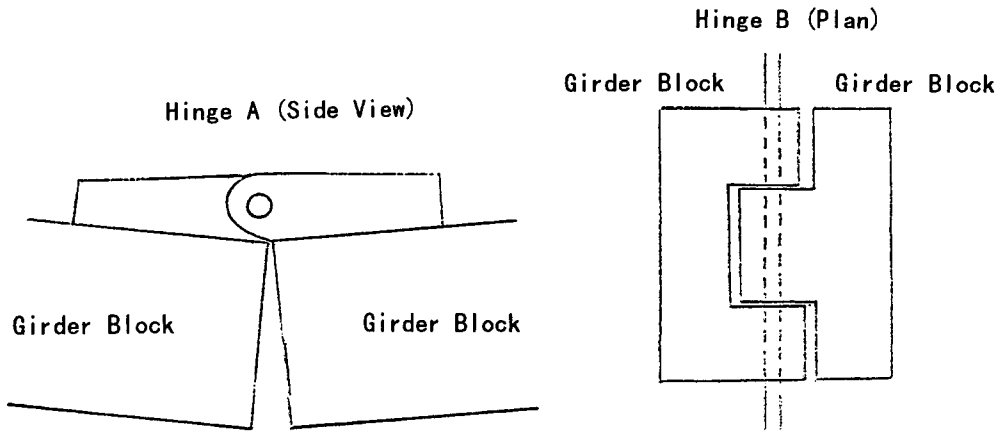


Fig.-2 Hinge System between Girder Blocks during Erection

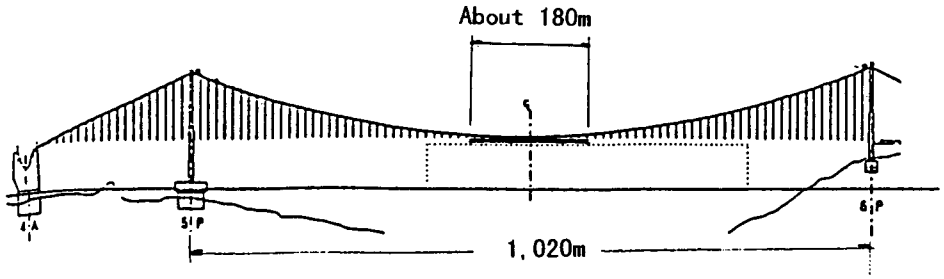


Fig.-3 Girder Erection Stage

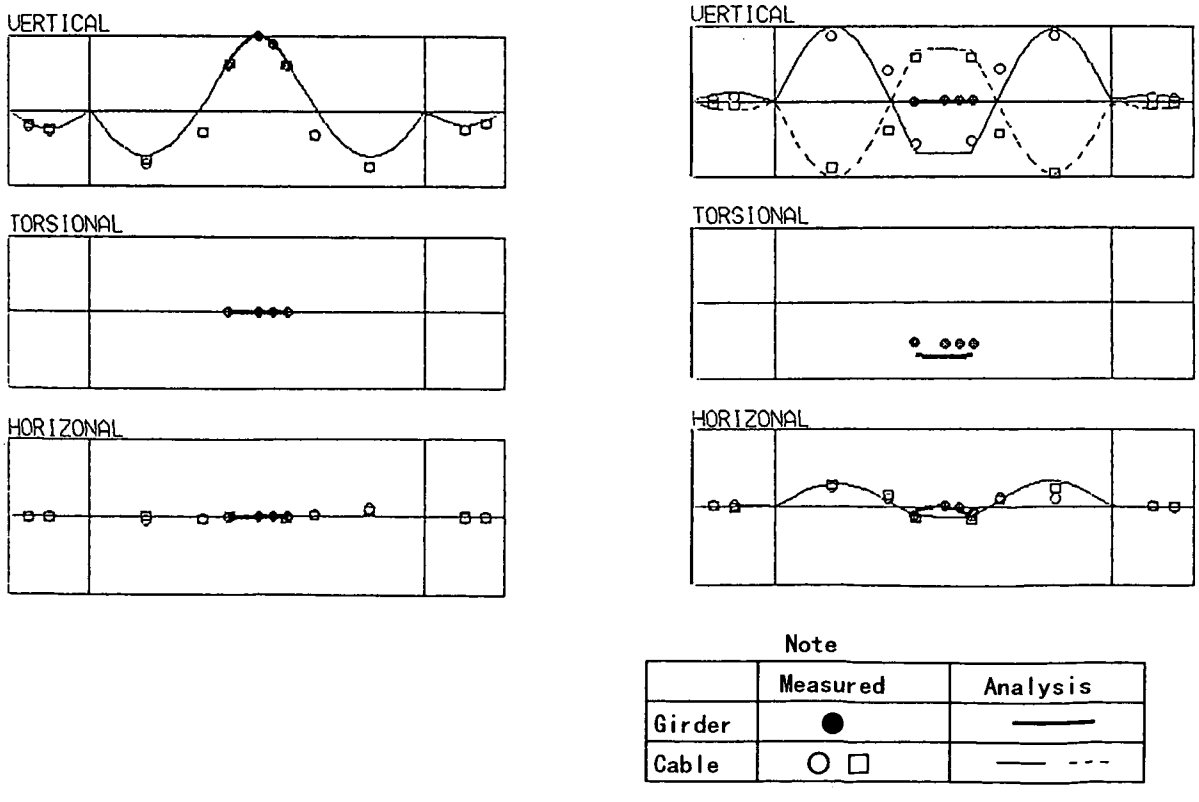


Fig.-4 Natural Mode Shape

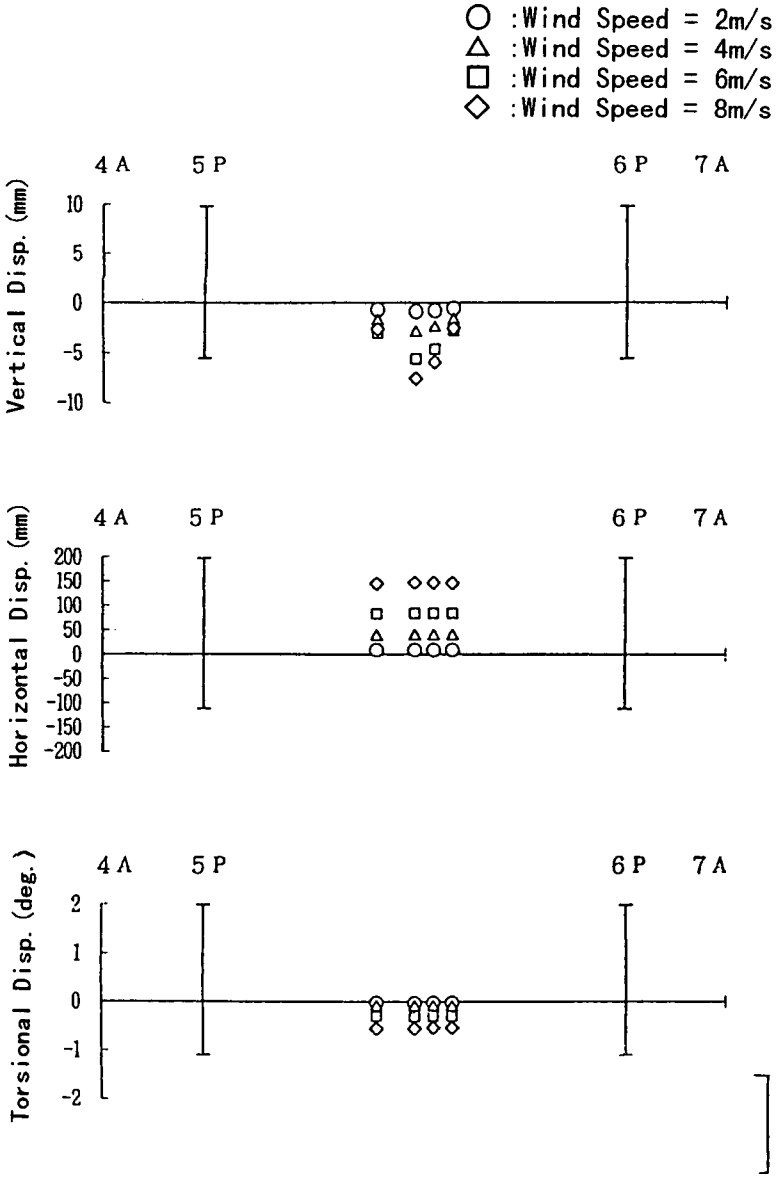


Fig.-5 Static Displacement (α =0°)

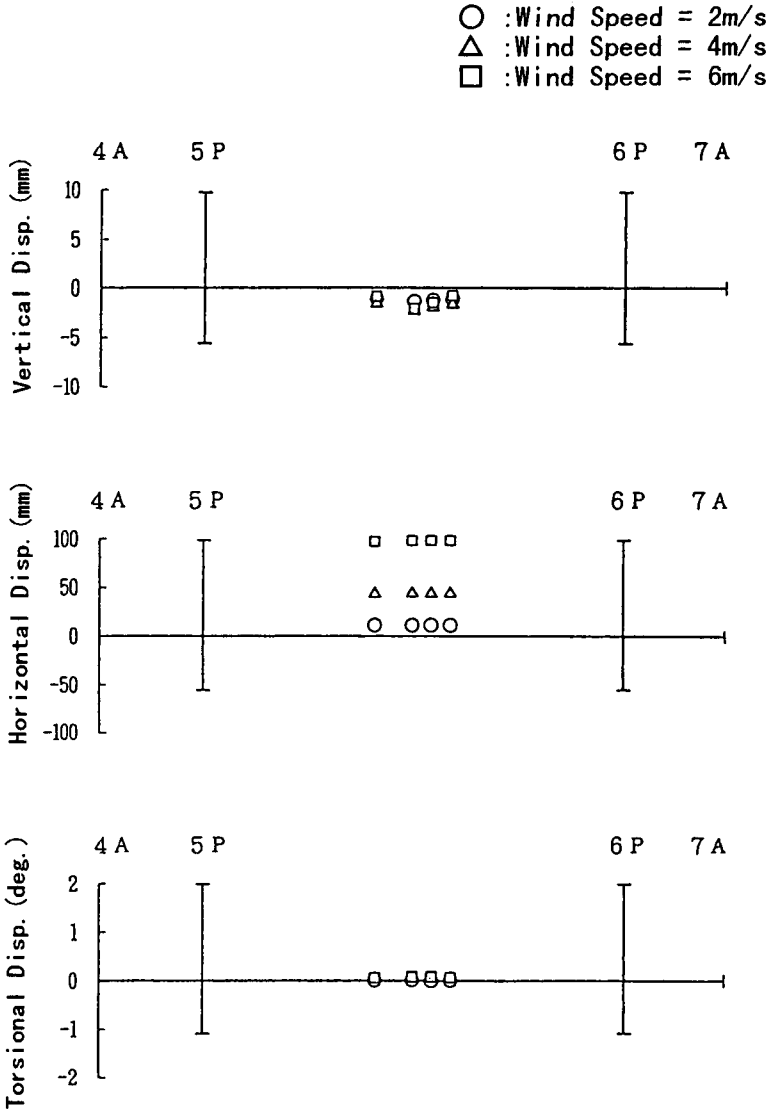


Fig.-6 Static Displacement (α =+3°)

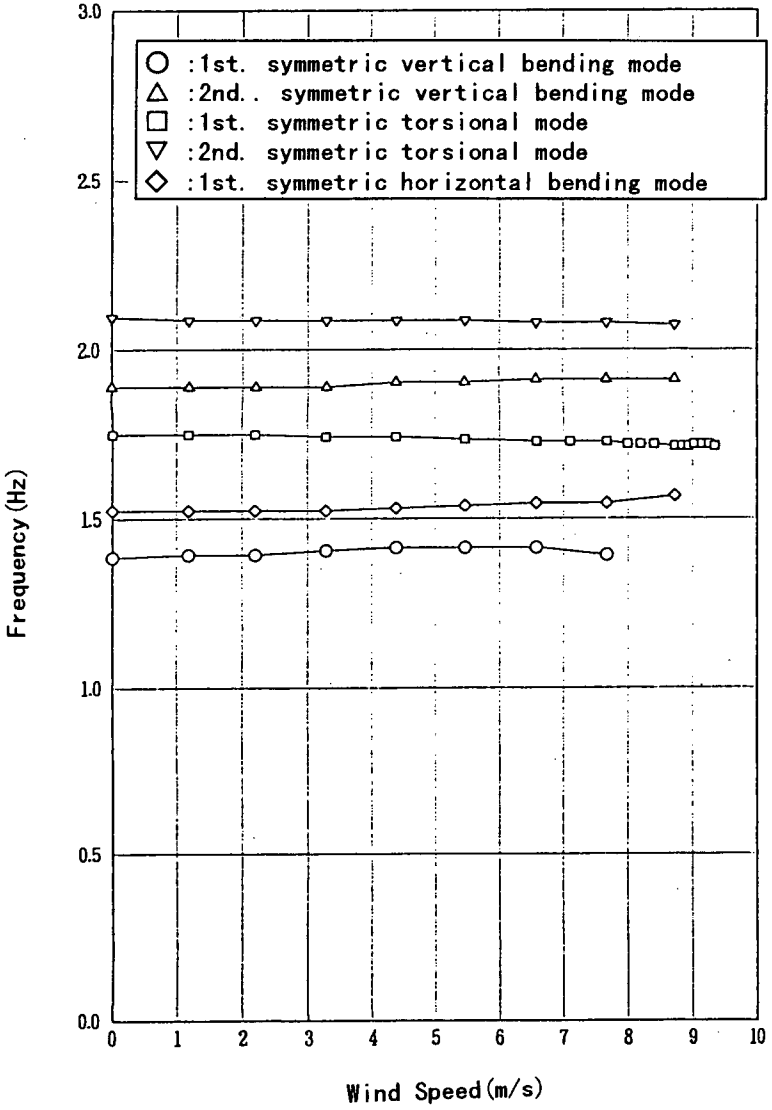


Fig.-7 Natural Frequency - Wind Speed (Test Result)

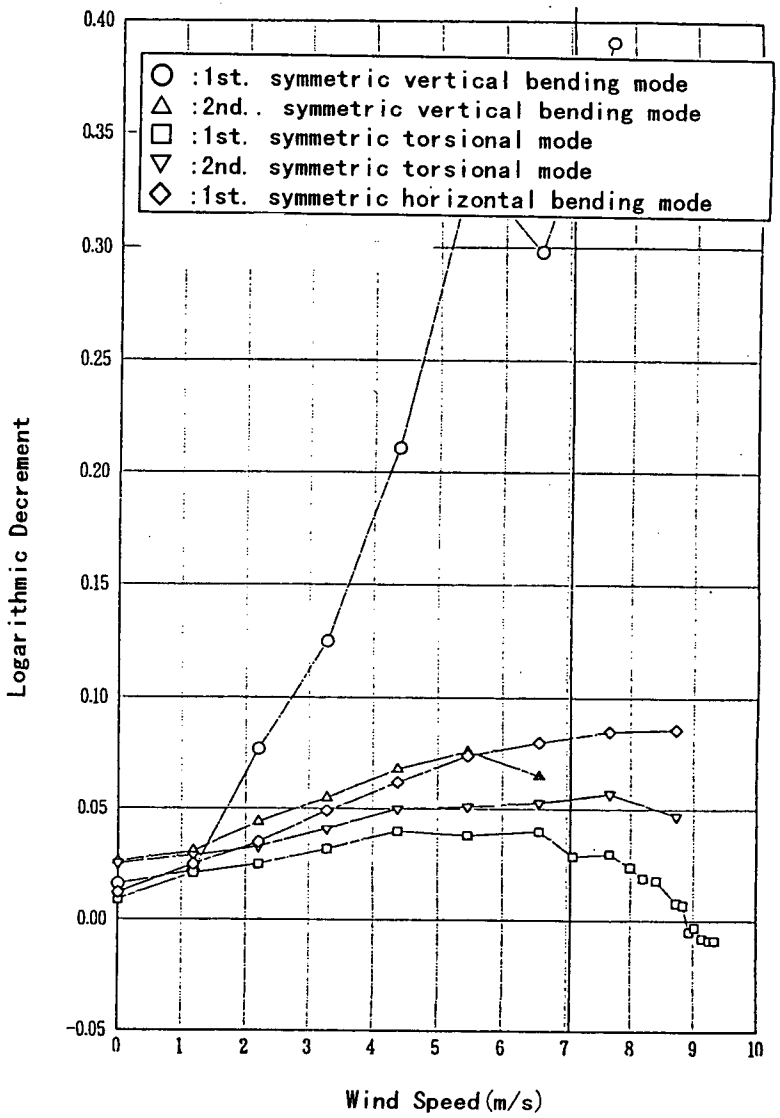


Fig.-8 Apparent Damping - Wind Speed (Test Result)

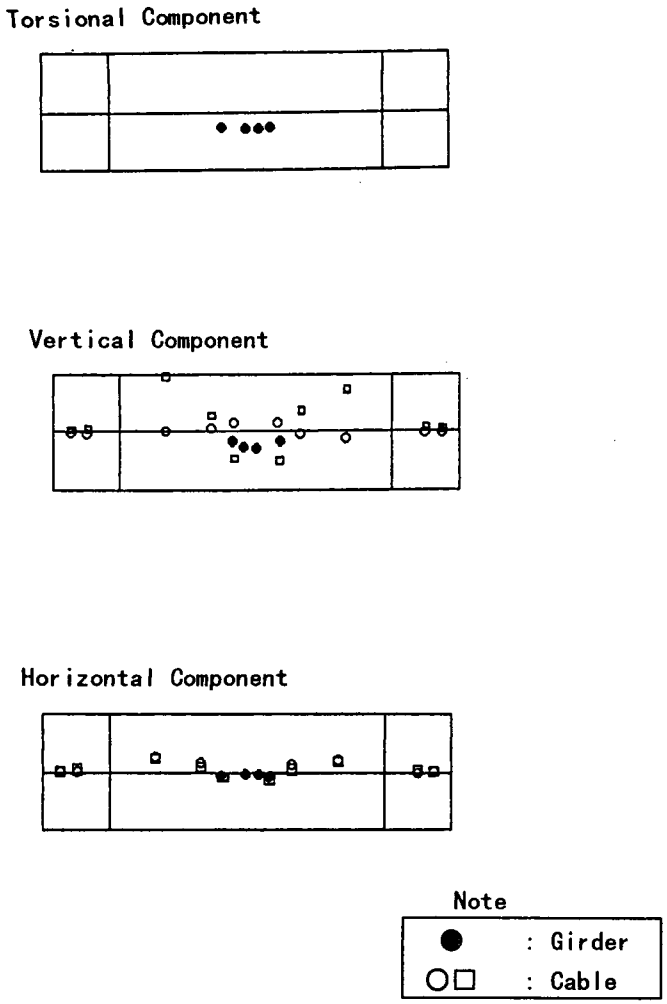
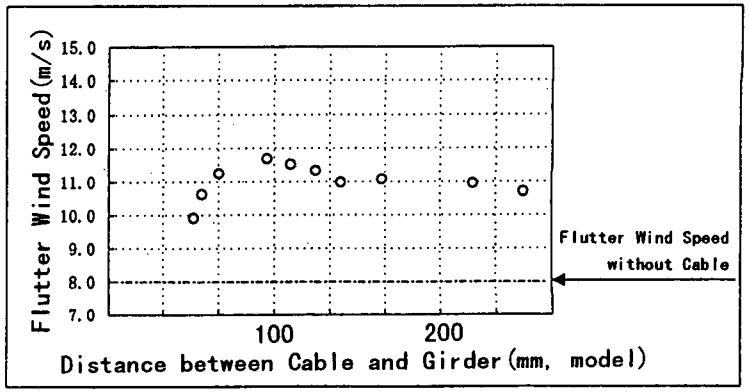
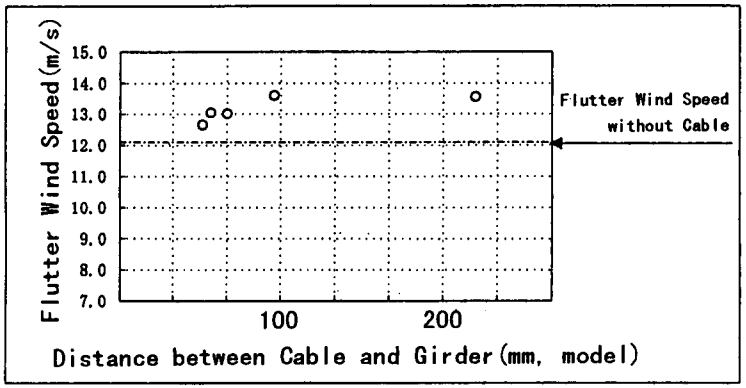


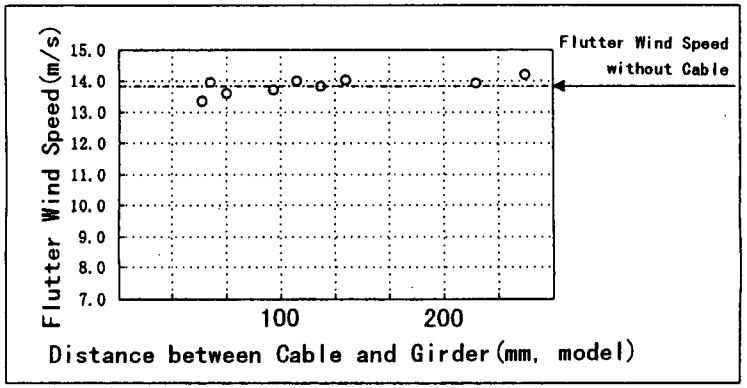
Fig.-9 Flutter Vibration Shape (Test Result)



Angle of Attack = +3°



Angle of Attack = 0°



Angle of Attack = -3°

Fig.-10 Spring Mounted Section Model Test (Effect of the Cat Walk)

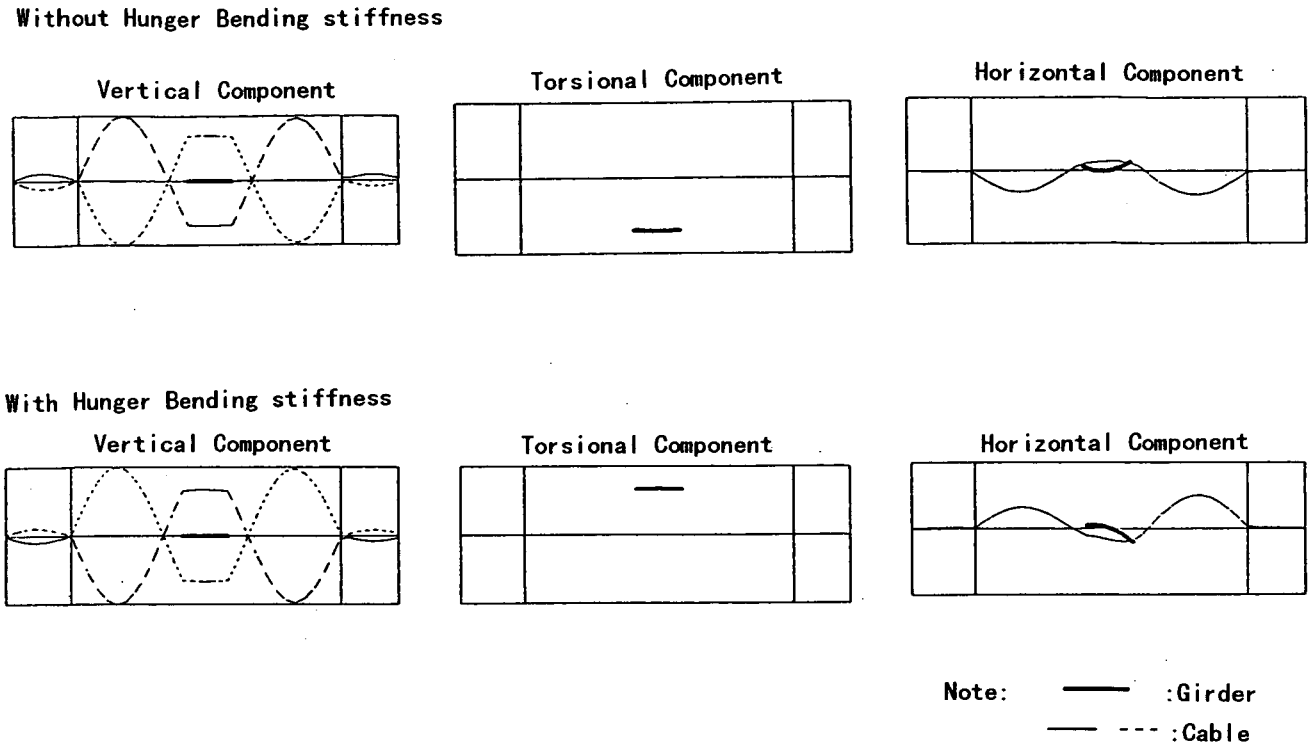


Fig.-11 Torsional Natural Mode Shape(Effect of Hunger Bending Stiffness)

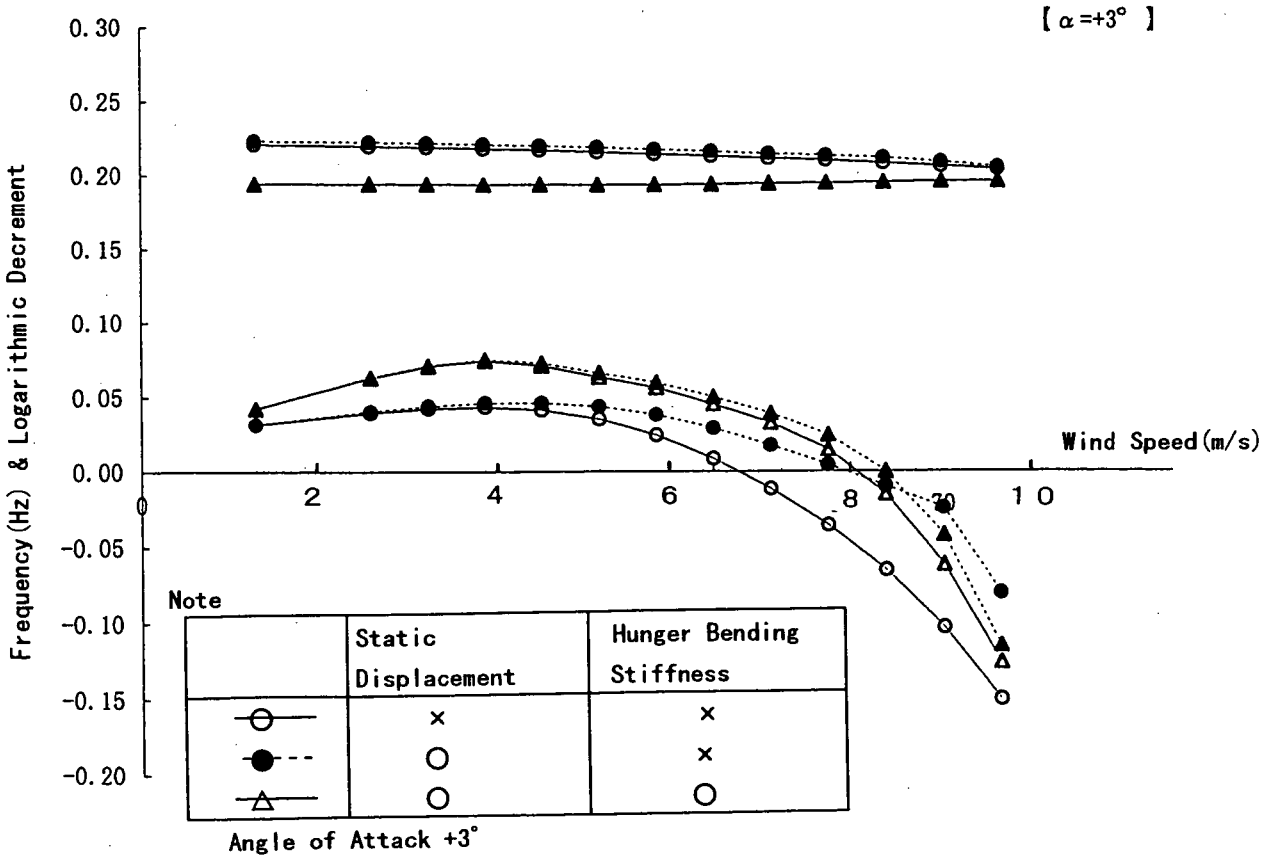


Fig.-12 Natural Frequency, Apparent Damping - Wind Speed(Analysis Result)

Table-1 Dynamic Characteristics of the Model

Mode	Natural Frequency (Hz)		Logarithmic Decrement
	Required	Measured	
1st. symmetric vertical bending mode	1.402	1.337	0.019
2nd. symmetric vertical bending mode	1.844	1.886	0.022
1st. symmetric torsional mode	1.712	1.729	0.012
2nd. symmetric torsional mode	1.991	2.080	0.023
1st. symmetric horizontal bending mode	0.403	0.410	0.009

Table-2 Flutter Wind Speed (m/s)

		Angle of Attack	
		0°	+3°
Experiment		9.4	8.7
Flutter analysis	Case-1	—	6.7
	Case-2	—	7.9
	Case-3	—	8.1

Notes: Case-1, Bending Stiffness of Hungers and Static Deformation are not considered
Case-2, Bending Stiffness of Hungers is considered, Static Deformation is not considered
Case-3, Bending Stiffness of Hungers and Static Deformation are not considered

Table-3 Flutter Analysis Condition

Analysis MethodMode used in the Analysis	Mode Analysis 0 ～ 30 mode
Angle of Attack	+3 °
Aerodynamic Forces	Girder: Lift and Moment Unsteady Aerodynamic Forces (Measured) Drag Quasi-Steady Aerodynamic Forces Cable: Drag and Lift Quasi-Steady Aerodynamic Forces
Air Density	0.12 kgf・s^2/ m^4

Table-4 Effect of Static Displacement and Bending Stiffness of Hungers

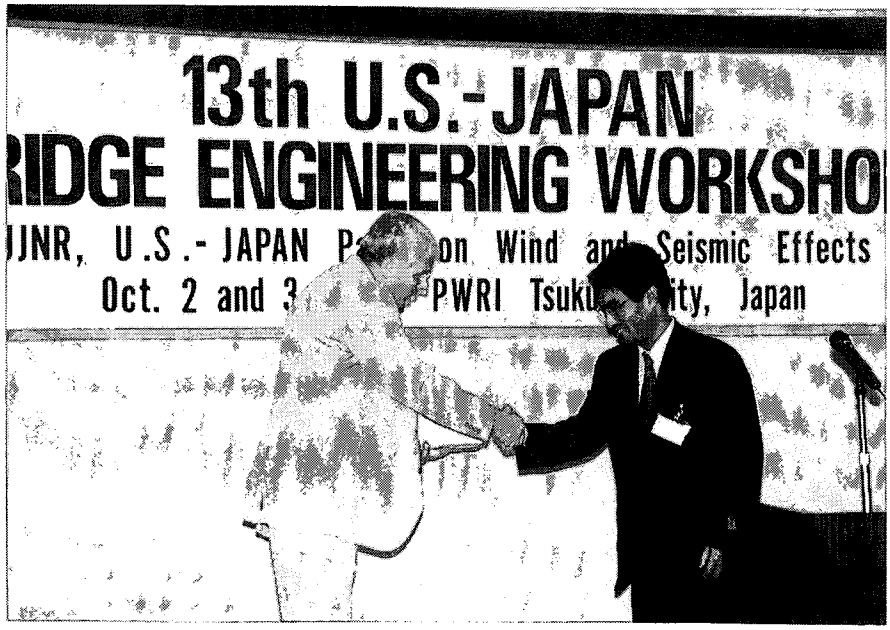
		Case-1	Case-2	Case-3
Static Displacement		×	×	○
Bending Stiffness of Hungers		×	○	○
Natural Frequency				
1st. symmetric vertical bending mode	Hz	1.402	1.402	1.387
1st. symmetric torsional mode	Hz	1.712	1.727	1.720
Equivalent Mass				
1st. symmetric vertical bending mode	kg・s^2/m/m	1.05	1.08	1.09
1st. symmetric torsional mode	kg・m・s^2/m	0.077	0.086	0.089
Flutter Wind Speed	m/s	6.7	7.9	8.1

SESSION 12: CLOSING SESSION

Settlement of Resolution

Remarks: James D.Cooper (Chairman for the U.S. Side)

Closing Remarks: Kazuhiro Nishikawa (Chairman for the Japan Side)



RESOLUTION

RESOLUTION OF THE THIRTEENTH U.S.-JAPAN BRIDGE ENGINEERING WORKSHOP

Tsukuba, Ibaraki, Japan

October 2 and 3, 1997

The following resolutions are proposed by organizers of the 13th U.S.-Japan Bridge Engineering Workshop to the Task Committee J of UJNR

1. The 13th U.S.-Japan Bridge Engineering Workshop provided valuable exchange of technical information which was beneficial to bridge engineering communities of both countries.

2. The workshop agreed to continue cooperative activities through workshops in this format.

3. It is recommended to conduct the 14th U.S.-Japan Bridge Engineering Workshop in fall 1998 in U.S.

Workshop Program

13th U.S.-JAPAN BRIDGE ENGINEERING WORKSHOP
PROGRAM SCHEDULE

October 2 and 3, 1997
Tsukuba City, Japan

Thursday, October 2, 1997

Place: Conference Room (8F) PWRI

SESSION 1: OPENING SESSION 9:00 - 9:15

(Co-Chairmen: K.Nishikawa, J.D.Cooper)

Welcome Remarks: Seizo Tsuji (Director General, PWRI)
Remarks: James D.Cooper (Chairman for the U.S. Side)
Remarks: Kazuhiro Nishikawa (Chairman for the Japan Side)

COFFEE BREAK 9:15 - 9:30

SESSION 2: SEISMIC ISSUES (1) 9:30 - 10:30

(Co-Chairmen: M.Kaneko, D.H.Sanders)

(1) M. Yoshikawa, H. Kanaji (9:30 - 9:45)
"Technology to Restore a PC Viaduct Damaged by the Great Hanshin Earthquake"

(2) Ayaz H. Malik (9:45 - 10:00)
"Seismic Retrofitting of Bridges in New York "

(3) H. Komatsu, Y. Suzuki, K. Mizuguchi (10:00 - 10:15)
"Aseismic Behavior Assessment of Composite Extradossed Bridge"

DISCUSSION (10:15 - 10:30)

COFFEE BREAK 10:30 - 10:45

SESSION 3: SEISMIC ISSUES (2) 10:45 - 11:45

(Co-Chairmen: Y.Adachi, M.A.Haroun)

(1) K. Tamura, T. Azuma (10:45 - 11:00)
"Experimental Study of the Effects of Liquefaction-Induced Ground Flow on Bridge Foundation"

(2) W. Phillip Yen, John D. O'Fallon, James D. Cooper, Ian M. Friedland (11:00 - 11:15)
"Seismic Vulnerability Studies of Highway Structures"

(3) K. Kawashima, J. Sakai, H. Takemura (11:15 - 11:30)
"Evaluation of Seismic Performance of Japanese Bridge Piers Designed by the Previous Codes"

DISCUSSION (11:30 - 11:45)

PHOTOGRAPH *(Entrance of PWRI Main Building)* 11:45 - 12:00

LUNCH *(Conference Room, 1F)* 12:00 - 13:00

SESSION 4: SEISMIC ISSUES (3) 13:00 - 14:15

(Co-Chairmen: K.Tamura, W.P.Yen)

(1) K. Kawashima, G. Shoji (13:00 - 13:15)
"Interaction of Hysteretic Behavior between Isolator/Damper and Pier in an Isolated Bridge"

(2) T.Terayama, S.Unjoh, K.Tasaki (13:15 - 13:30)
"Nonlinear Seismic Response Characteristics of Two-Story Frame Piers"

(3) Nadim I.Wehbe, M.Saiid Saiidi, David H.Sanders (13:30 - 13:45)
"Displacement Issues of Seismically Loaded R/C Bridge Columns"

(4) Y.Adachi, S.Unjoh, (13:45 - 14:00)
"Damping Characteristics of a Long-Span Suspension Bridge Identified by Strong-motion Data"

DISCUSSION (14:00 - 14:15)

COFFEE BREAK 14:15 - 14:30

SESSION 5: SEISMIC ISSUES (4) 14:30 - 15:45

(Co-Chairmen: S.Unjoh, Y. Xiao)

(1) K. Nishikawa, J. Murakoshi, Y. Josen, M. Takahashi (14:30 - 14:45)
"Ductility Improvement of Steel Bridge Columns Based on Large-Scale Cyclic Loading Tests"

(2) Medhat A. Haroun, Maria Q. Feng (14:45 - 15:00)
"Lap Splice and Shear Enhancements in Composite-Jacketed Bridge Columns"

(3) H. Hanno, H. Tajima, K. funamoto (15:00 - 15:15)
"Experimental Studies on Ductility Properties of Steel Rectangular Piers"

(4) T. Takaku, S. Ikeda, T. Okamoto, H. Matsuda, H. Noto, Y. Kawai (15:15 - 15:30)
"A Comparative Study of Elastic-Plastic Seismic Response Analysis and Pseudo-Dynamic Testing of Steel Bridge Piers"

DISCUSSION (15:30 - 15:45)

COFFEE BREAK 15:45 - 16:00

SESSION 6: MANAGEMENT (1) 16:00 - 16:45

(Co-Chairmen: J.Murakoshi, D.M.Frangopol)

(1) Arunprakash M. Shirole (16:00 - 16:15)
"Network Level Comprehensive Bridge Safety Assurance and Management"

(2) F. Wayne Klaiber, Terry J. Wipf, Brent M. Phares, Jeff R. Reid (16:15 - 16:30)
"Bridge Alternatives for Low Volume Roads"

DISCUSSION (16:30 - 16:45)

RECEPTION AT GRAND SHINONOME 18:30 - 20:30
(HOSTED BY JAPAN SIDE)

Friday, October 3, 1997

Place: Conference Room (8F) PWRI

SESSION 7: MANAGEMENT (2)

9:00 - 10:00

(Co-Chairmen: K.Nishikawa, R.Betti)

(1) Stuart S. Chen, Michael F. Lamanna (9:00 - 9:15)
"Net-Capable Informatics for Instrumented Bridges"

(2) H. Sato, K. Ogihara (9:15 - 9:30)
"Development of a Bridge Management System"

(3) Dan M. Frangopol, Allen C. Estes, Kai-Yung Lin (9:30 - 9:45)
"Optimal Bridge Management under Uncertainty in a Life-Cycle Perspective"

DISCUSSION (9:45 - 10:00)

COFFEE BREAK 10:00 - 10:15

SESSION 8: MANAGEMENT (3)

10:15 - 11:30

(Co-Chairmen: H.Sato, E.M.Maragakis)

(1) Andrzej S. Nowak, Sangjin Kim, Vijay Saraf (10:15 - 10:30)
"Evaluation of Bridges by Field Testing"

(2) M. Ishida, N. Akita, A. Watanabe, J. Fukui (10:30 - 10:45)
"Development of Survey Method for Bridge Foundations"

(3) Terry D. Philbin (10:45 - 11:00)
"Detection of Concrete Bridges Using Micropower Impulse Radar and Multi-Frequency Diffraction Tomography"

(4) Raimondo Betti, Maciej P. Bieniek, Paul F. Duby,
Alan C. West, Scott C. Barton, Garry Veermaas (11:00 - 11:15)
"Hydrogen Embrittlement and Deterioration Effects on Wires in Cable-Supported Bridges"

DISCUSSION (11:15 - 11:30)

LUNCH *(Conference Room, 1F)* 11:30 - 12:30

SESSION 9: ADVANCED MATERIALS 12:30 - 14:00

(Co-Chairmen: J.Murakoshi, F.W.Klaiber)

(1) Malcolm T. Kerley, Jose P. Gomez (12:30 - 12:45)
"The Use of High Performance Materials in Virginia's Bridges"

(2) A. Zureick (12:45 - 13:00)
"Test Methods and Long-Behavior of Polymer Composites for Bridge Structures"

(3) T. Hoshijima, H. Sakai, H. Otaguro, S. Matsui (13:00 - 13:15)
"Experimental Study on Strengthening Effect of High-Modulus Carbon Fiber Sheet on Damaged Concrete Deck Slab"

(4) Adam Matteo, Peter Massarelli, Jose Gomez,
William Wright, James Cooper (13:15 - 13:30)
"Preliminary Evaluation of an Aluminum Bridge Deck Design for Highway Bridges"

(5) Dennis R. Mertz, John W. Gillespie,Jr. and William A. Edberg (13:30 - 13:45)
" The Design and Construction of Composite-Material Bridges in Delaware"

DISCUSSION (13:45 - 14:00)

COFFEE BREAK 14:00 - 14:15

SESSION 10: SEISMIC ISSUES (5) 14:15 - 15:45

(Co-Chairmen: T.Terayama, D.R.Mertz)

(1) Y. Xiao, H. Wu (14:15 - 14:30)
"Compressive Behavior of Concrete Stub Columns Confined by Carbon Fiber Composite Jackets"

(2) F. Hakamada (14:30 - 14:45)
"Design Considerations on the Retrofit of RC Columns with CFRP Sheet"

(3) Thomas Post, Mohsen Sultan (14:45 - 15:00)
"California's Program for the Use of Composite Materials for Seismic Retrofit"

(4) H.Hayashi, K. Kosa, Y. Kimura, H. Kitahara (15:00 - 15:15)
"Evaluation of Foundations on the Hanshin Expressway Kobe Route Damaged by the Great Hanshin Earthquake"

(5) E. Manos Maragakis, Bruce M.Douglas, Qingbin Chen, Ray Zelinski (15:15 - 15:30)
"Retrofitting of Railway Bridges"

DISCUSSION (15:30 - 15:45)

COFFEE BREAK 15:45 - 16:00

SESSION 11: WIND 16:00 - 17:15

(Co-Chairmen: H.Sato, A.S.Nowak)

(1) H. Sato, T. Mabuchi (16:00 - 16:15)
"Development of Expert System for Wind Resistant Design of Highway Bridges"

(2) Y. Inoshita, T. Yokota (16:15 - 16:30)
"Wind Characteristics for Structural Design in Osaka City"

(3) S. Nakazaki, H. Yamaguchi (16:30 - 16:45)
"Very Long Suspension Bridges Using the Temporary Mass Method"

(4) R. Toriumi, M. Takeguchi (16:45 - 17:00)
"On Aerodynamic Stability of a Suspension Bridge with Box Girder during Erection Stage"

DISCUSSION (17:00 - 17:15)

SESSION 12: CLOSING SESSION 17:15 - 17:30

(Co-Chairmen: K.Nishikawa, J.D.Cooper)

Settlement of Resolution
Remarks: James D.Cooper (Chairman for the U.S. side)
Closing Remarks: Kazuhiro Nishikawa (Chairman for the Japan side)

RECEPTION AT HOURAN 19:00 - 21:00
(HOSTED BY U.S. SIDE)

List of Participants

- U.S. SIDE -

Dr. Raimondo Betti
Assistant Professor
Dept. of Civil Engineering
610 SW Mudd Building
Columbia University
New York, NY 10027
Phone: 212-854-6388
Fax: 212-854-6267
E-mail: betti@columbia.edu

Dr. Dan Frangopol
Professor
Department of Civil Engineering
Campus Box 428
University of Colorado
Boulder, CO 80309-0428
Phone: 303-492-7165
Fax: 303-492-7317
E-mail: dan.frangopol@colorado.edu

Dr. Stuart S. Chen
Associate Professor
Department of Civil Engineering
212 Ketter Hall
University of Buffalo
Buffalo, NY 14260-4300
Phone: 716-645-2114 x 2428
Fax: 716-645-3733
E-mail: liechen@acsu.buffalo.edu

Dr. Medhat A. Haroun
Professor
University of California, Irvine
Civil Engineering Department
Irvine, CA 92697

Mr. James D. Cooper
Chief of Structures Division (HNR-10)
Federal Highways Administration
6300 Georgetown Pike
McLean, VA 22101
Phone: 703-285-2060
Fax: 703-285-2766
E-mail: jim.cooper@fhwa.dot.gov

Mr. Malcolm Kerley
State Structure and Bridge Engineer
Virginia Department of Transportation
1401 East Broad Street
Richmond, VA 23219
Phone: 804-786-2635
Fax: 804-786-2988
E-mail: aharris3@erols.com

Mr. David Densmore
Chief, Bridge Division (HNG-30)
Federal Highways Administration
7th and D Streets, N.W.
Washington D.C. 20509
Phone: (202)366-4589
Fax: (202)366-9981

Dr. F. Wayne Klaiber
Professor
Department of Civil and Construction Engineering
Iowa State University
Ames, IA 50011
Phone: 515-294-8763
Fax: 515-294-8213
E-mail: Klaiber@iastate.edu

Mr. Ayaz Malik
Project Engineer
NYDOT, Structures Division
1220 Washington Ave.
State Campus Building 5-600
Albany, NY 12232
Phone: (518)457-6465
Fax: (518)485-7826
E-mail: amalik@gw.dot.state.ny.us

Dr. E. Manos Maragakis
Chair and Professor
Department of Civil Engineering
Mail Stop 258
University of Nevada, Reno
Reno, NV 89557
Phone: 702-784-6937
Fax: 702-784-1390
E-mail: maragaki@scs.unr.edu

Dr. Dennis Mertz
Associate Professor
Department of Civil and Environmental Engineering
137 Dupont Hall
University of Delaware
Newark, DE 19716
Phone: 302-831-2735
Fax: 302-831-3640
E-mail: ztrem@ce.udel.edu

Dr. Andrzej Nowak
Professor
Department of Civil & Environmental Engineering
University of Michigan
2340 G. G. Brown Building
Ann Arbor, MI 48109-2125
Phone: 313-764-9299
Fax: 313-764-4292
E-mail: Nowak@engin.umich.edu

Mr. Terry D. Philbin
Structural Engineering
FHWA Region 8
555 Zang Street, Room 400 Code HES-08
Lakewood, Colorado 80228
Phone: 303-969-5772 Ext.351
Fax: 303-696-6727
E-mail: terry.philbin@fhwa.dot.gov

Mr. Tom Post
Chief Officer of Earthquake Engineering
Engineering Service Center, Mail Stop 9
1801-30th Street / P. O. Box 942874
CALTRANS
Sacramento, CA 95816-001
Phone: (916)227-8728
Fax: (916)227-8898
E-mail: tpost@trmx3.dot.ca.gov

Dr. David H. Sanders
Associate Professor
Department of Civil Engineering
Mail Stop 258
University of Nevada, Reno
Reno, NV 89557
Phone: 702-784-4288
Fax: 702-784-1390
E-mail: sanders@unr.edu

Mr. Arunprakash Shirole
Executive Director
National Steel Bridge Alliance
4527 Robin Circle N.
Robbinsdale, MN 55422
Phone: 612-537-7073
Fax: 612-537-4997
E-mail: shirole@aiscmail.com

Dr. Yan Xiao
Assistant Professor
University of Southern California
Civil Engineering Department
3620 S. Vermont Ave. KAP 210
Los Angeles, CA 90089-2531
Phone: 213-740-0603
Fax: 213-744-1426
E-mail: yanxiao@rcf.usc.edu

Dr. Abdul Zureick
Head of Structural Engineering and Mechanics
Georgia Institute of Technology
Civil and Environmental Engineering
Atlanta, Georgia 30332-0335
Phone: 404-894-2294
Fax: 404-894-2278
E-mail: azureick@ce.gatech.edu

Dr. Wen-Huei (Phil) Yen
Structures Division (HNR-10)
Federal Highways Administration
6300 Georgetown Pike
McLean, VA 22101
Phone: 703-285-2315
Fax: 703-285-2766
E-mail: wen-huei.yen@fhwa.dot.gov

- JAPAN SIDE -

(Public Works Research Institute)

Address: 1 Asahi, Tsukuba-shi Ibaraki-ken 305, Japan
TEL: (0298)64-2211
FAX: (0298)64-2840

Seizo Tsuji

Position: Director - General

Toshinori Mizutani

Position: Deputy Director - General

Koichi Yamamoto

Position: Assistant Director - General

Shigeo Kanwo

Position: Assistant Director - General for Geosphere

Kunihiko Takada

Position: Director, Planning and Research Administration Department

Makoto Nakamura

Position: Director, Road Department

Kiyoshi Katawaki

Position: Director, Materials and Construction Department

Michio Okahara

Position: Director, Structure and Bridge Department

Koichi Yokoyama

Position: Director, Earthquake Disaster Prevention Research Center

Masahiro Nishitani

Position: Advisory Engineer for Bridge, Planning and Research Administration Department

Hiroyuki Sakamoto

Position: Head, Chemistry Division
Materials and Construction Department

Hirotaka Kawano

Position: Head, Concrete Division
Materials and Construction Department

Yoshiki Tanaka

Position Research Engineer, Concrete Division
Materials and Construction Department

Jiro Fukui

Position: Head, Foundation Engineering Division
Structure and Bridge Department

Yoshitomi Kimura

Position: Senior Research Engineer, Foundation Engineering Division
Structure and Bridge Department

Masahiro Ishida

Position: Research Engineer, Foundation Engineering Division
Structure and Bridge Department

Masahiro Shirato

Position: Research Engineer, Foundation Engineering Division
Structure and Bridge Department

Hiroshi Sato

Position: Head, Structure Division
Structure and Bridge Department

Jyunzo Inoue

Position: Senior Research Engineer, Structure Division
Structure and Bridge Department

Katsuya Ogihara

Position: Senior Research Engineer, Structure Division
Structure and Bridge Department

Toshiaki Mabuchi

Position: Research Engineer, Structure Division
Structure and Bridge Department

Kenichi Ohgi

Position: Research Engineer, Structure Division
Structure and Bridge Department

Kazuhiro Nishikawa

Position: Head, Bridge Division
Structure and Bridge Department

Jun Murakoshi

Position: Senior Research Engineer, Bridge Division
Structure and Bridge Department

Yasushi Josen

Position: Research Engineer, Bridge Division
Structure and Bridge Department

Arata Hiromatu

Position: Research Engineer, Bridge Division
Structure and Bridge Department

Hideki Sugita

Position: Head, Earthquake Disaster Prevention Technology Division
Earthquake Disaster Prevention Research Center

Tomofumi Nozaki

Position: Senior Research Engineer, Earthquake Disaster Prevention Technology Division
Earthquake Disaster Prevention Research Center

Tadashi Hamada

Position: Research Engineer, Earthquake Disaster Prevention Technology Division
Earthquake Disaster Prevention Research Center

Keiichi Tamura

Position: Head, Ground Vibration Division
Earthquake Disaster Prevention Research Center

Masahiro Kaneko

Position: Senior Research Engineer, Ground Vibration Division
Earthquake Disaster Prevention Research Center

Takuo Azuma

Position: Research Engineer, Ground Vibration Division
Earthquake Disaster Prevention Research Center

Akihiro Nakao

Position: Research Engineer, Ground Vibration Division
Earthquake Disaster Prevention Research Center

Shigeki Unjoh

Position: Head, Earthquake Engineering Division
Earthquake Disaster Prevention Research Center

Toru Terayama

Position: Senior Research Engineer, Earthquake Engineering Division
Earthquake Disaster Prevention Research Center

Yukio Adachi

Position: Senior Research Engineer, Earthquake Engineering Division
Earthquake Disaster Prevention Research Center

Masuo Kondoh

Position: Research Engineer, Earthquake Engineering Division
Earthquake Disaster Prevention Research Center

Jun-ichi Hoshikuma

Position: Research Engineer, Earthquake Engineering Division
Earthquake Disaster Prevention Research Center

Michio Ohsumi

Position: Research Engineer, Earthquake Engineering Division
Earthquake Disaster Prevention Research Center

Kazuhiko Murai

Position: Visiting Researcher, Earthquake Engineering Division
Earthquake Disaster Prevention Research Center

Kenji Tasaki

Position: Visiting Researcher, Earthquake Engineering Division
Earthquake Disaster Prevention Research Center

Masahiro Koshitoge

Position: Visiting Researcher, Earthquake Engineering Division
Earthquake Disaster Prevention Research Center

(Tokyo Institute of Technology)

Kazuhiko Kawashima

Position: Professor, Department of Civil Engineering
Address: 2-12-1,O-okayama, Meguro-ku, Tokyo, 152, Japan
TEL: 03-5734-2922
FAX: 03-3729-0728

Gaku Shoji

Position: Research Associate, Department of Civil Engineering
Address: 2-12-1,O-okayama, Meguro-ku, Tokyo, 152, Japan
TEL: 03-5734-2922
FAX: 03-3729-0728

(Japan Highway Public Corporation)

Kazuyuki Mizuguchi

Position: Assistant Manager, Bridge Engineering Division,
Construction Department 2, Nagoya Construction Bureau
Address: 4-1-1, Sakae, Naka-ku, Nagoya-shi, 460 Japan
TEL: 052-262-7383
FAX: 052-241-4530

(Metropolitan Expressway Public Corporation)

Hitoshi Tajima

Position: Section Chief, Design and Research Division, Engineering Department
Address: 1-4-1,Kasumigaseki, Chiyoda-ku,Tokyo, 100, Japan
TEL: 03-3502-7311
FAX: 03-3502-2411

(Hanshin Expressway Public Corporation)

Fumio Hakamada

Position: Senior Engineer, First Construction Division

Address: 1-2-4, Nishi Shinsaibashi, Chuo, Osaka, 542, Japan

TEL: 06-243-9861

FAX: 06-243-9888

Hidesada Kanaji

Position: Engineer, Design Sectioin, Osaka First Construction Division

Address: 1-2-4, Nishi Shinsaibashi, Chuo, Osaka, 542, Japan

TEL: 06-243-9863

FAX: 06-243-9888

Kenji Kosa

Position: Senior Engineer, Design Section, Engineering Division

Address: Osaka Center Bldg., Kyutaro 4-1-3, Chuo, Osaka, 541, Japan

TEL: 06-252-8121

FAX: 06-252-4583

(Honshu-Shikoku Bridge Authority)

Shuichi Suzuki

Position: Manager, Engineering Research Division, Tokyo Office

Address: Toranomon 45 Mori Bldg., 5-1-5, Toranomon, Minato-ku, Tokyo, 105, Japan

TEL: 03-3434-7281

FAX: 03-3578-9298

Ryuichi Toriumi

Position: Acting Manager, First Design Division, Design Department

Address: Urban-Ace San-nomiya Building, 4-1-22, Onoe-dori, Chuo-ku, Kobe, 651, Japan

TEL: 078-291-1000

FAX: 078-291-1362

(Tokyo Metropolitan Government)

Sentarou Takagi

Position: Major Engineer, Road and Bridge Construction Section,
Branch of North Tama-Area Construction, Bureau of Construction
Address: 2-15-19, Shibazaki-mati, Tachikawa City, Tokyo-Pref, Japan
TEL: 0425-25-9811 3630
FAX: 0425-25-9746

Hiroki Minamikawa

Position: Senior Engineer, Road and Bridge Construction Section, Bureau of Construction
Address: 2-8-1, Nishi-Sinjyuku, Shinjyuku City, Tokyo-Pref, Japan
TEL: 03-5320-5355
FAX: 03-5388-1531

(Osaka Municipal Government)

Tetsuya Yokota

Position: Staff Officer of Elevated Crossing Dept.
Roads and Streets Division, Public Works Bureau
Address: 1-2-2-500, Umeda, Kita-ku, Osaka, 530, Japan
TEL: 06-208-9484
FAX: 06-343-1384

Hiroshi Tanaka

Position: Manager, Bridge Design Department, Hitachi Zosen Corporation
Address: 1-5-1, Chikko-Shinmachi, Sakai City, Osaka, 592, Japan
TEL: 0722-43-6808
FAX: 0722-43-6834

(Japan Association of Steel Bridge Construction)

Shunzo Nakazaki

Position: Manager, Research Laboratory of Engineering Division, Kawada Industries, Inc.
Address: 1-3-11 Takinogawa, Kita-ku, Tokyo, 114, Japan
TEL: 03-3915-3301
FAX: 03-3915-3771

Shigeru Echigo

Position: Director, Manager of Engineering Division, Kawada Industries, Inc.

Address: 1-3-11 Takinogawa, Kita-ku, Tokyo, 114, Japan

TEL: 03-3915-3301

FAX: 03-3915-3771

Tatsumasa Takaku

Position: Principal Engineer, Steel Structure, Machinery and Construction Division, NKK Corp.

Address: 2-1, Suehiro-cho, Tsurumi-ku, Yokohama, 230, Japan

TEL: 045-505-7554

FAX: 045-505-7561

Soichiro Imai

Position: Engineer of Bridge Construction and Engineering Department, NKK Corp.

Address: 2-1, Suehiro-cho, Tsurumi-ku, Yokohama, 230, Japan

TEL: 045-505-7555

FAX: 045-505-7561

Kenji Watanabe

Position: Staff, Bridge Construction and Engineering Department, NKK Corp.

Address: 2-1, Suehiro-cho, Tsurumi-ku, Yokohama, 230, Japan

TEL: 045-505-7581

FAX: 045-505-7561

Shingo Mizutani

Position: Research Engineer,
Civil & Building Technology Research Department Applied Technology Research Center,
NKK Corp.

Address: 1-1, Minamiwatarida-cho, Kawasaki-ku, Kawasaki, 210, Japan

TEL: 044-322-6221

FAX: 044-322-6519

Keiji Terao

Position: Chief Research Engineer, Technical Maintenance Office, Yokogawa Maintenance Corp.

Address: 27, Yamano-cho, Funabashi-shi, Chiba-ken, 273, Japan

TEL: 0474-37-3821

FAX: 0474-37-3824

(Japan Prestressed Concrete Contractors Association)

Kazumasa Yano

Position: Design Department 2, Civil Engineering Design Division, Construction Group, Kajima Corp.

Address: 6-5-30, Akasaka, Minato-ku, Tokyo, 107, Japan

TEL: 03-5561-2189

FAX: 03-5561-2156

(Japanese Association for Steel Piles)

Takeshi Katayama

Position: Head, Foundation Engineering Service Dept., Construction Materials, Development & Engineering Service Div., Nippon Steel Corpotation

Address: 6-3 Otemachi 2-chome, Chiyoda-ku, Tokyo, 100-71, Japan

TEL: 03-3275-7745

FAX: 03-3275-5636

Osami Hashimoto

Position: Manager, Construction Materials & Engineering Services Dept., Construction Materials Center, Kawasaki Steel Corp.

Address: 2-3, Uchisaiwai-cho 2-chome, Chiyoda-ku, Tokyo, 100, Japan

TEL: 03-3597-4517

FAX: 03-3597-4530

(Carbon Fiber Repair & Reinforcement Research Association)

Masahiko Uemura

Position: Deputy General Manager Tow Sheet Marketing & Engineering Dept., Tonen Corporation
Chief Secretary of Carbon Fiber Repair & Reinforcement Research Association

Address: Ebisu Prime Square Tower, 1-1-39, Hiroo, Shibuya-ku, Tokyo, 150, Japan

Akira Kobayashi

Position: Manager, Engineering Group, Tow Sheet Marketing & Engineering Dept. Tonen Corpration

Address: W/I Tonen Corporation Elise Prime Square Tower,
1-1-39, Hiroo, Shibuyaku, Tokyo, 100, Japan

TEL: 03-3286-5186

Tokitaro Hoshijima

Position: General Manager, Composites Materials Division, Mitsubishi Chemical Corporation
Secretary of Carbon Fiber Repair & Reinforcement Research Association

Address: 5-2, Marunouchi 2-chome, Chiyoda-ku, Tokyo, 100, Japan

TEL: 03-3283-6838

FAX: 03-3283-6769

Hirofumi Otaguro

Position: Assistant Manager, Composite Materials Group, Kurosaki Plant,
Mitsubishi Chemical Corporation

Address: 1-1, Shiroichi, Kurosaki, Yahatanishi-ku, Kitakyushu, Fukuoka-ken, 806, Japan

TEL: 093-643-2500

FAX: 093-643-2030

Minoru Shimokawachi

Position: Deputy Director, Oyo Corporation

Address: 4-2-6, Kudankita, Chiyoda, Tokyo

TEL: 03-3234-0811

FAX: 03-3234-6485

Photos of Study Tour





